UNIVERSITY OF SOUTHAMPTON

DAMAGE STRUCTURES AND FAULT EVOLUTION AROUND STRIKE-SLIP FAULTS

by Young-Seog Kim

Thesis for Doctor of Philosophy

School of Ocean and Earth Science

July 2000

UNIVERSITY OF SOUTHAMPTON

ABSTRACT

FACULTY OF SCIENCE
SCHOOL OF OCEAN AND EARTH SCIENCE

Doctor of Philosophy

DAMAGE STRUCTURES AND FAULT EVOLUTION AROUND STRIKE-SLIP FAULTS

by Young-Seog KIM

Damage zones around strike-slip fault show a variety of fracture patterns related to stress concentration and accommodation of displacement. Damage zone structures can be classified into three main groups according to their location along a strike-slip fault - tip zone, wall zone and linking zone structures. Tip damage zones can be sub-divided according to fault tip modes such as along-strike tips (Mode II) and up- and down-dip tips (Mode III). Wall zone damage structures patterns that reflect the propagation of the fault and slip-induced deformation (kinematic damage). Linking zone damage structures are developed between adjacent tip zones of two parallel or sub-parallel faults and vary between dilational and contractional oversteps. Lens-shaped structures evolve from old fault segment tips.

Analysis of maximum displacement (d_{max}) - length (L) relationships for fault populations shows that strike-slip fault systems evolve from isolated faults through segmented faults to interacting faults. Most geologic faults have a much higher ratio of d_{max}/L than for single slip events (u/L).

Reactivation with the opposite sense of slip modifies the pattern of damage structures around strike-slip faults. Evidence for reverse reactivation includes two groups of tip cracks with different orientations and very low or negative displacements at fault tips.

Fractal analysis shows self-similarity over 6 orders of magnitude. Fractal dimensions for damage zones are higher than for the main fault traces. Strike-slip faults share many similar geometric features over a wide scale range.

ACKNOWLEDGEMENT

First of all, I am grateful to Dave Sanderson for his excellent supervision and guidance, both during preliminary fieldwork and the preparation of this thesis. Warm discussion and fieldwork with Jim Andrews and his reviews were of great benefit to me. I acknowledge Prof. J. H. Kim for his endless encouragement and love over the period for my PhD in UK, and structural geology supervision in SNU. I also thank Bill Fitchers for recommending and encouraging me with this project.

Many other people have contributed to my thesis. In particular I would like to thank Members of the Geomechanics Research Group: Paul Kelly, Gavin Day, Cat Greenfield, Joe Lenham, Rory Quinn, Danny Hyam, George Tuckwell and Xing Zhang for discussion and help. Also I thank David Peacock for useful data and many helpful comments, and suggestions on an early draft of Chapter 2. John Murray, Andy Barker, Bob Nesbitt, John Bull, Clive Boulter and Norman Hamilton are thanked for their advice and concerns through the project. I would like to thank Barry Marsh for all of the photographic processing. Chapter 5 is partly composed of Rachel Mills' painful contribution at Rame Head.

I am indebted to my mother, all other family and friends for all of their support. In particular, I would like to thank Youngmin Lee and Jung-suk Oh for their warm advice, which helped me to settle down in UK. Especially, I thank my wife for her support and love in spite of financial hardship and homesickness.

Finally, I would like to dedicate this thesis to my deceased father in heaven. Without his spiritual help, I could not have finished this project. I also thank Lord to be with me all the time.

CONTENTS

CHAPTER 4: STRIKE-SLIP FAULTING AND DAMAGE STRUCTURES TO THE WEST OF MARSALFORN IN GOZO ISLAND, MALTA **90**

CHAPTER 1: INTRODUCTION

1.1. BACKGROUND TO THE PROJECT

This thesis involves examination and interpretation of a number of exposure-scale strike-slip fault systems in the Devonian and Carboniferous rocks on the north and south coast of Cornwall, and in the Limestone of Miocene age in Gozo island. Structural analysis of these examples is compared with laboratory (analogue) experiments (e.g. Tchalenko, 1970; Bartlett *et al.*, 1981; Cox and Scholz, 1988; Schreurs and Colletta, 1998) and large-scale examples (e.g. Tchalenko and Ambraseys, 1970; Barka and Kadinsky-Cade, 1988; Nicholson *et al.*, 1986; Butler *et al.*, 1997; Little *et al.*, 1998; McClay and Khalil; 1998; Reijs and McClay, 1998). This thesis includes; kinematic analysis of damage zone structures, quantitative analysis of displacements, fractal analysis of the geometry of strike-slip fault systems and a study of scaling laws. The work is built on recent PhD work by Peacock (1991a; faulting) and Jackson (1992; veins) and is complementary to recent works by Kelly (1998; fault networks and strike-slip damage) and Day (1998; fault networks).

1.2. OBJECTIVES AND RESEARCH METHODS

The main purpose of this work is to describe and analyse damage zones around well-exposed strike-slip faults, and to build models of strike-slip fault evolution. The study of small-scale examples is used to provide insight into the development of larger scale faults. The field data are used to propose some kinematic and mechanical models for fault propagation and the development of damage structures.

Three main localities have been selected for this work, Crackington Haven in north Cornwall, Marsalforn in Gozo Island and Rame Head in south Cornwall. Crackington Haven was selected because it shows a spectrum of damage zone structures around strike-slip faults on a flat cleavage surface in the hinge zone of a recumbent fold. Here faults display damage zones of increasing complexity from a single isolated fault with horsetail splays to complex damage structures such as wing cracks, dilational and contractional jogs, overstep faults, block rotations, triangular

openings, fault bends and λ faults. Some of these strike-slip faults show reverse reactivation. Gozo, Malta was selected because strike-slip faults show a variety of damage structures and well preserved, detailed fracture patterns developed in a homogeneous host rock. Damage patterns are described and classified according to fault tip modes and associated fracture patterns. Rame Head was selected because several mature strike-slip faults are developed there. They are characterised by relatively long faults and displacements, and an evolved pattern of damage.

To determine the paleo-stress condition during faulting and to understand the fault evolution, detailed fault and fracture maps were constructed from photos. To understand the characteristics of displacement and propagation of faults, the amount of displacement was measured and marked on the maps. Displacement (d) - distance (x) profiles for the faults are used to quantify the effects of fault geometry on damage zones. Some population studies were performed to determine the distribution and growth characteristics of veins and faults. For a well exposed linked fault system, fractal analysis was carried out to determine the fractal dimensions. Fractal dimensions for fault segments are used to characterise the fault zone geometry and for comparison with the San Andreas Fault.

From the results, some fault evolution models are proposed to classify and explain the observed damage patterns around strike-slip faults and a conceptual model for the damage structures around a strike-slip fault is developed.

1.3. CHARACTERISTICS OF STRIKE-SLIP FAULT SYSTEMS

The importance of subsidiary structures associated with strike-slip faults is widely recognised particularly in the field of petroleum geology and earthquake studies (e.g. Sylvester, 1984, 1988; Biddle and Christie-Blick, 1985; King, 1986; Sibson, 1989; Scholz, 1990). In the past ten years much progress has been made in understanding the variation of displacement along faults and fault systems (e.g. Muraoka and Kamata, 1983; Peacock, 1991b; Peacock and Sanderson, 1991, 1992, 1996). This has led to new models of fault growth and evolution (Dey and Wang, 1981; King, 1986; Pollard and Segall, 1987; Cox and Scholz, 1988; Sibson, 1989; Aydin and Schultz, 1990; Peacock, 1991b; Peacock and Sanderson, 1991, 1992, 1996; Cowie and Scholz, 1992a, 1992c; Du and Aydin, 1995; Anders and Schlische, 1994;

Bürgmann *et al.*, 1994; Filbrandt *et al.*, 1994; Reches and Lockner, 1994; Cartwright *et al.*, 1995).

What are damage zones? They are deformed wall rocks close to the principal displacement surfaces of faults, which accommodate strains necessitated by slip and propagation of the faults. The accommodation strains can be related to changes in displacement along the fault and stress concentration at fault tips with zones of increased damage being associated with high displacement and with high displacement gradients, particularly where two faults overlap and tip out in the case of an isolated single fault.

An intensive damage zone is developed at fault tips, because fault termination and diminishing displacement increases the strain concentration of growth at fault tips (e.g. Cowie and Scholz, 1992b). The linkage via step faults, fault branches, and fault bends form important damage zones in strike-slip fault systems.

Why are they important? Faults are very important features in reservoir rocks. Faults often present barriers to fluid migration depending on their sealing characteristics, and cross-fault permeability may be low. Fluid flow within fault-bound compartments is likely to be controlled by enhanced porosity and permeability in damage zones around faults.

An understanding of damage zones and stress accommodation is important in earthquake activity, and in the determination of porosity and permeability in reservoir rocks. Strong stress drops or nucleation happens around damage zones, because the stress is dissipated to accommodate the loaded stress at damage zone (Sibson, 1986, 1989; King and Nabelek, 1985; King, 1986).

1.4. LAYOUT OF THE THESIS

Most of this thesis is based on data from three main study areas mentioned. The data are presented from each of these areas and two discussion chapters follow. Chapter 2 describes a variety of damage structures around several well-exposed strike-slip faults at Crackington Haven, north Cornwall. This study provides some information about various damage patterns, displacement variation along several segment faults, relationship between maximum displacements and fault lengths, and

distribution of fractures and veins within rotated blocks. The material in this chapter is basis of Kim *et al.*, (2000). Chapter 3 describes along-strike displacement variations and reactivation of strike-slip faults at Crackington Haven, north Cornwall. This study provides new evidence with which to recognise reactivated strike-slip faults using fracture geometry and displacement distributions. Chapter 4 describes a variety of damage zone patterns and their related tip modes around strike-slip faults on Gozo. From this study a model of a conceptual strike-slip fault and its damage zones, and some fault evolution models are proposed. Chapter 5 describes damage patterns around mature strike-slip faults at Rame Head, north Cornwall. This study identifies the development of lens-shaped structures and discusses displacement variation along faults. Chapter 6 synthesises the classification of all damage structures observed in the study areas, and compares several large-scale examples with such small-scale structures. Chapter 7 discusses the several issues of fault evolution such as scaling relationships and fractal analysis for a fault comparing it with a large-scale fault. Some ideas about fault evolution and growth of faults with different magnitudes are presented. Chapter 8 summarises the main conclusions of the thesis from each chapter.

REFERENCES

Anders, M. H. and Schlische, R. W. 1994. Overlapping faults, intra-basin highs, and the growth of normal faults. *J. Geol.* **102**, 165-180.

Aydin, A. and Schultz, R. A. 1990. Effect of mechanical interaction on the development of strike-slip faults with echelon patterns. *J. Struct. Geol.* **12**, 123-129.

Barka, A. A. and Kadinsky-Cade, K. 1988. Strike-slip fault geometry in Turkey and its influence on earthquake activity. *Tectonics* **7**, 663-684.

Bartlett, W. L., Friedman, M. and Logan, J. M., 1981. Experimental folding and faulting of rocks under confining pressure. Part IX. Wrench faults in limestone layers. *Tectonophysics* **79**, 255-277.

Biddle, K. T. and Christie-Blick, N. 1985. Glossary - Strike-slip deformation, basin formation, and sedimentation. In *Strike-slip Deformation, Basin Formation, and Sedimentation*: Eds: Biddle, K. T. and Christie-Blick, N. *Society of Economic Paleontologists and Mineralogists Special Publication,* **37**, 375-386.

Bürgmann, R., Pollard, D. D. and Martel, S. J. 1994. Slip distributions on faults: effects of stress gradients, inelastic deformation, heterogeneous host-rock stiffness, and fault interaction. *J. Struct. Geol.* **16**, 1675-1690.

Butler, R. W. H., Spencer, S. and Griffiths, H. M. 1997. Transcurrent fault activity on the Dead Sea Transform in Lebanon and its implications for plate tectonics and seismic hazard. Journal of the Geological Society of London **154**, 757-760.

Cartwright, J. A., Trudgill, B. D. and Mansfield, C. S. 1995. Fault growth by segment linkage: an explanation for scatter in maximum displacement and trace length data from the Canyonlands Grabens of SE Utah. *Journal of Structural Geology* **17**, 1319-1326.

Cowie, P. A. and Scholz, C. H. 1992a. Physical explanation for the displacement-length relationship for faults using a post-yield fracture mechanics model. *J. Struct. Geol.* **14**, 1133-1148.

Cowie, P. A. and Scholz, C. H. 1992b. Displacement-length scaling relationship for faults: data synthesis and discussion. *J. Struct. Geol.* **14**, 1149-1156.

Cowie, P. A. and Scholz, C. H. 1992c. Growth of faults by accumulation of seismic slip. *J. geophys. Res.* **97**, 11,085-11,095.

Cox, S. J. D. and Scholz, C. H. 1988. Rupture initiation in shear fracture in rocks: an experimental study. *Journal of Geophysical Research* **93**, 3307-3320.

Day, G. K.1998. The Development of fault network geometry (unpublished PhD thesis in Univ. of Southampton). 208pp.

Dey, T. N. and Wang, C. 1981. Some mechanisms of microcrack growth and interaction in compressive rock failure. *Int. J. Rock Mech. & Mining Sci.* **18,** 199-209.

Du, Y. and Aydin, A. 1995. Shear fracture patterns and connectivity at geometric complexities along strike-slip faults. *J. geophys. Res.* **100**, 18,093-18,102.

Filbrandt, J. M., Richard, P. D. and Franssen, R. C. M. W. 1994. Growth and coalescence of faults: numerical simulations and sand-box experiments. In: *TSG Special Meeting on Fault Populations*, Edinburgh, U. K., Extended Abstracts, 57-59.

Jackson, R. 1992. Geometries and mechanics of veins and dykes (unpublished PhD thesis in Univ. of Southampton). 183pp.

Kelly, P. G. 1998. Development and interaction of segmented fault systems. (unpublished PhD thesis in Univ. of Southampton). 167pp.

Kim, Y. -S., Andrews, J. R. and Sanderson, D. J. 2000. Damage zones around strike-slip fault systems and strike-slip fault evolution, Crackington Haven, southwest England. *Geoscience Journal* **4,** 53-72.

King, G. C. P. 1986. Speculations on the Geometry of the Initiation and Termination Processes of Earthquake Rupture and its Relation to Morphology and Geological Structure. . *Pure and Applied Geophysics* **124,** 567-585.

King, G. C. P. and Nabelek, J. 1985. Role of fault bends in the initiation and termination of earthquake rupture. Science **228**, 984-987.

Little, T. A., Grapes, R. and Berger, G. W. 1998. Late Quaternary strike slip on the eastern part of the Awatere fault, Soputh Island, New Zealand. *Geological Society of America Bulletin* **110**, 127-148.

McClay, K. and Khalil, S. 1998. Extensional hard linkages, eastern Gulf of Suez, Egypt. *Geology* **26**, 563-566.

Muraoka, H. and Kamata, H. 1983. Displacement distribution along minor fault traces. *Journal of Structural Geology* **5**, 483-495.

Nicholson, C., Seeber, L., Williams, P. and Sykes, L. R. 1986. Seismic evidence for conjugate slip and block rotation within the San Andreas fault system, southern California. *Tectonics* **5**, 629-648.

Peacock, D. C. P. 1991a. Displacement and segment linkage in fault zones (unpublished PhD thesis in Univ. of Southampton). 129p.

Peacock, D. C. P. 1991b. Displacement and segment linkage in strike-slip fault zones. *J. Struct. Geol.* **13**, 1025-1035.

Peacock, D. C. P. and Sanderson, D. J. 1991. Displacement and segment linkage and relay ramps in normal fault zones. *Journal of Structural Geology* **13**, 721-733.

Peacock, D. C. P. and Sanderson, D. J. 1992. Effects of layering and anisotropy on fault geometry. *J. Geol. Soc. London.* **149**, 793-802.

Peacock, D. C. P. and Sanderson, D. J. 1996. Effects of propagation rate on displacement variations along faults. *J. Struct. Geol.* **18**, 311-320.

Pollard, D. D. and Segall, P. 1987. Theoretical displacements and stresses near fractures in rock: With applications to faults, joints, veins, dikes, and solution surfaces. In *Fracture Mechanics of Rock (ed. B. K. Atkinson). Academic Press Geology Series*, Academic Press. 277-349.

Reches, Z. and Lockner, D. A. 1994. Nucleation and growth of faults in brittle rocks. *Journal of Geophysical Research* **99**, 18159-18173.

Reijs, J. and McClay, K. 1998. Salar Grande pull-aprt basin, Atacama Fault System, northern Chile. In: Holdsworth, R. E., Strachan, R. A. & Dewey, J. F. (eds*). Continental Transpressional and Transtensional Tectonics*. Greological Society, London, Special Publications, **135**, 127-141.

Scholz, C. H. 1990. *The Mechanics of Earthquakes and Faulting.* New York: Cambridge University Press. 439p.

Schreurs, G. and Colletta, B. 1998. Analogue modelling of faulting in zones of continental transpression and transtension. *Geol. Soc. London. Special. Pub.* **135**, 59-79.

Sibson, R. H. 1986. Earthquake and lineament infrastructure. *Phil. Trans. R. Soc. Lond.* **A317**, 63-79.

Sibson, R. H. 1989. Earthquake faulting as a structural process. *J. Struct. Geol.* **11**, 1-14.

Sylvester, A. G. (compiled) 1984. *Wench Fault Tectonics. Am. Ass. Petrol. Geol. Spec. Publ.* 374p.

Sylvester, A. G. 1988. Strike-slip faults. *Bulletin Geological Society of America* **100.** 1666-1703.

Tchalenko, J. S. 1970. Similarities between shear zones of different magnitudes. *Geol. Soc. of America Bull.* **81**, 1625-1640.

Tchalenko, J. S. and Ambraseys, N. N. 1970. Structural analysis of the Dasht-e Bayaz (Iran) earthquake fractures: *Geol. Soc. of America Bull.* **81**, 41-60.

CHAPTER 2: DAMAGE ZONES AND FAULT EVOLUTION AROUND STRIKE-SLIP FAULTS, CRACKINGTON HAVEN, SOUTHWEST ENGLAND

Abstract

A well-exposed outcrop of Upper Carboniferous greywackes and slates at Crackington Haven, north Cornwall, shows several episodes of strike-slip faulting. Exposure-scale structures display many features typical of strike-slip fault systems including: splay faults, wing cracks, jogs, fault bends, fault branches, λ-faults, rotated blocks, together with layer-parallel slip, and deformation of the wall-rocks.

The strike-slip faults developed with a remote NNE-SSW trending maximum compressive principal stress (σ_1). Interactions between anisotropic layering and faults with different orientations are important factors in controlling slip. Displacement (d) - distance (x) analysis indicates that variations in displacement gradient and the material anisotropy of the wall-rocks control the development and nature of damage structures.

The strike-slip fault system shows an evolving pattern from isolated faults through segmented faults to interacting faults, an analysis of which is supported by the maximum displacement (d_{max}) - length (L) relationships for the fault population.

2.1. INTRODUCTION

The importance of structures associated with strike-slip faults has been widely recognised particularly in petroleum geology and earthquake studies (e.g. Biddle and Christie-Blick, 1985; King, 1986; Sylvester, 1988; Sibson, 1989). In the past ten years much progress has been made in understanding variation of displacement along faults and fault systems (e.g. Muraoka and Kamata, 1983; Marrett and Allmendinger, 1991; Peacock, 1991a). This has led to new models of fault growth and evolution (Pollard and Segall, 1987; Cox and Scholz, 1988; Sibson, 1989; Aydin and Schultz, 1990; Peacock and Sanderson, 1991, 1992, 1996; Cowie and Scholz, 1992a, 1992c; Anders and Schlische, 1994; Bürgmann *et al.*, 1994; Filbrandt *et al.*, 1994; Reches *et al.*,

1994; Du and Aydin, 1995; Cartwright *et al.*, 1995).

This paper describes the geometry and evolution of natural damage zones around several exposure-scale strike-slip faults. This detailed work will provide a significant understanding for strike-slip fault evolution. Damage zones are deformed wall-rocks close to faults, which accommodate strains necessitated by changes in displacement along the fault. Zones of increased damage are associated with high displacements and with high displacement gradients (e.g. at fault tips), particularly where two faults interact (e.g. linkage via step faults, fault branches, and fault bends; Pollard and Segall, 1987; Bilham and King, 1989; Sibson, 1989).

Damage zone geometry around faults can provide useful information on how faults propagate, interact and are arrested. An understanding of damage zones and stress accommodation is important in modelling earthquake activity (King, 1986; Aki, 1989; Thatcher and Bonilla, 1989). This small-scale detailed work and scaling relationships suggest that study of small-scale examples provide insights into larger scale faults (e.g. Tchalenko, 1970).

2.2. GENERAL DESCRIPTION OF LOCALITY AND GEOLOGIC SETTING

A well-exposed outcrop at the southern side of Crackington Haven in northern Cornwall (UK grid reference SX 138973) was selected for this study (Fig. 2.1). A number of strike-slip faults are exposed on flat-lying cleavage surfaces in the hinge zone of a recumbent fold (Fig. 2.2). Most of the faults occur in a 5 × 6 m area (Fig. 2.3), but some additional faults were measured and mapped 5 - 20 m along strike to the west (F18 and F20).

Many of the faults are exposed from tip to tip and steeply dipping beds, at a high angle to faults, provide good markers for determination of displacement. The faults display damage zones of varying complexity, from single isolated faults with horsetail splays and interacting faults with wing cracks, through linked faults with overstepping segments, dilational and contractional jogs, to complex regions of damage including block rotations, triangular openings, fault bends and λ faults (Kim *et al.*, 1998).

The host rocks are interbedded sandstones and shales of the Crackington

Formation of Upper Carboniferous age (e.g. Freshney *et al.*, 1972; Selwood *et al.*, 1985; Enfield *et al.*, 1985). They are part of the older fill of the Culm Basin whose origins have been interpreted variously as a foreland basin (Hartley and Warr, 1990; Warr, 1989), a thrust-sheet top basin (Gayer and Jones, 1989) or a pull-apart basin (Andrews, 1993).

The basin was inverted during the Variscan Orogeny at the end of Carboniferous period and then affected by several minor episodes of deformation including late Tertiary movements (Andrews *et al.*, 1998). During the Variscan event, south-facing recumbent folds (Sanderson, 1979) were generated with associated thrusts (Whalley and Lloyd, 1986).

The age of the strike-slip faults can only be constrained from field observations; to post-date the main Variscan folding because the faults cross-cut the Variscan folds. Therefore they may be related to late Cretaceous or Alpine Tertiary north - south shortening (Lake and Karner, 1987; Peacock and Sanderson 1998; Chadwick, 1993; Willemse *et al.*, 1997).

2.3. RESEARCH METHODS AND FAULT PATTERNS

A series of maps at approximately 1:20 to 1:40 scale were made for each major fault system. The maps were made from field photographs with removal of photographic distortions being made in the laboratory using measured distances in the field. A map of the main part of the exposure (Fig. 2.3) was compiled using simple trilateration of selected reference points on the individual faults.

In the field, direct measurement was made of the displacements (d) between marker beds across a fault, and the distances (x) along the fault from one tip to the marker beds. The maximum displacement, usually near the centre of a fault, was also recorded and the fault length defined as the length between two fault-tips. On occasions when a fault is only partly exposed, the length from the tip of a fault to the maximum displacement was taken as a measure of the half-length of the fault. The accuracy of measurement is ~1 mm for vein thickness and fault displacement, and ~1 cm for fault length and distance from a fault tip. In addition to fault data, joints and veins were mapped, particularly in regions around the faults.

Strike orientations of right-lateral strike-slip faults range from N345° to N040^0,

and left-lateral strike-slip faults range from N020° to N075° (Fig. 2.4a). Joints show a similar spread of orientation as the faults (Fig. 2.4b), and are interpreted as a hybrid shear / extension system formed under the same stress system as faults. The general orientation of the far-field stress may be determined from the acute bisector of right-lateral and left-lateral faults, in which σ_1 (maximum compressive stress) is an approximately N030° with σ_2 sub-vertical and σ_3 ~N120°. Some of the faults may have originated from pre-existing joints or fractures due to local variation in the orientation of principal stress in both space and time (Segall and Pollard, 1983a; Granier, 1985).

Figure 2.3 shows a right-lateral fault (F2; NNE trend) cross-cut by a later left-lateral fault (F3; NE trend) implying an age relationship. The faults in Figure 2.3 can be viewed as two groups with slightly different orientation patterns reflecting variation in local stress distribution. During an early stage σ_1 is ~ N060° (horsetails at the tips of fault F8), and most of the right-lateral faults in the northern part of Figure 2.3 were developed (F1, F2, F8, F9 and F11). Some mode I fractures might have been generated during this stage (subsequently reactivated as F3 and F5). At a later stage σ_1 rotated anticlockwise to N020° (wing cracks at the tip of fault F3), and the faults and joints in southern part of Figure 2.3 were developed (F3, F4, F5, F6, F7 and F10). During the later stage, the fault F2 was offset by the left-lateral fault F3 reflecting the change of stress pattern with time.

In this paper the faults are described in order of increasing complexity of their interaction and damage zone development.

2.4. TIP DAMAGES

2.4.1. Definition of isolated faults

Isolated faults are faults where both tips are exposed, with no other faults mapped which cross-cut, abut or branch from the main fault. They are separated from other faults by distances greater than the fault displacement and at least 25% of the fault length. This definition does not preclude interaction of the faults outside the plane of observation, but, since the faults are generally sub-vertical and viewed on a horizontal plane, any interaction would be at a considerable distance from the mapped

trace.

2.4.2. Horsetails and wing cracks

Fault F8 (Fig. 2.5) is a right-lateral isolated fault, striking N032° and dipping 78° NW. The trace is 2 m long, with both tips exposed. It has a maximum displacement of 2 mm and is over 2 m from the nearest adjacent fault (F2). Although this fault has a small jog in the centre of the fault, the fault is mechanically a fault system. At both tips, the fault displays *horsetail fractures* - curved fault splays near the end of a fault that merge with that fault (e.g. Christie-Blick and Biddle, 1985; Sylvester, 1988; Granier, 1985; McGrath and Davison, 1995). They occur in the extensional quadrants of the faults (e.g. Bilham and King, 1989), and are associated with loss of displacement around the tips. The angles between the main fault and the horsetail fractures range from 25° to 40°. The local orientation of the maximum principal compressive stress (σ_1) during failure is assumed to have been parallel to the orientation of the tip cracks (c. N060°).

Branch fractures have been interpreted as propagating towards the direction of the maximum remote principal stress (σ_1) (Brace and Bombolakis, 1963). This is because near a shear plane the stress state changes orientation (e.g. Anderson, 1951; Rispoli, 1981), so the cracks show a change of direction with respect to the direction of regional σ_1 (Granier, 1985). Horsetail fractures splaying from the faults may indicate either former tip points, or sticking points, and may be used to track the propagation direction of the fault (Friedman and Logan, 1970; McGrath and Davison, 1995).

Fault F3 (N052°/87°SE) (Fig. 2.6) is left-lateral with rapidly diminishing displacement towards its north-east tip where a quartz-filled dilated *wing crack* is developed in the extensional quadrant (Fig. 2.6b; note the change of polarity between this and the right-lateral example above). *Wing cracks* are defined as extensional fractures which are wing-shaped in cross-section, and initiate at a high angle to the fault plane. They are assumed to form and propagate away from the fault terminations at an angle which maximises the local tensile stress acting across the incipient crack path (Erdogan and Sih, 1963; Pollard and Segall, 1987).

Wing fracture patterns (Fig. 2.6b) have been reported in association with strike-

slip faults (Rispoli, 1981; McGrath and Davison, 1995). Theoretical studies and laboratory experiments on glasses and ceramics with Mode II fault tips (Brace and Bombolakis 1963, Lajtai, 1971; Horii and Nemat-Nasser 1986, Pollard and Segall, 1987; Petit and Barquins, 1988) indicate that wing cracks propagate from the fault tip and curve away towards the remote maximum principal stress direction (Mode I type). Experiments on glass indicate that formation of wing cracks occurs in uniaxial compressive tests, whereas horsetail fractures are produced in biaxial compressive tests (Petit and Barquins, 1988). Therefore, wing cracks may be formed in tensional stresses under high pore pressure conditions or low confining pressures (McGrath and Davison, 1995), and may form when the end zones are comparatively small (Willemse and Pollard, 1998) due to abrupt changes in frictional strength (Cooke, 1997).

Stress concentrations resulting from slip on small faults often cause veins and solution surfaces to form and propagate away from the fault termination (e.g. Pollard and Segall, 1987). Wing cracks and horsetail splays are both generated by Mode I fractures, although there are some differences between these two structures in orientation and geometry. Wing cracks form at a higher angle to the fault, and have thick, short, wing-shaped openings, whereas horsetail splays form at lower angles to the fault and are long, thin branch fractures (Fig. 2.3).

2.4.3. Displacement-distance (d - x)

The relation between displacement (d) and distance (x) from the fault tips depends on the rock properties and fault interaction. Therefore, changes of observed d-x profile shape are to be expected if faults undergo a change in the geometry of fault or material properties (e.g. Peacock and Sanderson, 1991; Dawers *et al.*, 1993; Willemse *et al.*, 1996). Wing cracks occur where there is a rapid decrease of displacement, and hence high displacement gradient ($\partial d/\partial x$), towards fault tips (Fig. 2.7). The SW end of the profile has the C-type profile shape (cone-shaped) (see Peacock, 1991b) while the NE end has the E-type profile shape (elevated above the C-type), because it has a wing crack at the NE end of the fault tip. The maximum displacement is close to the tip with the wing crack where $\partial d/\partial x > 0.15$, whereas towards the other tip there is a steady displacement gradient ($\partial d/\partial x \approx 0.03$). This kind of fault produces a markedly asymmetrical d-x profile.

2.5. FAULT LINKAGE

Many faults are made up of sub-parallel, non-coplanar segments, which generally are separated by *oversteps* (e.g. Aydin and Nur, 1985; Biddle and Christie-Blick, 1985). Strike-slip faults stepping in the same sense as the fault-slip produce dilational oversteps, which when linked by fractures often produce dilational jogs, whereas those stepping in the opposite sense to fault-slip produce contractional oversteps.

2.5.1. Dilational jogs

The right-stepping segmentation of the right-lateral fault (F2, Fig. 2.6 inset a) has produced a *dilational jog* (e.g. Sibson, 1986, 1989). The quartz-filled openings with fracture filling fibres indicate that the fault was reactivated by repeated movements. The *d-x* profile of F2 fault is M-type (mesa-shaped) (Fig. 2.8; Muraoka and Kamata, 1983; Peacock, 1991b), with steep gradients at tips and a broad, more or less constant displacement region around the maximum displacement value. It is complicated by the effect of a crossing fault (F3), and interaction with fault F9 at its NE end. Measurement of displacement (d) with distance (x) shows displacement is conserved across the jog and the intersection with fault F3. It suggests that two segments were linked through the jog in early stage of the fault evolution, and the fault system reactivated as a fault system. The smooth slope and relatively low displacement around the intersection point of the two faults (F2 and F3) indicates a time gap between activation times of the two faults.

2.5.2. Dilational oversteps

Fault F20 (Fig. 2.9a) is a over 2 m in length and located 30 m west of the main mapped area. It consists of dilational oversteps and its profile of total slip has no displacement minimum at the dilational overstep zone, indicating that displacement is transferred systematically from one fault to the other.

Fault F18 (Fig. 2.9b) lies about 5 m north-west from fault F1 on the main map. The whole length of the fault system is about 6 m. It consists of several, unconnected, sub-parallel overstepping faults. The complex *d-x* profile may result from the interaction between soft-linked faults (Fossen and Hesthammer, 1997) and the linkage

of fault segments (Peacock and Sanderson, 1996). The total displacement profile shows a central minimum reflecting the effect of overstepping faults and jogs. Although complicated by oversteps and jogs, the total displacement is well conserved through soft-linked faults.

2.5.3. Contractional Oversteps

Two right-lateral faults (F2 and F9; Fig. 2.10) strike and dip N033°/80°NW and N027°/79°NW, respectively, and transfer displacement across a left-stepping contractional overstep. The ratio between overstep length (L) and offset (s) is very high (~10). High L/s ratios may occur between faults that form at different times, have a limited down-dip dimension, or where there is a large zone of increased fault strength (Olson and Pollard, 1989; Willemse, 1997).

Although there are no conspicuous fault bridges, which are defined as inclined sectors of unfaulted rock lying between the en-echelon faults, developed in the overstep zone (Ramsay and Huber, 1987), there is an overall displacement decrease where the segments overstep (Fig. 2.11). The linkage profile of F2 and F9 shows a D-type profile (depressed below the cone-shaped C-type) (Peacock, 1991b) and the gradients of each fault become slightly more gentle towards the tips at the relay zone (Willemse *et al.*, 1996; Willemse, 1997). The minimum in the total displacement profile is typical of contractional oversteps (Peacock, 1991a, 1991b; Peacock and Sanderson, 1991) and indicates that slip is transferred between the overstepping faults.

2.5.4. Displacement-distance (d - x) characteristics of linked faults

The distribution of total slip along an array of fault segments usually resembles that of a single larger fault (Fig. 2.9b; Walsh and Watterson, 1991; Bürgmann *et al.*, 1994; Dawers and Anders, 1995; Willemse *et al.*, 1996). The changes in slip distribution near a relay zone are systematic and depend on spacing, down-dip fault height, mechanical properties and the nature of the fault overstep (Peacock and Sanderson, 1991; Willemse *et al.*, 1996). The intensity of the mechanical interaction is influenced by the fault shape, the spatial arrangement of multiple segments, and the distribution of shear strength on the fault (Willemse *et al.*, 1996; Willemse, 1997).

The total d-x profiles at Crackington Haven show that the pattern of displacement transfer between fault segments is strongly dependent on the nature of

the overstep (Figs. 2.9a and 2.11). In contractional oversteps (Figs. 2.10 and 2.11), there is a total displacement minimum within the overstep zone, whereas in dilational oversteps (Fig. 2.9a) there is no displacement minimum. This difference in the total displacement profile might depend on the nature of the propagation of fault tips (Fig. 2.12). In a contractional overstep zone, the tips are pinned within the overstep zone so that the fault propagates from the opposite ends of the fault segments, whereas in dilational oversteps, the tips within overstep zone can propagate onwards to create a more extensive overstep. Therefore, in contractional oversteps, two maximum displacement nodes move back from the overstep zone producing a total displacement minimum.

2.6. ROTATED FAULT BLOCKS

Fault F1 (Fig. 2.13) is a right-lateral fault (strike/dip; N032°/88° NW), which has a relatively large amount of displacement (max. 270 mm) and shows a highly damaged western wall. Wall-rock strain has been accommodated by a combination of left-lateral slip along bedding planes and a right-lateral slip along a subsidiary fault, causing rotation of blocks bounded by the faults and bedding.

Slip along bedding is a dominant feature; the boundaries between thick slate layers and thin greywacke beds acting as detachment surfaces. Blocks of wall-rock adjacent to the fault rotate where locally slip occurs along all sides of the rotated block. A rectangular jog filled with vein quartz is developed at the intersection of the principal displacement surface (F1) with two bed-parallel left-lateral slip surfaces on either side of the main fault (inset (b) in Fig. 2.13).

Several triangular quartz veins are developed along the main fault plane (F1), where subsidiary left-lateral bedding-parallel faults intersect the main fault (inset (b), Fig. 2.13). At least four rotated blocks along the main right-lateral fault can be recognised. The opposing shear couples acting on the bounded blocks have internally deformed them producing arrays of extensional veins. During faulting, the evidence of compensatory vein development suggests enhanced porosity and permeability of the west wall which would have facilitated transfer of considerable volumes of fluid up or down the fault (e.g. Sibson, 1996).

These features are related to bending and block rotation of the wall-rocks (Fig. 2.13; McGrath and Davison, 1995). Detailed observations of the relation between slip

planes indicate that as bedding-plane slip progressed the blocks were internally deformed (inset (a) in Fig. 2.13). The curved slip plane and cross-cutting relationships indicate that both sets of slip surfaces were active at the same time.

The major east-bounding strike-slip fault is not truncated except where the rectangular quartz vein is developed, but the subsiding west-bounding fault is truncated by the bedding-parallel faults at block boundaries. Thus, the western bounding fault was offset by bedding-parallel slip during fault growth (inset (a) in Fig. 2.13). As a result of this mechanism, the triangular shaped veins are generally developed only along the major east-bounding faults.

2.6.1. Displacement - distance profile for F1

Figure 2.14a shows a fairly steady increase in displacement from the NE tip of fault F1, with a displacement gradient, $\partial d/\partial x \approx 0.08$. The profile is a good example of a constant displacement gradient or C-type profile (Peacock, 1991b). Figure 2.14b shows a kinematic model of how the steady increase in displacement along fault F1 can be produced by block rotation. Δd is the increased displacement accompanying each block rotation and $d + \Delta d$ is the total displacement at the end point of each block. Δd depends on the amount of rotation and the block thickness. The amount of rotation in these blocks ranges from 5° to 10° and the block thicknesses vary from 40 to 70 cm.

2.6.2. Veins within rotated blocks

Right-lateral en echelon vein arrays are developed by local maximum compressive stresses (σ_1) within the rotated blocks. The orientation of the vein arrays is nearly north-south trending and the angle between the arrays and master fault (F1) is ~ 30°, although individual veins are sub-parallel to the master fault.

A log-log plot of the maximum thicknesses (T) and lengths (L_v) of quartz veins within rotated blocks shows a very scattered distribution (Fig. 2.15a); the aspect ratio (T/L_V) ranging from 10^{-1} to 10^{-3}. Vein thicknesses show a good power-law distribution (slope $C \approx 0.91$) (Fig. 15b), while the length distribution (median length ~ 0.2 m) is log-normal (Fig. 2.15c). This length distribution is possibly due to vein length being restricted to within rotated blocks that are bounded between bedding layers. Some vein thicknesses may be increased by the connection of adjacent veins,

whereas lengthening was prohibited by the bounded bedding.

The damage zones around fault F1 show block rotation, triangular openings and conjugate Mode I fractures. The combination of local compressive stress (in the compressive quadrant) generated along F1 and block rotation with sympathetic bedding plane slip produced mixed Mode (I and III) fractures. The comparative lack of wall-rock deformation on the eastern side might be due to the failure of Mode I fractures to develop in the dilational quadrant.

In a fault propagation mechanism proposed by King and Sammis (1992), en echelon tension fractures separate slabs of rock which are bent due to shearing. This bending would produce a second series of extensional fractures orientated at right angles to the original set. An early stage model of this mechanism has been described as generating kink bands (Dewey, 1966) and reactivation of pre-existing joints (Rispoli, 1981). The en echelon fractures act in a similar way to domino faults and rotation causes locking of the faults once they have rotated almost normal to the σ_1 direction (McGrath and Davison, 1995). Therefore, the sigmoidal shapes of veins within rotated blocks indicate that they are generated by the Mode I fracturing (Pollard *et al.,* 1982) and influenced by block rotation and conjugate shear.

2.7. FAULT BENDS

The linked left-lateral fault system F5 - F4 - F10 (Fig. 2.16) is remarkable because fault F5 bends around by 48° to follow the bedding (F10), creating a listric fault with fault F4 propagating a short distance (~ 600 mm) onwards. This linked fault set shows a maximum amount of displacement (~ 500 mm) at the fault bend; a small amount of displacement (~30 mm) is accommodated by fault F4. Most of the displacement on fault F5 (strike/dip: N052°/87° SE) is transferred onto fault F10 (strike/dip: N080°/63° SW) which runs parallel to bedding for about 5 m before returning to a north-easterly trend (to the east of Fig. 3). Along fault F10, horizontal slickenside lineations on the bedding indicate left-lateral movement and displacement is defined by tracing marker beds A, B, and X. Interaction with a right-lateral fault (F2 - described previously) may be, in part, responsible for some loss of displacement on left-lateral fault F5.

2.7.1. λ-faults

λ-faults (Du and Aydin, 1995) are produced when one fault approaches and intersects another of a different orientation to define a 'λ' shape. The two faults may merge over a range of angles (see Du and Aydin, 1995). This structure is well developed where fault F5 merges into fault F10 (Fig. 2.16). The pre-existing discontinuity or fault (F10) can be defined as the major fault, because the bedding planes show frequent evidence of slip, as on the western side of the fault F1.

Assuming the direction of σ_1 as ~ N030° (see section **3** above), the angle between σ_1 and merging fault (F5), φ, is ~ 25°; within the orientation range propagation is predicted by Du and Aydin (1995, fig. 10). Where two faults are propagating towards each other (with λ shape), if the angle (between the maximum compressive stress and an approaching fault) is ~ 30°, the propagation path of the approaching fault rotates and becomes parallel to the main fault (λ faults; Fig 2.16).

The propagation path of the shear fracture depends not only on the applied stress orientation and the coefficient of friction but also on the specific geometric configurations (Du and Aydin, 1995).

2.7.2. Conjugate faults associated with strike-slip movement

A zone of damage extends up to 2 m from fault F10 in the southern wall (Fig. 2.17), which contains a conjugate pair of faults (F6 and F7; striking N005° and N050°). These conjugate faults extend bedding and can be attributed to movement around the fault bend in a manner similar to the development of "crestal-collapse graben" in listric extensional fault systems (McClay and Ellis, 1987). As the displacement on the conjugate faults decreases to zero where they intersect F10, the conjugate faults must have initiated in southern wall and propagated towards fault F10. The driving stress must have been sufficient to allow the conjugate faults to propagate into fault F10, but insufficient to cross-cut the strong anisotropic layer of bedding.

A balanced restoration for the south wall was constructed to estimate the amount of extension parallel to bedding (Fig. 2.17). The calculated average extension (*e*) for this block, by line balancing, is about 25%. The extension on bed X is a little bit higher than measured displacement along the fault (*d*) (Fig. 2.17) (Williams and Vann,

1987). Therefore, the maximum displacement might be located near the junction point with fault F6 and fault F7, because farther to the east the displacement decreases again.

The shaded area (Fig. 2.17b) at the left-hand end of the section is smaller than the area analogous to that between the regional dip and the rollover anticline in listric normal fault system (Fig. 2.17a). The ratio of shaded area / original area is about 80% based on bed B. The space deficit between the two areas probably results from dilation and formation of numerous small quartz veins.

Deformation in the southern wall is enhanced by the additional slip component transferred into fault F10 from the mergers, fault F5 and F6. On merging into a detachment fault, the above block of the detachment fault rotates as slip is transferred from the merging faults. Similar kinematic models have been reported in normal fault systems (e.g. Gross *et al.,* 1997) and thrust fault systems (e.g. Wojtal, 1994).

2.8. FAULT POPULATION ATTRIBUTES

2.8.1. Fault length and maximum displacement distribution

It is generally accepted that many populations of faults have power-law fault size - cumulative frequency distributions (e.g. Scholz and Cowie, 1990; Scholz *et al.,* 1993; Yielding *et al.,* 1996). That is, the number of faults (N) of length greater than or equal to L is given by

$$N = aL^{-C} \qquad (1)$$

where a is a constant and C is the power-law exponent. Ideally, when plotted on log-log axes, such distributions appear linear with slope $-C$.

The fault length data (Fig. 2.18a) show a poor fit to a power-law distribution ($C \approx 0.85$). Whilst the departure from a power-law can be in part due to censoring of fault lengths due to unexposed tip, the data are best described by a log-normal distribution with median length ~ 2m.

The maximum displacement data (Fig. 2.18b) show a better fit to a power-law distribution ($C \approx 0.4$), the departure being attributed to the "finite range effect" (Pickering *et al.,* 1995). Alternatively a log-normal distribution with median ~30 mm could also fit the data.

Thus for both data sets, the narrow band width makes distinction of an underlying power-law distribution difficult (Segall and Pollard, 1983b, Pickering *et al.*, 1995).

2.8.2. Maximum displacement (d_{max}) and fault length (L) relationship

The general expression of the relationship between the maximum cumulative displacement on a fault (d_{max}) and the maximum linear dimension of the fault surface (L or W) is given as;

$$d_{max} = cL^n, \qquad (2)$$

where the value of c is dependent on rock properties (including shear modulus) (Cowie and Scholz, 1992a, 1992b; Gillespie *et al.*, 1992) and the range of the exponent value, n, is from 0.5 to 2.0 (n=2.0, Watterson, 1986; Walsh and Watterson, 1988; n=1.5, Marrett and Allmendinger, 1991; Gillespie *et al.*, 1992; n=1, Cowie and Scholz, 1992a, 1992b; Dawers *et al.*, 1993; Scholz *et al.*, 1993; Clark and Cox, 1996; Schlische *et al.*, 1996; n=0.5 for deformation band, Fossen and Hesthammer, 1997). The value of the exponent, n, is important as $n = 1$ indicates a linear scaling law (i.e. self-similarity).

Although the maximum displacement against length distribution (Fig. 2.18c) is scattered, it can be separated into two main groups: isolated faults, which have no obvious interaction with other faults, and interacting faults including linked faults. Isolated faults have d_{max}/L (the ratio of maximum displacement / fault length) $\approx 10^{-2}$ ~ 10^{-3} whereas interacting faults have $d_{max}/L \approx 10^{-1}$ to 10^{-2}. This suggests that fault interaction allows proportionately greater displacement for a fault of given length. The trend line for the isolated faults follows approximately $n = 0.5$ line. This is very similar to the slope for deformation bands in porous sandstones in south-eastern Utah ($n = 0.54$, 0.1-100 m in length; Fossen and Hesthammer, 1997) showing relatively low displacement compared with faults with similar lengths.

Many recent researchers have suggested that faults are scale-invariant and have a constant d_{max}/L ratio (Cowie and Scholz, 1992b; Dawers *et al.*, 1993; Scholz *et al.*, 1993; Anders and Schlische, 1994; Dawers and Anders, 1995). Many factors are thought to influence the d_{max}/L ratio: measurement errors (Gillespie *et al.*, 1992);

material properties and tectonic settings (Cowie and Scholz, 1992b); mechanical stratigraphy and kinematics (Bürgmann *et al.*, 1994; Gross *et al.*, 1997); kinematic interaction in linkage faults (Peacock, 1991b; Peacock and Sanderson, 1991; Bürgmann *et al.*, 1994; Cartwright *et al.*, 1995; Wojtal, 1996; Willemse *et al.*, 1996; Willemse, 1997); propagation history (Peacock and Sanderson, 1996); size variation (Wojtal, 1994, 1996). Thus, the interpretation of data sets from many different environments on a single plot is debatable, as suggested by several workers (Scholz and Cowie, 1990; Pacheco *et al.*, 1992; Cowie and Scholz, 1992b; Wojtal, 1994; Clark and Cox, 1996). Even for the case of a simple single slip event in a homogeneous isotropic rock, because faults are not infinite in extent and so may interact with neighbouring faults, a variation in d_{max}/L ratio should be expected (Willemse *et al.*, 1996).

Filbrandt *et al.*(1994) demonstrate that d_{max}/L ratios change significantly during the early stages of fault growth. Gross *et al.*(1997) reported that, in contrast to small faults, displacement on large faults is independent of fault length.

In linked faults, the displacement is concentrated on the main fault (Sibson, 1989; Cowie and Scholz, 1992a), which interacts with adjacent minor faults during growth. Mechanical interaction among adjacent faults and linked faults is considered to increase the d_{max}/L ratio (Peacock and Sanderson, 1996; Willemse *et al.*, 1996).

Three stages can be identified in the growth of linked fault segments (Peacock and Sanderson 1991) (Fig. 2.19a). Initially isolated faults (stage 1) can propagated towards each other so that *soft-linking,* interacting without obvious connection, occurs (stage 2). This has intermediate evolution slope. The segment faults either evolve themselves without obvious *hard-linking* or hard-link to act as a linked fault when other neighbour segments exist near the segment. The soft-linked segment faults grow by interacting with adjacent faults with relatively high d_{max}/L ratios (higher slope) whereas hard-linked segments rapidly increase their length (low slope) (Fig. 2.19b), because all the segments are linked as a whole fault. The linked segments rapidly accumulate their displacement rather than length (steep slope; stage 3). Therefore, the linkage of segmented faults in strike-slip fault system shows a *step-like* growth path (Fig. 2.19b) as demonstrated in normal fault system by Cartwright *et al.* (1995).

The separation of the d_{max}/L data from Crackington Haven into isolated faults

and interacting faults (Fig. 2.18c) suggests that fault linkage and interaction are factors affecting the ratio between maximum displacement and fault length. A schematic fault growth model by linkage and interacting between adjacent segment faults in strike-slip fault system is illustrated in Fig. 2.19. The maximum displacement (d_{max}) - fault length (L) relationship evolves from isolated faults through segmented faults to interacting faults with a step-like route of two alternative ways depending on fault evolution stages.

2.9. CONCLUSIONS

1. Complex networks of strike-slip faults at Crackington Haven display a range of structures attributable to damage associated with displacement on the faults
2. Fault slip and associated damage geometries were produced by NNE (~N030°) maximum horizontal compressive stress (σ_1).
3. At low fault displacement, wall-rock deformation is mainly confined to the tips of faults (as in F8), where displacement gradients in the dilational quadrants produce horsetails and wing cracks. The latter accommodate larger displacement gradients at the tips (F3).
4. Overstepping of fault segments leads to linkage of fault displacement. At dilational oversteps and jogs, damage is localised within the overstep with displacement on the faults generally being conserved across the overstep with no displacement minimum (Fig. 2.9a). Contractional oversteps are characterised by well defined displacement minima (Fig. 2.11).
5. With increasing displacement, a wide variety of structures develop to accommodate wall-rock strains. Complex zones of veining and block rotation occur in broad regions in the contractional quadrants of faults where displacement gradients are relatively constant (e.g. F1).
6. Fault bends (λ-faults) are characterised by local patterns of strain controlled by pre-existing structure (e.g. bedding as in F10).
7. Maximum displacement (d_{max}) - fault length (L) plots of strike-lip faults show a step-like fault evolution from isolated faults through segmented faults to linked faults as a similar manner to normal fault system.

REFERENCES

Aki, K. 1989. Geometric features of a fault zone related to the nucleation and termination of an earthquake rupture. *U. S. Geological Survey Open -File Report* **89-315.**1-9.

Anders, M. H. and Schlische, R. W. 1994. Overlapping faults, intra-basin highs, and the growth of normal faults. *Journal of Geology.* **102**, 165-180.

Anderson, E. M. 1951. *The Dynamics of Faulting.* Olivier and Boyd, Edinburgh.

Andrews, J. R. 1993. Evidence for Variscan right-lateral transpression in the Pilton Shales, Croyde Bay, north Devon. *Proceedings of the Ussher Society* **8**, 198-199.

Andrews, J. R., Isaac, K. P., Selwood, E. B., Shail, R. K. and Thomas, J. M. 1998. Variscan structure and regional metamorphism. *The Geology of Cornwall.* Exter, University of Exter Press, 298 pp (edited by E. B. Selwood, E. M. Durrance and C. M. Bristow).

Aydin, A. and Nur, A. 1985. The types and role of stepovers in strike-slip tectonics. In *Strike-slip Deformation, Basin Formation, and Sedimentation*: eds: Biddle, K. T. and Christie-Blick, N. *Society of Economic Paleontologists and Mineralogists Special Publication*, **37**, 35-44.

Aydin, A. and Schultz, R. A. 1990. Effect of mechanical interaction on the development of strike-slip faults with echelon patterns. *Journal of Structural Geology* **12**, 123-129.

Biddle, K. T. and Christie-Blick, N. 1985.. Glossary - Strike-slip deformation, basin formation, and sedimentation. In *Strike-slip Deformation, Basin Formation, and Sedimentation*: Eds: Biddle, K. T. and Christie-Blick, N. *Society of Economic Paleontologists and Mineralogists Special Publication,* **37**, 375-386.

Bilham, R. and King, G. 1989. The Morphology of Strike-slip Faults: Examples from the San Andreas Fault, California. *Journal of Geophysical Research,* **94**, 10,204-10,216.

Brace, W. F. and Bombolakis, E. G. 1963. A note on brittle crack growth in compression. *Journal of Geophysical Research* **68**, 3709-3713.

Bürgmann, R., Pollard, D. D. and Martel, S. J. 1994. Slip distributions on faults: effects of stress gradients, inelastic deformation, heterogeneous host-rock stiffness, and fault interaction. . *Journal of Structural Geology* **16**, 1675-1690.

Cartwright, J. A., Trudgill, B. D. and Mansfield, C. S. 1995. Fault growth by segment linkage: an explanation for scatter in maximum displacement and trace length data from the Canyonlands Grabens of SE Utah. *Journal of Structural Geology* **17**, 1319-1326.

Chadwick, R. A. 1993. Aspects of basin inversion in southern Britain. *Journal Geological Society of London* **150.** 311-322.

Christie-Blick, N. and Biddle, K. T. 1985. Deformation and basin formation along strike-slip faults. In *Strike-slip Deformation, Basin Formation, and Sedimentation*: Eds: Biddle, K. T. and Christie-Blick, N. *Society of Economic Palaeontologists and Mineralogists Special Publication* **37,** 1-34.

Clark, R. M. and Cox, S. J. D. 1996. A modern regression approach to determining fault displacement-length scaling relationships. *Journal of Structural Geology* **18**, 147-152.

Cooke, M. L. 1997. Fracture localisation along faults with spatially varying friction. *J. Geophys. Res.*

102, 22,425-22,434.

Cowie, P. A. and Scholz, C. H. 1992a. Physical explanation for the displacement-length relationship for faults using a post-yield fracture mechanics model. *Journal of Structural Geology* **14**, 1133-1148.

Cowie, P. A. and Scholz, C. H. 1992b. Displacement-length scaling relationship for faults: data synthesis and discussion. *Journal of Structural Geology* **14**, 1149-1156.

Cowie, P. A. and Scholz, C. H. 1992c. Growth of faults by accumulation of seismic slip. *Journal of Geophysical Research* **97**, 11,085-11,095.

Cox, S. J. D. and Scholz, C. H. 1988. Rupture initiation in shear fracture of rocks: An experimental study. *Journal of Geophysical Research* **93**, 3307-3320.

Dawers, N. H. and Anders, M. H. 1995. Displacement-length scaling and fault linkage. . *Journal of Structural Geology* **17**. 607-614.

Dawers, N. H., Anders, M. H. and Scholz, C. H. 1993. Growth of normal faults: Displacement-length scaling. *Geology*. **21**. 1107-1110.

Dewey, J. F. 1966. Kink-bands in Lower Carboniferous Slates of Rush, Co. Dublin. *Geological Magazine* **103**, 138-142.

Du, Y. and Aydin, A. 1995. Shear fracture patterns and connectivity at geometric complexities along strike-slip faults. *Journal of Geophysical Research* **100**, 18,093-18,102.

Enfield, M. A., Gillcrist, J. R., Palmer, S. N. and Whalley, J. S. 1985. Structural and sedimentary evidence for the early tectonic history of the Bude and Crackington Formations, north Cornwall and Devon. *Proceedings of the Ussher Society* **6,** 165-172.

Erdogan, F. and Sih, G. C. 1963. On the crack extension in plates under plane loading and transverse shear. *J. Basic Eng.* **85**, 519-527.

Filbrandt, J. M., Richard, P. D. and Franssen, R. C. M. W. 1994. Growth and coalescence of faults: numerical simulations and sand-box experiments. In: *TSG Special Meeting on Fault Populations*, Edinburgh, U. K., Extended Abstracts, 57-59.

Fossen, H. and Hesthammer, J. 1997. Geometric analysis and scaling relations of deformation bands in porous sandstone. *Journal of Structural Geology* **19**, 1479-1493.

Friedman, M. and Logan, J. M. 1970. Microscopic feather fractures *Bulletin Geological Society of America* **81**, 3417-3420.

Freshney, E. C., McKeown, M. C. and Williams, M. 1972. Geology of the coast between Tintagel and Bude. *Mem. Geol. Surv. Gt. Br.*

Gayer, R. and Jones, J. 1989. The Variscan foreland in South Wales. *Proceedings of the Ussher Society* **7.** 177-179.

Gillespie, P. A., Walsh, J. J. and Watterson, J. 1992. Limitations of dimension and displacement data from single faults and the consequences for data analysis and interpretation. *Journal of Structural Geology* **14**, 1157-1172.

Gross, M. R., Gutiérrez-Alonso, G. Bai, T., Wacker, M. A., Collinsworth, K. B. and Behl, R. J. 1997. Influence of mechanical stratigraphy and kinematics on fault scaling relations. *Journal of*

Structural Geology **19**, 171-183.

Granier, T. 1985. Origin, Damping, and Pattern of Development of Faults in Granite. *Tectonics* **4**, 721-737.

Hartley, A. J. and Warr, L. N. 1990. Upper Carboniferous foreland basin evolution in SW Britain. *Proceedings of the Ussher Society* **7**, 212-216.

Horii, H. and Nemat-Nasser, S. 1986. Brittle failure in compression: splitting, faulting and brittle-ductile transition. *Philosophical Transections Royal Society of London* **319**, 337-374.

Kim, Y. -S., Andrews, J. R. and Sanderson, D. J. 1998. Field excursion to study damage zones around strike-slip faults at Crackington Haven, north Cornwall. *Geoscience in south-west England* **9**, 272-275.

King, G. C. P. 1986. Speculations on the Geometry of the Initiation and Termination Processes of Earthquake Rupture and its Relation to Morphology and Geological Structure. . *Pure and Applied Geophysics* **124,** 567-585.

King, G. C. P. and Sammis, C. 1992. The mechanisms of finite brittle strain. *Pure and Applied Geophysics* **138**, 611-640.

Lake, S. D. and Karner, G. D. 1987. The structure and evolution of the Wessex Basin, southern England: an example of inversion tectonics. *Tectonophysics* **137,** 347-378.

Lajtai, E. Z. 1971. A theoretical and experimental evaluation of the Griffith theory of brittle fracture. *Tectnophysics* **11**, 129-156.

Marrett, R. and Allmendinger, R. W. 1991. Estimates of strain due to brittle faulting: sampling of fault populations. *Journal of Structural Geology* **13**, 735-738.

McClay, K. R. and Ellis, P. G. 1987. Analogue models of extensional fault geometries. In: *Continental Extensional Tectonics,* Eds: M. P. Coward, J. F. Dewey and P. L. Hancock. *Geological Society of London Special Publication*, **28**, 109-125.

McGrath, A. G. and Davison, I. 1995. Damage zone geometry around fault tips. *Journal of Structural Geology* **17**, 1011-1024.

Muraoka, H. and Kamata, H. 1983. Displacement distribution along minor fault traces. *Journal of Structural Geology* **5**, 483-495.

Olson, J. E. and Pollard, D. D. 1989. Inferring paleostresses from natural fracture patterns: A new method. *Geology* **17**, 345-348.

Pacheco, J. F., Scholz, C. F. and Sykes, L. R. 1992. Changes in frequency-size relationship from small to large earthquakes. *Nature* **355,** 71-73.

Peacock, D. C. P. 1991a. Displacement and segment linkage in fault zones (unpublished PhD thesis in Univ. of Southampton). 129p.

Peacock, D. C. P. 1991b. Displacement and segment linkage in strike-slip fault zones. *Journal of Structural Geology* **13**, 1025-1035.

Peacock, D. C. P. and Sanderson, D. J. 1991. Displacement and segment linkage and relay ramps in normal fault zones. *Journal of Structural Geology* **13**, 721-733.

Peacock, D. C. P. and Sanderson, D. J. 1992. Effects of layering and anisotropy on fault geometry. *J.*

Geol. Soc. London. **149**, 793-802.

Peacock, D. C. P. and Sanderson, D. J. 1996. Effects of propagation rate on displacement variations along faults. *Journal of Structural Geology* **18**, 311-320.

Peacock, D. C. P. and Sanderson, D. J. 1998 Deformation history and basin-controlling faults in the Mesozoic sedimentary rocks of the Somerset coast. *Proceedings Geological Association* **110**, 41-52.

Petit, J. -P. and Barquins, M. 1988. Can natural faults propagate under Mode II conditions? *Tectonics* **7**, 1243-1256.

Pickering, G., Bull, J. M. and Sanderson, D. J. 1995. Sampling power-law distributions. *Tectonophysics* **248**, 1-20.

Pollard, D. D. and Segall, P. 1987. Theoretical displacements and stresses near fractures in rock: With applications to faults, joints, veins, dikes, and solution surfaces. In *Fracture Mechanics of Rock (ed. B. K. Atkinson). Academic Press Geology Series*, Academic Press. 277-349.

Pollard, D. D., Segall, P. and Delaney, P. 1982. Formation and interpretation of dilatant echelon cracks. *Bulletin Geological Society of America* **93,** 1291-1303.

Ramsay, J. G. and Huber, M. I. 1987. *The Techniques of Modern Structural Geology.* Volume 2. 700p.

Reches, Z. and Lockner, D. A. 1994. Nucleation and growth of faults in brittle rocks. *Journal of Geophysical Research* **99**, 18,159-18,173.

Rispoli, R. 1981. Stress fields about strike-slip faults inferred from stylolites and tension gashes. *Tectonophysics* **75**, T29-T36.

Sanderson, D. J. 1979. The transition from upright to recumbent folding in the Variscan fold belt of south-west England: a model based on the kinematics of simple shear. *Journal of Structural Geology* **1**, 171-180.

Schlische, R. W., Young, S,. S., Ackermann, R. V. and Gupta, A. 1996. *Geology* **24,** 683-686.

Scholz, C. H. and Cowie, P. A. 1990. Determination of geologic strain from fault slip data. *Nature* **346**, 837-839.

Scholz, C. H., Dawers, N. H., Yu, J.-Z., Anders, M. H. and Cowie, P. A. 1993. Fault Growth and Fault Scaling Laws: Preliminary Results. *Journal of Geophysical Research* **98**. 21,951-21,961.

Segall, P. and Pollard, D. D. 1983a. Nucleation and growth of strike-slip faults in granite. *Journal of Geophysical Research* **88**, 555-568.

Segall, P. and Pollard, D. D. 1983b. Joint formation in granitic rock of the Sierra Nevada. *Geol. Soc. of Am. Bull.* **94**, 563-575.

Selwood, E. B., Stewart, I. J. and Thomas, J. M. 1985. Upper Palaeozoic sediments and structure in north Cornwall - a reinterpretation. *Proceedings Geologists Association* **96,** 129-141.

Sibson, R. H. 1986. Earthquake and lineament infrastructure. *Philosophical Transections Royal Society of London.* **A317**, 63-79.

Sibson, R. H. 1989. Earthquake faulting as a structural process. *Journal of Structural Geology* **11**, 1-14.

Sibson, R. H. 1996. Structural permeability of fluid-driven fault-fracture meshes *Journal of Structural Geology* **18**, 1031-1042.

Sylvester, A. G. 1988. Strike-slip faults. *Bulletin Geological Society of America* **100.** 1666-1703.

Tchalenko, J. S. 1970, Similarities between shear zones of different magnitudes. *Geol. Soc. Am. Bull.*, **81**, 1625-1640.

Thatcher, W. and Bonilla, M. G. 1989. Earthquake fault slip estimation from geologic, geodetic and seismologic observations: Implications for earthquake mechanics and fault segmentation. *U. S. Geological Survey Open -File Report* **89-315**.386-399.

Walsh, J. J. and Watterson, J. 1988. Analysis of the relationship between displacements and dimensions of faults. *Journal of Structural Geology* **10**, 239-247.

Walsh, J. J. and Watterson, J. 1991. Geometric and kinematic coherence and scale effects in normal fault systems. In: *The Geometry of Normal Faults* (edited by Roberts, A. M., Yielding, G. and Freeman, B.). *Special Publication Geological Society of London* **56,** 193-203.

Warr, L. N. 1989. The structural evolution of the Davidstow Anticline, and its relationship to the Southern Culm Overfold, north Cornwall. *Proc. of the Ussher Society,* **7,** 136-140.

Watterson, J. 1986. Fault dimensions, displacements and growth. *Pure and Applied Geophysics* **124,** 365-373.

Whalley, J. S. and Lloyd, G. E. 1986. Tectonics of the Bude Formation, North Cornwall - the recognition of northerly directed decollement. *Journal Geological Society of London* **143,** 83-89.

Willemse, E. J. M. 1997. Segmented normal faults: Correspondence between three-dimensional mechanical models and field data. *Journal of Geophysical Research* **102,** 675-692.

Willemse, E. J. M., Peacock, D. C. P. and A. Aydin, N. 1997. Nucleation and growth of strike-slip faults in limestones from Somerset, UK *Journal of Structural Geology* **19**, 1461-1477.

Willemse, E. J. M. and Pollard, D. D. 1998. On the orientation and patterns of wing cracks and solution surfaces at the tips of a sliding flaw or fault. *J. Geophys. Res.*, **103**, 2427-2438.

Willemse, E. J. M., Pollard, D. D. and Aydin, A. 1996. Three-dimensional analyses of slip distributions on normal fault arrays with consequences for fault scaling. *Journal of Structural Geology* **18**, 295-309.

Williams, G. and Vann, I. 1987. The geometry of listric normal faults and deformation in their hangingwalls. *Journal of Structural Geology* **9**, 789-795.

Wojtal, S. F. 1994. Fault scaling laws and the temporal evolution of fault systems *Journal of Structural Geology* **16**, 603-612.

Wojtal, S. F. 1996. Changes in fault displacement populations correlated to linkage between faults. *Journal of Structural Geology* **18**, 265-279.

Yielding, G., Needham, T. and Jones, H. 1996. Sampling of fault populations using sub-surface data: a review. *Journal of Structural Geology* **18**, 135-146.

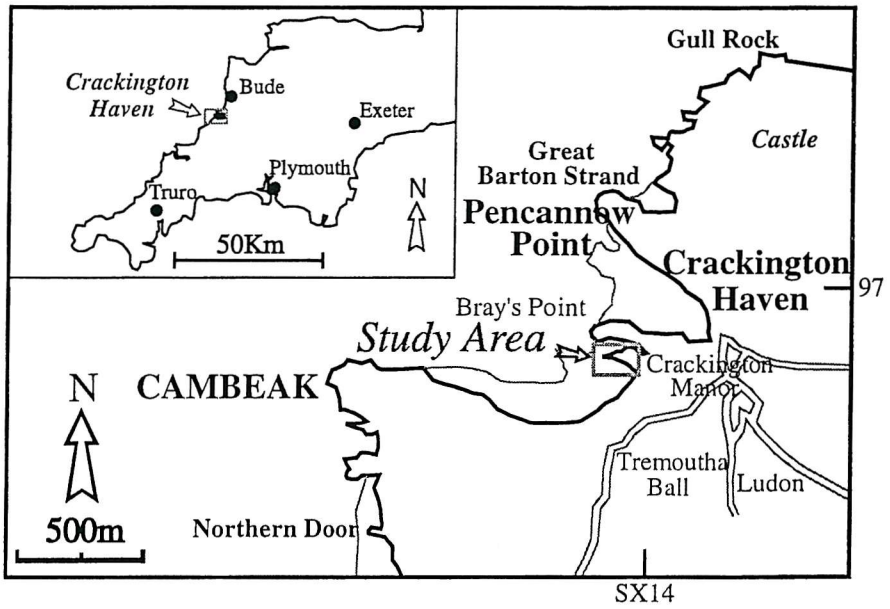

Fig. 2.1. Map showing the location of strike-slip faults at Crackington Haven (SX 138973). The faults lie within the boxed area indicated by the arrow, beneath a low hill to the east and just above the wave-cut platform. Thick line mean high water, and thin line mean low water.

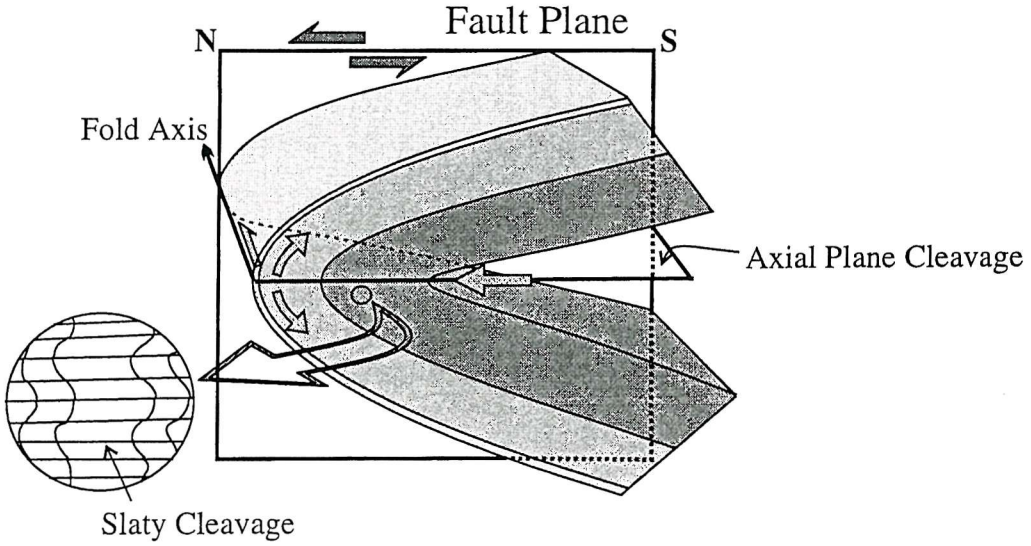

Fig. 2.2. A schematic illustration of the relationship of flexural slip folding to sinistral strike-slip faulting on the south side of Crackington Haven. The studied outcrop is ocated on a flat surface eroded along the early axial-plane cleavage.

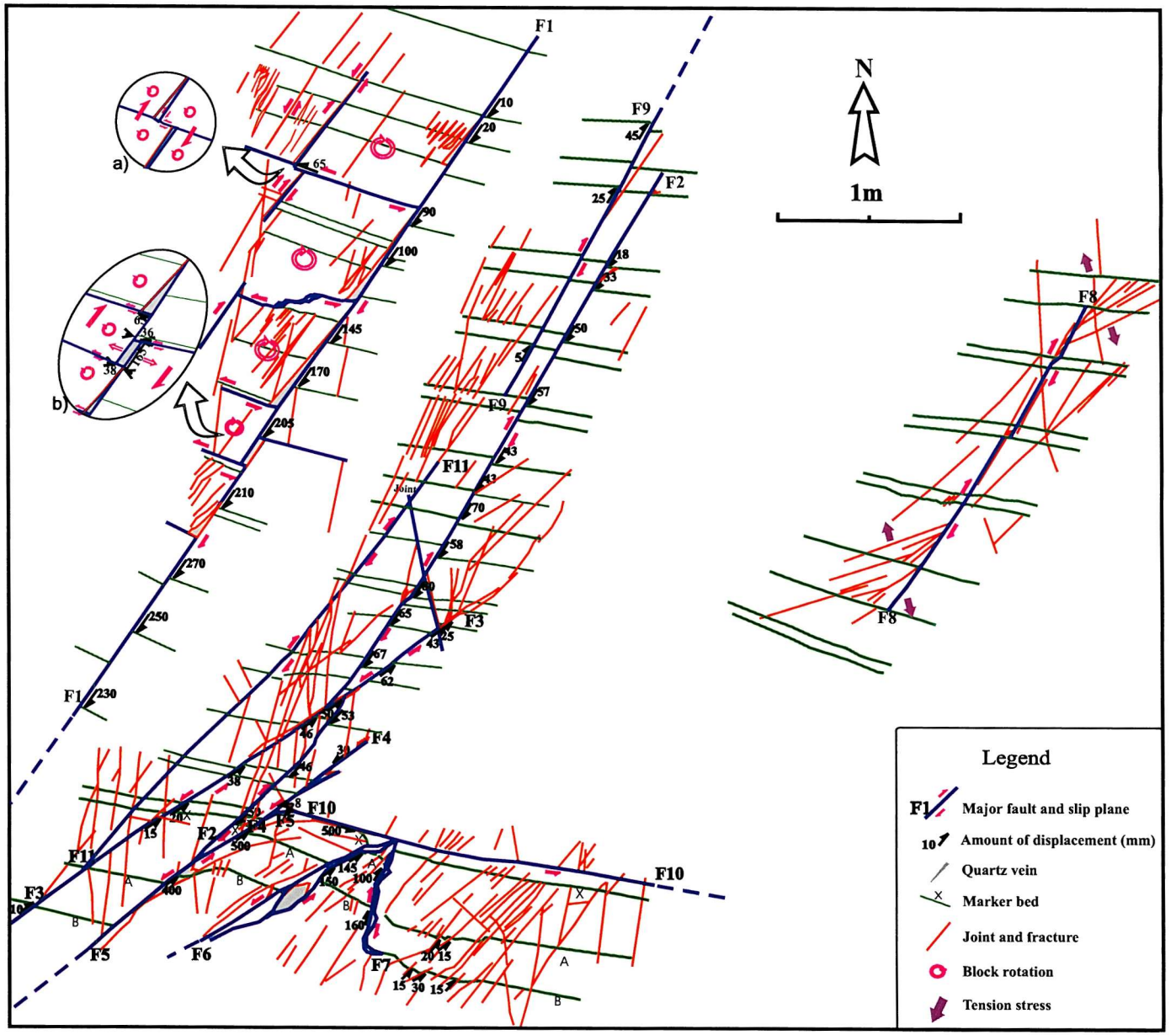

Fig. 2.3. Detailed map of strike-slip faults at Crackington Haven. It shows a variety of damage zone structures. The faults are located within the studied area shown on Fig. 1. The main fault slip directions and displacements at each location are marked by arrows and magnitudes in mm.

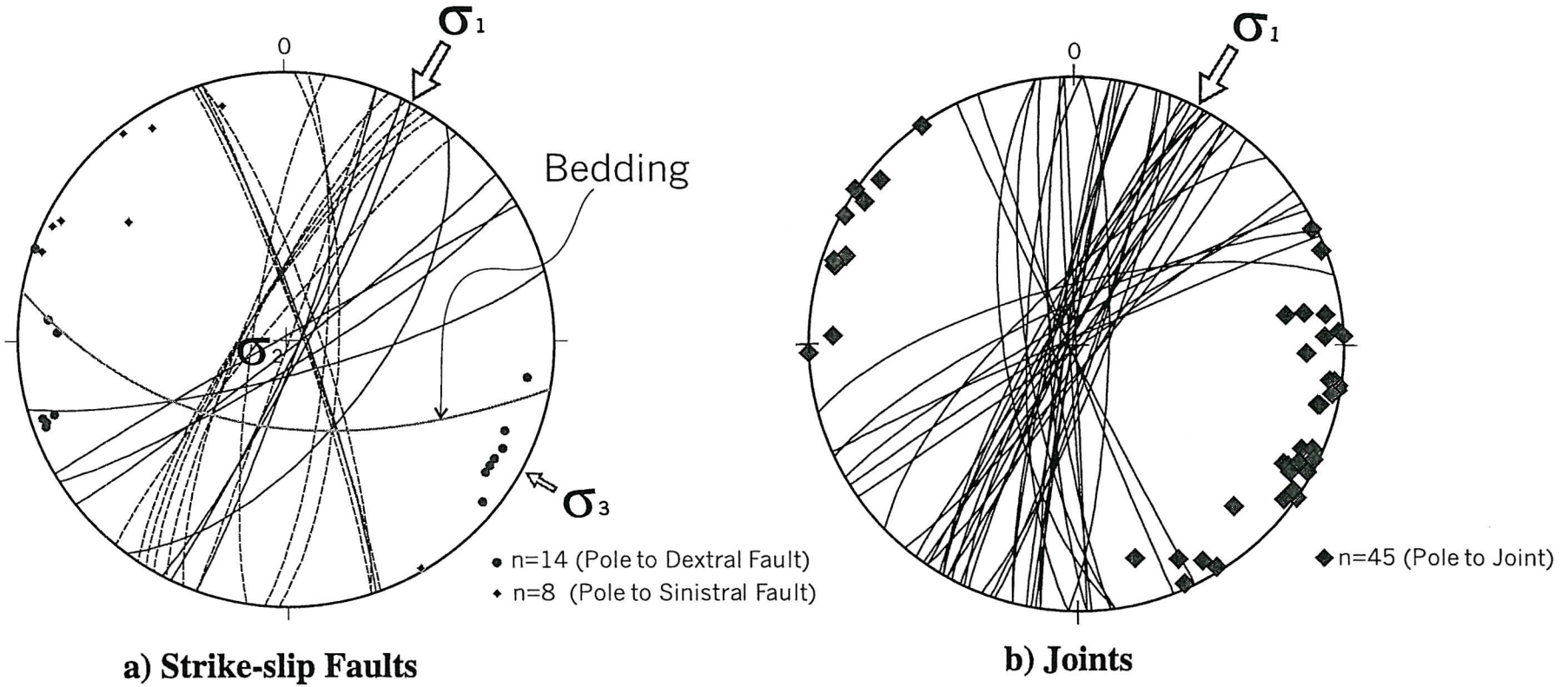

Fig. 2.4. Stereograms of structural data. a) strike-slip faults, and b) joints measured over the mapped area at Crackington Haven. Faults show mainly NE-SW orientation for sinistral (solid lines) and NNE-SSW for dextral (dashed lines). Assuming conjugate faulting, the orientations of σ_1 (maximum compressive stress) and σ_3 (minimum compressive stress) are about N30°(E and N60°(W, respectively. The bedding strikes nearly E-W and joints have similar orientations to strike-slip faults.

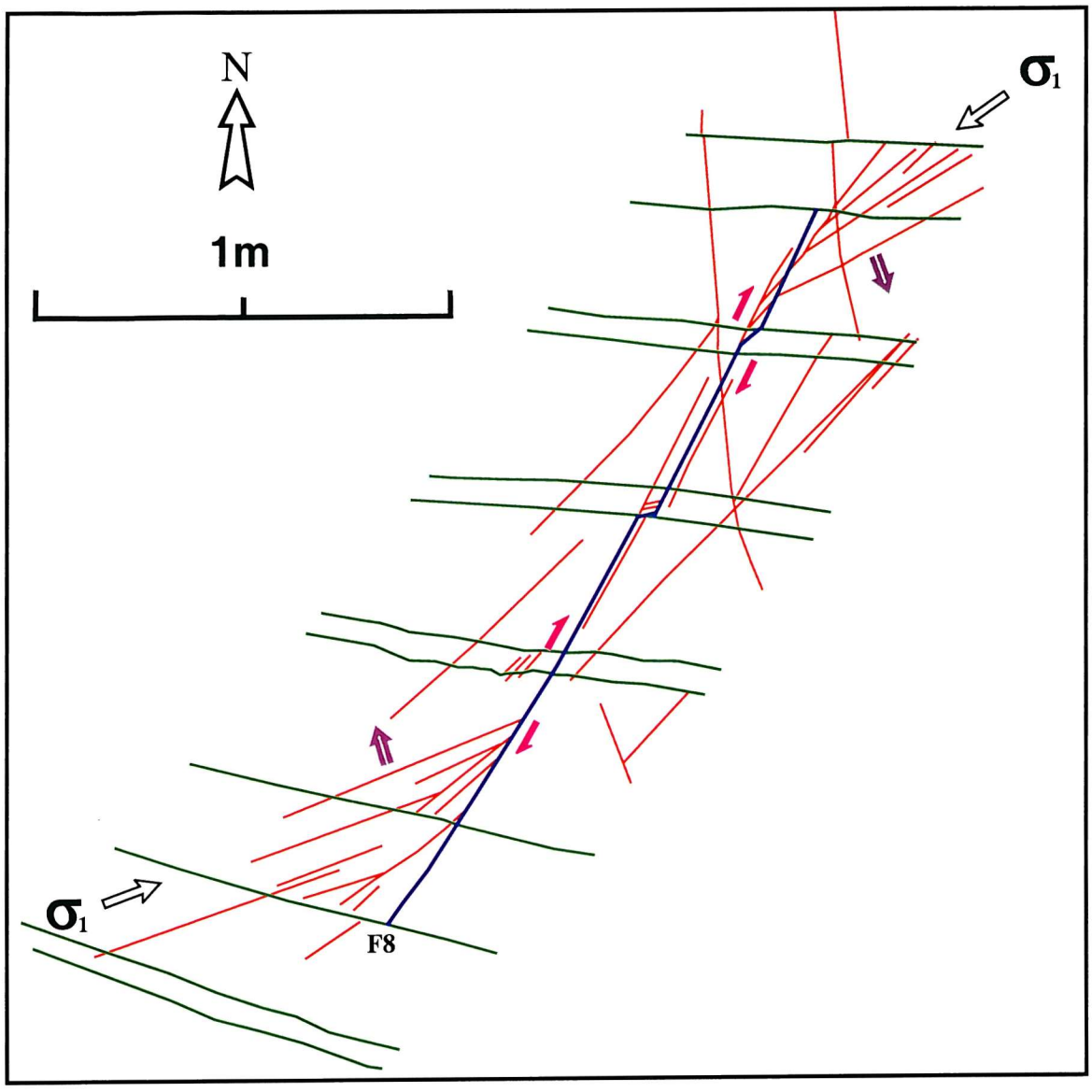

Fig. 2.5. Detail of fault F8 (see Fig. 3) and associated fractures. Although the maximum displacement along the fault is only 2 mm, it shows typical horsetail tip damage. Most of the displacement is compensated by the development of Mode I or mixed Mode cracks in the extensional quadrant. The main fault slip directions are marked by arrows.

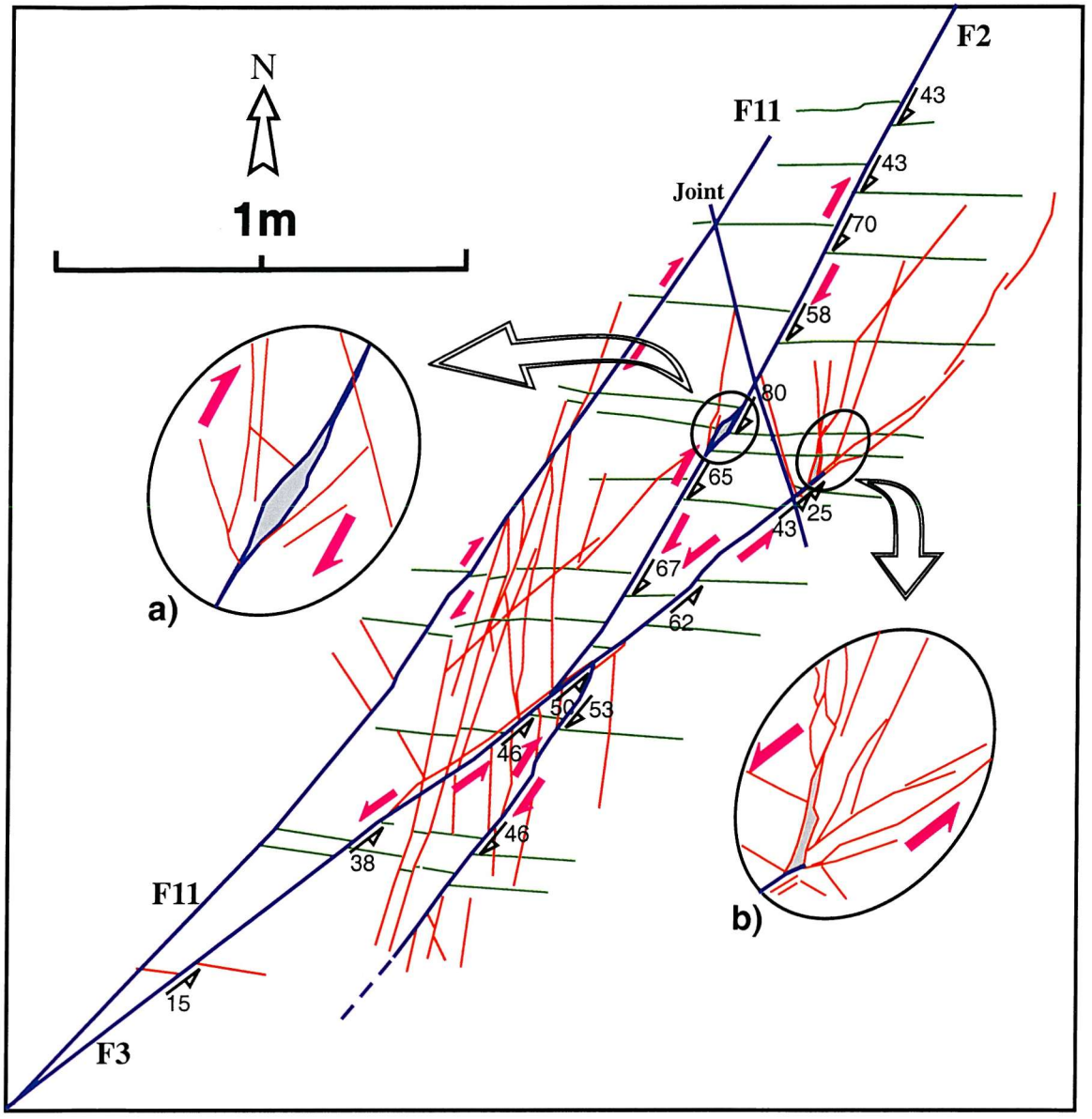

Fig. 2.6. Plan view of faults F2, F3 and F11 (see Fig. 3). It shows two dextral and one sinistral strike-slip faults with associated wing cracks and jogs. The displacement gradient along these faults is generally large and rapidly decreases between the wing cracks and the tips. This kind of fault geometry shows an unusual displacement - distance distribution along the fault (Fig. 7). The slip distribution along fault F2 (Fig. 8) is complicated by the effect of the intersection with fault F3 and a dilational jog. The main fault slip directions and displacements at each location are marked by arrows and magnitudes in mm.

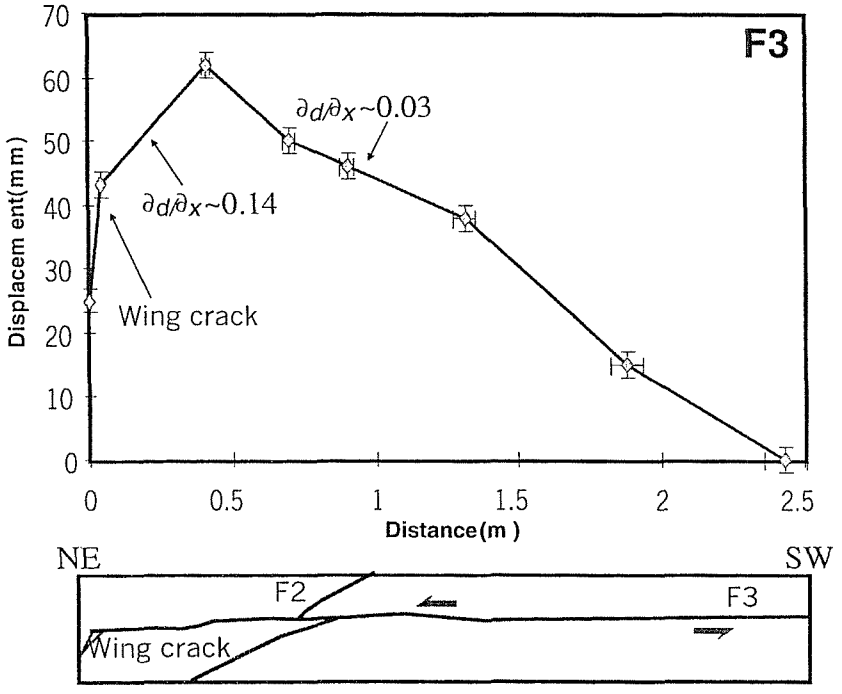

Fig. 2.7. Displacement (d) -distance (x) relationship for fault F3. The wing crack is developed where the displacement gradient reaches a maximum value near the NE tip.

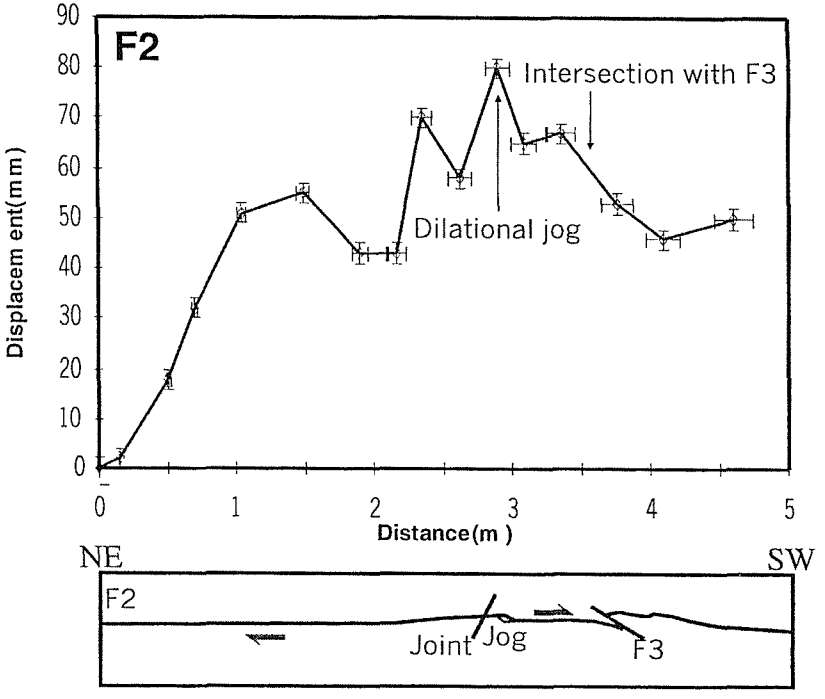

Fig. 2.8. Displacement (d) -distance (x) graph for fault F2. The profile has peak displacement at the dilational

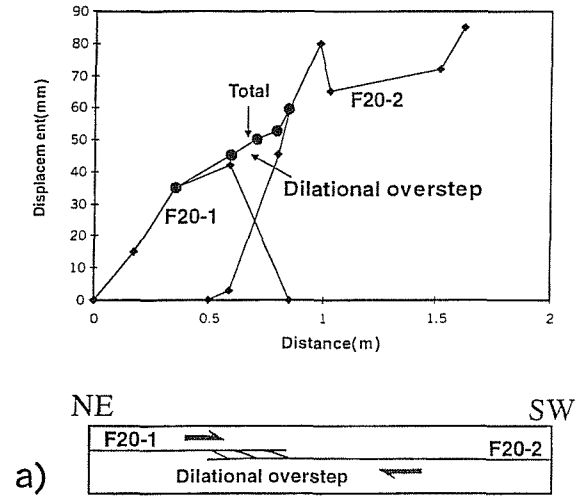

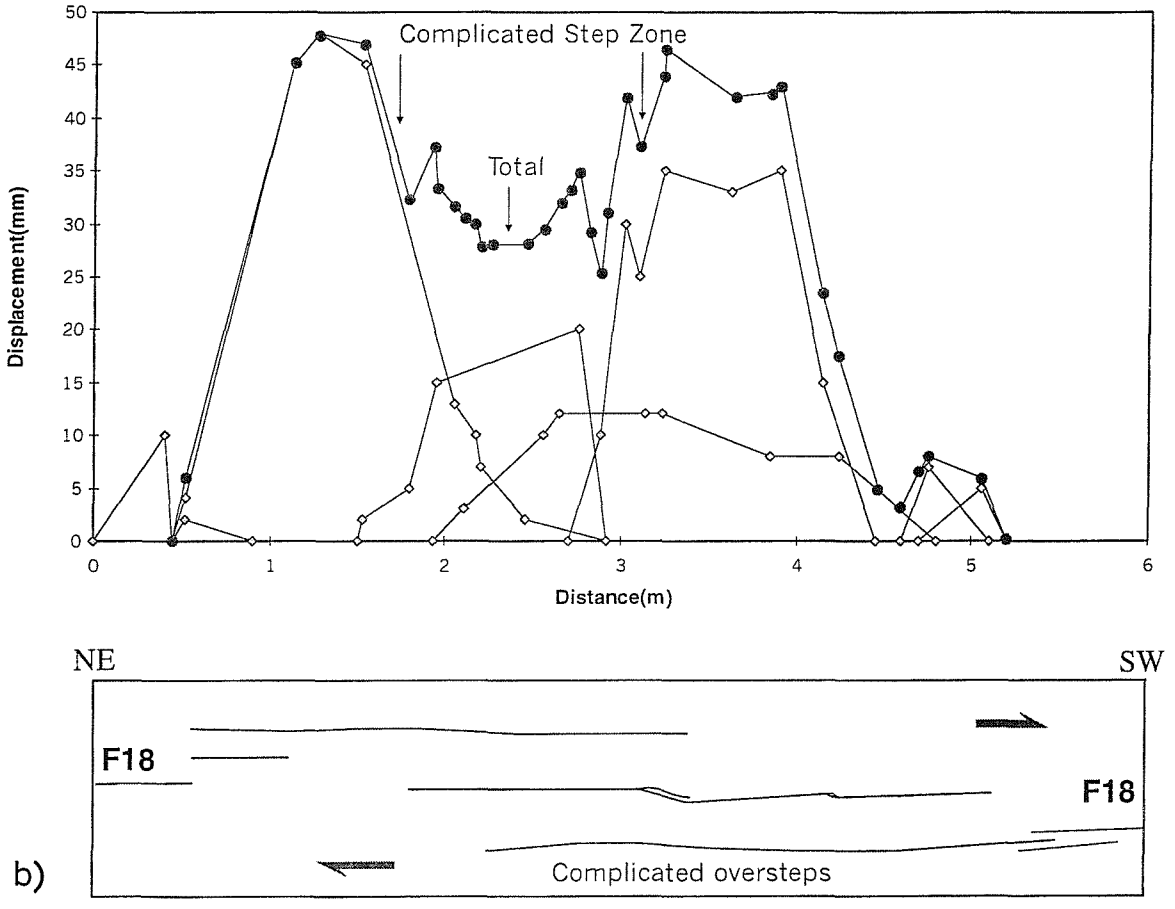

Fig. 2.9. Displacement (d)-distance (x) profiles for F20 (a) and F18 (b) overstep faults about 5-20 m northwest from the fault F1. a) The displacement is transferred between fault segments in the dilational overstep (F20). b) The total displacement is generally conserved through soft- / hard-linked multi-steps and jogs (F18). The central part of the total displacement graph is complicated by several minor steps and jogs.

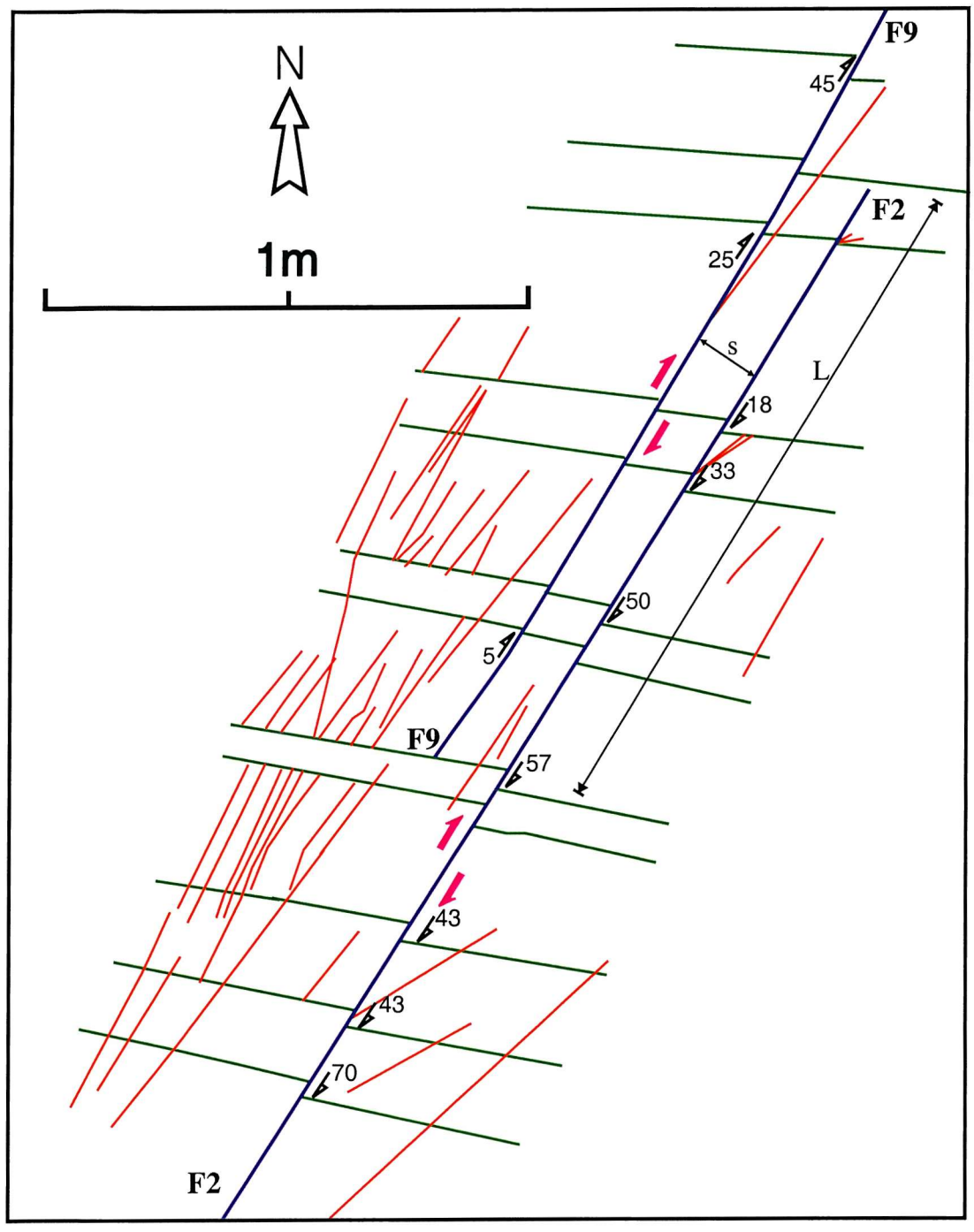

Fig. 2.10. Plan view of dextral left-stepping overstep faults, F2 and F9, and associated fractures. The faults have a high ratio of overstep length (L)/ spacing (s). Maximum displacement (d_{max}) of fault F2 is 80 mm occurring further to the SW. The main fault slip directions and displacements at each location are marked by arrows and magnitudes

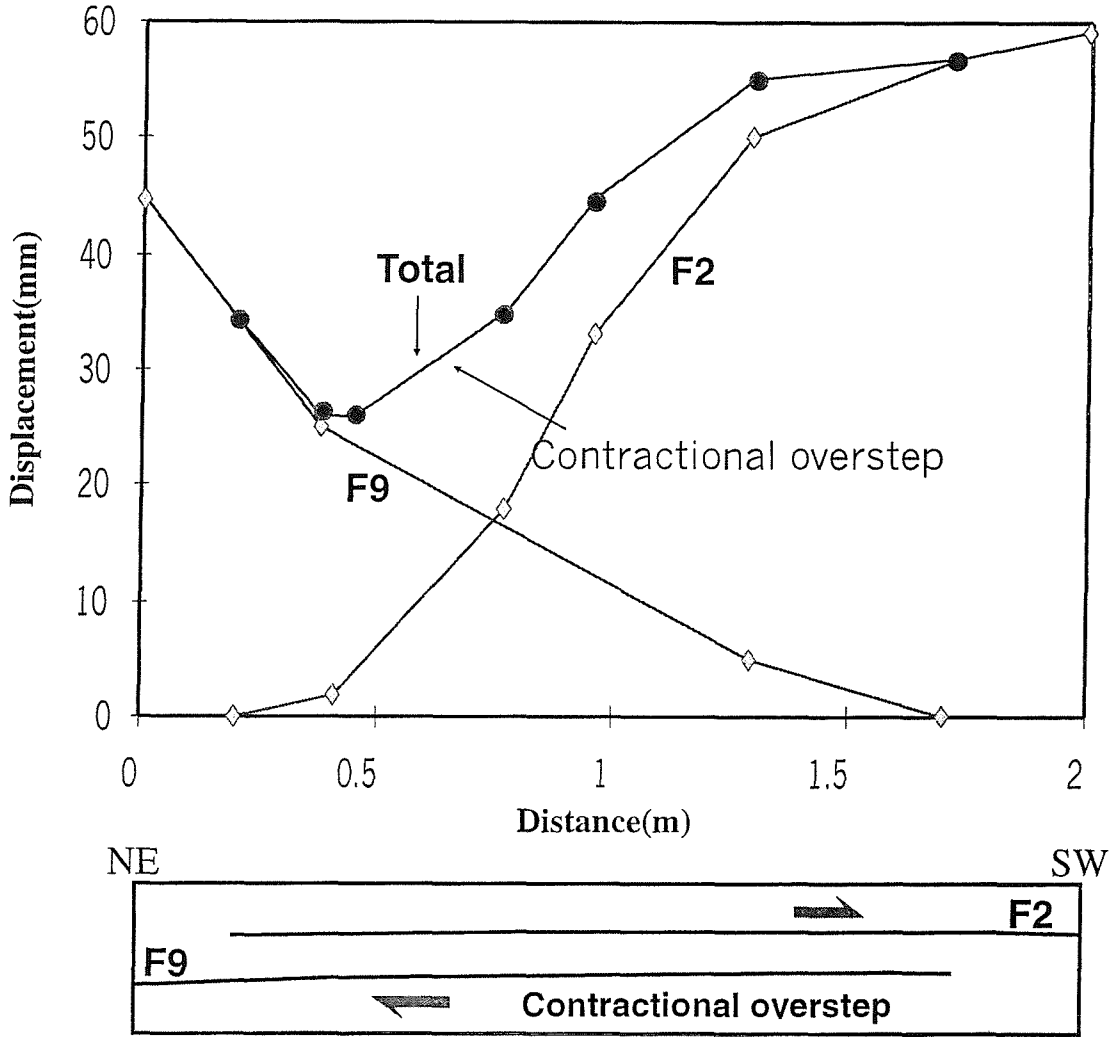

Fig. 2.11. Displacement (d) - distance (x) relationship for contractional overstep faults (F2 and F9). The segments show gentle displacement gradients at the tips within the overstep zone and the total displacement profile is depressed at the contractional offset.

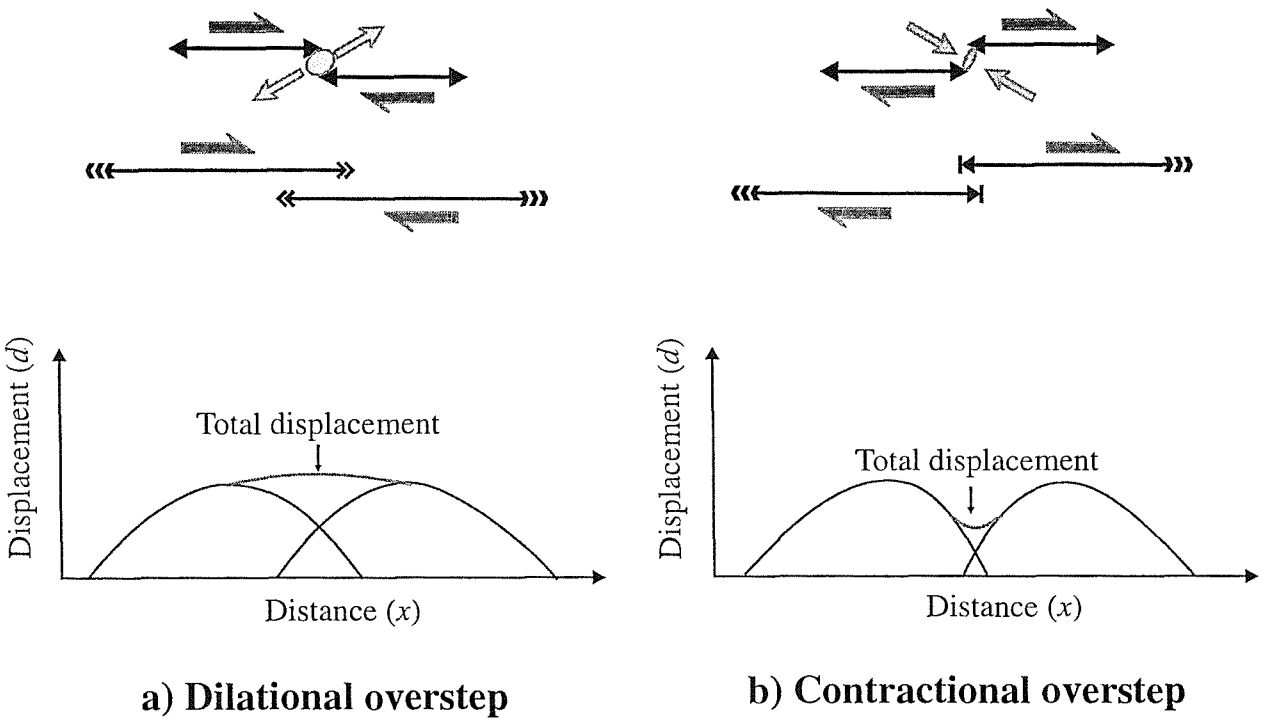

Fig. 2.12. Strike-slip fault linkages and their influence on the displacement (d) - distance (x) profile. a) Dilational overstep shows no displacement minina in the overstep zone. b) Contractional overstep shows displacement minima in the overstep zone. This might originate from the nature of fault propagation in the overlap zone. In the contractional overstep, the fault tips are pinned by compressive stresses and the fault segments propagate from the opposite ends.

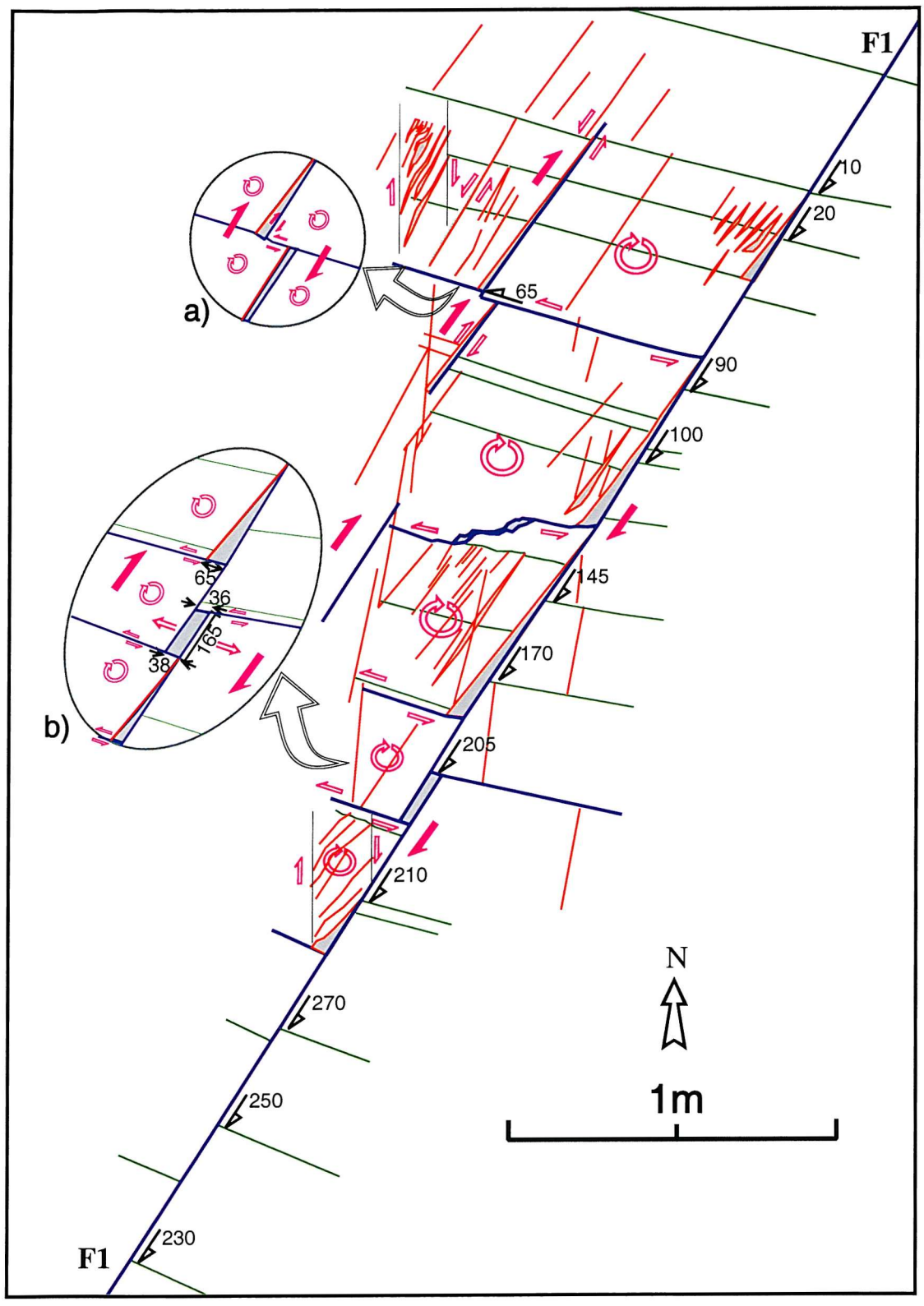

Fig. 2.13. Plan view of structure around fault F1. The boundary between thick slate layers and thin graywacke beds has acted as a preferred slip surface during faulting so that blocks in the wall rock are rotated. Detailed observation indicates that the step faulting and layer parallel slip were active simultaneously (inset a). A rectangular vein quartz is developed by later layer parallel slip (inset b). See text for further discussion

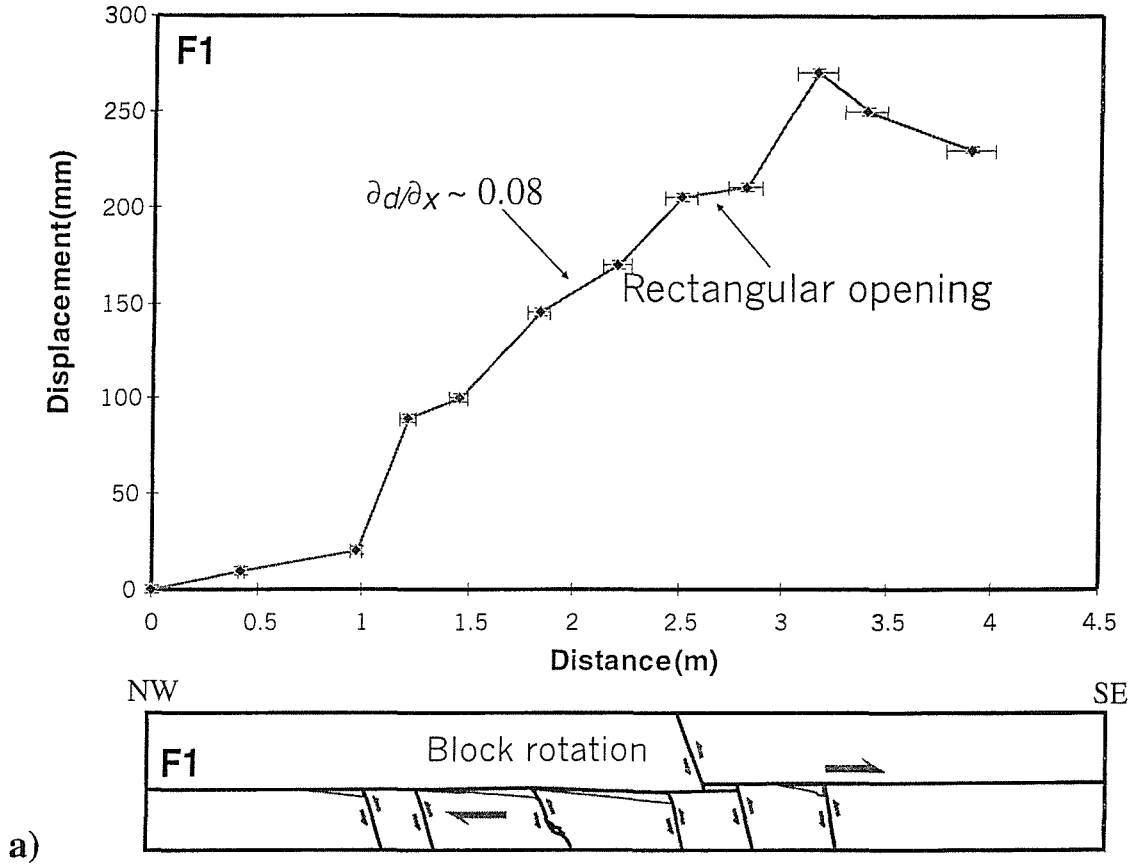

a)

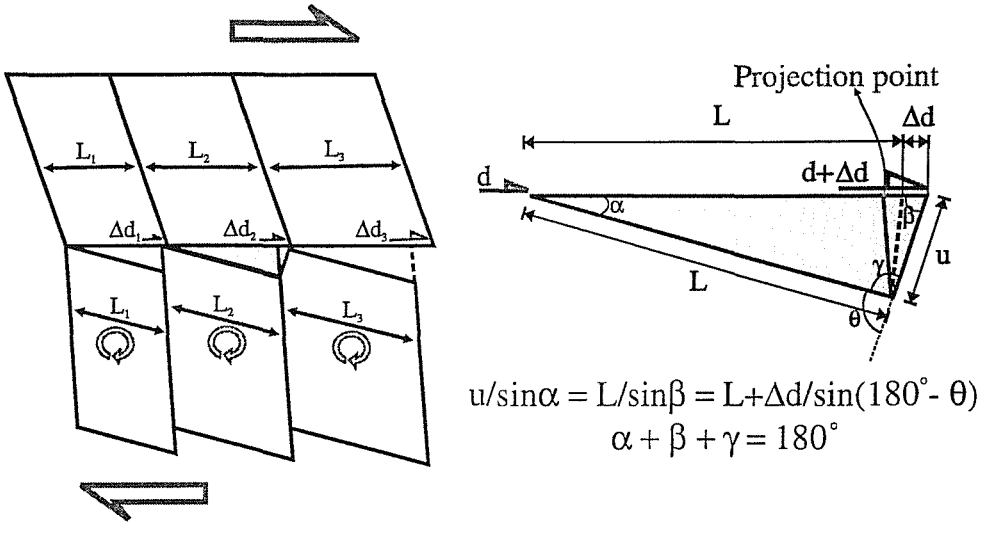

b)

Fig. 2.14. (a) Displacement (d) - distance (x) relationship of fault F1. It shows a fairly steady increase in displacement with a displacement gradient $du \sim 0.08$ to $d_{max} \cong 270$ mm. (b) A schematic cartoon for block rotation with a steady increase of displacement. d is displacement and Δd is incremental displacement. See text for further discussion.

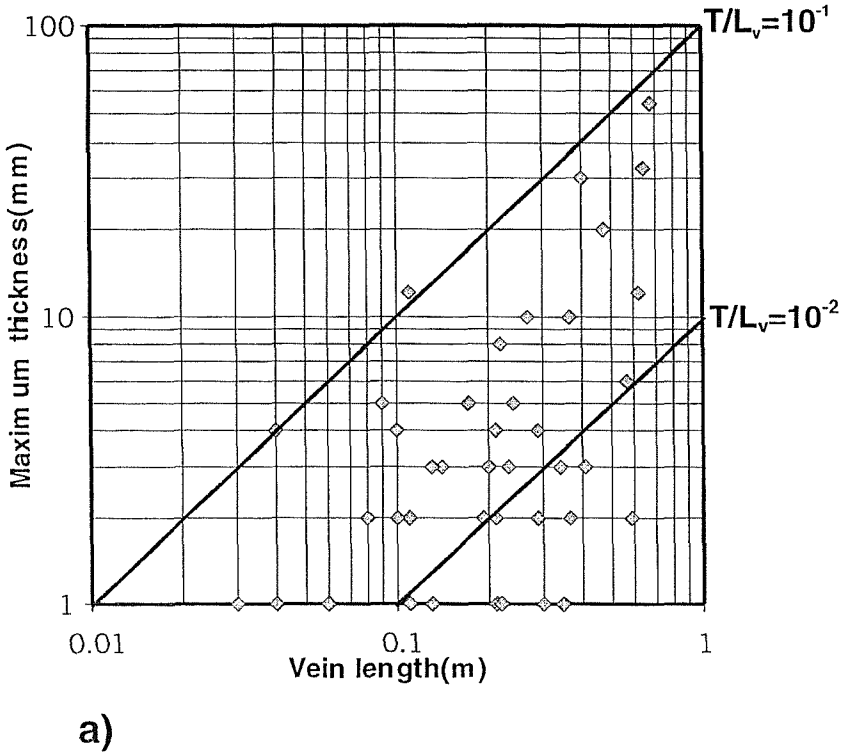

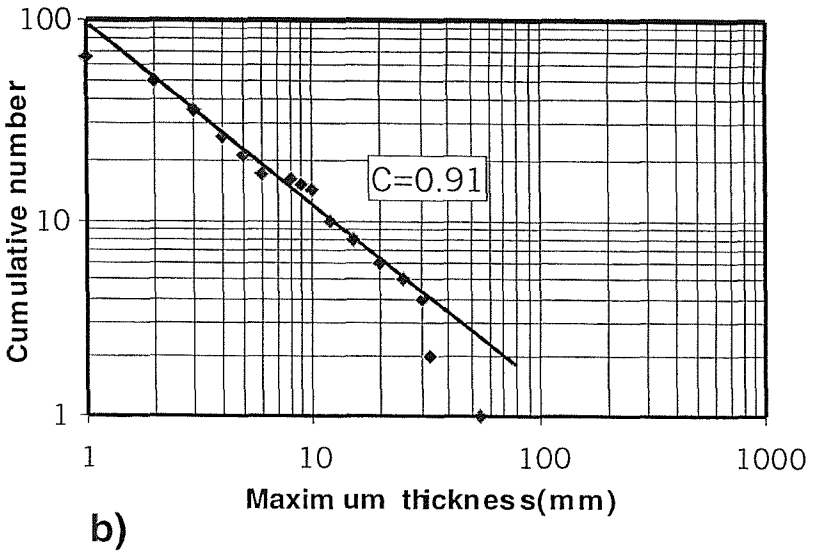

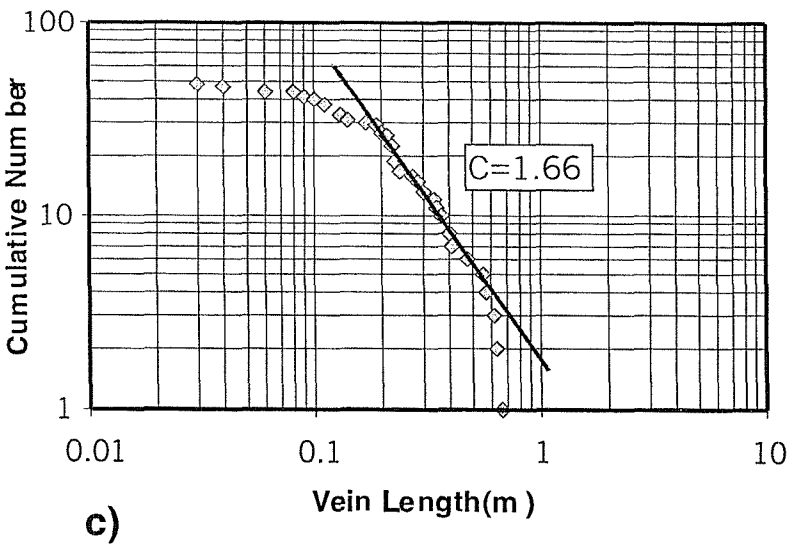

Fig. 2.15. Vein attributes in rotated blocks. a) Logarithmic plot of maximum thickness (*T*) against vein length (*Lv*) for veins in rotated blocks. b) Logarithmic plot of cumulative number of veins against vein thickness. c) Logarithmic plot of cumulative number of veins against vein length. See text for further discussion.

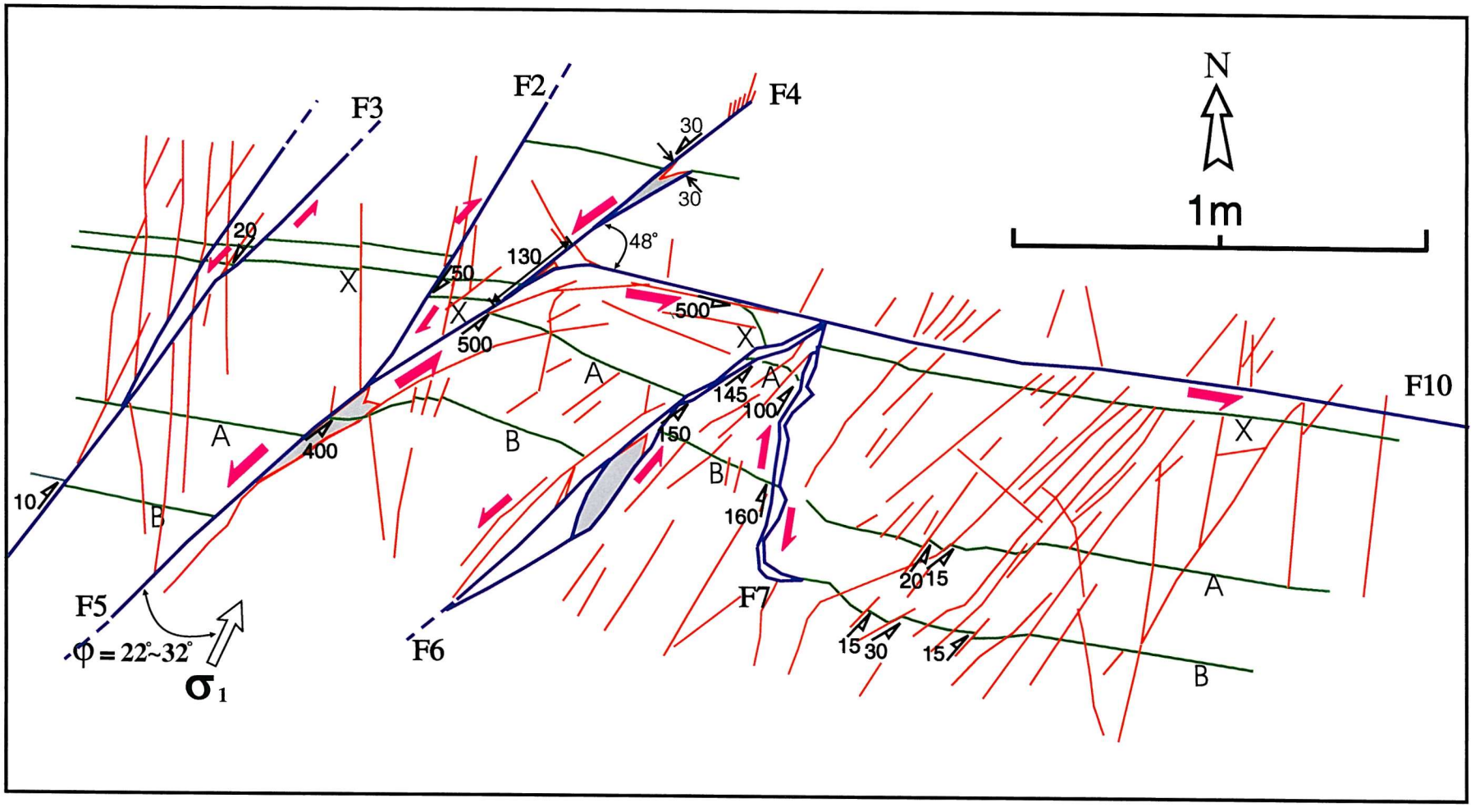

Fig. 2.16. Plan view of interacting dextral (F2, F7) and sinistral (F3, F4, F5, F6, and F10) faults. The angle between the minor-fault (F5) and fault F10 which follows bedding is 48°. Assuming the direction of σ_1 as N20°-30°E from joint and fault analyses, the angle (φ) between σ_1 and merging fault (F5) is 22°-32°, so that the propagation direction of the minor fault is in accord with the predicted direction

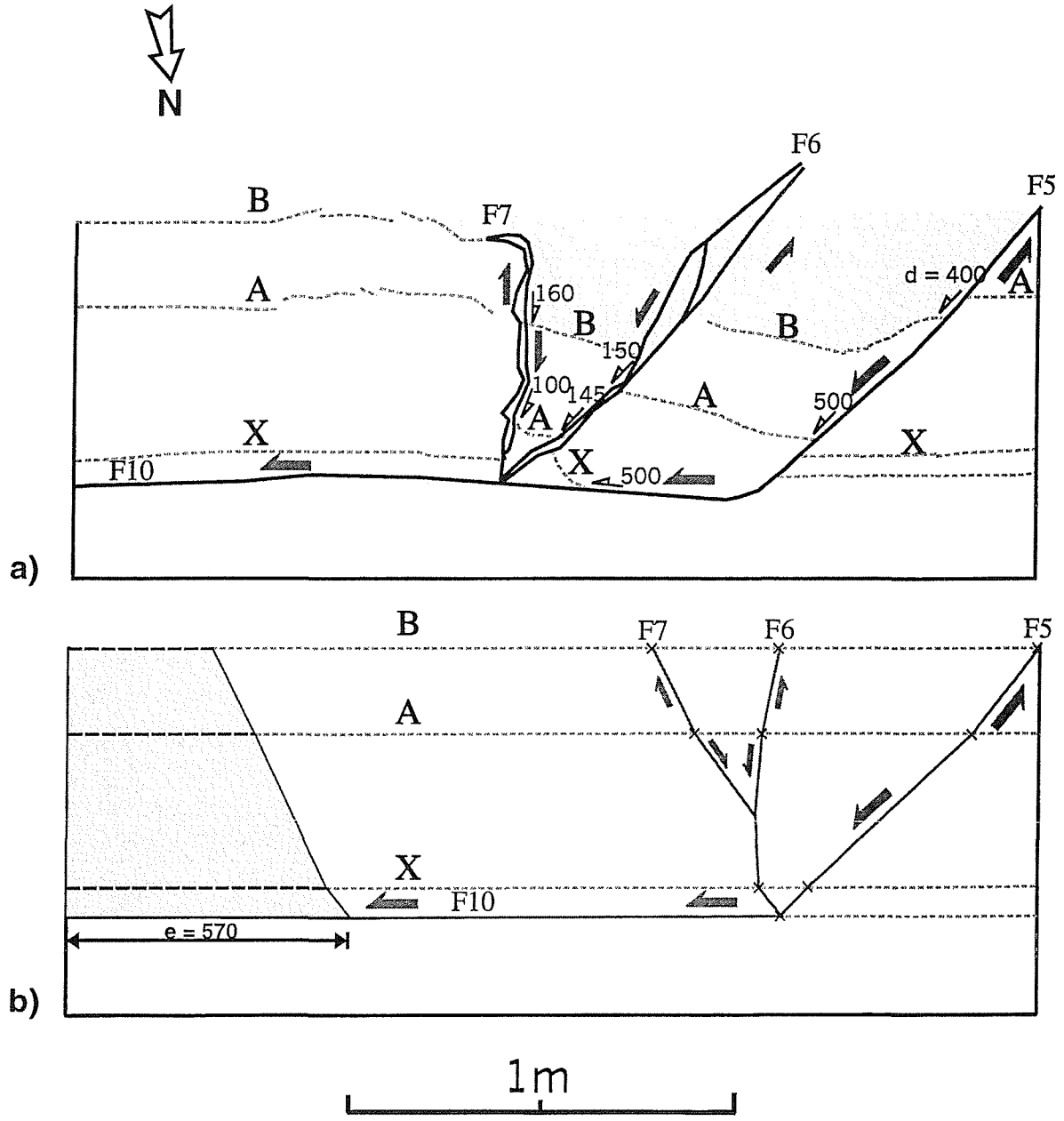

Fig. 2.17. Restoration of faults F4, F5, F6, F7 and F10. The estimated total amount of extension (*e*) is nearly similar to the measured displacement (*d*) along the fault, but the *e* value is a little bit larger than the *d* value. Solid lines represent fault planes. The dashed lines represent marker beds, and the shaded area represents the amount of extension along the beds. Faults F6 and F7 form a conjugate sinistral and dextral pair. Imagine this as a cross section through an extensional fault system (shown in figure as viewed from the north), and they are analogous to a "crestal-collapse graben" developed as the hanging (south) wall moves around the fault bend.

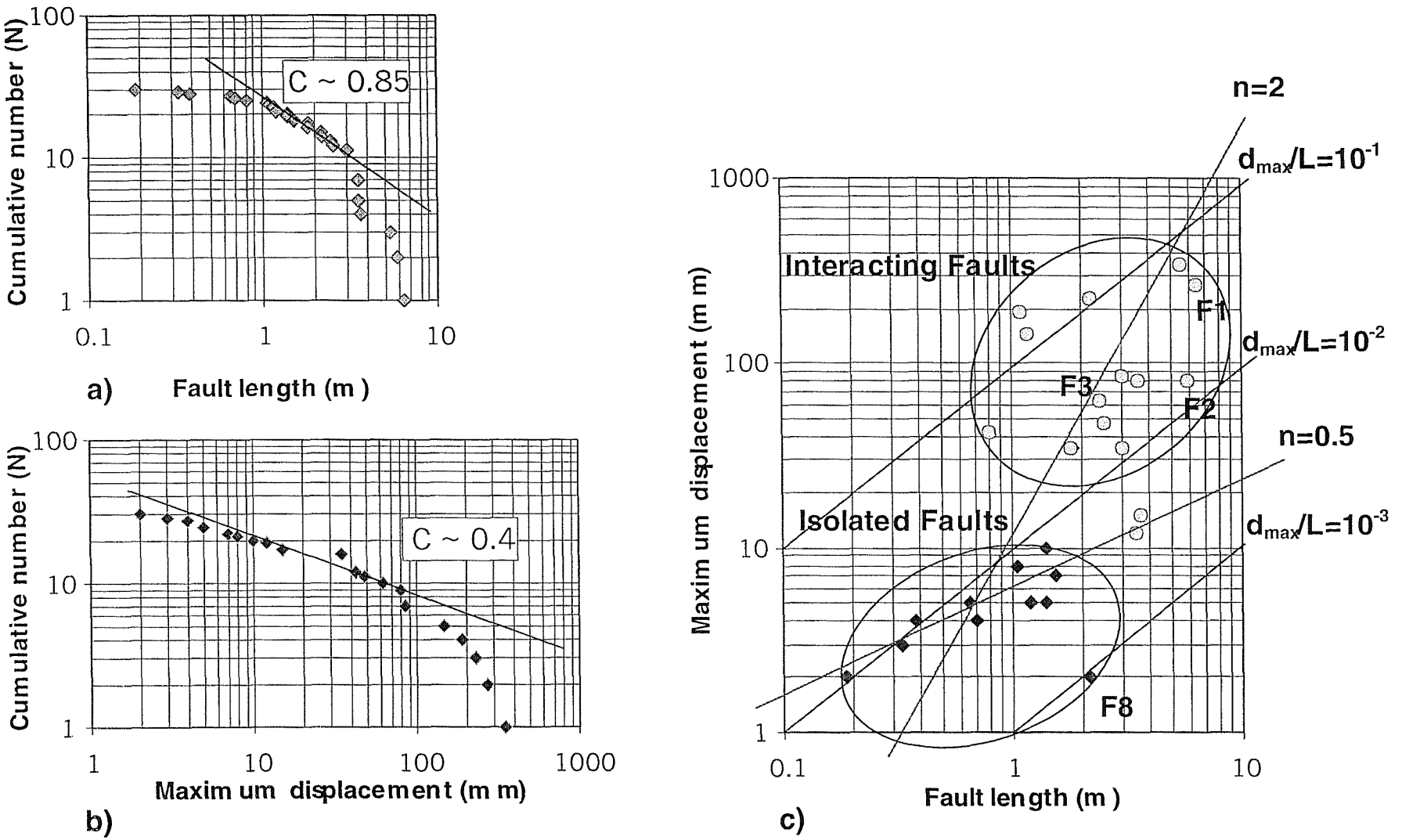

Fig. 2.18. Fault attributes of all strike-slip faults on and near map (Fig. 3). a) Logarithmic plot of fault lengths showing log-normal distribution due to censoring. b) Logarithmic plot of maximum displacements of faults. It maybe power-law with "finite range effect". c) Logarithmic plot of maximum displacement against fault length. The ratio of maximum displacement to fault length (d_{max}/L) is generally higher in interacting faults (circles) than isolated faults (diamonds). *C* and *n* denote slopes for log-log plots. See text for further discussion.

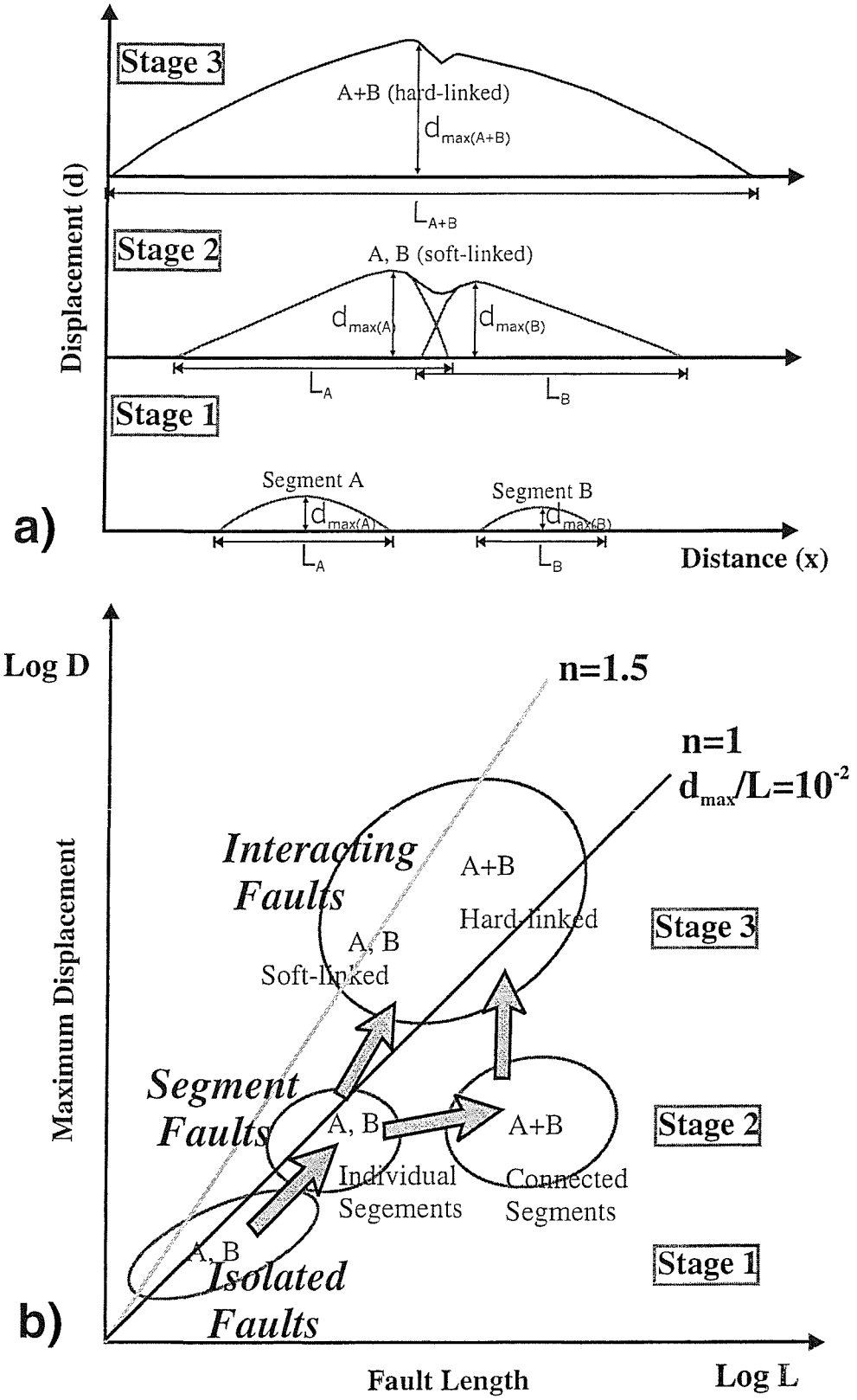

Fig. 2.19. A fault growth model by linkage and interaction between segmented faults from Crackington Haven for three stages of growth. (a) Linkage and evolution of fault segments. (b) d_{max}/L distribution and strike-slip fault evolution model for Crackington Haven. Isolated faults, segmented faults and interacting faults have distinctive d_{max}/L ratios. Each group evolves towards another group (arrows) along different slopes during the process of fault evolution.

CHAPTER 3: REACTIVATED STRIKE-SLIP FAULTS AT CRACKINGTON HAVEN, SOUTHWEST ENGLAND

Abstract

Several strike-slip faults at Crackington Haven show evidence of right-lateral movement with tip cracks and dilational jogs which has been reactivated by left-lateral strike-slip movement. Evidence for reactivation includes two slickenside striae on a single fault surface, two groups of tip cracks with different orientations and very low or negative displacements (left-lateral) at fault tips.

Evidence for the relative age of the two strike-slip movements is 1) the first formed tip cracks associated with right-lateral slip are deformed, whereas the tip cracks formed during left-lateral slip show no deformation; 2) some of the tip cracks associated with right-lateral movement show left-lateral reactivation; 3) left-lateral displacement is commonly recorded at the tips of dominant right-lateral faults.

The orientation of the tip cracks to the main fault is 30° - 70° clockwise for right-lateral slip, and 20° - 40° counter-clockwise for left-lateral slip. The structure formed by this process of strike-slip reactivation is named as "*tree structure*" because it is similar to a tree with branches. The angular difference between these two groups of tip cracks could be interpreted as due to different stress distribution (e.g. transtension/transpression, near-field/far-field stress and fracture modes) or pre-existing weakness.

Most of the d - x profiles have similar patterns which show low or negative displacement at the segment fault tips. Although the d - x profiles are complicated by fault segments and reactivation, they provide clear evidence for reactivation. Profiles which experience two opposing slip movements show various shapes depending on the amount of displacement and slip sequence. For a larger slip followed by a smaller slip with opposite sense, the profile would be expected to record very low or reverse displacement at fault tips due to late-stage tip propagation. Whereas for a smaller slip followed by larger slip with opposite sense, the d - x profile would be M-shape with no

reverse displacement at the tips. Such reactivation decreases the ratio of d_{max}/L by reducing d_{max} along a fault with increasing fault length.

3.1. INTRODUCTION

There has been increasing interest in studies of fault geometry and fault attributes during the last decade, leading to an appreciation of scaling relationships (e.g. Scholz and Cowie, 1990), fault growth models (e.g. Pollard and Segall, 1987; Cowie and Scholz, 1992; Martel and Boger, 1998), fault linkage (e.g. Peacock and Sanderson, 1991, 1992, 1996), and damage structures (e.g. McGrath and Davison, 1995; Kim *et al.*, 2000) around faults. However, no one has reported any damage structures related with reactivation of strike-slip faults and the displacement distribution along strike-slip fault during reactivation.

Several strike-slip faults, with tip cracks on both sides of a fault tip, are described from Crackington Haven. The aim of this chapter is to describe the characteristics of the fracture geometry resulting from reactivation and to interpret reactivated strike-slip faults. Also, the displacement (d) - distance (x) distribution for reactivated faults is examined and some simple conceptual models are suggested. Finally data of fault length (L) and maximum displacement (d_{max}) are used to suggest a growth model for reactivated strike-slip faults. A large scale example of reactivated strike-slip faults from the Atacama Fault System, Chile is compared with the examples from Crackington Haven.

In some brittle, homogeneous, isotropic materials, experimental studies have shown that a planar flaw loaded in shear or under combined normal and shear stress forms a crack at one or both of its ends (Brace and Bombolakis, 1963; Erdogan and Sih, 1963; Paterson, 1978; Nemat-Nasser and Horii, 1982). The term 'wing crack' (e.g. Brace *et al.*, 1966; Rispoli, 1981; Willemse and Pollard, 1998) has been applied to wing-shaped tip cracks at a high angle (> 60°) to the main fault, whereas 'horsetail splay'(e.g. Granier, 1985) has been used for secondary fractures which curve approaching main fault with various angles, generally low (< 20° ~ 50°). In this chapter these structures are referred to collectively as *tip cracks*.

Despite the large amount of theoretical (e.g. Rice, 1980; Willemse and Pollard, 1998) and experimental work (e.g. Paterson, 1978; Reches and Lockner, 1994) on

fault and crack growth, there is relatively little published work on the geometry of naturally induced brittle damage zones around the fault tips in rocks (Segall and Pollard, 1983; Granier, 1985; McGrath and Davison, 1995; Kim *et al.*, 2000). Furthermore there is no description and analysis of reactivated strike-slip faults, although Granier (1985) predicted such structures.

Some studies (McGarr *et al.*, 1979; Segall and Pollard, 1980; Mavko, 1982; Segall and Pollard, 1983; Cooke, 1997) have indicated that the structure and geometry of fault zones greatly influence the distribution of stress and slip along faults. Accurate analysis of damage zone structures around faults can determine whether experimental and theoretical studies are applicable to natural fault propagation and evolution. Furthermore, detailed investigation of exposure scale structures may provide a basis for the interpretation of large-scale reactivated strike-slip faults.

3.2. STRIKE-SLIP FAULTS AT CRACKINGTON HAVEN

A well exposed outcrop at the southern side of Crackington Haven (SX138973) in northern Cornwall was selected for this study (Fig. 3.1). Steeply dipping beds, normal to fault slip, provide good markers for quantifying displacement and damage structures. A variety of damage zone structures are reported around these strike-slip faults (Chapter 2; Kim *et al.*, 2000).

The host rock consists of inter-bedded sandstone and shale of the Crackington Formation of Upper Carboniferous age (Freshney *et al.*, 1972; Selwood *et al.*, 1985; Enfield *et al.*, 1985). The region was deformed during the Variscan (end Carboniferous) and by several episodes of Mesozoic and Tertiary movement (Selwood *et al.*, 1998). Most of the data were collected from wave cut exposures where erosion along the penetrative axial plane cleavage occurs in the core of a recumbent fold (Fig. 3.2).

In this area several strike-slip faults with a variety of orientations are interpreted as developed by the maximum compressive stress orientation of N030° (Fig. 3.3, Chapter 2; Kim *et al.*, 2000), although there might be a slight change of orientation of maximum compressive stress with time. There are a group of strike-slip faults, orientated at about N160° and dipping steeply east, which show mainly right-lateral slip, but with some later left-lateral reactivation (Fig. 3.3).

3.3. RESEARCH METHODS

1:10 to 1:40 scale maps were made from field photographs. Maps were calibrated in the laboratory with measured data to remove photographic distortions. Data were collected to establish displacement (d) - distance (x) relationships by measuring the displacement (d) between marker beds across the fault, and the distance (x) along the fault from one tip to the marker beds. The maximum displacement (d_{max}), is usually near the centre of the fault, and the fault length (L), defined as the length between two fault tips, was also measured. On occasions when a fault is only partly exposed, the fault length is estimated from the half-length that is taken from the tip of a fault to the maximum displacement. The accuracy in the measurement of displacement is about ±1 mm, and about ±1 cm for distance and fault length. The angular relationship between the main faults and tip cracks was examined and slickenside striae were measured on some fault surfaces.

3.4. STRIKE-SLIP REACTIVATION GEOMETRY

Five strike-slip faults were mapped for this work, each with a principal fault trace ranging from 2.5 m to 5.5 m in length. All have asymmetric tip cracks on both sides of the fault tips, but the cracks formed by right-lateral movement predominate, except in fault F26. Tip cracks have varying angles with the master fault, implying different stress origins and conditions. Because tip cracks are formed parallel to the orientation of maximum compressive stress, tip cracks on both sides of a fault are an indication of fault reactivation (Granier, 1985). Vein quartz fills most of the cracks formed during right-lateral slip, whereas it is rare in those associated with left-lateral slip.

3.4.1. Fault F22

Fault F22 (Fig. 3.4) trends N162° and is about 3.5 m long, with a maximum displacement of 105 mm with right-lateral sense. This fault has a single main segment showing a strong development of tip cracks, mainly formed during early right-lateral slip, and filled with vein quartz (red in Fig. 3.4). The longest tip crack is about 3 m in length, i.e. almost as long as the fault itself, with about 15 mm dilation. The angle of

the tip cracks ranges from 30° to 60° clockwise from the main fault. On the opposite side of the fault tip, a few tip cracks are formed by left-lateral movement (blue in Fig. 3.4). They strike at a low angle (10° ~ 20° anticlockwise) to the main strike-slip fault.

The right-lateral tip cracks have displacements of up to 27 mm. In general, the displacement along the tip cracks decreases away from the branching point with the master fault. In addition they have dilation of up to 20 mm. This suggests that the tip cracks are of mixed mode, I/II (McGrath and Davison, 1995; Willemse and Pollard, 1998). Detailed observation of fibre growth in quartz veins gave no clear evidence supporting the mixed mode nature of the splays. However, some en echelon vein arrays indicate right-lateral shear sense along the trend of tip cracks.

The displacement (d) - distance (x) profile (Fig. 3.5) for fault F22 is M-shape (Muraoka and Kamata, 1983) with a depression in the middle of the profile. The gradient is steeper to NW ($du/dx \approx 0.12$) than that to SE ($du/dx \approx 0.03$), which may result from relatively low reactivation and large damage development at NW tip. Although there is no direct evidence of left-lateral displacement in the d-x profile, the tip crack geometry at both fault tips indicates incipient left-lateral reactivation. Furthermore, left-lateral (negative) displacement is recorded along several minor tip cracks at the northern end of the fault associated with left-lateral movement (Fig. 3.4).

3.4.2. Fault F23

Fault F23 (Fig. 3.6) is a reactivated right-lateral fault trending N160° parallel to fault F22. Maximum displacement along this fault is 140 mm and the 3.5 m long exposed part comprises two segments separated by a dilational (during right-lateral slip) overstep zone or jog. NE trending tip cracks up to 2 m long are related to right-lateral movement; some are filled with vein quartz up to 50 mm wide. Subsidiary tip cracks formed by left-lateral slip are also apparent. It is very difficult to determine age relationships because the two sets of tip cracks are developed on different sides of the fault tip, and rarely display clear crosscutting relationship. The only evidence that left-lateral slip may be later in age is that the associated tip cracks are only developed at the final tip zones of the fault segments.

There are two slightly different fracture sets trending N-S and NE-SW (Fig. 3.6). The NE-SW set (at ~ 60° to the main fault) are confined to the tip origin, whereas the

more N-S fractures occur more widely. The N-S trending fracture set are interpreted as later fractures, because they are more widespread and cross-cut all early structures with opening mode, although some minor fractures abut earlier large discontinuities. The NE-SW fractures are interpreted as tip cracks developed during right-lateral slip on the main fault segments, and are similar in orientation to those seen in fault 22. The NW-SE tip cracks are also steeply dipping, 20° - 40° counter-clockwise from the main fault trace, and are related to the left-lateral slip movement.

The *d* - *x* profile (Fig. 3.7) shows that the point of maximum displacement (140 mm) is located near the overstep zone (jog), and the displacement of the other segment rapidly increases at the overstep zone. The combined *d-x* profile shows only a small displacement minimum with a high displacement gradient at the jog, suggests that the faults may be hard-linked (Nicol, *et al.,* 1996). At the north-western end of the fault, the profile shows an abnormally low displacement gradient ($du/dx \approx 0.02$) rather than the average gradient ($du/dx \approx 0.06$). This might result from later left-lateral strike-slip displacement superimposed on initial right-lateral displacement (see section 3.4.3 and 3.4.4).

3.4.3. Fault F24

Fault F24 (Fig. 3.8) trending N160° is exposed for about 5.5 m, and comprises 3 main segments separated by dilational jogs. The maximum displacement along the fault is 130 mm with right-lateral sense. Two of the three principal segments are connected through brecciated bridges as perpendicular, dilated quartz-filled jogs across the overstep. One of the segments is subdivided into two left-stepping sub-segment faults (B' and B"). The southern end of the fault is truncated by a left-lateral, bedding-parallel fault with a couple of triangular openings produced by accompanying block rotation (McGrath and Davison, 1995; Chapter 2; Kim *et al.*, 2000). These openings are a mirror image of triangular structures formed along a right-lateral strike-slip fault (Chapter 2; Kim *et al.*, 2000). However, there is no clear age relationship between these two faults.

Two sets of interfering slickenside striae with different plunge angles and slip senses occur on the fault plane (Fig. 3.9), providing further evidence that the fault underwent reactivation. The plunge of the two slickenside lineations are 160/03 and

160/23, respectively. However, there is no evidence of the age relationship between these two lineations.

Tip cracks are developed on both sides of the northern tip. Tip cracks associated with right-lateral movement (red in Fig. 3.8) are predominant, some reaching 2 m in length, and strike 50° ~ 70° clockwise from the main fault trace. The tip cracks associated with left-lateral movement (blue) strike 20° ~ 40° counter-clockwise from the main fault trace and are only developed at the northern tip of the fault, although other segment tips curve towards the dilational quadrant with left-lateral slip sense. Since faults generally propagate from the centre to the tips, the curved tip cracks at the end of a fault may indicate a later stage of left-lateral slip. However, there is little damage associated with left-lateral slip on the southern tips of the segments, probably because slip is accommodated through pre-existed damage.

A linkage pattern, similar to that of fault F23, is shown in the middle part of this fault set. As the slip along the fault increased, the bridge was broken through by a second-generation shear zone (Gamond, 1987). The displacement (Fig. 3.10) along the individual fault segments rapidly decreases in the bridge zone and is transferred to the adjacent segment with right-stepping sense. The maximum displacement along the fault is located along the southernmost fault segment (C) and the displacement is still high along the segment fault at the final stage, whereas the displacement along the segment B" is relatively low. This might be related to the segment stepping, that is, right-lateral slip is most easily transferred through right-stepping segments, whereas left-lateral slip is most easily transferred through left-stepping segments. The *d-x* profile is truncated by bedding-parallel slip at the SE end.

The segment pattern and damage distribution around the segment faults, and the *d-x* profiles provide clues for interpretation of the segment development and linkage. The predominant right-lateral displacements for all the segments and left-lateral displacements at the segment tips suggest right-lateral slip is early, and is transferred through right-stepping segments, mainly accumulated on the right-stepping segments (A-B'-C). Later left-lateral slip reactivated each segment producing curved tip cracks at the ends of segments. The net result is that segment tips show left-lateral displacement of up to 30 mm.

Segment A-B'-C are a right-stepping system and appear to transfer the right-slip efficiently, and accumulate 80 ~ 120 mm of displacement. The segment B'-B" are left

stepping and little right-lateral displacement (~ 30 mm) is transfer to B". However, the overstep between B'-B" accumulates much of the displacement (~ 13 mm) during left-lateral reactivation.

3.4.4 Fault F25

Fault F25 (Fig. 3.11) trends N162° and is about 5 m long with a maximum right-lateral displacement of 95 mm. The fault is composed of two main overstepping segments with minor sub-parallel subsidiary segments. The two main segments are linked through fractured dilational jogs filled with vein quartz. Two groups of obvious tip cracks are developed on the both sides of the northern tip producing an asymmetric pattern of tip cracks (both clockwise and anticlockwise to the main fault).

Tip cracks formed by right-lateral slip are predominant. They lie 40° - 50° clockwise from the main fault, whereas the tip cracks associated with left-lateral slip lie 20° - 30° counter-clockwise from the main fault. At the northern tip of the southern main segment, only a couple of tip cracks indicate later left-lateral slip, as at Ⓐ in Figure 3.11, where left-lateral slip of ~3 mm is developed. This is interpreted as a result of tip cracks formed during the early right-lateral movement being reactivated (Granier, 1985), with early formed tip cracks acting as pre-existing weakness.

At its southern end, the fault is terminated at a bedding-parallel slip surface without any extension fractures. Some dilation resulting from block rotation is developed along the bedding-parallel fault.

The relative age of right- and left-lateral slip is inferred from several field observations. Firstly, the segment faults show left-lateral displacements (up to 10 mm) only at their tips, though right-lateral displacement is predominant (up to 95 mm) near the centre of segment. Secondly, some tip cracks associated with right-lateral slip are deformed and show left-lateral displacement. Thirdly, the tip cracks associated with left-lateral slip are developed only on the western side of the segment tips, because the displacement during left-lateral slip could be accommodated by the early formed jogs (associated with right-lateral slip).

Although the d - x profile (Fig. 3.12) for fault F25 is complicated by reactivation and segment linkage, the total displacement is well preserved across the whole fault due to linkage through jogs. The d-x profile shows abnormally low or negative displacements at the fault tips. Although the fault shows predominantly right-lateral

offset with a maximum displacement of 95 mm, the sense of net slip is reversed at segment fault tips, where about 10 mm of left-lateral displacement occurs.

3.4.5. Fault F26

Fault F26 (Fig. 3.13) is a left-lateral fault striking N160°. It is about 2.5 m in length with a maximum displacement of 13 mm. The fault is composed of four left-stepping segments separated by overstep zones breached by secondary fractures. Tip cracks formed during left-lateral slip occur, particularly at the northern end of the fault and strike 20° - 30° counter-clockwise of the fault (blue in Fig. 3.13). Some short cracks oriented ~ N045° occur at 50° ~ 60° to the fault (red in Fig. 3.13).

The significance of this fault is that it is in the same orientation as the other faults (Fig. 3.4, 3.6, 3.8 and 3.11), but is dominantly left-lateral in movement. The only evidence of early right-lateral slip is the short cracks at 50° ~ 60° clockwise to the main fault segments, which resemble the right-lateral tip cracks of the other faults although they are not clearly related to segment tips.

The d - x profile of this fault is typical of a left-stepping, left-lateral fault linked by breached relays with a displacement minimum (Fig. 3.14).

On the basis of its evolution and early 'right-lateral' cracks, the fault interpreted as originating as a right-lateral fault with a series of left-stepping segments but with very little displacement. These fault segments were then reactivated by left-lateral slip, with linkage at oversteps to produce a larger fault with larger left-lateral displacement.

3.4.6. Discussion for all faults

All faults are steeply dipping and trend approximately N160°. With the exception of F26 they all show clear evidence of early right-lateral slip reactivated by later left-lateral slip. During right-lateral slip the maximum compressive stress (σ_1) must be oriented NE-SW, whereas during left-lateral slip σ_1 was oriented NW-SE. These slip events produce tip cracks, which are clockwise (NE-SW) for right-lateral and counter-clockwise (NW-SE) for left-lateral slip. Where both sets occur at the same tip, they produce a characteristic *tree structure* (Fig. 3.16).

In general right-lateral displacement (of ~ 100 mm) exceeds left-lateral, with net left-lateral movement being seen in the propagating tips of the fault segments. The

exception to this is fault 26 (Fig. 3.14), in which all segments have net left-lateral slip (of ~10 mm). Fault 26 has a series of left-stepping segments, whereas the other faults have right-stepping segmentation. Right stepping allows large right-lateral displacement across dilational jogs, whereas left-stepping accommodates less right-lateral displacement (Fig. 3.5, 3.7, 3.10 and 3.12) (Segall and Pollard, 1980; Cruikshank *et al.*, 1991; Moore and Lockner, 1995). During left-lateral reactivation the opposite is true, thus F26 (Fig. 3.14) accumulates net left-lateral displacement.

3.5. CHARACTERISTIC FEATURES AROUND REACTIVATED STRIKE-SLIP FAULTS

3.5.1. Evidence for strike-slip reactivation

There are four lines of evidence for reactivation: 1) There are two sets of tip cracks, with different orientations (Fig. 3.15), developed at fault tip zones producing a distinctive 'tree structure' (Fig. 3.16b). This implies that the fault experienced reverse reactivation, because tip cracks are developed normal to the orientation of maximum tensile stress. Granier (1985) suggested that if a strike-slip fault is activated subsequently in a opposite sense, the pre-existing tip cracks will reactivate with opposite sense. However, if the pre-existing tip cracks are filled with vein quartz, this may inhibit reactivation, and instead new tip cracks may develop on the other side of a fault tip (Fig. 3.16).

2) Two slickenside striae with different plunges are developed on fault F24 plane; striae indicating reversal slip senses occur, plunging horizontal and 023°. These two lineations strongly support the interpretation of a two-stage deformation, even though the sequence is not recognised on the surface.

3) Extensional tip cracks formed during the early right-lateral strike-slip movement were reactivated with left-lateral slip movement (of ~10 mm) during the later left-lateral strike-slip event.

4) The *d-x* profiles show abnormally low gradients or negative (left-lateral) displacements at fault tips (Fig. 3.7, 3.10 and 3.12). This results from later accumulation of slip with an opposite sense at the fault tips.

The geometry and nature of arrays of pre-existing fractures are important in controlling the nucleation and growth of some faults (Segall and Pollard, 1983). Several authors (e.g. Byerlee, 1967; Segall and Pollard, 1983) have worked on the failure of rocks with planes of discontinuity and showed that it is generally easier to reactivate a pre-existing fractures than to generate a new one. The tip cracks formed by left-lateral slip are more obvious for fault F24, F25 and F26 rather than fault F22 and F23. The difference between these structures might be partly dependent on the pre-existing structures. If any fault system has strong early-formed cracks or linkage structure to accommodate later stress, these pre-existing structures rather than developing new cracks may accommodate the stress. Also, segment stepping is another important factor. If segment stepping has the same sense with slip sense, displacement is well transferred into neighbour segment.

3.5.2. Tip cracks and their angles with the main faults

A shear fracture starts with the propagation of small flaws in the direction of σ_1 (Scholz, 1968). Final failure accompanies the linking of these small flaws along a shear plane, which in the laboratory is commonly at 25°-30° to σ_1 (Segall and Pollard, 1983; Engelder, 1989). Loading of a pre-existing flaw with sufficient stress to cause slip will produce a local concentration of tensile stresses near the tips (Griffith, 1924). Within intact rock, such as adjacent to faults, these opening-mode fractures initiate where local stress concentration exceed the fracture toughness (e.g., Jaeger and Cook, 1979; Lawn, 1993; Cooke, 1997).

In this chapter, 'branch fractures' (e.g. Brace and Bombolakis, 1963), 'wing cracks' (e.g. Willemse and Pollard, 1998) or 'tension gashes' (e.g. Rispoli, 1981) and 'horsetail splays' (e.g. Granier, 1985) structures are all considered as 'tip cracks'. 'Wing crack' is usually applied to a single thick, wing-shaped, tip crack at a high angle ($\theta_t > 60°$) with main fault, whereas the term 'horsetail splay' is used for splay fractures which curve at various angles, generally low ($\theta_t < 50°$), from main fault. Some studies (Petit and Barquins 1988; McGrath and Davison 1995; Kim *et al.*, 2000; Chapter 2) have tried to distinguish these two structures.

In general, *d-x* profiles with an abrupt decrease in slip at the tips develop wing cracks, whereas a gradual decrease of displacement towards the tip develops horsetail splays (Chapter 2; Kim *et al.*, 2000). Experiments on glass suggest that formation of

wing cracks occur in uniaxial compressive tests, whereas horsetail cracks are produced in biaxial compressive tests (Petit and Barquins 1988). Hence, tensional effective stresses are thought to induce wing-crack formation, which may form in rocks under high pore pressure conditions, or low confining pressures (McGrath and Davison 1995).

The tip cracks described in this study can be divided into two groups depending on their slip sense and orientation. The average orientation of the tip cracks during right-lateral slip is N040° (60° clockwise of the main fault plane) and during left-lateral slip is N130° (30° counter-clockwise of the main fault plane) (Fig. 3.15). Thus, the average angle between the two groups of the tip cracks is about 90°.

Various criteria have been proposed to predict the angle of a tip crack to a fault. These criteria include; the maximum circumferential tensile stress (Erdogan and Sih, 1963; Thomas and Pollard, 1993), maximum energy release rate (Hussain *et al.*, 1974), minimum strain energy density (Sih, 1974), $K_{II} = 0$ (Cotterell and Rice, 1980), and maximum principal stress (Cooke and Pollard, 1996). The stress intensity factors (K), in turn, depend on the loading conditions and the flaw geometry (Irwin, 1957; Williams, 1957).

The maximum circumferential stress criterion (Erdogan and Sih, 1963) postulates that (i) the crack propagates radially from the fault tip, and (ii) it starts in the plane perpendicular to the direction of greatest tension. This implies that the crack starts to grow from the tip in the direction θ_t (Fig. 3.16a) along which the circumferential stress is maximum and the shear stress is zero. However, during consecutive stress loading tip cracks generally experience mixed mode loading (McGrath and Davison, 1995; Willemse and Pollard, 1998). A similar condition was found to hold for solution seams, in which case, the circumferential stress corresponds to the minimum principal stress in the direction θ_c (Fig. 3.16a) (Willemse and Pollard, 1998).

Standard linear elastic fracture mechanics (LEFM) theory, in which the stresses rise to infinity at the flaw tip (Irwin, 1957; Rice, 1968), predicts that pure mode II faults produce tip cracks at the fault tip with angles of 70.5° (Pollard and Segall, 1987). Field description indicates that tip fractures often form at angles less than 50° to the primary fault (c.f. Cruikshank *et al.*, 1991; Martel *et al.*, 1988; Segall and

Pollard, 1983). The predicted angle may be reduced with incorporation of mixed-mode fracture propagation (Cruikshank *et al.*, 1991) or strong fault end zones that reduce the stress at the tip singularity (Martel, 1997; Cooke, 1997; Willemse and Pollard, 1998). In general, remote flaw-parallel compression tends to reduce the intersection angle between master fault and tip cracks, so that the tip crack is at a lower angle to the fault (Willemse and Pollard, 1998).

Individual structures together may form a distributed shear zone across the fault. In the "cohesive end zone" (CEZ) model (Tada *et al.*, 1985; Anderson, 1991; Cowie and Scholz, 1992; Rubin, 1993), a zone of high cohesive strength or friction is postulated near the fault tip (Dugdale, 1960; Barenblatt, 1962; Ida, 1972; Palmer and Rice, 1973; Cowie and Scholz, 1992). In some instances there is localisation of tip cracks and solution surfaces at the flaw tip and in specific quadrants. Such fracture patterns may form when the end zones are comparatively small (Willemse and Pollard, 1998) due to abrupt changes in frictional strength (Cooke, 1997).

In consequence, the angle that tip cracks make with the main fault may depend on the material properties (such as the rock plasticity), stress conditions and fault surface geometry (Lin and Parmentier 1988, Bilham and King, 1989, McGrath and Davison 1995; Willemse and Pollard, 1998).

3.5.3. Why do the 2 sets of tip cracks have different angles?

In the examples from Crackington Haven, the orientations of measured tip cracks have consistently different angles depending on the slip sense (Fig. 3.15). There are four possibilities for the angular difference between two sets.

1) The two crack tips are produced by different 'far-field' stress (Fig. 3.18A). For right-lateral slip the normal stress (σ_n) is large and shear stress (τ) is small (i.e. transpressional), therefore the tip cracks form at a higher angle to the main fault ($\theta_t >> 45°$). Whereas for left-lateral slip, the normal stress (σ_n) is small and shear stress (τ) is large (i.e. transtensional), therefore the tip cracks are at a lower angle to the main fault ($\theta_t << 45°$) (e.g. Sanderson and Marchini, 1984; Schreurs and Colletta, 1998).

2) The two tip cracks are caused by different 'near-field' stress concentration at tips (Fig. 3.18B). There could be difference between internally pressured cracks and frictionally sliding cracks. However, the 'near-field' stress is mainly controlled by the 'far-field' stress, and they show the same pattern as 1).

3) The two tip cracks are caused by different fracture mechanism (Fig. 3.18C). For example, during right-lateral slip σ_1 is at ~ 60° to the main fault, and cracks are mode I. Therefore, θ_t is ~ 60° to the main fault. Whereas during the left-lateral slip σ_1 is at ~ 60° to the main fault, but cracks are mode II/III. Therefore, θ_t is ~ 30° to the main fault. This is not supported by observed displacements along both tip cracks.

4) Tip cracks are caused by pre-existing plane of weakness (e.g. solution seams) (Fig. 3.18D). Solution surfaces form at 90° to tensional tip cracks in CEZ flaw models (Willemse and Pollard, 1998). The tip crack angle to the main fault (θ_t) is ~ 60° during right-lateral slip, and solution surface angle (θ_c) may be ~ 30° based on the CEZ model. Therefore, tip cracks formed during left-lateral slip may utilise these solution surfaces during reactivation. This hypothesis is not supported by clear evidence of solution surface during right-lateral slip.

By elimination of 3) and 4), the difference in tip crack angles to the main fault is attributed to variation in the loading orientation of the fault during the two slip events. This may be due to a combination of 'far-field' stress and internal fluid pressure, providing differences in the 'near-field' stress at the crack tips.

3.5.4. Displacement (d) - distance (x) characteristics for reactivated strike-slip faults

Displacement (*d*) - distance (*x*) data for the four faults (F22 ~ F25) show abnormally low or negative displacement at the tips of many faults. This suggests that the tips of faults propagate onwards during left-lateral reactivation, but that in the middle of the main fault reactivation is not large enough to exceed the early right-lateral movement.

d - *x* profiles of several fault segments develop from the non-coherent multi-peak type profile through a plateau-type profile to a coherent single-peak profile (Childs *et al.*, 1995; Dawers and Anders, 1995; Fossen and Hesthammer, 1997). Most of the profile shapes shown in this chapter are similar to the hard-linked multi-peak type. However, any other model has not predicted the abnormal low or negative displacement at the fault tips.

Four possible models for single faults and segment linkages are presented to explain the profile shapes (Fig. 3.19 and 3.20). The models assume that the faults propagate through fault tips (i.e. increasing length), from stage 1 to stage 2.

If the fault has a large right-lateral displacement (stage 1) followed by a small left-lateral displacement (stage 2) (Fig. 3.19a), the result *d-x* profile will be as in Fig. 3.19b. The propagation of the fault results in the left-lateral displacement occurring along the entire length of the fault trace, with the right-lateral displacement diminish in the central part. This produces the negative (left-lateral) displacement at the fault tips.

If the fault has an early left-lateral slip (stage 1) followed by a much greater right-lateral slip (stage 2) (Fig. 3.19c), the resulting *d-x* profile is as in Fig. 3.19d. The fault has a net right-lateral slip along its entire trace, the early left-lateral displacement producing a flat (*M*-type) central part to the profile.

For segmented faults, two similar models are illustrated (Fig. 3.20), essentially involving 2 overlapping faults of the type described in Figure 3.19. A larger right-lateral displacement followed by a smaller left-lateral displacement (Fig. 3.20b) produces a negative (left-lateral) displacement at both fault tips and reduced displacement at the overlapping zone. Whereas that of the fault experiencing a smaller left-lateral displacement followed by larger right-lateral displacement (Fig. 3.20d) would show a depression in the overlapping zone and no negative displacement at the tips. The first linkage model (Fig. 3.20a and 3.20b) is applicable to the cases of predominant slip recorded at the first stage, and is very similar to F24 and F25. On the other hand, Figures 3.20c and 3.20d shows the case for later slip is predominant, which is applicable to the fault F26. In these two cases, the *d* - *x* profiles are completely different, so that the slip history can be interpreted from the *d-x* profile of reactivated faults. These models may be applicable to all scale fault systems.

3.5.5. Maximum displacement (d_{max}) - fault length (L) relationship for reactivated strike-slip faults

The maximum displacement (d_{max}) and length (L) for the five faults are plotted in Figure 3.21a. Some of the fault lengths were obtained from the *d-x* profile, assuming fault length is twice distance from d_{max} to observed tip. The four right-lateral faults plot between $10^{-2} < d_{max}/L < 10^{-1}$ and are similar to the wide interacting fault region discussed in Chapter 2. The left-lateral fault plots with a relative low d_{max}/L ($< 10^{-2}$). F22 and F23, showing relatively weak reactivation, have relatively high d_{max}/L ratios compared with F24 and F25 in spite of their shorter fault lengths, although some

studies suggested increasing ratio with increasing fault length for general faults (e.g. Gillespie *et al.*, 1992; Peacock and Sanderson, 1996). It is interpreted that F24 and F25 have more reverse reactivation than F22 and F23 as shown dotted lines in Figure 3.21b.

Three stages can be identified in the growth of linked faults in general (Peacock and Sanderson 1991; Cartwright *et al.*, 1995; Chapter 2; Kim *et al.*, 2000). Isolated faults tend to propagate rapidly as the accumulated displacement increases e.g. producing $d_{max}/L \sim 0.005$ (Fig. 3.21b). Linkage initially occurs by overlap producing strike-slip relay ramp (Peacock and Sanderson, 1995), pull-aparts or jogs (Aydin and Nur, 1982; Sibson, 1989; Peacock, 1991) and soft-linked segments (Walsh and Watterson, 1991). These may evolve to produce through-going faults (i.e. hard-linkage, Walsh and Watterson, 1991 or breached relay ramp, Peacock and Sanderson, 1995). Soft-linked fault segments evolve along a step-like profile (Cartwright *et al.*, 1995; Chapter 2; Kim *et al.*, 2000) with periods of displacement accumulation with little propagation in relay ramp and periods of rapid increase in length due to hard-linkage. d_{max}/L profiles for interacting faults in Crackington Haven typically have $d_{max}/L \sim 0.04$ (Chapter 2; Kim *et al.*, 2000).

In faults that are reactivated with opposite sense, the net displacement is reduced as propagation continues (see earlier discussion). Although the slope of the reactivation path is not known; it may be estimated from the extended fault tips (10 to 20 % of original fault length) in the d - x profile for faults 24 and 25, and is about $d_{max}/L = 0.025$. This implies that the ratio of d_{max}/L decreases with progressive reactivation as shown in Figures 3.19e and 3.21b. For faults such as F26, which have little early right-lateral displacement, the evolution may be along the path $d_{max}/L \approx 0.005$ (Fig. 3.21b) with reactivation producing a net left-lateral slip as in Figure 3.21b.

3.6. A LARGE SCALE STRIKE-SLIP REACTIVATION IN THE SALAR GRANDE PULL-APART BASIN, ATACAMA FAULT SYSTEM, NORTHERN CHILE

The Salar Grande basin is a strike-slip pull-apart basin along the northern end of the Atacama Fault System (AFS) of the northern Chile (21°S, 70°W), which is mainly composed of Lower Jurassic to Lower Cretaceous arc-related rocks (Fig. 3.22). Salar

Grande is a recent salt pan with a N-S elongate shape of 50 km in length and 5-8 km wide. The pull-apart basin has undergone a long and complex history of polyphase strike-slip movement including reverse reactivation (Reijs and McClay, 1998).

The Salar Grande basin is cross-cut by the Salar Grande Fault (SGF), consisting of active fault traces that produce monoclines, sag basins and push-up swells. Stream-cuts into the alluvium are right-laterally offset by *c.* 300 m in the northern part of the SGF. A sidewall rip-out with left-lateral asymmetry (Swanson, 1989) has formed west of the SGF (Fig. 3.22) (Reijs and McClay, 1998).

Maps and LANDSAT TM imagery indicate a perfect match of the northern and southern blocks and the three N-S faults, assuming a 6 km left-lateral displacement (Reijs and McClay, 1998). This reconstruction supports the interpretation that the basin was dissected by a NNW-SSE left-lateral fault. The SGF dies out into curved horsetail splays of extensional faults north-west of Salar Grande, which reflect a left-lateral displacement history. The splay faults show later reactivation at the tip zone. Also, the Cerro Chuculay Fault displaces both the eastern normal faults and Salar de Llamara Border Fault right-laterally by *c.* 1 km. The Cerro Chuculay Fault is parallel to the active trace of the SGF and probably formed at the same time. This overprinting relationship shows that the eastern normal faults were active before the recent right-lateral NNW-SSE faulting phase (Reijs and McClay, 1998).

Reconstruction of the plate vector for the subducting Nazca plate at the north Chilean active margin shows a decrease in the convergence rate and obliquity in the Oligocence-Early Miocene (Pardo-Casas and Molnar, 1987; Buddin *et al.*, 1993). This time coincides with the initiation of the Salar Grande basin and the Quillagua Trough (Jensen *et al.*, 1995), and left-lateral strike-slip motion on the Pre-cordillera Fault System around Calama (Reutter *et al.*, 1996; May *et al.*, 1996). Plate reconstructions for the Miocene to recent show an increased convergence rate of the subducting slab at the Chilean active margin (Pardo-Casas and Molnar, 1987; Buddin *et al.*, 1993). These changes may have triggered the switch from left-lateral to right-lateral slip along the Atacama Fault System (Reijs and McClay, 1998).

After the Pleistocene, NNW-SSE faults were dextrally reactivated (SGF) and new NNW-SSE dextral faults formed (e.g. Cerro Chuculay Fault). This recent deformation produced active pressure ridges and sag basins in the rock salt of the Oligocene-Pleistocene Soledad Formation, and pull-aparts, scarps and stream offsets

in the Miocene to Quaternary alluvium. Right-lateral strike-slip offsets of 300 m along the SGF and 1 km along the Cerro Chuculay Fault are recorded as a result of the later reactivation (Reijs and McClay, 1998).

The right-lateral displacement is recorded only at the northern and southern tips of the SGF, and the reactivation along the other splay faults is very similar to the reactivated faults at Crackington Haven. The Cerro Chuculay Fault just records right-lateral displacement, and it indicates that the fault is generated at the later right-lateral stage or that any left-lateral displacement is completely recovered by later right-lateral displacement as the case of F26 at Crackington Haven.

3.7. CONCLUSIONS

1. Five sub-parallel (N160° trending) faults at Crackington Haven show evidence of right-lateral strike-slip movement with tip cracks and dilational jogs, which has been reactivated by left-lateral strike-slip movement.
2. Evidence for reactivation includes: two slickenside striae on a fault surface; two groups of tip cracks with different orientations; and opposite senses, and low or negative displacement at fault tips. Also, some early tip cracks formed by right-lateral movement show reactivation with a left-lateral slip sense.
3. The relative age of the two strike-slip movements are deduced from; 1) the right-lateral tip cracks are deformed, whereas the tip cracks formed by left-lateral slip show no deformation, 2) some tip cracks associated with right-lateral slip show left-lateral reactivation, 3) most of the examined faults (except F26) show very low or left-lateral displacement at fault tips whereas right-lateral displacement predominates along the central part of the faults.
4. The orientation of the tip cracks is 30° ~ 70° clockwise for right-lateral slip whereas 20° ~ 40° counter-clockwise for left-lateral slip from the main fault. The intersection angle of tip cracks with the master fault may depend on the stress state, material properties, and influence of any pre-existing planes of weakness. The angular difference between the two sets of tip cracks is interpreted as due to different far- and near-field stress distribution such as transpression/ transtension and cohesive/non-cohesive. The resulting asymmetric tree structure is a useful geometry for recognition of reverse reactivation in the strike-slip fault systems.

5. Most of the d - x profiles (except F26) have similar patterns that show low or negative (left-lateral) displacement at the segment fault tips. Profiles that experience two opposing slip movements show various shapes depending on the amount of displacement and the slip sequence. For a larger slip followed by smaller slip with opposite sense, the profile would be expected to record very low or reverse displacement at fault tips due to late-stage tip propagation. Whereas for a smaller slip followed by larger slip with opposite sense the d - x profile would be M-shape with no negative displacement at the tips.
6. Reverse reactivation decreases the ratio of d_{max}/L, because the opposite slip (negative displacement) reduces d_{max}, whereas continued propagation increases L.
7. The Salar Grande Fault formed as a left-lateral fault with large displacement in the central region. Later right-lateral reactivation is preserved at the fault tips and at the smaller sub-parallel Cerro Chuculay Fault. These faults resemble those seen at Crackington Haven.

REFERENCES

Anderson, T. L. 1991. *Fracture Mechanics: Fundamentals and Applications*. 793 pp. CRC Press, Raton, Fla.

Aydin, A. and Nur, A. 1982. Evolution of pull-apart basins and their scale independence. *Tectonics* **1**, 91-105.

Barenblatt, G. I. 1962. Mathematical theory of equilibrium cracks in brittle fracture. *Adv. Appl. Mech.*, **7**, 55-129.

Bilham, R. and King, G. 1989. The morphology of strike-slip faults: Examples from the San Andreas fault, California. *J. Geophys. Res.* **94**, 10,204-10,216.

Brace, W. F. and Bombolakis, E. G. 1963. A note on brittle crack growth ion compression. *J. Geophys. Res.* **68**, 3709-3713.

Brace, W. F., Paulding, B. W. and Scholz, C. H. 1966. Dilatancy in the fracture of crystalline rocks. *J. Geophys. Res.* **71**, 3939-3942.

Buddin, T. S., Stimpson, I. G. and Williams, G. D. 1993. North Chilean forearc tectonics and Cenozoic plate kinematics. *Tectonophysics*, **220**, 193-203.

Byerlee, J. D. 1967. Theory of friction based on brittle fracture. *J. Appl. Phys.*, **38**, 2928-2934.

Cartwright, J. A., Trudgill, B. D. and Mansfield, C. S. 1995. Fault growth by segment linkage: an explanation for scatter in maximum displacement and trace length data from the Canyonlands Grabens of SE Utah. *Journal of Structural Geology* **17**, 1319-1326.

Childs, C., Watterson, J. and Walsh, J. J. 1995. Fault overlap zones within developing normal fault systems. *J. Geol. Soc. London*, **152**, 535-549.

Cooke, M. L. 1997. Fracture localization along faults with spatially varying friction. *J. Geophys. Res.* **102**, 22,425-22,434.

Cooke, M. L. and Pollard, D. D. 1996. Fracture propagation paths under mixed mode loading within rectangular blocks of polymethyl methacrylate. *J. Geophys. Res.* **101**, 3387-3400.

Cotterell, B. and Rice, J. R. 1980. Slightly curved or kinked cracks. *Int. J. Fract.*, **16**, 155-169.

Cowie, P. A. and Scholz, C. H. 1992. Physical explanation for the displacement-length relationship of faults, using a post-yield fracture mechanics model. *J. Struct. Geol.*, **14**, 1133-1148.

Cruikshank, K. M., Zhao, G. and Johnson, A. M. 1991. Analysis of minor fractures associated with joints and faulted joints. *J. Struct. Geol.*, **13**, 865-886.

Dawers, N. H. and Anders, M. H. 1995. Displacement-length scaling and fault linkage. *J. Struct. Geol.*, **17**, 607-614.

Dugdale, D. S. 1960. Yielding of steel sheets containing slits. *J. Mech. Phys. Solids,* **8**, 100-104.

Enfield, M. A., Gillcrist, J. R., Palmer, S. N. and Whalley, J. S. 1985. Structural and sedimentary evidence for the early tectonic history of the Bude and Crackington Formations, north Cornwall and Devon. *Pro. of the Ussher Soc.* **6**, 165-172.

Engelder, T. 1989. Analysis of pinnate joints in the Mount Desert Island granite: implications for post-intrusion kinematics in the coastal volcanic belt, Maine. Geology, 17, 564-567.

Erdogan, F. and Sih, G. C. 1963. On the crack extension in plates under plane loading and transverse shear. *J. Basic Eng.*, **85**, 519-527.

Fossen, H. and Hesthammer, J. 1997. Geometric analysis and scaling relations of deformation bands in porous sandstone. *J. Struct. Geol.*, **19**, 1479-1493.

Freshney, E. C., McKeown, M. C. and Williams, M. 1972. Geology of the coast between Tintagel and Bude. *Mem. Geol. Surv. Gt. Br.*

Gamond, J. F. 1987. Bridge structures as sense of displacement criteria in brittle fault zones. *J. Struct. Geol.*, **9**, 609-620.

Gillespie, P. A., Walsh, J. J. and Watterson, J. 1992. Limitations of dimension and displacement data from single faults and the consequences for data analysis and interpretation. *Journal of Structural Geology* **14**, 1157-1172.

Granier, T. 1985. Origin, damping, and pattern of development of faults in granite. *Tectonics,* **4**, 721-737.

Griffith, A. A. 1924. Theory of rupture. in *First International Congress on Applied Mechanics,* edited by C. B. Biezeno, J. M. Burgers, and J. Waltman Jr., 55-63, Delft.

Hussain, M. A., Pu, S. L. and Underwood, J. H. 1974. Strain energy release rate for a crack under combined mode I and mode II, in *Fracture Analysis: Proceeding of the 1973 National Symposium on Fracture Mechanics II, ASTM Spec. Tech. Publ.*, **560**, 2-28.

Ida, Y. 1972. Cohesive force across the tip of longitudinal shear crack and Griffith's specific surface energy. *J. Geophys. Res.* **77**, 3796-3805.

Irwin, G. R. 1957. Analyses of stresses and strains near the end of a crack traversing a plate. *J. Appl. Mech.*, **24**, 361-364.

Jaeger, J. C. and Cook, N. G. W. 1979. *Fundamental of Rock Mechanics.* 593pp., Oxford Univ. Press, New York.

Jensen, A., Dorr, M. J., Gotze, H. J., Kiefer, E., Ibbeken, H., and Wilke, H. 1995. Subsidence and sedimentation of a forearc-hosted, continental pull-apart basin: the Quillagua Trough between 21°30 and 21°45'S, northern Chile. *In : A. Saez (ed.) Abstracts GLOPALS-IAS Meeting, Antofagasta, 12-18 November, Chile,* 5-6.

Kim, Y. -S., Andrews, J. R. and Sanderson, D. J. 2000. Damage zones around strike-slip fault systems and strike-slip fault evolution, Crackington Haven, southwest England. *Geoscience Journal* **4,** 53-72.

Lawn, B. 1993. *Fracture of Brittle Solids,* 2nd ed., 378pp., Cambridge Univ. Press, New York.

Lin, J. and Parmentier, E. M. 1988. Quasistatic propagation of a normal fault: a fracture mechanics model. *J. Struct. Geol.,* **10**, 249-262.

Martel, S. J. 1997. Effects of cohesive zones on small faults and implications for secondary fracturing and fault trace geometry. *J. Struct. Geol.,* **19**, 735-747.

Martel, S. J. and Boger, W. A. 1998. Geometry and mechanics of secondary fracturing around small three-dimensional faults in granitic rock. *Journal of Geophysical Research* **103**, 21,299-21,314.

Martel, S. J., Pollard, D. D. and Segall, P. 1988. Development of simple strike-slip fault zones, Mount Abbot quadrangle, Sierra Nevada, California. *Geol. Soc. Am. Bull.,* **100**, 1451-1465.

Mavko, G. M. 1982. Fault interaction near Hollister, California, *J. Geophys. Res.,* **87**, 7807-7816.

May, G., Hartley, A. J. and Stuart, F. M. 1996. Oligocene-Recent sedimentary and tectonic evolution of the Calama basin, N. Chilean forearc. *Third International Symposium on Andean Geodynamics, Saint-Malo (France), 17-19 September 1996*, 435-437

McGarr, A., Pollard, D. D., Gay, N. C. and Ortlepp, W. D. 1979. Observations and analysis od structures in exhumed mine-induced faults. Analysis of Actual Fault Zones in Bedrock, *U. S. Geol. Surv. Open File Rep.,* **79-1239**, 101-120.

McGrath, A. G. and Davison, I. 1995. Damage zone geometry around fault tips. *J. Struct. Geol.,* **17**, 1011-1024.

Moore, D. E. and Lockner, D. A. 1995. The role of microcracking and shear-fracture propagation in granite. *J. Struct. Geol.,* **17**, 95-114.

Muraoka, H. and Kamata, H. 1983. Displacement distribution along minor fault traces. *J. Struct. Geol.* **5**, 483-495.

Nemat-Nasser, S. and Horii, H. 1982. Compression-induced nonplanar crack extension with application to splitting, exfoliation and rockburst, *J. Geophys. Res.,* **87**, 6805-6821.

Nicol, A., Watterson, J., Walsh, J. J. and Childs, C. 1996. The shapes, major axis orientations and displacement patterns of fault surfaces. *J. Struct. Geol.* **18**, 235-248.

Palmer, A. C. and Rice, J. R. 1973. The growth of slip surfaces in the progressive failure of overconsolidated clay. *Proc. R. Soc. London.* **A, 332**, 527-548.

Pardo-Casas, F. and Molnar, P. 1987. Relative motion of the Nazca (Farallon) and South American plates since late Cretaceous time. *Tectonics*, **6**, 233-248.

Paterson, M. S. 1978. *Experimental Rock Deformation-The Brittle Field.* 254pp., Springer-Verlag, New York.

Peacock, D. C. P. 1991. Displacement and segment linkage in strike-slip fault zones. *Journal of Structural Geology* **13**, 1025-1035.

Peacock, D. C. P. and Sanderson, D. J. 1991. Displacements, segment linkage and relay ramps in normal fault zones. *J. Struct. Geol.* **13**, 721-733.

Peacock, D. C. P. and Sanderson, D. J. 1992. Effects of layering and anisotropy on fault geometry. *J. Geol. Soc. London.*, **149**, 793-802.

Peacock, D. C. P. and Sanderson, D. J. 1996. Effects of propagation rate on displacement variations along faults. *J. Struct. Geol.* **18**, 311-320.

Peacock, D. C. P. and Sanderson, D. J. 1995. Strike-slip relay ramps. *J. Struct. Geol.* **17**, 1351-1360.

Petit, J. P. and Barquins, M. 1988. Can natural faults propagate under mode-II conditions?. *Tectonics,* **7**, 1243-1256.

Pollard, D. D. and Segall, P. 1987. Theoretical displacements and stresses near fractures in rock: with applications to faults, joints, veins, dykes and solution surfaces. In: *Fracture Mechanics of Rock* (edited by Atkinson, B. K.). Academic Press, London, 277-349.

Reches, Z. and Lockner, D. A. 1994. Nucleation and growth of faults in brittle rocks. *Journal of Geophysical Research* **99**, 18,159-18,173.

Reijs, J. and McClay, K. 1998. Salar Grande pull-aprt basin, Atacama Fault System, northern Chile. In: Holdsworth, R. E., Strachan, R. A. & Dewey, J. F. (eds). *Continental Transpressional and Transtensional Tectonics.* Greological Society, London, Special Publications, **135**, 127-141.

Reutter, K. J., Schreuber, E. and Chong, C. 1996. The Procordilleran fault system of Chuquicamata, Northern Chile: evidence for reversals along arc-parallel strike-slip faults. *Tectonophysics*, **258**, 213-228.

Rice, J. R. 1968. Mathematical analysis in the mechanics of fracture. in *Fracture: An Advanced Treatise*, edited by H. Liebowitz, 191-311, Academic, San Diego, Calif.

Rice, J. R. 1980. The mechanics of earthquake rupture. in *Physics of the Earth's Interior,* edited by A. M. Dziewonski and E. Boschi, 555-649, Italian Physical Society, North Holland, Amsterdam.

Rispoli, R. 1981. Stress fields about strike-slip faults inferred from stylolites and tension gashes. *Tectonophysics* **75**, T29-T36.

Rubin, A. M. 1993. Tensile fracture of rock at high confining pressure: Implications for dike propagation, *J. Geophys. Res.*, **98**, 15,919-15,935.

Sanderson, D. J. and Marchini, W. R. D. 1984. Transpression. *J. Struct. Geol.*, **6**, 449-458.

Schreurs, G. and Colletta, B. 1998. Analogue modelling of faulting in zones of continental transpression and transtension. *In:* Holdsworth, R. E., Strachan, R. A. & Dewey, J. F. (eds) 1998. *Continental Transpressional and Transtensional Tectonics.* Geological Society of London Special Publications, **135**, 59-79.

Scholz, C. H. 1968. Microfracturing and the inelastic deformation of rock in compression, *J. Geophys. Res.*, **73**, 1417-1432.

Scholz, C. H. and Cowie, P. A. 1990. Determination of geologic strain from fault slip data. *Nature*, **346**, 837-839.

Segall, P. and Pollard, D. D. 1980.The mechanics of discontinuous faults. *J. Geophys. Res.*, **85**, 4337-4350.

Segall, P. and Pollard, D. D. 1983. Nucleation and growth of strike-slip faults in granite. *J. Geophys. Res.*, **88**, 555-568.

Selwood, E. B., Stewart, I. J. and Thomas, J. M. 1985. Upper Palaeozoic sediments and structure in north Cornwall - a reinterpretation. *Proc. Geol. Ass.* **96**, 129-141.

Selwood, E. B., Durrance, E. M. and C. M. Bristow. 1998. *The Geology of Cornwall.* Northweste. 288p.

Sibson, R. H. 1989. Earthquake faulting as a structural process. *Journal of Structural Geology* **11**, 1-14.

Sih, G. C. 1974. Strain-energy-density factor applied to mixed mode crack problems. *Int. J. Fract. Mech.*, **10**, 305-321.

Swanson, M. T. 1989. Sidewall ripouts in strike-slip faults. *Journal of Structural Geology* **11**, 933-948.

Tada, H., Paris, P. C. and Irwin, G. R. 1985. *The Stress Analysis of Cracks Handbook.* Paris Prod. Inc. (and Del Res. Corp.), St. Louis, Mo.

Thomas, A. L. and Pollard, D. D. 1993. The geometry of echelon fractures in rock: implications from laboratory and numerical experiments. *J. Struct. Geol.*, **15**, 323-334.

Walsh, J. J. and Watterson, J. 1991. Geometric and kinematic coherence and scale effects in normal fault systems. In: *The Geometry of Normal Faults* (edited by Roberts, A. M., Yielding, G. and Freeman, B.). *Special Publication Geological Society of London* **56,** 193-203.

Willemse, E. J. M. and Pollard, D. D. 1998. On the orientation and patterns of wing cracks and solution surfaces at the tips of a sliding flaw or fault. *J. Geophys. Res.*, **103**, 2427-2438.

Williams, M. L. 1957. On the stress distribution at the base of a stationary crack. *J. Appl. Mech.*, **24**, 109-114.

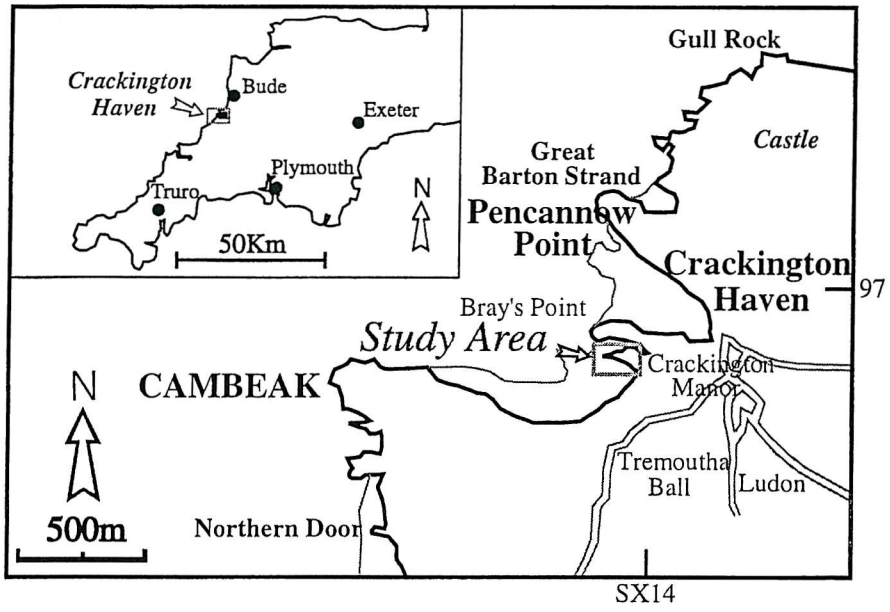

Fig. 3.1. Locality map of the studied area (SX138973) showing the location of reactivated strike-slip faults at Crackington Haven. Thick line means high water, and thin line means low water.

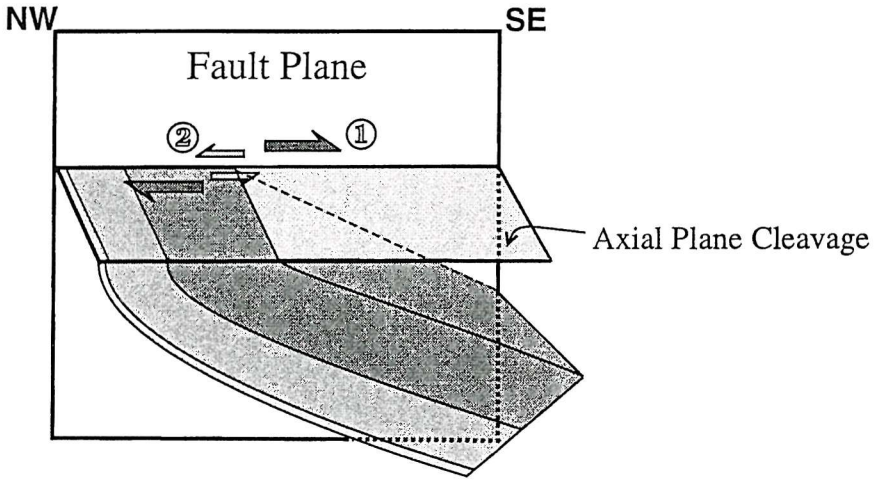

Fig. 3.2. A schematic illustration of the relationship of flexural slip folding to reactivated strike-slip faulting on the south side of Crackington Haven. The studied outcrop is located on a flat surface of the early axial-plane cleavage. The bullet numbers denote each strike-slip movement stage.

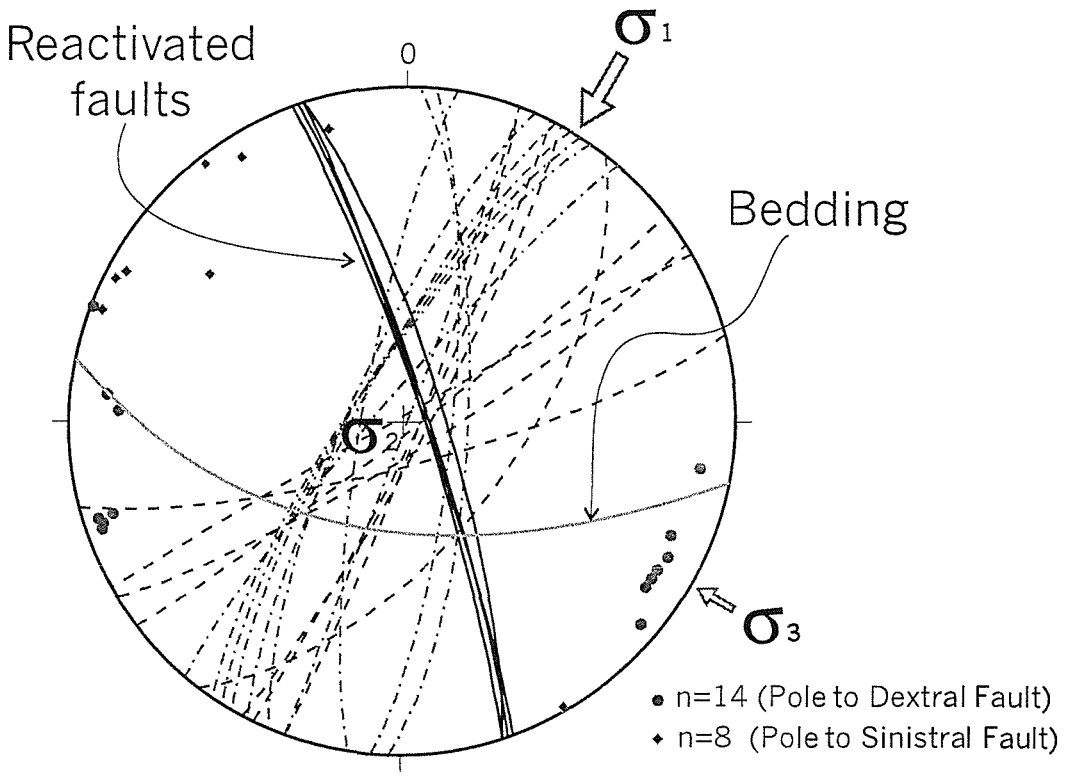

Fig. 3.3. Stereographic projection for strike-slip faults from studied area. The strike-slip faults show a conjugate set by NNE trend maximum compressive stress (σ_1). The NW-SE trending right-lateral strike-slip faults are reactivated in later stage.

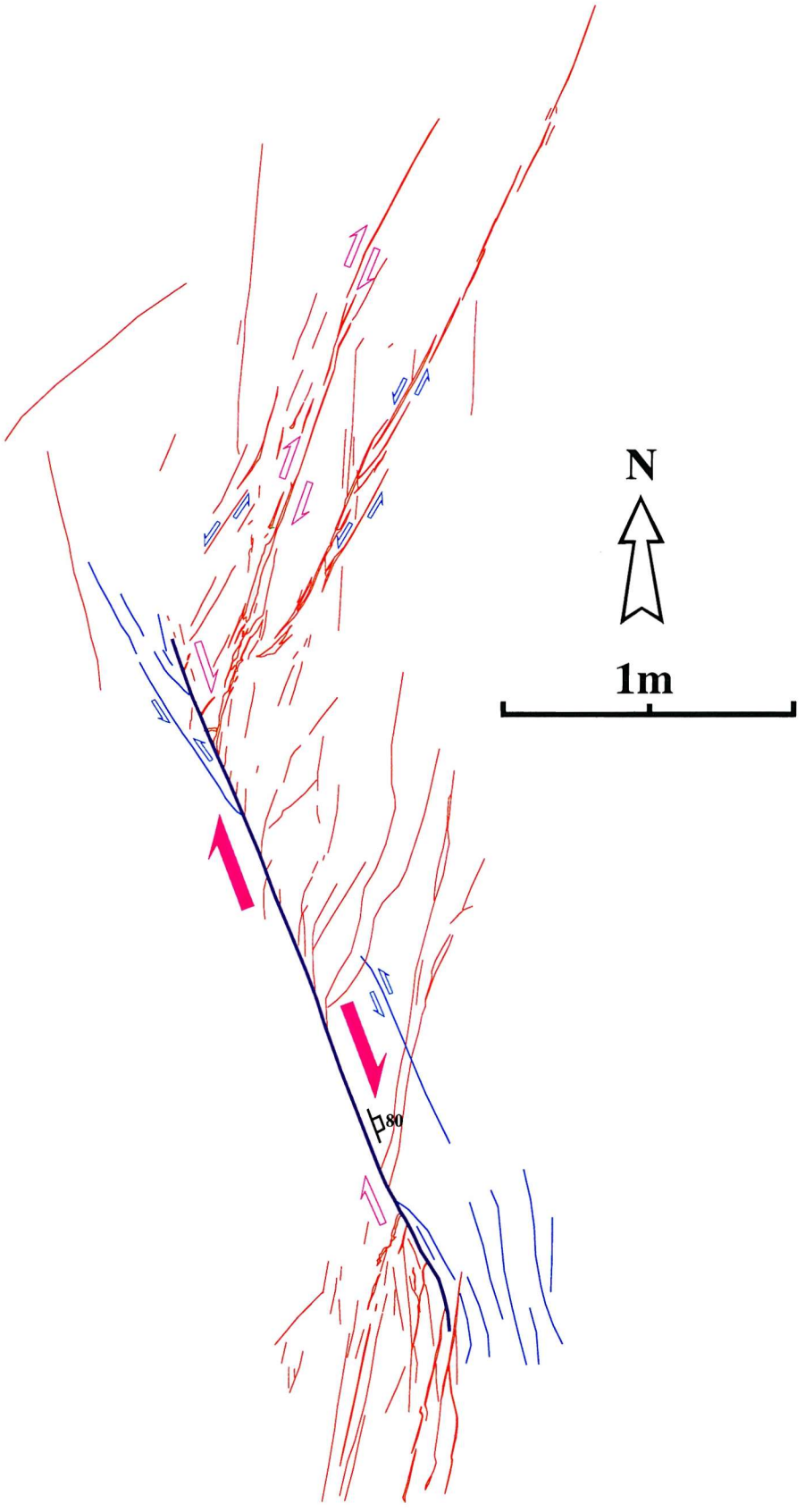

Fig. 3.4. Map showing a reactivated strike-slip fault (F22) with tip cracks filled with vein quartz. Tip cracks associated with right-lateral movment are predominant. Bold blue line denotes main strike-slip fault. Red line denotes tip cracks associated with right-lateral slip, and light blue line denotes tip cracks associated with left-lateral slip. This colour coding is applied to all the following figures.

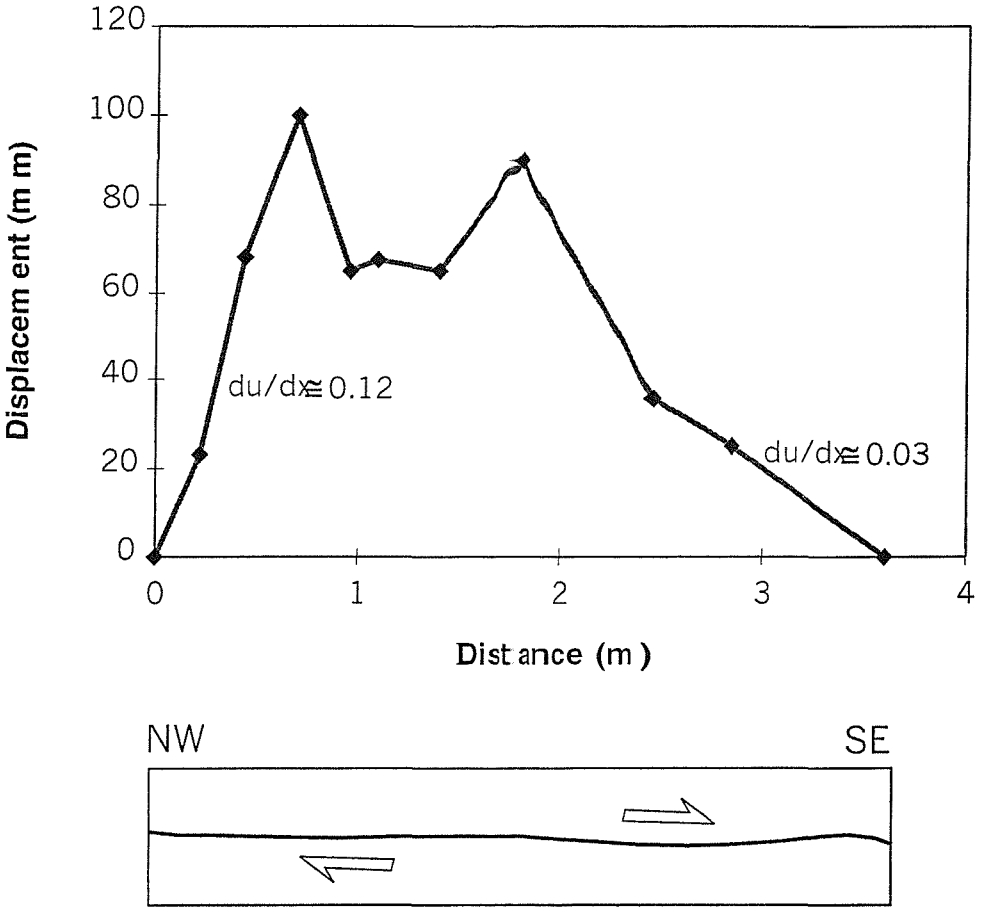

Fig. 3.5. Dispacement (d)-distance (x) plot for the fault F22. The profile shows slight depression in the middle of the fault. There is no strong indication of reverse reactivation at the fault tips.

Fig. 3.6. A strike-slip fault (F23) showing tip cracks on both sides of the main fault tip. Although tip cracks associated with right-lateral movement are predominant, minor tip cracks associated with left-lateral reactivation are evident.

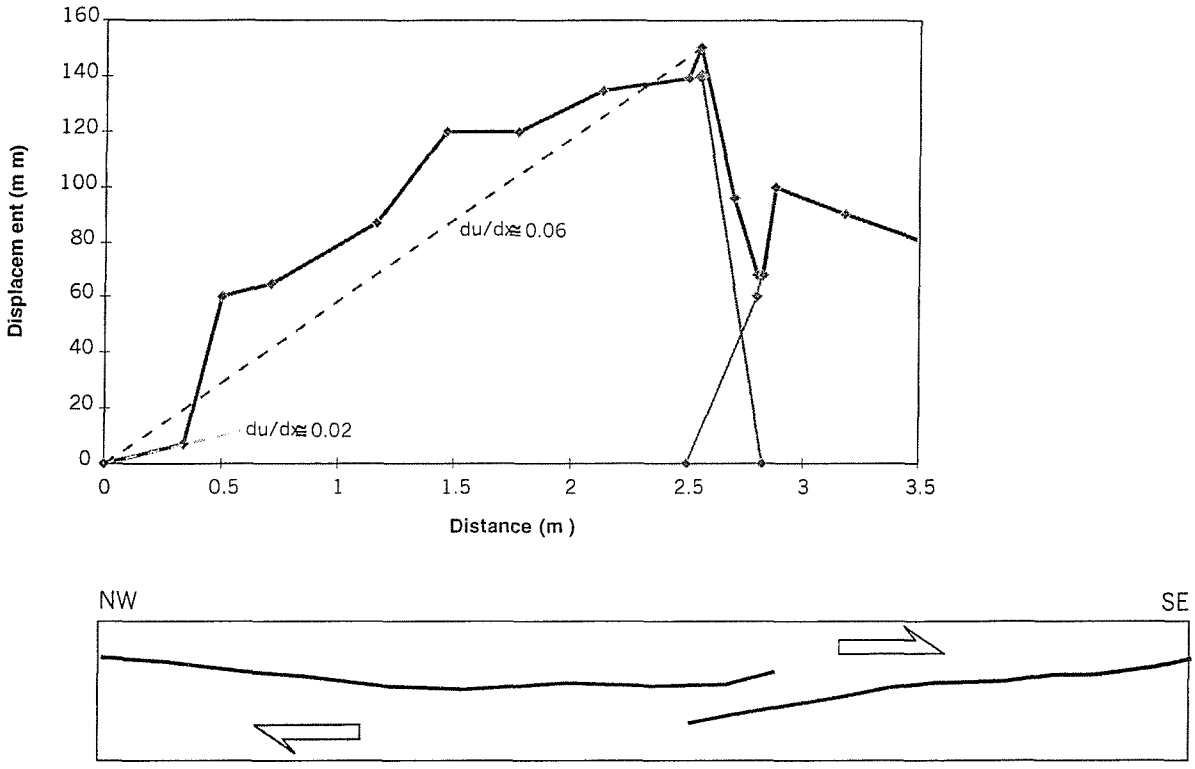

Fig. 3.7. Dispacement (d)-distance (x) plot for the fault F23. The profile shows good displacement transfer through the overstep zone and low displacement at a segment fault tip.

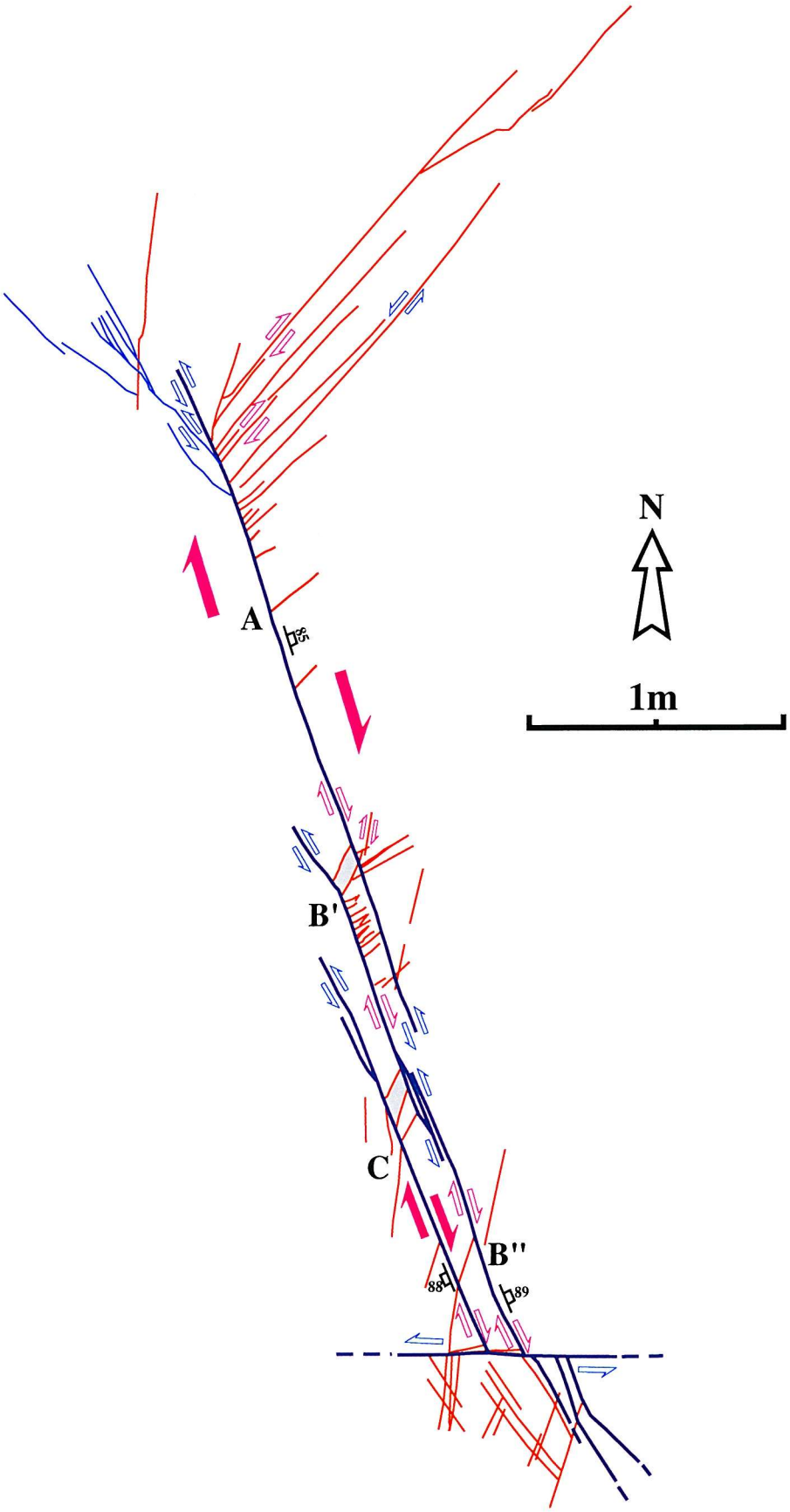

Fig. 3.8. A fault (F24) showing evidence of reverse reactivation. Tip cracks are developed on both sides of the northern tip. Tip cracks associated with right-lateral slip are predominant. It shows left-lateral slip sense at most of the segment fault tips.

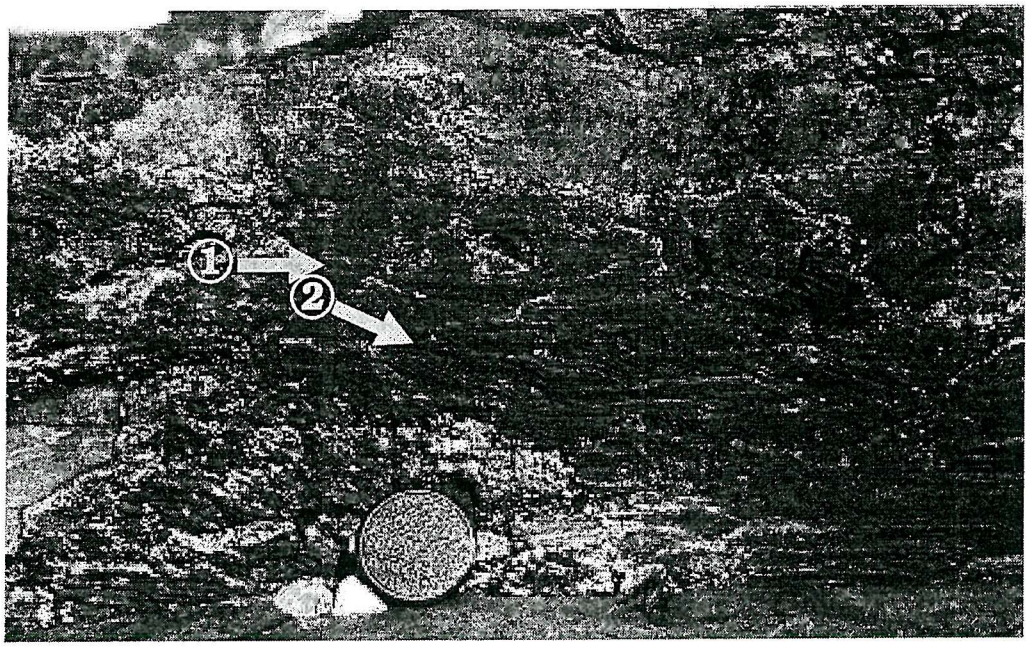

Fig. 3.9. An exposed fault (F24) plane. It shows two different generations of slickenside striae with different senses and plunges. One of the two striae has a small dip slip component. The two slickenside striae sets supply a clear evidence for strike-slip reverse reactivation.

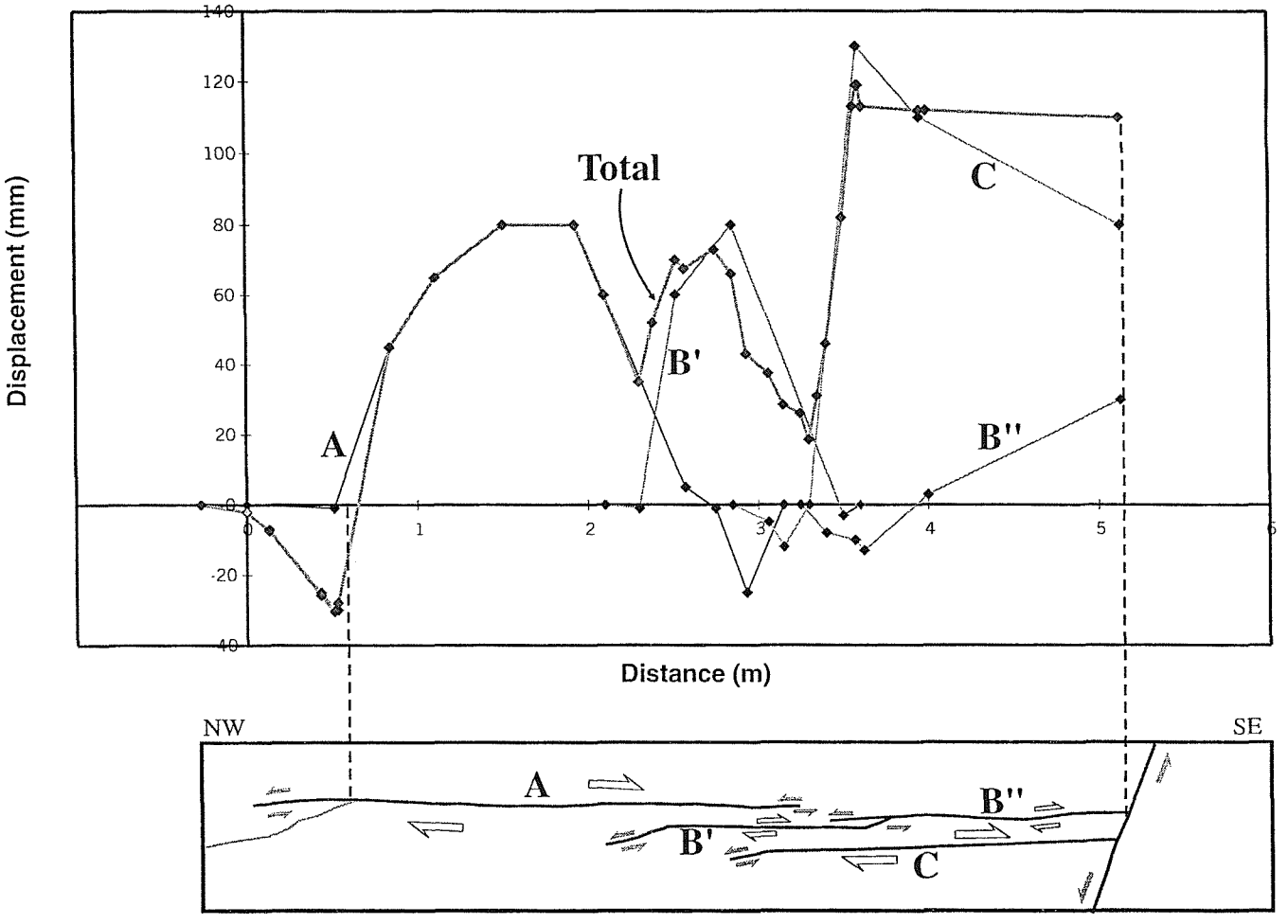

Fig. 3.10. Displacement (x) - distance (x) profile for fault F24. Displacement is transferred between fault segments. Most of fault segments show negative displacement or low displacement at fault tips. The bold line indicates a total displacement. Dashed lines denote the point of branching a left-lateral tip crack and truncation of main the fault.

a)

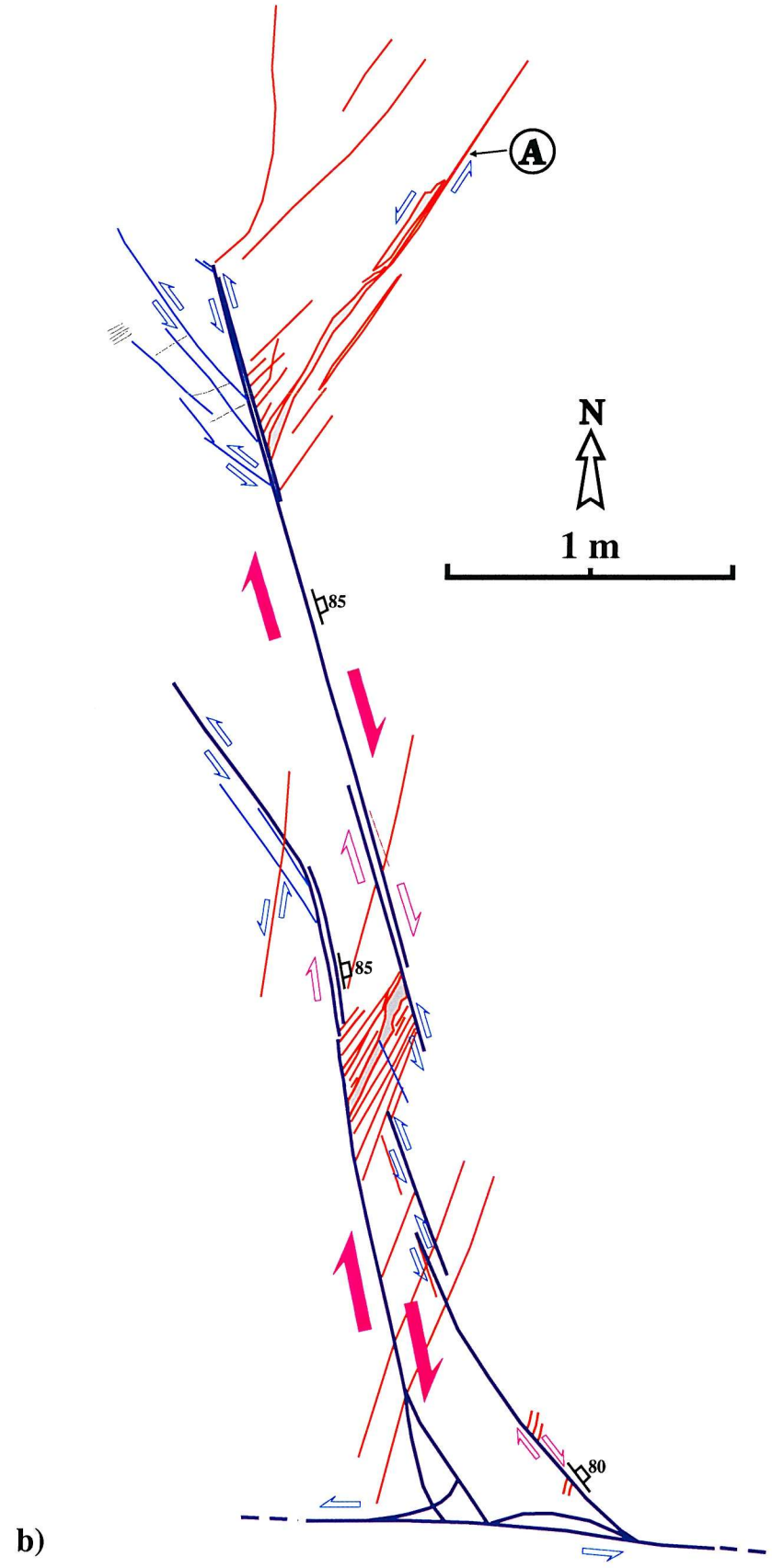

Fig. 3.11. A strike-slip fault (F25) showing two set of tip cracks on both sides of the fault tip. a) Photograph of a reverse reactivated strike-slip fault. Ruler in photograph is 50 cm long. b) Line drawing of the strike-slip fault with tip cracks. Although tip cracks formed by right-lateral slip are predominant, tip cracks formed by left-lateral slip are also very obvious. Some structures like solution surface are observed around the tip cracks associated with left-lateral slip.

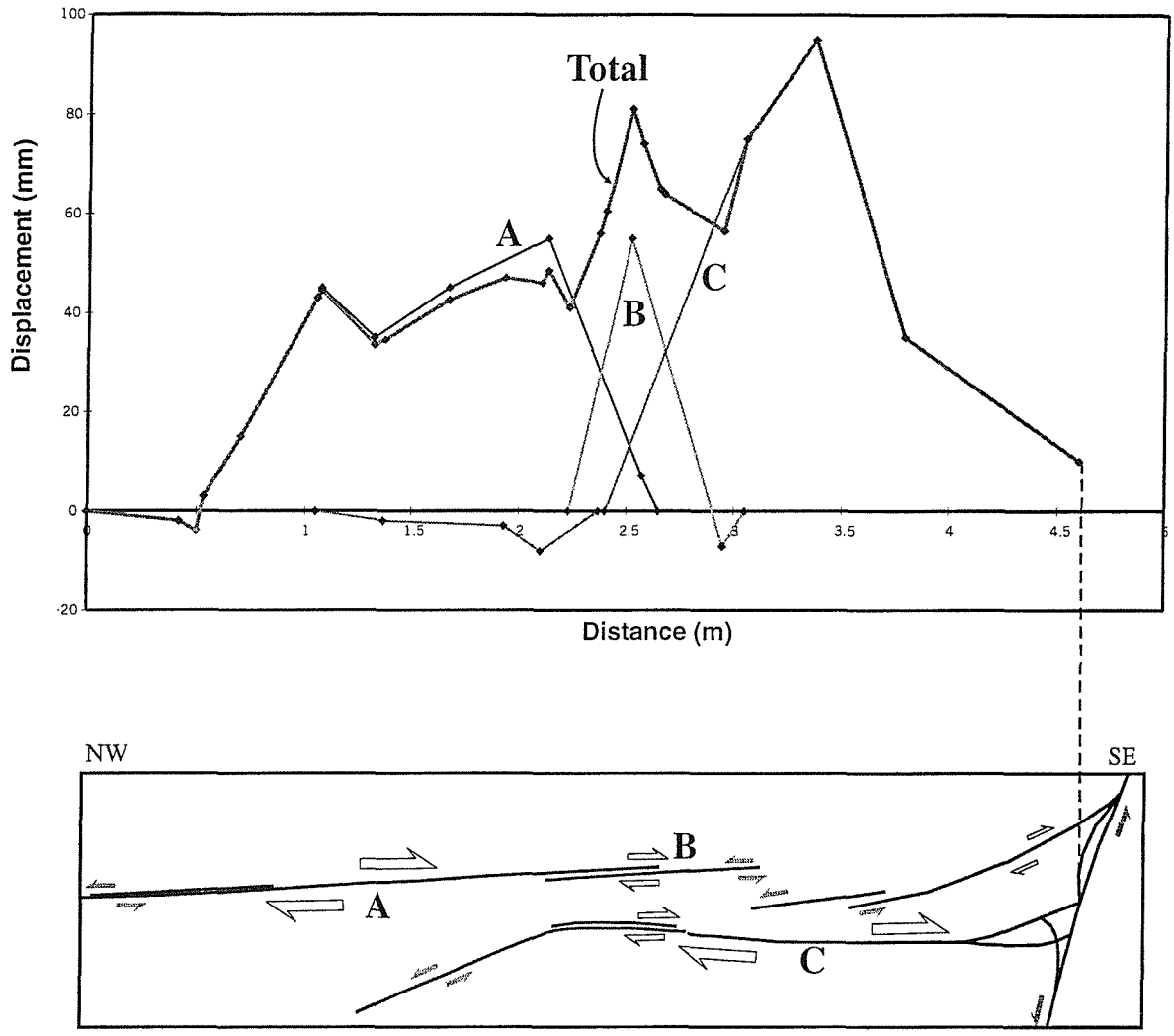

Fig. 3.12. Displacement (d) - distance (x) profiles for fault F25. The displacement is transferred between segment faults. Most of segment faults show negative or very low displacement at fault tips. The bold line indicates the total displacement for the whole faults. The dashed line denote the truncated point.

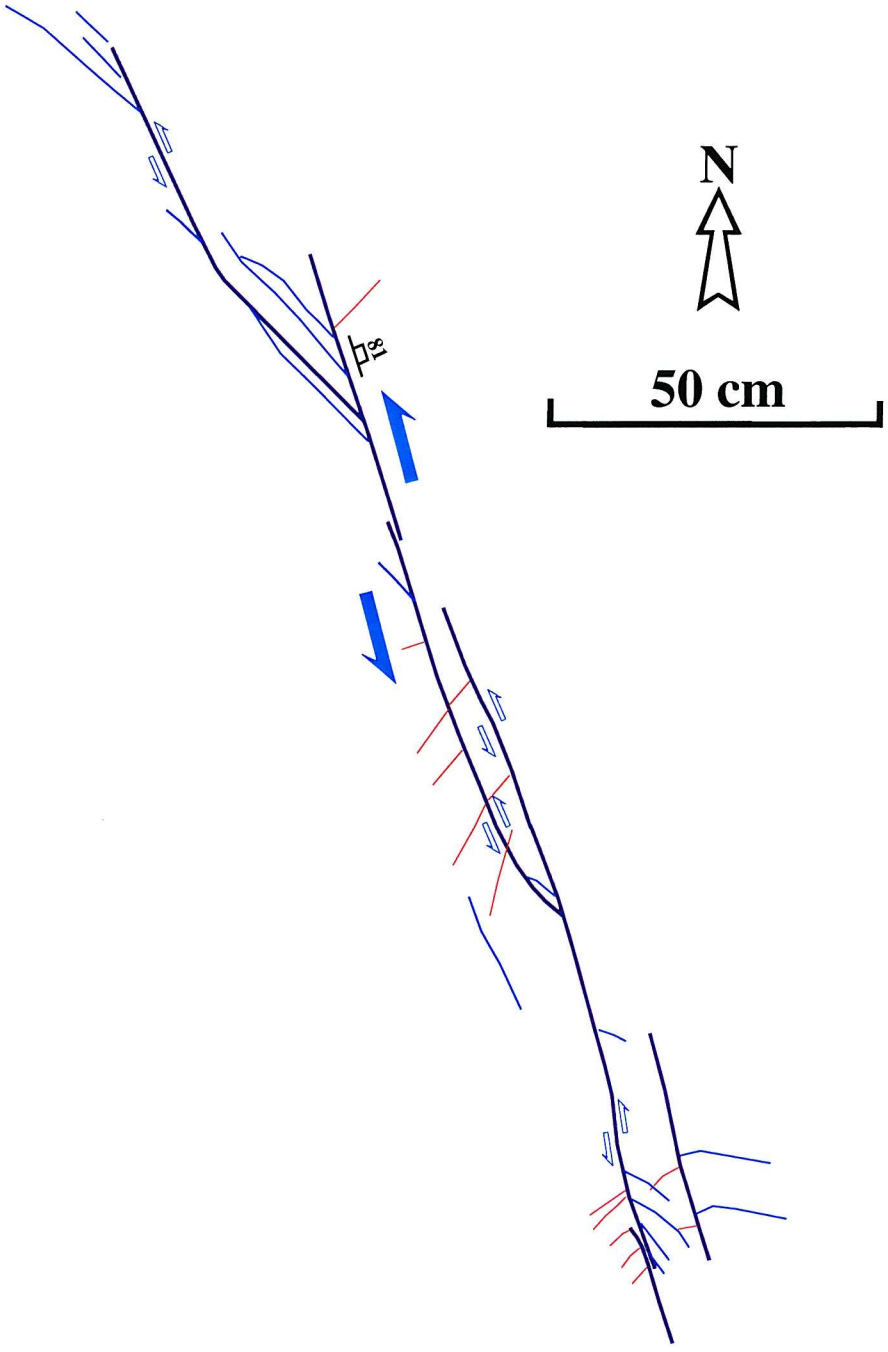

Fig. 3.13. A strike-slip fault (F26) showing left-stepping segment faults. It shows tip cracks on both sides of tips, but the tip cracks associated with left-lateral slip are predominant.

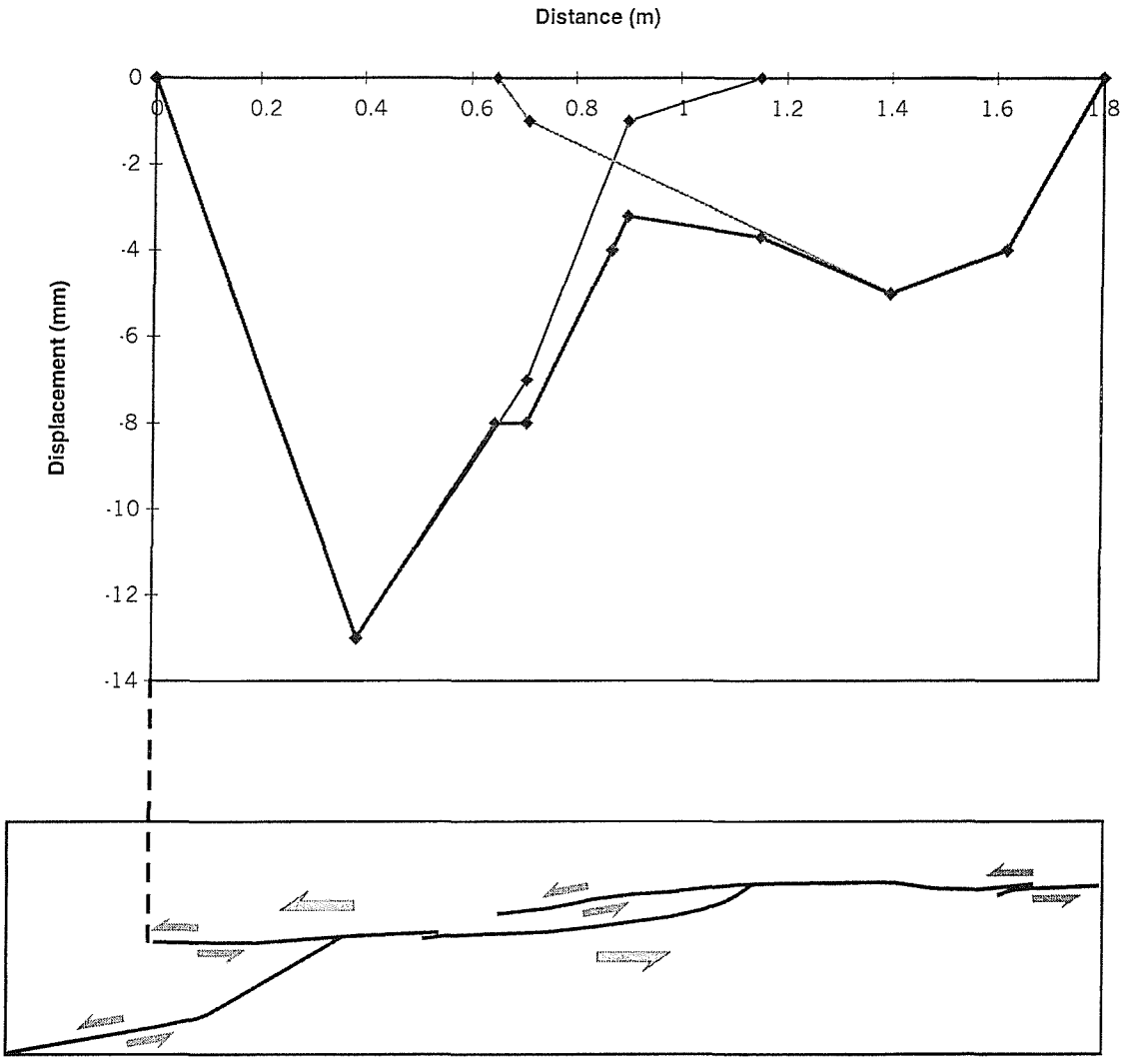

Fig. 3.14. Displacement (d) - distance (x) profiles for fault F26. All the displacements along the segment faults show negative (left-lateral) values. The displacement is very low compared with right-lateral dominant strike-slip faults.

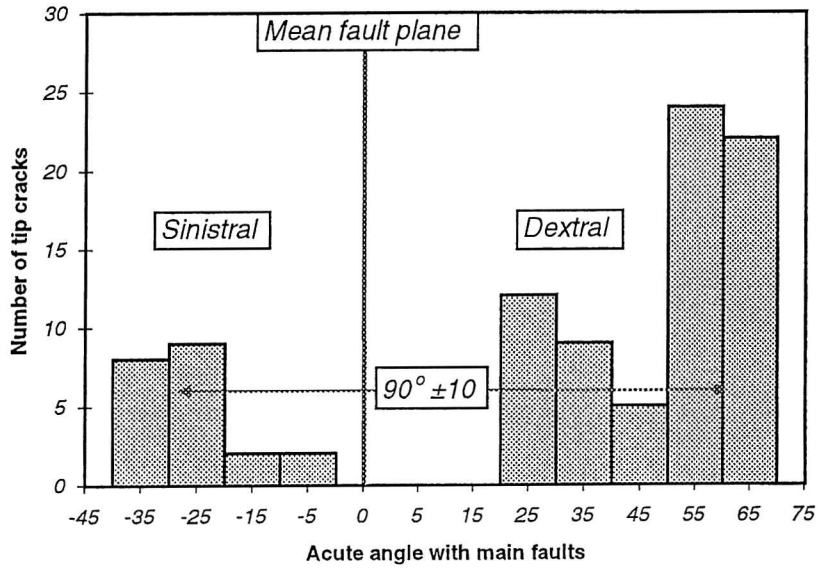

Fig. 3.15. Orientation of tip cracks associated with the reverse reactivated strike-slip faults.The value indicates the angle between tip crack and main fault.The average angle between the two group of tip cracks is about 90°.

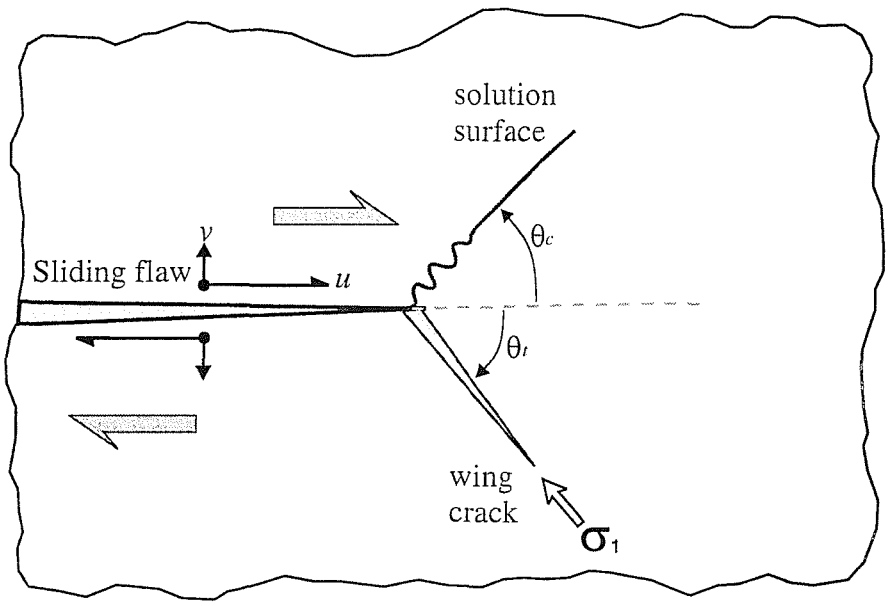

a)

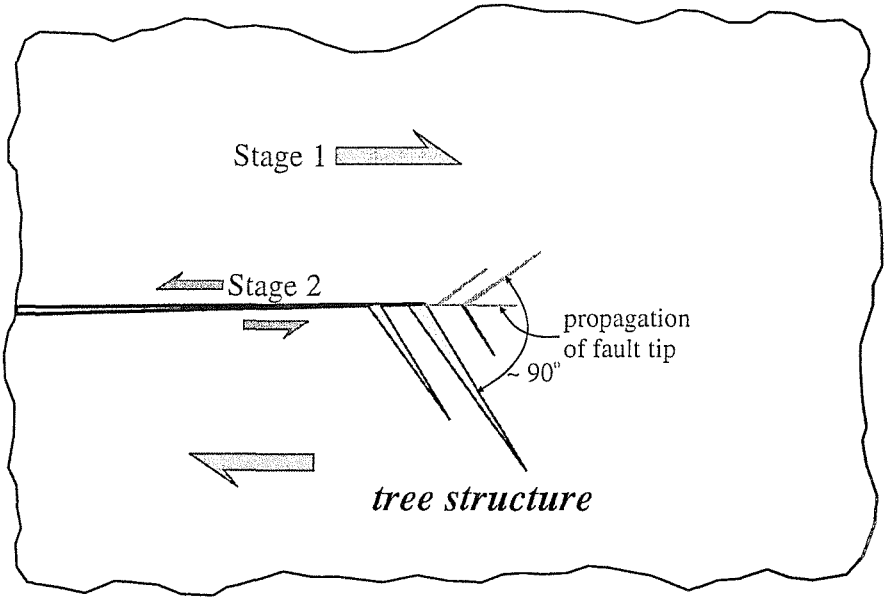

b)

Fig. 3.16. Idealized diagram of flaw tip region and reactivation model for cracks at a tip region. a) Angles θ_t and θ_c describe the orientation of wing cracks and solution surfaces, respectively, with respect to the sliding flaw. Here, u and v are displacements in a direction parallel and perpendicular to the flaw, respectively (modified from Willemse and Pollard, 1998). b) Cracks are developed on both sides of the fault with different orientations (tree structure). The left-lateral strike-slip movement followed by a right-lateral strike-slip movement along the fault.

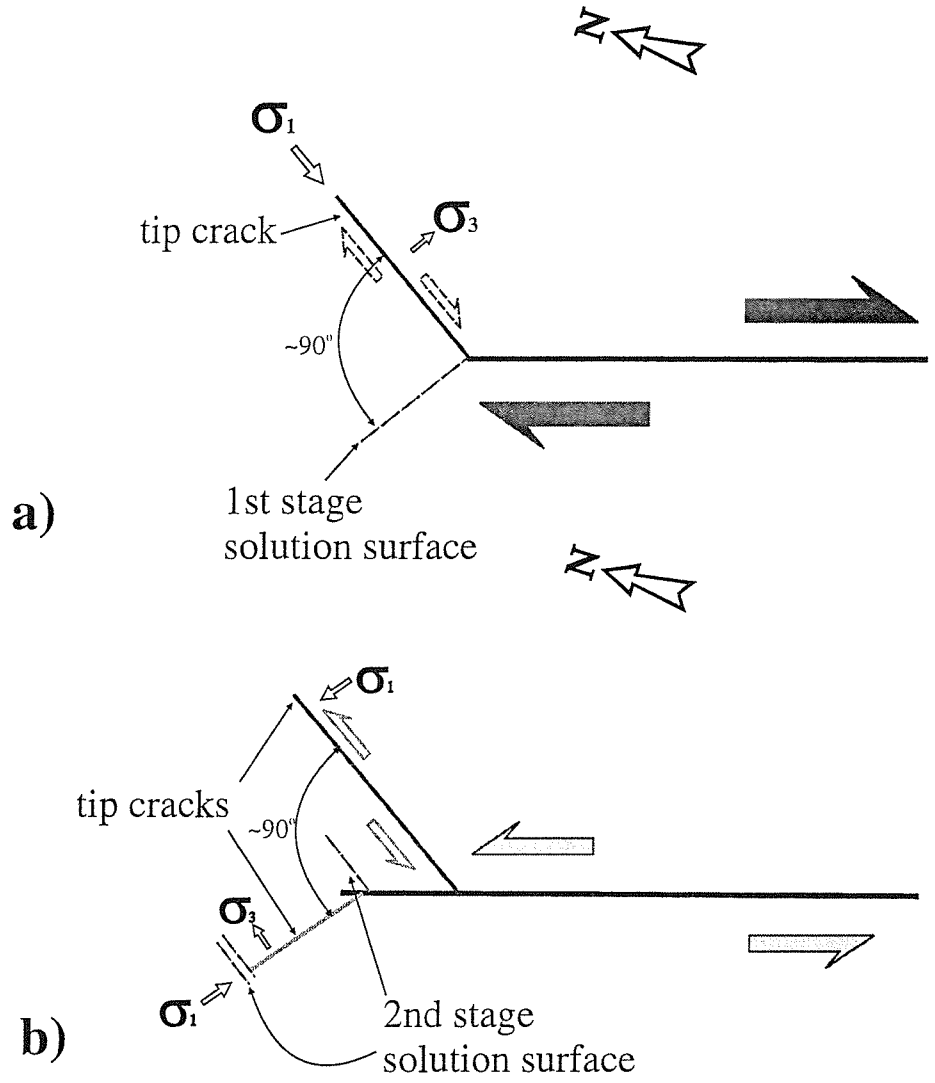

Fig. 3.17. The kinematic relationship at a tip of reactivated faults. a) The first stage of right-lateral strike-slip movement. b) The second stage of left-lateral strike-slip movement. The early formed extensional fracture experiences left-lateral slip.

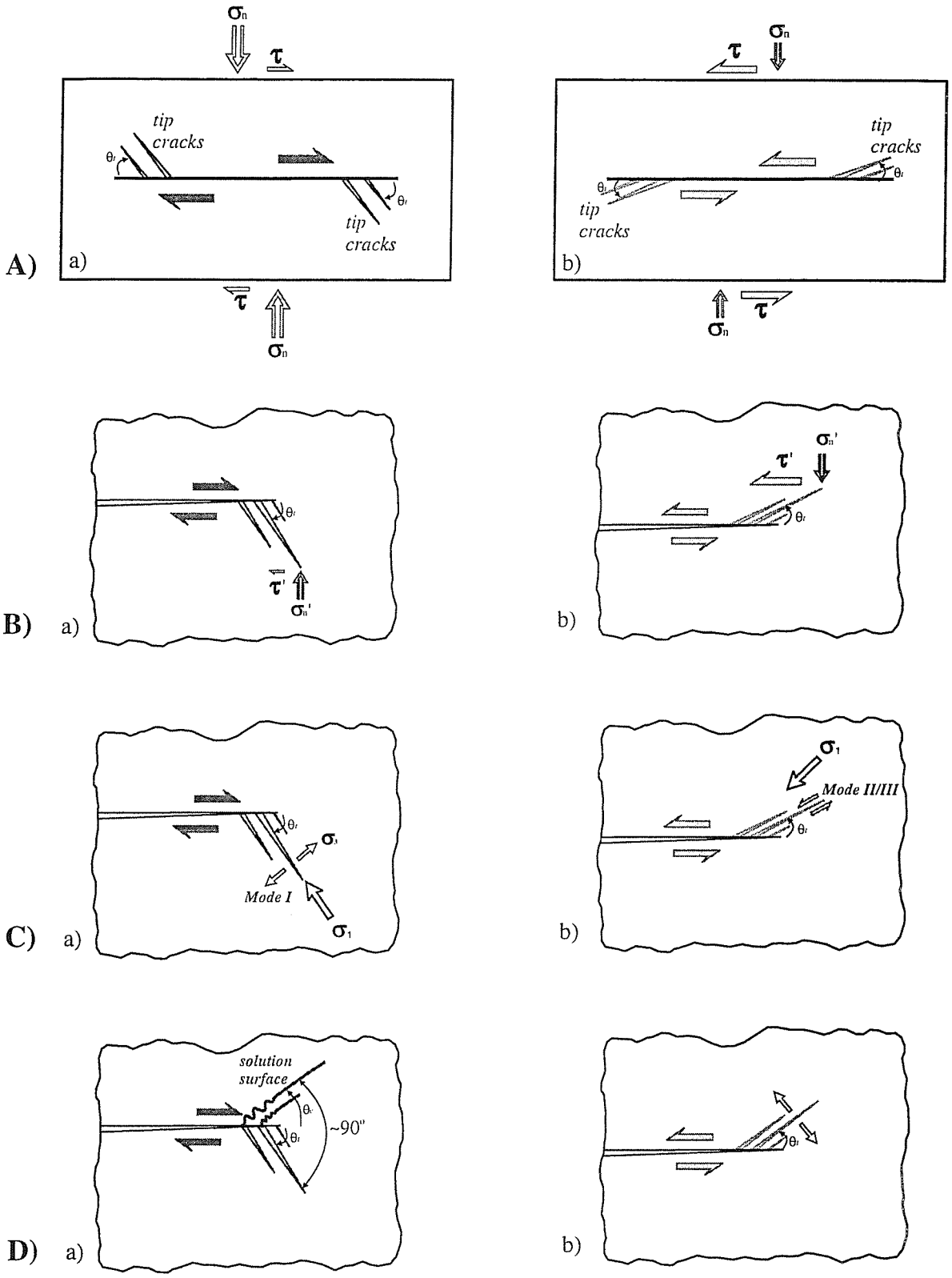

Fig. 3.18. Four possible kinematic models for different tip angles. A) Two crack tips are loaded by different 'far-field' stress. B) Two tip cracks are caused by only different 'near-field' stress concentration at tips. C) Two tip cracks are caused by different fracture mechanism. D) Tip cracks are caused by pre-existing plane of weakness. a) Tip cracks formed during early right-lateral stage. b) Tip cracks formed during later left-lateral stage. θ_t and θ_c denote the angle of tip crack and pressure solution to the main fault, respectively. σ_n, normal stress; σ_1, maximum compressive stress; τ, shear stress.

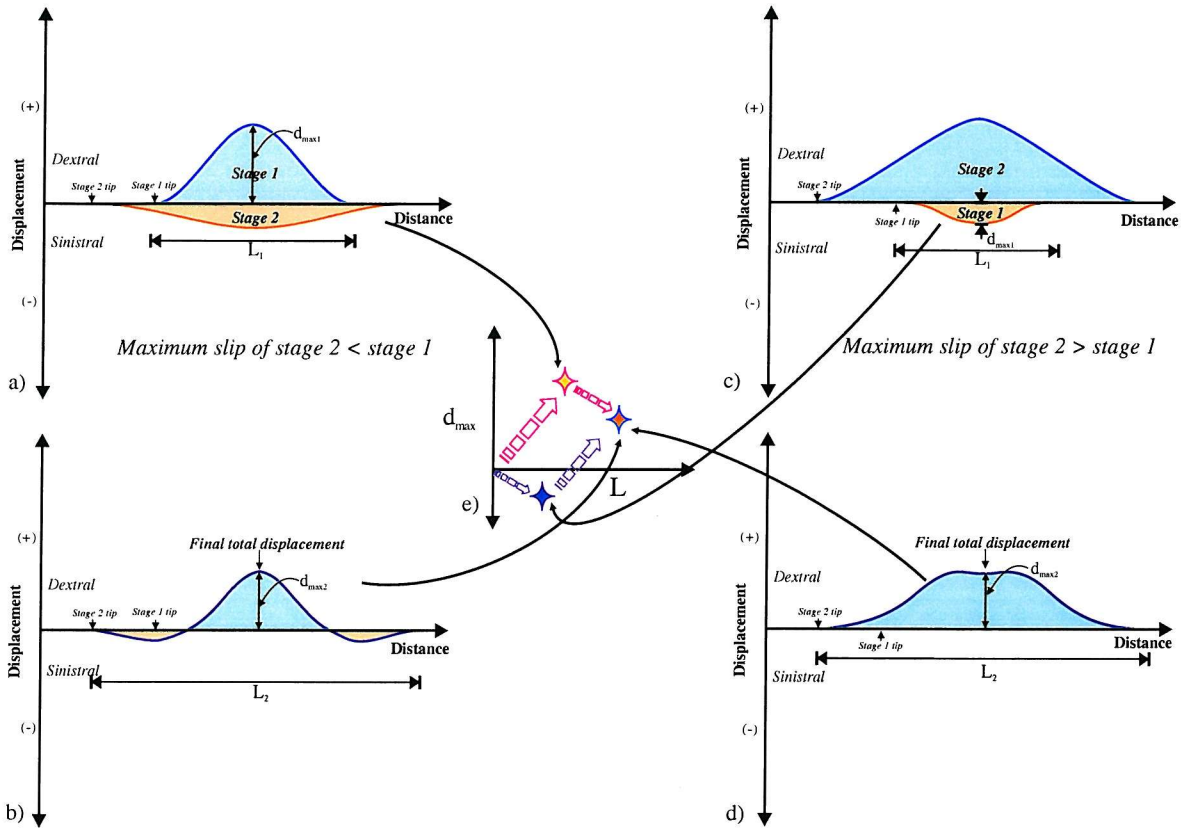

Fig. 3.19. A simple conceptual model for displacement and distance relationship of strike-slip fault reactivation. a) Two stages of fault displacement along a fault. It shows negative displacement at the tip zones. Stage 1 (blue shade) shows dextral movement and stage 2 (yellow shade) shows sinistral movement along the pre-existing fault plane. b) The total displacement profile after the final stage. c) Two stages of fault displacement along a fault. d) The total displacemnt profile at the final stage. e) d_{max}/L evolution during reactivation for the two cases. Compare with a) and b). This final total displacement profile shows no net negative slip at the fault tips. Stage 1 (yellow shade) shows sinistral movement and stage 2 (blue shade) shows dextral movement along the pre-existed fault plane. Dextral displacement is dedicated as positive sign (+) and sinistral is dedicated as negative sign (-).

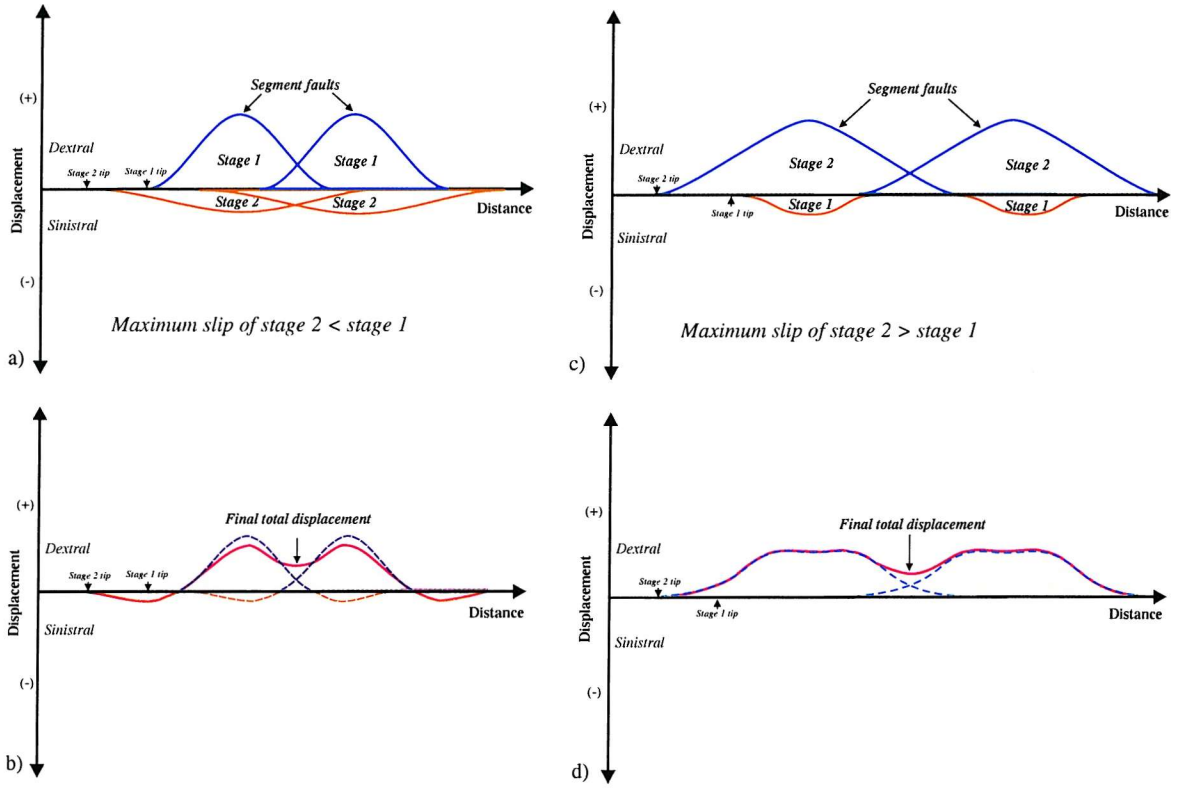

Fig. 3.20. A simple conceptual model for displacement and distance relationship of linked segment fault reactivation. a) Two stages of fault displacement along a fault. It shows negative displacement at the tip zones. Stage 1shows dextral movement and stage 2 shows sinistral movement along the pre-existing fault plane. b) The total displacement profile for linked segment faults after the final stage. Shaded area is final total displacement. c) Two stages of fault displacement along segment faults. d) The total displacemnt profile for segment faults at the final stage. Compare with a) and b). This final total displacement profile shows no net negative slip at the fault tips. Stage 1shows sinistral movement and stage 2 shows dextral movement along the pre-existed fault plane. Dextral displacement is dedicated as positive sign (+) and sinistral is dedicated as negative sign (-). Shaded area is total displacement at final stage.

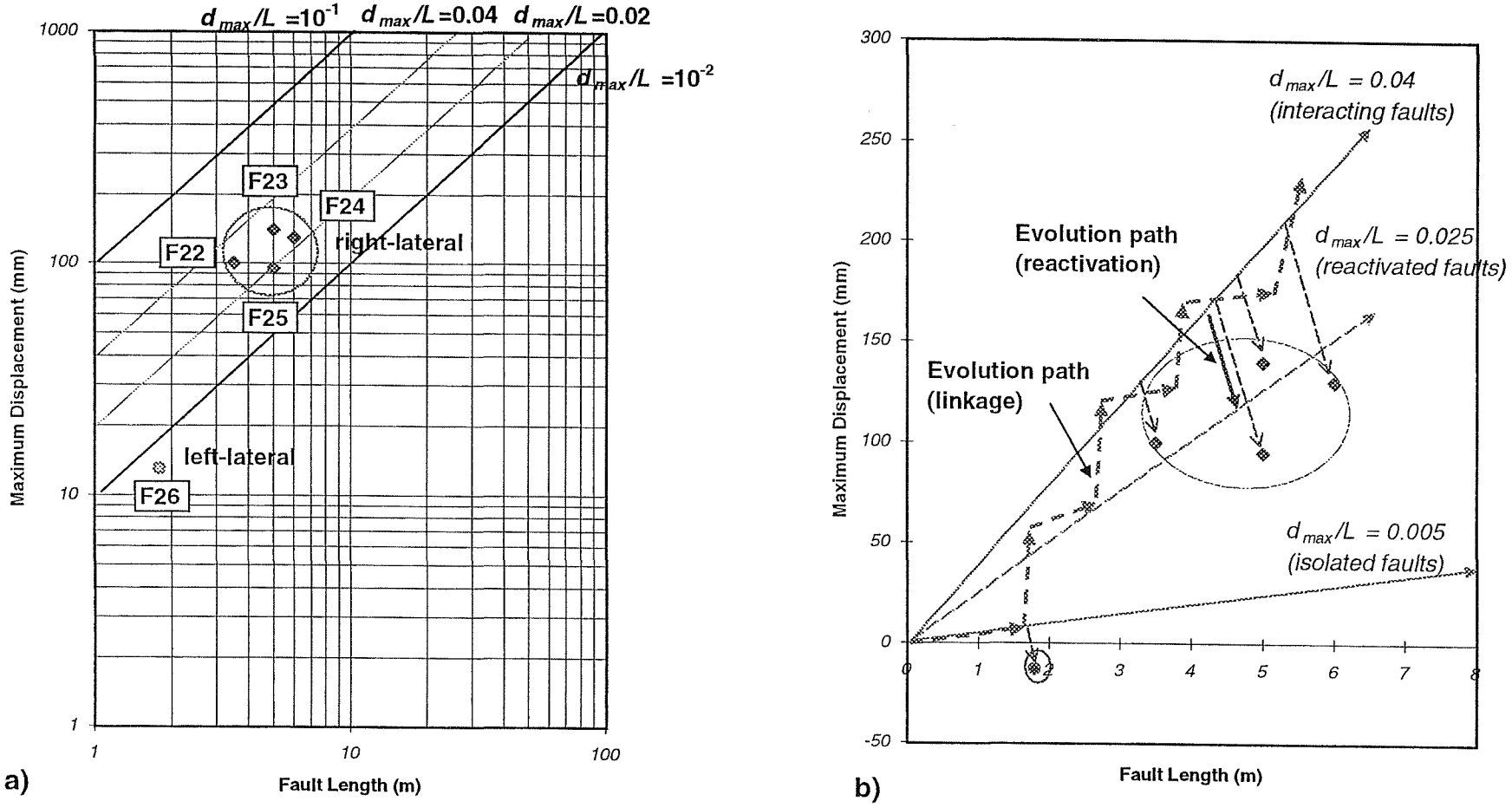

Fig. 3.21. Maximum displacement (d_{max}) - fault length (L) relationship for reactivated strike-slip faults at Crackington Haven. a) Log-log plot of d_{max}/L for the five faults. The small left-lateral fault shows relatively low d_{max}/L ratio. The d_{max}/L ratios for F24 and F25 are lower than F22 and F23. b) The evolution of d_{max}/L during reactivation on normal plot. Two reference lines are drawn from average d_{max}/L of interacting faults and isolated faults at Crackington Haven (Chapter 1; Kim *et al*., in press). See text for details.

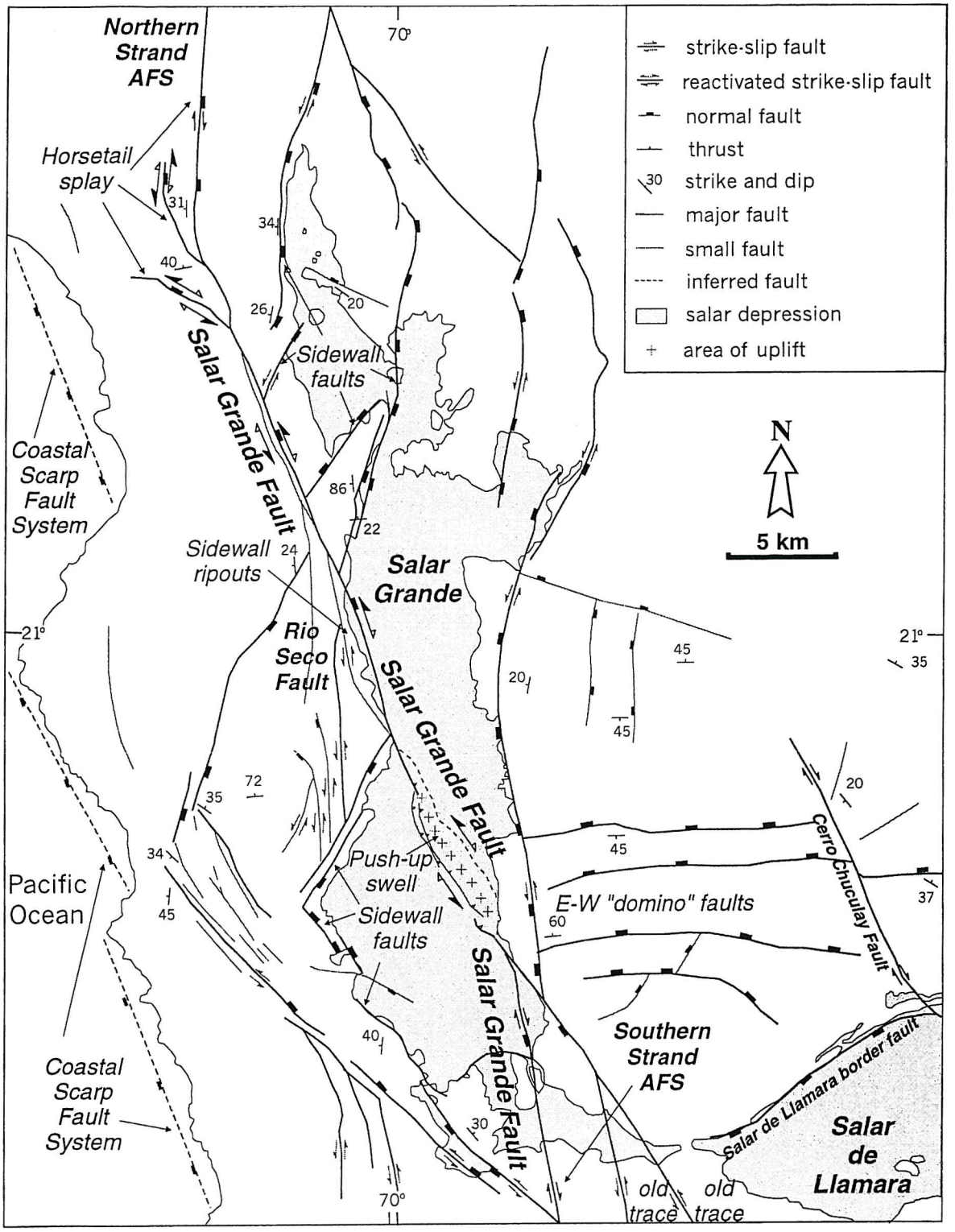

Fig. 3.22. Fault map of the Salar Grande area. The Salar Grande basin is offset left-laterally. The both strands of AFS and the Cerro Chuculay Fault show right-lateral displacement at fault tips (modified after Reijs and McClay, 1998).

CHAPTER 4: STRIKE-SLIP FAULTING AND DAMAGE STRUCTURES TO THE WEST OF MARSALFORN IN GOZO ISLAND, MALTA

Abstract

Well-exposed strike-slip faults in the north-western part of Gozo Island show very typical damage zone structures. The studied area is composed of the gently dipping Lower Member of the Miocene Globigerina Limestone Formation. The regional stress which controlled the faulting had a maximum horizontal compressive stress of ~ N070°.

Damage structures can be grouped into three main categories based on their location along faults; distributed damage, tip damage and linkage damage. The tips of faults consist of two basic modes; mode II (sliding) and mode III (tearing) or a mixture of these. The predominant fracture types within damage zones include extension fractures (T), R, R' and P shears. The dominant damage structures in distributed damage zones are the classical Riedel shear pattern, whereas at the tips of faults show predominantly wedge-shaped antithetic fractures (R') and T fractures, often accompanied by block rotation. Tip cracks (mode I) develop at the tips of some shear fractures and faults indicating the shear sense.

Similar damage styles can be developed at different scales, with distinct orders of damage structures and rotation of stress axes. Fractal analysis shows that relatively high fractal dimensions ($D \approx 1.4$) characterise fault linkage zones.

Based on these observations, evolutionary models for strike-slip fault systems are suggested. The form of natural fault tip damage varies strongly with fault tip mode, exposed level and evolutionary stage. A 3-D conceptual damage model around a strike-slip fault is suggested from the observation at Gozo.

4.1. INTRODUCTION

Damage zones around faults occur because of stress concentrations particularly at fault tips (Cowie and Scholz, 1992; Gupta and Scholz, 2000) and the need to accommodate displacement variation along faults (Chapter 2). They can provide key information on fault evolution including propagation and termination. The aim of this field-based study was to provide an observational basis for models of the evolution of strike-slip fault systems.

The section between Reqqa Point (^{4}312 ^{39}935) and Xwieni Bay (^{4}325 ^{39}932) was selected for study (Fig. 4.1), because there is good flat outcrop showing well developed strike-slip deformation structures. Displacements associated with the faults are essentially strike-slip, as over-all vertical displacements are negligible. The damage zones vary in length from several centimetres to several tens of meters and in width from < 1 cm to a few meters.

Fracture development associated with fault growth has been studied in experiments (e.g. Brace and Bombolakis, 1963; Tchalenko, 1970; Gamond, 1983; Horii and Nemat-Nasser, 1985; Petit and Barquins, 1988; Cox and Scholz, 1988). In addition, theoretical studies have explored the processes of strain localisation and rupture in rock (e.g. Segall and Pollard, 1983; Pollard and Segall, 1987; Reches and Lockner, 1994). These studies have shown that secondary fractures often initiate oblique to the master fault. These fractures nucleate around a fault, commonly where the tensile stresses are highest (e.g. Martel and Boger, 1998), and can link originally discontinuous faults both mechanically (Segall and Pollard, 1983; Martel, 1990; Bürgmann *et al.*, 1994; Martel, 1997) and hydraulically (Long and Witherspoon, 1985; National Academy of Science, 1996). As a result, secondary fractures must greatly influence how faults grow and how fluids circulate in the Earth's crust (Martel and Boger, 1998).

Relatively little published work using detailed field investigations of naturally occurring faults has been undertaken to determine how damage nucleates and grows in rocks. Some field studies (Rispoli, 1981; Segall and Pollard, 1983; Granier, 1985; Martel *et al.* 1988) have focused on tip damage structures of strike-slip faults. Recently, a few researchers (McGrath and Davison, 1995; Martel and Boger, 1998) have published 3-D interpretations of fault damage structures.

This chapter describes the geometry of natural damage structures around well-exposed strike-slip faults in limestone. Maps of strike-slip faults were made, particularly of segmentation, linkage (relay ramps and pull-aparts) and fault tips. These data were collected as part of a wide investigation into the processing of fluid flow, fault propagation and fault termination in strike-slip fault system. All data were collected from 2-D mapping in horizontal or vertical sections. A mode I (opening), mode II (sliding) and mode III (tearing) terminology is used to describe fault tips. Along-strike tips of strike-slip faults are interpreted as mode II fault tips, and up- and down- dip tips of strike-slip faults are mode III tips (Atkinson, 1987; Pollard and Segall, 1987; McGrath and Davison, 1995; Martel and Boger, 1998). Fractures are described using a terminology (T, P, R and R' shears) associated with simple shear for kinematic description and interpretation.

4.2. GEOLOGIC SETTING

The host rock of the study area is Lower Globigerina Limestone Member of Miocene age (Fig. 4.1b) (Debono and Xerri, 1993). The maximum thickness of the member probably exceeds 100 m in the Valletta Basin of Malta, but on Gozo the thickness does not exceed 40 m (5 - 40 m). The member is a pale cream to yellow, massive bedded, planktonic, foraminiferal packstone, becoming wackestone a short distance above the base. The top of the member is marked by a ubiquitous hard ground (Pedley *et al.*, 1976; Debono and Xerri, 1993).

Two main structural trends of the Sicily Channel area (Fig. 4.1a) are NW-SE trending tectonic depressions which might relate to large-scale pull-apart opening (Boccaletti *et al.*, 1987), and a NE-SW trend related to rifting (Illies, 1981) and left-lateral transcurrent displacements of Pleistocene age (Winnock, 1981).

According to Illies (1981), the two tensional trends are related to two-phases of intraplate rifting; an intra-Miocene phase producing NE-SW trending structures and a supra-Miocene-Quaternary phase producing NW-SE trending structures. Winnock (1981) has reported that the deformation of this area occurred in Plio-Pleistocene times, and rifting associated with volcanic activity is of Quaternary age. Finetti (1984) described a more complex deformation history of extension perpendicular to the axis of a rift extending from Pantelleria to the Medina Graben, and right-lateral strike-slip motion along E-W trending faults (Fig. 4.1a). Another model by Cello *et al.* (1985)

and Boccaletti *et al.* (1987) is that the Pantelleria Trough and the Sicily Channel developed in a right-lateral shear zone where crustal thinning and associated magmatic activity are linked to the opening of large-scale complex pull-apart basins. Malta is located on the south-eastern edge of one of these pull-apart structures.

The island of Gozo is characterised by a gentle regional dip to the NE. Major normal faults, ENE-WSW trending, predominate in most of Malta and Gozo, cutting the entire Oligo-Miocene succession, and there is considerable evidence of movement since Miocene times. Fresh fault-scarp faces with striae, negligible scarp recession, and the development of local raised beaches suggest that the faulting must, in part, be recent (Pedley *et al.*, 1976). But in the north-western part of Gozo these normal faults are replaced locally by strike-slip faults also produced by a NNW-SSE extension.

4.3. RESEARCII METHODS

For this study, field photographs were used to make fault maps. To make the M-00 map, for example, about 50 photographs were combined. The maps were adjusted using field measurements to reduce distortion. Some of the detailed maps were drawn from single photos.

Some displacements were measured from the offset of trace fossils or early veins across faults. The angular relationship and geometry of secondary fractures were classified and described. For each order, the maximum compressive stress direction (σ_1) was estimated from the relationship between fractures, and the type of fracture determined from the fracture pattern where possible. For the fault M-00, fractal analysis was carried out using the Circle Method (Mandelbrot, 1977; Okubo and Aki, 1987). Finally, based on these observations some models are suggested for fault propagation and damage patterns.

4.4. ORIENTATION OF FAULTS AND FRACTURES

Orientation data from 122 major faults and fractures (longer than 1 m and showing no lower order faults) can be grouped into three sets: right-lateral strike-slip (21), left-lateral strike-slip (39) and extension fractures (62) (Fig. 4.2). Strike orientation of right-lateral strike-slip faults ranges from N020° to N080° (with a modal orientation of N045°), left-lateral strike-slip faults from N070° to N130° (mode

N100°), and extensional faults from N050° to N090° (mode 070°). Therefore, the average orientation of the maximum horizontal compressive stress (σ_1) is ~ N070°, which is concordant with the major fault trends of the Malta and Gozo area (ENE trending normal faults, Pedley *et al.*, 1976).

To examine the angular relationships of fractures to faults, data were plotted in terms of the master fault traces (Fig. 4.3). Because most of the data are collected from left-lateral strike-slip faults, data collected from right-lateral strike-slip faults are reflected into left-lateral relationship to show the general relationship to master faults. The mean angle between P shears and the master fault is 10°, and the angle for Riedel shears (R) is -15°. The angle for extensional fractures (T) is -40°, and that for conjugate Riedel shears (R') is -65° to master fault. The fracture pattern can be compared with a simple shear fracture pattern (Fig. 4.4a) (Tchalenko and Ambraseys, 1970; Wilcox *et al.*, 1973; Bartlett *et al.*, 1981; Davis *et al.*, 2000).

The kinematically classified fractures could be related to associated fracture tip modes. There are three fundamental fracture tip modes (Fig. 4.4b). T fractures are extensional fractures (mode I), which commonly have vein filling or open space. P, R and R' are shear fractures (mode II/III), which generally have no veining or opening. Extension fractures propagate by growth with the plane of the fracture, whereas shear fractures commonly develop tip cracks oblique to the fracture plane.

Several well exposed strike-slip faults and their associated damage zone structures were mapped and described. The main locations of these are shown in Figure 4.1b. The damage structures are classified and described in terms of their arrangement along the faults and dominant fracture types in damage zones. The damage styles will be described in the order of *distributed* damage, *tip* damage and *linkage* damage.

4.5. DISTRIBUTED DAMAGE

The distributed damage is damage that develops along the fault zone and has been widely described from *simple shear* zones (e.g. Tchalenko, 1970; Tchalenko and Ambraseys, 1970; Wilcox, *et al.*, 1973; Bartlett *et al.*, 1981; Christie-Blick and Biddle, 1985; Davis *et al.*, 2000) based on both natural examples and analogue modelling. Distributed damage is generally characterised by long, narrow, symmetric

damage zones along the whole fault trend. Fractures may combine to form a "principal displacement zone" (PDZ) in which Riedel shears (R), conjugate Riedel shears (R'), T and P shears can be recognised.

4.5.1. Extension fracture (T) dominant distributed damage (M-04 and M-03-total)

En echelon extensional (mode I) fracturing distributed along fault trend is common in many strike-slip fault systems (e.g. Mollema and Antonellini, 1999). M-04 (Fig. 4.5) and M-03-total (Fig. 4.6) belong to this damage style, which consists of an array of en echelon extension fractures, with little additional damage or shearing around the fractures. In both cases, the mean trend of the fault system is ~ N100° and extension fractures form at ~ N070° (i.e. at 30°~40° to the master fault). Most extensional fractures are parallel to the orientation of regional compressive stress (Fig. 4.2). Some extension fractures bend to make progressively lower angles with the master fault farther away from the fault plane. These extensional fractures are intersected by later linking fractures. They do not show any strong development of R' shears in the central parts. Although most of the extensional fractures show no displacement, the tips of some fractures are kinked clockwise implying a small component of right-lateral slip.

M-04 fault is an array of en echelon fractures (Fig. 4.5) with no central master fault. Some of the extensional fractures have kinked tips or show sigmoidal shape suggesting later shear and rotation. In Figure 4.6, straight master fault is well developed with overstep in the middle of the fault system. There is a difference of 10° ~20° between the extensional fractures in the wall zone and tip fractures at the western end of the fault, suggesting different processes were responsible for generating the two sets.

4.5.2. Riedel (R) and conjugate Riedel (R') shears dominant distributed damage (M-16, M-N02, M-22 and M-28)

This type of damage (Figs. 4.7 - 4.10) is a predominant pattern in distributed damage zones at Gozo. The damage zones show a long, narrow, generally symmetric shape along the fault trend with no master fault. They are characterised by the classic Riedel shear model with frequent high-angle antithetic shear fractures (R'). The angle

between the en echelon antithetic shear fractures (R') and the main fault is generally ~ 65°.

Along the whole fault system R' shear fractures are dominant, and P and R shears intersect some of the R' shear fractures. The R' shear fractures developed earlier than P and R shear fractures as some of relicts of R' shears are observed on both side of P and R shear planes. The slip-sense of the antithetic shear fractures can be inferred from the curved tips, which are higher order T fractures. Most of the antithetic shear fractures have a similar spacing and fracture length. The damage zones do not show any obvious wedge-shaped pattern, neither increasing nor decreasing in length of R' shear fractures, except at some along-strike fault tips (Fig. 4.10).

Several straight segments are developed in the central part of some faults, where there are few R' fractures around segments. These segments are aligned and linked through transfer zones with more intensive R' fractures (Fig. 4.9). Systematic variation in fracture length is interpreted as due to overlapping wedge-shaped zones that propagate away from some segment tips (e.g. Fig. 4.8).

The fault M-N02 and M-22 (Figs. 4.8 - 4.9) show some central en echelon fault segments (R shears) which may represent the fault tip breaking through the tip zone. This processing continues further in Figure 4.10 where P shear and T (or R) fractures link to form a principal displacement zone (PDZ). The combination of fault segments (R shears) with T (or P) fractures develops some pull-aparts. At the eastern tip, antithetic fractures, extensional fractures and some synthetic branch fractures form a wedge-shaped damage zone.

Three main observations can be noted in these examples. Firstly, in most of the examples (Fig. 4.8 - 4.10), short fault segments frequently develop, which are not shown in the fault M-16 (Fig. 4.7). Secondly, some early R' shears are observed on the P or R shear fracture planes. Thirdly, some damage zones show combinations of two mode (II & III) of tip damage (Figs. 4.7 and 4.10; see section 4.6).

4.5.3. Attributes of distributed damage

It is often difficult to distinguish the characteristics of the en echelon fractures developed within a distributed damage zone such as in Figures 4.5, 4.8 and 4.9. Some studies denote such fractures as R' shears (e.g. Tchalenko, 1970; Tchalenko and

Ambraseys, 1970; Davis *et al*, 2000), whereas other researchers (e.g. Segall and Pollard, 1983; Harding *et al.*, 1985; Moore and Lockner, 1995; Mollema and Antonellini, 1999) classified them as extensional fractures. Although most of the fractures do not show any clear evidence for slip, some of the fracture tips are bent or generate higher order tip cracks indicating the slip sense (e.g. Fig. 4.7).

In this study, distributed damage zones which consists of en echelon fractures are divided into two groups such as T dominant damage (Figs. 4.5 - 4.6) and R' dominant damage (Figs. 4.7 - 4.10). T dominant damage zones show relatively long fracture length, and a wide damage zone, with fractures having rare tip cracks and forming at a lower angle to the master faults (30° ~ 40°). R' dominant damages show relatively short fracture length, and a narrow damage zone, with fractures having frequent tip cracks and forming at a higher angle to the master faults (~ 65°). However, some T fractures also display tip cracks and sigmoidal shapes, which are interpreted as early extensional fractures that have experienced some subsequent shear and rotation.

Figure 4.5 and 4.6 show that extensional fractures (mode I) form before the generation of the master fault. Local tensile stresses greater than the toughness of materials would promote secondary fracture formation. Moore and Lockner (1995) have reported, in laboratory experimental work, that those fractures formed prior to the nucleation of the fault are roughly parallel to the loading direction, whereas those generated in the tip zone make angles averaging 20° to the far-field loading axis and reflect the local stress field. Therefore, extensional fractures striking N070° might be developed in the early stages by the regional compression, whereas pinnate or tip fractures developed to accommodate the displacement along the master fault in slightly later stage (Cox and Scholz, 1988). For example, fault M-04 (Fig. 4.5) shows extensional fractures in an initiation stage of fault generation. Similarly oriented fractures are seen along the wall of fault M-03 (Fig. 4.6), but with slightly differently oriented extensional fractures at the tip. In some conjugate shear zones, extension fractures form at ~ 45° to each zone, often at 15 –20° to the far field maximum compressive stress (Beach, 1975; Rothery, 1988).

In mode III tips, even if the high-angle fractures initiate as extensional fractures, parallel to maximum compressive stress, they might experience slip and rotation in a

later stage by subsequent shears. This idea is also supported theoretically, because brittle failure of natural rocks depends on the tensile strength in generation stage, but after that it is easier to slip along a pre-existing shear plane (e.g. Hancock, 1985; Segall and Pollard, 1983; Sibson, 1985).

R' shear dominant distributed damage (mode III fault tip) structures follow Riedel shear fracture pattern in a shear zone starting from en echelon R' shears and followed by R and P shears (e.g. Tchalenko, 1970; Wilcox *et al.*, 1973; Swanson, 1988). The long, narrow, symmetric, distributed damage zone and the absence of a through-going fault suggest stress distribution related to a mode III fault tip above or below the location of exposure (Figs. 4.4 and 4.7). Some of the en echelon fractures evolve into mode III tip damage with central fracture segments in a later stage (Fig. 4.8 - 4.10; Martel and Boger, 1998).

Tchalenko (1970) suggested that conjugate Riedels (R') become passive and distorted into an *S* shape or closed, because they make large angle with the general direction of movement. If the main fault propagates across the zone, propagation of early-formed antithetic shear fractures (R') is prohibited by localisation of displacement along the master faults. Therefore, R' shears are very rare in the walls of segmented faults (e.g. Fig. 4.9).

Antithetic fractures are especially abundant in segment transfer zones (Davis *et al.*, 2000) (Fig. 4.8 and 4.9), and indicate where faults have propagated by linkage of segments (Peacock and Sanderson, 1991; Cartwright *et al.*, 1995; Kim *et al.*, 2000). Several fault segments start to develop in the central part of the distributed damage zones. They initiate from small linking fractures (Fig. 4.7) and evolve through P, R or T en echelon fractures (Fig. 4.8 and 4.9), to linked zigzag faults (Fig. 4.10). The damage structure of M-28 (Fig. 4.10) is regarded as typical of a mature fault where initial mode III tip damage has been cut by fault segments, which link to produce a fault with mode II tip pattern at the south-eastern end. The R' shear relicts along the fault and the linked zigzag geometry (Bilham and Williams, 1985; Moore and Lockner, 1995) of the fault trace are good evidence for this evolution. At the tips of fault segments, the damage structure shows more complicated pattern due to combination of mode II and III tips.

4.6. TIP DAMAGE

Because strike-slip faults are almost vertical and the slip direction is horizontal, along-strike tips are commonly exposed in map view. For these reasons, most studies (e.g. Brace and Bombolakis, 1963; Nemat-Nasser and Horii, 1982; Granier, 1985; Pollard and Segall, 1987; Cooke, 1997) have concentrated on along-strike tips, where damage is common and shows a variety of fracture patterns.

4.6.1. Extension fracture (T) dominant tip damage (M-07, M-15 and M-14)

These three examples (Figs. 4.11 - 4.13) show predominantly extensional fractures at fault tips. This type of tip damage shows mode I fractures generally attached singly (e.g. wing cracks) or multiply (e.g. horsetail) near the master fault tip. The angle between the fractures and the fault is generally ~ 40°, although some fractures have higher angles. The tips of the extensional fractures are straight and show little damage.

Figures 4.11 - 4.13 show left-lateral slip trending N110° ~ N125° with several extensional fractures at fault tips. The extensional fractures strike ~ N070° parallel to regional maximum compressive stress, and shorter pinnate fractures make a wide range of high angles with the main faults (e.g. Fig. 4.13). Although it is apparent that the two fracture sets are mode I dominate fractures, they have different orientations. Therefore, the two fracture sets might have originated from different local stress fields or in different stages of fault propagation.

There are some different features in each tip damage zone. At the western fault tip in Figure 4.11, high angle fractures striking N040° are dominant, whereas at the eastern tip extensional horsetail style fractures striking N070° are dominant. Several smaller en echelon fractures are also developed at both tips. In Figure 4.12, extensional fractures striking N076° are the predominant secondary fractures developed around the fault tip with one branch fault striking N308° developed on the opposite side of the tip as a manner of type A_1 of Chinnery (1966b). The tip fractures in this fault system generally decrease in length towards the fault tip. In Figure 4.13, short pinnate style fractures and long extensional fractures are coexisting in the dilational quadrant.

4.6.2. Conjugate Riedel shear (R') dominant damage (M-01, M-03, M-08, M-26 and M-24)

This type of damage is characterised by a wedge-shaped damage zone of antithetic fractures widening from the fault tip (Figs. 4.14 - 4.18). The size of the wedge is generally proportional to the fault length.

Dominant damage zone fractures can be grouped into four sets; antithetic shear fractures (R' shear or Type B of Chinnery, 1966b), synthetic branch faults aligned as an array continuing sub-parallel to the main fault zone (Type A), synthetic shear fractures (R shear), and extensional fractures (T). The fracture distributions for this type damage zones show predominant second order antithetic faults and some T fractures. Several second-order shear fractures (R) link the second-order antithetic fractures.

In this type of tip damage zone, antithetic shears (type B or R') are the predominant fracture (as in McGrath and Davison, 1995, fig. 11). Synthetic shears (Type A of Chinnery, 1966b) and extensional fractures (T) often occur, but tend to be shorter and less frequent. Some higher-order fractures are also developed.

The movement sense of the antithetic faults can be inferred from the angular relationship with higher or lower order faults and the tip cracks. Antithetic fractures lie about 60°-70° from the main fault. The tip cracks open up at approximately 45° to the antithetic fracture plane. Some antithetic fractures show smooth sigmoidal shapes indicating slip sense and rotation.

This type of damage zone shows a slight rotation in its trend away from dilational quadrant toward the compression quadrant. This phenomenon is more obvious in larger faults such as Figures 4.14 and 4.15. Although the reason for this is not clear, it might be due to shear at the cohesive end zone (Cowie and Scholz, 1992; Martel and Boger, 1998). In the damage zone, displacement from the main fault is accommodated by antithetic shears and extensional tip fractures.

In Figure 4.17, branch fractures and antithetic shear fractures combine to form a wedge-shaped damage pattern. The two fracture sets intersect. Most of the antithetic shear fractures are located in the dilational quadrant and the major fault trace bends towards the dilational site. M-24 (Fig. 4.18) consists of several segmented branch faults, and each wedge-shaped zone at segment tips has different fracture spacing and

lengths. This indicates that each wedge-shaped zone can be matched to a fault segment tip whether or not all the fault segments developed coevally.

4.6.3. Conjugate Riedel shears (R') and extensional fractures (T) dominant tip damage (M-35, M-31 and M-05)

The combination of several fractures with different fracture patterns in a damage zone is very common. Some faults show more complicated mixed fracture patterns at tips. In this section, mixed tip damage structures of antithetic shear fractures (R') and extensional fractures (T) are described.

Figures 4.19 - 4.21 show several long extensional fractures with relatively small antithetic shear fractures. Higher order extensional fractures are developed at the tips of some second order antithetic fractures allowing determination of the slip sense of the fractures. The antithetic fractures dominate away from the fault tip, with several sets of wedge-shaped zones of higher order antithetic shear fractures developed at some segment tips. Several second-order shear fractures crosscut antithetic fractures (Fig. 4.19 - 4.21).

Along fault system M-35 (Fig. 4.19), zones of antithetic shears are developed, particularly at oversteps and tip zones of fault segments. Extensional branch faults are predominant on the NE side of the main fault, and these fractures are distributed along the whole fault. This indicates that the north-western side of the wall was a dilational zone during the entire branch fault propagation. In the central section of the fault M-31 (Fig. 4.20), a few pinnate fractures and branch faults are developed. The damage zone around the western fault tip shows a combination of branch fractures and antithetic shear fractures, whereas at the other end a wedge-shaped antithetic fracture set striking about N060° is developed.

Several early studies (McKinstry, 1953; Moody and Hill, 1956; Chinnery, 1966b; Arboleya and Engelder, 1995; Davis *et al.*, 2000) have described plausible higher-order fractures, similar to those developed around secondary antithetic faults in the study area (Figs. 4.14, 4.15 and 4.21). The inferred stress axes for higher-order fracture sets differ systematically from those of the lower-order fractures (Fig. 4.22). The pattern can be explained assuming that the higher-order fractures form at 15° to the maximum compressive stress (σ_1) and that there is a 15° rotation of σ_1 at each fracture tip. Displacement and shear along a fault generates a shear-induced stress

which result in a rotation of the sub-regional direction of maximum principal stress into a local direction of maximum principal stress (Mandl, 1988; Davis *et al.*, 2000). Thus the examples in Figure 4.14 show second order antithetic fractures (R') striking ~ N105° related to a first order right-lateral fault, with σ_1 at ~ N080°. Third order fractures to second order left-lateral fractures (R') have σ_1 at about ~ N060° (Fig. 4.14b-f). A similar relationship is also shown in Figure 4.21 for a left-lateral fault system.

4.6.4. Attributes of tip damage

Recent studies by Granier (1985), McGrath and Davison (1995), and Martel and Boger (1998), based on detailed field observation, have led to greater understanding of tip damage structures. Many authors (e.g. Granier, 1985; Petit and Barquins, 1988; Cox and Scholz, 1988) have argued that natural faults do not propagate as shear fractures, however, such propagation has been induced in computer modelling (Chinnery 1966a, 1966b) and in glass at high differential loading and confining pressures to produce horsetails and wing cracks (Petit and Barquins, 1988). For a fault with a cohesive zone, the total stress field reflects contributions from gravity, regional tectonic stresses, thermal stresses, and the perturbations arising from slip on the fault (Martel and Boger, 1998).

Experimental and computer modelling studies (e.g. Brace and Bombolakis, 1963; Reches and Lockner, 1994; Moore and Lockner, 1995) have shown that tensile microcracking often precedes the development of continuous faults in various rock types. Similar processes of localisation and linking of opening mode fractures, followed by macroscopic failure along a fault surface, has been observed by others (e.g. Horii and Nemat-Nasser, 1985; Granier, 1985; Mollema and Antonellini, 1999).

Two different mechanisms are recognised. 1) Favourably orientated pre-existing discontinuities, such as microcracks, joints or bedding planes, may slide under compression forming mode I cracks at their tips (tip cracks or wing cracks). The tip cracks may link the sliding fractures to produce a continuous failure plane (Horii and Nemat-Nasser, 1985; Granier, 1985; Segall and Pollard, 1983; Martel, 1990). 2) In the absence of pre-existing discontinuities, a through-going fault may be formed by the linking of microcracks via grain boundaries (Moore and Lockner, 1995) or by

breaking of bridges between the en-echelon microcracks or joints (Reches and Lockner, 1994; Mollema and Antonellini, 1999).

Antithetic tip damage patterns are located in the dilational quadrant of a fault tip region in general (Fig. 4.16 and 4.17), where fracture density is higher (Figs. 4.11 - 4.19) (Moore and Lockner, 1995). Antithetic fractures at fault tips generally increase in length and spacing away from fault tips, producing a wedge-shaped zone of damage at mode II fault tips (Figs. 4.14 - 4.21). The slip sense of these antithetic shear fractures can be inferred from tip cracks (higher order) developed at the tips of related fractures.

Because the nucleation and termination of earthquake rupture is strongly dependant on fault geometry (Aki, 1989), fault propagation direction might influence tip damage pattern. Cartwright and Mansfield (1998) have suggested that faults at active tips of normal faults in Utah propagate asymmetrically. In brittle faulting, the propagation direction of faults can be determined from the orientations of microfractures formed within the process zone (Vermilye and Scholz, 1999). In most of the tip damage structures, the density and pattern of fractures is different at both tips. Therefore, although there is no clear evidence for the fault propagation, this different tip damage might indicate the main propagation direction.

4.6.5. Attributes of transitional damage zone pattern (mode II + III tip)

Mixed damage pattern in transition zones is a very common phenomenon between the two end members of pure tip modes. In fact, natural along-strike tips or up- or down-dip tips are very rare, because most of exposed tips necessarily have other tip component depending on the location of the exposed surface around master fault surface.

Segmented fault patterns show characteristic damage that comprises overlapping R' shear fractures (Fig. 4.7, 4.10, 4.18 and 4.19). The damage pattern of these faults shows strong wedge-shaped patterns as well as distributed R' shear fractures intersecting fault segments. The damage pattern, especially in Figure 4.7, is very similar to along-strike tip damage pattern. However, there is no master fault, suggesting that this shear zone is a mode III tip, with a mode II tip component.

The wedge-shaped patterns (Fig. 4.7, 4.18, and 4.19) in these examples show a consistent lengthening of fractures away from the main fault, suggest that branch faults

have only one tip, the other tip terminating against the main fault. Therefore, the branch faults may form a half-loop of a single isolated fault loop, which could be evidence for the fault propagation direction, because the branch faults may grow from the main fault. Also, as shown in several examples (e.g. Fig. 4.6, 4.10 and 4.16), most strike-slip faults show different tip damage patterns at both fault tips. It might imply propagation direction.

At the ends of some up- and down-dip tips (mode III), the damage pattern shows a combined style, with mode II and III, because the rock experienced two types of fault tip modes. At a later stage, the damage zone is wider and P and R shears predominate over R'. The mode III tip zone is moved upward or downward and the mode II tips laterally propagate away from the centre to evolve into a larger fault.

4.7. LINKAGE DAMAGE

At the linking zones of two fault segments, intensive damage is developed. This may be an important conduit for fluid flow and migration of minerals (Sibson, 1996; Martel and Boger, 1998) due to abundant fracturing and the combination of various fractures.

4.7.1. Extensional fracture dominant linkage damage (M-00)

This type of damage style is characterised by a high density of extensional fractures at overstep zones. The M-00 fault (Fig. 4.1b) consists of several left-lateral strike-slip fault segments (Fig. 4.23) linked through highly fractured oversteps. The measured maximum displacement from the offset of burrows is ~ 220 mm, indicating that the displacement is relatively small, with $d_{max}/L \approx 0.006$.

Although dilational oversteps are dominant, some minor contractional overstep zones are developed. The dilational overstep zone is dominated by extensional (mode I) fractures and pull-aparts trending N060° ~ N080°, i.e. at 40-50° to the main fault zone. Some of these fractures, particularly within the dilational jogs, are partially filled with calcite. H-shaped fracture bridge patterns, where younger fractures abut older ones (Hancock, 1985), provide evidence of the secondary extension of bridges (Gamond, 1987).

4.7.2. Conjugate Riedel shears (R') and branch fractures (Type A) dominant linkage damage (M-25, M-19 and M-MAP02)

This type of damage style is characteristic of two non-overlapping sub-parallel fault segments. Examples (Figs. 4.24 - 4.26) show a high density of overlapping tip damage zones linking two fault segments. The damage zones mainly consist of branch fractures and antithetic shear fractures (R'), corresponding to type A and B secondary faults of Chinnery (1966b), respectively. The antithetic fractures are at a high angle to the branch fractures, and some show sigmoidal shapes and have tip cracks, from which the slip sense can be inferred. Although the two fracture zones overlap, the time relationship is not clear. Some of the splay fractures terminated against antithetic faults and *vice versa,* suggesting both fault sets are active contemporaneously.

Between east-west trending left-lateral strike-slip branch fractures (bounding fractures), shorter north-south trending fractures (cross-fractures) have a right-lateral slip sense. Fracture density around fault tips is generally higher on the side of the dilational quadrant. Cross-faults may form blocks with anti-clockwise rotations in mature stage (Fig. 4.26) under regional left-lateral shearing (c.f. Nicholson *et al.*, 1986), as in the experimental studies (Schreurs, 1994). Hence, if the sense of block rotation is known, the orientation and sense of the main fault can be determined, and *vice versa.*

4.7.3. Pull-aparts (M-06, M-05, M-41 and M-42)

Several types of pull-aparts are observed (Figs. 4.27 - 4.30). They are generally developed by a combination of three fractures (P, R and T) to form open spaces. Some straight segments, generated individually at an early stage, link together to form the fault plane. The zigzag geometric pattern of these examples is analogous to the geometry of some active faults (Bilham and Williams, 1985), and laboratory shear fractures (Moore and Lockner, 1995).

Although displacement along the fault in Figure 4.27 could not be determined from offset markers, two tip cracks and the pull-aparts along segment linkages indicate right-lateral slip. The character of the linking fractures between P shears is not obvious. Figure 4.28 shows a pair of conjugate faults linked through dilational jogs or releasing bends producing pull-aparts. To the east of their intersection, the faults show no segmentation and overstep, but a series of fractures, generally striking between the

two main faults, produced a network with some open spaces. A few secondary fractures show higher-order structures at their tips (wing-cracks), indicative of a strike-slip origin. Some resemble synthetic branch fractures in tip zones. Damage indicative of high strain is developed near the intersection of conjugate fault sets (Watterson *et al.*, 1998). These damage structures are developed between the two conjugate fault sets to accommodate the stress and slip. Although the conjugate faults are developed under the same regional stress condition, higher-order secondary fractures reflect different local stress conditions (Fig. 4.28). Thus, the orientation patterns depend on the order of the local stress distribution (Fig. 4.22; Hancock, 1972; Willemse *et al.*, 1997).

M-41 and M-42 (Figs. 4.29 and 4.30) are located along the same E-W trending left-lateral fault system. M-41 shows a good example of P and R shears combining to generate pull-aparts (Gamond, 1983). The fault trace is kinked depending on the orientation of the main linking fractures. P fracture segments strike N110°, and R fracture segments strike N092°, so that the general trend of the fault is between these two orientations. The opening of the pull-aparts is dependent on slip along the P segments, the amount of extension, and the σ_1 direction

M-42 (Fig. 4.30) shows pull-aparts caused by interacting P and T fracture segments. P segments terminate at T segments suggesting they post-date (Segall and Pollard, 1983; Hancock, 1985), with the T segments continuing as extensional fractures. The opening of the pull-aparts is dependant on the amount of extension perpendicular to the extension fracture segments and slip along the P fracture segments. Peacock and Sanderson (1995) have described a similar combination of pull-aparts in Somerset, England. They suggested that the variation in the geometry of pull-apart arrays varies with the amount of transtension and transpression.

The pull-apart shape caused by the linkage of P and R fault segments (Fig. 4.29) is a relatively long narrow trapezoid, whereas P and T sets (Fig. 4.30) produce a wide trapezoid with higher intersection angle (θ).

4.7.4. Attributes of linkage damage

Faults are not generally planar surfaces but consist of linked arrays of en-echelon fractures (Gamond 1987), which have been described at all scales (e.g. Peacock, 1991; Peacock *et al.*, 2000). The pattern of linkage depends on material properties, stress

condition (e.g. Naylor *et al.* 1986; Du and Aydin, 1995), fault evolution stage (e.g. Peacock, 1991; Peacock and Sanderson, 1995), relationship between segments (e.g. Du and Aydin, 1995), and relative motion of associated fractures. In this study, three main linkage styles have been described: extensional fracture dominant linkage (at mode II tip); R' and branch fractures dominant linkage (at mode II tip); and pull-aparts with combination of P, R and T fractures (at mode II & III tips).

The M-00 fault system (Fig. 4.23) involves dilational oversteps, linked by extensional fractures producing pull-aparts and highly fractured zones. Concentrated stress at segment tips (Cowie and Scholz, 1992; Gupta and Scholz, 2000) might be accommodated in oversteps by secondary fracturing (King, 1986). Where faults are overlapping in map view, they curve sharply away from the main fault tip towards the adjacent fault and terminate in extensional fractures. This produces high displacement gradients at fault tips, and indicates that the principal stress orientations are markedly different at tips, or where interference between two faults occurs (Peacock and Sanderson, 1991; McGrath and Davison, 1995).

Slip along pre-existing joints can result in the formation of fractures at the tip of the reactivated joint (tail cracks) and the fragmentation of the rock bridges between the slip planes (*granite*, Segall and Pollard, 1983; Granier, 1985; Martel *et al.*, 1988; Martel, 1990; *sandstone*, Cruikshank, 1991; Myers and Aydin, 1996; Cooke *et al.*, 1999; *shale*, Dholakia *et al.*, 1998). Therefore, secondary fractures play a critical role in fault growth and fluid flow.

The antithetic fracture arrays are not bounded by other fractures (Figs. 4.14b-f and 4.16) at an early stage in evolution, but at a mature stage they may be bounded and linked by branch fractures. A combination of branch fractures and antithetic fractures at overlapped fault tips could produce an appropriate condition for block rotation in a mature stage of linkage (Fig. 4.26). The sigmoidal shape of the antithetic fractures (Fig. 4.26) might have originated from the shear stress distribution (Chinnery, 1966a), propagation of fractures within shear zone (Ramsay and Huber, 1987), or block rotation by simple shear (McGrath and Davison, 1995). All these mechanisms do not exclude shearing along the fault.

Fluid flow along faults would tend to be anisotropic and channelled, with "chimneys" of highly fractured rock oriented normal to the slip vector being regions of elevated hydraulic conductivity (Sibson, 1996; Martel and Boger, 1998). Hence fault

plane hydraulic conductivity arising from linkages would be low parallel to slip and high normal to slip (Martel and Boger, 1998).

4.7.5. Block rotation

In general, slip on faults takes place as deformation proceeds, and is associated with the rotation of the blocks between faults and rotation of the faults themselves (Nur *et al.,* 1986). If two sub-parallel faults are developed as fault tips or oversteps, there might be a strong potential for block rotation (Rispoli, 1981), accomplished by faults that are antithetic to the main fault. Some of the mapped examples (Fig. 4.24 - 4.26) show a developing series of block rotation. Most of the rotated blocks result from a combination of processes between branch faults and antithetic faults at overlapped fault tips.

These types of blocks may not rotate much before new fractures form (Nur *et al.*, 1986). Cross-faults acquire a sigmoidal shape and usually terminate against earlier formed master faults. As strain increases, cross-faults separated by unfaulted domains undergo clockwise rotation about vertical axes (Schreurs, 1994). Some antithetic fractures have high angular relationship because of later rotation (e.g. Fig. 4.26; about 100°), indicating rotational strain in the relay ramps, with the sense of rotation consistent with that of the fault zone (Fig. 4.26) (Peacock and Sanderson, 1995)

The geometrical model for rotated blocks predicts that synthetic, antithetic slips, and rotation occur coevally. Triangular voids may form at the junction between the rotated and unrotated blocks (Luyendyk *et al.,* 1980; Chapter 2). For a wide range of (reasonable) values of the coefficient of friction, cohesive strength, and depth, Nur *et al.* (1986) suggested that the rotations are likely to be in the range of 20° to 40°; rotations of more than 45° require other process such as multiple sets of rotating faults with angles of 20° to 45° between them.

4.8. CROSS SECTIONAL FEATURES OF STRIKE-SLIP FAULT TIPS

Most studies of strike-slip fault systems have discussed faults seen in map view (e.g. Crowell, 1974; Tchalenko, 1970; Segall and Pollard, 1983; Mollema and Antonellini, 1999). There are just a few studies (e.g. Wilcox *et al.*, 1973; Sylvester and

Smith, 1976; Bartlett, *et al.*, 1981; McGrath and Davison, 1995) describing vertical cross-sections of strike-slip fault geometries. On Gozo there are several cross-sections of strike-slip fault planes accessible for detailed field study in cliffs. Two of the best examples are examined to understand the three dimensional geometry of strike-slip fault structures.

The two cross-sectional views of up-dip tips of strike-slip faults are shown in Figures 4.31 and 4.32. Both show cone-shaped damage zones diverging from main fault tips, with several branch fractures spreading out from the master fault. At the tip, two symmetric branching fractures diverge upwards forming mostly symmetric cone-shape, reflecting the stress propagation from the tips. The damage density decreases downwards.

Figure 4.32 shows a slightly higher density of sub-horizontal fractures on the NW side, but the damage geometry is almost symmetric, whereas Figure 4.31 shows a more asymmetric damage fracture pattern. This suggests that the cross-section M-38 (Fig. 4.32) might be located near the central part along the fault trace.

These cone-shaped damage patterns are very similar to 'flower structures' (Wilcox *et al.*, 1973; Sylvester and Smith, 1976; Bartlett, *et al.*, 1981; Sylvester, 1988) and an observed up-dip tip of a strike-slip fault exhibiting a series of bifurcating fractures (McGrath and Davison, 1995). Also an analogous structure was reported in seismic section (Naylor *et al.,* 1986). These fractures are terminated in the vertical plane parallel to σ_1 (McGrath and Davison, 1995), or interpreted to be Riedel shears with a helicoidal geometry (e.g. Naylor *et al.*, 1986). The main fractures branching from the master fault tips probably correspond to P or R shears (see the supposed map views in Fig. 4.31 and 4.32).

Generally a mode III tip is relatively symmetric along a fault trace, except at transition zones with mode II tip. The symmetric, cone-shaped, branch fracture geometry (Figs. 4.31 –4.32) and distributed damage zone pattern at mode III tip (Figs. 4.8 - 4.10) supports this idea.

4.9. FRACTAL GEOMETRY OF FAULT LINKAGE

If geometrical complexity, or irregularity, is an important parameter, then it may be useful to quantify this complexity. Fractal analysis has been applied to sites selected to determine the fractal dimension and explore its relationship to the fault geometry.

4.9.1. Determination of the fractal dimension

For a given set, a number of different fractal dimensions can be defined, which are measures of the set's complexity or irregularity. These can be determined in a number of ways (Mandelbrot, 1977). Once the fractal dimension of a set has been determined, it provides a quantitative means of characterising the fractal nature of that set (Okubo and Aki, 1987).

Several methods have been suggested to define the fractal dimension of fault geometry and fracture density (Aviles *et al.*, 1987; Okubo and Aki, 1987; Barton and Larsen, 1985; La Pointe, 1988). Aviles *et al.* (1987) applied Mandelbrot's ruler method to the San Andreas Fault. Although this method is useful for a simple single fault trace, it is difficult to apply to a complex fault network. Okubo and Aki (1987) developed a circle method based on Mandelbrot's idea, which is used here. The basic concept is very similar to box counting method which counts the number of boxes that include part of the fault traces (see Barton and Larsen, 1985; La Pointe, 1988).

Ruler method

Mandelbrot (1977) analysed the lengths of coastlines, elaborating observation by L. F. Richardson. These curves are measured using a chain of line segments of equal length ε. As ε becomes smaller, it is observed that the length of curve $L(\varepsilon)$ tends to increase without limit. Plotted on log-log axes, a power-law relationship between $L(\varepsilon)$ and ε is represented by a straight line of the form

$$Log_{10} L(\varepsilon) = a + b \, log_{10} \varepsilon \qquad (1)$$

A further interpretation of this result is that in order to approximate a coastline by a number of straight-line segments of length ε, two constants A and D are required. To achieve a total length $L(\varepsilon)$ from segments of length ε requires a total number $A\varepsilon^{-D}$ of such segments, so that

$$L(\varepsilon) = A\varepsilon^{1-D} \quad (2)$$

Comparing (1) and (2), it follows that $a = log_{10} A$ and $b = 1 - D$. It also follows that $L(\varepsilon)$ increases more rapidly for larger D, so that larger values of D are directly associated with more complicated curves. Mandelbrot suggested that D, the exponent in equation (2), could be thought of as a fractal dimension following the approach of Hausdorff.

Circle method

This method involves covering all the faults and fractures in a selected fault zone. Circles of a chosen radius r are drawn in order to cover the fault and fracture traces using a minimum number $N(r)$ of such circles. Fracture length (L) is a function of circle radius r and is defined as the total area of the N circles, divided by the diameter of a single circle. That is,

$$L(r) = N(r)\pi r^2/2r \quad (3)$$

Normalising $L(r)$ by a factor of $\pi/4$, the fault length estimates are given by

$$L°(r) = 2N(r)r \quad (4)$$

Length $L°(r)$ are plotted as a function of measuring radius r on log-log axes, and the fractal dimension D is estimated from the slope b of the best straight-line fit to the data as

$$D = 1 - b \quad (5)$$

D is thus a measure of the rate of change of log (fault length) with respect to log (measurement resolution) (Okubo and Aki, 1987).

4.9.2. Fractal dimension of fault system M-00

Application of the circle method to Fault M-00 (Fig. 4.23) is described in this section. In Figure 4.33 the fault system has been divided into seven regions of equal area. A range of circle radii has been used, from an upper cut-off of 2 m (or 4 m for entire fault) to a lower cut-off of 0.125 m. Fault length is measured as a function of measuring radius in the manner as described earlier. Normalised fault length, number of circles and measuring radius data are presented in Table 1 and plotted on log-log axes in Figure 4.34. The fractal dimension D is estimated from the slopes of straight-line that fitted by least squares to the data. D ranges from 1.14 to 1.40 (Table 1).

The differences in fault complexity between different segments are reflected by the variations in measured fractal dimensions (Fig. 4.35). It is obvious that master fault segments (segments B and D) have small fractal dimensions that imply less complexity, whereas the segment boundaries (segment A, C and E) have large fractal dimensions and more complex geometry. This implies a relation between fault segmentation and the complexity of fault geometry as suggested for the surface trace of the Dixie Valley - Pleasant Valley normal fault system by Zhang *et al.* (1991).

Segment boundaries are often associated with stepovers or discontinuities within the fault zone. Although the eastern fault tip zone shows complex tip damage (segments F and G), the fractal dimensions are lower than those of the fault linkage zones (segments A, C and E). The fractal dimension is most sensitive to the number of fractures or blocks, rather than their size, orientation or size variability (La Pointe, 1988). Therefore, the results indicate that segment linkage increases fracture density within a narrow zone, although the result is poorly constrained and speculative because of limited data.

4.10. STRIKE-SLIP FAULT EVOLUTION MODELS AT GOZO

Most studies of the propagation of faults and fractures have concentrated on the secondary fracture mechanism around fault tips (Brace and Bombolakis, 1963; Chinnery, 1966a; 1966b; Rispoli, 1981; Nemat-Nasser and Horii, 1982; Segall and Pollard, 1983; Granier, 1985; Pollard and Segall, 1987; Petit and Barquins, 1988; Willemse and Pollard, 1998). A number of recent publication are concerned with two- or three-dimensional propagation models of entire faults including damage structures (Moore and Lockner, 1995; McGrath and Davison, 1995; Willemse *et al.*, 1997; Martel and Boger, 1998; Mollema and Antonellini, 1999). These studies enhance understanding of how faults nucleate and grow in natural rock, which is very important to earthquake and fluid flow studies.

In this section, three models of fault propagation are proposed for the strike-slip faults in Gozo, Malta (Fig. 4.36 - 4.38). The width and complexity of the strike-slip zone is determined by the total displacement and by the initial stress state (Naylor *et al.*, 1986).

In the first model, faults initiate from arrays of extensional fractures (Fig. 4.36), which generate a fault due to mechanical interaction (Cox and Scholz, 1988; Reches and Lockner, 1994; Mollema and Antonellini, 1999). Cox and Scholz (1988) suggested that a shear fracture zone might extend in length in its own plane. They produced a fracture pattern (fig, 9 of Cox and Scholz, 1988), which is analogous to the observed fracture patterns in study area (e.g. Fig. 4.5). They attribute tension fractures to the initial stress field, with linking fractures forming later as the deformation increased. Minor fractures, which include R and P shear fractures, link into a through-going large fault (PDZ) in a late stage (Figs. 4.6 and 4.23). Extension fractures are generally parallel to the local σ_1 direction, whereas shear fractures or faults are orientated at 45° - $\phi/2$ to σ_1 (Scholz, 1968; Naylor *et al.,* 1986). The geometry of this shear fracturing is analogous to the form of en echelon tension cracks in small-scale shear zones (Knipe and White 1979, Pollard *et al.,* 1982).

The second model (Fig. 4.37) involves the growth of mode II (shearing) fault tips by the development of tip cracks and linkage (Peacock, 1991; Moore and Lockner, 1995; Cartwright *et al.*, 1995; Kim *et al.*, 2000) producing zigzag geometry. These examples have been documented at microscopic scales (Moore and Lockner, 1995) and tectonic scales (Bilham and Williams, 1985). This model postulates that faults or shear flaws propagate predominantly through secondary fractures, and overstep zones are linked through cross-faults in a later stage. Examples of this growth pattern are well observed in Figures 4.23 - 4.28.

Opening-mode splay fractures develop as secondary features along and within fault zones (Cooke, 1997). They can serve as conduits for the transport of hydrocarbons (e.g., Nelson, 1985), geothermal fluids (e.g., Takahashi and Abe, 1989) or groundwater (e.g., Long and Wood, 1986). Both field observations and mechanical considerations indicate that strike-slip faults link more readily through mode II tips, because fractures associated with mode II loads are larger than those for mode III (Martel and Boger, 1998).

The third model (Fig. 4.38) follows the classical Riedel shear fracture pattern (e.g. Tchalenko, 1970); the orientations of the early Riedel shears are determined by the initial stress state (Naylor *et al.,* 1986). For early R and R' shears, σ_1 lies within a horizontal plane at about 45° to the imposed shear direction (Fig. 4.4) (Schreurs, 1994). The R and R' shears created at the peak stage are both unfavourably oriented to

sustain large relative displacements, and further straining and shearing must take place to accommodate increased over-all movements (Tchalenko, 1970). Several shear models (Morgenstern and Tchalenko, 1967; Gamond, 1983, 1987; Swanson, 1988; Sims *et al.*, 1999) have shown that the discontinuity is composed of first-generation fractures of the R type joined by second-generation P fractures.

The conjugate Riedels in particular, being nearly at right angles to the general movement, respond passively to post-peak deformations by rotation and distortion due to at a high angle to the main fault trend (Fig. 4.26). The combination of displacement along the R and P shears leads to the formation of the zigzag shaped fault traces orientated in the general direction of movement (Figs. 4.29 and 4.30). Pull-aparts are generally formed by the combination of any two of the three fractures (Riedel shears, P shears and tension fractures).

4.11. 3-D CONCEPTUAL MODEL OF A STRIKE-SLIP FAULT AND ITS DAMAGE ZONES

4.11.1. Possible reasons for different damage patterns

In the above section, the obvious differences between the three main patterns of fault zone development are described. These differences could result from several reasons.

1) *Different material properties such as frictional coefficient*: This is not likely, because most of the structures from the study area are developed in a small region and in the same rock layer.

2) *Different orientation of fault zone to far-field stress*: This is not likely, because σ_1 is consistent for the strike-slip faults in this area (Fig. 4.2), with the exception of zones of overlapping extension fractures close to σ_1, little systematic relationship exists between fault zone orientation and geometry (Fig. 4.39). Although the mapped faults and shear zones can be grouped based on shear sense, there is no other relationship between the angle to the maximum compressive stress and particular damage pattern.

3) *Relation to strain or maturity*: This is not likely, because most of structures are found with low displacement (< 200 mm) and low d_{max}/L ratio of $< 10^{-2}$.

4) *Different styles could reflect positions in relation to main fault* (i.e. mode II and mode III tips). Although it is not possible to relate the examples directly to a master fault, mode II and mode III fault tip damage zones are recognised on the bases of:

(i) d*ifferent damage zone orientations*. Mode II tip damage zones curve towards dilational quadrant, whereas mode III tip damage zones are parallel to main fault trend.

(ii) *different damage zone shapes*. Mode II tips are dominated by extensional fractures in the dilational quadrant or by asymmetrical wedge-shaped zones antithetic fracture which increase in length from the fault tip, whereas mode III tips show long symmetrical zones of distributed damage.

(iii) *different relation with master fault*. Mode II tips are developed at the end of a straight master fault, whereas mode III tips rarely show any clear through-going master faults. When some segmented, relay fractures or faults exist, they are developed in the middle of the damage zone and overlapped with other en echelon fractures.

4.11.2. Attributes of 3-D damage patterns

A mode II fault tip (sliding) is an along-strike tip of a strike-slip fault, whereas a mode III fault tip (tearing) is an up- or down-dip tip (Lawn, 1993; McGrath and Davison, 1995). While the stress concentration at a propagating mode II tip is asymmetric across the fault plane (Reches and Lockner, 1994; Vermilye and Scholz, 1999) with dilational and contractional quadrants, the stress concentration for mode III tips is symmetrical on both sides of the fault trace (Pollard and Segall, 1987). Because of these basic differences in fault slip modes, the associated damage orientation, geometry and fracture generation are different. Therefore, different fracture propagation models should be applied to different fault tip modes.

A three-dimensional conceptual model (Fig. 4.40) for a strike-slip fault with two tip modes (II and III) is extrapolated to explain this variety of damage structures. It shows different damage styles at different tip modes (A-D in Fig. 4.40), also shows a simple vertical cross-section showing mode III tip damage of a strike-slip fault (E in Fig. 4.40).

Extensional fractures (T) might be the first to initiate (C & D in Fig. 4.40) (e.g. Cox and Scholz, 1988; Reches and Lockner, 1994; Mollema and Antonellini, 1999),

and arrays of these en echelon extensional fractures produce a fault. Extension fractures (T) are mainly developed by remote regional compressive stress (~ N070°), and the intersection angles between the fractures and the main fault trend are ~ 45° (Fig. 4.3). Most of these fractures are long and straight, and abut against the master fault without any tip cracks. In addition to these extensional fractures, another type of extensional fractures is localised at mode II tips forming 'wing crack' or 'horsetail splay', although some of the latter may be mixed mode, with a shear component. The orientation of extension fractures at mode II fault tips, is controlled by local stress redistribution and is slightly different from the extensional fractures at wall zones (Moore and Lockner, 1995).

It is generally difficult to interpret deformation at the surface of exposure in terms of fault movements below or above. Conjugate Riedel shears are usually first fracture to appear in a simple shear zone, which is propagating upwards (A in Fig. 4.40) (e.g. Tchalenko, 1970). This may be considered as a mode III (tearing) tip of a master fault. The reconstructed structural evolution follows a pattern basically similar to that ones observed in the classical Riedel experiment (Riedel, 1929), and in shear box tests and earthquake fractures (Tchalenko, 1970; Tchalenko and Ambraseys, 1970).

The larger angles of conjugate Riedel shears (R') to the general movement direction, shown at the early stage of mode III tip, cause them to be subsequently distorted and rotated (Tchalenko, 1970). At increased displacements, P shears interconnect Riedel shears with orientation approximately symmetrical to the Riedels (R). Although R and P shears are observed at mode III tips, they are not dominant fractures at early stages (A in Fig. 4.40). At a mature stage or at a slightly lower level from the up-dip tip, R and P shears are combined with extensional fractures (T) to produce a zigzag geometry of the fault (e.g. Moore and Lockner, 1995). This type of fault usually has pull-aparts and relicts of R' shears on later fault planes (e.g. Figs. 4.29 and 4.30).

In this chapter, the en echelon fractures along mode III tips of strike-slip fault (A in Fig. 4.40) are referred as R' shears not T fractures for the following reasons, although it is still debatable (Section 4.5.3). Firstly, the intersection angles of the fractures and main shear zone trend are typically 65° ± 10° (e.g. Figs. 4.3, 4.8 and 4.9). Secondly, most of the R' fractures do not accumulate much slip since R and P shears

generated, and they are just passively distorted or rotated (e.g. Fig. 4.8, 4.29 and 4.30). Thirdly, at some of the fracture tips, tip cracks are developed indicating shear slip (e.g. Figs. 4.7 and 4.8). Fourthly, the fracture pattern at mode III tip (tearing) is very similar to classical Riedel shear model (e.g. Tchalenko, 1970).

The mode II near-tip stress concentration has a characteristic form (Lawn, 1993) that has been widely used to predict the distribution and orientation in which secondary fractures propagate (Pollard *et al.*, 1982; Ingraffea, 1987; Segall and Pollard, 1987; Cruikshank, 1991; Reches and Lockner, 1994). Secondary fracture should nucleate toward the fault perimeter, where tensile stresses are greatest, rather than near the fault centre. Furthermore, any secondary fracture that nucleates on the fault face should preferentially propagate toward the perimeter (Martel and Boger, 1998). Tensile stress is also concentrated ahead of the fault tip (Kassir and Sih, 1975), and secondary fractures should be able to propagate some distance beyond the fault perimeter (C and D in Fig. 4.40) (Cooke, 1997; Martel and Boger, 1998).

At mode II tips, varying damage patterns occur (D in Fig. 4.40) (e.g. Chinnery, 1966b; Granier, 1985; McGrath and Davison, 1995; Martel and Boger, 1998). R' shears commonly develop at mode II tips, but show a wedge-shaped damage pattern. Although these fractures have similar angular relationship with R' at mode III tip, they increase in length and spacing away from the fault tip showing wedge-shaped pattern (McGrath and Davison, 1995). Also, some synthetic branch faults commonly occur at mode II fault tips (D in Fig. 4.40), and sometimes they contribute as bounding faults to develop rotated blocks. The combination of these two faults provides a good condition for block rotation.

To summarise, the shear zone model, with Riedel shears (e.g. Tchalenko, 1970; Wilcox *et al.*, 1973; Schreurs, 1994), is applicable to mode III tips, whereas tip crack or wing crack model with pre-existing flaws (Brace and Bombolakis, 1963; Chinnery, 1966a, 1966b; Nemat-Nasser and Horii, 1982; Segall and Pollard, 1983; Petit and Barquins, 1988; Willemse and Pollard, 1998) is mainly applicable to mode II fault tips. Thus the damage zone geometries and the damage fracture patterns of strike-slip faults are different depending on the locations around a master fault plane and fault evolution stages (Fig. 4.40).

The model shown in Figure 4.40 can be used to interpret natural fault zones. Figure 4.41, for example, shows a left-lateral strike-slip fault, cut by a slightly later

right-lateral fault. The left-lateral fault shows considerable variation in the tips of damage. The eastern tip shows a series of wedge-shaped zones of R' shears in the dilational quadrant that is fairly typical of a mode II tip. Similar sets of structures when traced westwards probably represent former mode II tips (N.B. their wedge-shaped form and concentration of damage in the dilational quadrant). The centre of the fault shows a typical contractional overstep or strike-slip relay dominated by R' shears. The western tip shows a series of zones of damage with no obvious wedge-shaped pattern. The damage develops as a series of R' shears, probably above (or below) fault segments (R shears – blue dashed line). Therefore, the eastern tip damage pattern shows propagation of mode II dominant tip damage (corresponding to plane D in Fig. 4.40), whereas the western tip shows mode III dominant tip damage pattern (corresponding to plane B in Fig. 4.40).

4.12. CONCLUSIONS

1. The faulting in Miocene Limestone, Gozo, to the west of Marsalforn comprises conjugate sets of strike-slip faults showing a wide range of secondary fractures and damage zones.
2. The inferred regional maximum compressive stress orientation (σ_1) from the fault data is about N070°. Most of the extensional fractures formed prior to the nucleation of the fault are roughly parallel to this orientation. These fractures are distinguished from the tip cracks developed in local stress field at along-strike tip zones.
3. Damage zones around strike-slip faults are divided into three styles; distributed damage, tip damage, linkage damage. Distributed damage shows antithetic fracture dominant long, narrow damage pattern along the fault trend. Tip damage shows extensional dominant fractures in dilational quadrant or antithetic wedge-shaped damage zone pattern at along-strike fault tips. Linkage damage shows a high density of fractures in relay zones of fault segments.
4. Dominant damage patterns at along-strike tips are wedge-shaped antithetic shear fractures (R') widening away from a tip, often accompanied by block rotation in linking zones. Tip cracks develop at the tips of some shear fractures indicating the

slip sense. At up- or down-dip tips early developed R' later P or R shears intersect. The shear fractures often combined with T fractures to form pull-aparts.

5. Similar damage structures are developed at different scales. There are distinct orders of damage fractures and rotation of stress axes within individual faults.
6. Fractal analysis using circle method for the whole fractures and faults of fault M-00 shows relatively high fractal dimensions ($D \approx 1.4$) characterising linkage zones.
7. Three fault growth models are proposed to interpret the observed fracture patterns in damage zones: extensional fracture dominate model, along-strike propagation model, and up- and down-dip propagation model. These models are dependent on the master fault tip modes as well as the level of exposure in relation to the master fault.
8. A three dimensional conceptual model is proposed for strike-slip fault damage structures, and shows different damage patterns depending on the fault tip mode and exposed section level.

REFERENCES

Aki, K. 1989. Geometric features of a fault zone related to the nucleation and termination of an earthquake rupture. *U. S. Geological Survey Open -File Report* **89-315**. 1-9.

Arboleya, M. -L. and Engelder, T. 1995. Concentrated slip zones with subsidiary shears: their development on three scales in the Cerro Brass fault Zone, Appalachian Valley and Ridge. *Journal of Structural Geology* **17**, 519-532.

Atkinson, B. K. 1987. Introduction to fracture mechanics and its geophysical applications. In *Fracture Mechanics of Rock (ed. B. K. Atkinson). Academic Press Geology Series*, Academic Press. 1-26.

Aviles, C. A., Scholz, C. H. and Boatwright, J. 1987. Fractal analysis applied to characteristic segments of the San Andreas fault. *Journal of Geophysical Research* **92**, 311-344.

Barton, C. C. and Larsen, E. 1985. Fractal geometry of two-dimensional fracture networks at Yucca Mountain, Southwest Nevada. In*: Fundamentals of Rock Joints* (edited by Stephannson, O.). Proceedings of the International Symposium on Fundamentals of Rock Joints, Bjorkkliden, Sweden, 77-84.

Bartlett, W. L., Friedman, M. and Logan, J. M., 1981. Experimental folding and faulting of rocks under confining pressure. Part IX. Wrench faults in limestone layers. *Tectonophysics* **79**, 255-277.

Beach, A. 1975. The geometry of en-echelon vein arrays. *Tectonophysics* **28**, 245-263.

Bilham, R. and Williams, P. 1985. Sawtooth segmentation and deformation processes on the southern San Andreas fault, California. *Geophys. Res. Lett.***12**, 557-560.

Boccaletti, M., Cello, G. and Tortorici, L. 1987. Transtensional tectonics in the Sicily Channel. *Journal of Structural Geology* **9**, 869-876.

Brace, W. F. and Bombolakis, E.G. 1963. A note on brittle crack growth in compression. *Journal of Geophysical Research* **68**, 3,709-3,713.

Bürgmann, R., Pollard, D. D. and Martel, S. J. 1994. Slip distributions on faults: effects of stress gradients, inelastic deformation, heterogeneous host-rock stiffness, and fault interaction. . *Journal of Structural Geology* **16**, 1675-1690.

Cartwright, J. A. and Mansfield, C. S. 1998. Lateral displacement variation and lateral tip geometry of normal faults in the Canyonlands National Park, Utah. *Journal of Structural Geology* **20,** 3-19.

Cartwright, J. A., Trudgill, B. D. and Mansfield, C. S. 1995. Fault growth by segment linkage: an explanation for scatter in maximum displacement and trace length data from the Canyonlands Grabens of SE Utah. *J. Struct. Geol.* **17**, 1319-1326.

Cello, G., Crisci, G. M., Marabini, S. and Tortoici, L. 1985. Transtensive tectonics in the Strait of Sicily: structural and volcanological evidence from the island of Pantelleria. *Tectonics* **4**, 311-322.

Chinnery, M. A. 1966a. Secondary faulting: I. Theoretical aspects. *Canadian Journal of earth Sciences* **3**, 163-174.

Chinnery, M. A. 1966b. Secondary faulting: II. Geological aspects. *Canadian Journal of earth Sciences* **3**, 175-190.

Christie-Blick, N. and Biddle, K. T. 1985. Deformation and basin formation along strike-slip faults. In *Strike-slip Deformation, Basin Formation, and Sedimentation*: Eds: Biddle, K. T. and Christie-Blick, N. *Society of Economic Palaeontologists and Mineralogists. Special Publication.* **37,** 1-34.

Cooke, M. L. 1997. Fracture localization along faults with spatially varying friction. *Journal of Geophysical Research* **102**, 22,425-22,434.

Cooke, M. L., Mollema, P. N., Pollard, D. D. and Aydin, A. 1999. Joint localization in folds over basement faults: Results from numerical modeling and evidence from Kaibab Monocline, Utah, USA. In: *Forced (drape) Folds and Associated Fractures* (edited by Cosgrove, J.). Geological Society of London, Special Publication.

Cowie, P. A. and Scholz, C. H. 1992. Physical explanation for the displacement-length relationship for faults using a post-yield fracture mechanics model. *Journal of Structural Geology* **14**, 1133-1148.

Cox, S. J. D. and Scholz, C. H. 1988. On the formation and growth of faults: an experimental study. *Journal of Structural Geology* **10**, 413-430.

Crowell, J. C. 1974. Origin of late Cenozoic basins in southern California. *Wrench Fault Tectonics* (compiled by A. G. Sylvester, 1984). 195-209.

Cruikshank, K. M. 1991. Analysis of minor fractures associated with joints and faulted joints. *Journal of Structural Geology* **13**, 865-886.

Davis, G. H., Bump, A. B., Garcia, P. E. and Ahlgren, S. G. 2000. Conjugate Riedel deformation band shear zones. *Journal of Structural Geology* **22**, 169-190.

Debono, G. and Xerri, S. 1993. *Geological map of the Maltese islands.* Sheet 2, Gozo and Comino, 1:25,000.

Dholakia, S. K., Aydin, A., Pollard, D. D. and Zoback, M. D. 1998. Fault-controlled hydrocarbon pathways in the Monterey formation, California. *American Association of Petroleum Geologists Bulletin* **82**, 1551-1574.

Du, Y. and Aydin, A. 1995. Shear fracture patterns and connectivity at geometric complexities along strike-slip faults. *Journal of Geophysical Research* **100**, 18,093-18,102.

Finetti, I. 1984. Geophysical study of the Sicily Channel rift zone. *Boll. Geofis. teor. appl.* **101-102**, 3-28.

Gamond, J. F. 1983. Displacement features associated with fault zones: a comparison between observed examples and experimental models. *Journal of Structural Geology* **5**, 33-45.

Gamond, J. F. 1987. Bridge structures as sense of displacement criteria in brittle fault zones. *Journal of Structural Geology* **9**, 609-620.

Granier, T. 1985. Origin, damping and pattern of development of faults in granite. *Tectonics* **4**, 721-737.

Gupta, A. and Scholz, C. 2000. A model o normal fault interaction based on observations and theory. *Journal of Structural Geology* **22**, 865-879.

Hancock, P. L. 1972. The analysis of en-echelon veins. *Geol. Mag.* **109**, 269-276.

Hancock, P. L. 1985. Brittle microtectonics: principles and practice. *Journal of Structural Geology* **7**, 437-457.

Harding, T. P., Vierbuchen, R. C. and Christie-Blick, N. 1985. Structural styles, plate-tectonic settings, and hydrocarbon traps of divergent (Transtensional) wrench faults. In *Strike-slip Deformation, Basin Formation, and Sedimentation*: Eds: Biddle, K. T. and Christie-Blick, N. *Society of Economic Palaeontologists and Mineralogists. Special Publication.* **37,** 51-77.

Horii, H. and Nemat-Nasser, S. 1985. Compressive-induced microcrack growth in brittle solids: axial splitting and shear failure. *Journal of Geophysical Research* **90**, 3105-3125.

Illies, J. H. 1981. Graben formation - the Maltese Islands - a case history. *Tectonophysics* **73**, 151-168.

Ingraffea, A. D. 1987. Theory of crack initiation and propagation in rock, in *Fracture Mechanics of Rocks* (edited by B. K. Atkinson) pp.71-108, Academic Press, san Diego, California.

Kassir, M. K. and Sih, G. C. 1975. *Three-Dimensional Crack Problems.* 452 pp. Noordhoof, Leiden, Netherlands.

Kim, Y.-S., Andrews, J. R. and Sanderson, D. J. 2000. Damage zones around strike-slip fault systems and strike-slip fault evolution, Crackington Haven, southwest England. *Geoscience Journal* ***4***, 53-72

King, G. C. P. 1986. Speculations on the Geometry of the Initiation and Termination Processes of Earthquake Rupture and its Relation to Morphology and Geological Structure. *Pure Appl. Geophys.* **124,** 567-585.

Knipe, R. J. and White, S. H. 1979. Deformation in low grade shear zones in the Old Red Sandstone, SW Wales. *Journal of Structural Geology* **1**, 53-66.

La Pointe, P. R. 1988. A method to characterize fracture density and connectivity through fractal geometry. *Int. J. Rock Mech. Min. Sci. and Geomech. Abstr.* **25**, 421-429.

Lawn, B. 1993. *Fracture of Brittle Solids*, 2nd ed., 378 pp. Cambridge Univ. Press, new York.

Long, J. C. S. and Witherspoon, P. A. 1985. The relationship of the degree of interconnection to permeability in fracture networks. *Journal of Geophysical Research* **90**, 3087-3098.

Long, P. E. and Wood, B. J. 1986. Structures, textures and cooling histories of Columbia River basalt flows. *Geol. Soc. Am. Bull.* **97**, 1144-1155.

Luyendyk, B. P., Kamerling, M. J. and Terres, R. 1980. Geometric model for Neogene crustal rotations in southern California. *Geol. Soc. Am. Bull.* **91**, 211-217.

Mandl, G. 1988. The mechanics of tectonic faulting; models and basic concepts. In: Zwart, H. J. (ed.), *Developments in Structural Geology*, Elsevier, Amsterdam, 407p.

Mandelbrot, B. B. 1977. *Fractals: Form, Chance and Dimension.* 365pp. W. H. Freeman, San Francisco, (revised edition, *The Fractal Geometry of Nature*, 468 pp., 1983).

Martel, S. J. 1990. Formation of compound strike-slip fault zones, Mount Abbot quadrangle, California, *Journal of Structural Geology* **12**, 869-882.

Martel, S. J. 1997. Effects of cohesive zones on small faults and implications for secondary fracturing and fault trace geometry. *Journal of Structural Geology* **19**, 835-847.

Martel, S. J. and Boger, W. A. 1998. Geometry and mechanics of secondary fracturing around small three-dimensional faults in granitic rock. *Journal of Geophysical Research* **103**, 21,299-21,314.

Martel, S. J. Pollard, D. D. and Segall, P. 1988. Development of simple fault zones in granitic rock, Mount Abbot quadrangle, Sierra Nevada, California, *Geol. Soc. Am. Bull.* **100**, 1451-1465.

Myers, R. D. and Aydin, A. 1996. Progressive fracturing and fragmentation in faults formed from joint-zones in porous sandstone. *Geological Society of America Annual Meeting. Program with Abstracts* **28**, A-254.

McGrath, A. G. and Davison, I. 1995. Damage zone geometry around fault tips. *Journal of Structural Geology* **17**, 1011-1024.

McKinstry, H. E. 1953. Shears of the second order. American Journal of Science 251, 401-414.

Mollema, P. N. and Antonellini, M. 1999. Development of strike-slip faults in the dolomites of the Sella Group, Northern Italy. *Journal of Structural Geology* **21**, 273-292.

Moody, J. D. and Hill, M. J. 1956. Wrench-fault tectonics. *Bull. Geol. Soc. Am.* **67**, 1207-.

Moore, D. E. and Lockner, D. A. 1995. The role of microcracking in shear-fracture propagation in granite. *Journal of Structural Geology* **17**, 95-114.

Morgenstern, N. R. and Tchalenko, J. S. 1967, Microscopic structures in kaolin subjected to direct shear. *Geotechnique* **17**, 309-328.

National Academy of Science, 1996. *Rock Fractures and Fluid Flow: Contemporary Understanding and Application.* 551pp. Nat. Res. Counc. Washington, D. C.

Naylor, M. A., Mandl, G. and Sijpesteijn, C. H. K. 1986. Fault geometries in basement-induced wrench faulting under different initial stress states. *Journal of Structural Geology* **8**, 737-752.

Nelson, R. A. 1985. *Geological Analysis of Naturally Fractured Reservoirs*, Gulf, Houston, Tex.

Nemat-Nasser, S. and Horii, H. 1982. Compression-induced nonplanar crack extension with application to splitting, exfoliation, and rockburst. *Journal of Geophysical Research* **87**, 6805-6821.

Nicholson, C., Seeber, L., Williams, P. and Sykes, L. R. 1986. Seismic evidence for conjugate slip and block rotation within the San Andreas fault system, southern California. *Tectonics* **5**, 629-648.

Nur, A., Ron, H. and Scotti, O. 1986. Fault mechanics and the kinematics of block rotations. *Geology* **14**, 746-749.

Okubo, P. G. and Aki, K. 1987. Fractal Geometry in the San Andreas Fault System. *Journal of Geophysical Research* **92**, 345-355.

Peacock, D. C. P. 1991. Displacements and segment linkage in strike-slip fault zones. *Journal of Structural Geology* **13**, 1025-1035.

Peacock, D. C. P. and Sanderson, D. J. 1991. Displacement and segment linkage and relay ramps in normal fault zones. *Journal of Structural Geology* **13**, 721-733.

Peacock, D. C. P. and Sanderson, D. J. 1995. Strike-slip relay ramps. *Journal of Structural Geology* **17**, 1351-1360.

Peacock, D. C. P., Price, S. P., Whitham, A. G., and Pickles, C. S. 2000. The World's biggest relay ramp: Hold With Hoe, NE Greenland. *Journal of Structural Geology* **22**, 843-850.

Pedley, H. M., House, M. R. and Waugh, B. 1976. The Geology of Malta and Gozo. *Proc. Geol. Ass.*, **87** (3), 325-341.

Petit, J. -P. and Barquins, M. 1988. Can natural faults propagate under Mode II conditions? *Tectonics* **7**, 1243-1256.

Pollard, D. D. and Segall, P. 1987. Theoretical displacements and stresses near fractures in rock: With applications to faults, joints, veins, dikes, and solution surfaces. In *Fracture Mechanics of Rock (ed. B. K. Atkinson). Academic Press Geology Series*, Academic Press. 277-349.

Pollard, D. D., Segall, P. and Delaney, P. T. 1982. Formation and interpretation of dilatant echelon cracks. *Bulletin Geological Society of America* **93.** 1291-1303.

Ramsay, J. G. and Huber, M. I. 1987. *The Techniques of Modern Structural Geology.* Volume 2. 700p.

Reches, Z. and Lockner, D. A. 1994. Nucleation and growth of faults in brittle rocks. *Journal of Geophysical Research* **99**, 18159-18173.

Riedel, W. 1929. Zur Mechanik geologischer Brucherscheinungen. *Zentrablatt. f. Mineral. Geol. u. Pal.* **1929B**, 354-368.

Rispoli, R. 1981. Stress fields about strike-slip faults inferred from stylonites and tension gashes. *Tectonophysics* **75**, T29-T36.

Rothery, E. 1988. En echelon vein array development in extension and shear. *Journal of Structural Geology* **10**, 63-71.

Scholz, C. H. 1968. Microfractures, aftershocks, and seismicity. *Seismological Society of America Bulletin* **58**, 1117-1130.

Schreurs, G. 1994. Experiments on strike-slip faulting and block rotation. *Geology* **22**, 567-570.

Segall, P. and Pollard, D. D. 1983. Nucleation and growth of strike slip faults in granite. *Journal of Geophysical Research* **88**, 555-568.

Sibson, R. H. 1985. A note on fault reactivation. *Journal of Structural Geology* **7**, 751-754.

Sibson, R. H. 1996. Structural permeability of fluid-driven fault-fracture meshes. *Journal of Structural Geology* **18**, 1031-1042.

Sims, D., Ferrill, D. A. and Stamatakos, J. A. 1999. Role of a ductile decollement in the development of pull-apart basins: Experimental results and natural examples. *Journal of Structural Geology* **21**, 533-554.

Swanson, M. T. 1988. Pseudotachylyte-bearing strike-slip duplex structures in the Fort Foster Brittle Zone, S. Maine. *Journal of Structural Geology* **10**, 813-828.

Sylvester, A. G. 1988. Strike-slip faults. *Bulletin Geological Society of America* **100.** 1666-1703.

Sylvester, A. G. and Smith, R. R. 1976. Tectonic transpression and basement-controlled deformation in San Andreas fault zone, Salton Trough, California. *American Association of Petroleum Geologists Bulletin* **60**, .

Takahashi, H. and Abe, H. 1989. Fracture mechanics applied to hot, dry rock geothermal energy, in *Fracture Mechanics of Rock* (edited by B. K. Atkinson). 241-276, Academic Press, San Diego, California

Tchalenko, J. S. 1970. Similarities between shear zones of different magnitudes. *Geol. Soc. of America Bull.* **81**, 1625-1640.

Tchalenko, J. S. and Ambraseys, N. N. 1970. Structural analysis of the Dasht-e Bayaz (Iran) earthquake fractures: *Geol. Soc. of America Bull.* **81**, 41-60.

Vermilye, J. M. and Scholz, C. H. 1999. Fault propagation and segmentation: insight from the microstructural examination of a small fault. *Journal of Structural Geology* **21**, 1623-1636.

Watterson, J. Nicol, A., Walsh, J. J. and Meier, D. 1998. Strains at the intersections of synchronous conjugate normal faults. *Journal of Structural Geology* **20**, 363-370.

Wilcox, R. E., Harding, T. P. and Seely, D. R. 1973. Basic wrench tectonics. *American Association of Petroleum Geologists Bulletin* **57**, 74-96.

Willemse, E. J. M., Peacock, D. C. P. and Aydin, A. 1997. Nucleation and growth of strike-slip faults in limestones from Somerset, U. K. *Journal of Structural Geology* **19**, 1461-1477.

Willemse, E. J. M. and Pollard, D. D. 1998. On the orientation and patterns of wing cracks and solution surfaces at the tips of a sliding flaw or fault. *Journal of Geophysical Research* **103**, 2427-2438.

Winnock, E. 1981. Structure du Bloc Pelagien. In: *Sedimentary Basins of Mediterranean Margins* (edited by Wezel f. C.). Technip, Bologna, 445-464.

Zhang, P., Slemmons, D. B. and Mao, F. 1991. Geometric pattern, rupture termination and fault segmentation of the Dixie Valley-Pleasant Valley active normal fault system, Nevada, U. S. A. *Journal of Structural Geology* **13**, 165-176.

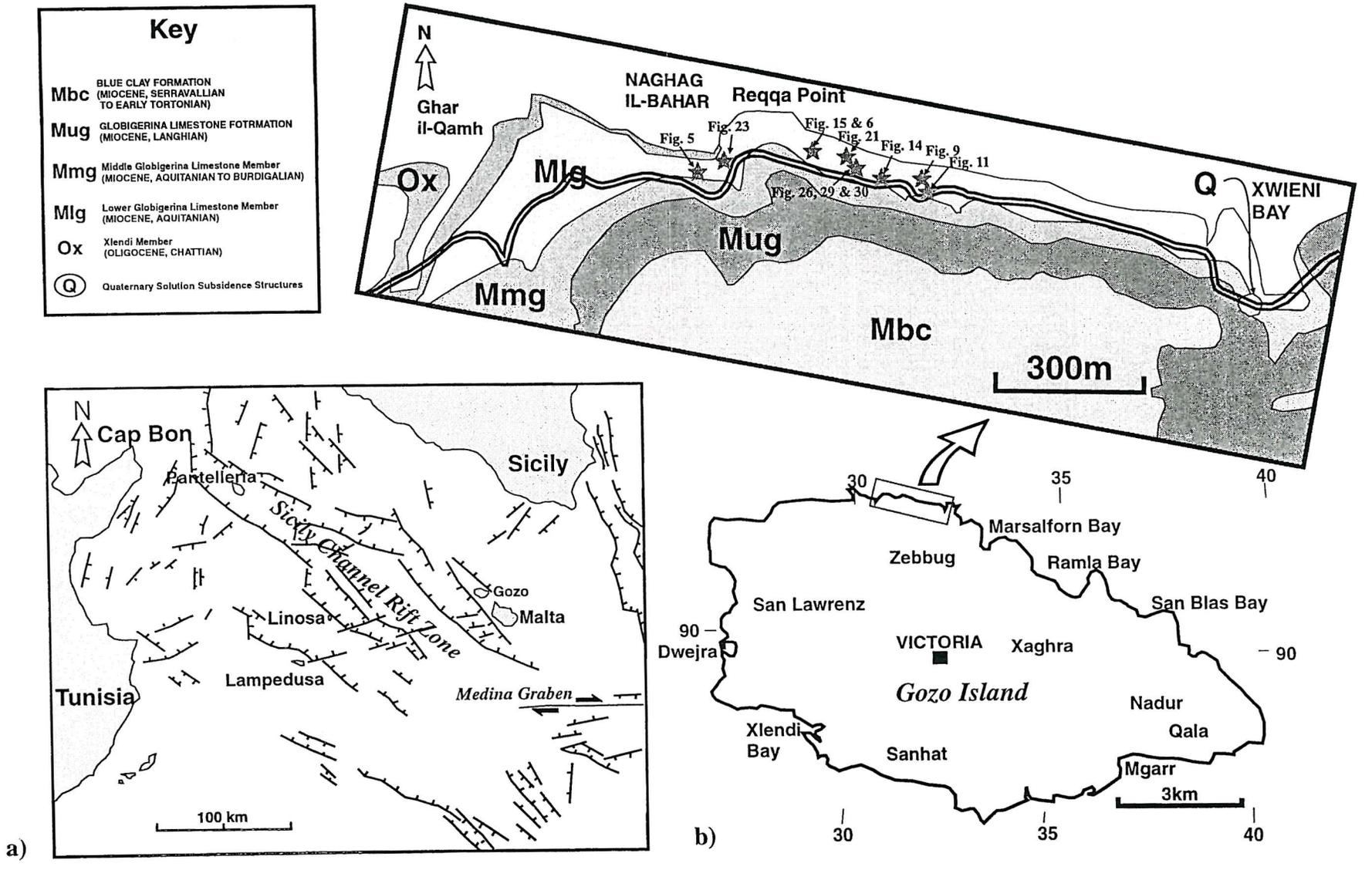

Fig. 4.1. a) Structural sketch map of the Sicily Channel Zone and the Pelagian Block (modified from Finetti, 1984; Boccaletti *et al.*, 1987). b) Locality map and geological map of the studied area, the west of Marsalforn, Gozo, Malta. The studied section is between Reqqa Point ($^{4}312\ ^{39}935$) and Xwieni Bay ($^{4}325\ ^{39}932$). The host rock is the Lower Globigerina Limestone Member (Miocene). Some of the mapped locations are denoted on the geological map.

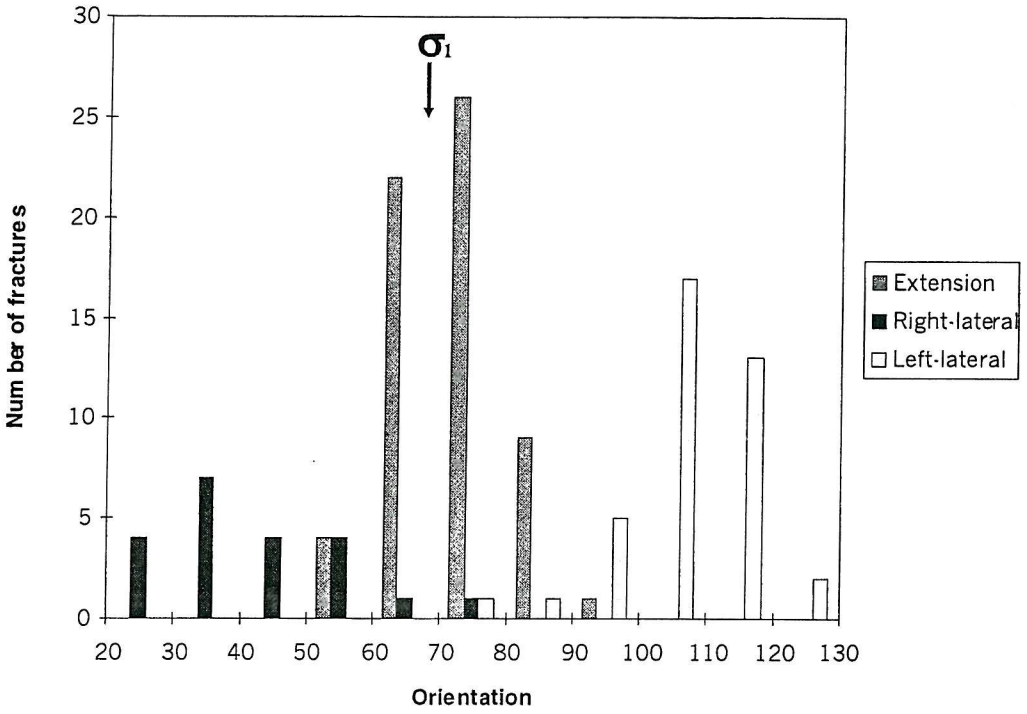

Fig. 4.2. Orientation of faults and fractures in the studied area. Right-lateral strike-slip faults range from N030° to N070°, left-lateral strike-slip faults range from N060° to N120° and extensional faults concentrated between N060° and N080°. Inferred maximum compressive stress (σ_1) is about N070°.

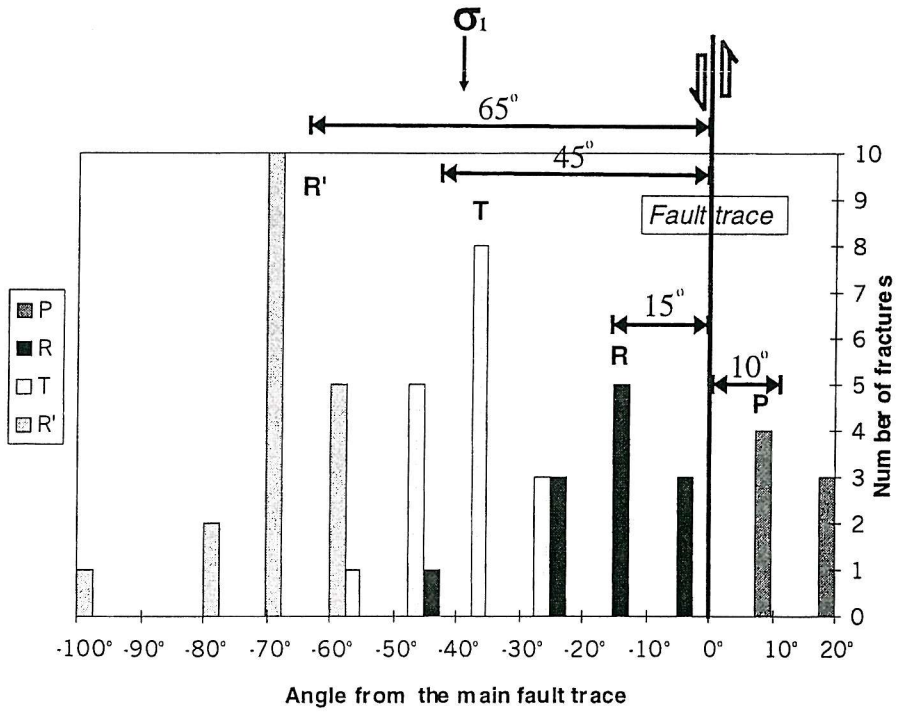

Fig. 4.3. Angular relationship of fracture orientations to each master fault in the studied area referenced to a left-lateral strike-slip fault. Positive (+) values indicate clockwise from each master fault and negative (-) values indicate anticlockwise from each master fault for left-lateral strike-slip sense. Antithetic Riedel shears concentrate between -75° and -50°, extensional fractures range from -50° to -25°, Riedel shears range from -25° to -05° and P shears range from 05° and 020°. The average intersection angle of master fault and extensional fracture is about 40°.

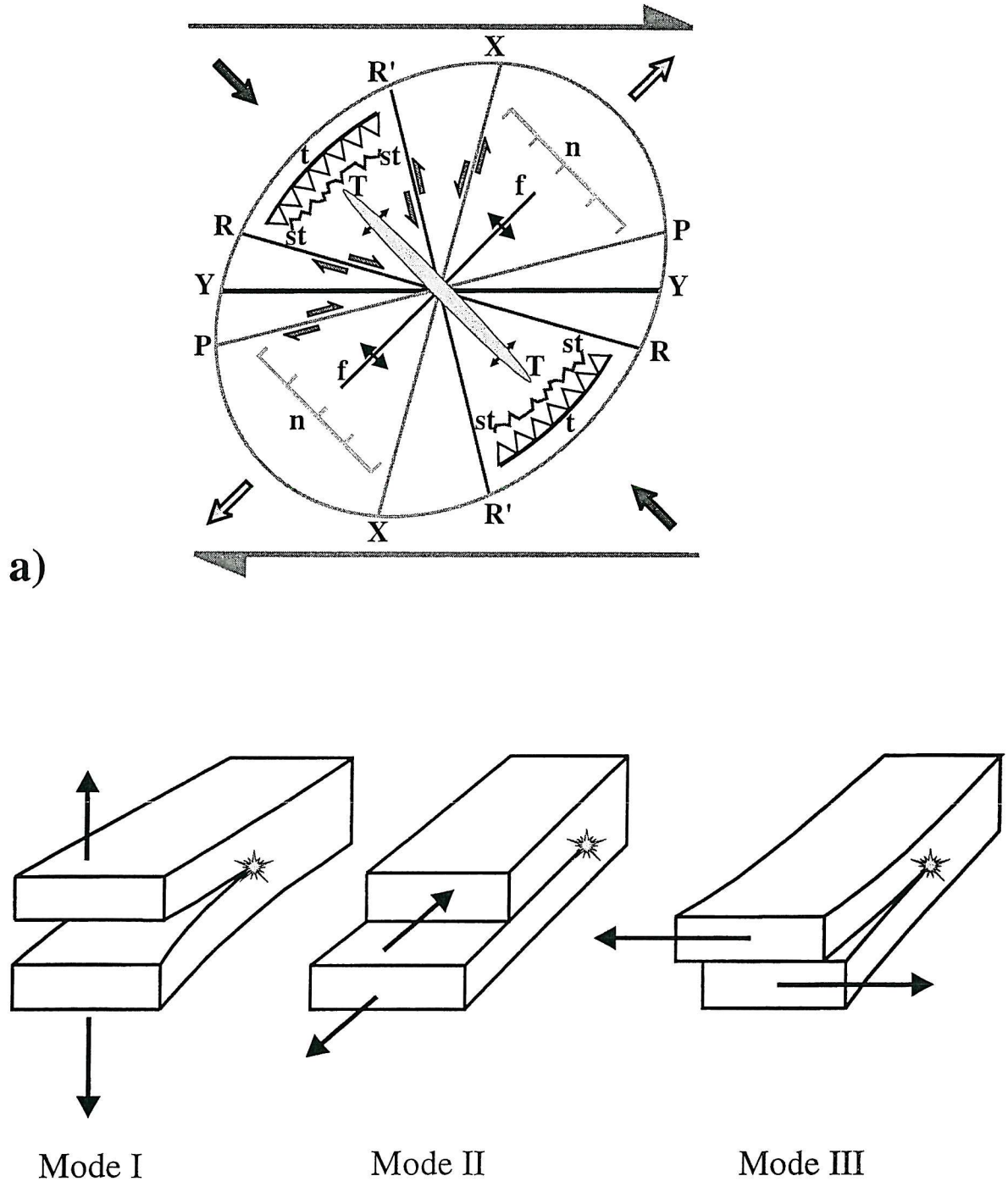

Fig. 4.4. a) Compilation diagram illustrating structures that tend to form in right-lateral simple shear under ideal conditions, compiled from clay-cake models and from geological examples (modified from Wilcox *et al.*, 1973; Tchalenko and Ambraseys, 1970; Bartlett *et al.*, 1981; Hancock, 1985). *R* and *R'*, Riedel and antithetic Riedel shears; *P, X* and *Y, P-, X-* and *Y*-shears; *T*, extension fracture; *n*, normal fault; *t*, thrust; *st*, stylolite; *f*, fold. b) Schematic drawing illustrating the three fundamental modes of fracture. Mode I, tensile or opening mode; Mode II, in-plane shear or sliding mode; Mode III, anti-plane shear or tearing mode (modified from Lawn and Wilshaw, 1975).

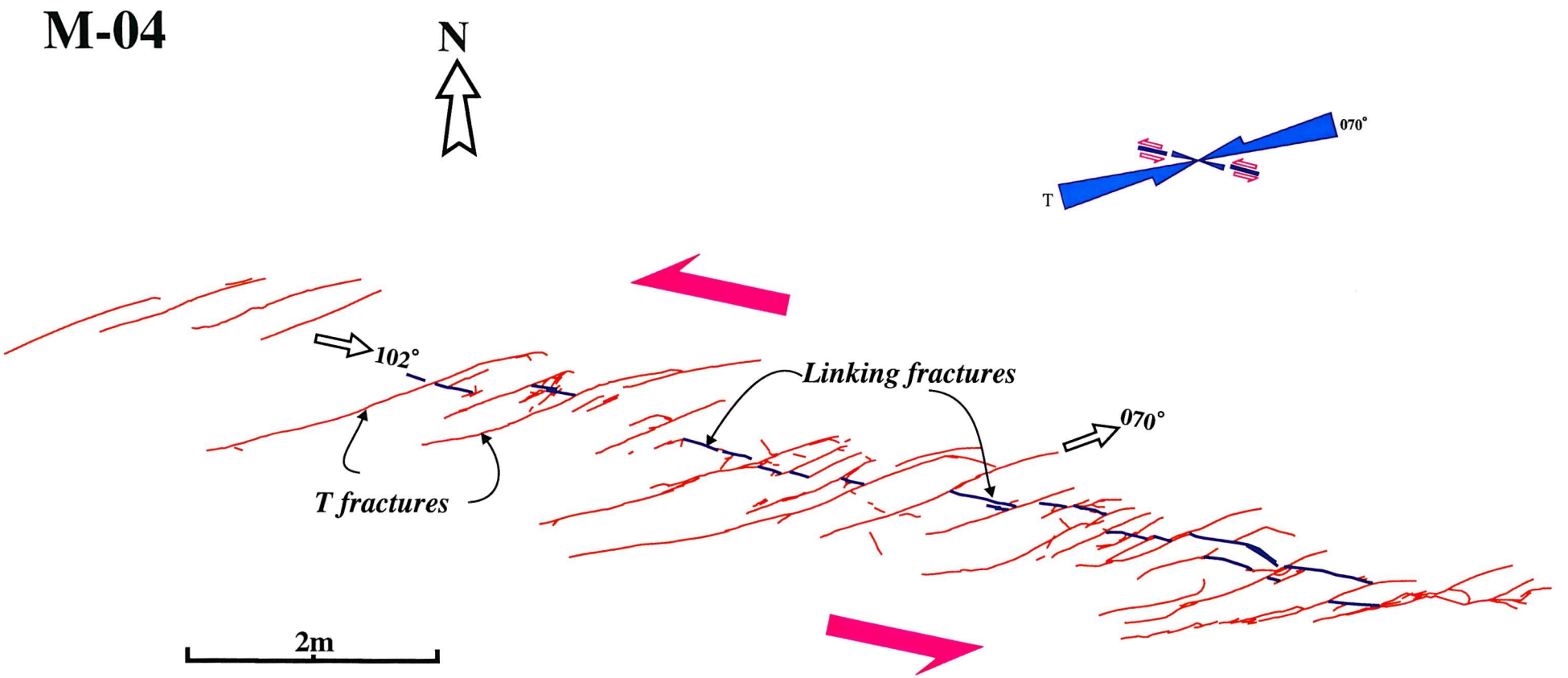

Fig. 4.5. A extensional fracture dominated fault map in the studied area. The whole fault system is about 12 m in length along the mean fault trend. The master fault trend is N102° and the predominant fractures are extensional fractures striking N070°. Some of the fractures show sigmoidal shapes and tail cracks at the fracture tips implying later rotation. Some linking fractures occur crossing the tensional fractures, which are later than the tensional fractures. This fracture pattern is similar to fracture patterns produced in experimental studies (Cox and Scholz, 1988).

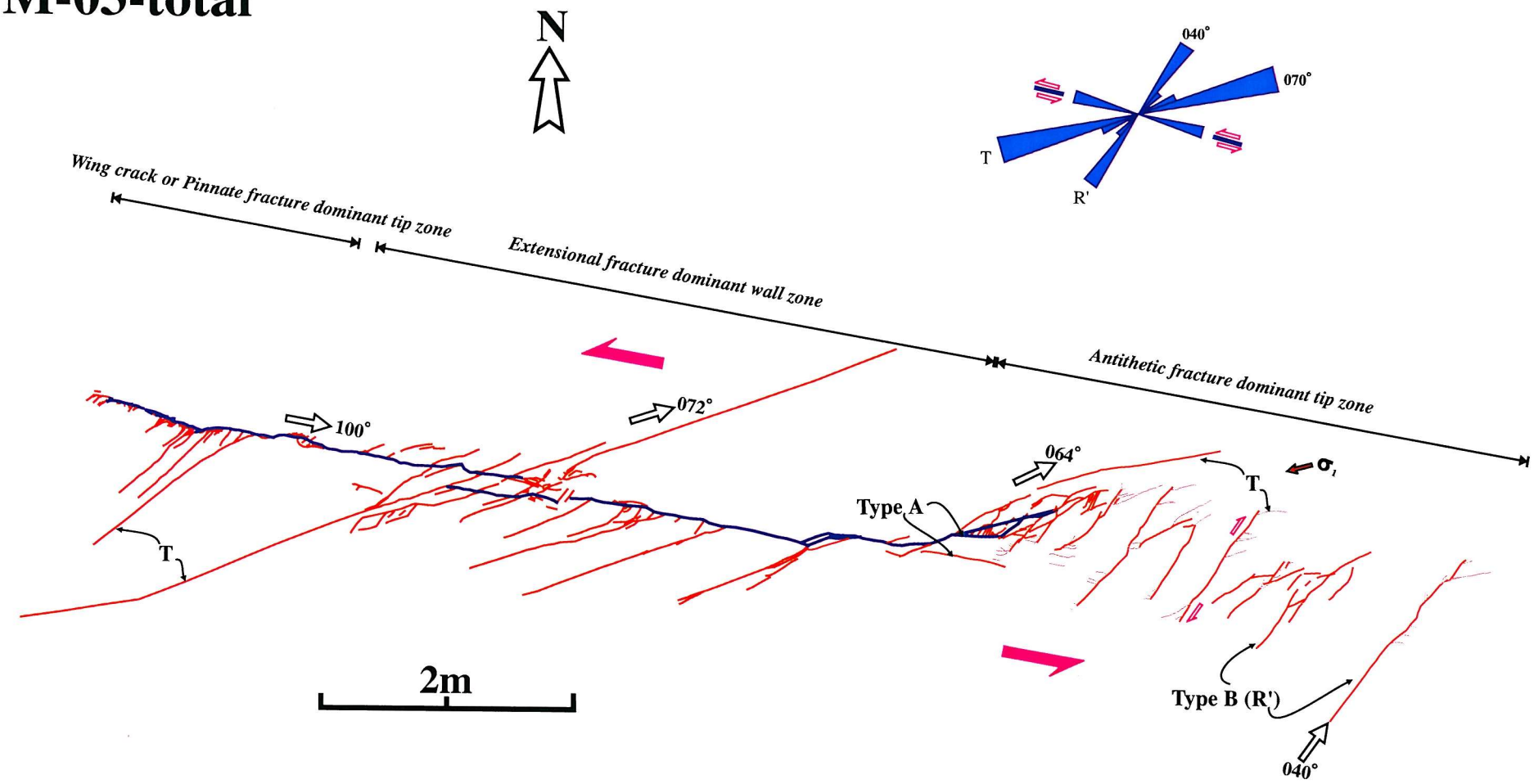

Fig. 4.6. Map showing a well exposed left-lateral strike-slip fault trending N100°. It shows a 13 m long left-lateral fault with several secondary fracture patterns. The fault can be divided into three parts according to the style of damage zone fractures; i) wing crack or pinnate style dominated fracturing, ii) extentional dominated fracturing and iii) antithetic dominated fracturing.

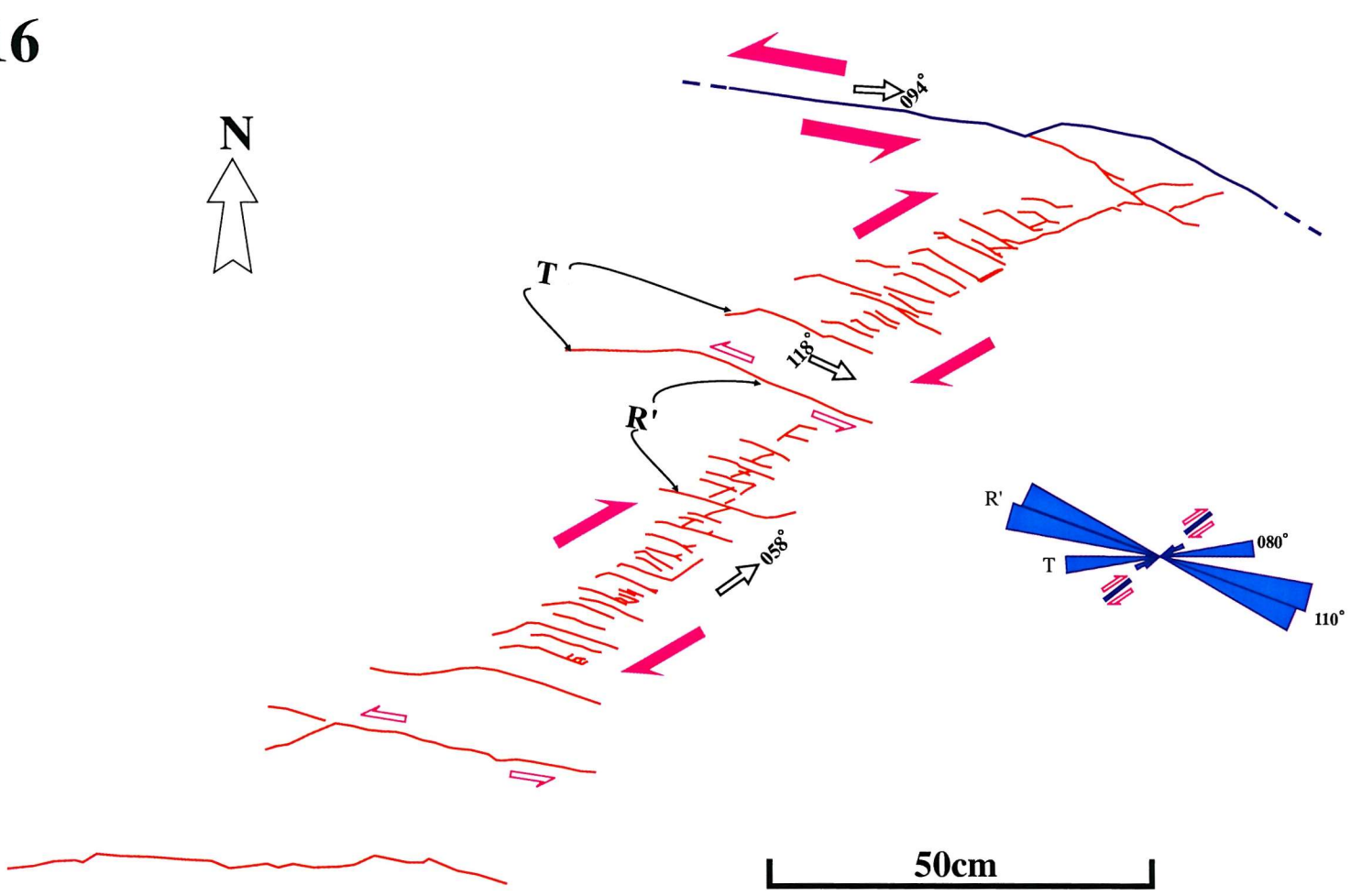

Fig. 4.7. A map showing right-lateral shear zone array defined by antithetic fractures. The trend of the shear zone with right-lateral slip is N058°, and the mapped shear zone is about 2 m in length. Some of the tips of the antithetic fractures are kinked indicating slip sense. The zone consists of two wedge-shaped zones slightly offset from each other.

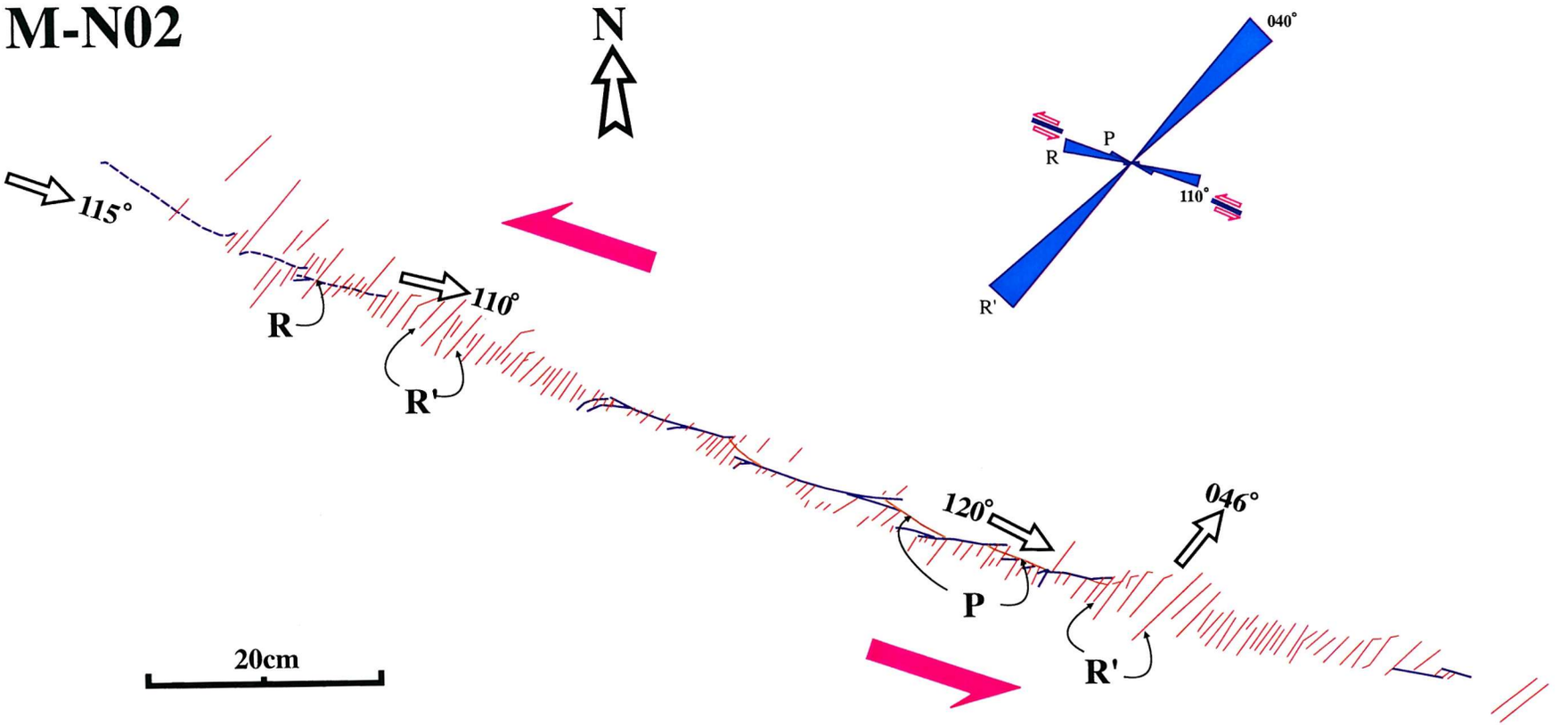

Fig. 4.8. A map showing a segmented left-lateral fault trending N115° with associated damage zone. In the damage zone, en echelon antithetic shear fractures (R') or extension fractures (T) trending N045° predominate. The main shear zone is about 1.2 m in length. Though antithetic shear fractures are predominate, there are some R shears (segments) and P shears linking segments.

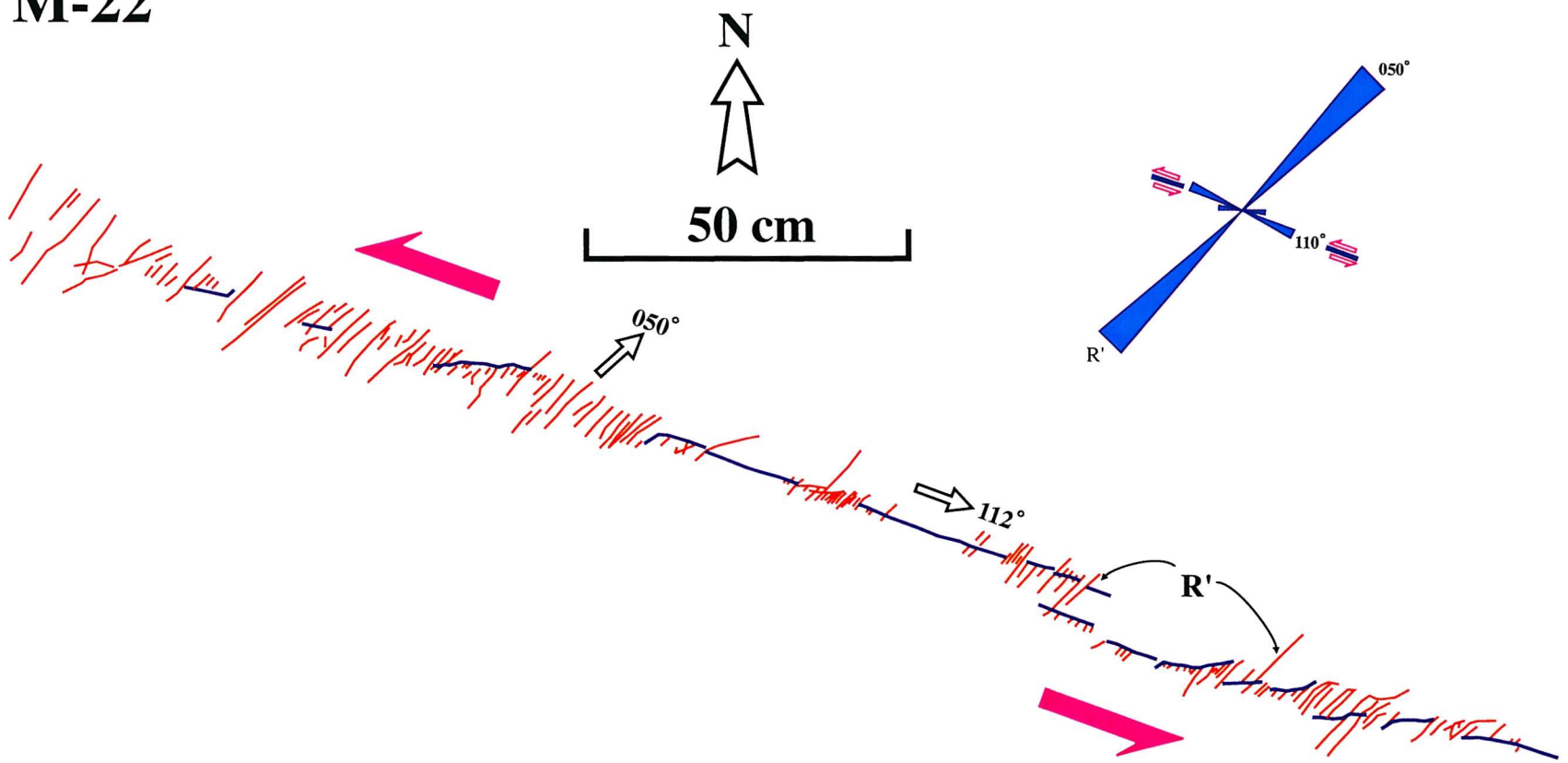

Fig. 4.9. A map showing a left-lateral fault segments with arrays of damage zone fractures. Although this map shows some along-strike tip damage patterns at the end of the fault zone, it mostly shows a up- or down dip tip damage pattern with en echelon antithetic shear fractures (R') or extension fractures (T) trending N050°. The main trend of the segment fault array is N112°, and the whole length of the damage zone is about 2.5 m. The damage zones do not form wedge-shaped fracture patterns, however, at the tips of the fault segments, there is a tendency to form incipient wedge-shaped array pattern.

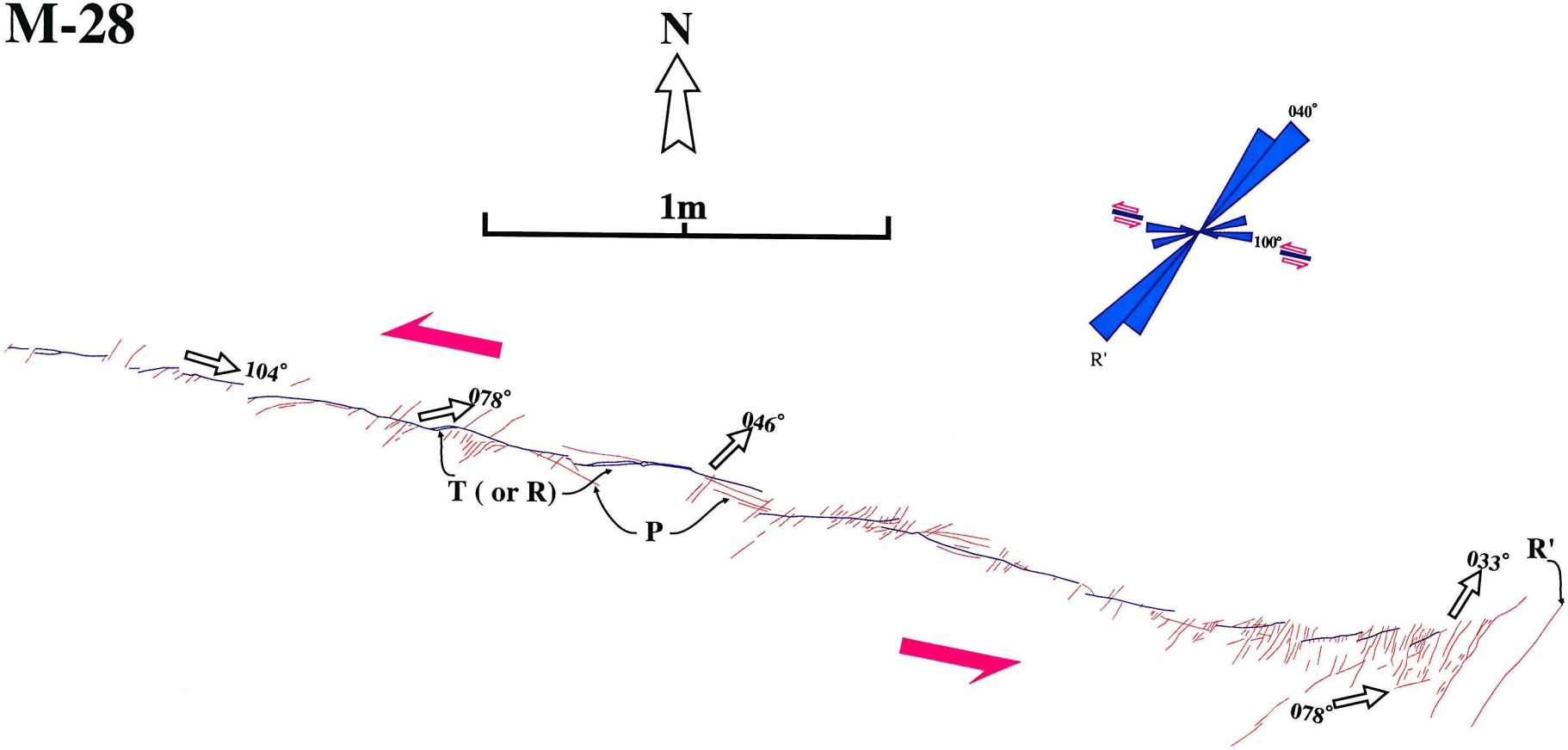

Fig. 4.10. An isolated left-lateral strike-slip fault striking N104° which shows with two well exposed tips. It is about 4 m long. One tip shows a wedge-shaped tip damage zone. Several segments are linked with antithetic shear fractures in the central part of the fault.

M-07

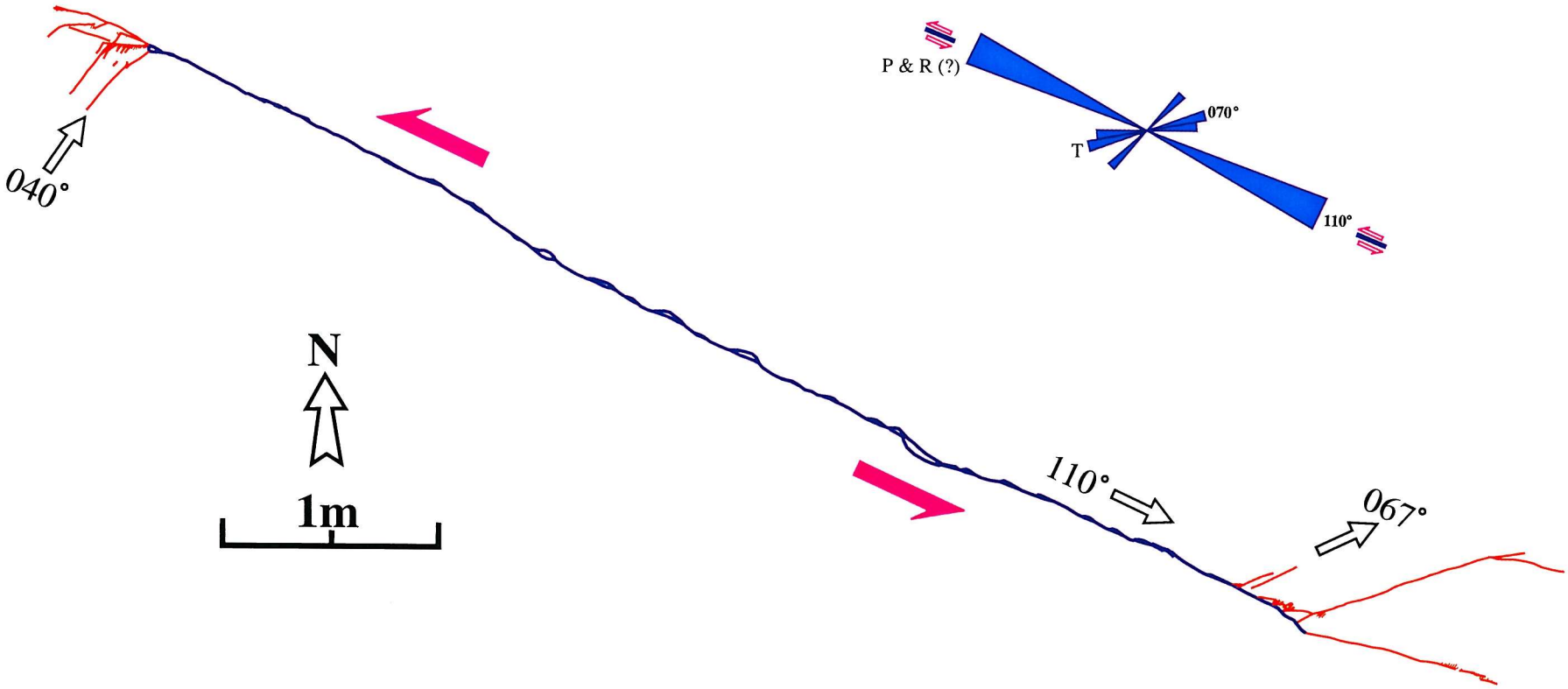

Fig. 4.11. A left-lateral strike-slip fault. It is about 8 m long, and the whole fault trace is exposed. The general trend of the fault is about N110° and shows some tip fractures around N070° and N040° at the fault tips. The orientational difference may reflect local stress redistribution.

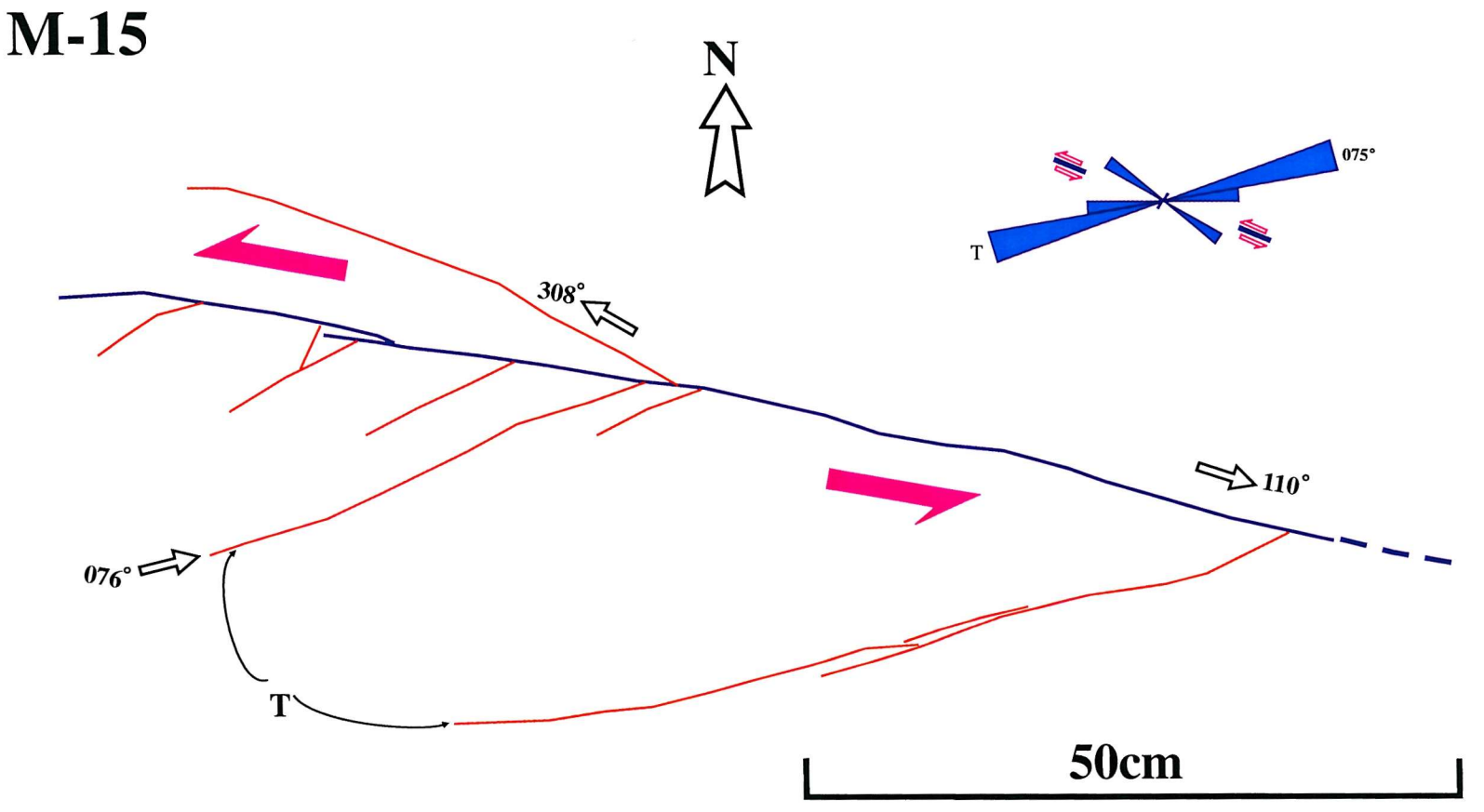

Fig. 4.12. A left-lateral fault showing branch style tip damage structures (Type A of Chinnery, 1966b). The trend of the main left-lateral strike-slip fault is N110°, and the mapped damage zone is about 1 m in length. Most of the branch faults are developed in the dilational quadrant.

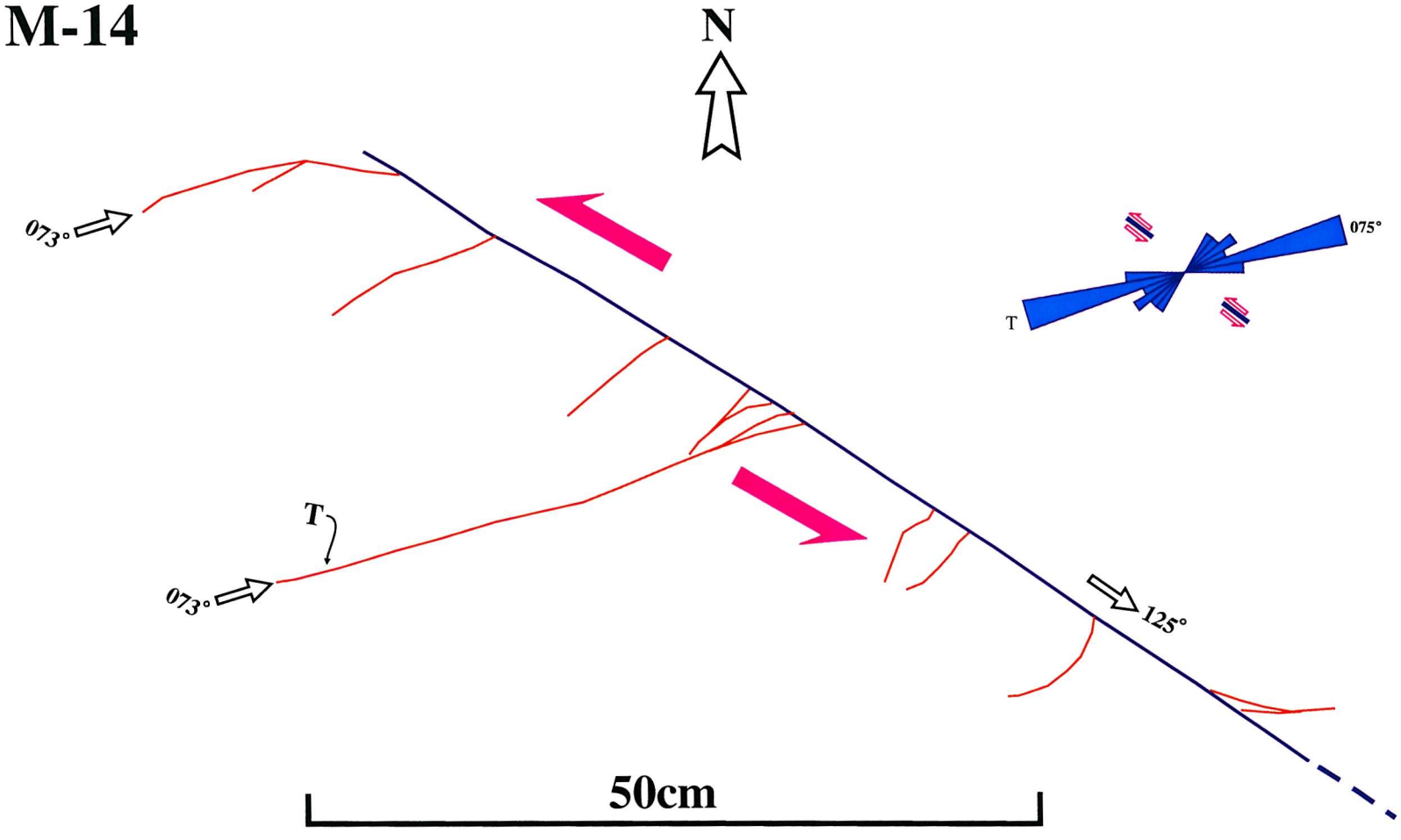

Fig. 4.13. A left-lateral fault showing two types of extensional fractures around the fault tip. The trend of the main left-lateral strike-slip fault is N125°, and the mapped damage zone is about 1 m in length. Long fractures strikes about N073°, whilst shorter fractures show high angular relationships to the master fault. Most of the fractures are developed in the dilational quadrant.

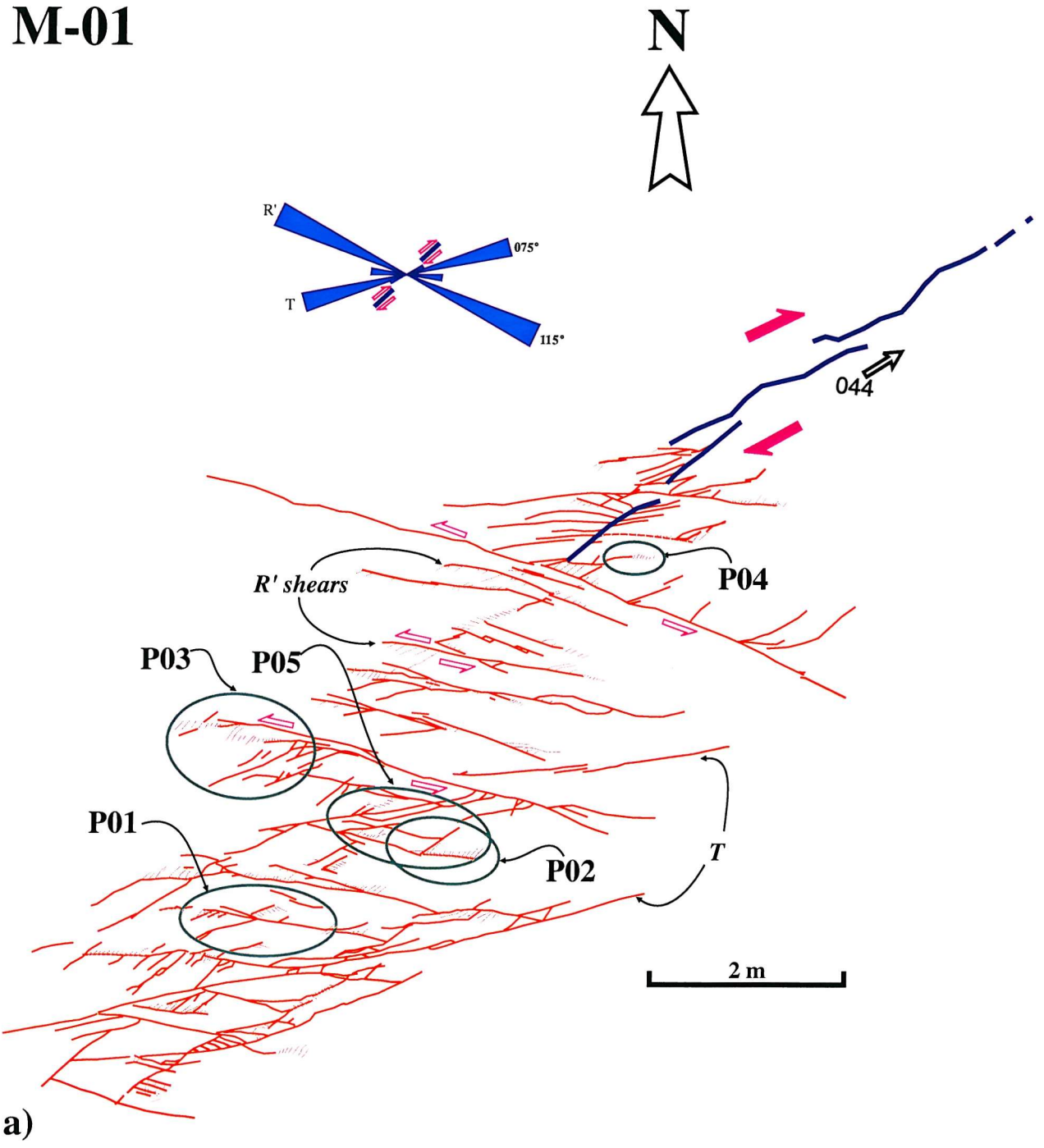

Fig. 4.14. A map showing intensive along-strike tip damage striking N044°. a) Map of the whole tip damage zone showing two orders of secondary fracturing. The exposed main fault is about 19 m in length and the mapped damage zone shows extensive damageof about 10 m parallel to the fault trend. The dominant structures in the tip region are antithetic shears striking N110° - 120° (type B or R'), which are the most common secondary fractures. Synthetic shears (type A) and extensional fractures (T) striking N070° - N080° also occur, but tend to be shorter and less frequent. It is taken from oblique photo. b), c), d), e) and f) Detailed maps of the secondary fractures. Synthetic branchfractures and antithetic fractures are dominant secondary fractures. R and R', Riedel shears; P, P-shear; σ_1, maximum compressive stress.

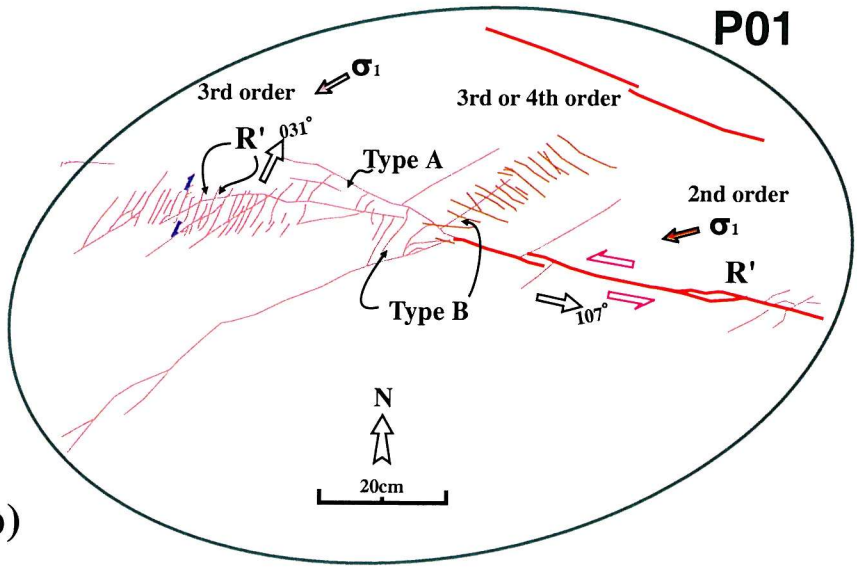
P01
3rd order
σ1
3rd or 4th order
R'
031°
Type A
2nd order
σ1
R'
Type B
107°
N
20cm

b)

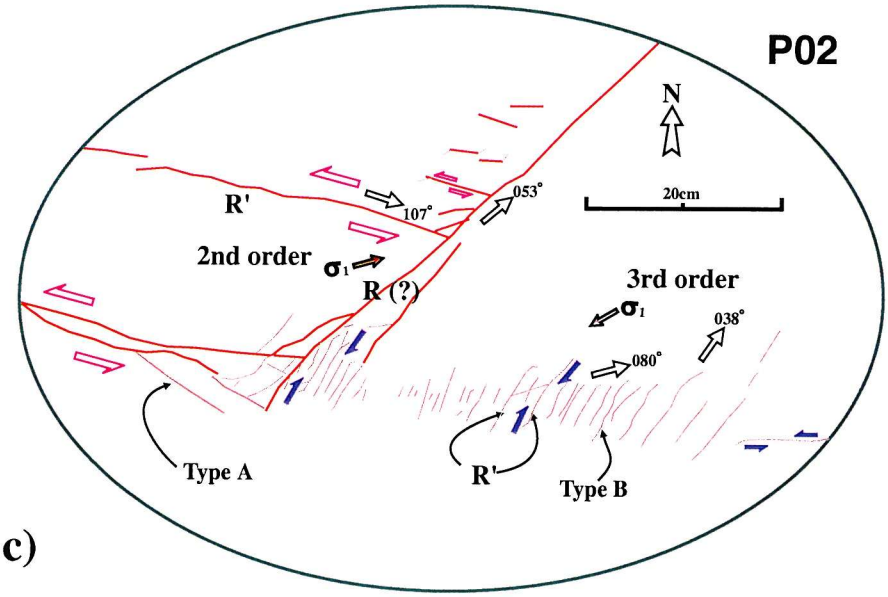
P02
N
20cm
R'
107°
053°
2nd order
σ1
R (?)
3rd order
σ1
038°
080°
Type A
R'
Type B

c)

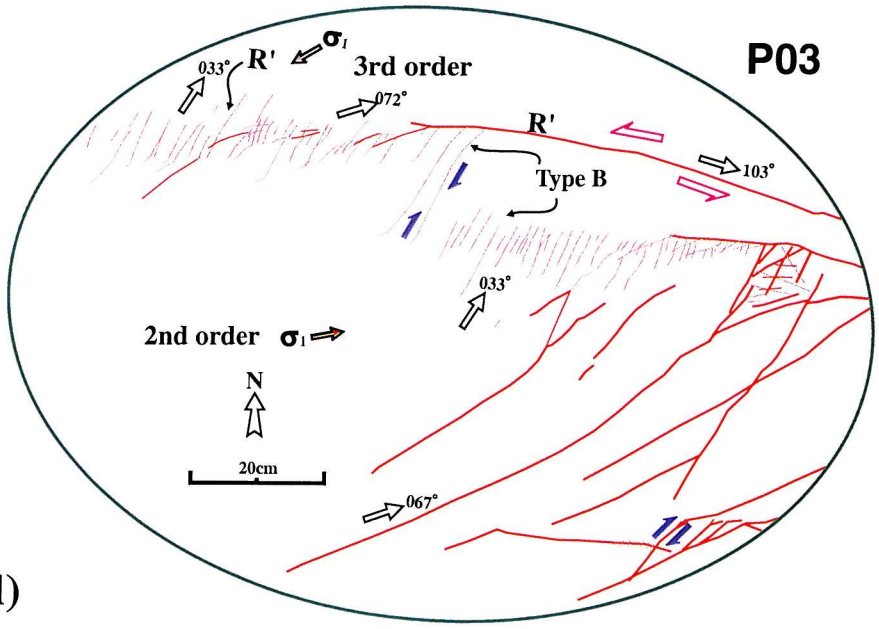
P03
033°
R'
σ1
3rd order
072°
R'
Type B
103°
033°
2nd order
σ1
N
20cm
067°

d)

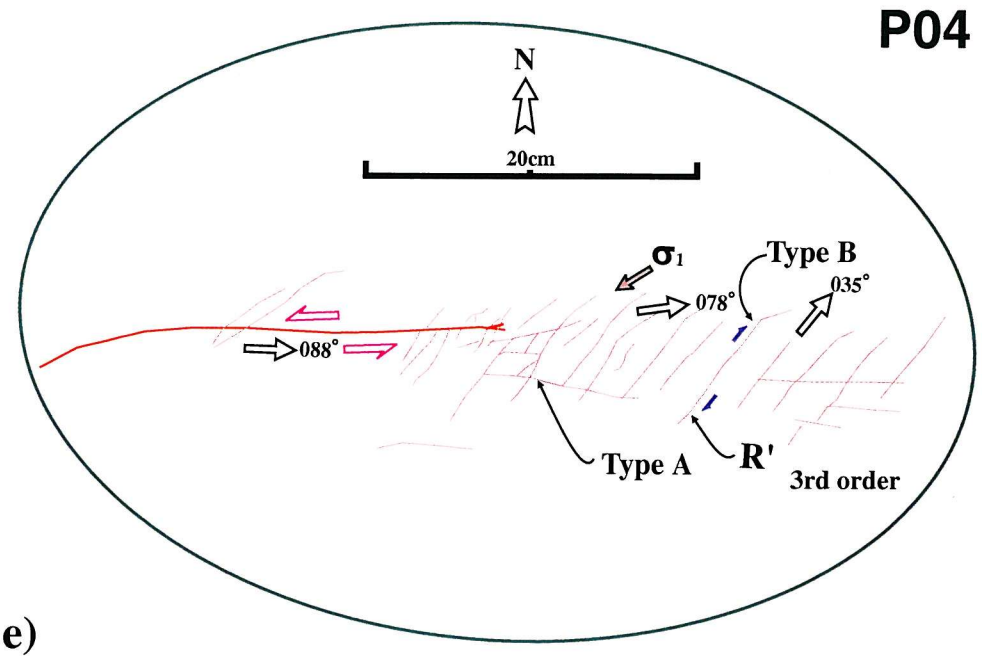
P04
N
20cm
σ1
Type B
078°
035°
088°
Type A
R'
3rd order

e)

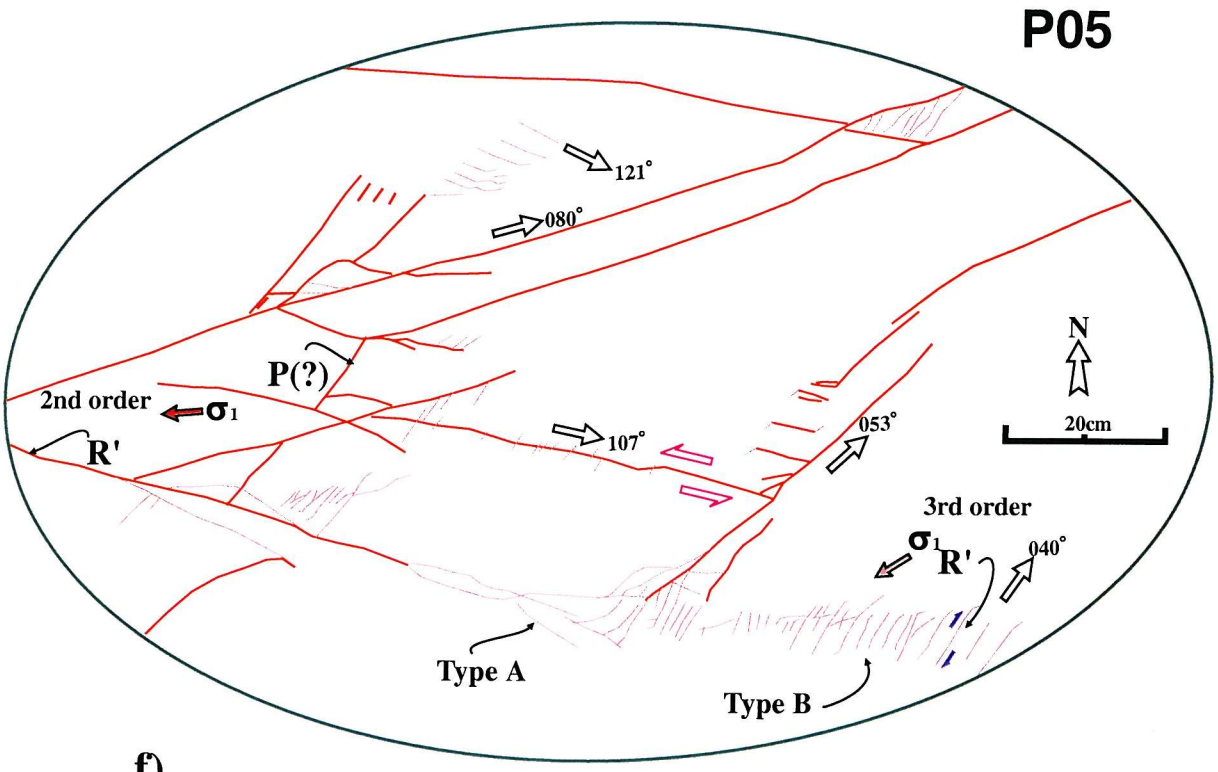
P05
121°
080°
P(?)
2nd order
σ1
R'
107°
053°
N
20cm
3rd order
σ1
R'
040°
Type A
Type B

f)

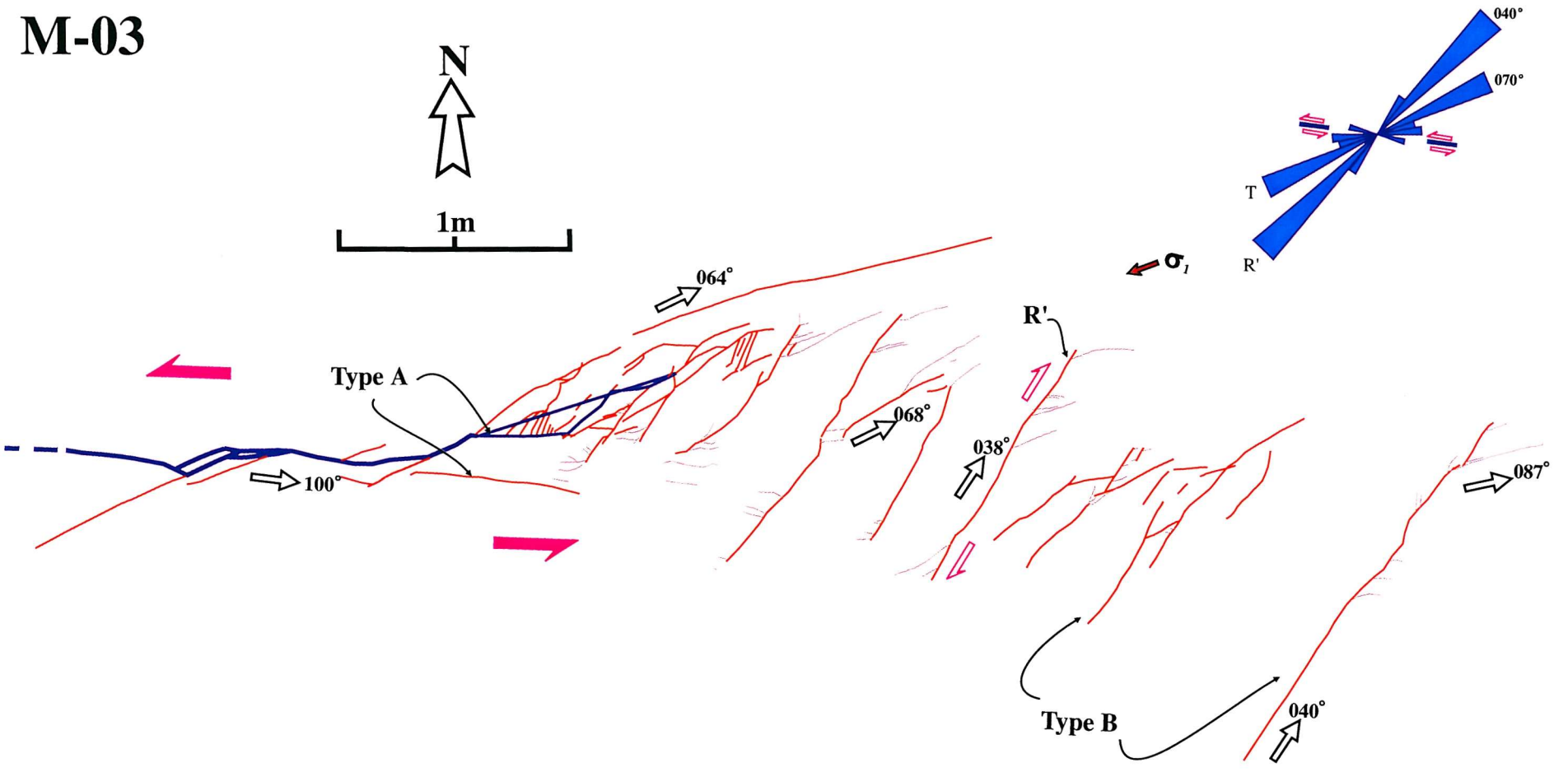

Fig. 4.15. Tip damage structures associated with a left-lateral strike-slip fault striking N100°. It shows generally increasing lengths of the antithetic fractures away from the main fault tip. Some connecting fractures and higher order secondary fractures are developed. Tip cracks at the termination of antithetic fractures indicate the slip sense of the fractures.

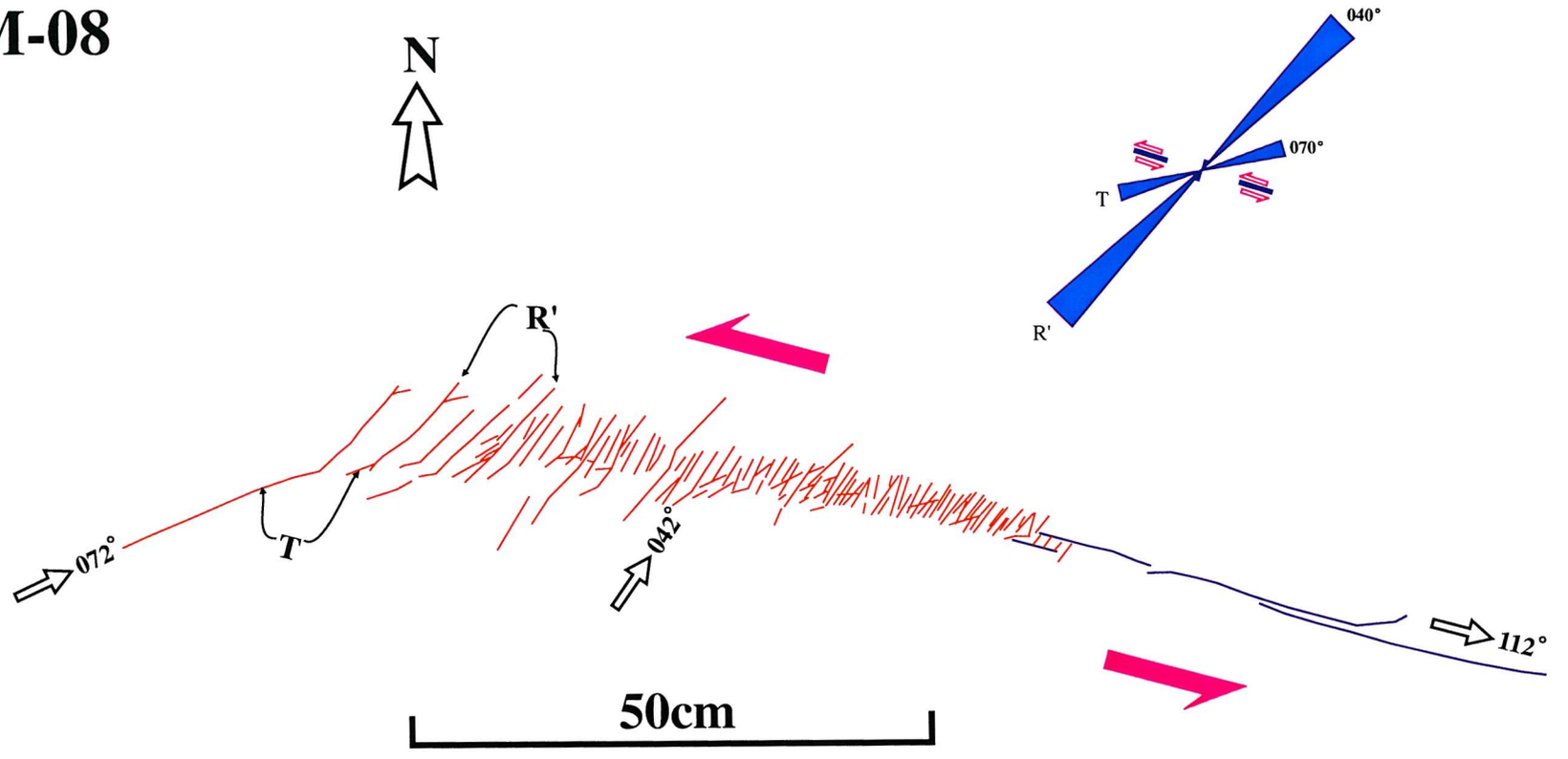

Fig. 4.16. Map of a left-lateral fault tip trending about N110°. The exposed tip damage zone is about 1 m long. It shows en echelon antithetic shear fractures at the western fault tip. Both the length and spacing of antithetic fractures increase away from the fault tip producing a wedge-shaped pattern.Tip cracks at some of antithetic fracture tips indicate a right-lateral sense. Some T fractures occur intersect the antithetic shear fractures.

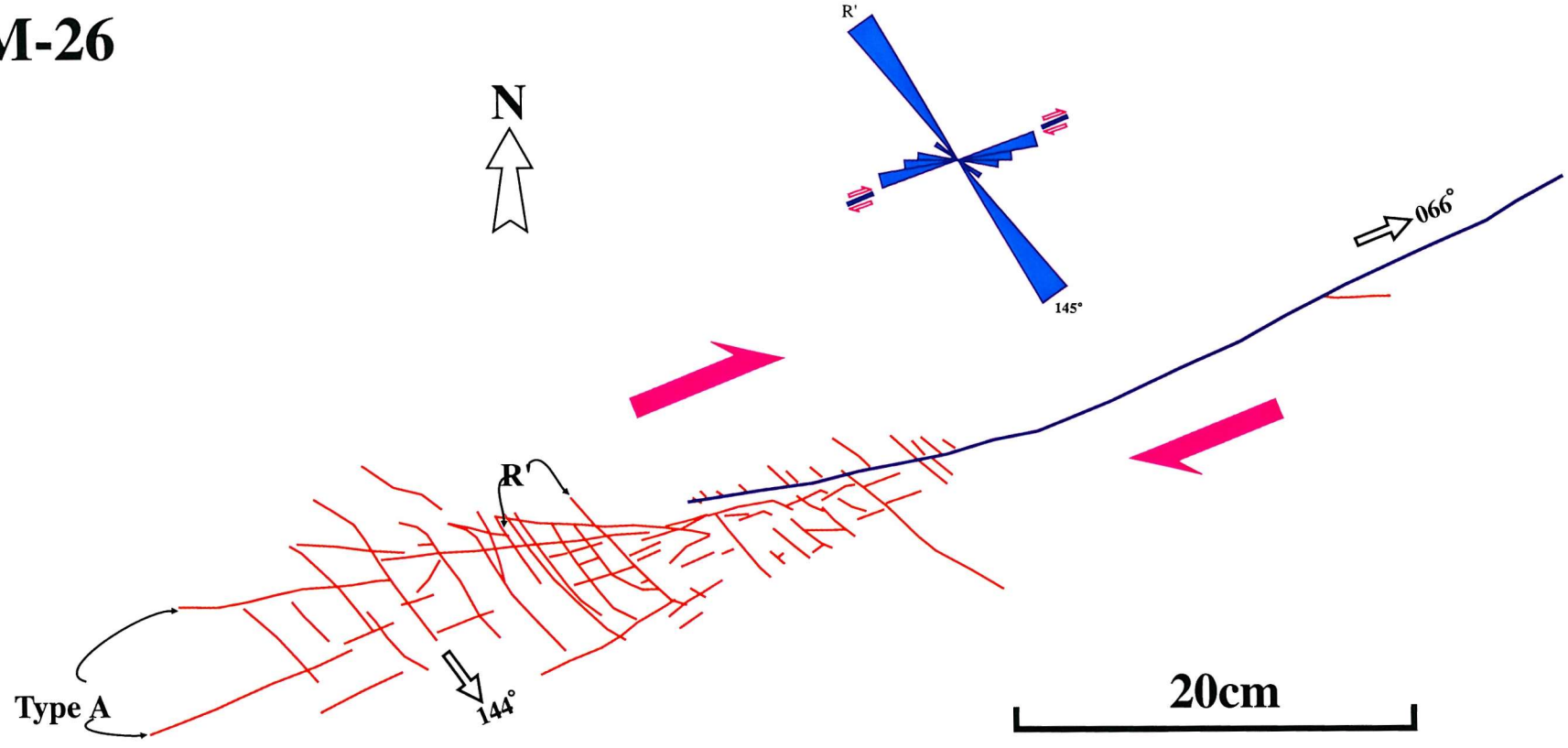

Fig. 4.17. A right-lateral fault with tip damage zone at western termination. The master fault is bent at the tip towards the dilational quadrant. The tip damage zone consists of en echelon antithetic shear fractures and some branch fractures at the fault tip. The main fault strikes N066°, branch faults have a mean trend of N080° and antithetic shear fractures have a mean trend of N145°. The antithetic shears generally increase in length away from the tip producing a wedge-shaped pattern.

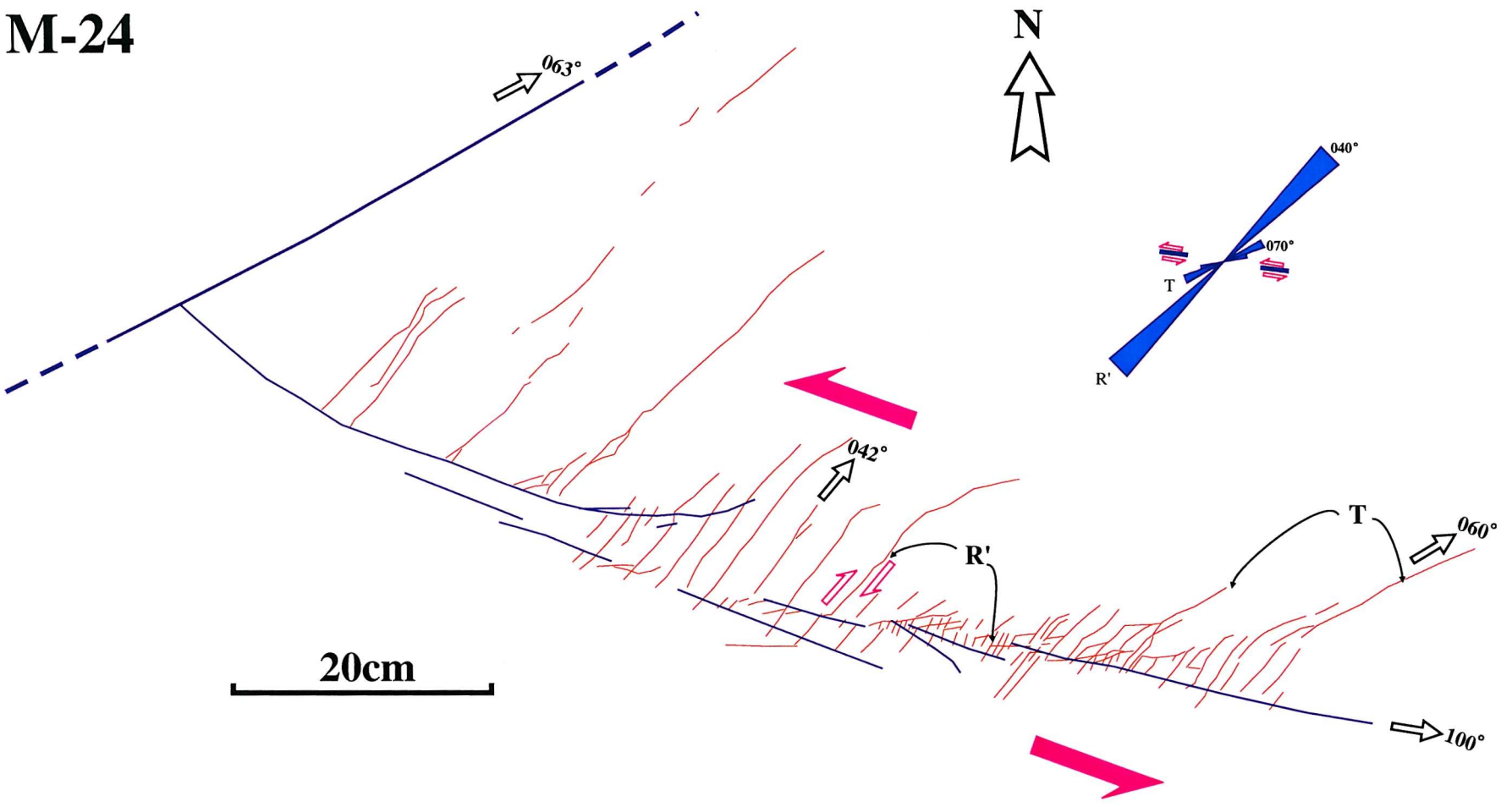

Fig. 4.18. A segmented left-lateral branch fault which displays predominantly wedge-shaped zones of antithetic fractures. The trend of the fault is N100°. The approximately 1 m long left-lateral branch fault interacts a larger right-lateral strike-slip fault striking N063°. Some secondary antithetic fractures show sigmodal shapes indicating a right-lateral slip sense.

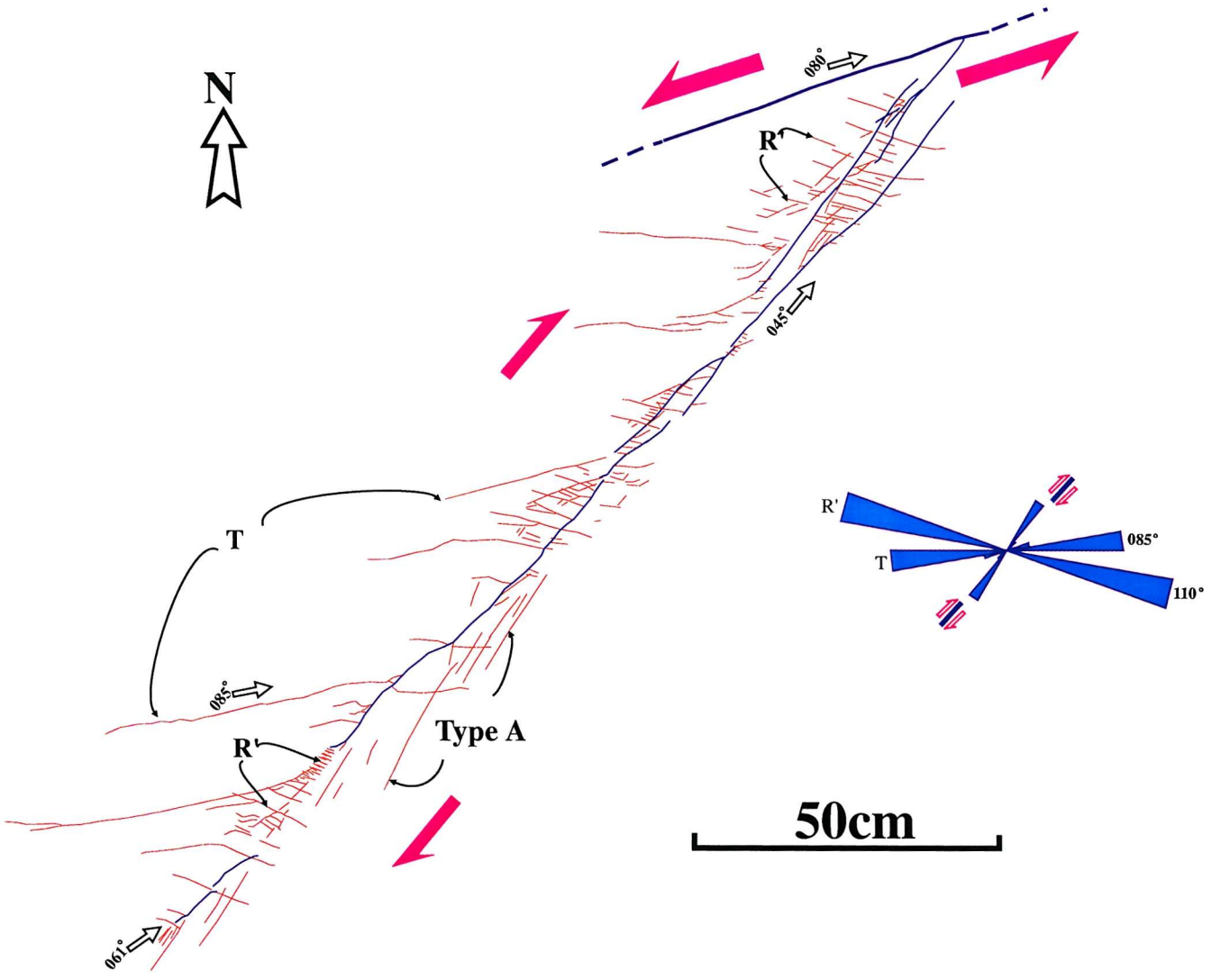

Fig. 4.19. A right-lateral branch fault (striking N045°) joining a left-lateral fault at its NE termination. It is about 3 m long. The south-western fault tip shows a mixed fracture pattern with branch faults and antithetic shear fractures. It shows several wedge-shaped tip damage structures combined with long extensional fractures.

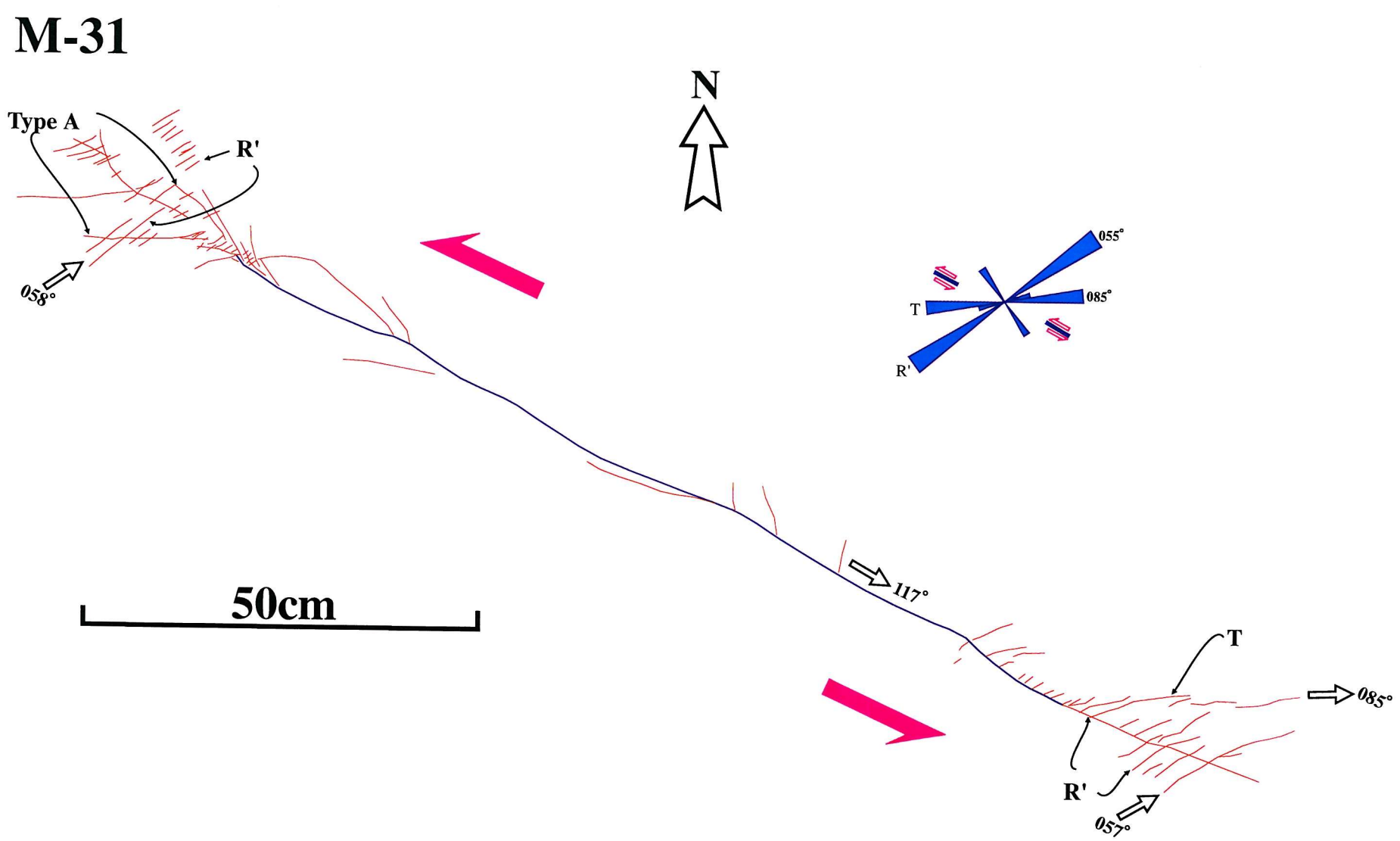

Fig. 4.20. Map showing an entirely exposed left-lateral fault zones with predominant wedge-shaped antithetic fracture pattern at the fault tips. It shows a left-lateral fault striking N117° exposed over its whole fracture length of 2 m. Some branch faults combined with antithetic fractures at the western tip.

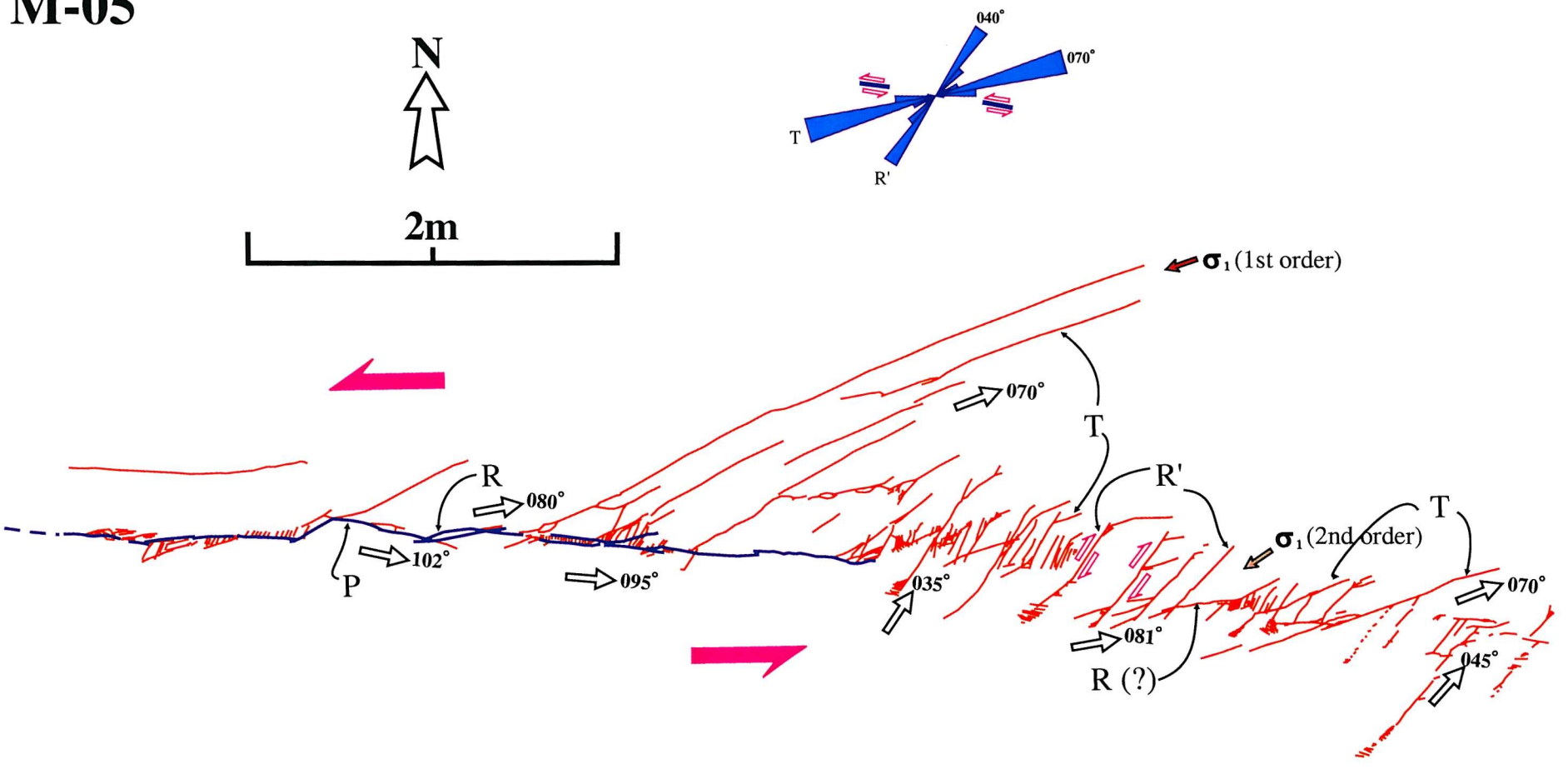

Fig. 4.21. Tip damage structures at the termination of a left-lateral strike-slip fault. The eastern tip damage zone for the left-lateral fault system is about 6 m long. The segmented main fault strikes about N100°, and has several long extensional fractures and smaller antithetic (right-lateral) fractures striking N070° and about N040°, respectively. Some long extensional fractures are developed at the tip parallel to σ_1. Some connecting fractures and higher order secondary fractures are developed. Tip cracks at the tips and sigmoial shapes of antithetic fractures indicate the slip sense of the fractures.

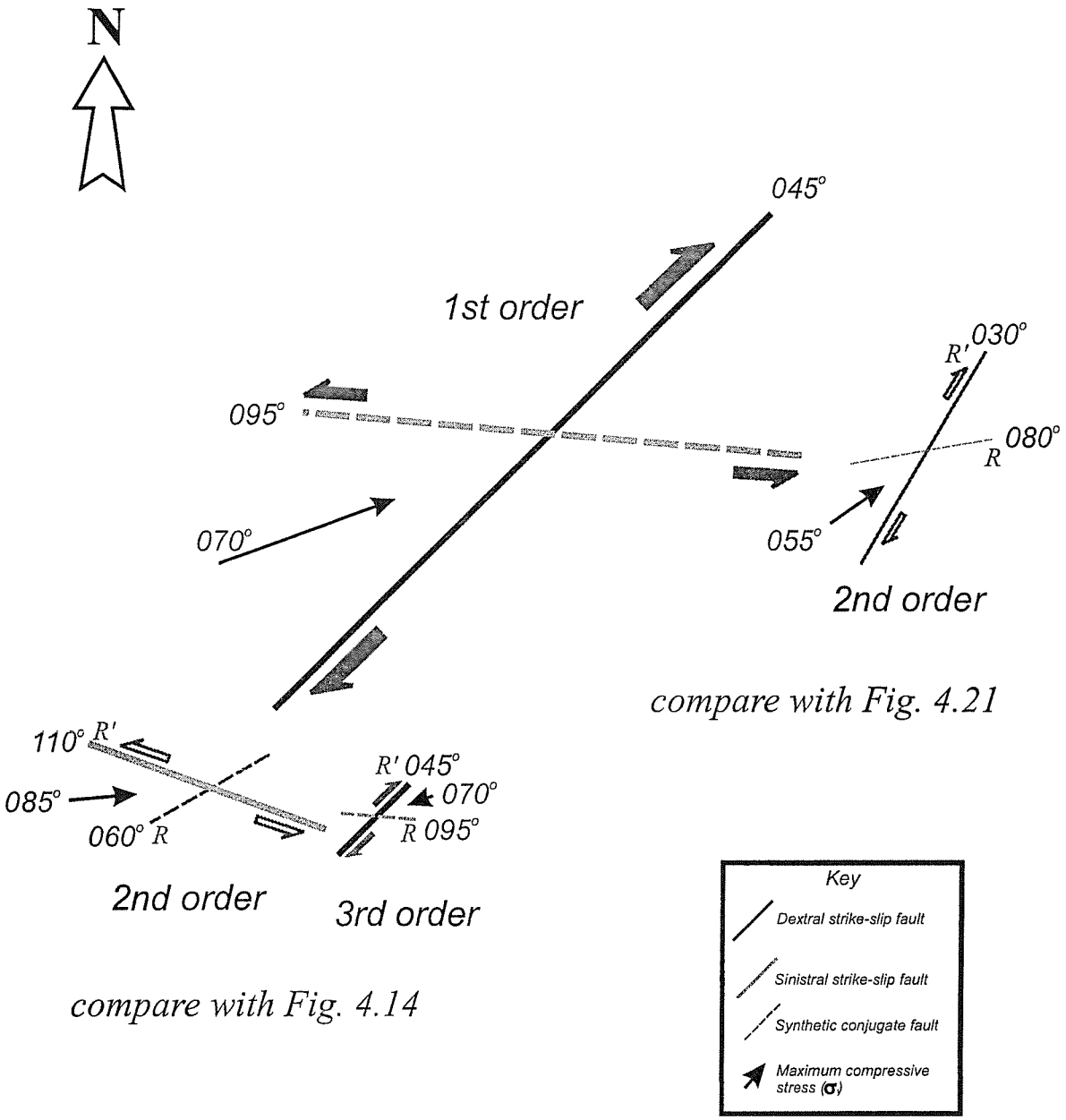

Fig. 4.22. Schematic description of the angular relationships and geometry of fractures with orders in tip damage. The stress distribution changes depending on the order of fracture generation. The main developing faults in higher order shows antithetic sense to the lower order main fault. The thickness of lines indicates the possibility of development, and dashed line is a synthetic conjugate fault set.

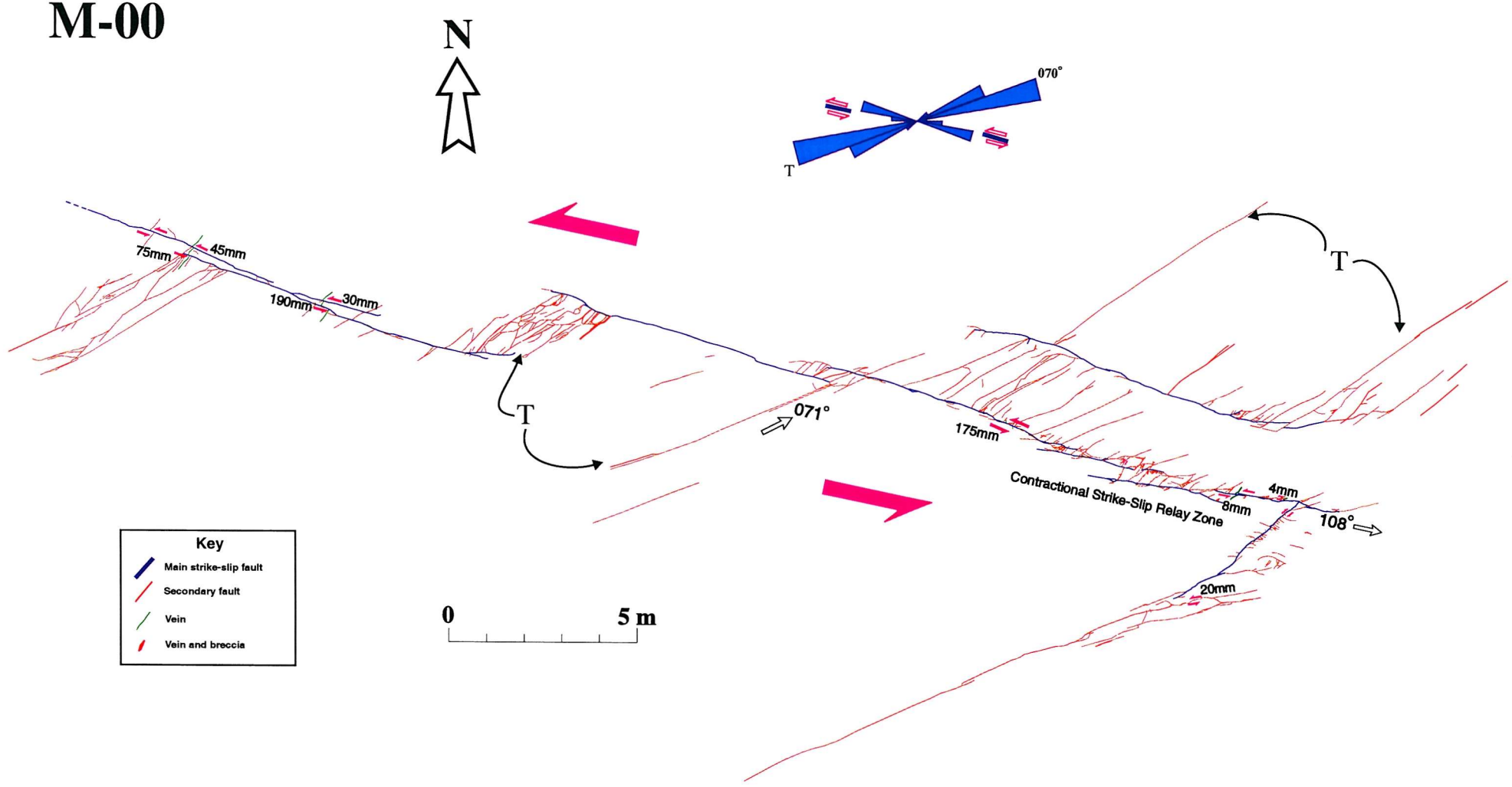

Fig. 4.23. Map of a left-lateral strike-slip fault system. Several fault segments are linked through mainly dilational oversteps with extensional secondary fractures. The segments are sub-parallel and have an average trend of N108. The length (L) of the whole fault system is over 30 m. Linkage zones show high fracture densities.

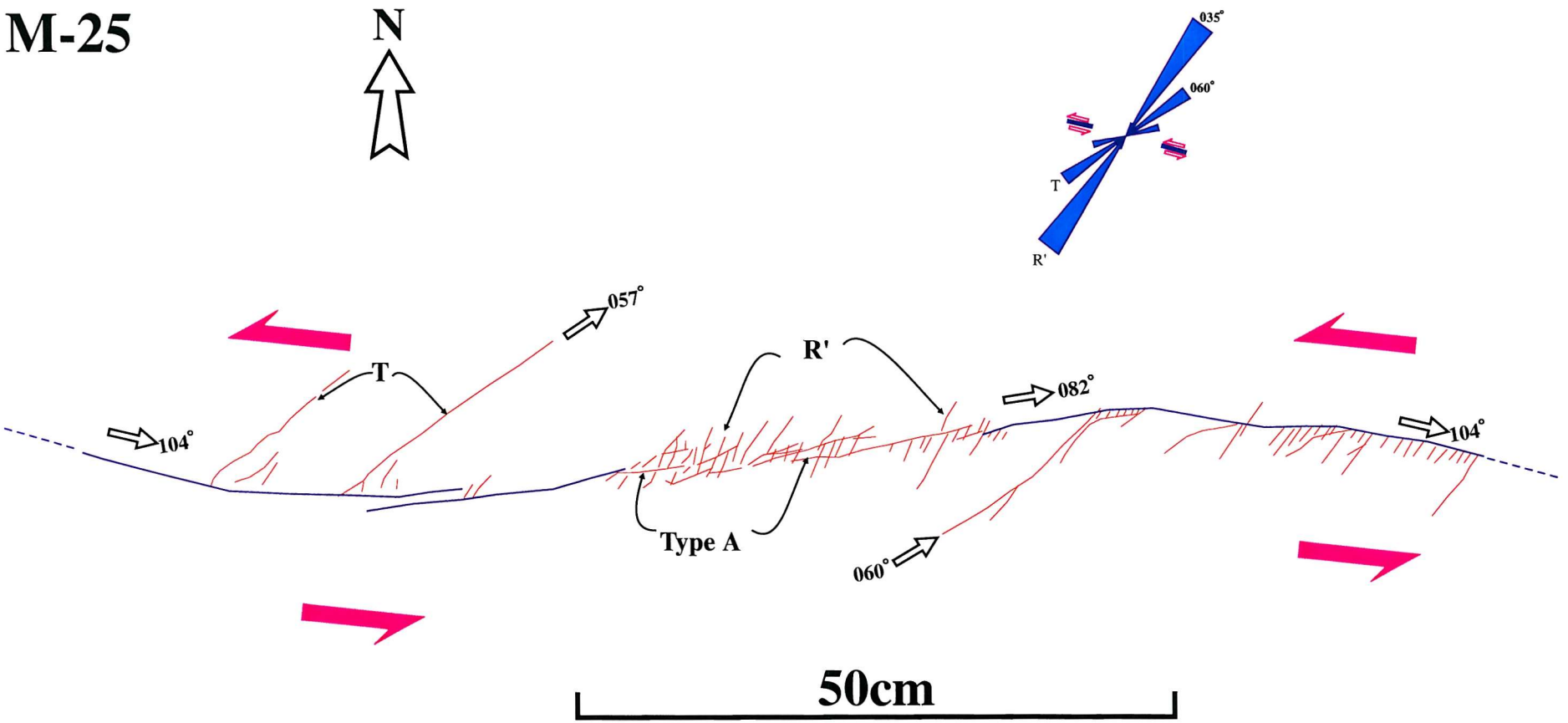

Fig. 4.24. Map showing two parallel but not quite overlapping left-lateral faults. The tip to the two faults show rotation anticlockwise away from a strike of N104° towards N082°. Some branch faults are combined with antithetic fractures in the combined tip zone.

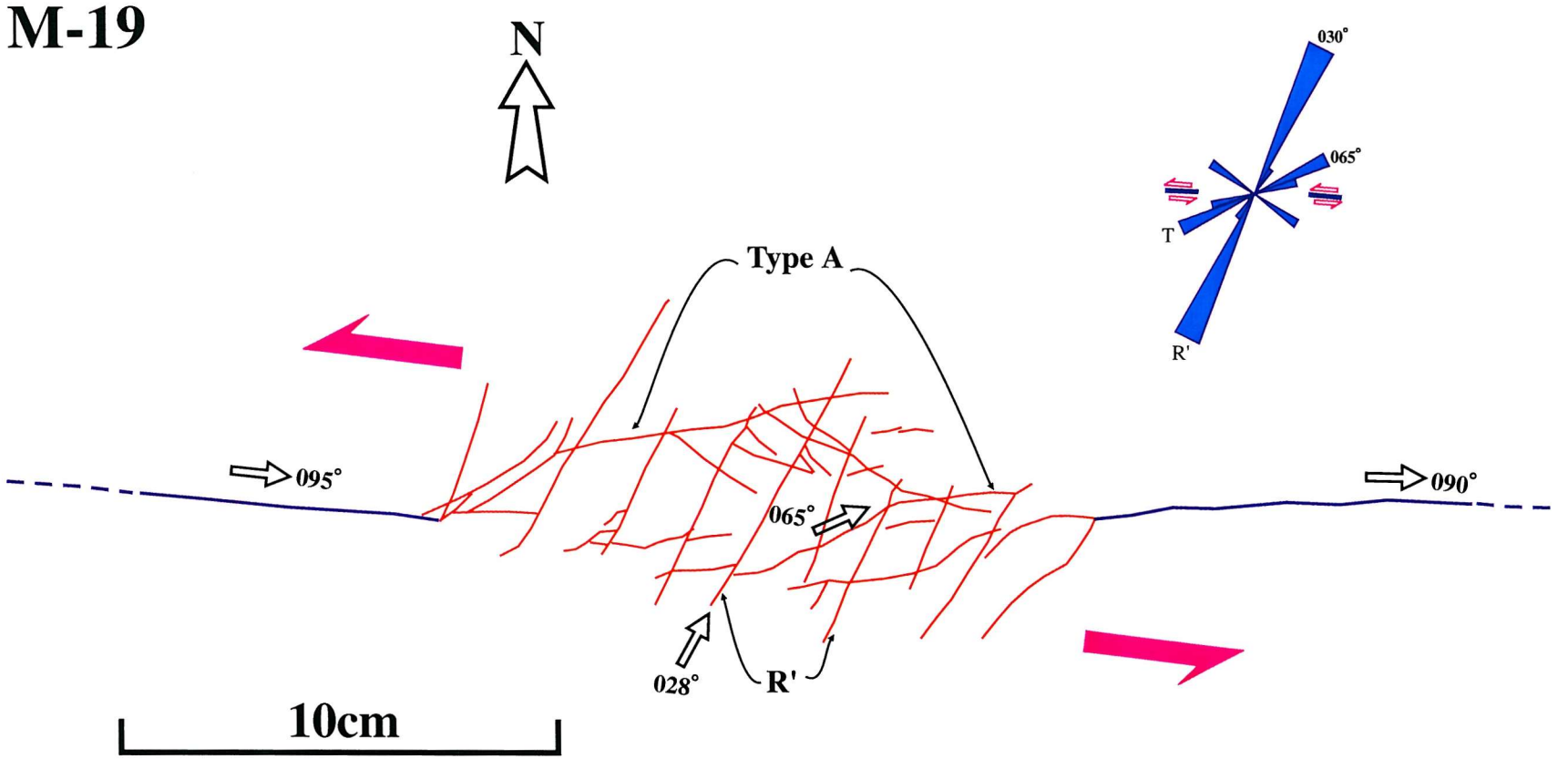

Fig. 4.25. Map showing two left-lateral strike-slip faults with overlapping tip damage zones. It shows 15 cm long overlapping tip damage zone between two faults striking E-W. Antithetic shear fractures strike N028°, and splay fractures range from N060° to N120°. The damage zone consists predominantly of antithetic fractures with some branch faults.

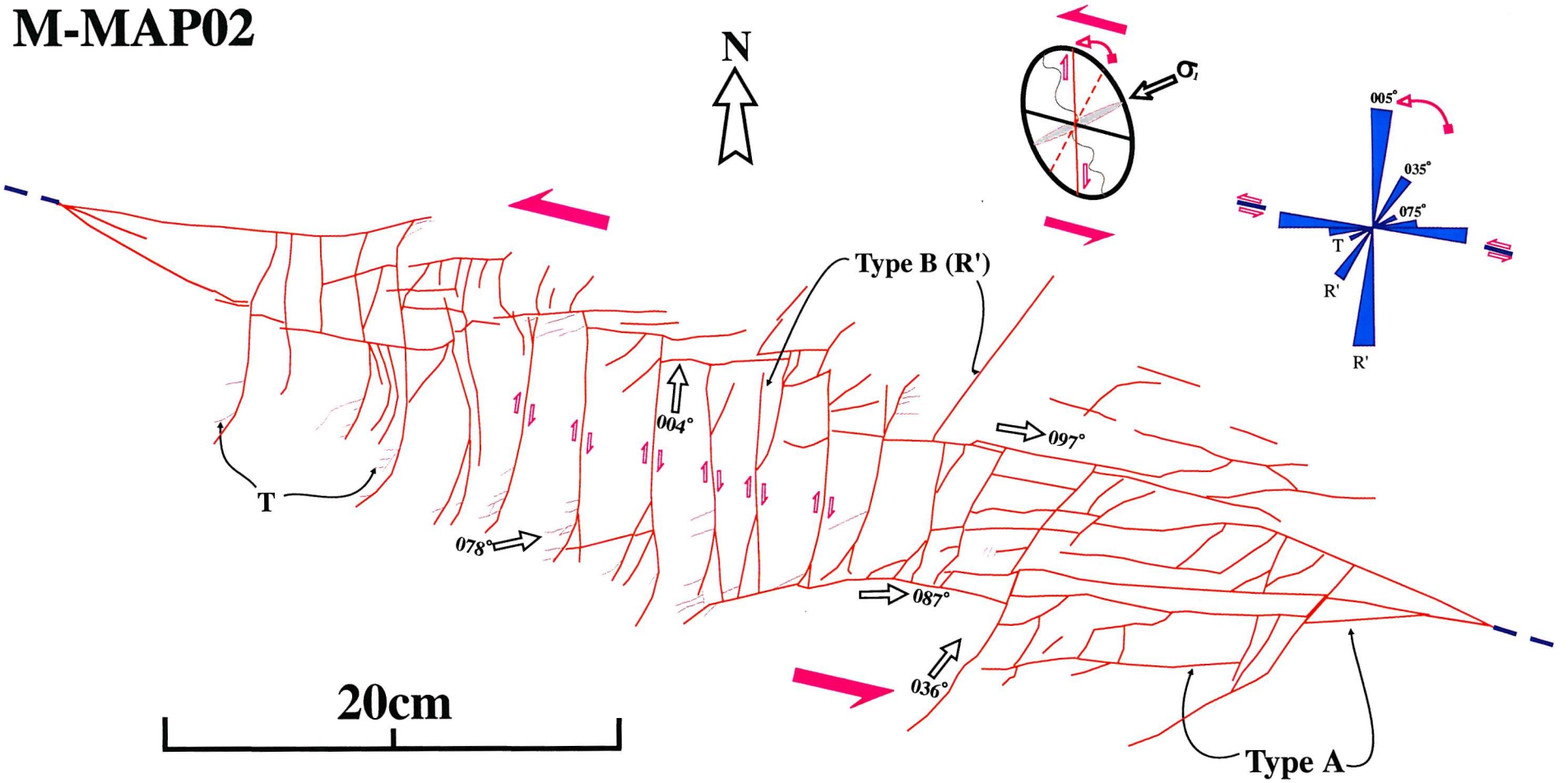

Fig. 4.26. Map showing a complex, linkage damage zone at the termination of two sub-parallel left-lateral faults. Synthetic branch faults and antithetic fractures predominate. Some of the antithetic fractures show sigmoidal shape and tail cracks at the fracture tips implying slip sense. Antithetic faults terminate against branch faults allowing the system to evolve into a series of rotated blocks. The angles between the branch faults and the antithetic fractures recorded unusually high anticlockwise of about 100°.

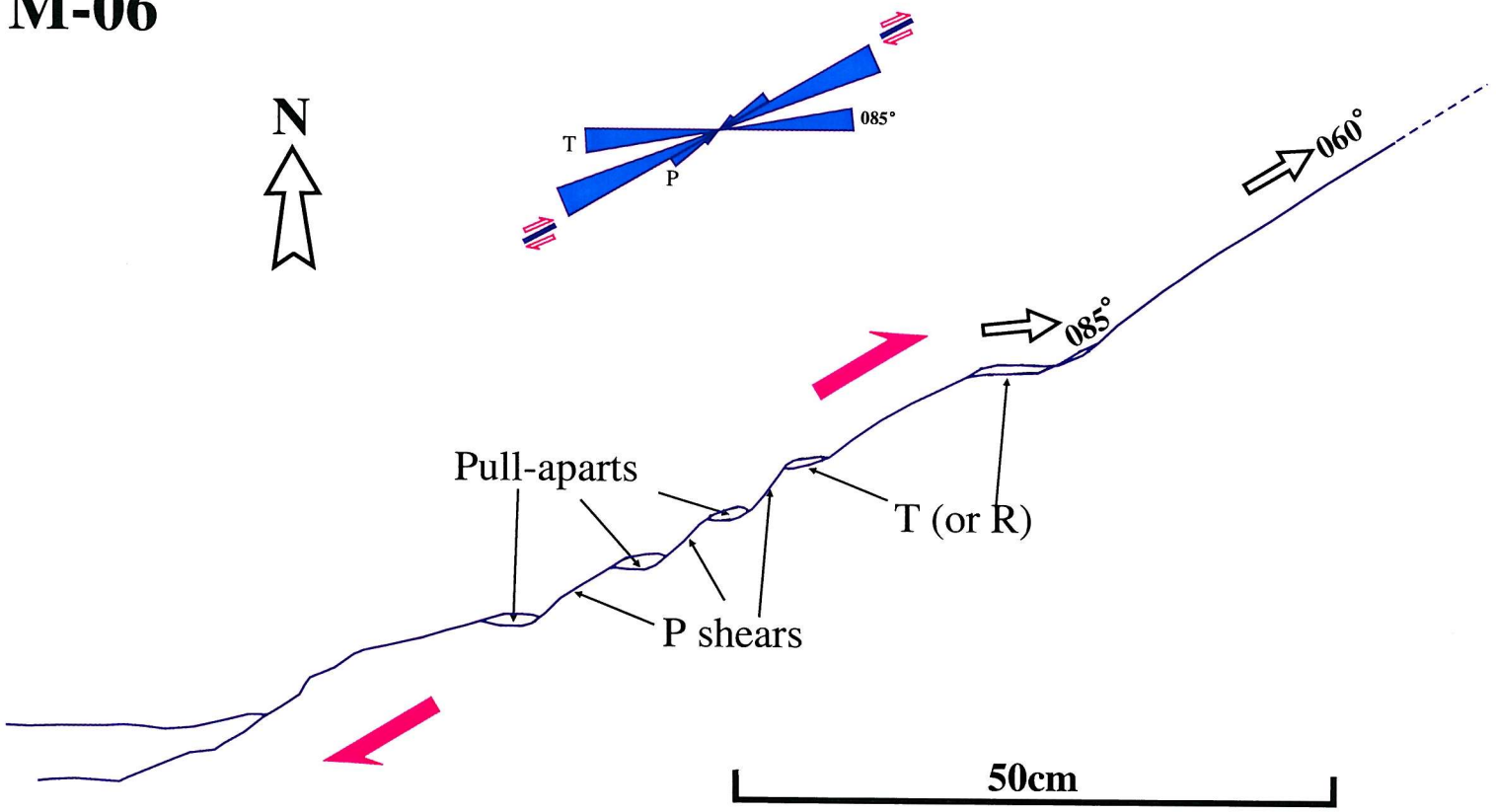

Fig. 4.27. A map showing a light-lateral fault of segment linkage connected through linking fractures. The main fault trend is N060 and the mapped fault is about 1.5 m in length along the mean fault trend.

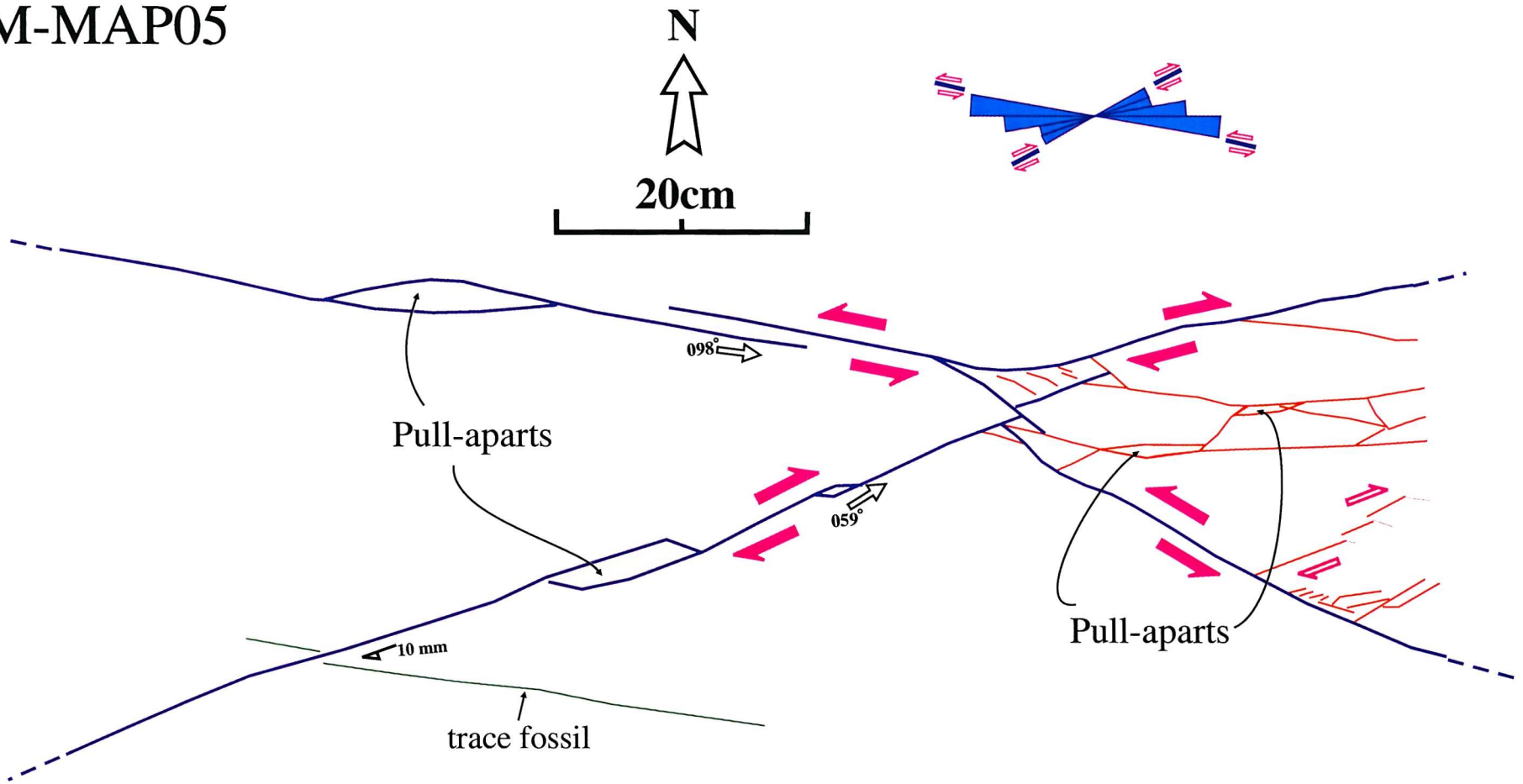

Fig. 4.28. Map showing an intersecting conjugate fault set and its damage structure. The right-lateral strike-slip fault strikes N059°, and the offset of a trace fossil indicates a displacement of 10 mm. The left-lateral fault strikes N098°. The western end of both faults connecting segments linked through dilational overstep. There is little damage between the faults. The eastern ends of both faults show no overstep but a high increase of damage structures in the intervening zone.

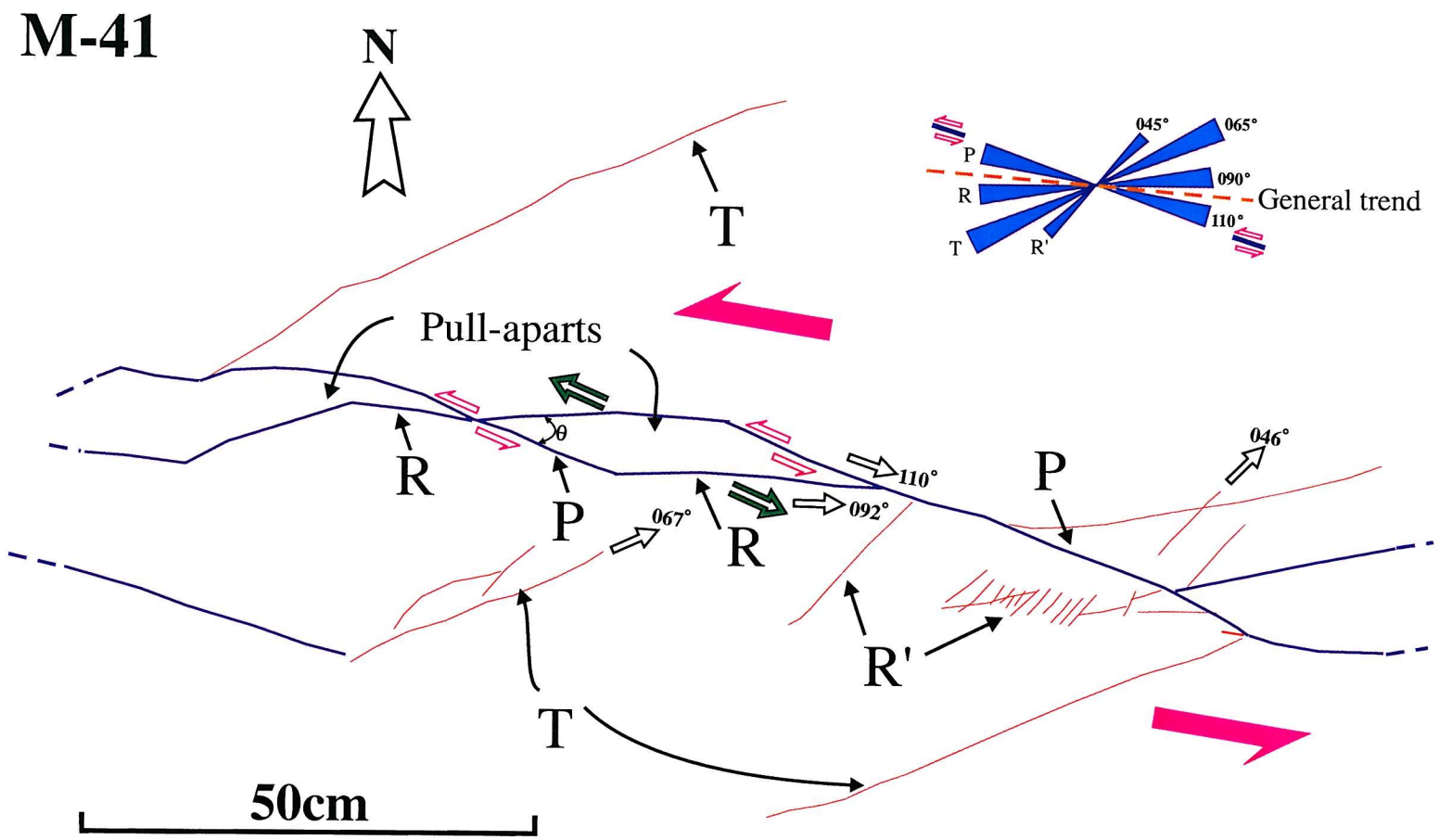

Fig. 4.29. Map of a complex left-lateral fault showing a 'zigzag' geometry. The fault consists of several secondary fractures including P- and R-shear fractures. Pull-aparts are developed by the combination of the fractures.

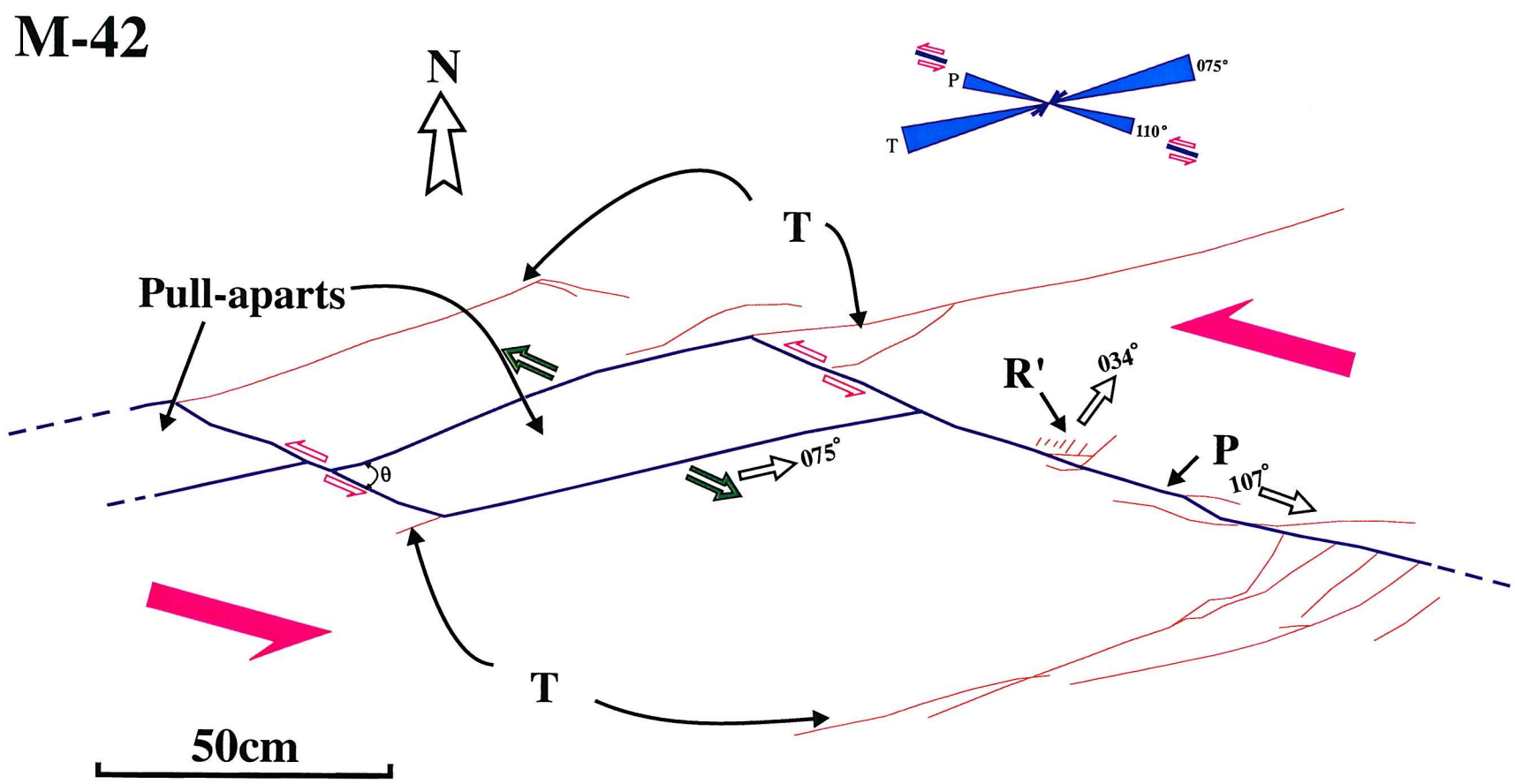

Fig. 4.30. Map of a complex left-lateral fault showing a 'zigzag' geometry. The fault zone mainly consists of P shears and T (extensional) fractures. Pull-aparts are developed by the combination of the two fractures.

M-34

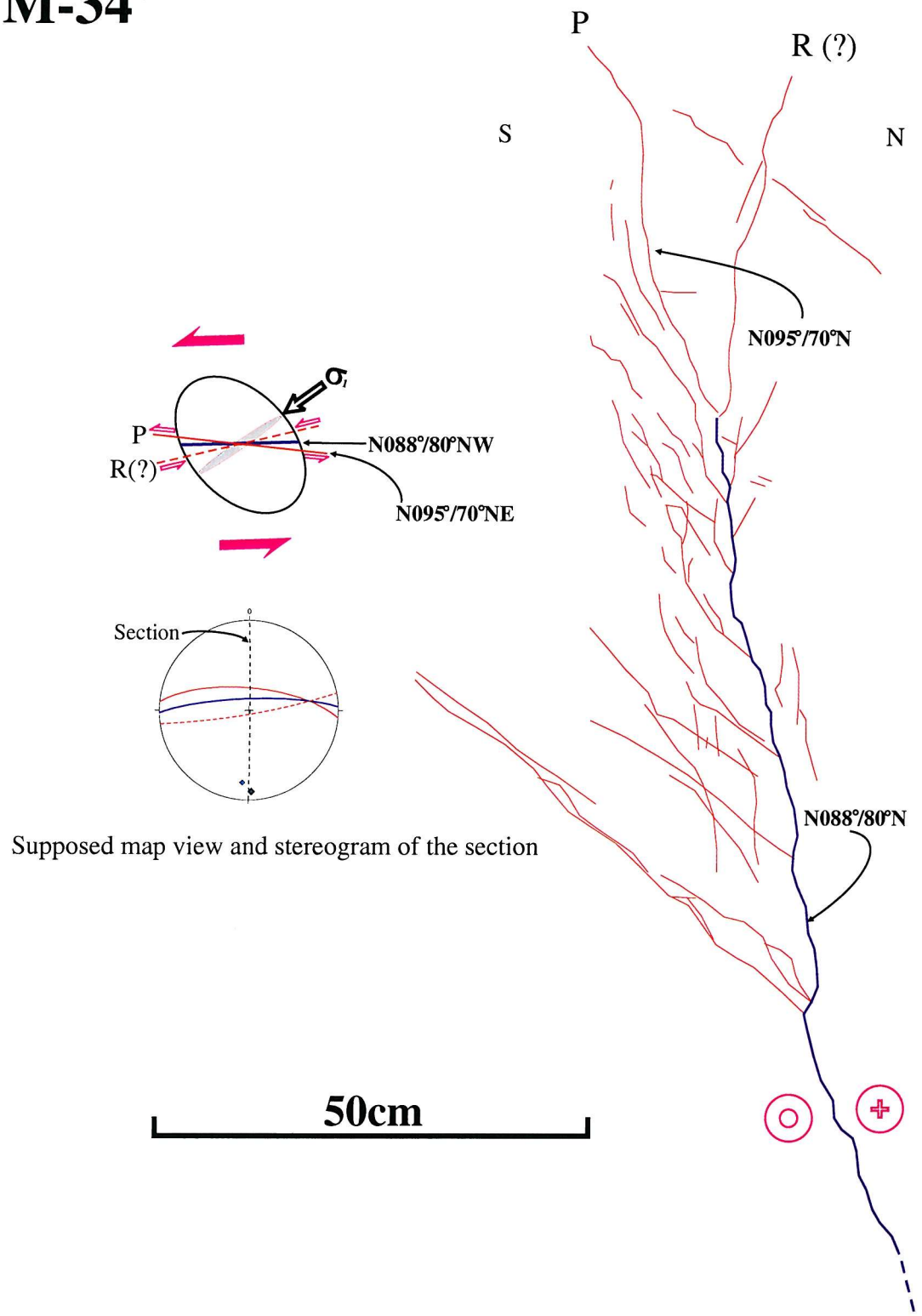

Supposed map view and stereogram of the section

Fig. 4.31. Vertical cross-section of the up-dip tip of a left-lateral strike-slip fault viewed from the east. It is a 1.5 m long vertical section of a strike-slip fault. The attitude of the strike-slip fault plane is N088°/80°NW. It shows an up-dip tip damage with an asymmetric fracture pattern. Above the fault tip, the fracture pattern is symmetric; below the tip most of the fractures are developed on the south side of the fault wall.

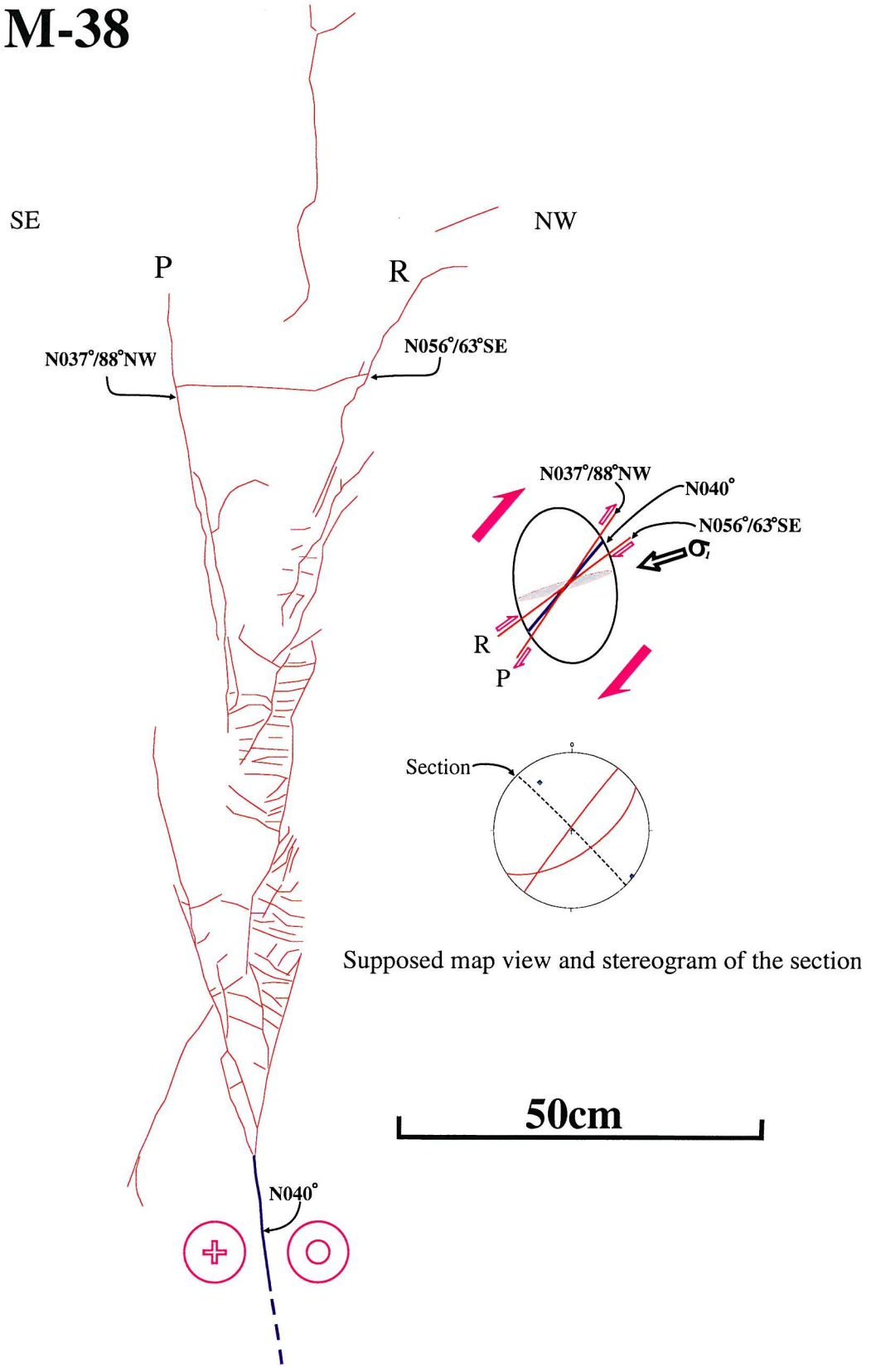

Fig. 4.32. A cross section of a right-lateral strike-slip fault terminating upwards into a fracture damage zone. The main strike-slip fault strikes N040°E, and the damage zone is about 1.5 m in length. Above the upper fault tip, many branch style fractures are developed with small flat lying linking cross fractures. The section dip 60°NE. The tip damage zone fracture geometry shows a relatively symmetric pattern.

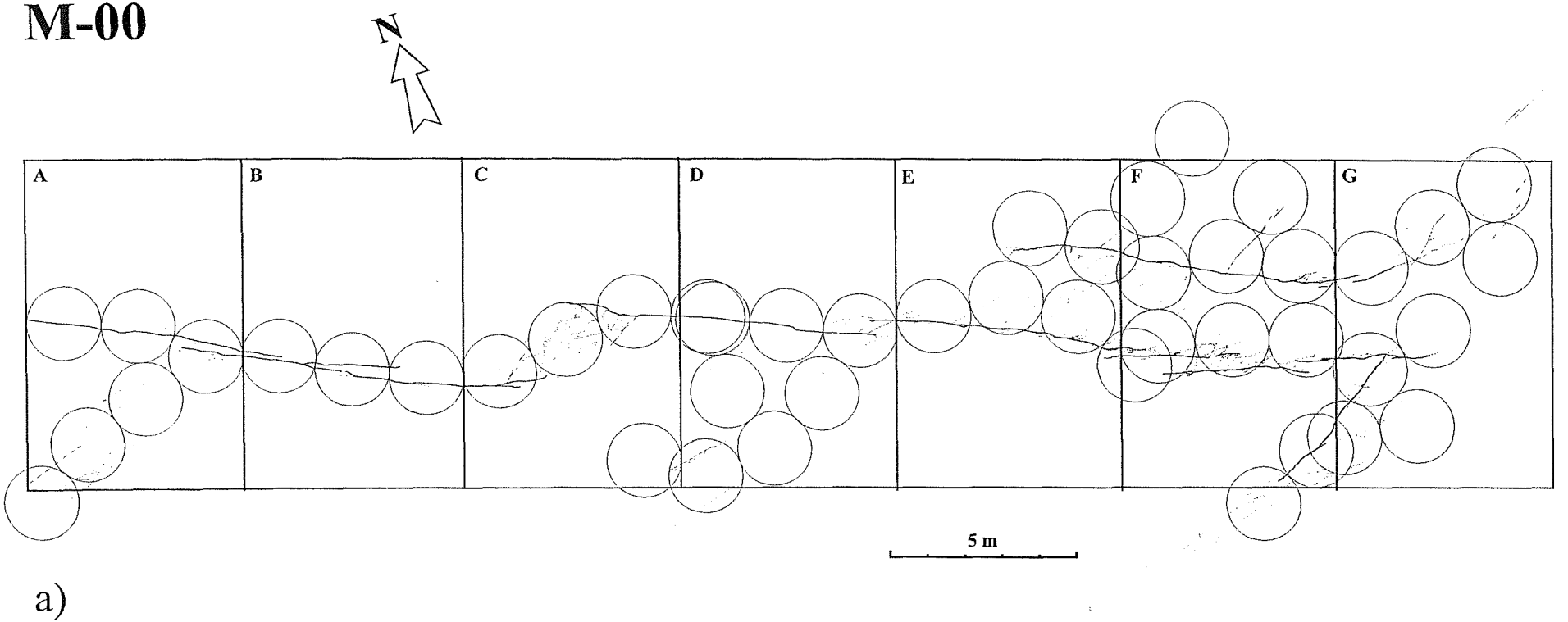

Fig. 4.33. Fracture map of fault M-00 in the studied area divided into seven subsets used for fractal analysis. The method of covering the fault and fracture traces by circles of radius r = 2 m (a) and 0.5 m (b) are shown as examples.

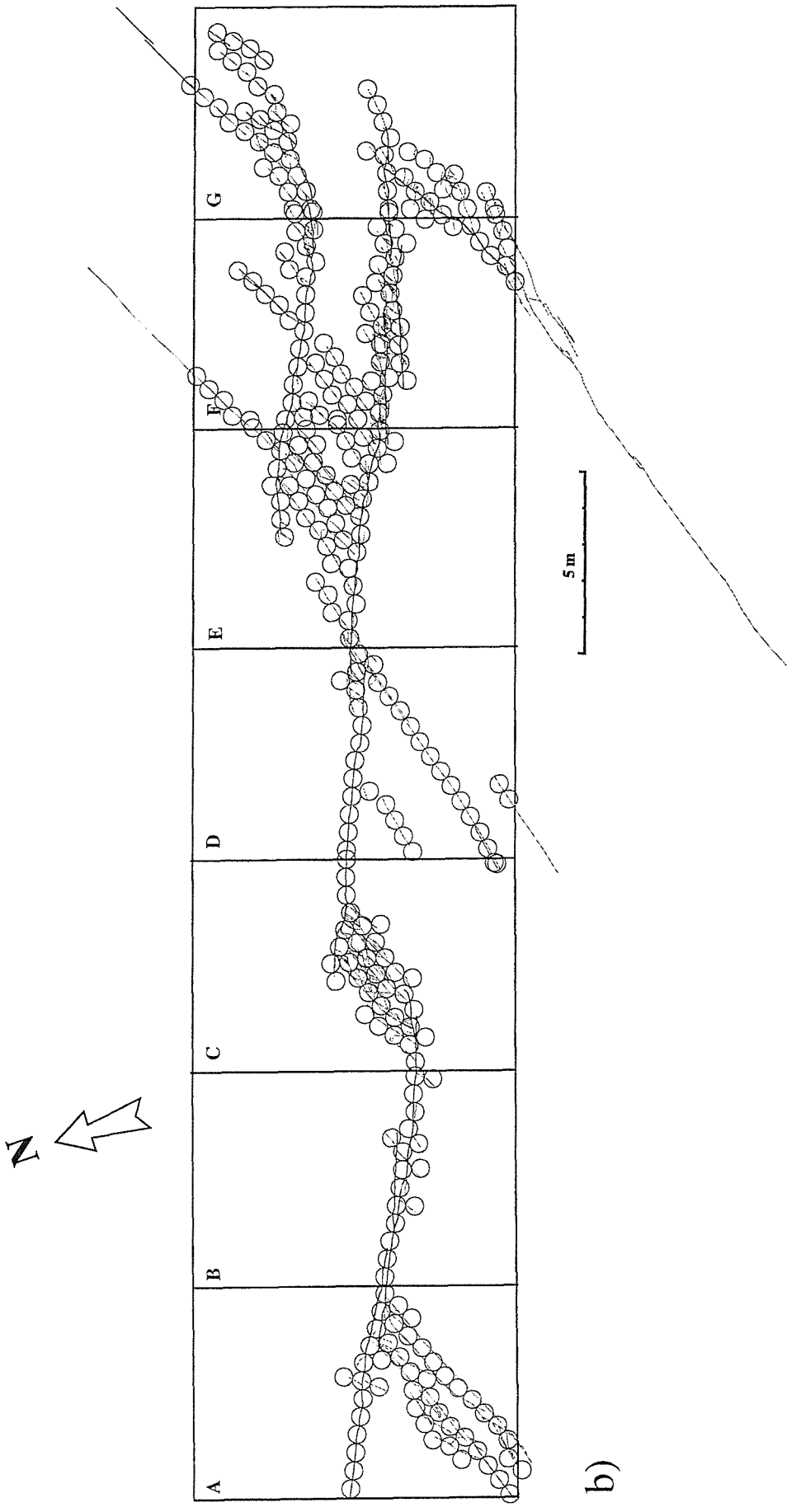
G
F
E
D
C
B
A
5 m
N
b)

Table 4.1. Fault lengths for the subsets of the fault M-00 mapped in the studied area. r, circle radius; N, number of circles; $L°$, normalised length in metre; $\boldsymbol{D}$, fractal dimension.

	Entire	Segment A	Segment B	Segment C	Segment D	Segment E	Segment F	Segment G
r = 4.000m								
N	*16*							
L°, m	*128*							
r = 2.000m								
N	*42*	*6*	*3*	*5*	*7*	*6*	*11*	*8*
L°, m	*168*	*24*	*12*	*20*	*28*	*24*	*44*	*32*
r = 1.000m								
N	*113*	*19*	*7*	*12*	*16*	*21*	*33*	*23*
L°, m	*226*	*38*	*14*	*24*	*32*	*42*	*66*	*46*
r = 0.500m								
N	*305*	*47*	*17*	*33*	*34*	*51*	*76*	*54*
L°, m	*305*	*47*	*17*	*33*	*34*	*51*	*76*	*54*
r = 0.250m								
N	*760*	*127*	*43*	*87*	*78*	*128*	*171*	*132*
L°, m	*380*	*63.5*	*21.5*	*43.5*	*39*	*64*	*85.5*	*66*
r = 0.125m								
N	*1777*	*285*	*100*	*232*	*164*	*307*	*406*	*290*
L°, m	*444.25*	*71.25*	*25*	*58*	*41*	*76.75*	*101.5*	*72.5*
D	***1.3697***	***1.388***	***1.2737***	***1.393***	***1.1386***	***1.3962***	***1.2785***	***1.2881***

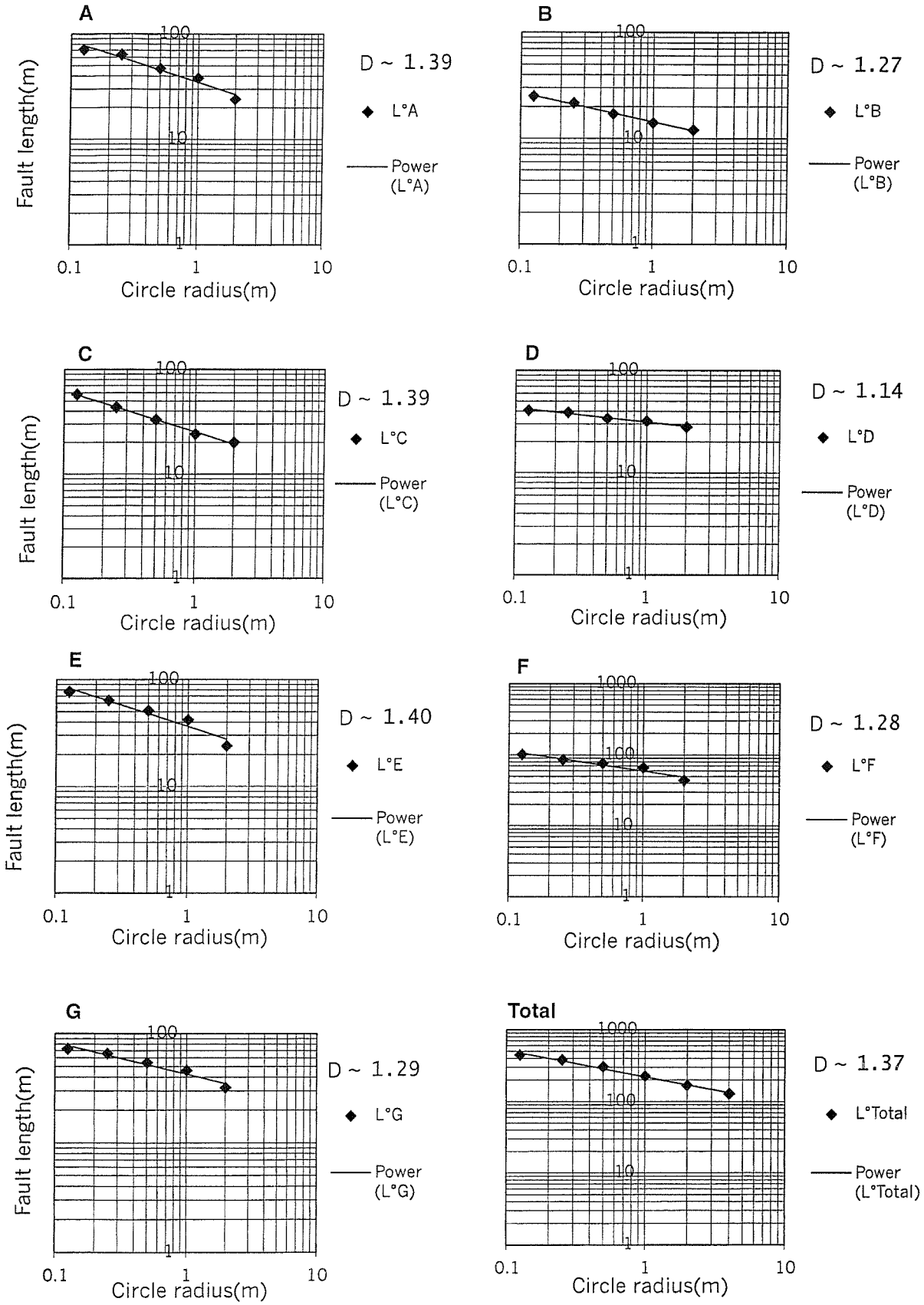

Fig. 4.34. Fault length L°(r) versus measuring radius data for fault M-00 and the seven subsets. Solid linesare best least squares fits to data.

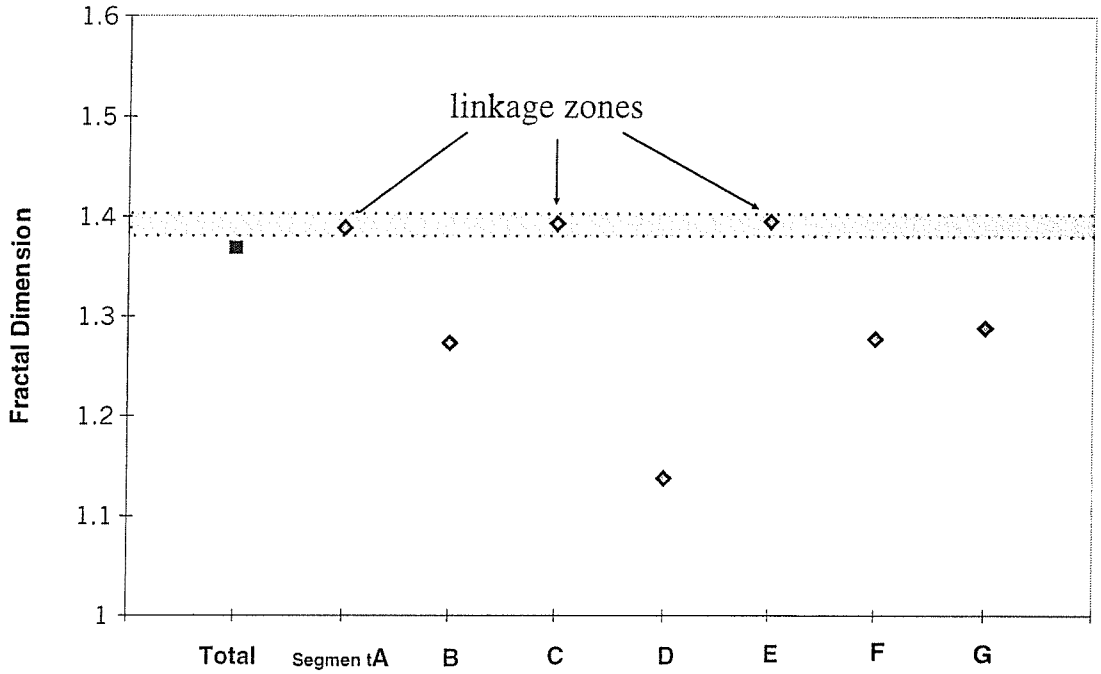

Fig. 4.35. Variation in fractal dimension, *D*, for the whole data sets.The total of fault M-00 and subsets (segments) are listed. High values of *D* (shaded) occur at linkage zones (segments A, C and E).

Fig. 4.36. A simple evolution model of a strike-slip fault predominated with extensional fractures in Gozo, Malta. First generated extensional factures are linked by later linking fractures. It presumably is a core zone of a strike-slip fault and initial generation stage of a fault system.

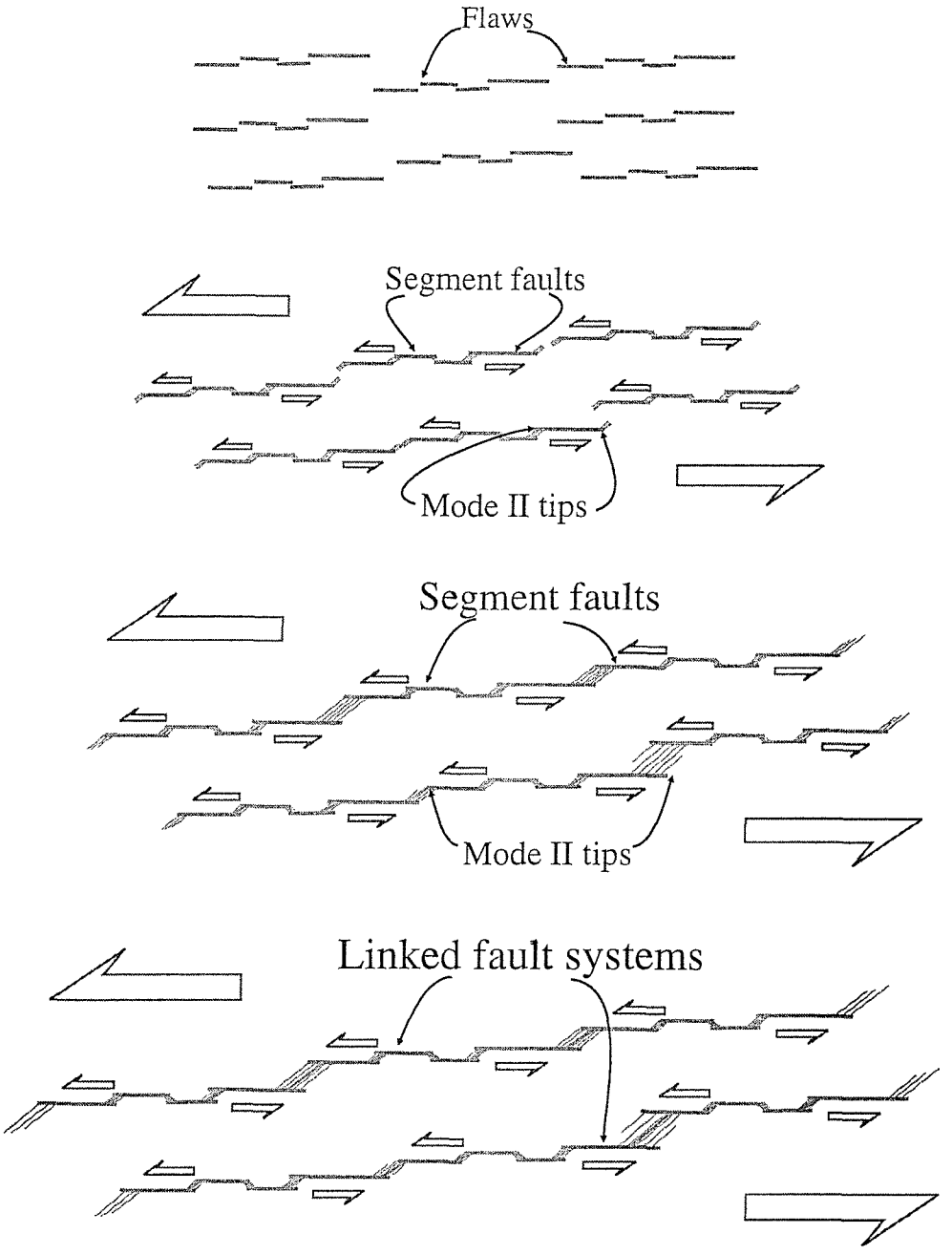

Fig. 4.37. A simple evolution model of a strike-slip fault as along-strike (mode II) tips propagating in Gozo, Malta. Pre-existing flaws are linked by later secondary fractures. The final fault geometry shows zigzag shape due to segment linkage.

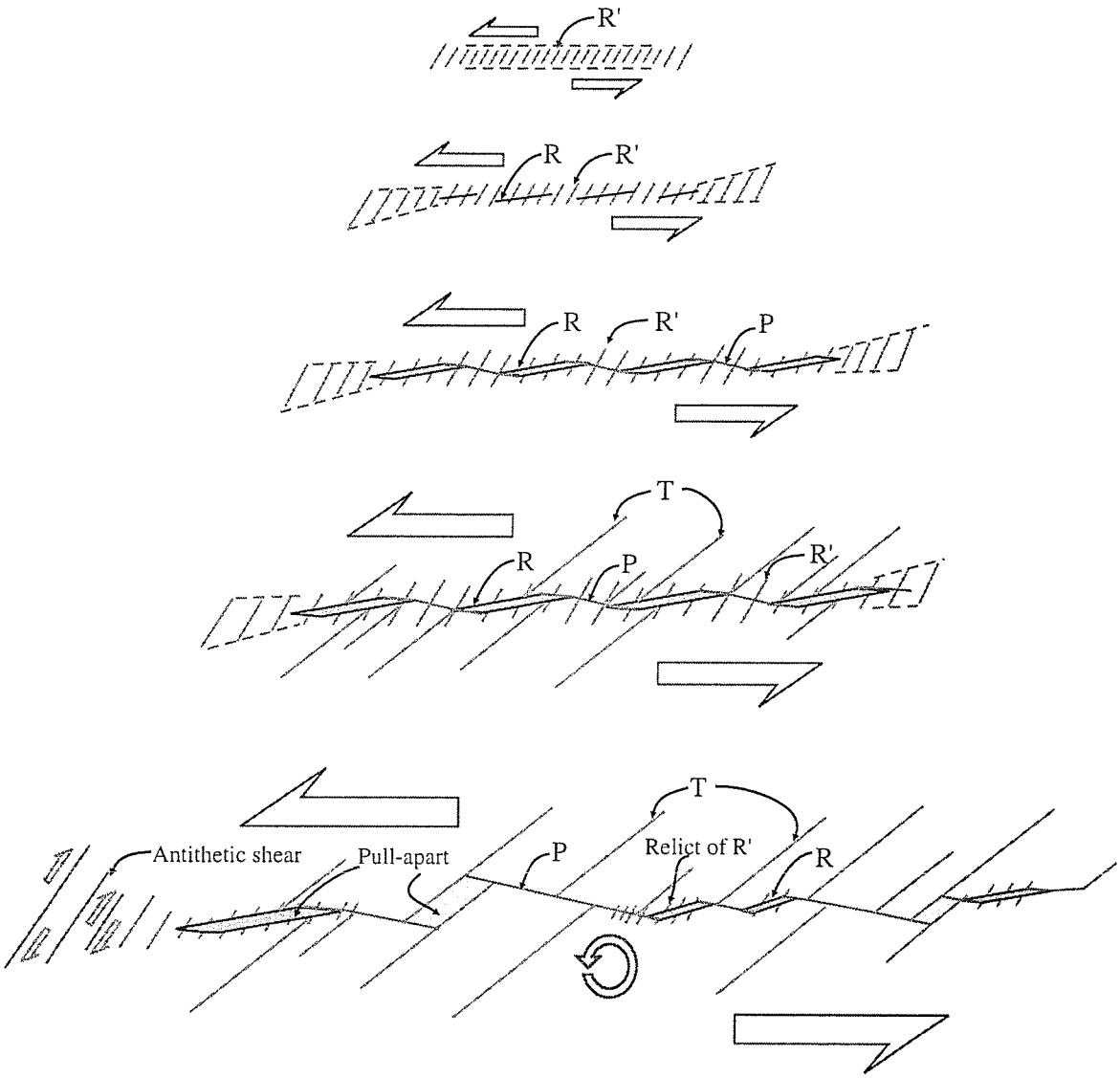

Fig. 4.38. Evolution model of up- or down-dip (mode III) tip of a strike-slip fault in Gozo, Malta. First generated R' shear are intersected by later R and P shears and extensional factures. R' shears are inactive in later stage and other fractures are combined to accommodate displacement and to form pull-aparts. The final fault trace shows zigzag shape.

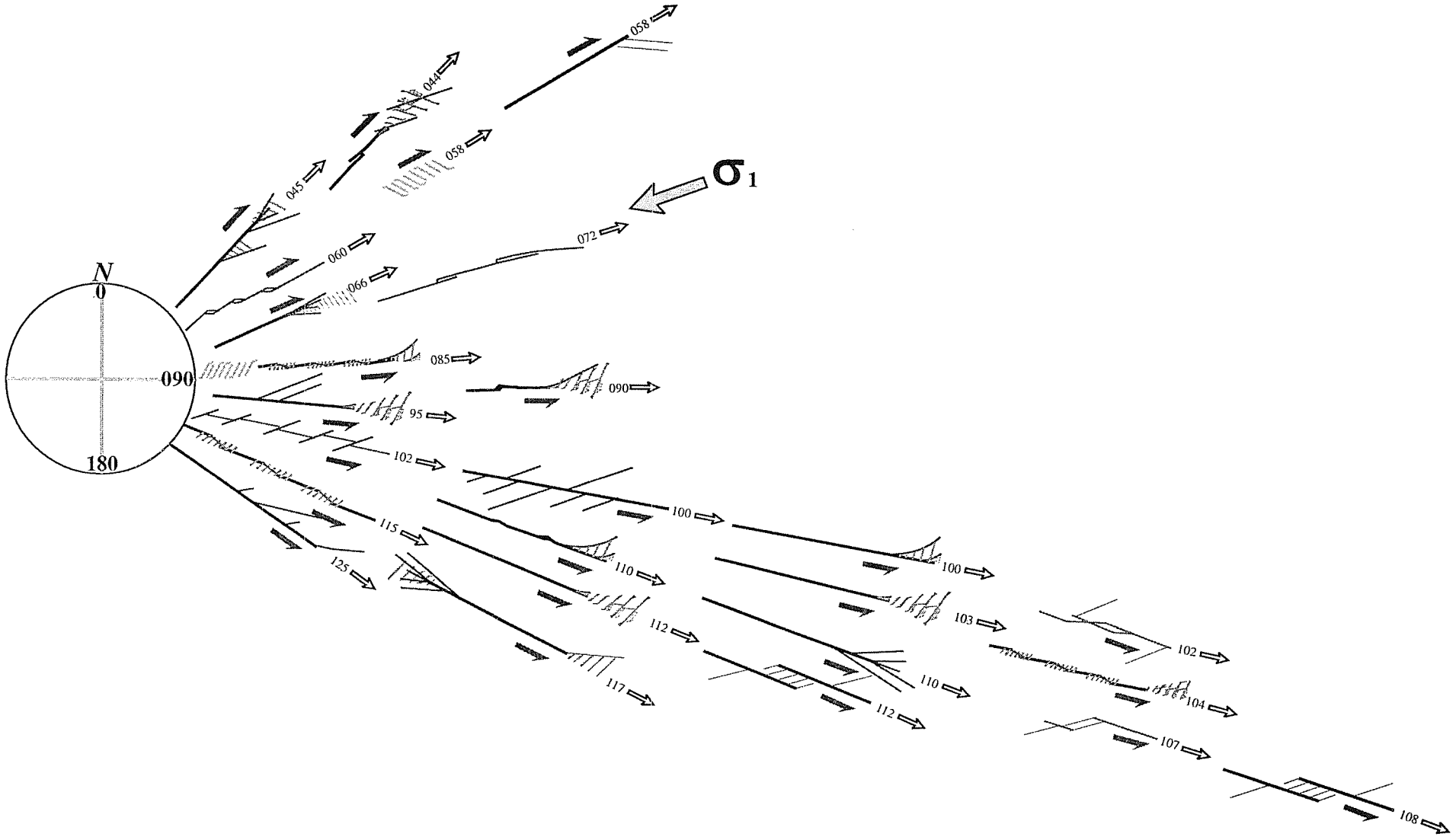

Fig. 4.39. A variety of damage structures around strike-slip faults at Marsalforn, Gozo. The damage structures are arranged according to the orientation of main faults. The damage pattern is not controlled by the master fault trend.

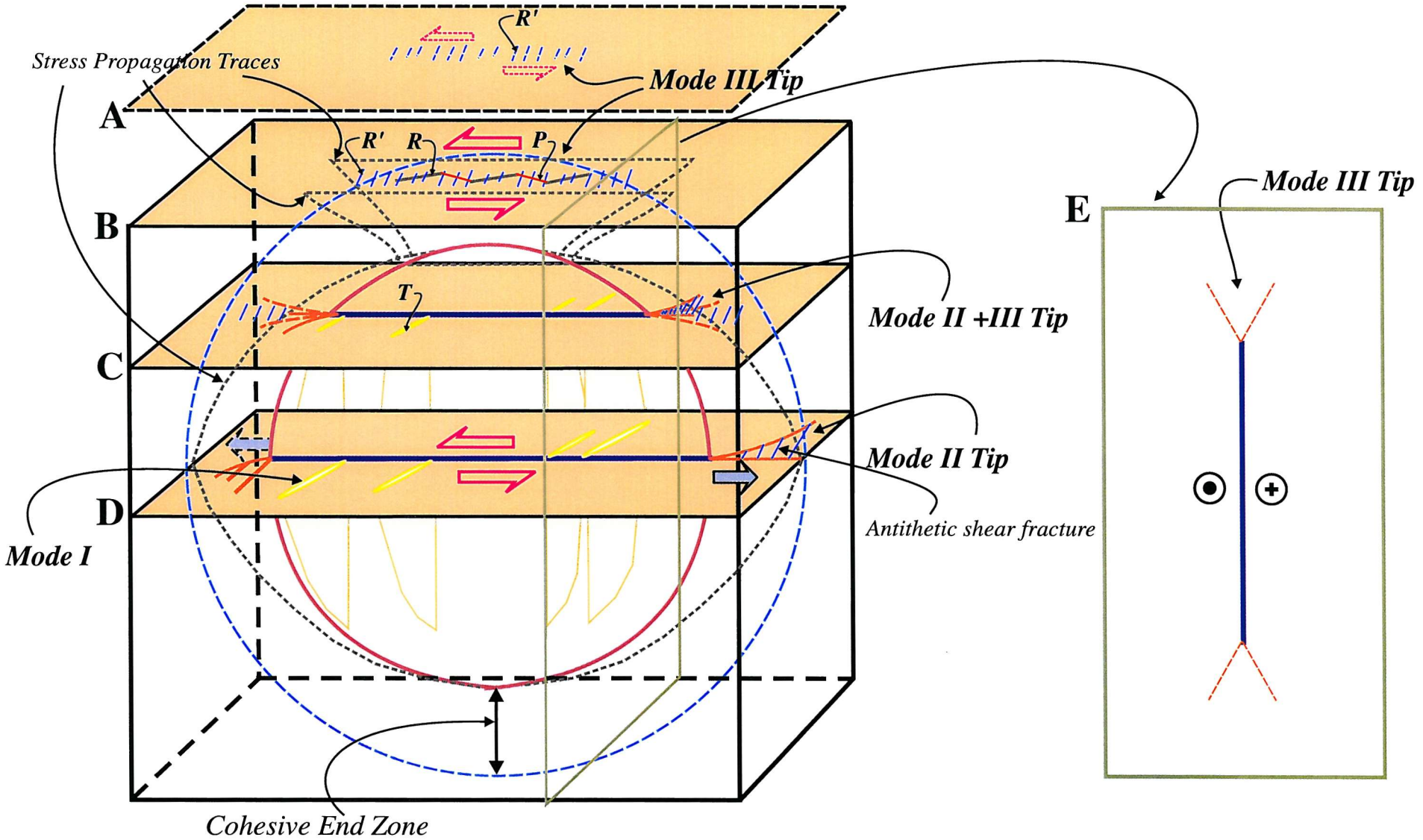

Fig. 4.40. Three dimensional conceptual model of a vertical strike-slip fault and its damage zone fractures. Damage structures depend on tip modes and exposed surfaces of the fault.

M-MAP07

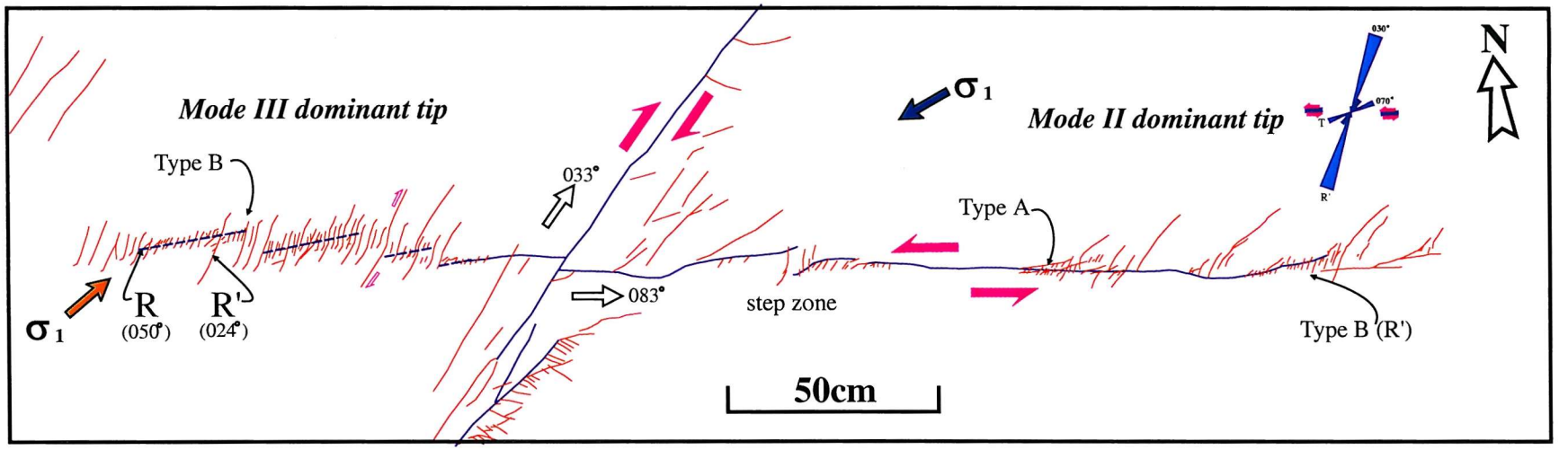

Fig. 4.41. A left-lateral strike-slip fault (striking N083°) showing both tips. This strike-slip fault is cross-cut by a right-lateral strike-slip fault (striking N033°). The left-lateral strike-slip fault is 4 m long. Both tips of this fault are well exposed and exhibit different damage structures. σ_1 is the inferred regional maximum compressive stress.

CHAPTER 5: SECONDARY FAULTS AND SEGMENT LINKAGE IN STRIKE-SLIP FAULT SYSTEMS AT RAME HEAD, SOUTHERN CORNWALL

Abstract

Right-lateral strike-slip faults with displacement of 0.1 ~ 5 m strike NW-SE. There are also several left-lateral conjugate faults and secondary fractures, include splay faults, antithetic high angle fractures (X or R'), and tensional fractures. The remote maximum compressive stress (σ_1) is about N160°.

Characteristic *lens-shaped structures* are developed, which often link fault segments. The *d-x* profiles show that displacement rapidly decreases when the fault meets these structures, with maximum displacements just before and after the lenses, suggesting that they evolve from old segment fault tips or relay zones. The *d-x* profiles for major strike-slip faults show very variable and irregular shapes, mainly caused from segment linkage through lens-shaped structures and branch faults.

At some exposed fault tips (mode II), damage structures are observed, but they are complicated by subsequent fault propagation. At wall zones, high angle fractures (R' or X) are the predominant fracture patterns. The maximum displacement / fault length (d_{max}/L) plot for the strike-slip faults in the study area shows a 'step-like growth path' typical of segment faults.

5.1. INTRODUCTION

Strike-slip faults at Rame Head (Fig. 5.1) are chosen because they show displacements of 0.1 ~ 5 m, and fairly straight overall traces, with few unlinked segments. The d_{max}/L ratios are fairly high (~ 4×10^{-2}). These were selected for comparison with the low-displacement segmented faults at Gozo.

Steeply dipping beds, at a high angle to faults, provide good markers for determination of slip sense and displacement, although the exposed surface is a gently undulating wave-cut platform with many steep erosional gullies (Fig. 5.1b). The

strike-slip fault systems show more complicate fault geometry than those at Crackington Haven and Gozo. Most faults comprise several linked segments.

Numerous recent studies from a variety of tectonic settings have presented slip distribution data and suggested the effects of fault geometry, segmentation and interaction on the shape of displacement profiles (Peacock, 1991; Bürgmann *et al.*, 1994; Cartwright, *et al.*, 1995; Nicol, *et al.*, 1996; Willemse, *et al.*, 1996; Peacock and Sanderson, 1996; Fossen and Hesthammer, 1997; Cartwright and Mansfield, 1998). A common feature is that irregular distributions of displacement have been attributed to fault segmentation generally marked by either intact or linked relay structures.

Detailed observation of the faults, some characteristic damage structures and measured displacement (d) - distance (x) data provide a basis for the interpretation of d-x profiles. A distinctive feature is the development of fault-bound *lens-shaped structures*. These structures may be compared with "sidewall ripouts" (Swanson, 1989), "open eye-structures" (Fossen and Hesthammer, 1997) or "strike-slip duplexes" (Woodcock and Fischer, 1986; Swanson, 1988; Cruikshank *et al.*, 1991). In normal fault systems, similar structures have been reported (Wernicke, 1981; Gibbs, 1984; Fossen and Gabrielsen, 1996; Walsh *et al.*, 1999) as "extensional duplexes", "isolated lenses" or "closed loops".

Numerous secondary fractures defining damage zones will be classified and compared with those described from other study areas (Chapter 2-4), although the scale is different. In this chapter several fault geometries, their d-x and d_{max}/L relationships are described. Three damage propagation models for lens-shaped structures are suggested.

5.2. RESEARCH METHODS

A series of maps at approximately 1:3 scale were made of tip damage zones, and approximately 1:100 scale maps were made for whole fault systems. The maps were made from field photographs, which were analysed in the laboratory using computer based processing. Errors arising from photographic distortion were adjusted by reference to field measurements.

In the field, direct measurement was made of the displacement (d) between marker beds across faults and the distance (x) along the fault from one tip to the marker beds. The maximum displacement, usually near the centre of a fault, was also

recorded if possible. In most cases faults are only partly exposed, so that the length from the tip of a fault to the maximum displacement was taken as a measure of the half-length of the fault length. The accuracy of measurement is ~10 mm for fault displacement, and ~100 mm for fault length because of surface relief. When integrating field data and photographic interpretations, a further error can arise due to the irregular nature of the exposure surfaces. At all times reference to field scale markers has been made to minimise these errors.

5.3. GENERAL DESCRIPTION OF LOCALITY AND GEOLOGIC SETTING

The studied area (SX 417487; Fig. 5.1) is the western coast of the Rame Peninsula between Queener Point and Rame Head Chapel. The host rock is interbedded slate and thin sandstone of the Dartmouth Group of Lower Devonian age (Bristow *et al.*, 1998). The slaty cleavage dips moderately to steeply southward throughout the area and is associated with early E-W major folds (D_1), inferred to be north- or upward-facing and gently east-plunging (Burton and Tanner, 1986). Several NW-SE trending strike-slip faults are related to the Portwrinkle and Cambeak-Cawsand fault zones (Burton and Tanner, 1986), and cut the D_1 cleavage and folding.

The principal structures measured are bedding, right-lateral strike-slip faults, subsidiary left-lateral conjugate faults, extensional veins, minor folds and slickenside striae. Bedding strikes ~ N075° and dips steeply SE consistently. Strike orientations of steep right-lateral strike-slip faults are concentrated around N120°, and steep left-lateral strike-slip faults concentrate around N035° (Fig. 5.2). Assuming that they were developed concurrently as a conjugate set, σ_1 (maximum compressive stress) is assumed to lie in the acute bisector of these right-lateral and left-lateral faults. From this analysis the inferred σ_1 orientation is ~ N160°. The measured extensional veins show this orientation (Fig. 5.2). Measured minor fold axes close to right-lateral strike-slip faults, suggesting 'parallel forced folds' (e.g. Harding *et al.*, 1985), plunge steeply SE.

5.4. DESCRIPTION OF STRIKE-SLIP FAULTS AND DAMAGE ZONES

Strike-slip faults on the scale of several tens of metres in length have been mapped together with damage structures. In this section, geometries of main fault traces, damage structures, *d-x* profiles and effective factors on the obtained profiles will be described.

5.4.1. Major strike-slip faults

Fault R12

Figure 5.3 shows a right-lateral strike-slip fault with an exposed tip at the north-western end. This tip is curved towards the dilational quadrant, with horsetail style fractures defining a tip damage zone. The fault trends N128° and is about 28 m long. It is composed of several segments; some cut by crosscutting high angle fractures. The maximum displacement is 320 mm for the whole fault system. The corresponding ratio of d_{max}/L is about 0.01. This is relatively low compared with other hard-linked faults in the area.

The fault R12 has at least four segments, which are soft- or hard-linked. Segment A is divided into two sub-segments (A' and A''), which are now a linked segment. Although they show a hard-linked pattern, they can be considered as two fault segments because the displacement at the linking point shows a displacement minimum. Segment B and C are considered as separate segments for the same reason. All the segments are left stepping.

Displacement of most of the fault segments decreases generally from the centre towards the fault tips. The d - x profile (Fig. 5.4) has several peaks (Fossen and Hesthammer, 1997) indicating overlapping of several segments. The total displacement profile shows local minima due to contractional segment oversteps. Although all the segments in this fault are not hard-linked, the profile has a maximum displacement in the centre suggests a coherent fault system. This fault system may be at an early stage of fault linkage, because the linkage pattern shows some soft-linked as well as hard-linked segments (Fossen and Hesthammer, 1997).

The segment linkage shows strike-slip relay ramps (Peacock and Sanderson, 1995). A similar profile pattern has been reported in normal fault systems in the Bishop Tuff, Volcanic Tableland, California (Willemse, *et al.*, 1996, fig. 8). The slip minima around overstep zones in the profile of fault R12 (Fig. 5.4) is very similar to the relay structures in the normal fault arrays.

Fault R09

Figure 5.5 shows part (about 17 m) of a long right-lateral strike-slip fault with one exposed tip. The master fault strikes N124° and the south-eastern fault tip curves away southwards, with a high density of horsetail fractures in the dilational quadrant.

The master fault anastomoses around several isolated lenses. The lens-shaped structures are developed at bends or slight misalignments of the fault segments, implying they were early relay zones. This is supported by the development of soft-linked segments in the middle and unlinked branch faults around some lenses, which imply they were originally, isolated early fault tips.

Since the master fault shows only one tip, the total fault length is estimated as double the length from this tip to the maximum displacement i.e. ~ 30 m. The corresponding ratio of d_{max}/L is about 0.007 for a maximum displacement of 200 mm.

Figure 5.5b shows typical tensional fractures (mode I) dominant tip damage structures. The main fault tip striking N122° curved toward the dilational quadrant and fracture density increases in the dilational quadrant (Moore and Lockner, 1995; Vermilye and Scholz, 1999). The general trend of the tensional fractures at the fault tip is consistent with the regional remote maximum compressive stress (σ_1) of N160° (Fig. 5.2). There are many secondary fractures trend N-S to ENE-WSW, which may represent antithetic shears (R') at around N030° and high angle (X) fractures (Logan *et al.*, 1979) at around N060°. The tip damage pattern is that of a horsetail splay style (e.g. Granier, 1985) as also occurs at Crackington Haven and Gozo.

The *d-x* profile (Fig. 5.6) for this fault shows several minima and maxima, but because of sampling limitation some minima and maxima may have been missed. The displacement does not show systematic distribution along the fault. However, the displacement is very low at branch faults and isolated lens zones indicating

displacement distribution into each splay fault. The well-defined minima correspond to the position of two lens-shaped structures.

Fault R02

R02 (Fig. 5.7) is a ~12 m long right-lateral strike-slip fault with a prominent branch fault at its SE tip. It strikes ~ N110°. The northern branch fault might extend through linkage, because the displacement along the branch fault is increasing eastward (from 40 mm to 50 mm), and maximum displacement (520 mm) along this fault occurs just before the branching. Both tips have a high-density zone of secondary fractures in the dilational quadrants. Branch faults at both segment tips are curved towards the dilational quadrants (c.f. Moore and Lockner, 1995; Vermilye and Scholz, 1999). Also, at least two lens-shaped structures are developed along the fault.

In the north-western part, displacement rapidly decrease from ~320 mm to ~180 mm due to branching. The two branch faults form a wedge-shape structure, where no obvious fracturing and rotation exist. It is interpreted that the intersection angle is too large to interact, or, alternatively, the minor branch fault did not rotate the intervening block.

The displacement generally decreases towards both fault tips from the centre, and the high displacements occur just before branch faults at both tips. These high displacements rapidly decrease as the fault goes into the branch faults. The fault is characterised by a damage zone consisting of extensional fractures at fault tips, and high angle fractures (X) to the main fault along the wall zone.

Fault R01

Fault R01 (Fig. 5.8) strikes N084° and the tips terminate with extensional secondary fractures parallel to σ_1 ~ N160° in the dilational quadrants. The eastern tip terminates with a prominent branch fault to form a fork-shaped structure. Within the enclosed wedge-shaped block, several minor secondary cross fractures developed, and are now rotated to show sigmoidal shapes filled with vein quartz.

The displacement generally decreases, from ~ 185 mm at the centre, towards both fault tips. The fault length between the tips is ~ 6.50 m and the ratio of d_{max}/L is about 0.028. The fault is characterised by a damage zone consisting of extensional fractures at fault tips, and branch fractures along the central section.

Fault R00

Figure 5.9 shows a tip zone of a right-lateral strike-slip fault. The exposed fault length is about 10 m. The main fault trend is ~ N095° and the western tip is curved towards the dilational quadrant (c.f. Moore and Lockner, 1995; Vermilye and Scholz, 1999), N112°, showing a splay fault style (Anderson, 1951; Type A of Chinnery 1966b).

The *d-x* profile (Fig. 5.10) shows a general displacement decreases towards the western fault tip, and the displacement gradient is variable producing local displacement maxima and minima. The main fault segment branches and joins forming several isolated lenses. The displacement does not systematically decrease towards the western fault tip; i.e. the maximum displacement is recorded just before the tip splay begins (670 mm). The displacement also decreases along each branch fault. As the main fault meets any branch fault (at a fault bend, tip or relay) the displacement on the main fault rapidly decreases. Clearly a significant component of the total displacement is taken up on the branch faults, indicating the fault is not an isolated fault but a linked segmented fault (e.g. Peacock, 1991).

Fault R07

Map R07 (Fig. 5.11) shows the best example of lens-shaped structures in the study area. Two sub-parallel left-lateral strike-slip faults are developed. The major fault is about 10 m long and the minor one is about 4 m long. The maximum displacements for the two faults are ~ 350 mm and ~ 130 mm, giving a ratio of d_{max}/L of about 0.035 and 0.033, respectively.

The major fault strikes ~ N040°, and the fault trace shows a zigzag geometry with several lens-shaped structures and unlinked branch faults along the fault. Lens-shaped structures occur where there are offsets of fault trace, and their geometry is very similar to strike-slip duplexes (Woodcock and Fischer, 1986; Swanson, 1988; Cruikshank *et al.*, 1991). The material within the isolated lenses is not exotic but the same as that of the adjacent wall. If the lenses are initiated as pull-aparts or jogs at relays or fault bends, the lenses should be filled with vein material or empty. Fracture density within the lens-shaped structures is relatively low suggesting well-transferred displacement through them.

This characteristic is also shown in *d-x* profile (Fig. 5.12) of this fault system. The effect of the main lens-shaped structure on the profile is well recorded in the central part of the *fault A*. The sum of the displacement of the two branches is depressed at the lens-shaped structure. It suggests a linked old fault tip where the entire displacement is transferred into the branch faults. The minor sub-parallel *fault B* also shows similar displacement pattern. The sum of the displacement of these two sub-parallel faults (*A+B*) is made to know the interaction and transferring of displacement between these two faults. Although it is increased, the displacement minimum at the lens-shaped structure is still obvious.

Therefore, this lens-shaped structure is interpreted as a structure of early stage 'strike-slip duplexes' (Woodcock and Fischer, 1986; Swanson, 1988; Cruikshank *et al.*, 1991), and this geometry is originated from old fault tip or relay zone of fault segments.

Fault R03

Figure 5.13 shows a right-lateral strike-slip fault, which has a complex geometry, dominated by two, fault bounded lenses. The general trend of the fault system is within the range of N110° ~ N120° and the exposed portion of the fault is about 10 m long. As the fault maintains an approximately constant displacement (Fig. 5.14), the tips probably lie some distance from either end of the exposure.

Along the fault two lens-shaped structures are developed, and around the lenses various damage patterns occur. The main fault trend curves from N110° to N120°, and the western lens is located in a restraining bend and the eastern lens is located in releasing bend. The fracture density is higher around the western lens than around the eastern lens.

The two lens-shaped structures show slightly different fracture pattern because they are located in different stress regimes. Along an isolated fault bend there are two structures usually classified as releasing or restraining depending on the tendency associated with the incremental slip transfer (Christie-Blick and Biddle, 1985; Sibson, 1989). A lot of extensional fractures and veins are developed at the western lens, and the fracture density is very high at the north-western part of the lens. Low slip along the fault plane may make a local shear zone producing tension gashes. The presumable stress distribution and its simple kinematic model is shown in Figure 5.13b, when it is

supposed that the main slip occurred along the main trace with larger displacements. However, there is only a low density of fractures around the eastern lens, because the lens is located at a dilational bend.

Secondary fractures are predominant in tension (T) fracture and high angle (X) fracture patterns (Fig. 5.13a). An interesting semi-circular fracture pattern is observed in the northern wall of the western lens-shaped structure. This type of fracture pattern has been reproduced by Chinnery (1966b) in a numerical modelling study.

The *d-x* profile (Fig. 5.14) for displacement along the main fault shows lower displacement around the lens-shaped structures. However, the total displacement is slightly higher and has a well-preserved, flat displacement profile along the lens-shaped structures. It indicates that the lens-shaped structures are in a mature stage. Relatively higher displacements occur along the straight branch than those of the more curved branch because the general fault trend is almost parallel to the straight fault trace. Therefore, the straight major branch fault takes over most of the displacement, because straight fault is more effective to slip transference.

Fault R05

Figure 5.15 shows the eastern tip of a branch fault of the largest fault (R05) in the study area. The mapped section is about 15 m in length, and the whole fault length is over 100 m. This right-lateral fault trends ~ N135°. The eastern fault tip zone is characterised by fractures developed at a high-angle to the main fault. The fault is offset by a later left-lateral fault in the north-west (Fig. 5.15), but it extends towards north-west with increasing displacement (Fig. 5.16). Several lens-shaped structures and branch faults are developed along the fault. Fractures developed around the fault include high angle antithetic fractures (X fractures). Other fractures observed in this map are tension fractures (mode I).

Although detailed mapping along all the fault system was not carried out, d - x data were collected until the fault reached the sea. The d - x profile (Fig. 5.16) resembles a single isolated fault profile. Assuming a symmetric d - x profile the total fault length is estimated to be ~ 120 m. This gives a ratio of d_{max} / L about 0.042; the highest value of any faults estimated at Rame Head.

5.4.2 Comparison of damage patterns

The aim of this section is to compare damage structures in this study area with those from other study areas. Several characteristic damage structures in process zone are described. The basic classification follows Riedel shear fracture grouping, and as a complementary way Chinnery (1966b)'s classification types will be used.

Wall zone damage (R04 & R51)

Figure 5.17 and 5.18 shows right-lateral strike-slip faults cut by later left-lateral faults. They show wall zone damage structures. Predominant fractures are antithetic fractures at a high angle (X fractures) to the master fault. Along the mapped section several lens-shaped structures and some branch faults are developed. These are observed around most of the faults described in the study area. The slip sense is left-lateral as indicated insets b) and c) of Figure 5.17, by the offset of beds and the development of tip cracks. In detailed drawing (inset a) in Fig. 5.17), some of minor high angle fractures (X) or higher order fractures linked to form pull-aparts in relay zones. The orientations of secondary fractures are slightly distorted by local stress re-distribution and pre-existing structures, because the final stage opening is not parallel to the secondary fracture orientations associated with the original master fault system.

Figure 5.18 (R51) is close to fault R05 and sub-parallel to a branch fault of the fault (R05-1). The antithetic fractures (X) dominate at wall zone and lower angle antithetic fractures (R') or extensional fractures (T) become dominant towards the fault tip.

Tip zone damage (R20, R08 & R21)

Figure 5.19 – 5.21 show some tip damage structures in this area. They consist of splay faults and antithetic shear fractures. The branch faults sometimes isolate a wedge-shaped block (Fig. 5.21) within which an array of fractures strikes at a high angle to the main structures. Although the sense of the antithetic fractures is not obvious on the map, predominant left-lateral shear can be inferred from higher order tip cracks. The fracture orientation is at a high angle to the main fault (R' or X fractures).

In Figure 5.19, near its northern termination, a branch fault propagates a short distance onwards where a fault curves away towards N032°. A further splay propagates away from these branch faults. Near the termination of the main fault unusual semi-circular

fractures occur. They resemble type C fractures of Chinnery (1966b). Figure 5.20 shows a fault (R08) with a tip damage pattern with some similarity to R20 (Fig. 5.19), but the orientation of antithetic fractures is slightly different.

At the end of tip zones in Figure 5.20 and 5.21, linear fractures occur often without any indication of shear displacement. These are producing extension fractures and can be used to imply the regional orientation of σ_1 (N160°).

Within the wedge-shaped block bounded by the two splays in Figure 5.21, there are two predominant secondary fracture trends. Some of the sigmoidal fractures, which make a high angle with the splay faults, imply rotation between the two right-lateral faults. Some extensional fractures are developed on both side-walls along the splay faults. Many barren fractures generally terminate against the antithetic fractures.

Linkage zone damage (R51-R06, R072-1 & R072)

Figure 5.22 – 5.24 show linkage zone damages with varying relay patterns. Figure 5.22 shows an oblique overstep zone with antithetic linking faults between two right-lateral faults. The angular relation between these two fault sets is about ~ 90°. Most of the linking faults terminate at the boundary faults.

Figure 5.23 and 5.24 are linkage zones showing hard-linkage of two misaligned segments. However, they show different linkage patterns. Figure 5.23 is a segment linkage pattern developed at a bend in relay zones. The eastern segment developed horsetail splays, and at a later stage linked with the western segment. This relay zone produced fault bends rather than lens-shaped structures, although small lenses were developed around fault bends. Figure 5.24 shows a lens-shaped dilational overstep. It is interpreted as a mature stage of evolution of a relay zone developed due to a slight misalignment between two right-lateral strike-slip faults (Olson and Pollard, 1989; Cruikshank *et al.*, 1991; Fossen and Hesthammer, 1997). After linkage, further slip promoted opening at the fault bends (c.f. dilational jog, Sibson, 1989) creating open spaces now filled with vein quartz. Some secondary fractures are developed around and within the lens-shaped structures implying extensional fractures (or R' shear fractures).

5.5. SUMMARY OF CHARACTERISTIC FEATURES OF STRIKE-SLIP FAULTS AT RAME HEAD

• *Orientation and displacement*: WNW-ESE trending right-lateral faults dominate (Fig. 5.2) with longer fault lengths and larger displacements than NE-SW trending left-lateral faults.

• *Age relationships*: Field relationships show right-lateral faults are cut by left-lateral faults, but not *vice versa*. Some left-lateral faults terminate against right-lateral faults and *vice versa*. Evidence for the contemporary formation of both fault sets is equivocal but measurement of isolated extensional veins support a paleo-stress σ_1 = NNW-SSE consistent with a conjugate origin of the two sets of strike-slip faults.

• *Fault segmentation*: Some segmented faults show hard- and soft-linked fault system (Fig. 5.3) before forming lens-shaped structures.

• *Lateral tip damage structures*: Horsetail fractures (Figs. 5.5, 5.7-5.9 and 5.23) and branch faults (Figs. 5.7-5.9, 5.19, 5.20 and 5.21) are dominant. Sometimes arrays of antithetic shear fractures occur (Figs. 5.19 and 5.20).

• *Wall zone damage structures*: High angle shear fractures predominate (X or R') (Figs. 5.13, 5.15, 5.17 and 5.18). Higher order secondary fractures may occur indicating the shear sense (Fig. 5.17). Moderate angle fractures occur around both contractional and dilational fault bends and lens-shaped structures, showing evidence of local extension (T fractures and tension veins) (Figs. 5.13, 5.21, 5.23 and 5.24).

• *Lens-shaped structures*: These structures commonly occur along a fault (Figs. 5.5, 5.7-5.9, 5.11, 5.13, 5.15, 5.17, 5.18 and 5.24). The shape ratio (short axis/long axis) of the structures is in a range of 1/3 ~ 1/10. Associated fracture patterns include branch faults and semi-circular fractures. Extensional veins occur at fault bends and leading/trailing edges. The mapped examples show some possible mechanisms for lens-shaped structures.

• *Fault interaction*: Antithetic faults are developed within oversteps between two sub-parallel faults (Fig. 5.21 and 5.22).

5.6. DISCUSSION

5.6.1. Tip damage

Tip damage structures at Rame Head are noteworthy because the strike-slip faults in this study area show larger displacements and more complicated fracture patterns. A variety of tip damage structures occur and they are more complicated at segment linkage zones.

As a master fault propagates, several secondary fractures are generated to release stress and slip around the main fault, especially at fault tips. Secondary faulting (McKinstry, 1953; Chinnery, 1966a, 1966b) is mainly associated with the end of a master fault, although McKinstry (1953) suggested that it may occur along the entire length of a fault. At the tips, the master faults curve towards the dilational quadrants (Figs. 5.3, 5.5, 5.7, 5.8 and 5.9) (Moore and Lockner, 1995; Vermilye and Scholz, 1999), and terminate commonly with horsetail splay fractures filled with vein quartz (Figs. 5.3, 5.5, 5.7 and 5.8).

Near mode II fault tips, the predominant sliding mode causes fractures to initiate obliquely to the fault plane forming splay fractures (McKinstry, 1953; Chinnery, 1966b; Freund, 1974; Arthaud and Matte 1977; Petit and Barquins, 1988). Linear elastic fracture mechanics theory predicts a concentration of stresses near mode II tips that promotes the initiation of secondary single (e.g. Broek, 1991; Lawn, 1993) or multiple splay fractures (e.g. Cooke, 1997), which are obliquely oriented opening-mode fractures. Theoretical prediction of the propagation paths of these fractures has been verified by laboratory experiments (Brace and Bombolakis, 1963; Erdogan and Sih, 1963; Nemat-Nasser and Horii, 1982; Thomas and Pollard, 1993), which show that tensional fractures (mode I) propagate in the direction parallel to the maximum principal stress (Segall and Pollard, 1983).

Chinnery (1966b) classified several secondary fault modes with more complex geometries (Fig. 5.25), which were derived from the results of a modelling study (Chinnery, 1966a). The *type A* fractures represents the basic tendency for a strike-slip fault to extend itself (c.f. 'splay faults' of Anderson, 1951), and includes branching "splay" or "horsetail" faults (Fig. 5.5, 5.7-5.9, 5.15, 5.19, 5.20 and 5.21). *Type B* fractures are antithetic and conjugate to type A, and occur frequently (Fig. 5.19, 5.20 and 21). The semi-circular *type C* fractures are seen around fault tips including old segment tips (Fig. 5.13 and 5.19). Other types of fractures have not been observed in this area.

Type B fractures arise from the conjugate directions of shearing associated with the near-field stress distribution, and they are analogous to R' shears or high angle (X) fractures. Type B fractures are divided into two groups, R' shears and high angle (X) fractures, depending on the fracture orientations based on Bartlett *et al.* (1981). R' shears are dominant at tip zones (Chapter 4), and high angle (X) fractures (Logan *et al.*, 1979) are frequently observed along fault walls (Figs. 5.13, 5.15, 5.17 and 5.18).

5.6.2. Wall zone damage

High-angle antithetic fractures (X) (Logan *et al.*, 1979; Bartlett, *et al.*, 1981) as a wall zone damage are shown in Figures 5.7, 5.13, 5.15, 5.17 and 5.18. Bartlett *et al.*, (1981) suggested, from analogue modelling, that high angle (X) shear fractures initiate in the post-peak region where fracture zones contain a higher percentage of R shears, P shears and gouge, and are not common in early stages of fault evolution. In consequence, high angle (X) fractures dominate in wall zone of main fault and R' or T fractures are predominant around fault tips and relay zones. Therefore, R' fractures occur at an early stage at mode III tips and at all stages in mode II tips (e.g. Chapter 4), whereas high angle (X) fracture frequently occurs at a mature stage of wall zones and tip zones.

Subsidiary faults or fractures, formed during distributed shear strain within the fault zone, rotate as passive markers during further shear strain (Arboleya and Engelder, 1995). The amount of rotation depends on the amount of displacement and on the initial orientation of each subsidiary fracture (Ramsay and Huber, 1987; Arboleya and Engelder, 1995). Therefore, rotation of R' shears may lead to fractures with the same orientation as later generated X fractures.

A fault system is the result of accumulation of small movements over a long period of time. Furthermore, irregularities along the fault plane will cause local stress concentration and local redistribution of stress. As a result, second order faults will not all make the same angle with the main fault (McKinstry, 1953). Fracture orientation depends on material properties (e.g. McKinstry, 1953), stress condition (e.g. Chinnery, 1966b; Bartlett *et al.* 1981; Schreurs and Colletta 1998), and amount of rotation (Arboleya and Engelder, 1995).

A large secondary fault may well give rise to new subsidiary faults (Chapter 4; Davis *et al.*, 2000). For example, in map R04 (Fig. 5.17), higher order secondary faults

are developed at a slightly different orientation from that of the larger faults (Chapter 4). Arboleya and Engelder (1995) suggested that once the boundary faults develop, the local stress field must reorient in the vicinity of the fault. Usually it seems that when a secondary fault propagates out of the region of influence of the master fault it curves to become parallel to the appropriate complementary shear direction (Chinnery 1966b).

In consequence, microcrack and fracture orientation may change with fracture order (Chapter 4; McKinstry, 1953; Chinnery, 1966b; Arboleya and Engelder, 1995; Willemse *et al.*, 1997), local stress re-distribution (Chapter 4; Moore and Lockner, 1995; Vermilye and Scholz, 1998) and in relation to pre-existing structures (Peacock and Sanderson, 1992; Du and Aydin, 1995). However, the mechanism of fracture is similar regardless of the orders in the same tectonic setting.

In the study area, the angular relationship between dominant right-lateral strike-slip faults and left-lateral strike-slip faults as conjugate or secondary faults is about 85°. Pinnate style fractures and veins are also developed, which are en-echelon structures that branch diagonally from one side of a master fracture. Some pinnate fractures are tension gashes or Riedel shears but others are conjugate, antithetic shears at about 60° ~ 90° to the master fracture (Hancock 1972).

5.6.3. Block rotation

Some of high-angle fractures form long antithetic linking faults within a overstep zone (Fig. 5.22). Although the characteristic of these linking fractures is not clear, they could be interpreted as slightly rotated R' fractures or conjugate fault sets, because high angle (X) fracture is already described as having a different orientation. The combination can allow later block rotation. For example, in Figure 5.19 the wedge-shaped area between the two faults is rotated by antithetic shear fractures (R' or type B of Chinnery, 1966b). Several similar fracture patterns have been described from Gozo (Chapter 4). In most examples, antithetic cross-fractures are generated as R' shears, but the fractures in Figure 5.21 show high angle (X) fracture orientation pattern.

Generally, as deformation proceeds, slip on the faults takes place, which is associated with the rotation of the faults and the blocks between the faults (Nur *et al.* 1986). Intersecting wedge-shaped branch faults and/or antithetic faults provide good

conditions for block rotation (Fig. 5.21). A similar model for block rotation has already been suggested in Gozo (Chapter 4) and in tectonic models (Nicholson *et al.*, 1986).

5.6.4. Lens-shaped structures

Lens-shaped structures in strike-slip fault system have been described by a number of workers and may be grouped as follows; i) "strike-slip duplexes" (Woodcock and Fischer, 1986; Swanson, 1988; Cruikshank *et al.*, 1991), ii) "sidewall ripouts" (Swanson, 1989), iii) "open eye-structures" (Fossen and Hesthammer, 1997). Lens-shaped structures are commonly developed at Rame Head and are interpreted as originating from old fault tips or relay zones.

Some possible mechanisms and evolution are suggested for the development of these lens-shaped structures (Fig. 5.26a). Two fault segments approach towards each other (stage 1). At the transfer zone between adjacent fault segments, the segments branch and lengthen to grow a linked fault (stage 2) (Fig. 5.3). One segment tip links to the other segment, with the other segment tip propagating onwards (stage 3) (Figs. 5.3, 5.5 and 5.23). The free tip is curved and eventually links with the other segment producing a lens (stage 4) (Fig. 5.24). By subsequent displacement along the fault, lens-structures generate other fractures within and/or outside the structures to form strike-slip duplexes (stages 5-7).

The connecting faults form different patterns and shapes, with different degrees of complexity and number of connectors (Cruikshank *et al.*, 1991). The observed thickening with the lens was interpreted as a result of original curvature and interaction between fault segments. Displacement along the fault generally decreases at the lens-shaped structures, because the displacement is transferred into two branch faults and due to bending, supporting the interpretation that the zones were old fault tips or relay ramps.

It is common to interpret faults as growing by segment linkage (e.g. Peacock, 1991; Peacock and Sanderson, 1991; Cartwright *et al.*, 1995; Fossen and Hesthammer, 1997; Kim *et al.*, 2000). Therefore, lens-shaped structures subsequently break down and induce duplexes.

The type of hard-linkage in joint system has been interpreted to indicate a relative age difference between the linking segments (Cruikshank and Aydin, 1995).

The straight segment is considered to be older, and the curved one veers as it approaches and becomes influenced by the local variation in stress field caused by the already existing straight segment.

Another model for lens-shaped structures is suggested (Fig. 5.26b) based on observed semi-circular fractures (Fig. 5.13 and 5.19). Some of the lens-shaped structures could be developed through these fracture patterns at fault bends with type C fault branches (Figs. 5.25 and 5.26b). This type of lens-shaped fracture geometry is very similar to 'sidewall ripouts' (Swanson, 1989). However, this type has little damage within the lens-shaped structures, and is usually located in one side of the fault wall with an asymmetric shape. For this type of lens-shaped structures, there might be no displacement minimum at the lens-shaped structures (Fig. 5.15).

Most of the lens-shaped structures in the study area fall within these two groups, but there are some others that show a slightly different pattern (Fig. 5.26c). This type shows slight misalignment of two fault segments (narrow separation) (Fig. 5.3), generally asymmetric lenses, and tip damage pattern around the lens-shaped structures producing low displacement (Fig. 5.13). One of the segment tips terminated against the other segment and transfer displacement through the linking fracture. The other tip is linked in a later stage to form a lens-shaped structure. Although this type is very similar to strike-slip duplexes, the narrow separation between two segments might not allow developing duplex structures in later stages.

5.6.5. Relationship between strike-slip fault geometry and displacement

The *d-x* profiles of strike-slip faults in the study area are highly variable as has also been described in normal fault systems (Cartwright and Mansfield, 1998). The variability is too large to be attributed to measurement errors.

Asymmetry and displacement minima in displacement profiles are typically associated with segment linkage and fault branching. Interaction between segments prior to linkage results in accentuation of displacement gradients in the region of segment overlap (Walsh and Watterson, 1990; Peacock, 1991; Peacock and Sanderson, 1991; Trudgill and Cartwright, 1994; Huggins *et al.*, 1995; Fossen and Hesthammer, 1997). Displacement profiles showing irregular distributions along strike occur at boundaries between adjacent segments (Peacock, 1991; Willemse *et al.*, 1996), splay faults (Huggins *et al.*, 1995; Cartwright and Mansfield, 1998), or lens-

shaped structures marked by substantial displacement minima. If total displacement profiles are obtained, they might produce smoother profiles than those of the main faults alone (e.g. Fig. 5.14) (Cartwright and Mansfield, 1998).

At Rame Head, most of the highly asymmetric profiles are interpreted as this type of interaction effect, because they show higher displacement gradients and displacement minima at oversteps, lens-shaped zones or branching zones (Figs. 5.4, 5.6, 5.12 and 5.14). This complex distribution is thought to be the result of the fault growth history involving the lateral propagation and linkage of early-formed segments (Chapter 2 and 4; Cartwright *et al.*, 1995, 1996; Kim *et al.*, 2000). As these early irregularities are smoothed out by the formation of lenses, the overall *d-x* profile becomes simpler, as has been described for normal faults (Dawers and Anders, 1995).

The large range of lateral displacement gradients in faults is mainly due to interactions between neighbouring faults (Willemse, *et al.*, 1996; Cartwright and Mansfield, 1998). Additional complexities may result from local variations in remote loading stresses and the frictional properties of the fault surfaces (Bürgmann *et al.*, 1994), from propagation rate (Peacock and Sanderson, 1996), from the distribution of friction coefficient (Cooke, 1997), and from processes related to non-planar or discontinuous segment linkage (Peacock, 1991; Peacock and Sanderson, 1991; Bürgmann *et al.*, 1994; Cartwright, *et al.*, 1995, 1996; Fossen and Hesthammer, 1997; Cartwright and Mansfield, 1998). In summary, slip along a fault may vary as a result of lithologic variations (Bürgmann *et al.*, 1994), interaction with nearby structures (Willemse *et al.*, 1996), and irregular fault geometries (Schultz and Aydin, 1990).

5.6.6. Maximum displacement / fault length (d_{max}/L) relationship

The general expression of the relationship between the maximum cumulative displacement on a fault (d_{max}) and the fault length (L) is given as;

$$d_{max} = cL^n , \qquad (1)$$

where the value of c is dependent on rock properties and the range of the exponent value, n, is from 1 to 2 (Chapter 2).

The relationship of d_{max}/L for measured strike-slip faults in the study area is plotted in Figure 5.27. Even though data are only available for seven faults, the distribution shows evidence for the pattern of fault growth. Most of the data have

values of d_{max}/L lying between 10^{-1} and 10^{-2}; two partly soft-linked faults plot near $d_{max}/L = 10^{-2}$ with hard-linked faults plotting near $d_{max}/L = 4 \times 10^{-2}$. From this result, two main points can be made. (1) The faults R01, R02, R05, R07(A) and R07(B) may be hard-linked faults forming a geometrically coherent system. (2) Displacement is concentrated along master faults (Sibson, 1989; Cowie and Scholz, 1992), if a fault system is mature. The hard-linked faults lie on a line of slope $n = 1$ and $d_{max}/L = 4 \times 10^{-2}$. Partly soft-linked faults (R12 and R09; Fig. 5.3 and 5.5) have lower ratios of d_{max}/L. This suggests that faults grow through segment linkage (e.g. Peacock and Sanderson, 1991), and that displacement is concentrated on the master fault as it increases. This result is similar to that obtained from Crackington Haven (Chapter 2). Therefore the argument for the 'step-like growth path' model (Cartwright *et al.*, 1995; Kim *et al.*, 2000) is still applicable to these mature strike-slip faults.

5.7. CONCLUSIONS

1. Several metres to tens of metre long right-lateral strike-slip faults strike WNW-ESE. NE-SW left-lateral strike-slip faults are also developed. The remote maximum compressive stress (σ_1) forming these conjugate strike-slip fault sets is about N160°. Extensional veins (mode I) are parallel to this orientation.
2. A lot of lens-shaped structures link fault segments.
3. *d-x* profiles are very variable and irregular resulting from segment linkage through lens-shaped structures and branch faults. These structures influence displacement along a fault, so that displacement rapidly decreases when the fault meets these shape structures. This suggests that the lens-shaped structures are developed from segment fault tips and relay ramps. If the fault system as a whole is considered, the *d-x* relationship more or less resembles that for a single fault. Where local displacement minima occur, they indicate relays, lens-shaped structures or branch faults.
4. Most of the major fault tips are mode II at which damage structures are dominated by horsetail splay fractures at a low angle to the main fault.
5. Along the faults damage is caused in the wall rock, where it is dominantly formed by high angle fractures (X or R').

6. The maximum displacement / fault length (d_{max}/L) plot for the strike-slip faults is higher for hard-linked relays with lens-shapes structures (~ 4×10^{-2}) than for soft-linked relays (~ 1×10^{-2}).

REFERENCES

Anderson, E. M. 1951. *The Dynamics of Faulting.* Olivier and Boyd, Edinburgh.

Arboleya, M.-L., and Engelder, T., 1995. Concentrated slip zones with subsidiary shears: their development on three scales in the Cerro Brass fault zone, Appalachian Valley and Ridge. *Journal of Structural Geology* **17**, 519-532.

Arthaud, F. and Matte, Ph. 1977, Late Palaeozoic strike slip faulting in southern Europe and northern Africa: result of a right lateral shear zone between the Appalachians and the Urals. *Bull. geol. Soc. Am.* **88**, 1305-1320.

Bartlett, W. L., Friedman, M. and Logan, J. M. 1981. Experimental folding and faulting of rocks under confining pressure. Part IX. Wrench faults in limestone layers. *Tectonophysics* **79**, 255-277.

Brace, W. F. and Bombolakis, E. G. 1963. A note on brittle crack growth in compression. *Journal of Geophysical Research* **68**, 3709-3713.

Bristow, C. M., Durrance, E. M. and Selwood, E. B. 1998. Introduction. In: *The Geology of Cornwall.* Exter, University of Exter Press, 298pp (edited by E. B. Selwood, E. M. Durrance and C. M. Bristow). 1-15.

Broek, D. 1991. *Elementary Engineering Fracture Mechanics.* 469 pp. Kluwer Acad,. Norwell, Boston.

Bürgmann, R., Pollard, D. D. and Martel, S. J. 1994. Slip distributions on faults: effects of stress gradients, inelastic deformation, heterogeneous host-rock stiffness, and fault interaction. *Journal of Structural Geology* **16**, 1675-1690.

Burton, C. J. and Tanner, P. W. G. 1986. The stratigraphy and structure of the Devonian rocks around Liskeard, east Cornwall, with regional implications. Journal of the Geological Society of London **143**, 95-105.

Cartwright, J. A. and Mansfield, C. S. 1998. Lateral displacement variation and lateral tip geometry of normal faults in the Canyonlands National Park, Utah. *Journal of Structural Geology* **20**, 3-19.

Cartwright, J. A., Mansfield, C. S. and Trudgill, B. D. 1996. Fault growth by segment linkage. In *Modern developments its structural interpretation*, eds P. C. Buchanan and D. A. Nieuwland, Vol. 99, 163-177. *Special Publication of the Geological Society of London.*

Cartwright, J. A., Trudgill, B. D. and Mansfield, C. S. 1995. Fault growth by segment linkage: an explanation for scatter in maximum displacement and trace length data from the Canyonlands Grabens of SE Utah. *Journal of Structural Geology* **17**, 1319-1326.

Chinnery, M. A. 1966a. Secondary faulting: I. Theoretical aspects. *Canadian Journal of earth Sciences* **3**, 163-174.

Chinnery, M. A. 1966b. Secondary faulting: II. Geological aspects. *Canadian Journal of earth Sciences* **3**, 175-190.

Christie-Blick, N. and Biddle, K. T. 1985. Deformation and basin formation along strike-slip faults. In *Strike-slip Deformation, Basin Formation, and Sedimentation*: Eds: Biddle, K. T. and Christie-Blick, N. *Society of Economic Palaeontologists and Mineralogists Special Publication* **37,** 1-34.

Cooke, M. L. 1997. Fracture localization along faults with spatially varying friction. *Journal of Geophysical Research* **102**, 22,425-22,434.

Cowie, P. A. and Scholz, C. H. 1992. Physical explanation for the displacement-length relationship for faults using a post-yield fracture mechanics model. *Journal of Structural Geology* **14**, 1133-1148.

Cruikshank, K. M. and Aydin, A. 1995. Unweaving the joints in Entrada Sandstone, Arches National Park, Utah, U. S. A. *Journal of Structural Geology* **17**, 409-421.

Cruikshank, K. M., Zhao, G. and Johnson, A. M. 1991. Duplex structures connecting fault segments in Entrada Sandstone. *Journal of Structural Geology* **13**, 1185-1196.

Davis, G. H., Bump, A. B., Garcia, P. E. and Ahlgren, S. G. 2000. Conjugate Riedel deformation band shear zones. *Journal of Structural Geology* **22**, 169-190.

Dawers, N. H. and Anders, M. H. 1995. Displacement-length scaling and fault linkage. *J. Struct. Geol.,* **17**, 607-614.

Du, Y. and Aydin, A. 1995. Shear fracture patterns and connectivity at geometric complexities along strike-slip faults. *Journal of Geophysical Research* **100**, 18,093-18,102.

Erdogan, F. and Sih, G. C. 1963. On the crack extension in plates under plane loading and transverse shear. *J. Basic Eng.,* **85**, 519-527.

Fossen, H. and Gabrielsen, R. H. 1996. Experimental modeling of extensional fault systems by use of plaster. *Journal of Structural Geology* **18**, 673-687.

Fossen, H. and Hesthammer, J. 1997. Geometric analysis and scaling relations of deformation bands in porous sandstone. *Journal of Structural Geology* **19**, 1479-1493.

Freund, R. 1974. Kinematics of transform and transcurrent faults. Tectonophysics **21**, 93-134.

Gibbs, A. D. 1984. Structural evolution of extensional basin margins. *Journal of Geological Society of London* **141**, 609-620.

Granier, T. 1985. Origin, damping and pattern of development of faults in granite. *Tectonics* **4**, 721-737.

Hancock, P. L. 1972. The analysis of en-echelon veins. *Geol. Mag.* **109**, 269-276.

Harding, T. P., Vierbuchen, R. C. and Christie-Blick, N. 1985. Structural styles, plate-tectonic settings, and hydrocarbon traps of divergent (transtensional) wrench faults - Strike-slip deformation, basin formation, and sedimentation. In *Strike-slip Deformation, Basin Formation, and Sedimentation*: Eds: Biddle, K. T. and Christie-Blick, N. *Society of Economic Paleontologists and Mineralogists Special Publication,* **37**, 51-77.

Huggins, P., Watterson, J., Walsh, J. J. and Childs, C. 1995. Relay zone geometry and displacement transfer between normal faults recorded in coal mine plans. *Journal of Structural Geology* **17**, 1741-1755.

Kim, Y.-S., Andrews, J. R. and Sanderson, D. J. 2000. Damage zones around strike-slip fault systems and strike-slip fault evolution, Crackington Haven, southwest England. *Geoscience Journal* **4**, 53-72.

Lawn, B. 1993. *Fracture of Brittle Solids*, 2nd ed., 378 pp. Cambridge Univ. Press, new York.

Logan, J. M., Friedman, M., Higgs, N., Dengo, C. and Shimamoto, T. 1979. Experimental studies of simulated gouge and their application to studies of natural fault zones. *U.S. geol. Surv. Open-File Report* **79-1239**, 305-343.

McKinstry, H. E. 1953. Shears of the second order. American Journal of Science 251, 401-414.

Moore, D. E. and Lockner, D. A. 1995. The role of microcracking in shear-fracture propagation in granite. *Journal of Structural Geology* **17**, 95-114.

Nemat-Nasser, S. and Horii, H. 1982. Compression-induced nonplanar crack extension with application to splitting, exfoliation, and rockburst. *Journal of Geophysical Research* **87**, 6805-6821.

Nicholson, C., Seeber, L., Williams, P. and Sykes, L. R. 1986. Seismic evidence for conjugate slip and block rotation within the San Andreas fault system, southern California. *Tectonics* **5**, 629-648.

Nicol, A., Watterson, J., Walsh, J. J. and Childs, C. 1996. The shapes, major axis orientations and displacement patterns of fault surfaces. *Journal of Structural Geology* **18**, 235-248.

Nur, A., Ron, H. and Scotti, O. 1986. Fault mechanics and the kinematics of block rotations. *Geology* **14**, 746-749.

Olson, J. E. and Pollard, D. D. 1989. Inferring paleostresses from natural fracture patterns: A new method. *Geology* **17**, 345-348.

Peacock, D. C. P. 1991. Displacement and segment linkage in strike-slip fault zones. *Journal of Structural Geology* **13**, 1025-1035.

Peacock, D. C. P. and Sanderson, D. J. 1991. Displacement and segment linkage and relay ramps in normal fault zones. *Journal of Structural Geology* **13**, 721-733.

Peacock, D. C. P. and Sanderson, D. J. 1992. Effects of layering and anisotropy on fault geometry. *J. Geol. Soc. London.* **149**, 793-802.

Peacock, D. C. P. and Sanderson, D. J. 1995. Strike-slip relay ramps. *Journal of Structural Geology* **17**, 1351-1360.

Peacock, D. C. P. and Sanderson, D. J. 1996. Effects of propagation rate on displacement variations along faults. *Journal of Structural Geology* **18**, 311-320.

Petit, J. -P. and Barquins, M. 1988. Can natural faults propagate under Mode II conditions? *Tectonics* **7**, 1243-1256.

Ramsay, J. G. and Huber, M. I. 1987. *The Techniques of Modern Structural Geology.* Volume 2, Folds and fractures. Academic Press, London. pp.309-700.

Schreurs G. and Colletta, B. 1998. Analogue modelling of faulting in zones of continental transpression and transtenstension. In: Holdsworth, R. E., Strachan, R. A. & Dewey, J. F. (eds). *Continental Transpressional and Transtensional Tectonics.* Geol. Soc. Lon. Spec. Pub. **135**, 59-79.

Schultz, R. A. and Aydin, A. 1990. Formation of interior basins associated with crved faults in Alaska. *Tectonics* **9**, 1387-1407.

Segall, P. and Pollard, D. D. 1983. Nucleation and growth of strike-slip faults in granite. *J. Geophys. Res.*, **88**, 555-568.

Sibson, R. H. 1989. Earthquake faulting as a structural process. *Journal of Structural Geology* **11**, 1-14.

Swanson, M. T. 1988. Pseudotachylyte-bearing strike-slip duplex structures in the Fort Foster Brittle Zone, S. Maine. *Journal of Structural Geology* **10**, 813-828.

Swanson, M. T. 1989. Sidewall ripouts in strike-slip faults. *Journal of Structural Geology* **11**, 933-948.

Thomas, A. L. and Pollard, D. D. 1993. The geometry of echelon fractures in rock: Implications from laboratory and numerical experiments. *Journal of Structural Geology* **15**, 323-334.

Trudgill, B. D. and Cartwright, J. A. 1994. Relay ramp forms and normal fault linkages - Canyonlands National Park, Utah. *Bulletin of the Geological Society of America* **106**, 1143-1157.

Vermilye, J. M. and Scholz, C. H. 1998. The process zone: A microstructural view of fault growth. *Journal of Geophysical Research* **103**, 12223-12237.

Vermilye, J. M. and Scholz, C. H. 1999. Fault propagation and segmentation: insight from the microstructural examination of a small fault. *Journal of Structural Geology* **21**, 1623-1636.

Walsh, J. J. and Watterson, J. 1990. New methods of fault projection for coalmine planning . Proceedings of the Yorkshire Geological Society 48, 209-219.

Walsh, J. J. and Watterson, J., Bailey, W. R. and Childs, C. 1999. Fault relays, bends and branch-lines. *Journal of Structural Geology* **21**, 1019-1026.

Wernicke, B. 1981. Low-angle normal faults in the Basin and Range Province: nappe tectonics in an extending orogen. *Nature* **291**, 645-648.

Willemse, E. J. M., Peacock, D. C. P. and Aydin, A. 1997. Nucleation and growth of strike-slip faults in limestones from Somerset, U. K. *Journal of Structural Geology* **19**, 1461-1477.

Willemse, E. J. M., Pollard, D. D. and Aydin, A. 1996. Three-dimensional analyses of slip distributions on normal fault arrays with consequences for fault scaling. *Journal of Structural Geology* **18**, 295-309.

Woodcock, N. H. and Fischer, M. 1986. Strike-slip duplexes. *Journal of Structural Geology* **8**, 725-735.

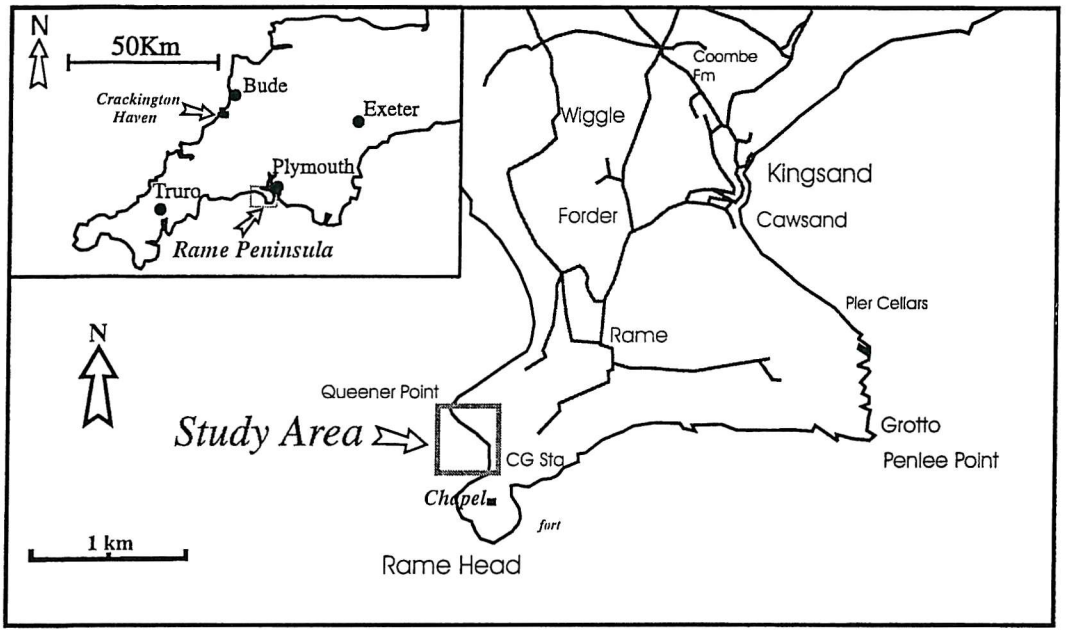

a)

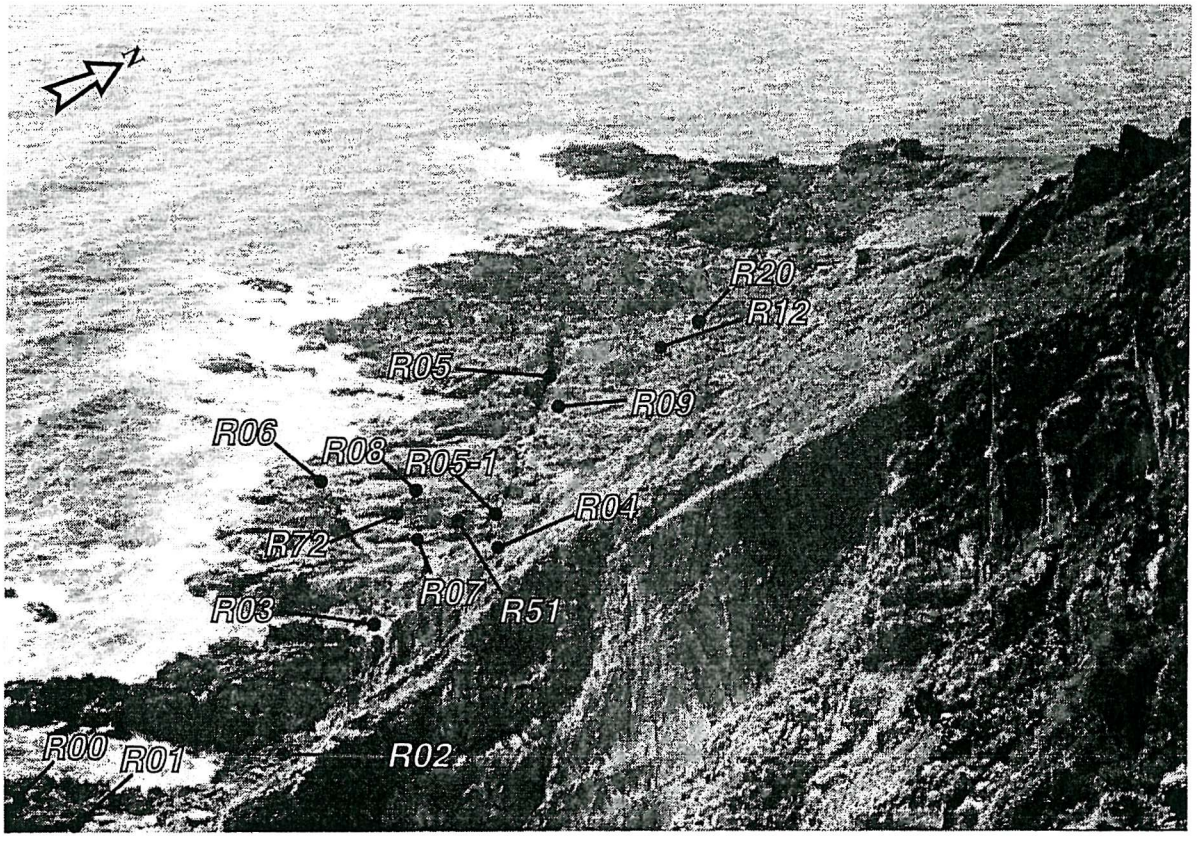

b)

Fig. 5.1. a) Map showing the location of strike-slip faults at Rame Head (SX 417487), southern Cornwall. b) Photo shows the location of studied strike-slip faults and outcrop exposure, within the boxed area in Fig. 5.1a).

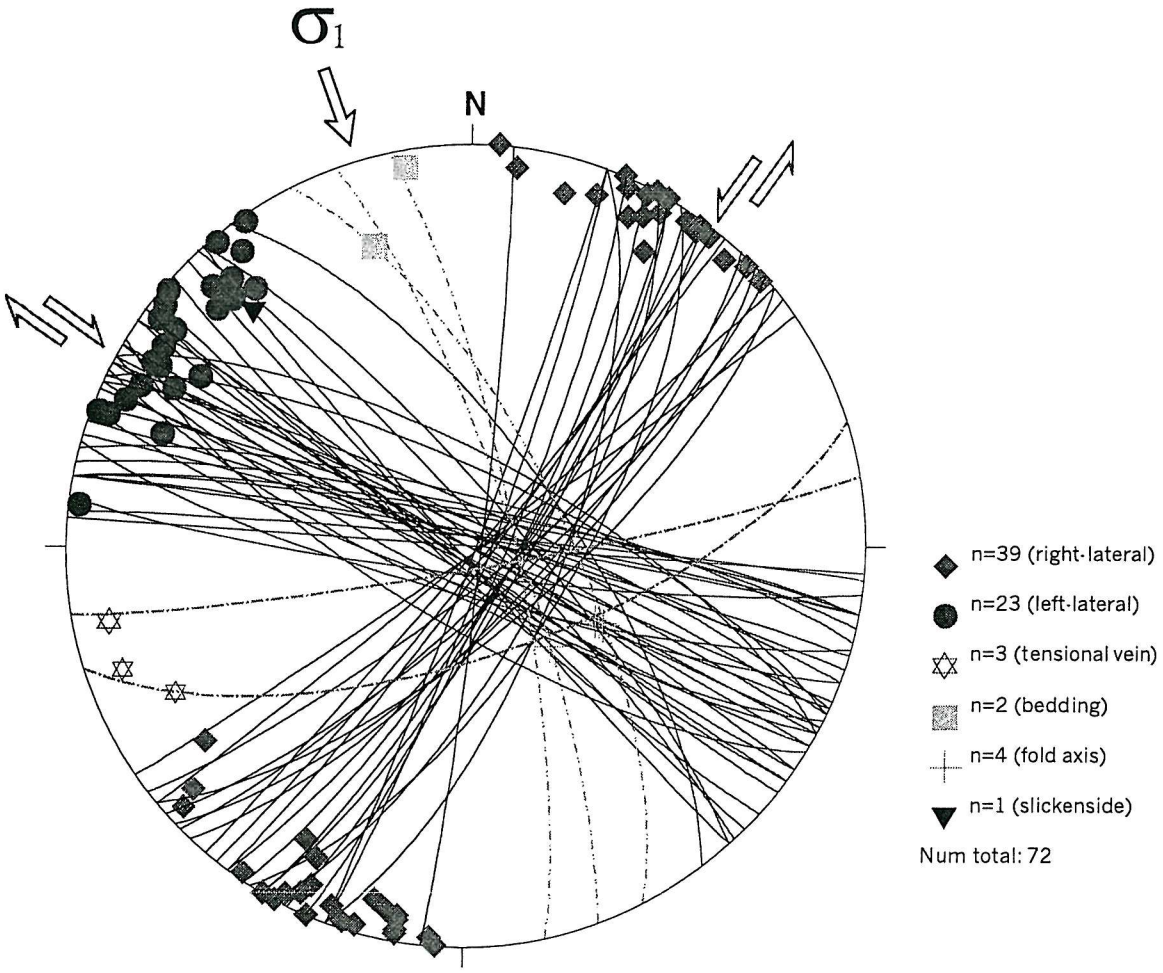

Fig. 5.2. Stereographic projection of bedding, strike-slip faults, tension veins, minor fold axes, and slickenside striae measured at Rame Head. Faults show mainly WNW-ESE orientation for right-lateral and NE-SW for left-lateral. The orientation of assumed σ_1 and extensional veins is about N160°. The general bedding strikes nearly N075°.

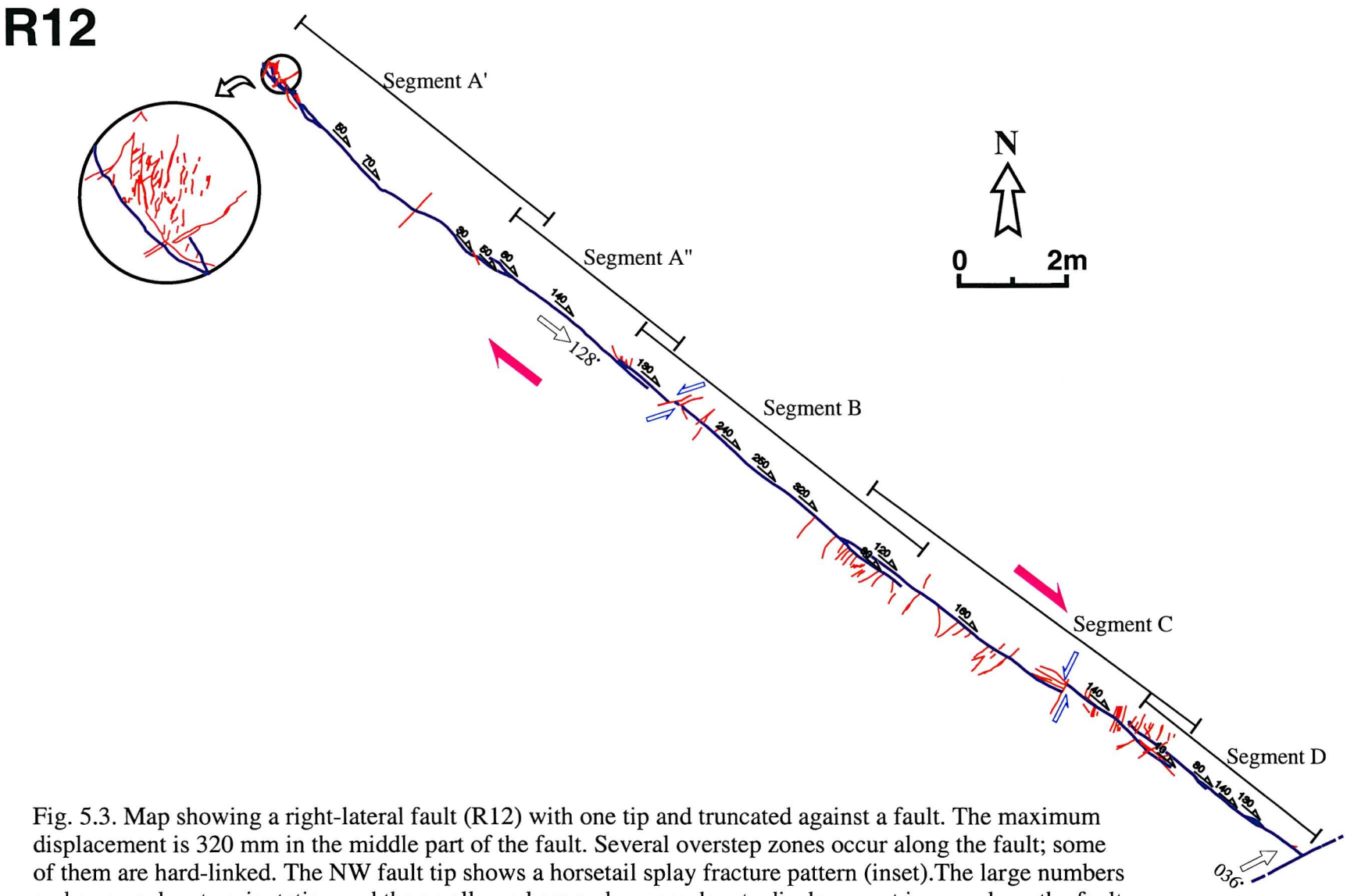

Fig. 5.3. Map showing a right-lateral fault (R12) with one tip and truncated against a fault. The maximum displacement is 320 mm in the middle part of the fault. Several overstep zones occur along the fault; some of them are hard-linked. The NW fault tip shows a horsetail splay fracture pattern (inset).The large numbers and arrows denote orientation and the small numbers and arrows denote displacement in mm along the fault for all the following maps.

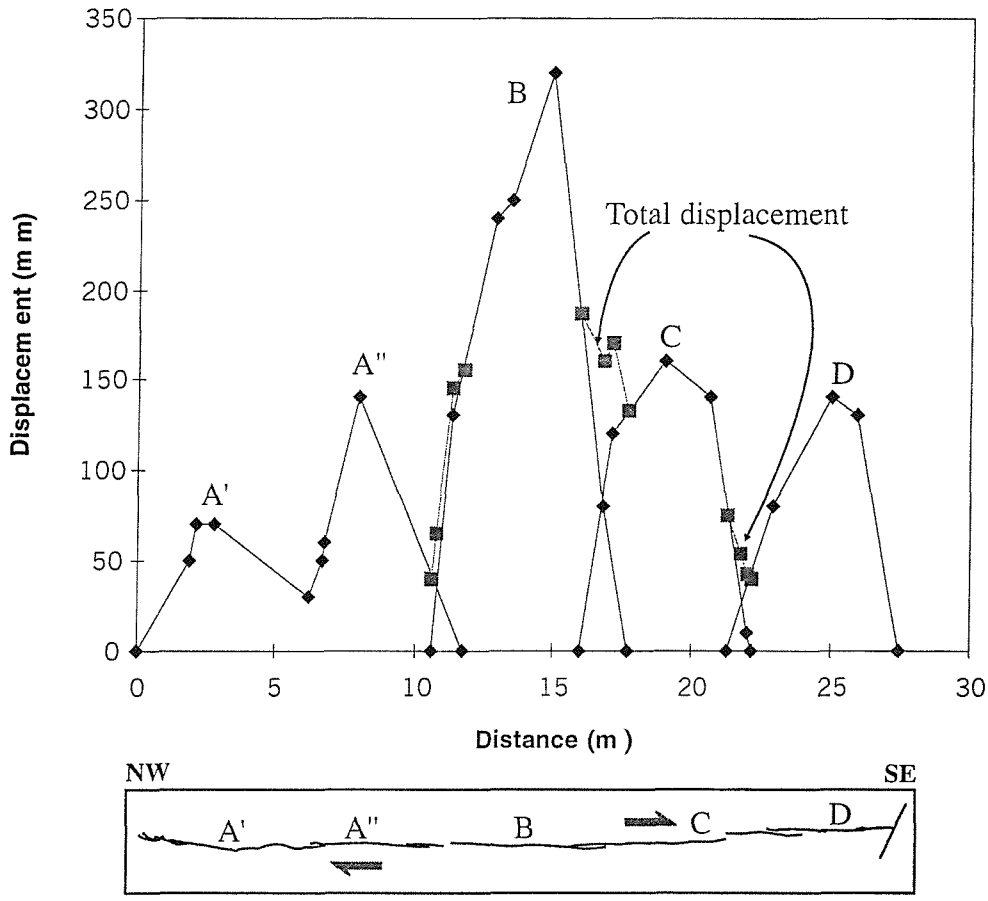

Fig. 5.4. Displacement (d) - distance (x) profile of fault R12; the minima characterize low displacements at relay zones.

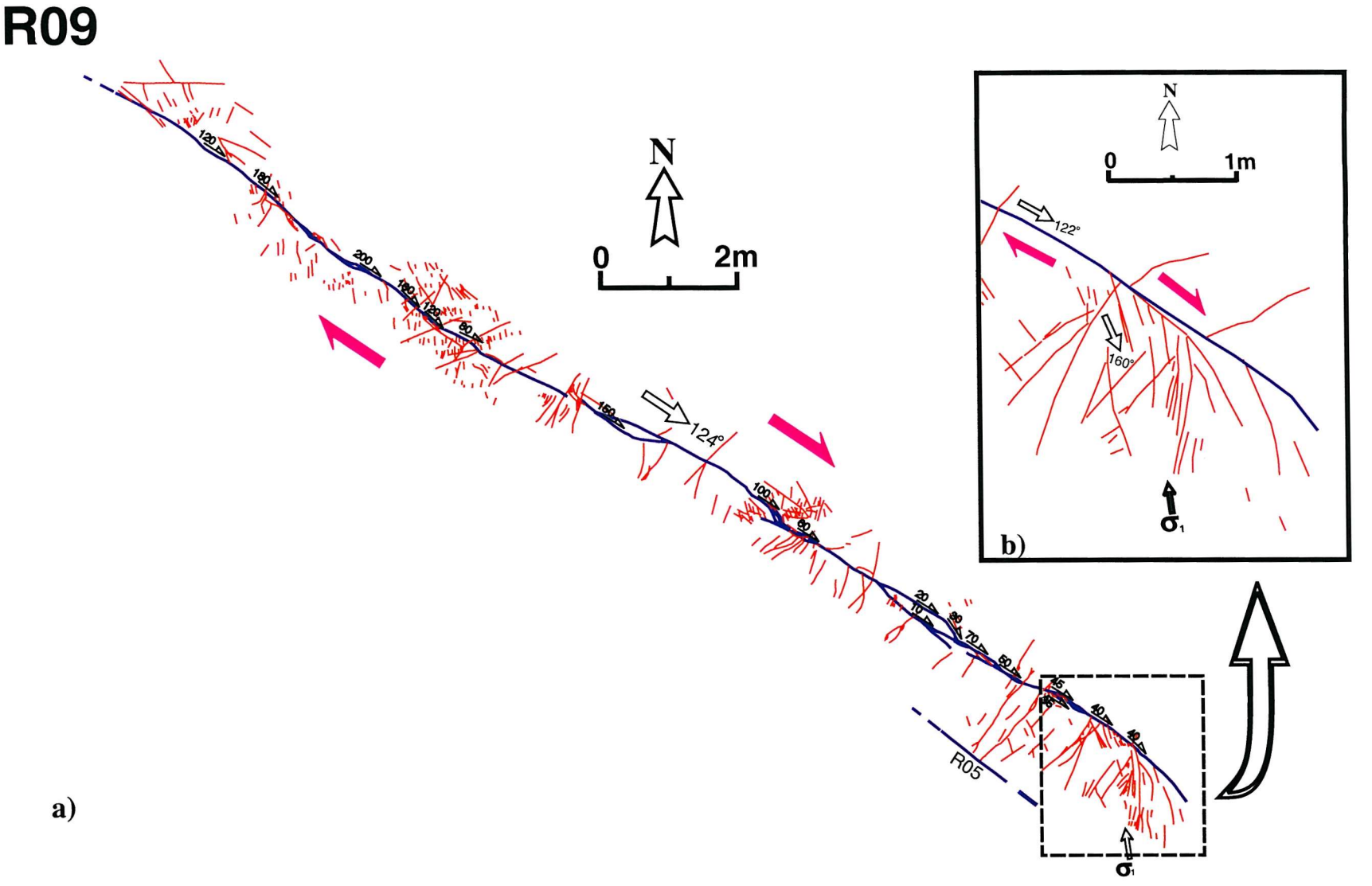

Fig. 5.5. Map view of right-lateral strike-slip fault R09. a) The map shows the fault consists of several linked segments separated by lens-shaped structures. Displacement varies along the fault rising to maximum value of 200 mm. Many secondary fractures are developed along the fault. b) The SE fault tip shows horsetail splay fractures composed of tensional fractures and shows some high angle fractures.

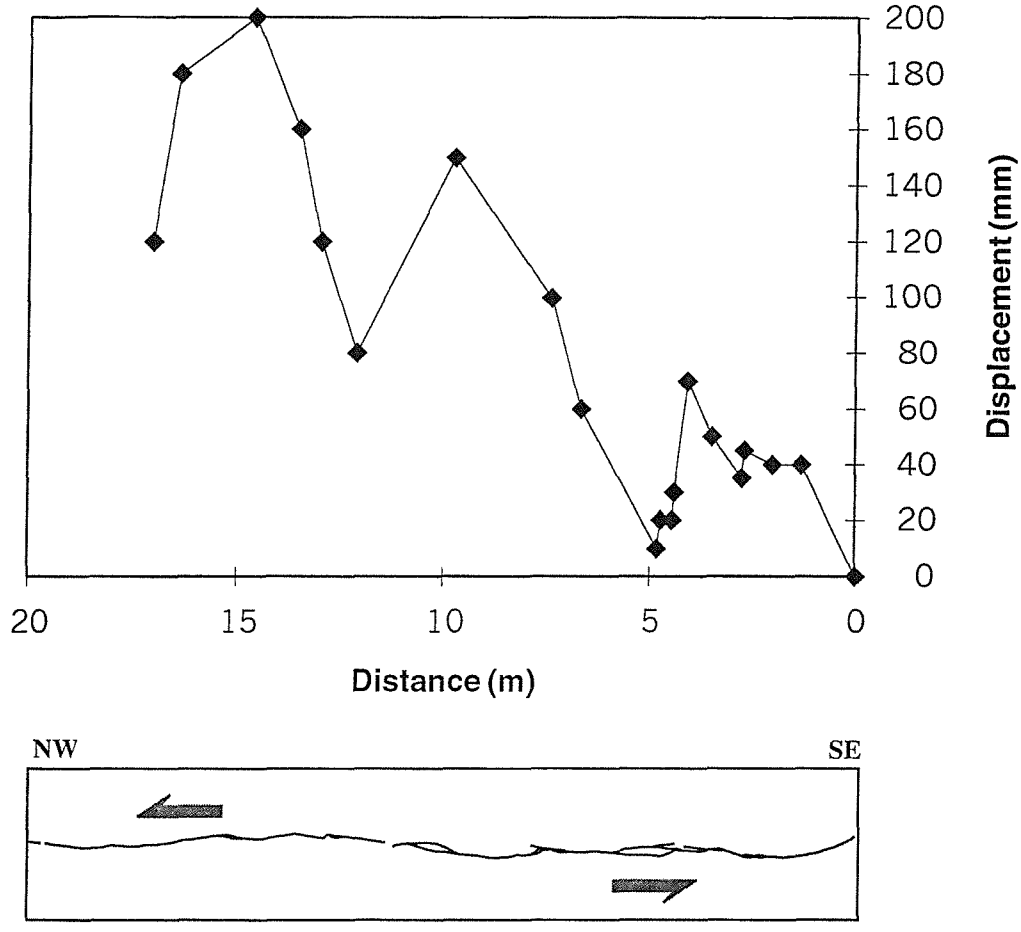

Fig. 5.6. Displacement (d) - distance (x) profile of fault R09, showing several local minima and maxima along the fault, reflecting lens-shaped zones. The general trend of the profile shows that the displacement increases towards the NW that starts to decrease towards the unexposed tip.

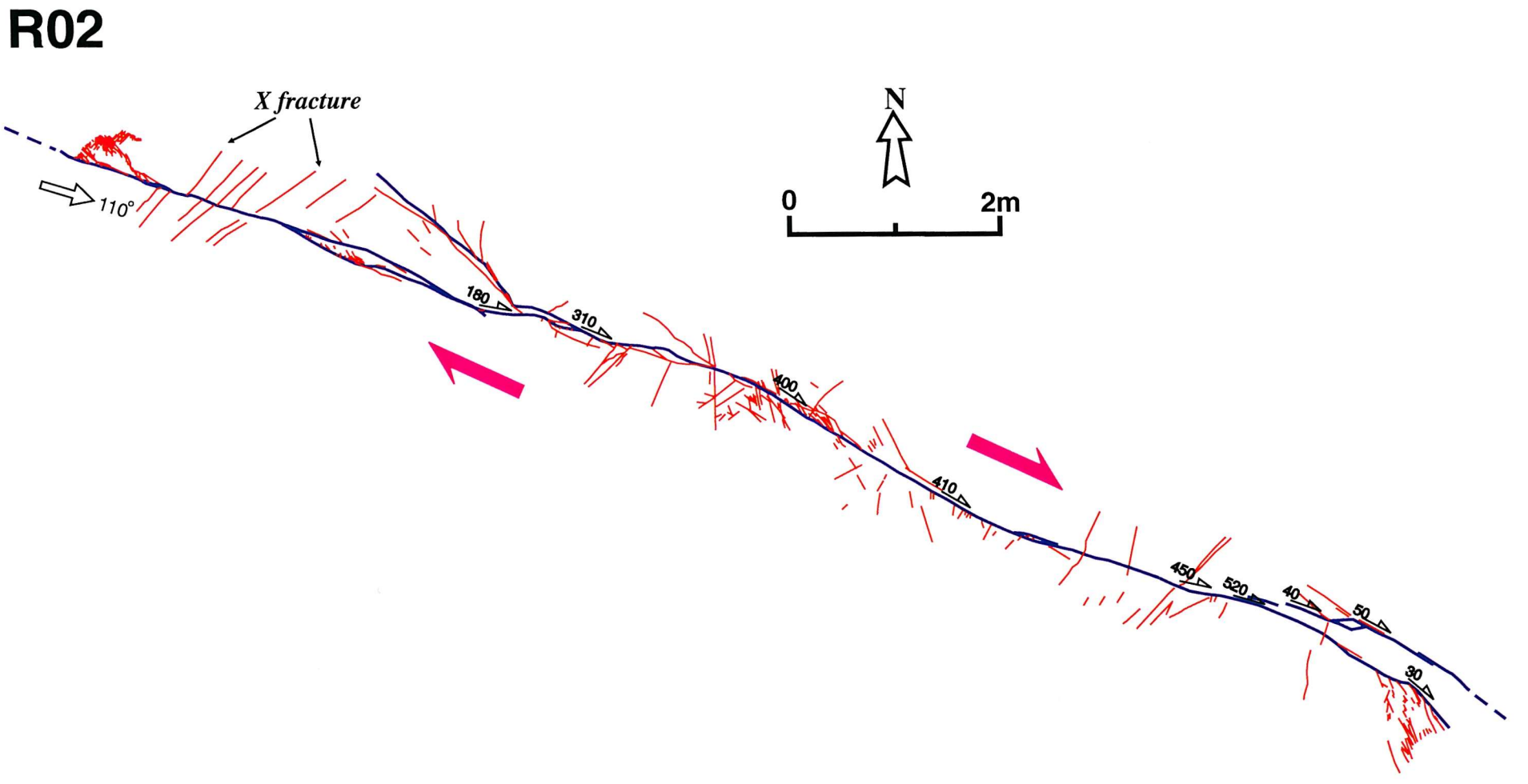

Fig. 5.7. Map of right-lateral strike-slip fault R02. Horsetail splay tip damage fractures occur at both segment tips, and branch faults and high angle fractures are present along the central section. The fault rapidly loses displacement where it branches. The south-eastern branch fault might extend away increasing displacement through linkage.

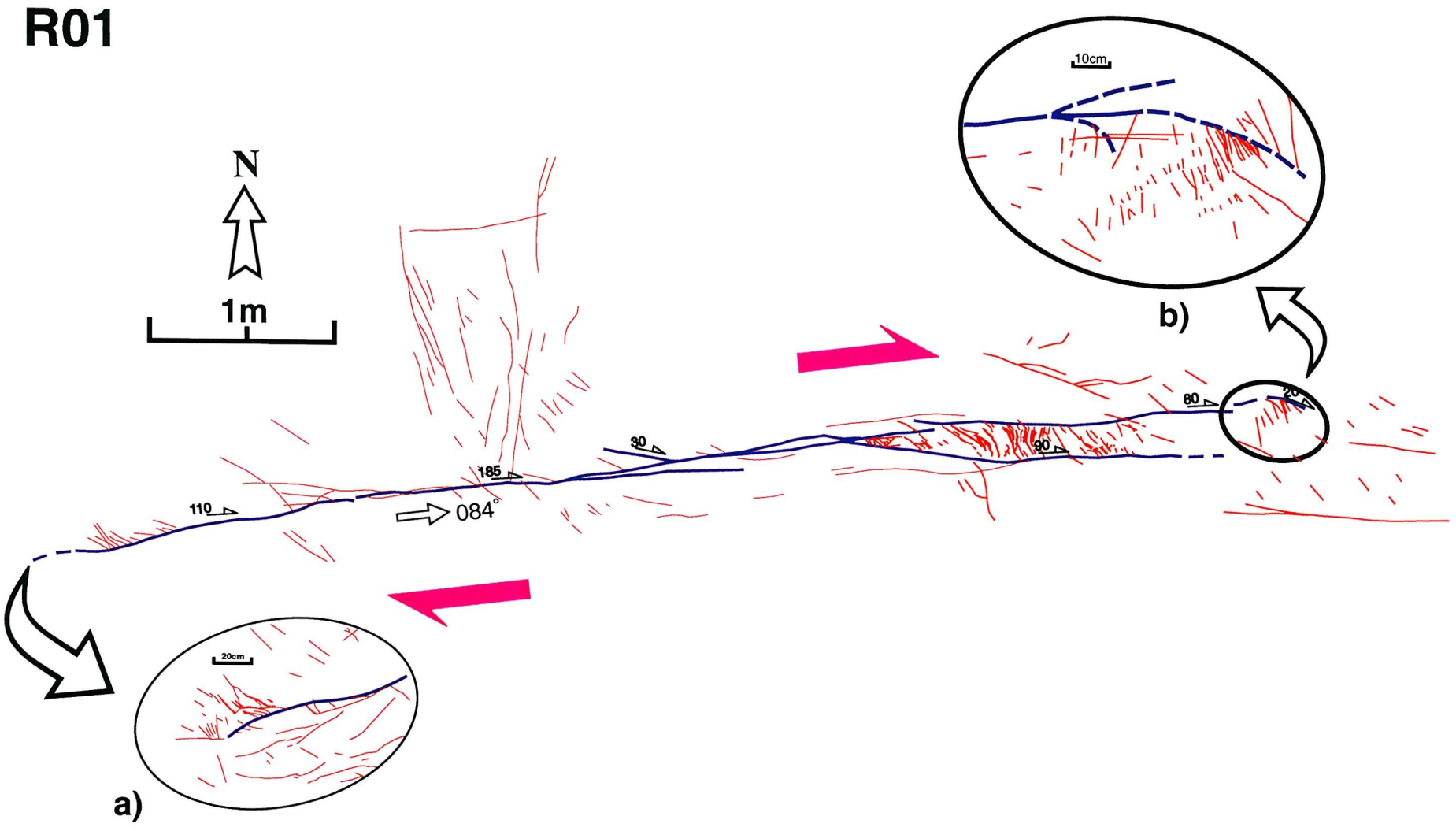

Fig. 5.8. Map of right-lateral strike-slip fault R01. The fault shows horsetail splay tip damage fractures at both tips. At its eastern termination the fault develops a prominant splay. The wedge-shaped block between these two faults is rotated and veined. The vein arrays show sigmoidal shapes.

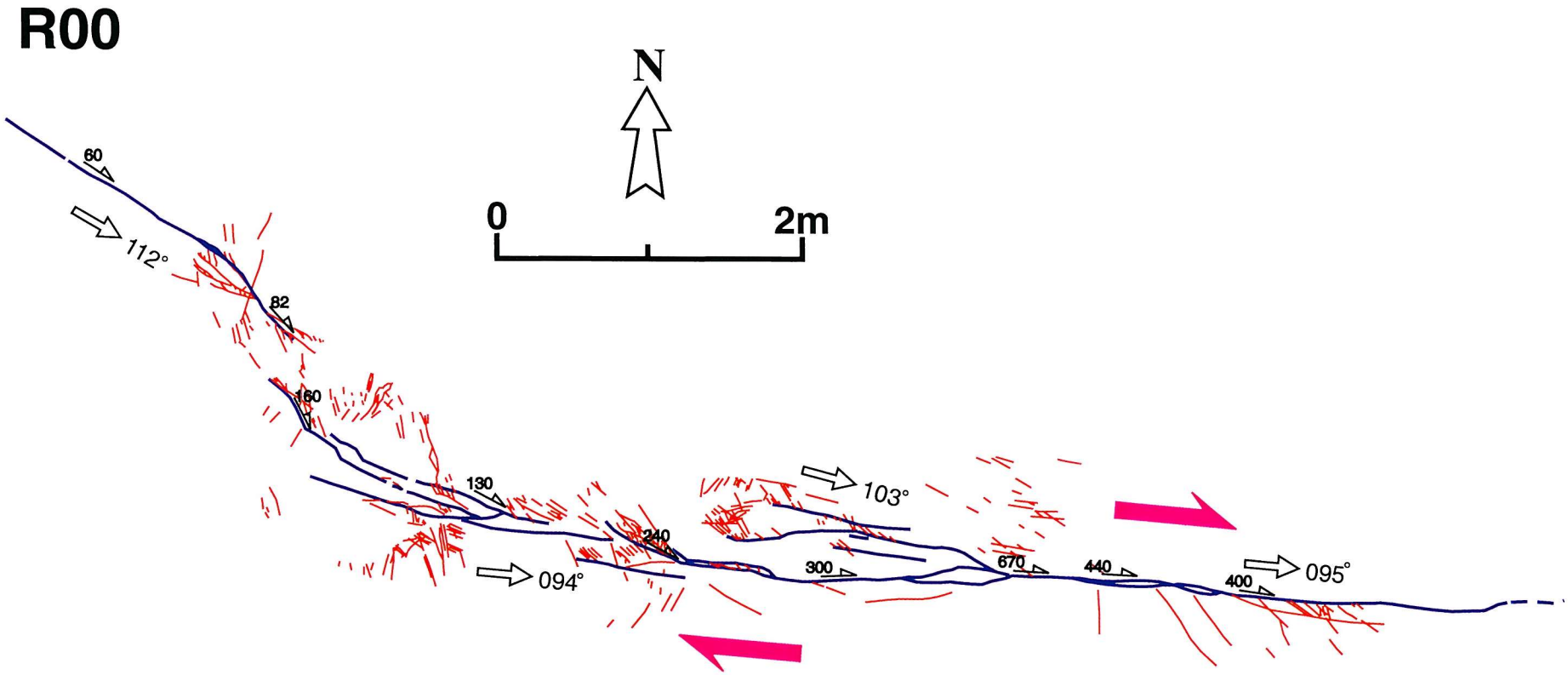

Fig. 5.9. Map of the right-lateral strike-slip fault R00; the central section and north-western termination of the fault are exposed. The fault tip curves toward the dilational quadrant and displacement generally increases toward fault centre.

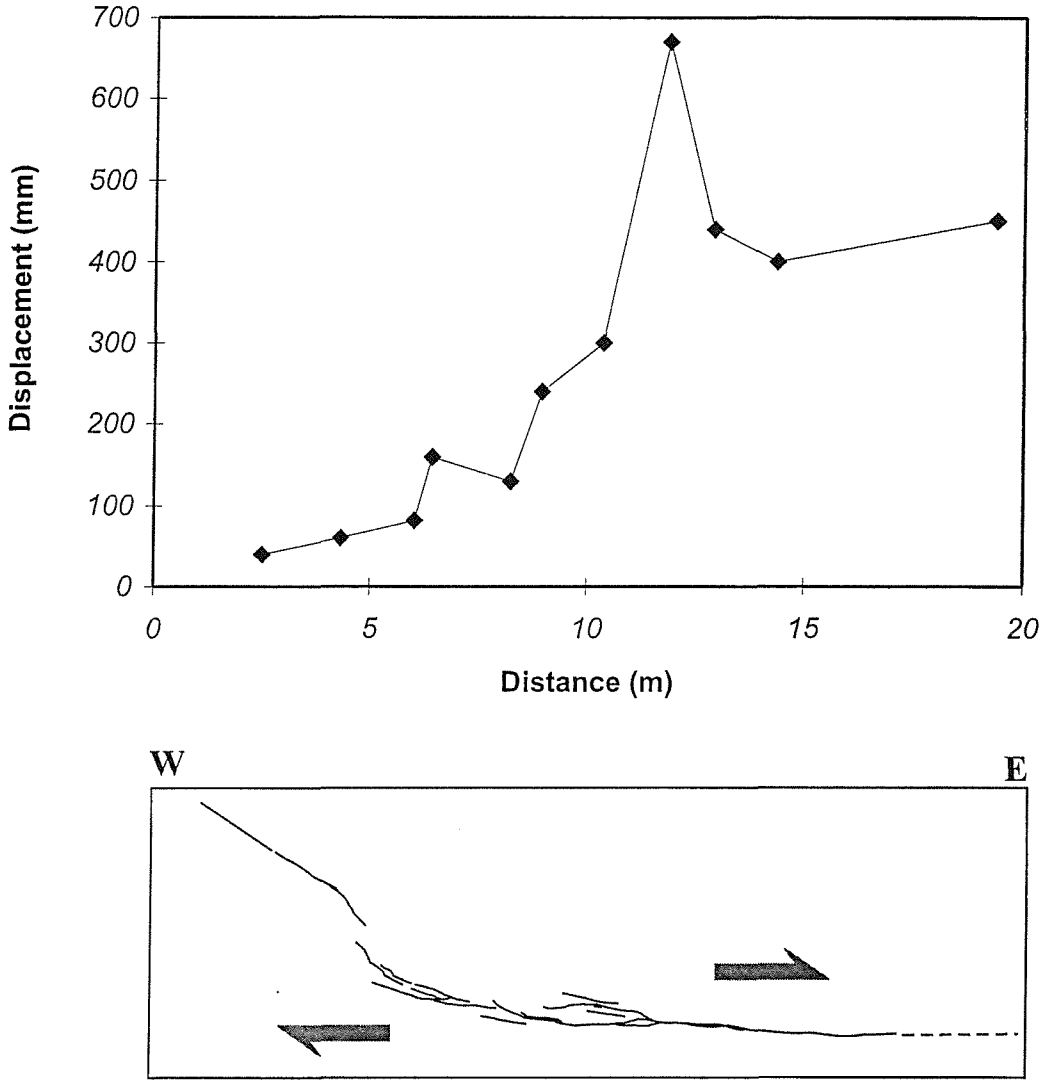

Fig. 5.10. Displacement (d) - distance (x) profile of fault R00 along the major fault trace, showing a steady increase in displacement towards the fault centre.

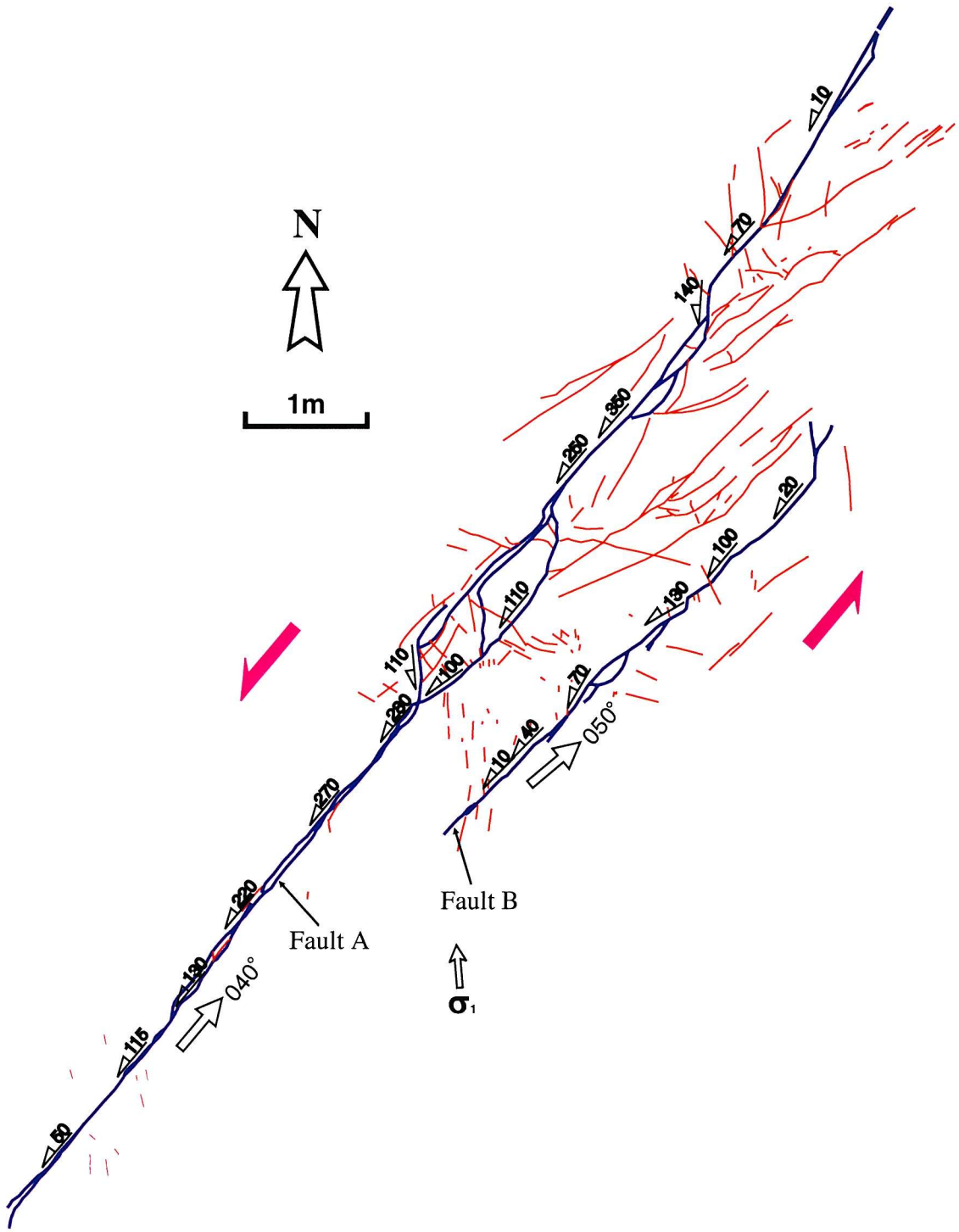

Fig. 5.11. A map of two subparallel antithetic left-lateral strike-slip faults R07. Several lens-shaped structures characterize this fault system. The major fault shows a dominance of dilational left-stepping segment linkage leading to development of strike-slip duplexes.

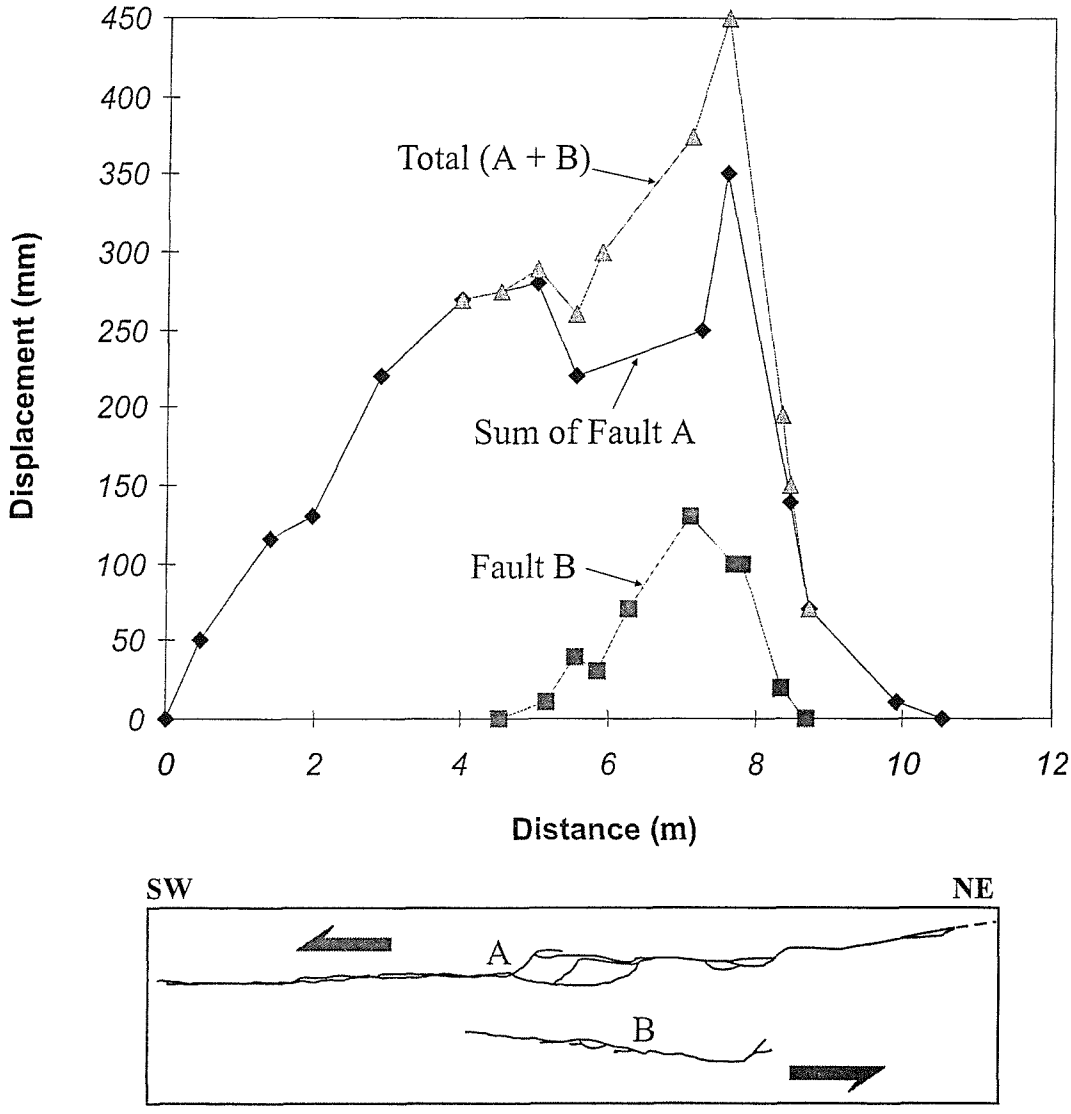

Fig. 5.12. Displacement (d) - distance (x) profile of fault R07. The major fault (A) shows a depression in the middle of the profile near a lense-shaped structure. The total displacement also shows a minima.

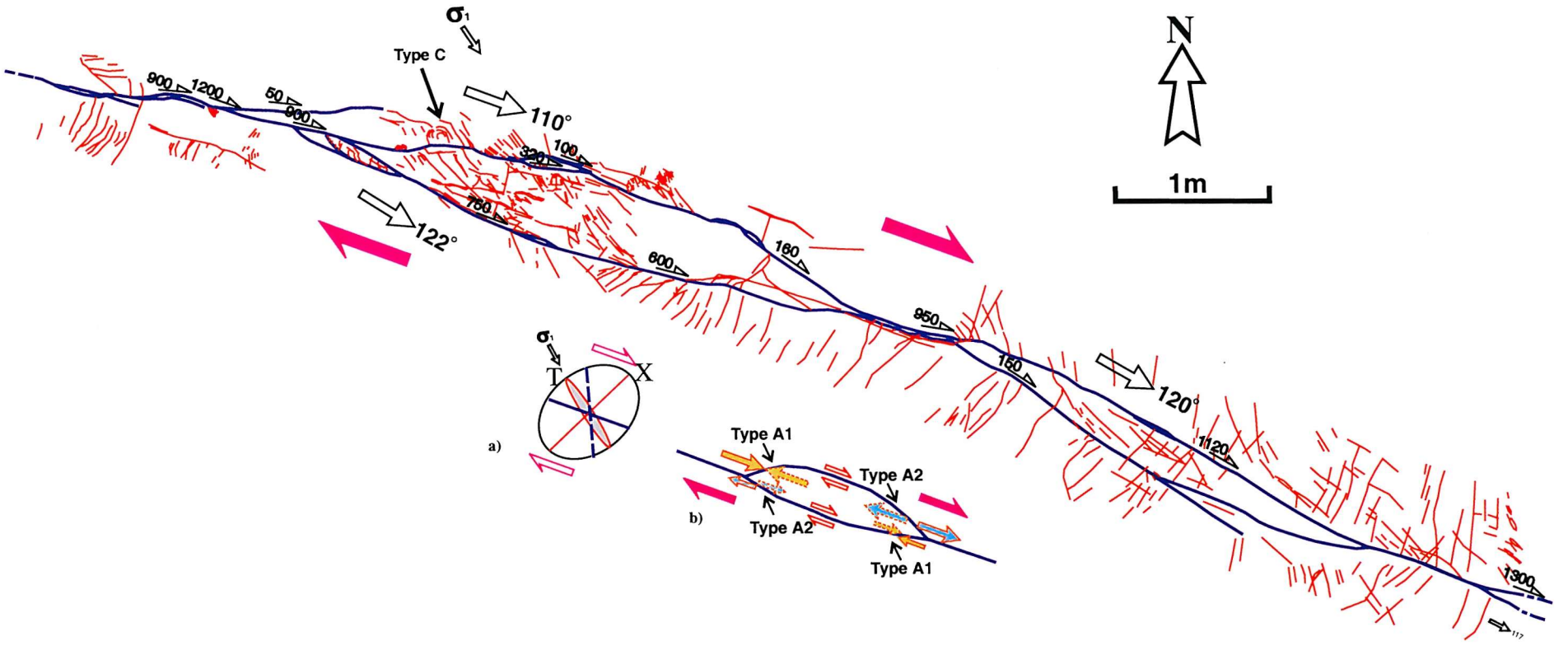

Fig. 5.13. Map view of right-lateral strike-slip fault (R03) with two prominent lens-shaped structures developed along the fault. There are several branch faults leading the main fault marking former segment tips. Many secondary fractures are present along the fault with orientation corresponding to type A and C of Chinnery (1966b), tensional fractures (mode I) and high angle (X) fractures. The displacement varies along the fault with minima at fault branches. a) A stress ellipse indicates maximum compressive stress and other fracture patterns. b) Local stress distribution around bends and lens-shaped structures.

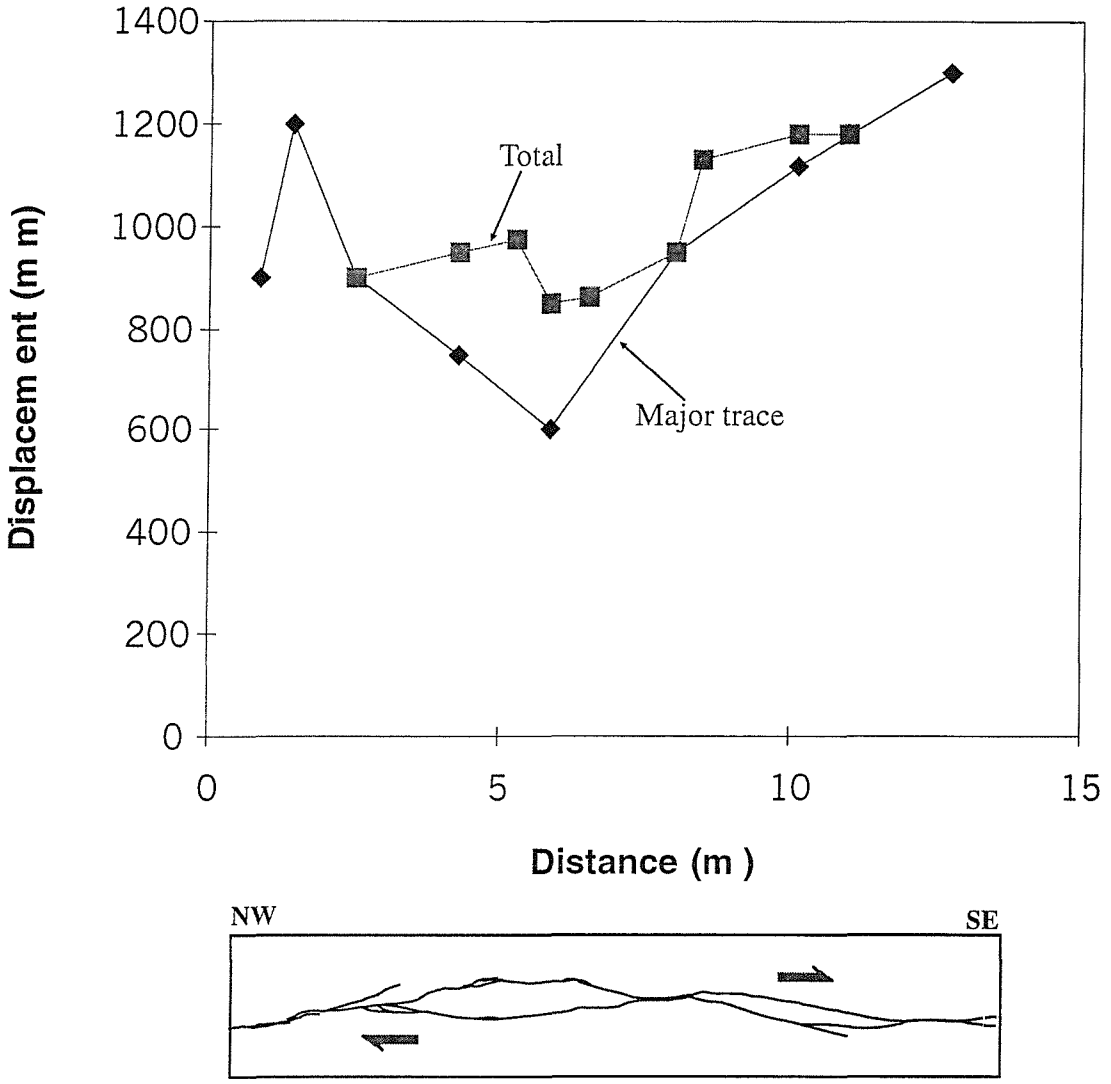

Fig. 5.14. Displacement (d) - distance (x) profile of fault R03, showing irregular shape. The profile for the main fault shows overall lower displacement at the lens-shaped zones.

R05-1 (branch)

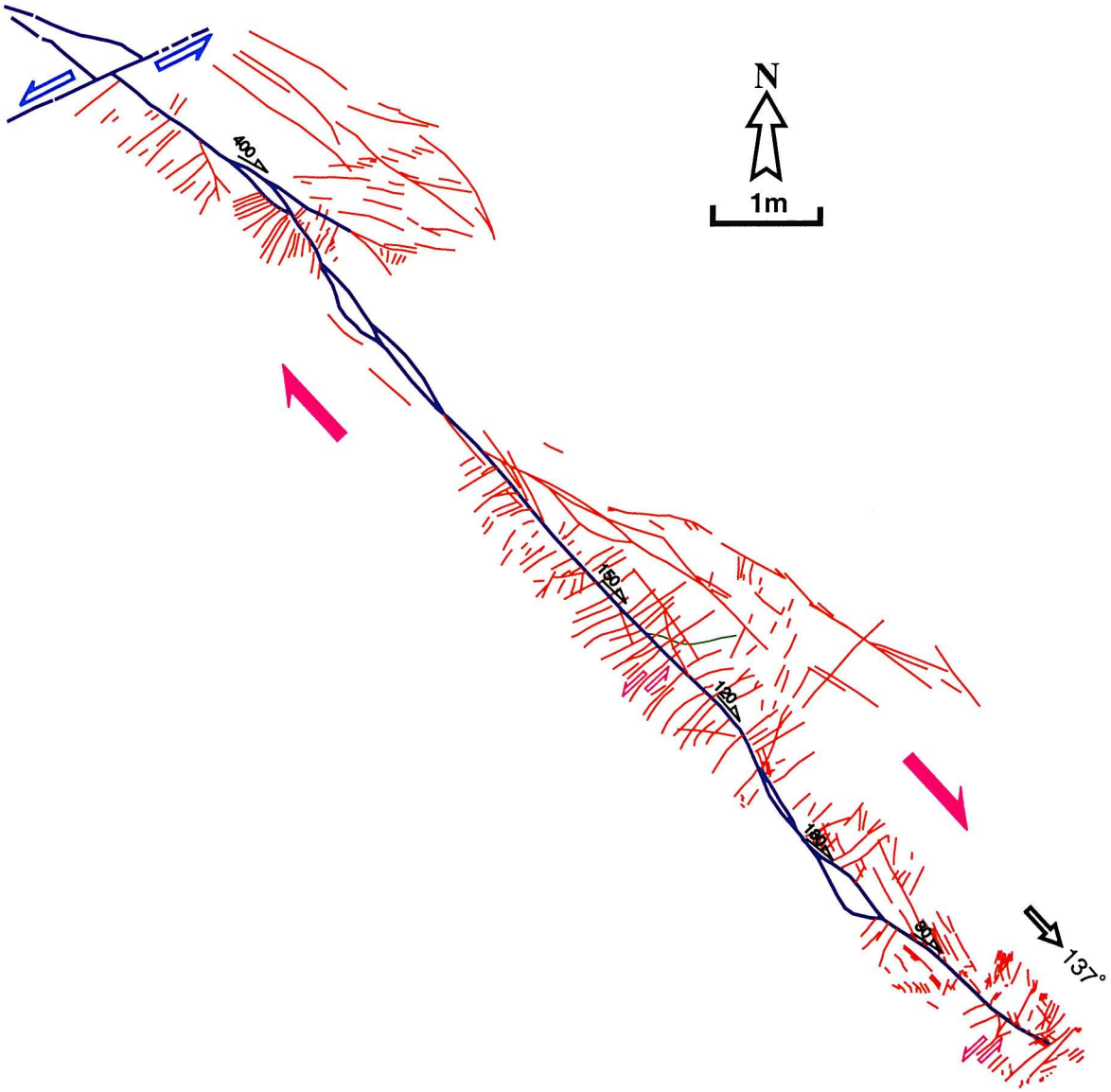

Fig. 5.15. Map view of part of ~100 m long right-lateral strike-slip fault (R05) showing several lens-shaped structures. The eastern fault tip is exposed with tip damage fractures making a high angle to the fault. The western end is truncated by a cross fault.

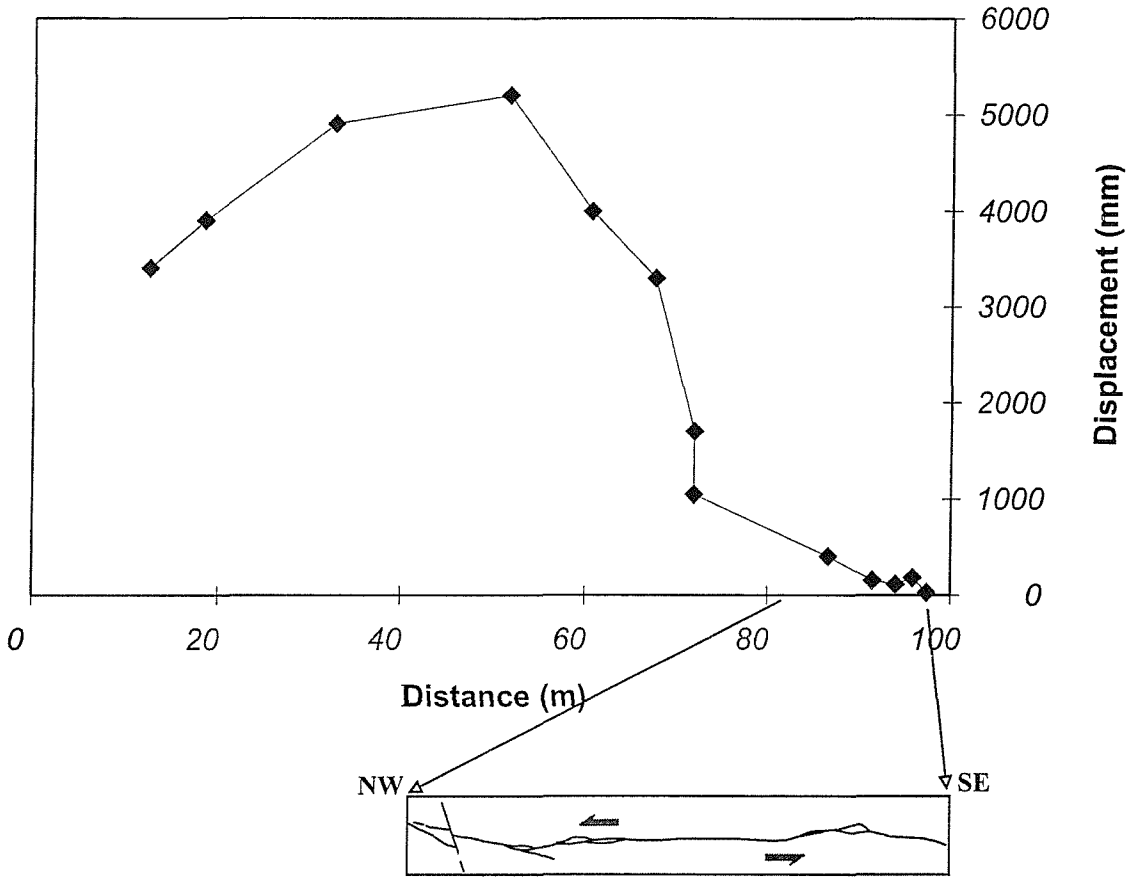

Fig. 5.16. Displacement (d) - distance (x) profile ofpart of fault R05. The profile shows smooth curve, although the measured data interval is long compared with other smaller faults in this area.

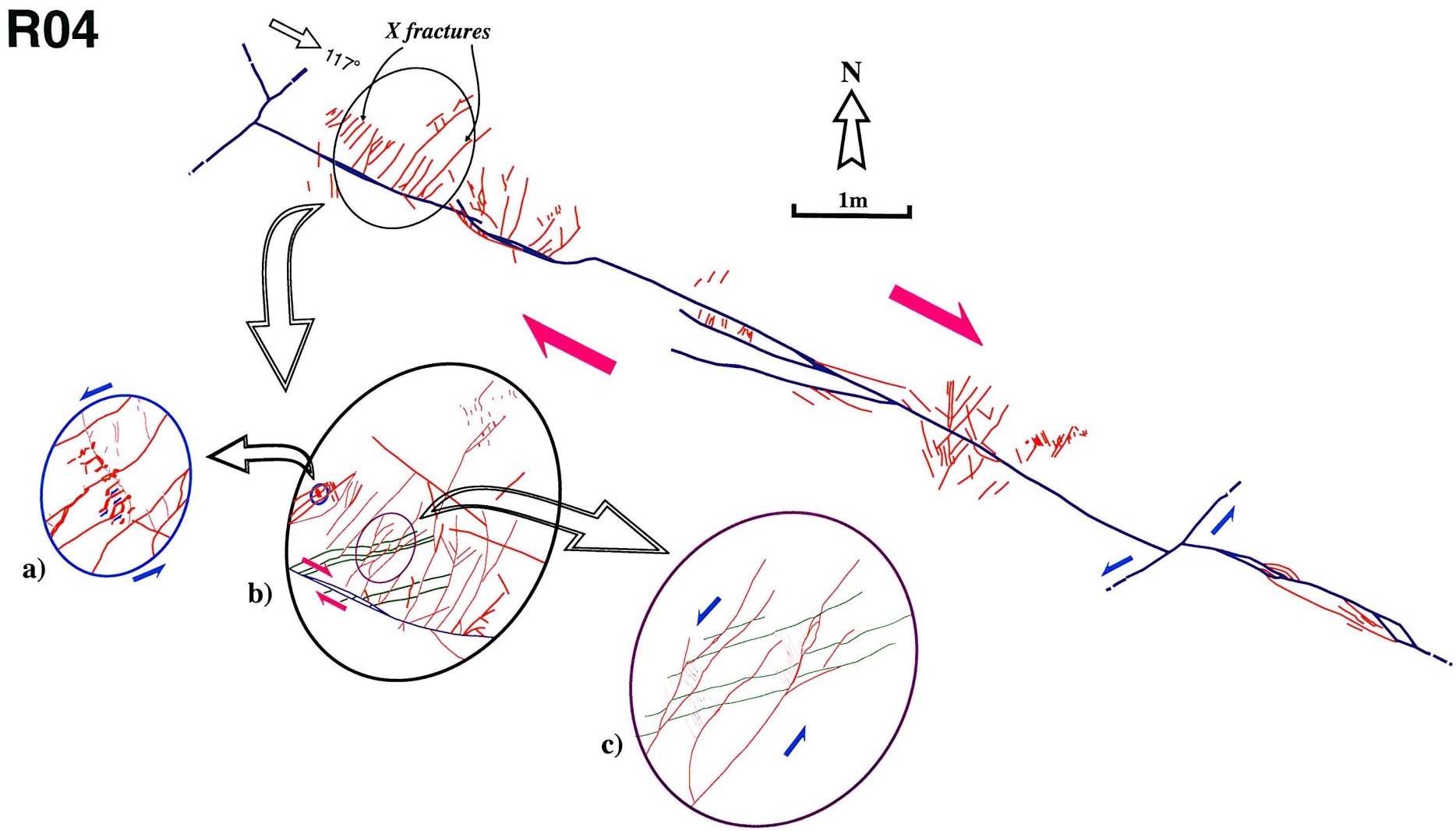

Fig. 5.17. Map of right-lateral strike-slip fault R04. The master fault is at least 14 m long, and strikes ~ N115°. It is truncated at the northwestern end and displaced by a later NE-SW trending fault towards its eastern end. Branch faults are developed along the middle of the section. Green lines denote bedding. Insets show details of fracture arrays.

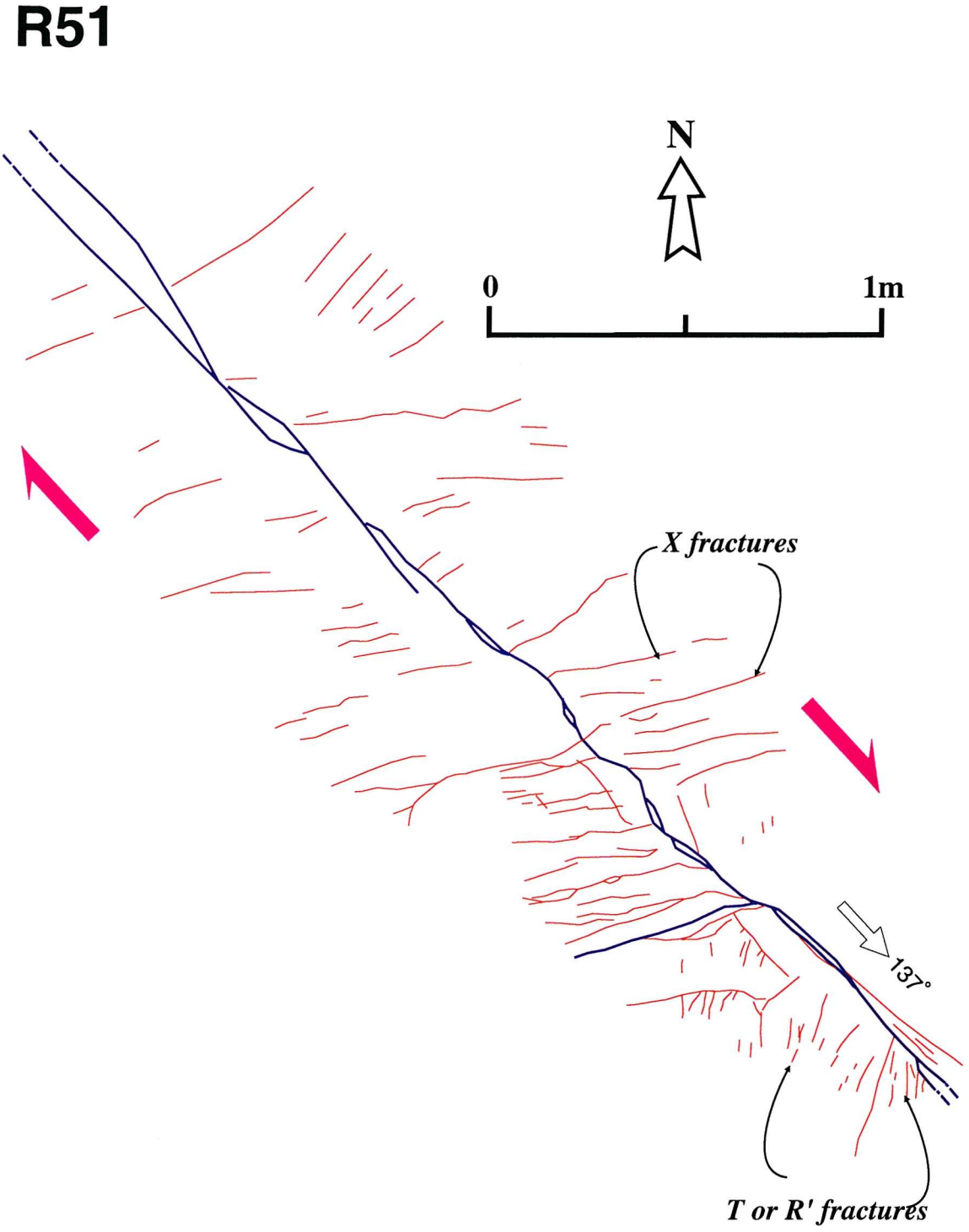

Fig. 5.18. Plan view of wall zone damage structures for a right-lateral strike-slip fault striking ~ N135°. This mapped section is about 3 m long and the fault tip is about 2 m to the south-east. High angle fractures striking about N070° within the wall zone, but the fracture pattern changes to lower angle antithetic fractures (R') or extensional fractures (T) striking ~ N020° at the fault tip.

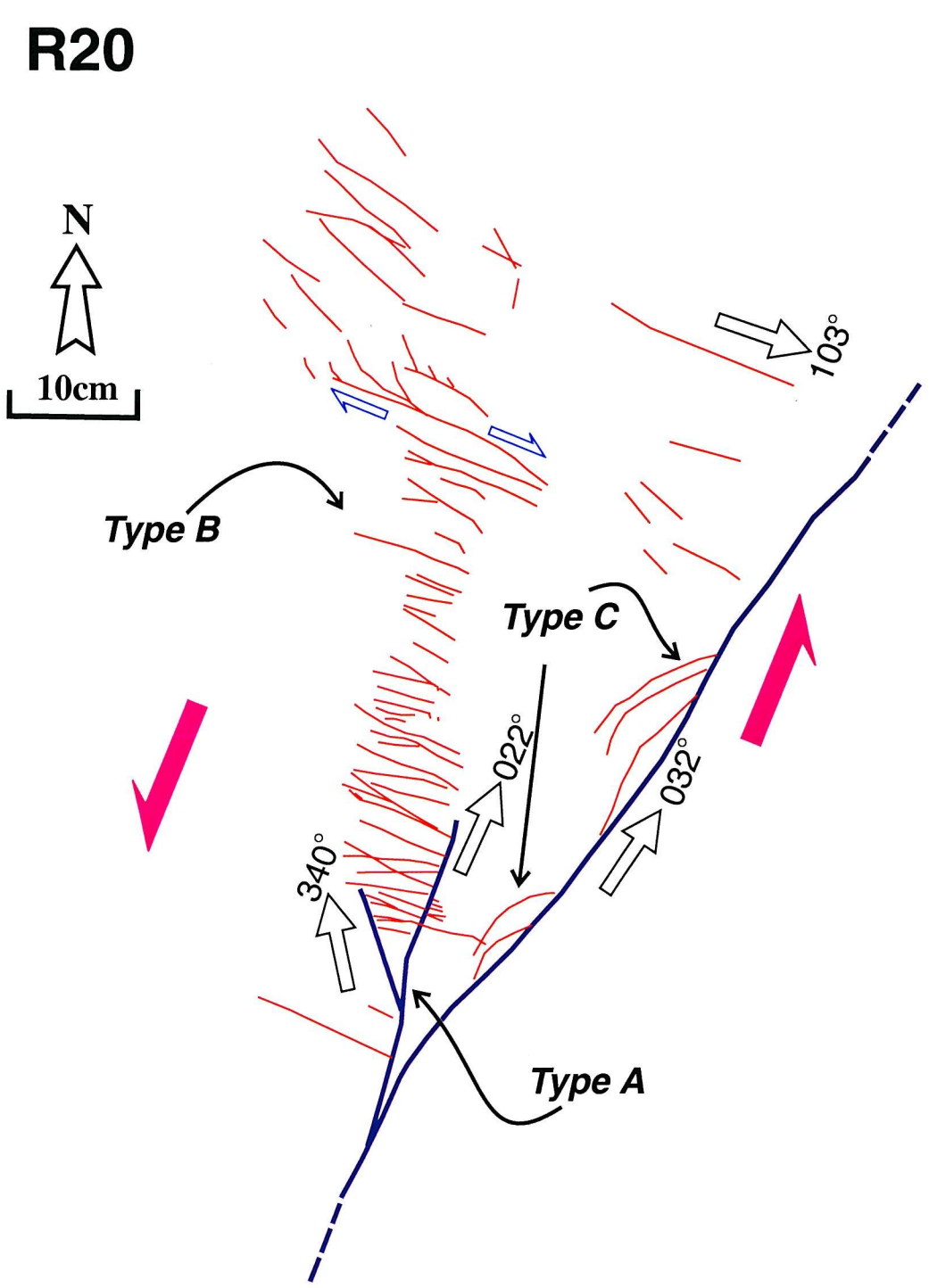

Fig. 5.19. Plan view of tip damage structures at the termination of a left-lateral strike-slip fault. The main fault strikes ~ N010°. Antithetic shear fractures are developed between branch faults.

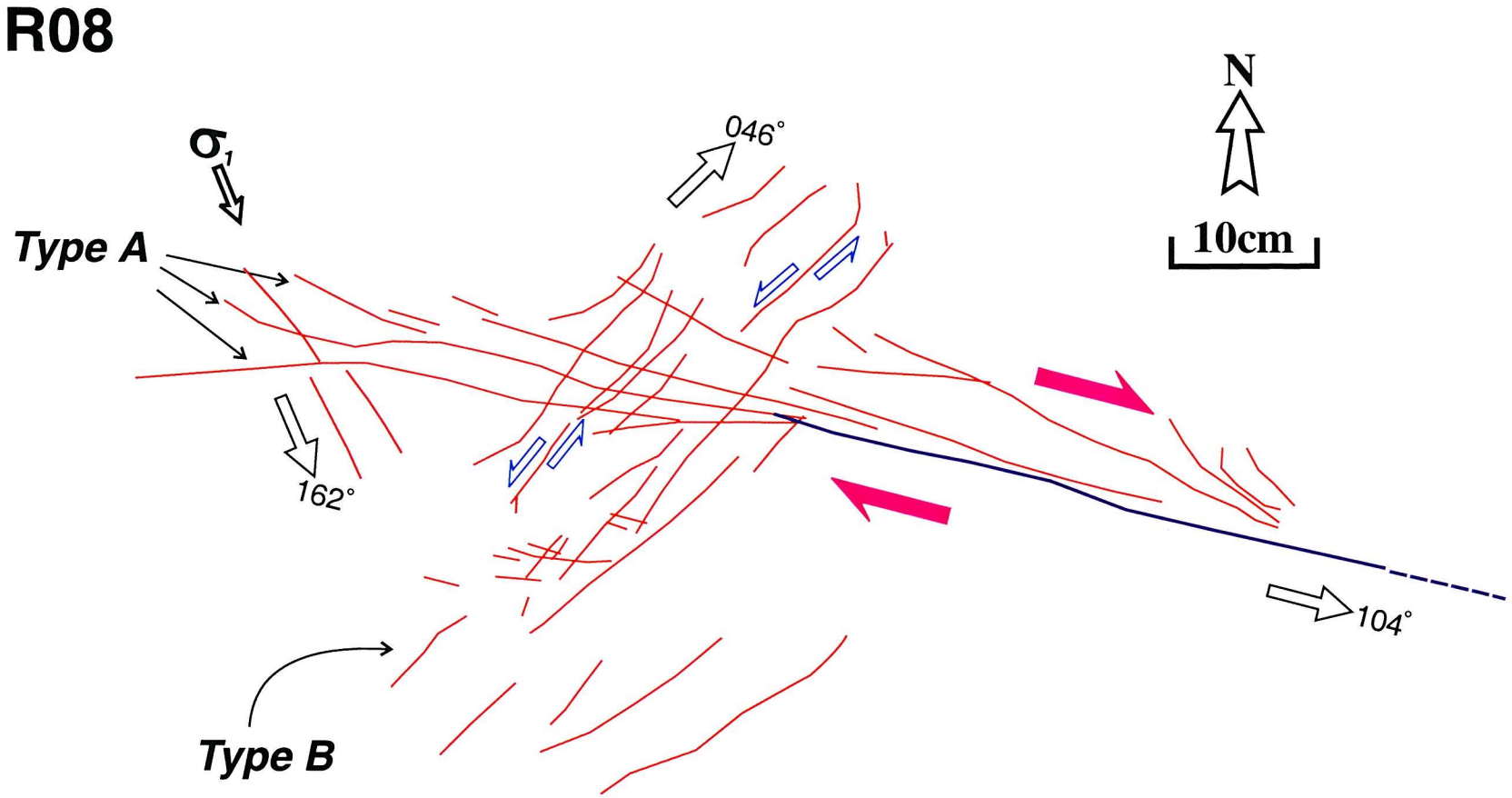

Fig. 5.20. Plan view of tip damage structures around a right-lateral strike-slip fault. The damage zone is about 1 m long. The main fault strikes ~ N105° with several splay faults, tensional fractures and antithetic fractures striking N045°.

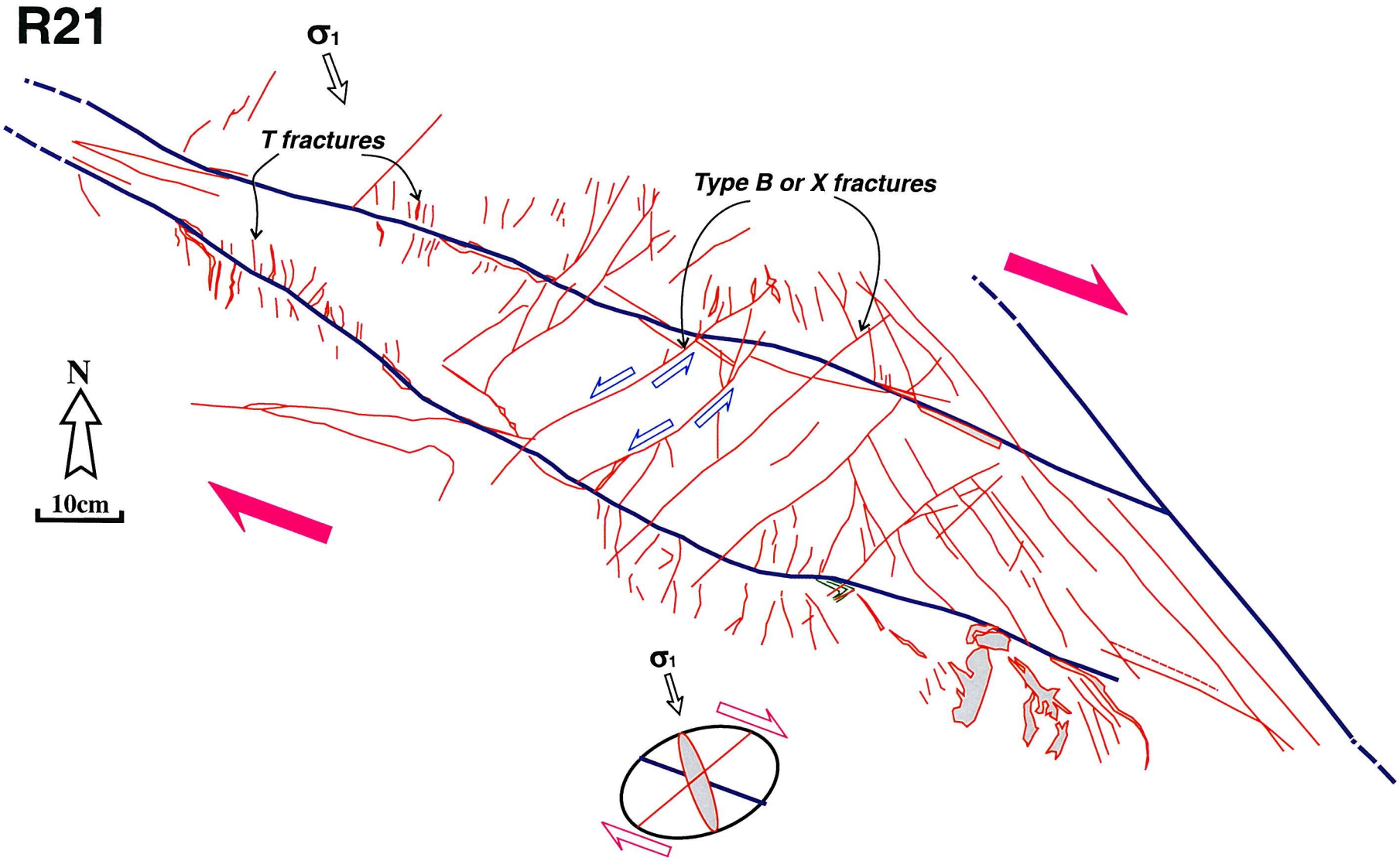

Fig. 5.21. Map of a wedge-shaped block between two ~ 1m long right-lateral strike-slip faults which form splays at the termination of a larger fault. Several antithetic faults are developed within the wedge-shaped block, displaying sigmoidal shapes implying rotation by right-lateral shear.

R05-1 & R06

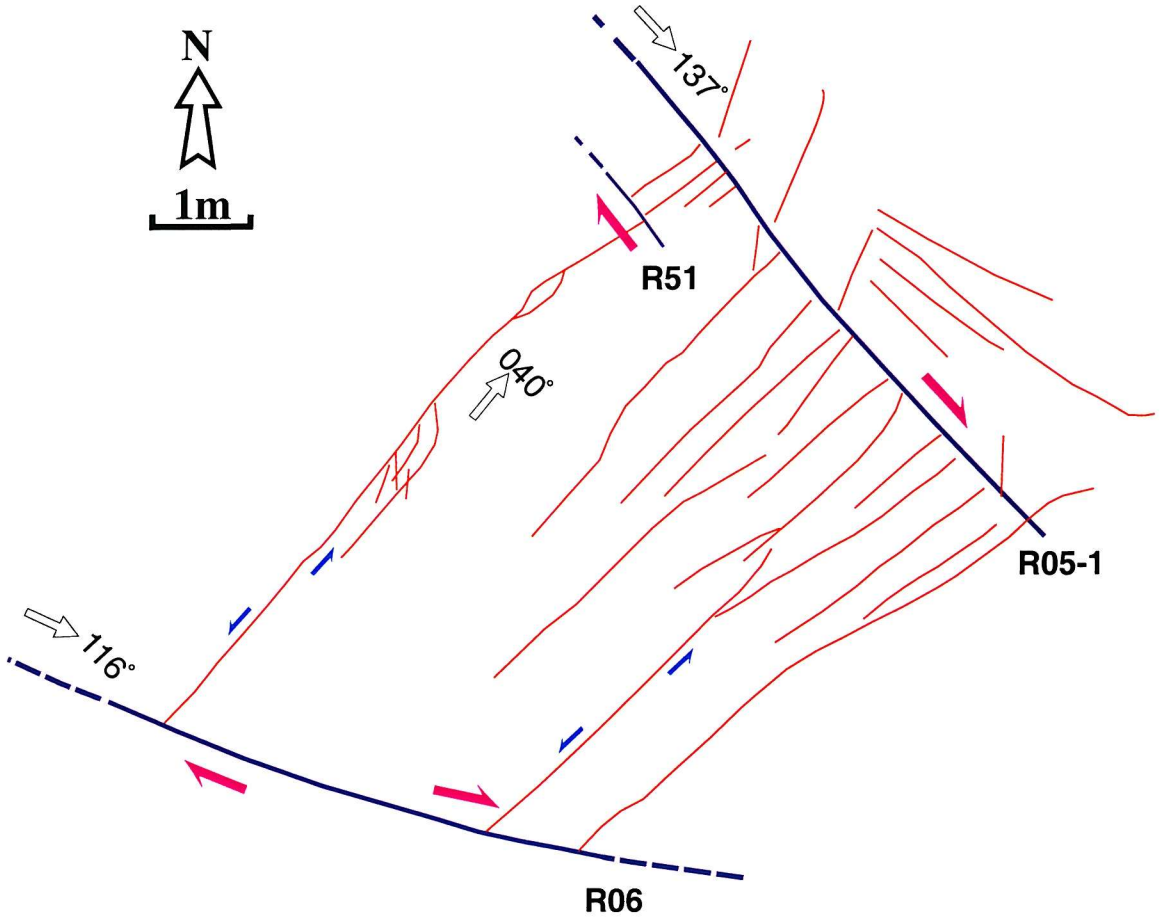

Fig. 5.22. Plan view of an overstep zone between two right-lateral strike-slip faults R05-1 & R06. The two right-lateral faults strike ~ N135° and ~ N115°, respectively. The antithetic cross-faults strike ~ N040, and have left-lateral displacements up to 350 mm. A series of linking antithetic faults almost perpendicular to the main faults are developed in the overstep zone.

R72-1

Fig. 5.23. Map of a linkage zone between two misaligned fault segments. One of the old segment fault tips shows a horsetail fracture pattern and the other shows extension fractures with development of vein quartz. The two segment tips are hard-linked and extensive open spaces are now filled with vein quartz at the fault bends.

R72

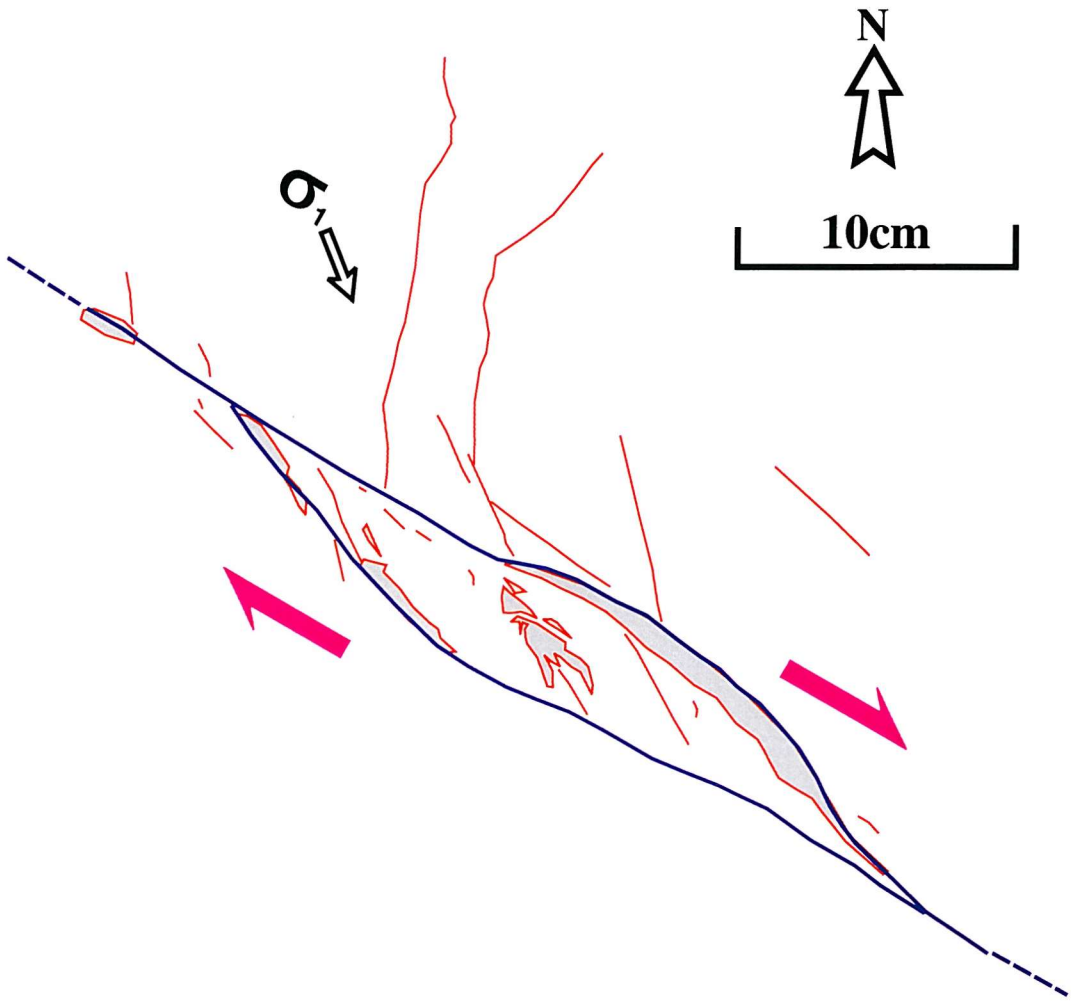

Fig. 5.24. Map of a lens-shaped dilational overstep structure at a linkage zone of two right-lateral strike-slip faults. Several secondary fractures are developed around and within the structure. Open spaces formed by dilation are now filled with vein quartz.

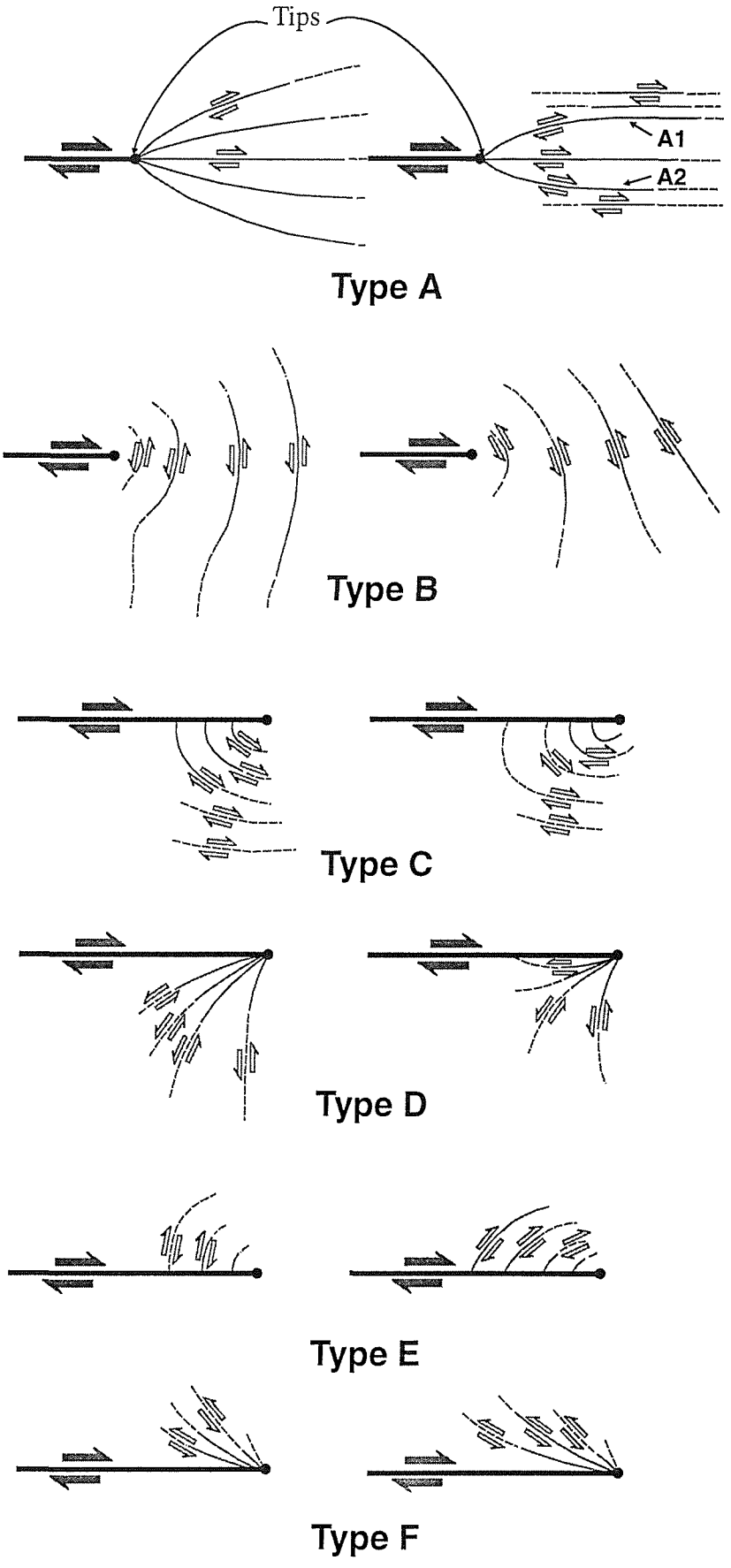

Fig. 5.25. Secondary faulting, deduced from the results of a modelling study (Chinnery, 1966a). The left-hand pattern corresponds to formation of the master fault under conditions of pure shear, and the right-hand pattern results from a uniaxial compression (after Chinnery, 1966b).

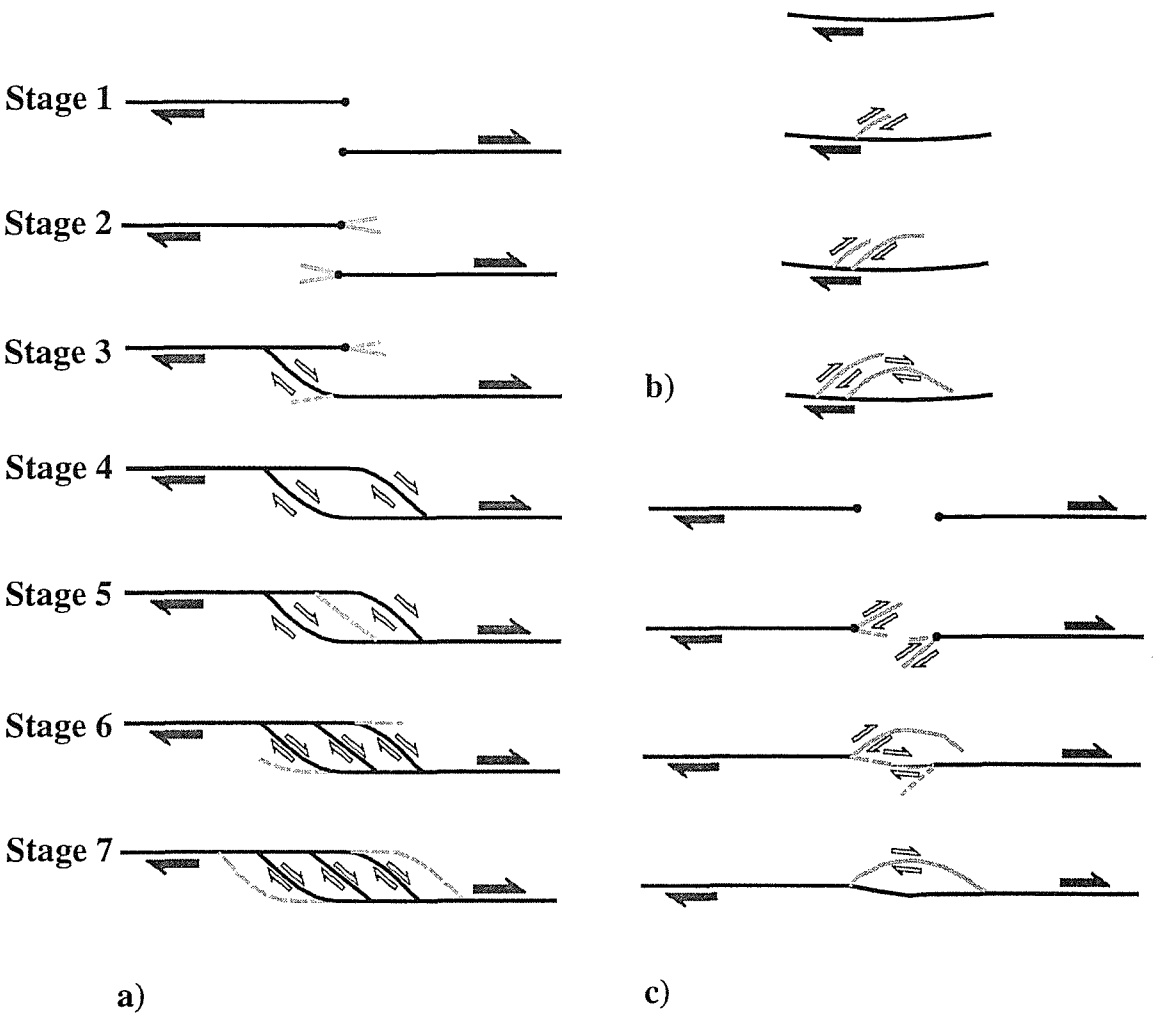

Fig.5.26. Three alternative models for development of an isolated fault bound lens. a) The isolated lensoriginates from overstep and evolves into a strike-slip duplex (modified from Woodcock and Fischer,1986). b) The isolated lens originates from semi-circular secondary fractures similar to ripouts (Swanson, 1989). c) The isolated lens originates from misaligned segments with secondary fractures such as branch faults in overstep zones.

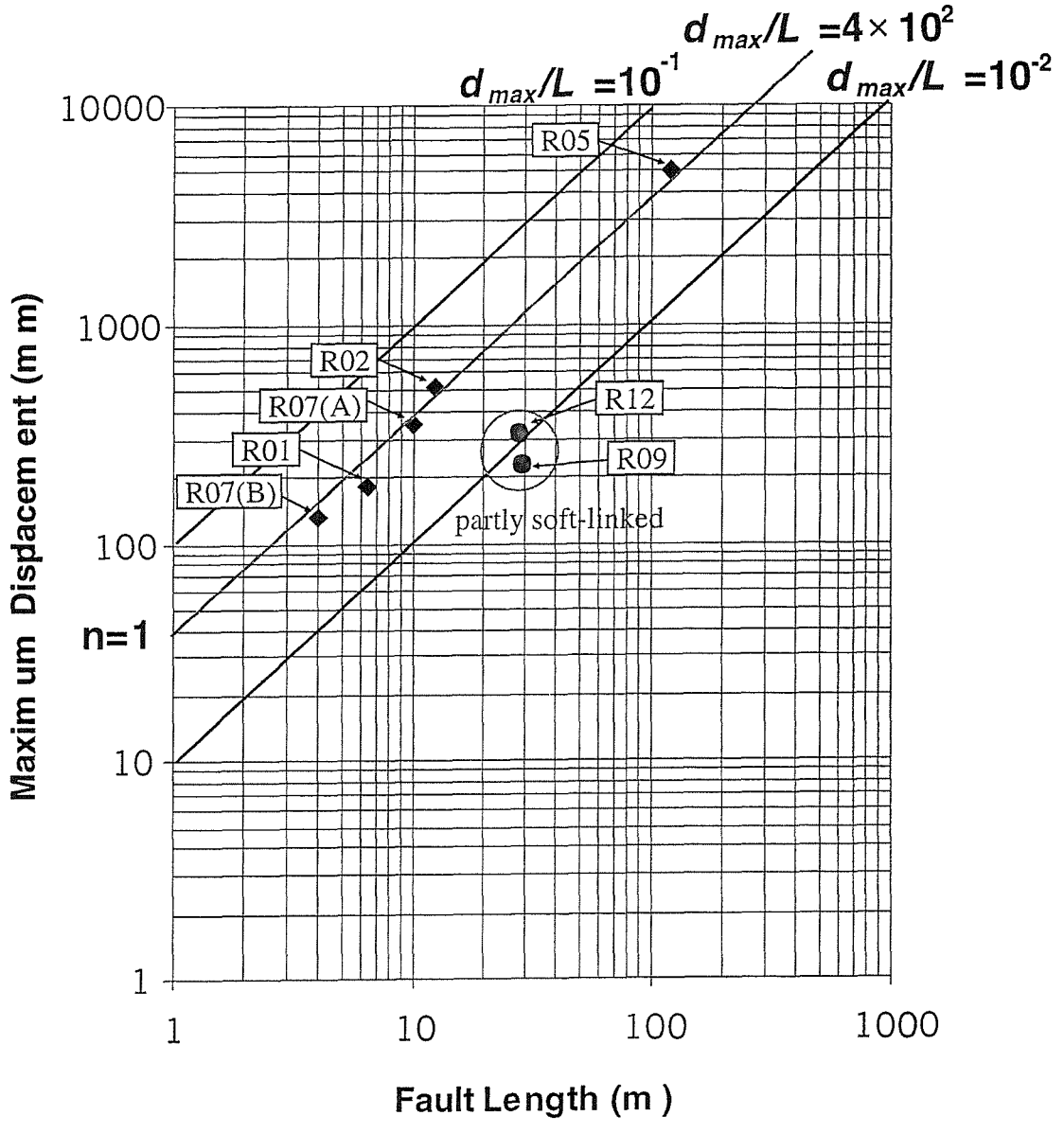

Fig. 5.27. Maximum displacement - fault length (d_{max}/L) relationship for all measured strike-slip faults in the study area. Diamonds are for hard-linked faults; circles for partly soft-linked faults. The ratio of d_{max}/L is lower for the partly soft-linked faults than for the hard-linked faults.

CHAPTER 6: CLASSIFICATION OF DAMAGE STRUCTURES AROUND STRIKE-SLIP FAULTS

Abstract

Damage zones around strike-slip faults show a variety of fracture patterns, which may be divided into three main zones according to their location: tip zone, wall zone, and linkage zone.

The tip zone damage structures can be classified by fracture patterns. At mode II tips (along-strike tips of a strike-slip fault) a variety of asymmetric damage structures such as 'wing cracks', 'horsetail splays', 'antithetic shear fractures', and 'synthetic branch faults' are observed.

Wall-zone damage structures generally show propagation of mode II and mode III tips, or kinematic damage associated with increased displacement. Structures include 'en echelon veins', 'extension fractures', 'antithetic faults', 'Riedel shears', 'rotated blocks' and 'triangular openings'.

Linkage zone damage structures are developed at oversteps or relay ramps between two parallel or sub-parallel faults. The damage geometries depend on the stress conditions in the zone such as dilational or contractional. In dilational oversteps, extension fractures (mode I) and 'pull-aparts' develop, whilst in contractional oversteps 'composite faults' are developed. 'Rotated blocks' and 'isolated lens' or 'strike-slip duplexes' are observed in both types of oversteps.

Strike-slip faults generated from extension fractures or joints and solution seams are linked and terminated in various damage structures. They evolve into fault networks with increasing displacement.

Several large-scale strike-slip faults and their damage structures are compared with damage patterns from small-scale examples. Most of the large-scale examples are consistent with the classification and interpretation for small-scale faults. The damage pattern is mainly dependant on the location along a fault system, the slip modes at fault tips, and the stress propagation at cohesive end zones, so that 3-D fault geometry and slip modes at tips should be considered to understand damage patterns around faults.

6.1. INTRODUCTION

Wall-rocks close to the principal displacement surfaces of faults are deformed to accommodate strains necessitated by changes in displacement and stress along the fault. Many damage structures around faults and their relationship to fault evolution have been described (Cruikshank *et al.*, 1991a, 1991b; Segall and Pollard, 1983; Granier, 1985; McGrath and Davison, 1995; Martel and Boger, 1998; Kim *et al.*, 2000). The development of different features, such as 'horsetail splays', 'wing cracks', 'synthetic and antithetic faults', 'oversteps', 'isolated lens' and 'rotated blocks', might give a clue to the understanding of fault propagation and growth (McGrath and Davison, 1995; Vermilye and Scholz, 1998, 1999), fluid flow (Sibson, 1996; Martel and Boger, 1998), as well as earthquake fault initiation and termination (King, 1986; Aki, 1989; Thatcher and Bonilla, 1989) for hazard assessment. In spite of much recent interest in damage structures there have been few studies and systematic classification of natural damage structures around faults.

A variety of damage structures around strike-slip faults have been described from Crackington Haven in northern Cornwall (Chapter 2 & 3), Gozo in Malta (Chapter 4) and Rame Head in southern Cornwall (Chapter 5), together with some subsidiary examples from Kilve in Somerset, and Rush near Dublin. Basically, the damage structures in each zone depend on the dominant fault tip modes, i.e. mode II (sliding) and mode III (shearing) (Fig. 6.1) (Lawn and Wilshaw, 1975; Chapter 4), location along a fault system (Fig. 6.2) and the nature of the fractures (extensional or shear).

Physical models for fault growth must address the fact that faults do not grow by simple propagation within the plane but form by a more complicated breakdown process, often resulting from the coalescence of opening-mode microfractures (Scholz, 1968; Cox and Scholz, 1988a, 1988b; Lockner *et al.*, 1991; Vermilye and Scholz, 1998, 1999). Therefore, several mixed modes and combined damage structures are developed by the coalescence with other fractures.

In this chapter the exposure scale damage structures are compared with larger scale examples. Also, some structural criteria for identification of natural damage structures are proposed.

6.2. PRINCIPAL LOCATION OF DAMAGE STRUCTURES

Fault growth produces two deformation zones: a *fault core* composed of slip surfaces and comminuted rock material, and a broader volume of more distributed deformation, known as the *damage zone* or the *process zone* (McGrath and Davison, 1995; Caine *et al.*, 1996; Vermilye and Scholz, 1998, 1999). The principal location of damage structures in plan view of a linked strike-slip fault can be divided into three main zones such as *tip zone*, *wall zone* and *linkage zone* (Fig. 6.2).

Tip zones show very intensive damage due to stress concentration at the fault tip, which is manifest as a variety of damage geometries that can provide indicators for the slip sense and other characteristics of the tip. The wall zone may record damage that results from either past location of the tips as the fault propagation or wall-rock deformation associated with slip (rotation, drag etc.). Linkage zones generally show a high fracture density due to overlapping of two segment tips in a narrow region. Depending on the interaction between the two segments the zone can develop a wide range of damage patterns.

When we consider a three-dimensional fault plane and damage structures (Chapter 4; McGrath and Davison, 1995; Martel and Boger, 1998), the above classification becomes more complicated (Fig. 6.3). Around a fault we can recognise several types of fractures (extensional or shear), arranged in different patterns depending on the fault tip modes. An understanding of the displacement modes at tips is very important in understanding and predicting the resulting damage structures.

6.3. DAMAGE DEVELOPMENT AT 'TIP ZONES' (MODE II)

The zone of microfracturing, formed in a volume of rock surrounding the fault tip is defined as the process zone (e.g. King 1986; Ingraffea, 1987; Reches and Lockner, 1994; Vermilye and Scholz, 1998, 1999). It is postulated that a rock will experience the highest stresses in the vicinity of the fault tip and that damage produced by this stress concentration might outweigh damage resulting from subsequent slip on the fault plane (Vermilye and Scholz, 1999). Basically, only two tip modes occur around a strike-slip fault tip line (Fig. 6.1 and 6.3). Mode II tip is an along-strike tip and mode III tip is up- and down-dip tip of the strike-slip fault. Between these two end

members, transitional fault tips that show mixed mode damage geometries, could occur. In this section only mode II dominant tip damage patterns are discussed and mode III tip damage will be discussed in the wall-zone damage section.

The mode II (sliding mode) tip of a strike-slip fault is the along-strike tip in plan view, which has been described and studied (Brace and Bombolakis, 1963; Erdogan and Sih, 1963; Segall and Pollard, 1983; Granier, 1985; Petit and Barquins, 1988; Cruikshank, 1991a, 1991b; McGrath and Davison, 1995; Willemse and Pollard, 1998) because the mode tips are well exposed on outcrops. This tip line is developed normal to slip direction. Four basic damage structures at mode II fault tips (Fig. 6.4) are described such as 'wing cracks', 'horsetail splays', 'synthetic branch faults' and 'antithetic faults (or fractures)'.

Wing cracks (Fig. 6.4a) occur where there is a rapid decrease in displacement at the tip (Chapter 2; Kim *et al.*, 2000), and *horsetail splays* or *pinnate fractures* (Fig. 6.4b) are developed where displacement gradually dies out. Wing cracks are described from Crackington Haven (Chapter 2, Fig. 6.5a), and typical horsetail splays occur at Crackington Haven (Chapter 2, Fig. 6.5b) and Rame Head (Chapter 5). Because these two tip damage fractures propagate with extensional (mode I) style, the two cracks grow along a curved path which becomes parallel with the direction of maximum compressive stress (e.g. Brace and Bombolakis, 1963; Erdogan and Sih, 1963; Segall and Pollard, 1983). Wing cracks may form in rocks under high pore pressure or low confining pressure conditions (McGrath and Davison, 1995) (Chapters 2 and 3).

Synthetic branch faults (Figs. 6.4c and 6.5c-e) are well described by Chinnery (1966a, b) as type A secondary faults (Chapter 5). Similar structures were described as 'splay faults' (Anderson, 1951) and 'shears of the second order' (McKinstry, 1953). The branch faults have the same slip sense as the main fault, and one may develop as a linking fault into another fault segment. Sometimes these branch faults combine with other tip damage fractures to produce complicated damage structures. They frequently combine with antithetic fractures (Fig. 6.5d & e) and some of the blocks between the branch fractures, experience block rotation (Fig. 6.5e).

Antithetic faults (or fractures) (Fig. 6.4d) are a very significant damage geometry in Gozo (Fig. 6.5c-f & i), and some similar tip damage structures are described from Rame Head (Fig. 6.5g & h), with slightly different angular relationship to the main fault. They generally consist of several antithetic fractures that widen,

increasing their length and spacing, away from the fault tip (McGrath and Davison, 1995; Chapter 4). The whole wedge-shaped antithetic damage cluster sometimes combines with branch faults in dilational quadrant (Fig. 6.5d & e), or curves away from dilational quadrant into compressional quadrant (Fig. 6.5f). This type of tip damage has been classified as 'type B' by Chinnery (1966b), and he argued that the fracture orientation would be different under different stress conditions (Chapter 5).

Shear zones with en echelon microcracks, widening away from fault tips, have been induced in glass under higher differential loading and confining pressures than those required to produce horsetails and wing cracks (Petit and Barquins, 1988). These fractures are interpreted as R' shears. Further fracturing occurred at the tips of the antithetic shears, with the most prominent extension (mode I) cracks branching off the antithetic shears at the fracture tips (Fig. 6.5f) (Chapter 4; McGrath and Davison, 1995). Because mode II is sliding mode, the slip distribution is generally asymmetric, and the stress propagation and damage structures at the fault tip are asymmetric (Fig. 6.1, 6.3 and 6.4).

Some combined tip damage structures occur. The most frequent combination is synthetic branch faults (or horsetail fractures) and antithetic faults (Fig. 6.4e & f and 6.5c-f). At Rame Head, the antithetic fractures are at higher angles (Fig. 6.5g & h) than in other areas, so that they are interpreted as an *X*-fractures (Logan *et al.*, 1979; Bartlett *et al.*, 1981) or due to rotation with increasing deformation. Also, some tip damage structures show mixed mode (II & III) tip damage structures (Fig. 6.4g) at the transition zone of the two end members (Fig. 6.5i and 6.7a).

6.4. DAMAGE DEVELOPMENT AT 'WALL ZONES'

Wall-zone damage (or distributed damage) occurs in a zone along the trace of the fault (Fig. 6.6). Such damage may result from three origins; propagation of mode II fault tip damage, mode III fault tip damage, and kinematic damage associated with high displacement. Although relatively little damage is shown in wall zone, the damage is complicated with increasing displacement at a mature stage.

6.4.1. Propagation of mode II tip

As faults propagate along mode II fault tips, the damage zone area extends and secondary faults and fractures increase. Therefore, damage zone size formed during

each slip event increases from the centre to the tips of the fault. As a result of the 'wake' of this fault propagation, wedge-shaped damage zones can occur at wall zones (Fig. 6.6a). This type of wall damage is conceptually plausible, but it is very rarely observed; only a few possible damage patterns are shown (Fig. 6.7b). The two central segments have small segment tip damage zones, formed at an early stage, and at a consecutive stage the two segments might activate as a fault system producing larger tip damage zones at both ends, forming a wedge-shaped 'wake'. However, there is some overlapping of mode III tip damage structures.

There are several reasons why this type of wall damage does not frequently occur. Firstly, it is very difficult to observe the 'wake' of the damage propagation, where sections are not through the centre of the fault plane, because tip damage develops only around fault tip lines. Secondly, because fault displacement and stress are accommodated at linkage zones of fault segments, early tip damage zones are linked and inactive. This may suggest that faults generally grow through linkage (e.g. Peacock and Sanderson, 1991, 1994; Cartwright *et al.*, 1995, 1996; Kim *et al.*, 2000) rather than radially propagate within their own planes.

6.4.2. Mode III fault tip

One of the developments of damage at wall zones is due to the preservation of mode III tip damage. The mode III fault tip of a strike-slip fault is an up-dip and down-dip tip with tearing mode (Figs. 6.1 and 6.3). Stresses are symmetric in terms of the master fault trace, so that most of the observed damage is generally symmetric in plan view (Figs. 6.6b-d, 6.7a, b & d) and cross-section (Fig. 6.7c). However, the damage zone could show slight asymmetry in plan view away from the fault centre due to the influence of the mode II fault tip. The damage structure in cross-section could also show an asymmetric shape, if the dip-slip component is involved or the exposed section is close to the mode II fault tip.

The classical Riedel shear experiment and most shear box or clay cake analogue modelling (Tchalenko, 1970; Wilcox *et al.*, 1973; Harding, 1974; Bartlett *et al.*, 1981) essentially involves a mode III tip with deformation above a lower fixed forcing plate. Therefore, damage fractures observed at the mode III fault tip are very similar to the structures illustrated from simple shear zone of a strike-slip fault (Fig. 6.3). Generally Riedel and conjugate Riedel shears (*R* and *R'*), extensional fractures (*T*), and some *P*

shears are observed with symmetric distribution (Fig. 6.6b-d and 6.7a-e). These damage structures are cut by a later *Y* shear and the former en echelon fractures move upwards or downwards with fault growth. When these en echelon structures evolve, they sometimes combine one another to make pull-aparts (they will be discussed in next section) (Fig. 6.9c & d).

En echelon vein arrays (Fig. 6.6b) (e.g. Ramsay and Huber, 1983; Hancock, 1985) often develop in the initial stages of fault growth, especially in more ductile conditions. Such a pattern is observed within rotated blocks at Crackington Haven (Fig. 6.7g). Ramsay and Huber (1983) claimed that planar veins at 45° to the zone margins are extension fractures formed normal to the maximum incremental extension within a zone of simple shear. They also show that continued shear along the zone produces veins with a sigmoidal shape.

Figures 6.6c and 6.7d & e shows wall-zone damage evolving from the mode III tip damage or from the central part of a fault system. *Extension fractures* in wall zones are well described in Gozo (Chapter 4). The tips of extension fractures are generally straight, but sometimes they show slightly different geometries with curved tips and cross-joints.

Microcracking and jointing parallel to σ_1 is postulated as the initial fracturing prior to formation of fault (e.g. Mollema and Antonellini, 1999), and may be linked through zone-parallel fractures as the deformation increases (Cox and Scholz, 1988b). This type of fracture is shown in wall zones of Figures 6.7d & e. Extensional fractures form at larger angles to the main fault with increasing normal loads (Cox and Scholz, 1988b). A similar fracture pattern with a central fault trace is described at mode III fault tips (Martel and Boger, 1998), although it is interpreted as conjugate Riedel shears or extension fractures reactivated as shear fractures in this study (Fig. 6.6d and 6.7a, b & d).

Riedel shear patterns (Figs. 6.6d and 6.7a-c) are observed in the wall zone of faults (Naylor *et al.*, 1986; Martel and Boger, 1998). They are well described near mode III fault tips, and are generally symmetric (Fig. 6.3). Although it is difficult to measure the slip sense of these fractures (Martel and Boger, 1998), especially in early stage, some of the fractures show extensional tip cracks splaying from the fracture tips implying antithetic shears. The tip cracks and angular relationship of these fractures

support R' shear pattern, but a possibility of reactivation of extension fractures is not excluded (McGrath and Davison, 1995).

En echelon shear fractures (Fig. 6.6d) with almost symmetric distribution along the shear zone (Fig. 6.7a, b & d) are common fracture type at mode III fault tips. Although the fractures show an antithetic shear sense at a more advanced stage, two alternative interpretations are possible. The fractures initiated as extension fractures (mode I) (Figs. 6.6a and 6.7d) and reactivated as antithetic shears (mode II/III) (McGrath and Davison, 1995). Alternatively, they initiate as antithetic R' shear fractures, which is supported by the angle of ~65° with the main fault and the tip cracks indicating shear sense (Fig. 6.7a & b).

Petit and Barquins (1988) argue that shear fractures cannot exist as a primary fracture mechanism but can only be a macroscopic fracture phenomenon that must necessarily involve tensile microcrack formation. However, other studies (Lawn and Wilshaw, 1975; Lin and Parmentier, 1988; Reches and Lockner, 1994; McGrath and Davison, 1995) suggest that in-plane mode II and III fault propagation can occur at high confining stress, low rock plasticity, and at high differential stress.

The cross-sectional view of both up- and down-dip tips of strike-slip faults are rarely seen, but some of the mode III fault tips are observed on steeply inclined surfaces at Gozo (Fig. 6.7c) (Chapter 4). They exhibit a series of bifurcating fractures, which terminate in the vertical fault plane. These are interpreted to be Riedel shears, which splay off from the main fault, possibly with a helicoidal geometry (Naylor *et al.*, 1986). Some flower structures (e.g. Wilcox *et al.*, 1973; Sylvester and Smith, 1976; Sylvester, 1988) may be developed in a similar manner to the mode III tip damage structures. Similar geometries are also produced through experimental work on rock (Bartlett, *et al.*, 1981) of a shear zone.

6.4.3. Kinematic damage

High density of damage in wall zones can also result from kinematic damage, i.e. damage formed due to increasing displacement on the fault. For example, Gozo faults (Chapter 4) have very low strain, and show little kinematic damage, whereas Crackington Haven (Chapter 2) and Rame Head (Chapter 5) have high displacement, and show more intensive kinematic damage.

Typical kinematic damage associated with high displacement is *block rotation* (Fig. 6.6f), which is observed at Crackington Haven (Fig. 6.7g). Similar damage patterns are also observed at Kilve (Fig. 6.7h & k) and Rush near Dublin (Fig. 6.7i & j) along shear zones or joints as a kink band type. At the wall zones along the master faults several segmented blocks are rotated, and triangular openings are developed along the master faults or shear zones. Antithetic cross-faults develop almost orthogonal to the main fault, and the blocks rotate synthetically (Fig. 6.7g-k). Under layer-parallel extension antithetically rotated blocks are developed (Martel *et al.*, 1988; Gross *et al.,* 1997), but this is rare. The angles of the antithetic cross-faults may change with increasing deformation and slip to allow displacement along the main fault to increase steadily toward the fault centre (Fig. 6.7g). Similar types of rotated blocks are also observed in sub-parallel faults or mode II tip zones with antithetic faults (Fig. 6.7k) (e.g. Nicholson *et al.*, 1986b; Ron *et al.*, 1986; McGrath and Davison, 1995; Watterson *et al.*, 1998), kink bands or shear zones (Fig. 6.7j) (Dewey, 1966), and overstep faults (Fig. 6.9e, f & h) (Terres and Sylvester, 1981). Linkage structures and opening up of linkage (pull-aparts) will be discussed in next section.

A slightly different type of antithetic fracture is observed at Rame Head (Figs. 6.6e and 6.7f). They are classified as *conjugate sets* to the main right-lateral strike-slip faults, but the bisector angle is $> 90°$. Therefore, they could be interpreted as *X* fractures with antithetic sense (Logan *et al.*, 1979; Bartlett *et al.*, 1981). This type of fracture is not observed in other study areas, and it might suggest a mature stage of fracture.

Joint drags (Figs. 6.6f and 6.7h-k) are to drag along shear zones or sub-parallel joints. They occur in a similar manner to block rotation in fault systems producing high angle antithetic shears and triangular openings along the joints or shear zones. Kinematic damage increases with increasing displacement and with progress in fault evolution.

6.5. DAMAGE DEVELOPMENT AT 'LINKAGE ZONES'

Damage structures in linkage zones (or oversteps, or relays) (Fig. 6.8) are well observed (Terres and Sylvester, 1981; Woodcock and Fischer, 1986; Swanson, 1988; Peacock and Sanderson, 1995a; Walsh *et al.*, 1999), and they show high fracture density and complexity (Chapter 4; Zhang, *et al.*, 1991) compared with other zones.

They evolve from two tips of adjoining faults, and complicated by interaction between the two faults with increasing deformation.

6.5.1. Dilational overstep

In dilational oversteps (or jogs) various types of structures develop. These include:

Extension fractures (mode I) (Fig. 6.8a) have well been described by Granier (1985) and occur in Gozo (Fig. 6.9a). The linkage is mainly controlled by extensional fractures approximately parallel to the local σ_1 orientation, which is developed dominantly in the dilational quadrants of fault segments. These fractures abut to the main faults, and some link the two fault segments.

Dilational jogs or pull-aparts develop (Figs. 6.8b, 6.9a-d) between two segments (e.g. Aydin and Nur, 1982; Peacock and Sanderson, 1995b) due to increasing deformation. The pull-apart shapes and angles are different depending on the fractures (i.e. P, R, T) associated with the pull-apart (Fig. 6.9c & d). In the linkage zone, extension fracture is the main linking structure.

Rotated Blocks (Fig. 6.8c) are observed at Rush, Dublin and Kilve (Fig. 6.9e & f). They show rotation of blocks as slip develops along the boundary faults. Cross-faults slip antithetically, and extension occurs across the fault zone. Antithetic cross-faults, initially striking at an acute (clockwise) angle to the main fault are rotated to over 90 degrees clockwise to the boundary fault (Fig. 6.9e), which is inferred from the unrotated fracture boundaries. The blocks rotate synthetically with the rotation angle increasing with increasing deformation and slip.

Martel et al., (1988) and Gross et al., (1997) have suggested two possible models for block rotation with different rotation senses along the boundary faults. It depends on the stress condition, such as extension or contraction. The examples shown (Fig. 6.9e & f) are developed in extensional conditions across the fault zone, so that they display a synthetic rotation sense. Several segmented blocks within the overstep zone are rotated, and triangular openings are developed along the master fault or the zone boundary.

Strike-slip duplexes or isolated lenses occur at Rame Head (Figs. 6.8d and 6.9g), and are similar to "sidewall ripout" (Swanson, 1989), "open eye-structure" (Fossen and Hesthammer, 1997) or "strike-slip duplexes" (Woodcock and Fischer, 1986; Swanson,

1988). This structure is interpreted to form from relay structures between two misaligned segment fault tips (Chapter 5). In dilational oversteps some open spaces formed along the lens and they are filled with vein materials. These structures are bridged by short ramp faults regardless of segment stepping (Cruikshank et al., 1991b).

6.5.2. Contractional overstep

In contractional oversteps (or jogs) various structures are also developed. They include:

Rotated Blocks (Fig. 6.8e) are observed in Gozo (Fig. 6.5e) and at Kilve (Fig. 6.9h). They show counter-clockwise rotation of blocks between cross-faults as sub-parallel boundary faults slip left-laterally. Between the antithetic cross-faults, each block displays a synthetic rotation sense. Several segmented blocks within overstep zones are rotated, and some of the cross faults show a sigmoidal shape, implying continuous simple shear (Fig. 6.5e) (Ramsay and Huber, 1983). Some third-order tip cracks (mode I) branch off from the antithetic fault tips indicating the slip sense.

Composite faults (Fig. 6.8f) are well described by Peacock and Sanderson (1995a) at East Quantoxhead, Somerset (Fig. 6.9i), where two sub-parallel faults develop a strike-slip relay ramp in contractional oversteps. Some veins, antithetic faults and pressure solution seams occur in the relay ramp. Further rotation and deformation causes the two overstepping faults to link across the relay ramp, and finally the relay ramp is completely broken by a single composite fault, with the same slip sense to the main fault.

Strike-slip duplexes or isolated lenses (Fig. 6.8g) occur in contractional overstep in Rame Head (Chapter 5), although it is more commonly developed in dilational oversteps (Fig. 6.9g). They may also be interpreted as an early stage of a strike-slip duplex (Chapter 5; Woodcock and Fischer, 1986; Swanson, 1988; Cruikshank *et al.*, 1991b), as described for dilational oversteps, although most of the structures show just a simple lens shape. This type of overlapping geometry is described in deformation bands in sandstone (Cruikshank *et al.*, 1991b; Fossen and Hesthammer, 1997). Similar structures develop in normal faults during experimental modelling (Fossen and Gabrielsen, 1996) and at a basin scale (Walsh *et al.*, 1999). Cruikshank *et al.*, (1991b) suggest that the kinematics of these structures are similar to duplex structures along

thrust faults (Boyer and Elliott, 1982), but they show different patterns and shapes with different degrees of complexity.

6.6. ATTRIBUTES OF DAMAGE ZONE STRUCTURES

In Table 6.1 many of the observed damage patterns are listed, and their locations along the fault, fracture modes and characteristic features summarised. Figure 6.10 shows the simplified pattern of damage structures around a linked strike-slip fault. Tip damage patterns are various, and depend on the fault-tip mode and propagation. Wall-zone damages may originate from the propagation of mode II and III fault tips, or due to kinematic damages associated with high displacements and joint drags. Linkage damage shows different damage patterns in terms of its overstep patterns such as dilational and contractional.

Two recent works (McGrath and Davison, 1995; Martel and Boger, 1998) have described secondary faults and damage structures around strike-slip faults. The damage structures are ascribed to fracture modes and locations along a three-dimensional fault. Based on the observation from the studied areas and the previous work, a more systematic classification and interpretation is suggested for the damage patterns around strike-slip faults, which are classified in terms of locations along the fault, fault tip modes, and fracture patterns (Table 6.1 and Fig. 6.3 and 6.10).

McGrath and Davison (1995) argued that the observed variation of damage zone geometries in strike-slip faults might be due to various stress regimes such as transpression, transtension and simple shear. However, the current work indicates that the difference of damage structures may depend mainly on the slip modes at each tip. Different damage patterns at the same tip mode may result from variation in fault propagation direction, material properties, confining pressure and differential stress.

McGrath and Davison (1995) suggested that faults propagate towards the zone with horsetail fractures, whereas Vermilye and Scholz (1998, 1999) and others propose that faults propagate from the centre to the tips. For some of the examined faults the damage zone structures at both tips show different patterns (Fig. 6.7e; Martel and Boger, 1998), and the damage pattern might be related to the fault propagation direction. Aki (1989) argued that the starting point and the stopping point of an earthquake rupture are dependent on fault trace geometry. Also, the main shock

epicentre, the initiation point of seismic rupture, is preferentially located towards the ends of the zone of surface faulting (e.g. Thatcher and Bonilla, 1989). Therefore, the different damage patterns at both tips might provide an indicator to track the fault propagation direction within a fault, if damage patterns are examined in detail for earthquake ruptures.

Mode II fault tip damage is typical at the along-strike tips of strike-slip faults (Fig. 6.1 and 6.3) (McGrath and Davison, 1995). The damage structures are predominant in the dilational quadrant at the tip. However, the antithetic fractures at mode II tip show generally wedge-shaped divergence pattern (McGrath and Davison, 1995; Martel and Boger, 1998) and the whole damage zone may curve from dilational quadrants towards contractional quadrants probably due to rotation related to simple shear (see Fig. 6.7e). The damage patterns around this type of fault tip show a variety of geometries, which depend on fault slip mechanism, fault propagation direction and evolution stage.

"Zipper crack bands" described by Martel and Boger (1998) are interpreted as due to Riedel shears and to the master fault plane at mode III tip of a strike-slip fault. An early stage of this type of fracture has been observed in Gozo (Fig. 6.7a, b & d). However, the fracture orientation is very variable such as *R*, *T* and *R'* depending on examples, and they might be related to location around a fault or stress components (e.g. transpression or transtension) or evolution stages (Chapter 4).

Martel and Boger (1998) suggested a conceptual model of a penny-shaped strike-slip fault and secondary fractures. Their model is mainly concentrated on the exposed shapes of the extension (mode I) fracture type attached as secondary fractures around fault tips. They argued that the different fracture patterns are mainly controlled by the three dimensional locations around a fault plane. However, several natural examples show more complicated damage patterns depending on stress regimes at tips. Their model can not explain several phenomena related with secondary fractures around a strike-slip fault: 1) wedge-shaped antithetic fractures at cohesive end zones of mode II fault tips, 2) several shear fractures (*P*, *R*, and *R'*) at cohesive end zones of mode III fault tips, 3) bifurcating fractures on cross sections of mode III fault tips, 4) overlapping fracture pattern at mode II fault tips with branch faults, antithetic fractures and extension (mode I) dominant fractures.

Mode II fault tip damage zone shows two lobes of damage (Reches and Lockner, 1994) (B in Fig. 6.11). In natural examples, some of the mode II tip damage zone is predominant with wedge-shaped antithetic shears similar to tensile stress lobe suggested by Reches and Lockner (1994) (Fig. 6.5f & i). They exhibit a damage zone, which widens away from the fault tip (McGrath and Davison, 1995) implying stress propagation at mode II fault tip. In the cohesive end zone of mode II tip, the stress mode is almost simple shear with wedge-shaped boundaries (Fig. 6.3). If branch faults develop into the boundary faults, shear is more localised, and block rotation and antithetic shears develop. Some of the examples (Fig. 6.5e & f; McGrath and Davison, 1995) show tip cracks (mode I) at the antithetic fault tips, which are the evidence for shear movement (mode II/III). Therefore, it is argued that the shear fractures are originated as antithetic fractures in simple shear condition at mode II tips rather than due to the reactivation of extension (mode I) fractures as suggested by McGrath and Davison, (1995). General damage zones around a linked strike-slip fault are illustrated (Fig. 6.11) from observed natural damages.

As a consequence, damage in strike-slip faults is strongly dependant on the fault tip modes (McGrath and Davison, 1995) and stress regimes in cohesive end zones, and three dimensional stress propagation patterns with two end members (mode II and III). In other words, mode II type slip at a fault tip is mainly accommodated with extension (mode I) cracks because there is no strong rotational component at the tip. Whereas, in the cohesive end zone away from the tip, the stress regime changes and wedge-shaped zones develop with antithetic shear fractures accommodating rotation (B in Fig. 6.11). Whereas, mode III type slip generates a symmetric simple shear zone, with Riedel shear style fractures accommodating the rotation of simple shear along the mode III fault tip (A in Fig. 6.11). In cross sections the cohesive end zone of mode III tip shows generally symmetric cone-shaped (convex downwards) stress regime, and the fracture pattern resembles bifurcating flower structures (Figs. 6.3 and 6.7c).

All these damage structures evolve into fault networks with continuing deformation. A flow chart for the main damage structures and their evolution related to fault interaction is shown in Figure. 6.12. Strike-slip faults may generate from extension fractures or joints (mode I) and solution seam (anti-mode I) (e.g. Segall and Pollard, 1983; Willemse *et al.*, 1997; Mollema and Antonellini, 1999). Faults terminate with two tip modes (mode II and mode III), but sometimes these two modes

are combined to show more complicated structures (Fig. 6.1 and 6.3). As faults propagate towards each other, the damage geometry that develops depends on the nature of the fault interaction (i.e. on the stepping and the angle between two approaching faults). If they are parallel or sub-parallel, they develop oversteps/relays producing extensive damage, including jogs, lenses and pull-aparts (Figs. 6.10 and 6.12), such segmented faults localise displacement and produce kinematic damage, such as pull-aparts and rotated blocks with triangular openings as displacements increase. In effect faults grow by this method of linkage to produce longer strike-slip faults with longer tip zones, repeating processes discussed previously. The growth of faults in more than one orientation will produce oblique linkage and λ faults. As displacement is localised on such non-coplanar structures, additional damage, due to bending of the wall rocks, etc., may result (e.g. crestal collapse graben style structures).

Table 6.1. Classification of damage structures around strike-slip faults

Name	*Location*	*Fracture Mode (type)*	*Remark*
Wing crack	Mode II tip	Extension (mode I)	**high displacement gradient, high angle**
Extensional fracture	Wall, Mode II & III tip, linkage zone	Extension (mode I)	**first generation fracture, secondary fracture**
Horsetail splay	Mode II tip	Extension (mode I), mixed Mode	**low displacement gradient, low angle to main fault**
Antithetic fault (R')	Mode II & III tip, early stage wall	R' shear (Type B)	**one of main secondary fractures**
Riedel shears	Mode III tip	Shears (mode II/III)	**simple shear zone**
Block rotation & Triangular opening	Mode II tip, wall, linkage zone	R' shear, combined shear (Type A + B)	**antithetic to main fault**
Branch fault	Mode II tip	Synthetic shear (Type A)	**low angle to main fault**

Jog or Pull-apart	Linkage zone	Opening with extension (mode I)	**bending**
Dilational overstep	Linkage zone	Extension (mode I) + R' shear	**no or weak displacement minima, pull-apart**
Contractional overstep	Linkage zone	Synthetic shear + R' shear	**displacement minima, internal volume change**
λ fault	Intersection zone of two faults	Shear (mode II/III)	**propagation angle depends on the angular relationship between two faults**
Rip-out	Linkage zone	Shear (mode II/III)	**old tips, dilational or contractional**
Conjugate fault	Between faults	Shear (mode II/III)	**high strain zone at the intersection zone**
Circular shear	Wall near tips	Synthetic shear (Type C)	**concentric shear circles**
Drag fold	Wall, Mode II tip	Transpression	**normal drag in ductile material**
En echelon fold	Wall, Mode II tip	Transpression	**orientation of fold axes sub-parallel to the main fault**

6.7. LARGE SCALE EXAMPLES

In this section several large-scale examples of damage structures will be described from the literature. The examples are compared with the exposure-scale examples in the studied areas and with suggested models for damage structures. The examples are described in order of increasing complexity.

6.7.1. The Lake Basin fault zone, Montana

The Lake Basin fault zone, Montana is described by Harding *et al.* (1985) (Fig. 6.13). The fault zone trends N100° and consists of a number of short faults that strike at angles of 30° to 70° to the overall trend (mostly N055° to N070°) and have been interpreted as normal faults (Smith, 1965; Harding *et al.,* 1985).

This type of fracture pattern is similar to wall damage zones from Gozo (Fig. 6.7d), comprising distributed extensional fractures in the wall-zone showing no wedge-shaped pattern. The Lake Basin fault zone is interpreted as a mode III fault tip zone (Fig. 6.6c) of a left-lateral strike-slip fault at depth (Smith, 1965; Harding *et al.,* 1985). The higher oblique en echelon faults are interpreted as normal faults or normal faults reactivated as R' shears as described in Gozo (Chapter 4).

6.7.2. The eastern Gulf of Suez, Egypt

The Araba-Abu Durba area on the eastern margin of the Gulf of Suez (Fig. 6.14) exhibits examples of horsetail splays. The Gulf of Suez is the northwestern arm of the Red Sea Cenozoic rift system with minimum extension in the north (Bosworth, 1995; McClay and Khalil, 1998).

Three large, domino-style, NE dipping fault blocks are developed associated with a series of major NW trending normal faults. These are offset by two NNE trending left-lateral oblique-slip transfer faults - the Ekma and Durba transfer faults that terminate in horsetail normal fault splays (McClay and Khalil, 1998). The north-west end of the faults splay into several curved faults that transfer the displacement, probably on oblique-slip extension. These splay faults link into the dominant NW rift-parallel fault system. Small-scale, steep reverse faults and flower structures also indicate oblique-slip motion along the transfer fault system. Several hundreds metres of strike-slip offset is observed along the faults.

Evidence that the normal faults are related to the transfer faults includes; extensional faults that terminated at the transfer faults; increase in the number of normal faults at the tips of the transfer faults; and predominance of faults in the dilational quadrant that curve away from the tips. Even though the transfer faults are not the main structural elements (McClay and Khalil, 1998), this example shows a clear geometry of horsetail splays (mode I dominant faults) at the mode II fault tip as described in small scale examples (Fig. 6.4b and 6.5b).

6.7.3. The Villefort's region, Northern Cevennes

Arthaud and Matte (1975) and Granier (1985) have described several strike-slip faults and associated horsetail structures in the Northern Cevennes, France (Fig. 6.15). The Villefort's Fault, that might have been active for about 20 million years (Arthaud and Matte, 1975), has a horizontal (left-lateral) displacement of about 12 km (Granier, 1985). The fault shows horsetail splays in the south, which resemble mixed mode fractures (McGrath and Davison, 1995; Willemse and Pollard, 1998; Chapter 3). The fault pattern may show a failed mode II fault tip, because the main fault tip propagates by curving into the dilational quadrant in the south, where horsetail splays are developed. Also, there are several right-lateral strike-slip faults as a conjugate set to the N-S trending left-lateral Villefort's fault. This conjugate fault pattern almost at 90° with the main fault, which is similar to the fault pattern at Rame Head (Chapter 5).

6.7.4. The Eastern Transverse Range, California

Several studies have suggested block rotation models for conjugate slip through the Eastern Transverse Ranges, California (Fig. 6.16) from paleomagnetic evidence (e.g. Dibblee, 1977; Luyendyk *et al.*, 1985) and from a variety of seismic and geologic evidence (e.g. Matti *et al.*, 1985; Nicholson *et al.*, 1986a, 1986b).

The kinematic model proposed to explain the seismic pattern (Fig. 6.16) accounts for the presence of north-east-striking left-lateral subsurface faults that terminate against major strike-slip fault boundaries. Earthquakes tend to cluster in areas where major faults splay, or define the nearly orthogonal, short, linear segments (Nicholson *et al.*, 1986b). Detailed mapping of existing geologic structures reveals a number of low-angle thrusts and left-slip faults, much like those suggested by the seismicity (Nicholson *et al.*, 1986a, 1986b). Clockwise rotation of material can also

account for the increased uplift observed from west to east along the presently active northward-dipping thrust faults that form the Banning fault zone through San Gorgonio Pass (Matti *et al.*, 1985).

Similar rotated blocks between sub-parallel faults are common in the small-scale examples from the studied areas (Figs. 6.5e and 6.7g-k). The slip sense of the most transverse faults is antithetic to the major thoroughgoing faults, and the orientation of the faults is at a high angle to the major faults (Fig. 6.6f).

6.7.5. The Marlborough fault system in northeastern South Island, New Zealand

Some examples with geometric similarity to lens-shaped structures are mapped in the Marlborough fault system in northern South Island, New Zealand (Fig. 6.17; Roberts, 1995; Little, 1996; Little and Jones, 1998; Little *et al.*, 1998). The obliquely convergent motion between Pacific and Australian plates is accommodated across the ~150 km wide Marlborough fault system. There are four principal right-lateral strike-slip faults in the Marlborough fault system (Fig. 6.17).

Like the Alpine fault, the trace of these oblique slip faults is broken into strike-slip and oblique reverse sections of differing strike. Norris and Cooper (1995) inferred that stress gradients caused by steep topography play an important role in controlling the position of these segments. Little *et al.* (1998) interpreted the bimodal segmentation pattern to be related to selective reactivation of older basement faults. These faults appear to undergo a progressive lateral change in the degree to which oblique plate motion is partitioned along the faults (Little *et al.*, 1998).

In the mapped region several fault bends and lens-shaped structures (Fig. 6.17) are shown with changing orientation. Also, some branch faults that are not linked to the main faults were mapped. Although mechanism for development of the structures shown on this map is not known, the geometry is almost the same as the lens-shaped structures from Rame Head (Fig. 6.9g; Chapter 5).

6.7.6. The Dasht-e Bayaz (Iran) Earthquake Fractures in the Nimbluk Valley

Ambraseys and Tchalenko (1969), and Tchalenko and Ambraseys (1970) mapped in detail a part of the Dasht-e Bayaz (Iran) Earthquake Fractures in the Nimbluk Valley (Fig. 6.18). The relative displacements observed in the fault zone, which is composed of en echelon shears, are up to 450 cm left-lateral and 250 cm

vertical. The structure was interpreted as a simple shear type of deformation (Ambraseys and Tchalenko, 1969; Tchalenko and Ambraseys, 1970). This large-scale natural example of damage structure shows both mode III and mode II fault tips.

Overstep zone is situated in southwest of the village, Dasht-e Bayaz (Fig. 6.18a & b). It dies out towards the west from the Cemetery and is replaced by a similar parallel zone to the south. A lozenge-shaped graben has developed between these two rectilinear zones. The boundaries of the lozenge are formed by the principal displacement zones and *T* fractures (Tchalenko and Ambraseys, 1970). The major fractures within this zone are *T* fractures, and subsidiary *R'* and *R* shear fractures are also frequently observed. The damage pattern of this zone shows a typical dilational overstep zone (c.f. Fig. 6.8), showing dominant extensional fractures, linked through a synthetic composite fault at a later stage.

Bending zone is located to the south of Chah Khundri pumping station (Fig. 6.18c). In the central segment the zone strikes N115°E and gradually bends into an east-west direction. Most of the shears are *R* shears, and the junction between adjacent *R* shears takes place through *P* shears (Tchalenko and Ambraseys, 1970). In the western segment, the general fracture pattern resembles that of the central segment, except for a few parallel cracks (*R'*), slightly *S*-shaped in plan, crossing the zone in a N040°E direction (Tchalenko and Ambraseys, 1970). In the eastern segment, the *R* shears are subdued and show only very small amounts of shearing, whereas the *R'* shears are well developed. The arrangement, and the distortion of linear features seen from the air, indicates a small right-lateral movement along each R' shears (Tchalenko and Ambraseys, 1970).

This zone shows a typical restraining bend predominating with *R* and *R'* shears. In the eastern segment, a characteristic damage pattern is observed, which is combined damage pattern of mode II/III tips showing predominant *R* and *R'* shears.

A mode II tip zone is situated about 5 km north-west of Ja'fari (Fig. 6.18d). The ground displacements associated with the earthquake are concentrated in a variety of shears (Ambraseys and Tchalenko, 1969; Tchalenko and Ambraseys, 1970). The prevailing right-lateral *R'* shears are composed of parallel zones formed of en echelon cracks and ridges, with *R* shears generally being less pronounced.

The widening at fault tip was not discussed by Tchalenko and Ambraseys (1970), however, it is very similar to the mode II tip damage structures at Gozo (Fig.

6.5d, f & i). The fracture (*R'*) distribution has a wedge-shaped pattern, and the whole damage area spreads from the fault tip in an asymmetric pattern, in a similar manner to that in Figures 6.4d and 6.5c-i.

6.7.7. Transcurrent fault along the Dead Sea Rift in Lebanon

Several researchers (Freund *et al.*, 1970; Garfunkel *et al.*, 1981; Girdler, 1990; Van Eck and Hofstetter, 1990; Sneh, 1996; Butler *et al.*, 1997) have described the strike-slip movement and seismicity along the Dead Sea rift. Detailed fault maps around the Dead Sea rift have been drawn from field data and satellite images (Fig. 6.19a; Dubertret, 1962; Freund *et al.*, 1970; Garfunkel *et al.*, 1981).

The transform fault system consists of three fundamental portions. The Yammouneh fault links the transtensional portion (Dead Sea fault) in the south and the Ghab fault. The two left-lateral faults are right-stepping (Segall and Pollard, 1980; Kim *et al.*, 2000) hence sub-parallel en echelon folds and uplift are formed (Garfunkel *et al.*, 1981). This forms a broad restraining bend where deformation has been accommodated by the strike-slip splay faults and distributed strain in the adjacent blocks (Garfunkel *et al.*, 1981; Butler *et al.*, 1997).

The linking Yammouneh fault and the recent active Roum fault (Butler *et al.*, 1997) are branch faults (type A of Chinnery, 1966b) at the northern tip of the Dead Sea fault. There are some other branches spreading out from the tip (Fig. 6.19a). These faults radially spread from the tip rather than sub-parallel to the main fault and predominant in the contractional quadrant with synthetic sense to the main fault.

On the other side of the tip near Haifa, normal faults are predominant as predicted in other examples in the dilational quadrant (Figs. 6.4a & b and 6.5a & b). The angle between the main fault and the normal faults is higher than that for the branches (Fig. 6.4c), and some faults show a left-lateral slip sense (Fig. 6.19a). Other interesting structures are high-angle right-lateral strike-slip faults mainly to the south of the Yammouneh fault. These faults are almost orthogonal to the main fault trend, and can be interpreted as antithetic faults at tip damage zones (c.f. Fig. 6.4d and 6.5f). In this area some anticlockwise rotations are observed (Hancock and Atiya, 1979).

The relative rare damage structures around the Ghab fault and its lower displacements (Freund *et al.*, 1970) indicate that the fault was generated later than the Dead Sea fault, and propagated into the Dead Sea fault facilitating one of the branch

faults around the old fault tip. During the period of consecutive deformation the Yammouneh fault region has been uplifted by transpression and the Roum fault has been activated by the influences of the orientation of the fault, stress directivity and maximum compressive stress. A simple diagram (Fig. 6.19b) explains this model.

6.7.8. Flower structures in the Moray Firth, Scotland and the Long Beach oilfield, California

Naylor *et al.*, (1986) showed some natural examples of flower structures (Fig. 6.20) from the Moray Firth, Scotland and the Long Beach oilfield in California. These faults curve into a main fault plane in depth showing cone-shaped structures. These flower structures are shown in other large-scale natural examples with a variety, which are commonly, loosely attributed to strike-slip faulting (Lowell, 1972; Sylvester and Smith, 1976).

The mechanism and the geometry of flower structures are basically the same as the mode III fault tip shown in cross-sections, especially in early stages of strike-slip faults. Some of these examples, showing similar fracture patterns, are described from Gozo (Fig. 6.7c). Although some of flower structures are reported across mature strike-slip faults (Sylvester, 1988), flower structure is a large-scale geometry of mode III fault tip damage.

6.8. CONCLUSIONS

1. Damage zones around strike-slip faults show a variety of fracture patterns. They are mainly divided into three main zones according to their location - tip zone, wall zone, and linkage zone.
2. The tip damage structures can be classified by geometric patterns of damage structures, which are mainly dependent on the slip modes at fault tips. At a mode II tip, a variety of damage structures are observed, such as 'wing cracks', 'horsetail splays', 'antithetic shear fractures', 'synthetic branch faults', and their combined types. These tip damage structures strongly depend on the fault tip mode and stress propagation at cohesive end zone of each tip.
3. Wall-zone damage may result from the propagation of mode II & III tips, or kinematic damage including joint drag. Structures include 'en echelon veins', 'extension

fractures', 'antithetic faults', 'Riedel shears', 'rotated blocks' and 'triangular openings'.

4. Linkage zone damage structures are developed between two parallel or sub-parallel fault segments. The damage geometries depend on the stress conditions, i.e. dilational or contractional oversteps. At dilational oversteps 'extension fractures (mode I)' and 'pull-aparts' form, whereas in contractional oversteps 'composite faults' are developed. 'Rotated blocks' and 'isolated lens' or 'strike-slip duplexes' are observed in both oversteps with slight differences in geometry.
5. Several large-scale strike-slip faults and their damage structures are compared with the classification from small-scale damage structures. Most of the large-scale examples are consistent with the classification and interpretation.

REFERENCES

Aki, K. 1989. Geometric features of a fault zone related to the nucleation and termination of an earthquake rupture. *U. S. Geological Survey Open -File Report* **89-315**.1-9.

Ambraseys, N. N. and Tchalenko, J. S. 1969. The Dasht-e Bayaz (Iran) earthquake of August 31, 1968: A field report. *Bulletin of the Seismological Society of America* **59**, 1751-1792.

Anderson, E. M. 1951. *The Dynamics of Faulting*. Olivier and Boyd, Edinburgh.

Arthaud, F. and Matte, Ph. 1975, Les decrochements tardi-hercyniens du S. W. de l'Europe. Geometrie et essai de reconstitution des conditions de la deformation. Tectonophysics 25, 139-171.

Aydin, A. and Nur, A. 1982. Evolution of pull-apart basins and their scale independence. *Tectonics* **1**, 91-105.

Bartlett, W. L., Friedman, M. and Logan, J. M., 1981. Experimental folding and faulting of rocks under confining pressure. Part IX. Wrench faults in limestone layers. *Tectonophysics* **79,** 255-277.

Bosworth, W. 1995. A high-strain rift model for the southern Gulf of Suez (Egypt), *in* Lambiase, J. J., ed., *Hydrocarbon habitat in rift basins: Geological Society of London Special Publication* **80**, P. 75-102.

Boyer, S. E. and Elliott, D. 1982. Thrust systems. *Bulletin of American Association of Petroleum Geology*. **66**, 1196-1230.

Brace, W. F. and Bombolakis, E. G. 1963. A note on brittle crack growth ion compression. *J. Geophys. Res.* **68**, 3709-3713.

Butler, R. W. H., Spencer, S. and Griffiths, H. M. 1997. Transcurrent fault activity on the Dead Sea Transform in Lebanon and its implications for plate tectonics and seismic hazard. Journal of the Geological Society of London **154**, 757-760.

Caine, J. S., Evans, J. P. and Forster, C. B. 1996. Fault zone architecture and permeability structure. *Geology* **24**, 1125-1128.

Cartwright, J. A., Mansfield, C. S. and Trudgill, B. D. 1996. Fault growth by segment linkage. In *Modern developments its structural interpretation*, eds P. C. Buchanan and D. A. Nieuwland, Vol. 99, 163-177. *Special Publication of the Geological Society of London.*

Cartwright, J. A., Trudgill, B. D. and Mansfield, C. S. 1995. Fault growth by segment linkage: an explanation for scatter in maximum displacement and trace length data from the Canyonlands Grabens of SE Utah. *Journal of Structural Geology* **17**, 1319-1326.

Chinnery, M. A. 1966a. Secondary faulting: I. Theoretical aspects. *Canadian Journal of earth Sciences* **3**, 163-174.

Chinnery, M. A. 1966b. Secondary faulting: II. Geological aspects. *Canadian Journal of earth Sciences* **3**, 175-190.

Cox, S. J. D. and Scholz, C. H. 1988a. Rupture initiation in shear fracture in rocks: an experimental study. *Journal of Geophysical Research* **93**, 3307-3320.

Cox, S. J. D. and Scholz, C. H. 1988b. On the formation and growth of faults: an experimental study. *Journal of Structural Geology* **10**, 413-430.

Cruikshank, K. M., Zhao, G. and Johnson, A. M. 1991a. Analysis of minor fractures associated with joints and faulted joints. *J. Struct. Geol.*, **13**, 865-886.

Cruikshank, K. M., Zhao, G. and Johnson, A. M. 1991b. Duplex structures connecting fault segments in Entrada Sandstone. *Journal of Structural Geology* **13**, 1185-1196.

Dewey, J. F. 1966. Kink-bands in Lower Carboniferous Slates of Rush, Co. Dublin. *Geological Magazine* **103**, 138-142.

Dibblee, T. W. Jr. 1977. Strike-slip tectonics of the San Andreas fault and its role in Cenozoic basin evolution. *in Late Mesozoic and Cenozoic Sedimentation and Tectonics in California*, edited by T. H. Nilsen, 26-38, San Joaquin Geological Society, Bakersfield, Calif.

Dobbin, C. E. and Erdman, C. E. 1955. Structure contour map of the Montana plains: United States Geological Survey Oil and Gas Investigation Map OM 178A, Scale 1:500,000.

Dubertret, L. 1962. Carte geologique du Liban, Syrie et bordure de pays voisins, au 1:1,000,000. Mus. d'Hist. Natur., Paris.

Erdogan, F. and Sih, G. C. 1963. On the crack extension in plates under plane loading and transverse shear. *J. Basic Eng.*, **85**, 519-527.

Fossen, H. and Gabrielsen, R. H. 1996. Experimental modeling of extensional fault systems by use of plaster. *Journal of Structural Geology* **18**, 673-687.

Fossen, H. and Hesthammer, J. 1997. Geometric analysis and scaling relations of deformation bands in porous sandstone. *Journal of Structural Geology* **19**, 1479-1493.

Freund, R., Garfunkel, Z., Zak, I., Goldberg, M., Weissbrod, T. and Derin, B. 1970. The shear along the Dead Sea rift. *Phil. Trans. Roy. Soc. Lond.* **A. 267**, 107-130.

Garfunkel, Z., Zak, I. and Freund, R. 1981. Active faulting in the Dead Sea rift. *Tectonophysics* **80**, 1-26.

Girdler, R. W. 1990. The Dead Sea transform fault system. *Tectonophysics* **180**, 1-13.

Granier, T. 1985. Origin, damping and pattern of development of faults in granite. *Tectonics* **4**, 721-737.

Gross, M. R., Gutiérrez-Alonso, G. Bai, T., Wacker, M. A., Collinsworth, K. B. and Behl, R. J. 1997. Influence of mechanical stratigraphy and kinematics on fault scaling relations. *Journal of Structural Geology* **19**, 171-183.

Hancock, P. L. 1985. Brittle microtectonics: principles and practice. *Journal of Structural Geology* **7**, 437-457.

Hancock, P. L. and Atiya, M. S. 1979. Tectonic significance of mesofracture system associated with the Lebanese segment of the Dead Sea transform fault. *Journal of Structural Geology* **1**, 143-153.

Harding, T. P. 1974. Petroleum traps associated with wrench faults. *The American Association of Petroleum Geologists Bulletin.* **58**, 1290-1304.

Harding, T. P., Vierbuchen, R. C. and Christie-Blick, N. 1985. Structural styles, plate-tectonic settings, and hydrocarbon traps of divergent (Transtensional) wrench faults. In *Strike-slip Deformation, Basin Formation, and Sedimentation*: Eds: Biddle, K. T. and Christie-Blick, N. *Society of Economic Palaeontologists and Mineralogists. Special Publication.* **37,** 51-77.

Ingraffea, A. D. 1987. Theory of crack initiation and propagation in rock, in *Fracture Mechanics of Rocks* (edited by B. K. Atkinson) pp.71-108, Academic Press, san Diego, California.

Kim, Y. S., Andrews, J. R. and Sanderson, D. J. 2000. Damage zones around strike-slip fault systems and strike-slip fault evolution, Crackington Haven, southwest England. *Geoscience Journal* **4**

King, G. C. P. 1986. Speculations on the Geometry of the Initiation and Termination Processes of Earthquake Rupture and its Relation to Morphology and Geological Structure. . *Pure and Applied Geophysics* **124,** 567-585.

Lawn, B. R. and Wilshaw, T. R. 1975. *Fracture of Brittle Solids.* 204pp., Cambridge Univ. Press, London.

Lin, J. and Parmentier, E. M. 1988. Quasistatic propagation of a normal fault: a fracture mechanics model. *J. Struct. Geol.*, **10**, 249-262.

Little, T. A. 1996. Faulting-related displacement gradients and strain adjacent to the Awatere strike-slip fault in New Zealand. *Journal of Structural Geology* **18**, 321-342.

Little, T. A. and Jones, A. 1998. Seven million years of strike-slip and off-fault deformation on the Awatere Fault, South Island, New Zealand. *Tectonics* **17**, 285-302.

Little, T. A., Grapes, R. and Berger, G. W. 1998. Late Quaternary strike slip on the eastern part of the Awatere fault, Soputh Island, New Zealand. *Geological Society of America Bulletin* **110**, 127-148.

Lockner, D. A., Byerlee, J. D., Kuksenko, V., Ponomarev, A. and Sidorin, A. 1991. Quazi-static fault growth and shear fracture energy in granite. *Nature* **350**, 39-42.

Logan, J. M., Friedman, M., Higgs, N., Dengo, C. and Shimamoto, T. 1979. Experimental studies of simulated gouge and their application to studies of natural fault zones. *U.S. geol. Surv. Open-File Report* **79-1239**, 305-343.

Lowell, J. D. 1972. Spitsbergen Tertiary orogenic belt and the Spitsbergen fracture zone. *Bulletin of Geological Society of America* **83**, 3091-3102.

Luyendyk, B. P., Kamerling, M. J., Terres, R. and Hornafius, J. S. 1985. Simple shear of southern California during Neogene time suggested by paleomagnetic declinations. *Journal of Geophysical Research* **90**, 12,455-12,466.

Martel, S. J. and Boger, W. A. 1998. Geometry and mechanics of secondary fracturing around small three-dimensional faults in granitic rock. *Journal of Geophysical Research* **103**, 21,299-21,314.

Martel, S. J., Pollard, D. D. and Segall, P. 1988. Development of simple strike-slip fault zones, Mount Abbot quadrangle, Sierra Nevada, California. *Geol. Soc. Am. Bull.*, **100**, 1451-1465.

Matti, J. C., Morton, D. M. and Cox, B. F. 1985. Distribution and geologic relations of fault systems in the vicinity of the Central Transverse Ranges, southern California. U.S. Geol. Surv. Open File Rep., 85-365, 27pp.

McClay, K. and Khalil, S. 1998. Extensional hard linkages, eastern Gulf of Suez, Egypt. *Geology* **26**, 563-566.

McGrath, A. G. and Davison, I. 1995. Damage zone geometry around fault tips. *Journal of Structural Geology* **17**, 1011-1024.

McKinstry, H. E. 1953. Shears of the second order. American Journal of Science 251, 401-414.

Mollema, P. N. and Antonellini, M. 1999. Development of strike-slip faults in the dolomites of the Sella Group, Northern Italy. *Journal of Structural Geology* **21**, 273-292.

Naylor, M. A., Mandl, G. and Sijpesteijn, C. H. K. 1986. Fault geometries in basement-induced wrench faulting under different initial stress states. *Journal of Structural Geology* **8**, 737-752.

Nicholson, C., Seeber, L., Williams, P. and Sykes, L. R. 1986a. Seismicity and fault kinematics through the eastern Transverse Ranges, California: Block rotation, strike-slip faulting and low-angle thrusts. *Journal of Geophysical Research* **91**, 4891-4908.

Nicholson, C., Seeber, L., Williams, P. and Sykes, L. R. 1986b. Seismic evidence for conjugate slip and block rotation within the San Andreas fault system, southern California. *Tectonics* **5**, 629-648.

Norris, R. J. and Cooper, A. F. 1995. Origin of small-scale segmentation and transpressional thrusting along the Alpine fault, New Zealand. *Geological Society of America Bulletin* **107**, 231-240.

Peacock, D. C. P. and Sanderson, D. J. 1991. Displacement and segment linkage and relay ramps in normal fault zones. *Journal of Structural Geology* **13**, 721-733.

Peacock, D. C. P. and Sanderson, D. J. 1994. Geometry and development of relay ramps in normal fault systems. *AAPG Bulletin* **78**, 147-165.

Peacock, D. C. P. and Sanderson, D. J. 1995a. Strike-slip relay ramps. *Journal of Structural Geology* **17**, 1351-1360.

Peacock, D. C. P. and Sanderson, D. J. 1995b. Pull-aparts, shear fractures and pressure solution. *Tectonophysics* **241**, 1-13.

Petit, J. P. and Barquins, M. 1988. Can natural faults propagate under mode-II conditions?. *Tectonics*, **7**, 1243-1256.

Ramsay, J. G. and Huber, M. I. 1983. *The Techniques of Modern Structural Geology.* Volume 1, Strain Analysis. Academic Press, London.

Reches, Z. and Lockner, D. A. 1994. Nucleation and growth of faults in brittle rocks. *Journal of Geophysical Research* **99**, 18159-18173.

Rispoli, R. 1981. Stress fields about strike-slip faults inferred from stylonites and tension gashes. *Tectonophysics* **75**, T29-T36.

Roberts, A. P. 1995. Tectonic rotation about the termination of a major strike-slip fault, Marlborough fault system, New Zealand. *Geophysical Research Letters* **22**, 187-190.

Ron, H., Aydin, A. and Nur, A. 1986. Strike-slip faulting and block rotation in the lake Mean fault system. *Geology* **14**, 1020-1023.

Scholz, C. H. 1968. Microfracturing and the inelastic deformation of rock in compression, *J. Geophys. Res.*, **73**, 1417-1432.

Segall, P. and Pollard, D. D. 1980. The mechanics of discontinuous faults. *Journal of Geophysical Research* **85**, 4337-4350.

Segall, P. and Pollard, D. D. 1983. Nucleation and growth of strike slip faults in granite. *Journal of Geophysical Research* **88**, 555-568.

Sibson, R. H. 1996. Structural permeability of fluid-driven fault-fracture meshes *Journal of Structural Geology* **18**, 1031-1042.

Smith, J. G. 1965. Fundamental transcurrent faulting in northern Rocky Mountains. *American Association of Petroleum Geologists Bulletin* **64**, 1398-1409.

Sneh, A. 1996. The Dead Sea Rift: lateral displacement and downfauting pharases. *Tectonophysics* **263**, 277-292.

Swanson, M. T. 1988. Pseudotachylyte-bearing strike-slip duplex structures in the Fort Foster Brittle Zone, S. Maine. *Journal of Structural Geology* **10**, 813-828.

Swanson, M. T. 1989. Sidewall ripouts in strike-slip faults. *Journal of Structural Geology* **11**, 933-948.

Sylvester, A. G. 1988. Strike-slip faults. *Bulletin Geological Society of America* **100.** 1666-1703.

Sylvester, A. G. and Smith, R. R. 1976. Tectonic transpression and basement-controlled deformation in San Andreas fault zone, Salton Trough, California. *American Association of Petroleum Geologists Bulletin* **60**, .

Tchalenko, J. S. 1970. Similarities between shear zones of different magnitudes. *Geol. Soc. of America Bull.* **81**, 1625-1640.

Tchalenko, J. S. and Ambraseys, N. N. 1970. Structural analysis of the Dasht-e Bayaz (Iran) earthquake fractures: *Geol. Soc. of America Bull.* **81**, 41-60.

Terres, R. R. and Sylvester, A. G. 1981. Kinematic analysis of rotated fractures and blocks in simple shear. *Bulletin of Seismological Society of America* **71**, 1593-1605.

Thatcher, W. and Bonilla, M. G. 1989. Earthquake fault slip estimation from geologic, geodetic and seismologic observations: Implications for earthquake mechanics and fault segmentation. *U. S. Geological Survey Open -File Report* **89-315**.386-399.

Van Eck, T. and Hofstetter, A. 1990. Fault geometry and spatial clustering of microearthquakes along the Dead Sea-Jordan rift fault zone. *Tectonophysics* **180**, 15-27.

Vermilye, J. M. and Scholz, C. H. 1998. The process zone: A microstructural view of fault growth. *Journal of Geophysical Research* **103**, 12223-12237.

Vermilye, J. M. and Scholz, C. H. 1999. Fault propagation and segmentation: insight from the microstructural examination of a small fault. *Journal of Structural Geology* **21**, 1623-1636.

Walsh, J. J. and Watterson, J., Bailey, W. R. and Childs, C. 1999. Fault relays, bends and branch-lines. *Journal of Structural Geology* **21**, 1019-1026.

Watterson, J., Childs, C. and Walsh, J. J. 1998. Widening of fault zones by erosion of asperities formed by bed-parallel slip. *Geology* **26**, 71-74.

Wilcox, R. E., Harding, T. P. and Seely, D. R. 1973. Basic wrench tectonics. *American Association of Petroleum Geologists Bulletin* **57**, 74-96.

Willemse, E. J. M. and Pollard, D. D. 1998. On the orientation and patterns of wing cracks and solution surfaces at the tips of a sliding flaw or fault. *Journal of Geophysical Research* **103**, 2427-2438.

Willemse, E. J. M., Peacock, D. C. P. and A. Aydin, N. 1997. Nucleation and growth of strike-slip faults in limestones from Somerset, UK *Journal of Structural Geology* **19**, 1461-1477.

Woodcock, N. H. and Fischer, M. 1986. Strike-slip duplexes. *Journal of Structural Geology* **8**, 725-735.

Zhang, P., Slemmons, D. B. and Mao, F. 1991. Geometric pattern, rupture termination and fault segmentation of the Dixie Valley-Pleasant Valley active normal fault system, Nevada, U. S. A. *Journal of Structural Geology* **13**, 165-176.

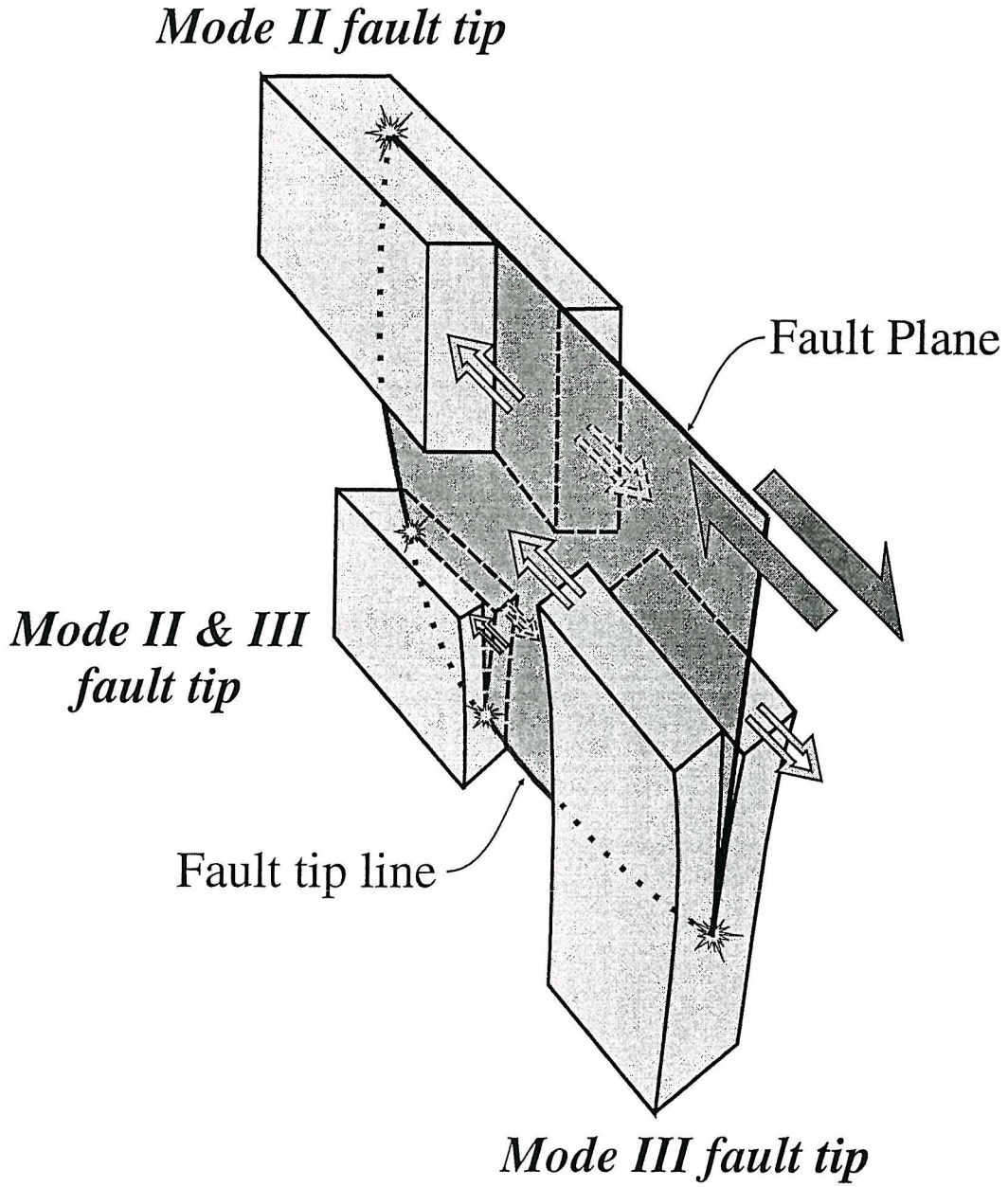

Fig. 6.1. Schematic drawing illustrating fault tip modes. Mode II, in-plane shear or sliding mode; Mode III, anti-plane shear or tearing mode; Mode II & III, mixed mode.

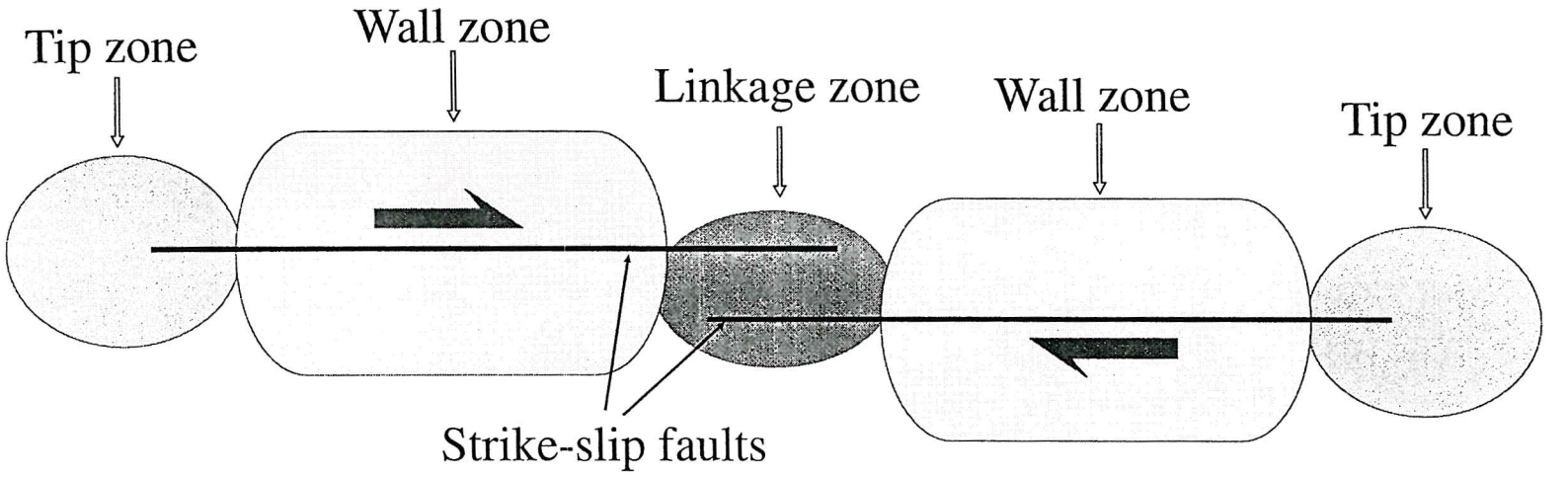

Fig. 6.2. The principal location of damage structures on plan view of a linked strike-slip fault. It shows two fault segments with overstep zone in the middle of the whole fault system.

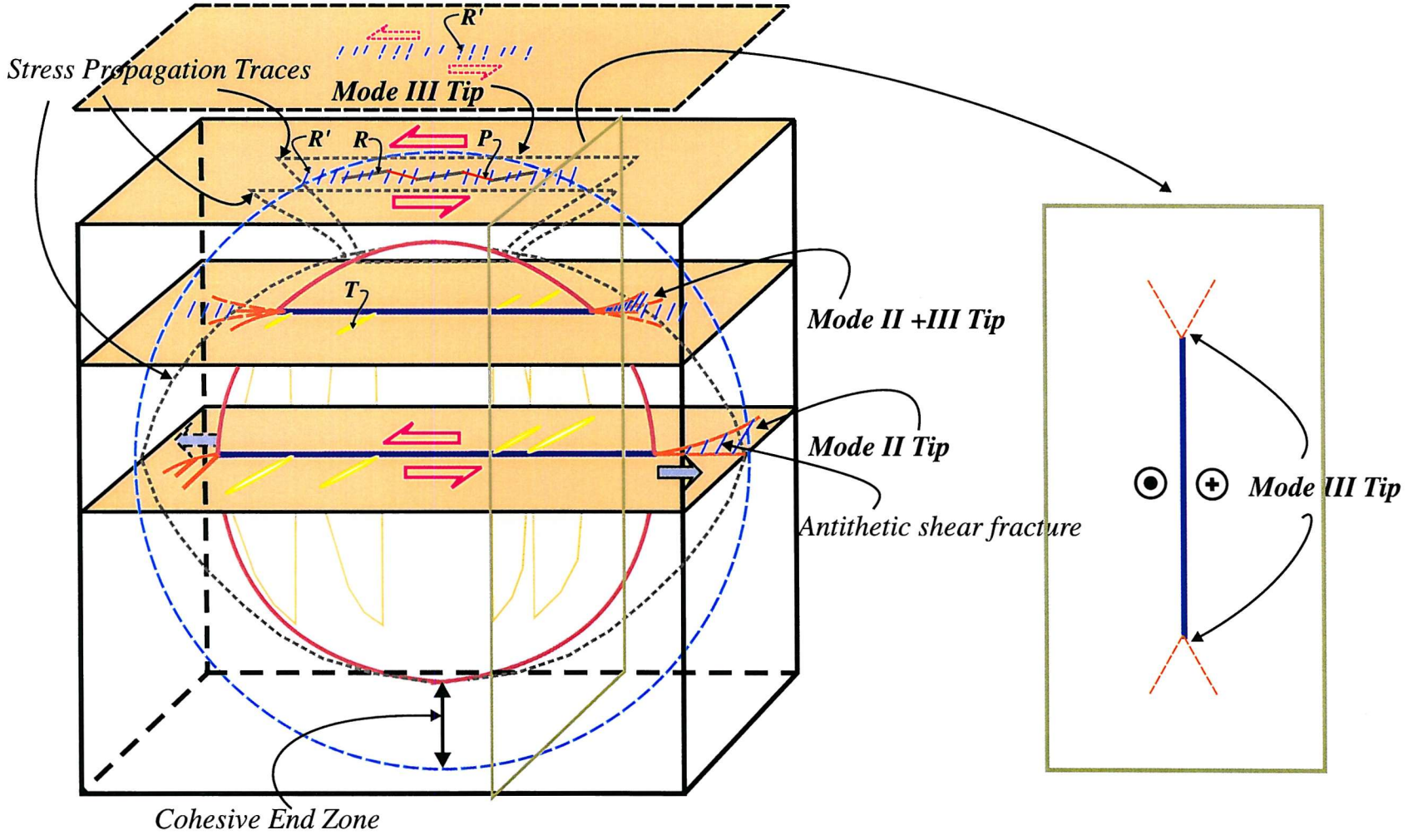

Fig. 6.3. A simplified block diagram showing typical damage structures around a single strike-slip fault on each level and on a vertical section. The tip damage structures have different damage geometries on each level depending on their tip modes. Some mixed modes can occur between two end members.

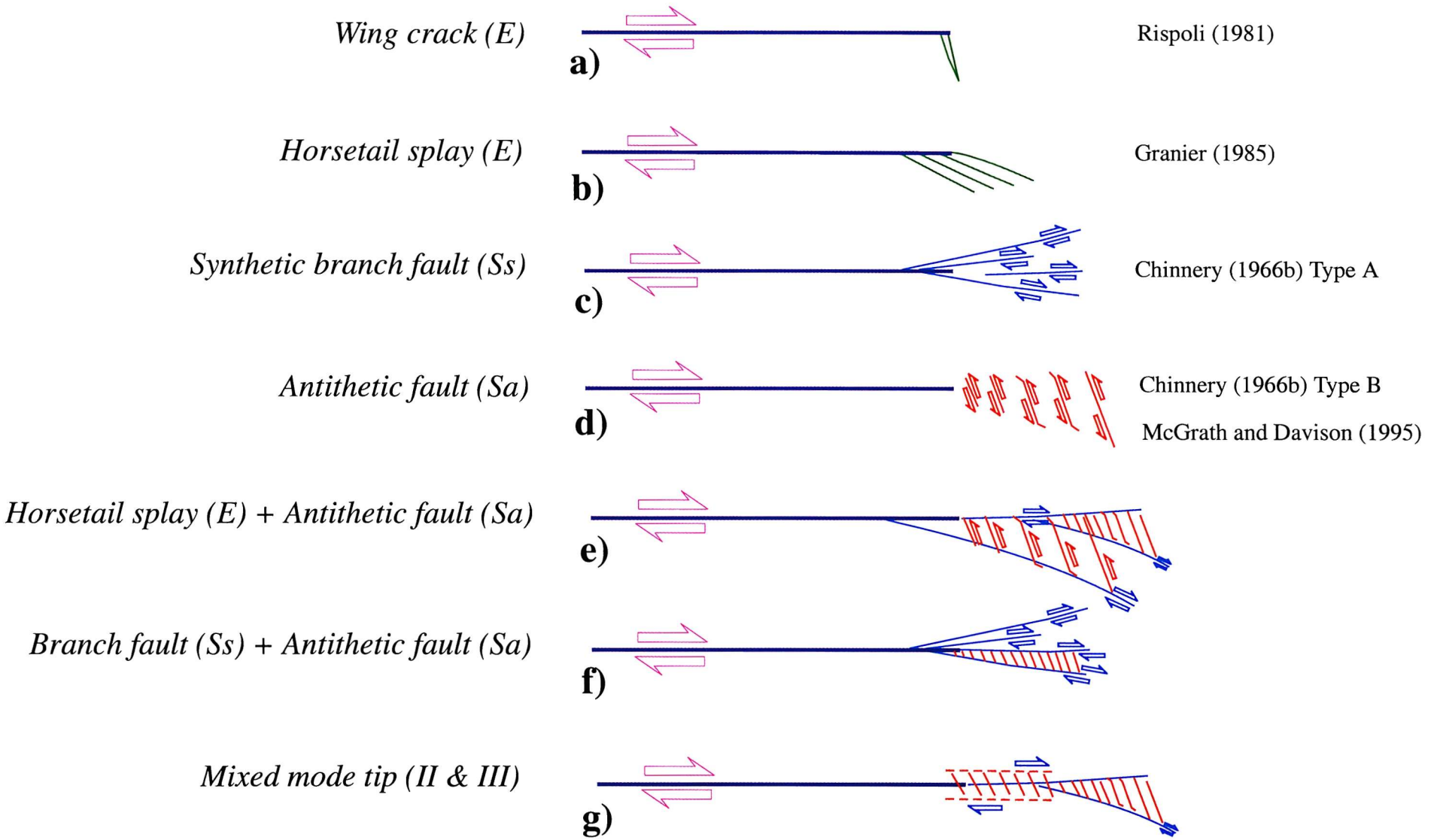

Fig. 6.4. Various tip damage structures at mode II dominant tip zone. Some damage structures show combined damage patterns and mixed modes. *E*, extensional fractures; *Ss*, synthetic shear fractures; *Sa*, antithetic shear fractures.

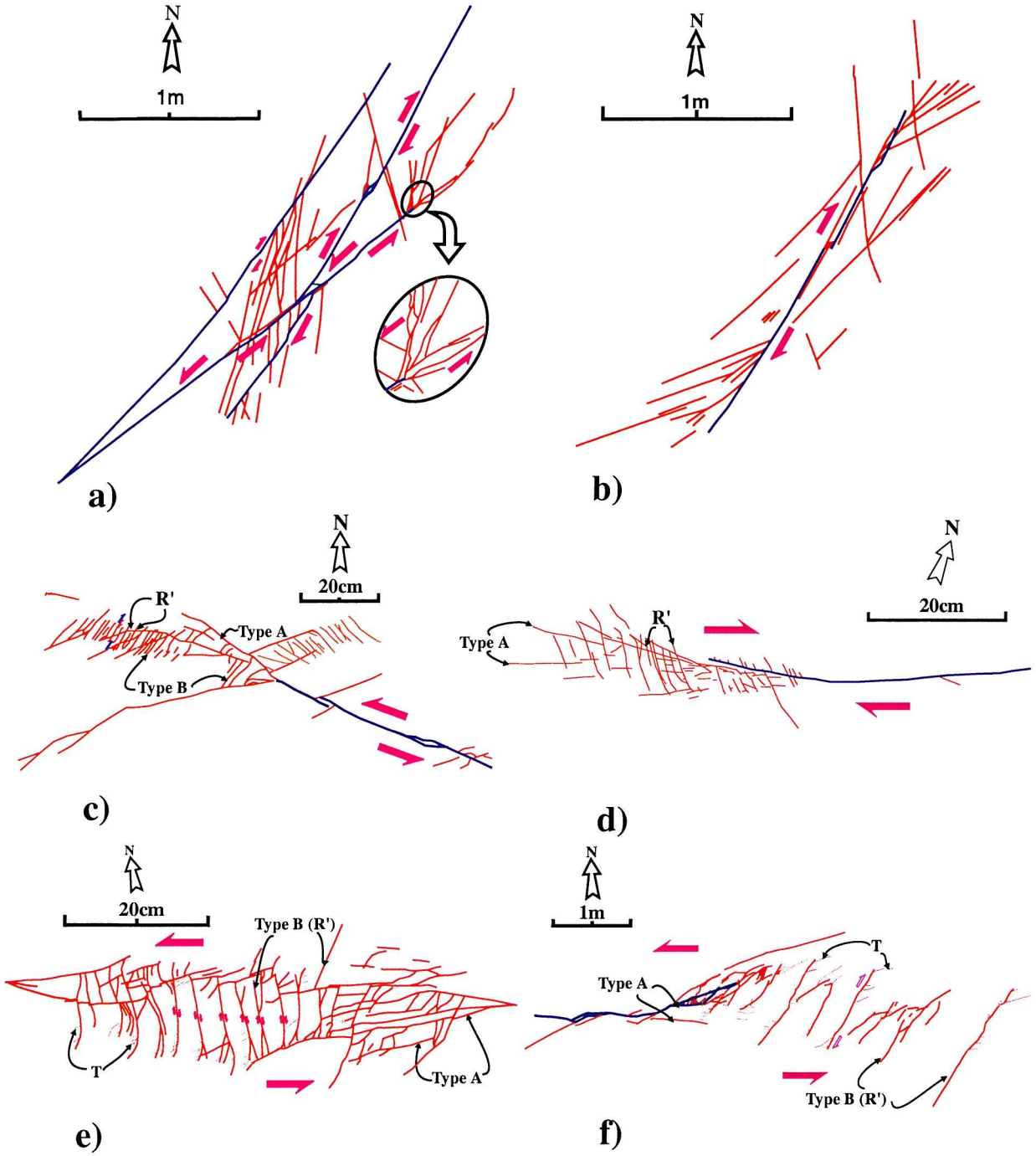

Fig. 6.5. Several exposure scale tip damage structures around strike-slip faults. a) Wing cracks from Crackington Haven. b) Horsetail splays from Crackington Haven. c) and d) Combined tip damage structure from Gozo. e) Combined tip damage and linkage damage structures showing block rotation from Gozo. f) Antithetic dominant tip damage structure from Gozo.

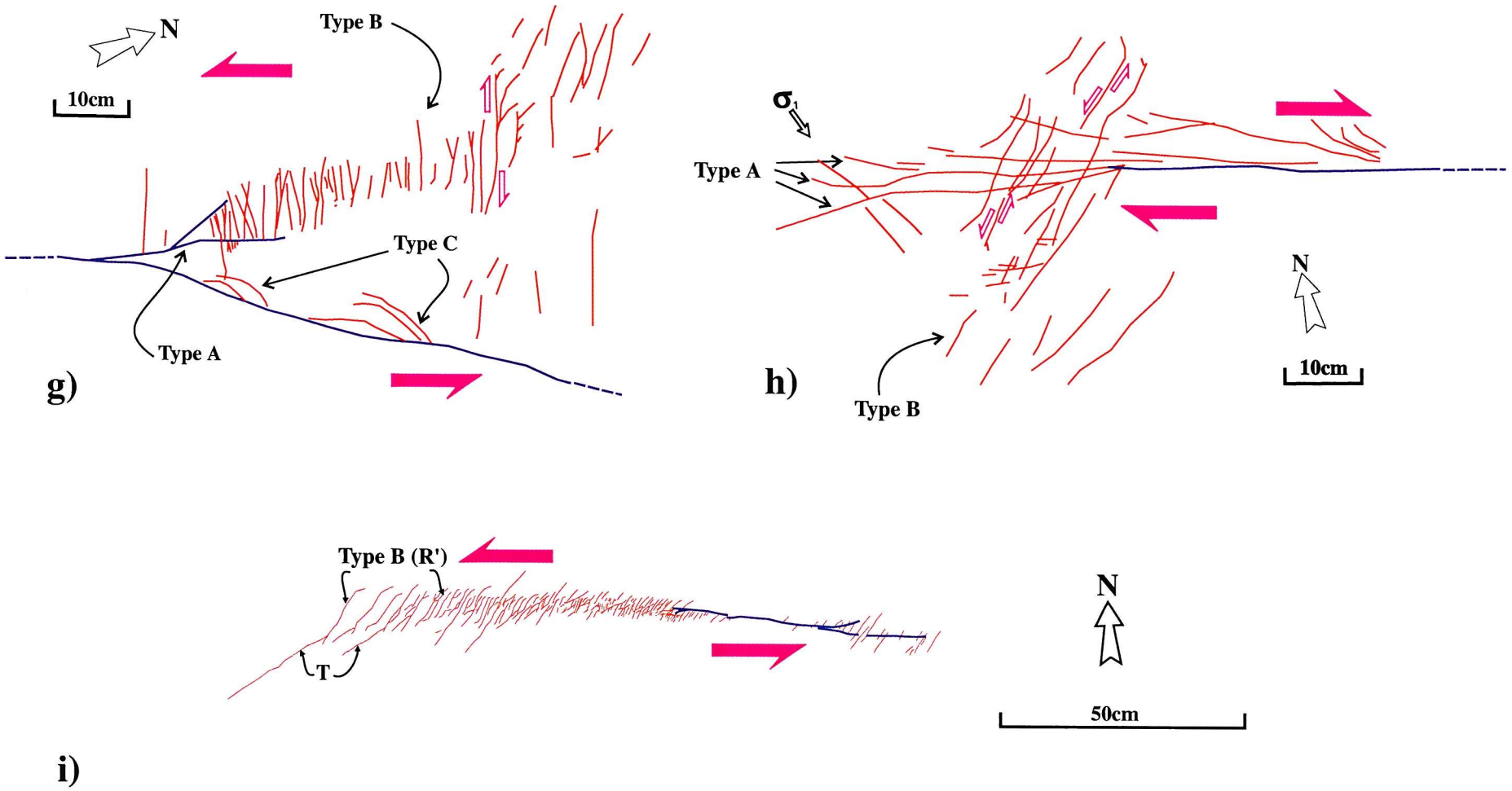

Fig.6.5. (continued). g), h) Combined tip damage structures from Rame Head showing different anglular relationship from other study areas. i) Mode II dominant mixed mode (II/III) tip damage structures from Gozo.

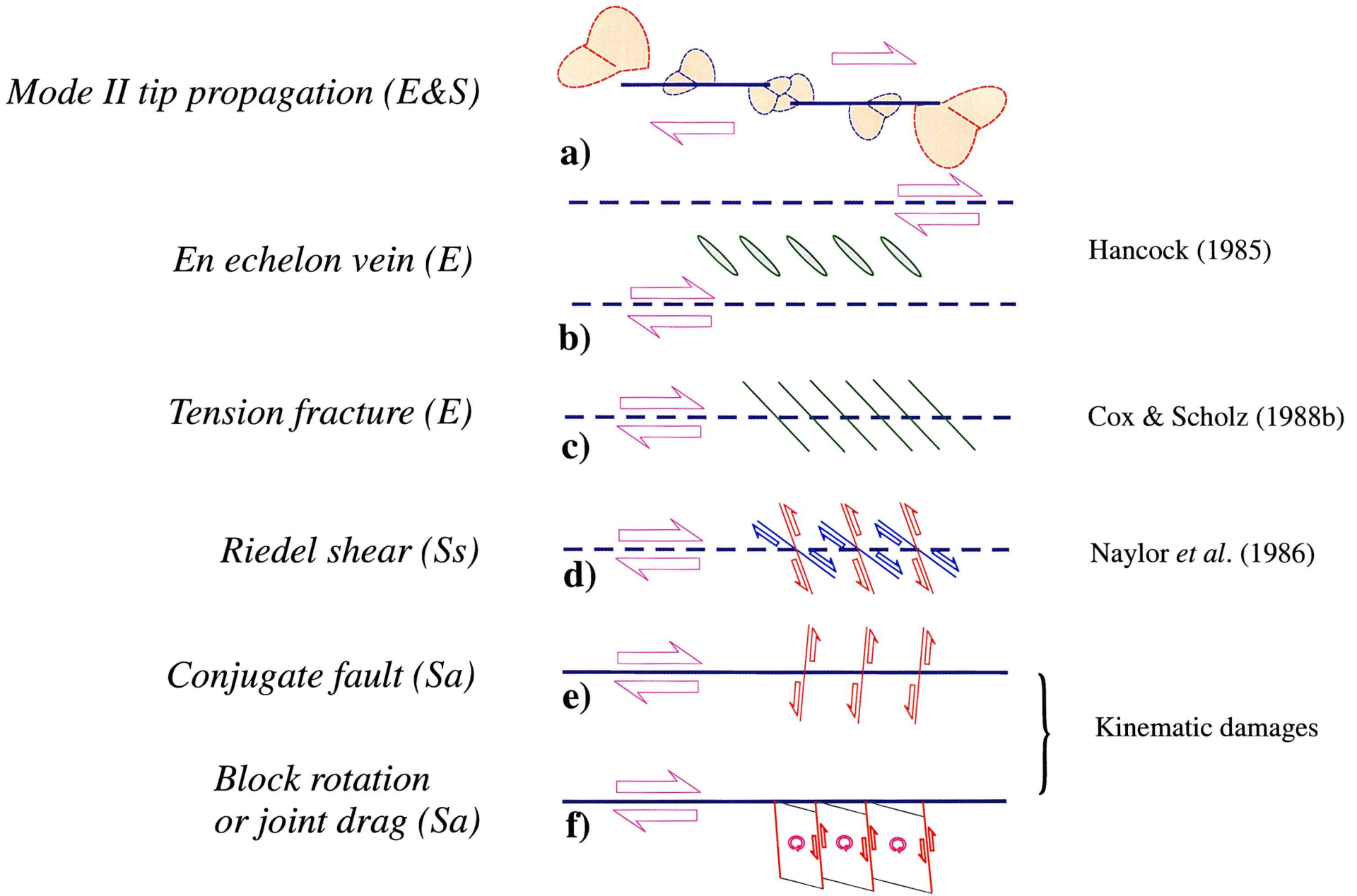

Fig. 6.6. Various wall zone damage structures. Some of the damage patterns show propagation of mode II tip, mode III fault tip damage structures, and others are kinematic damages.

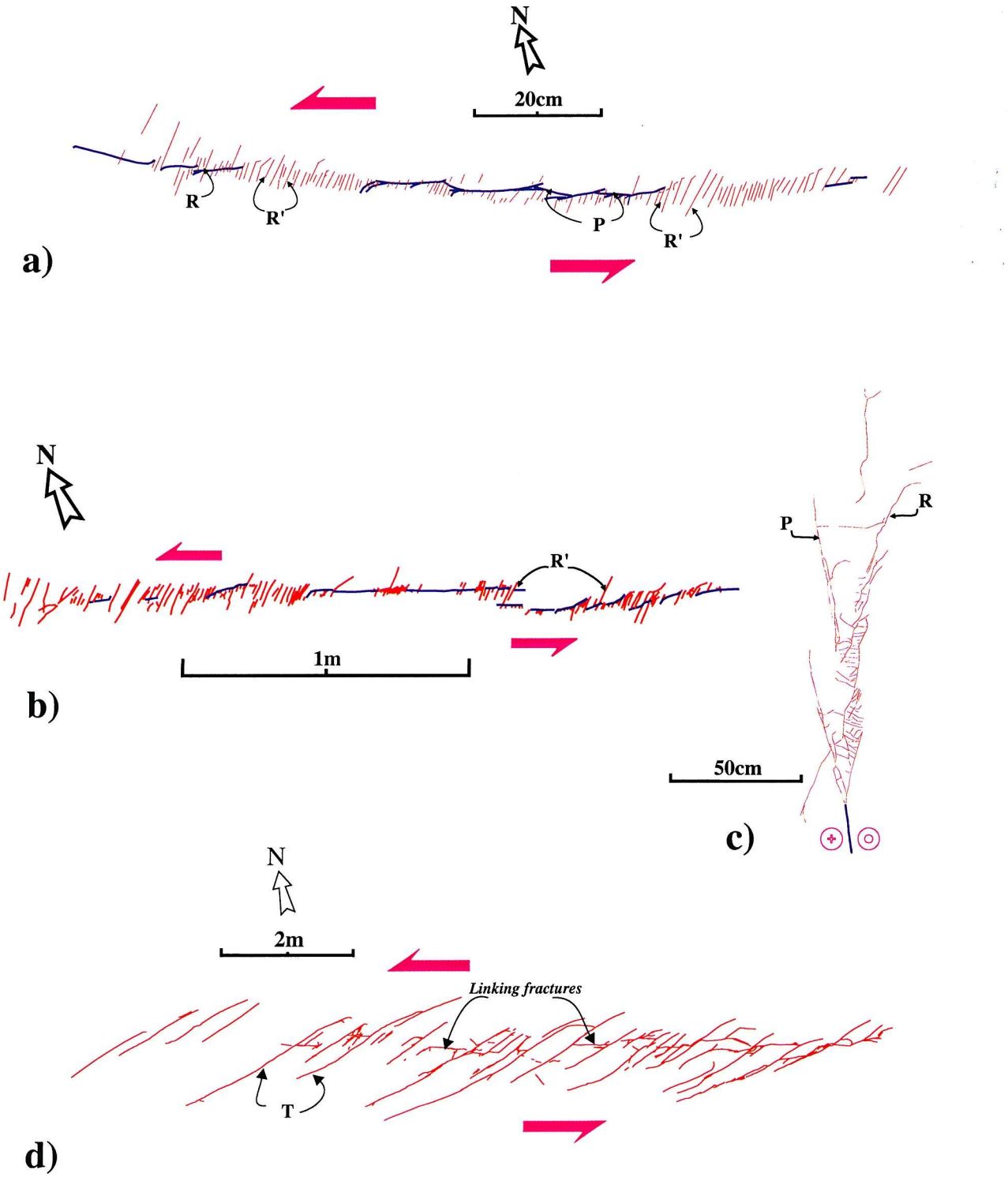

Fig. 6.7. Various wall zone damage patterns. a), b) Mode III fault tip damages on plan view with Riedel shears and fault segments. c) Symmetric damage pattern at mode III fault tip on a cross section. d) Extension fracture dominant wall zone damage structures from Gozo.

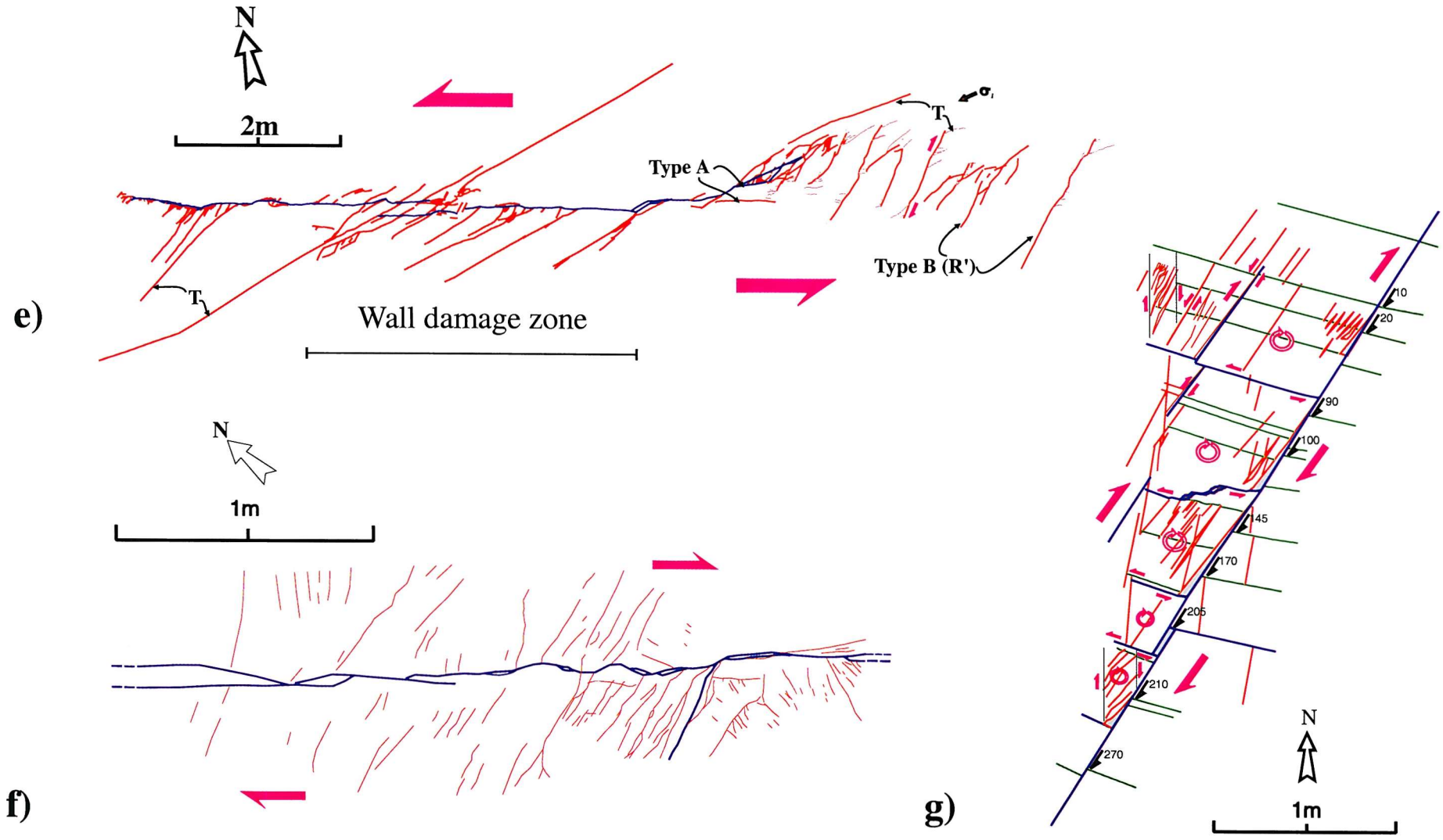

Fig. 6.7. (continued). e) Extensional fractures at wall zone at a mature stage from Gozo. f) Kinematic damages at wall zone showing high angle conjugate faults from Rame Head. g) Kinematic damages at wall zone showing block rotation with parallel boundary faults from Crackington Haven.

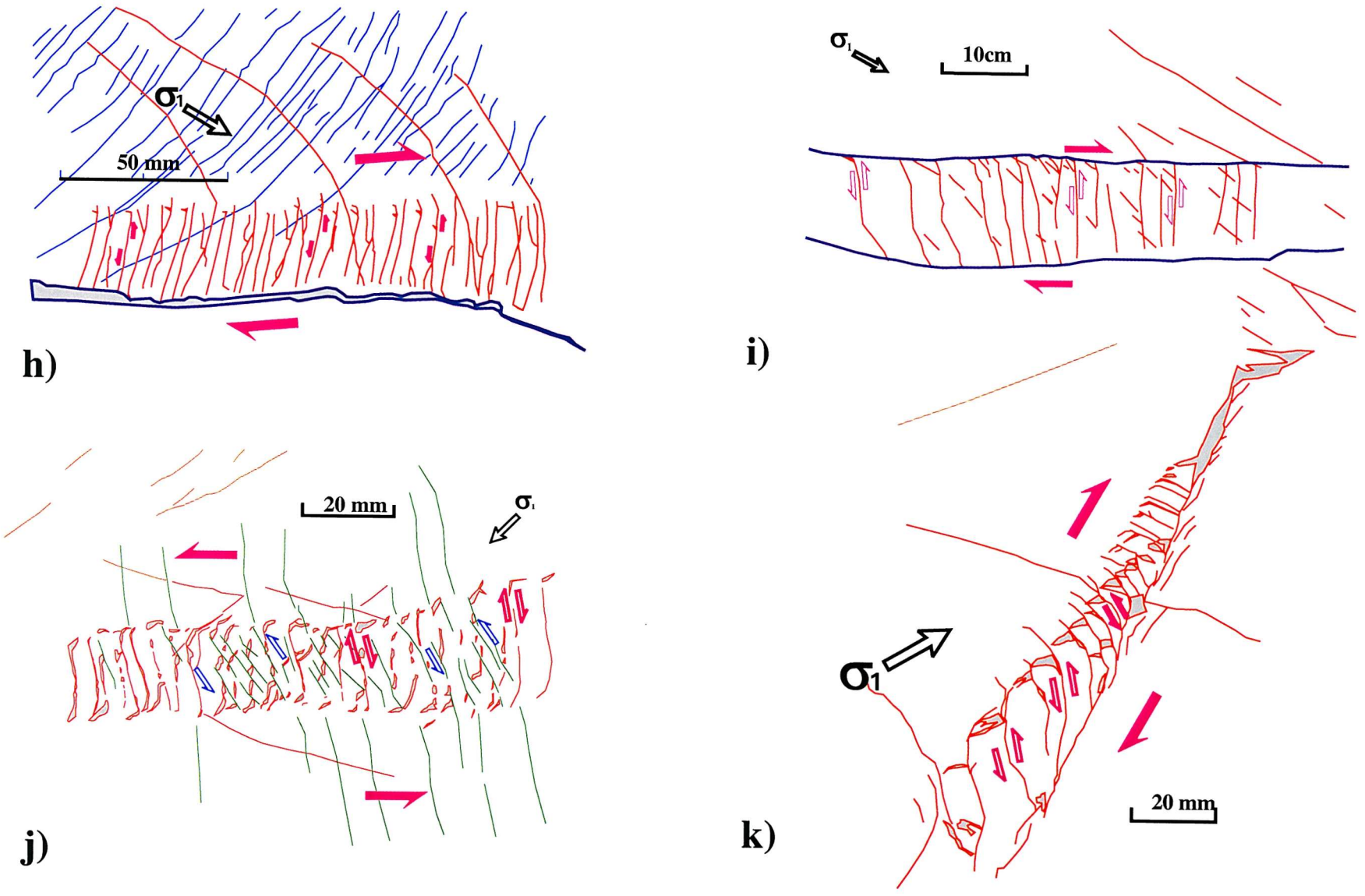

Fig. 6.7. (continued). h) Kinematic damage structures with antithetic transverse fractures from Kilve. i) Kinematic damage structures with antithetic transverse fractures and two boundary faults from Rush, Dublin. j) Shear zone (kink band) showing antithetic and synthetic transverse fractures from Rush, Dublin. k) Kinematic damage structures showing block rotation at sub-parallel faults from Kilve.

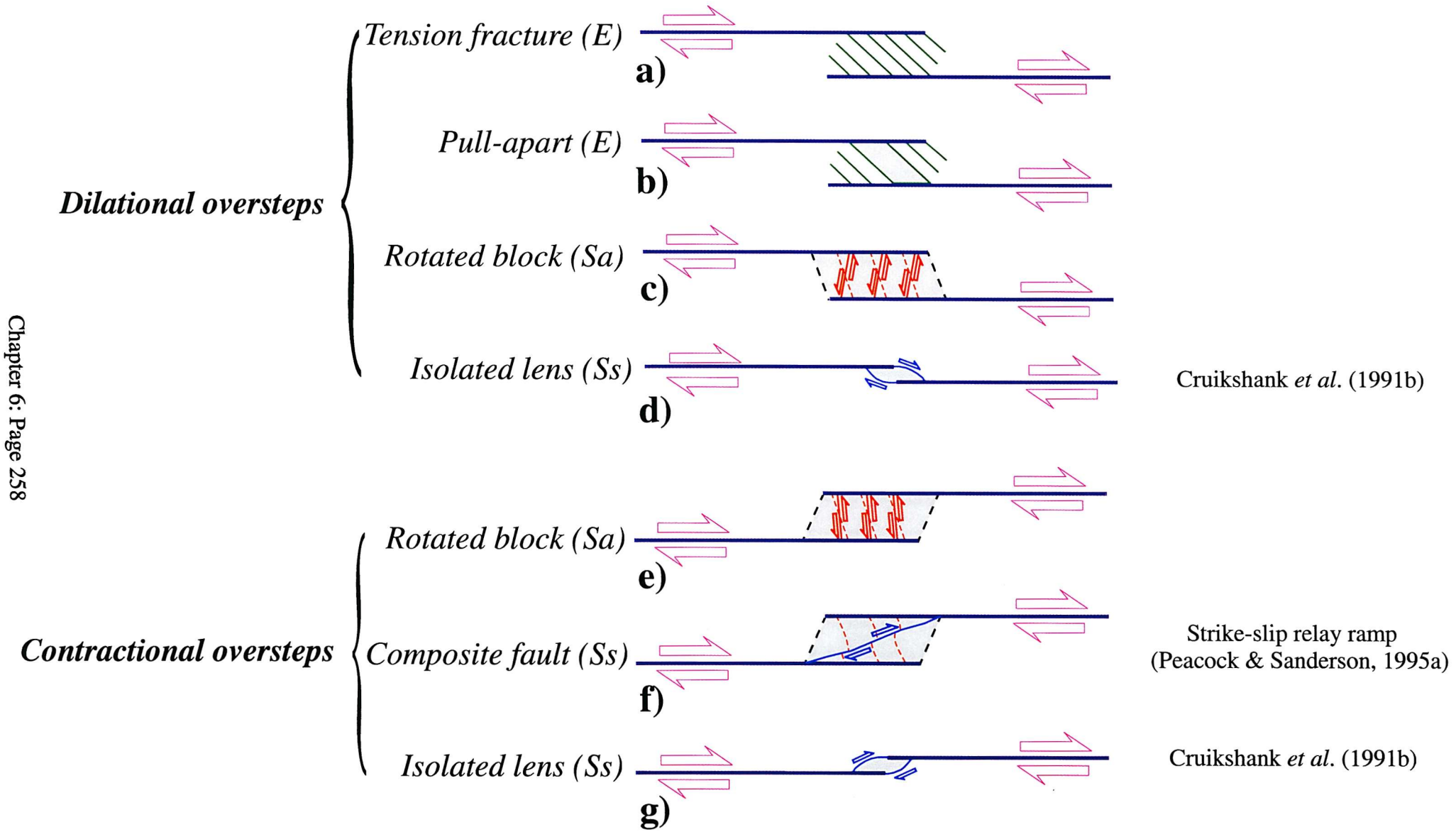

Fig. 6.8. Various damage structures at linkage zones. Linkage zone damage structures show most of the tip damage structures, because the zone is old tip zone. The damage structures are slightly different at dilational and contractional oversteps.

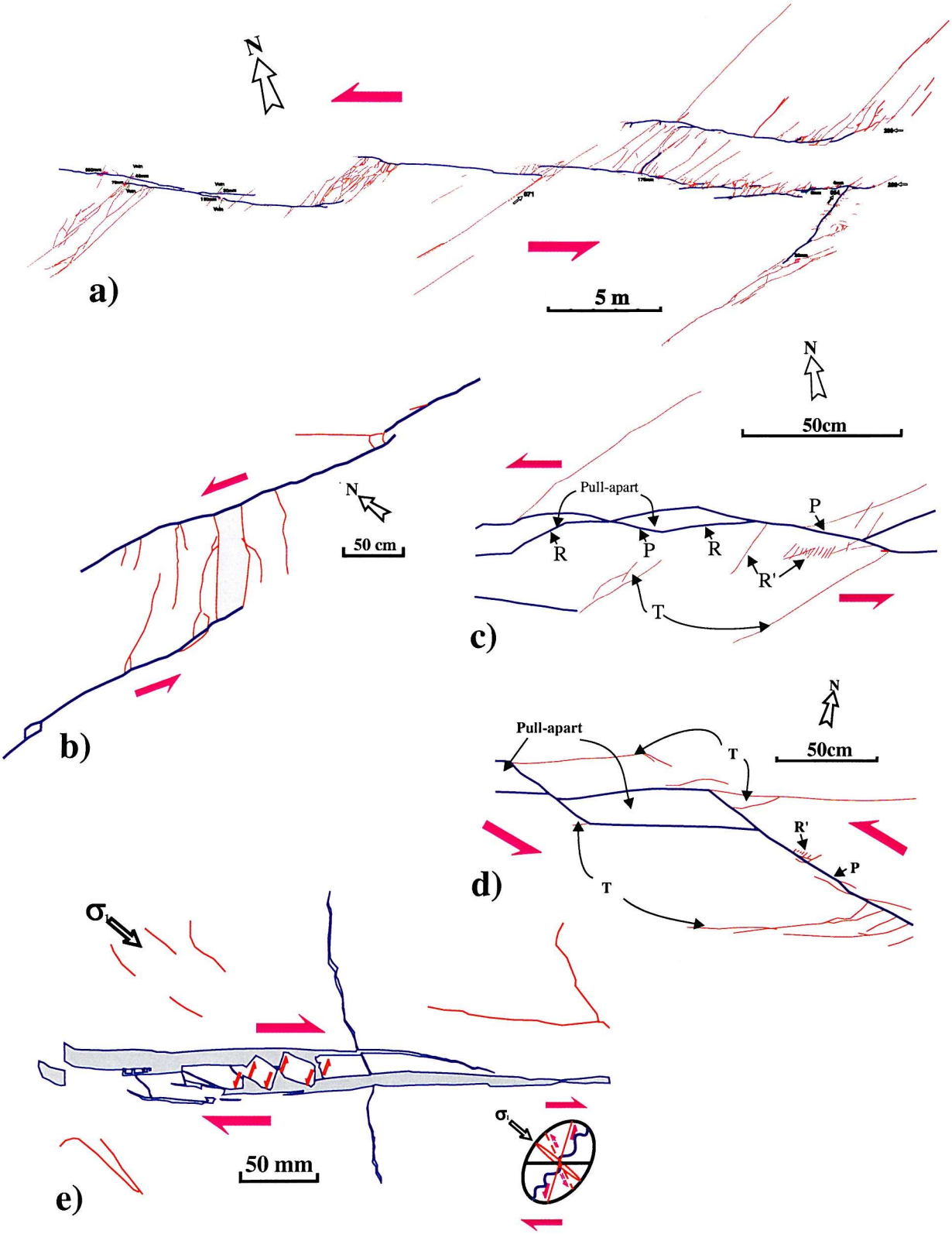

Fig. 6.9. Various linkage zone damage structures. a) Extensional fractures at dilational overstep from Gozo. b) Pull-aparts and extensional fractures at dilational overstep from Gozo. c), d) Pull-aparts composed of *R*, *T* and *P* fractures from Gozo. e) Block rotation at dilational overstep showing rotation of antithetic fractures from Rush, Dublin.

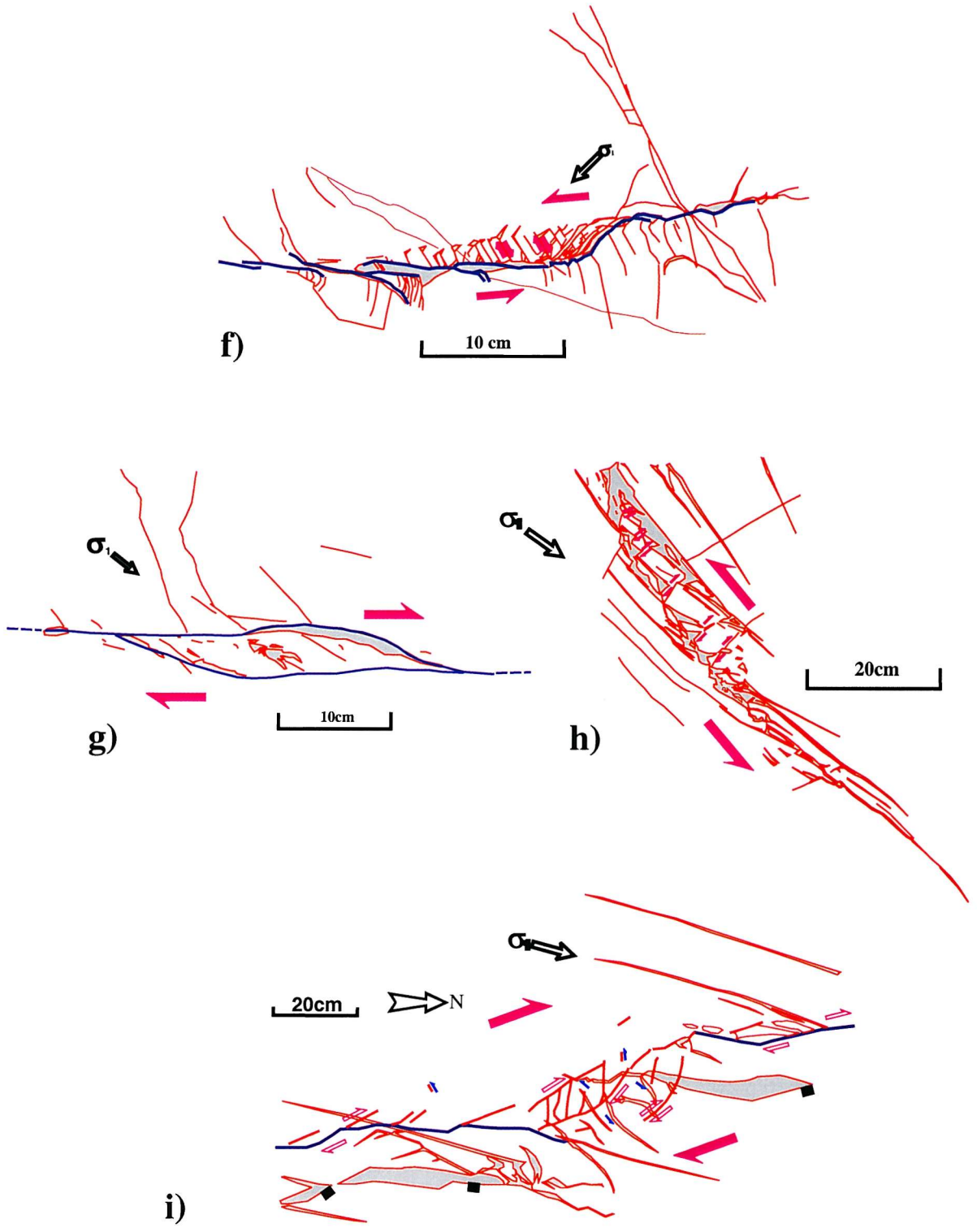

Fig. 6.9. (continued). f) Block rotation with triangular opening at sub-parallel dilational overstep from Kilve. g) Isolated lens at dilational overstep from Rame Head. h) Rotated blocks at contractional overstep from Kilve. i) Composite fault at contractional overstep from Kilve (modified from Peacock and Sanderson, 1995a).

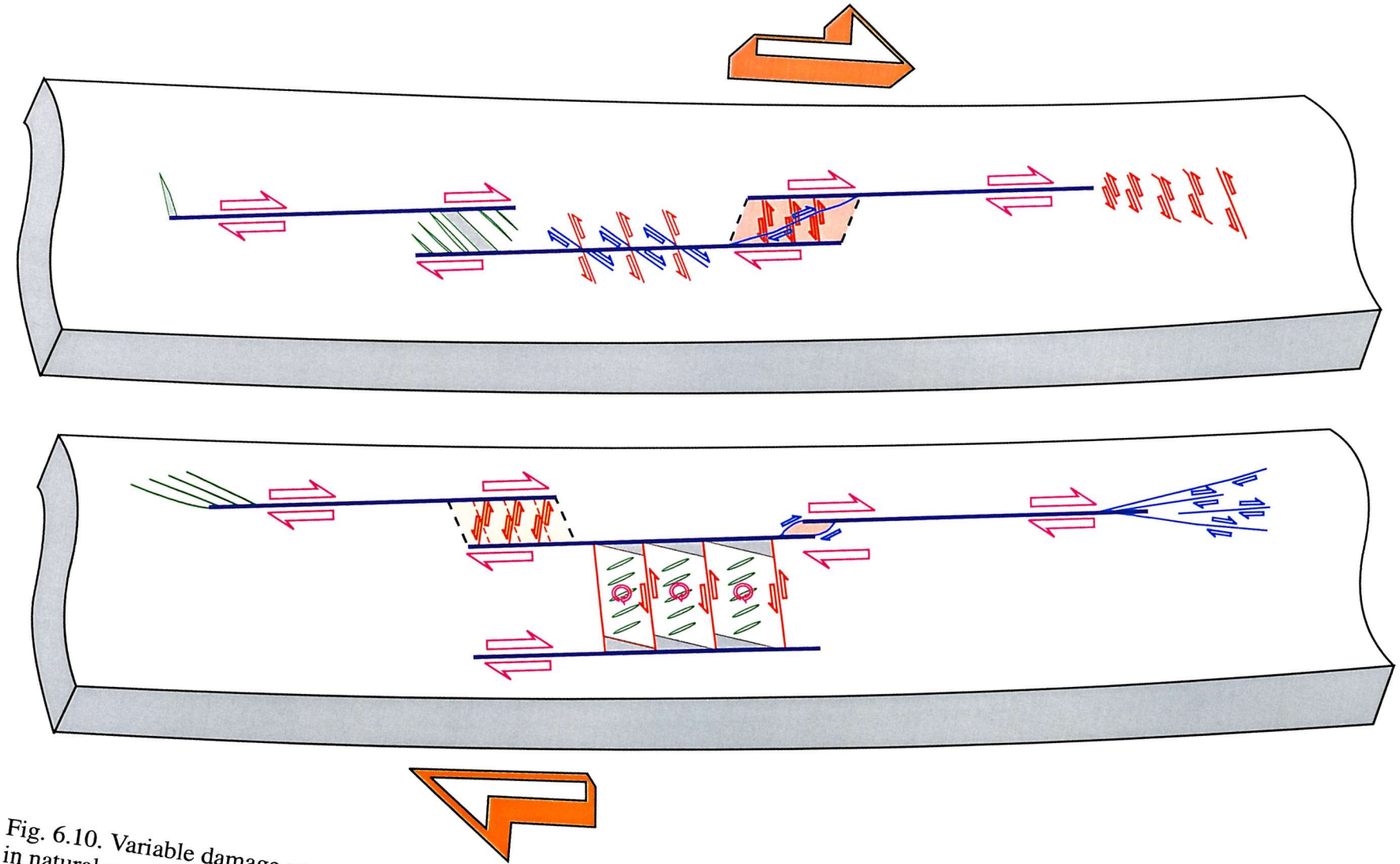

Fig. 6.10. Variable damage zone structures around strike-slip faults. The simple damage patterns shown are more complicated in natural examples due to several factors and combination with other structures.

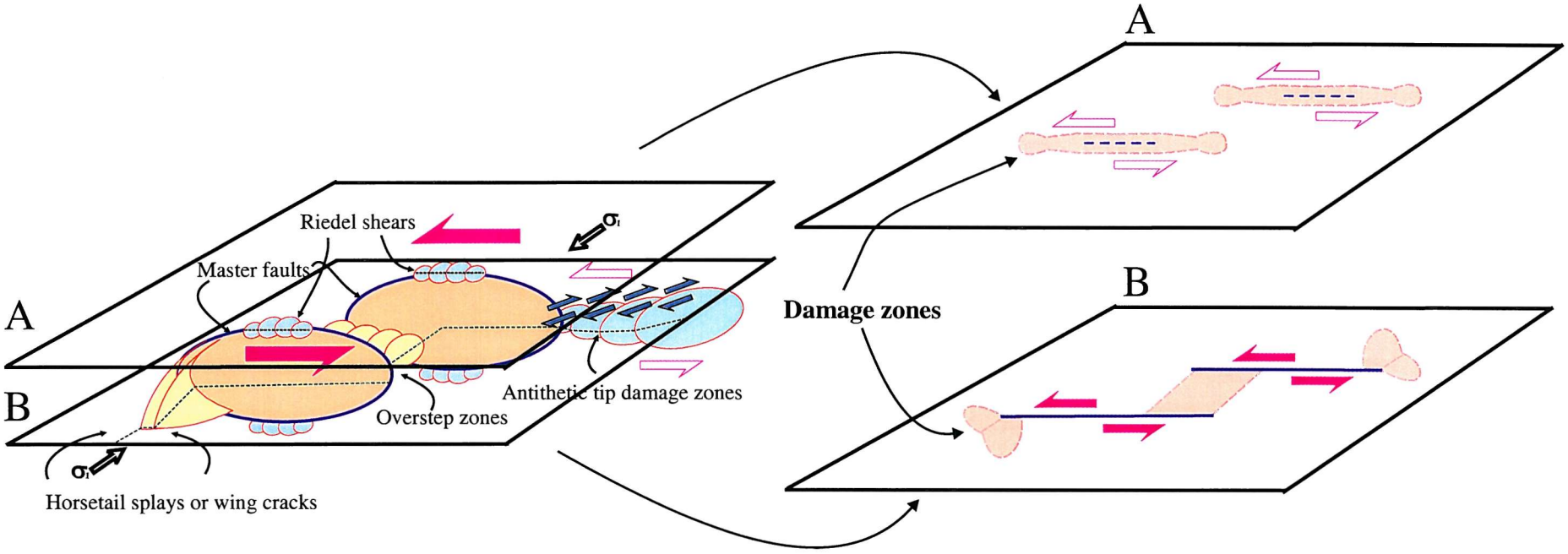

Fig. 6.11. A simple conceptual linked fault model and its damage regions at mode II and III fault tips. The distribution of damage zones is entirely different at the two fault tips. Mode III tip damage zone (A) is in general symmetric while mode II tip damage zone (B) is asymmetric. The three dimentional fault model shows secondary fractures around each fault tips such as Riedel shears, mode I cracks and antithetic fractures.

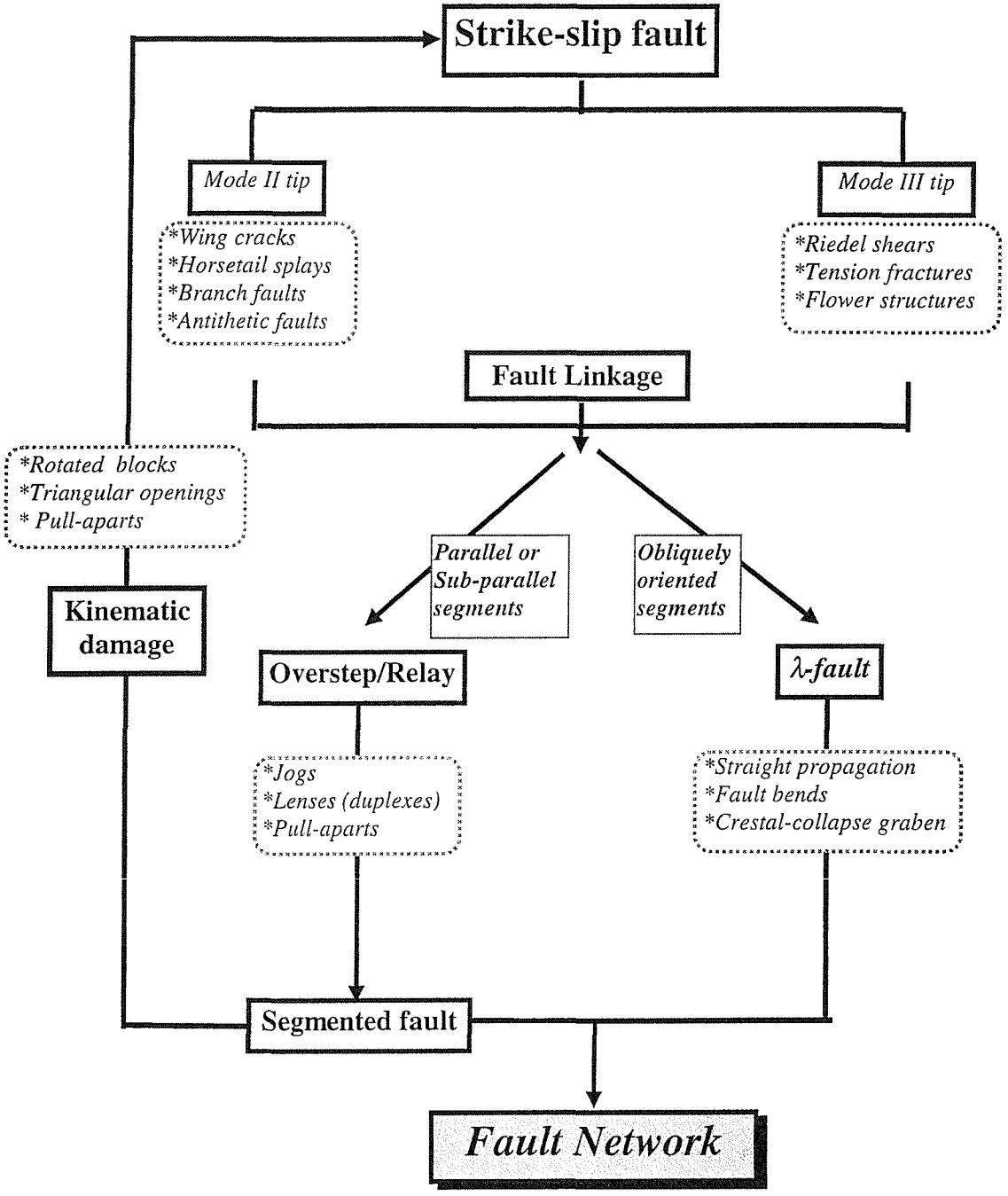

Fig. 6.12. Evolution of fault networks. The diagram shows a flow chart of fault evolution through linkage to fault network. Several damage structures are listed at appropriate stages.

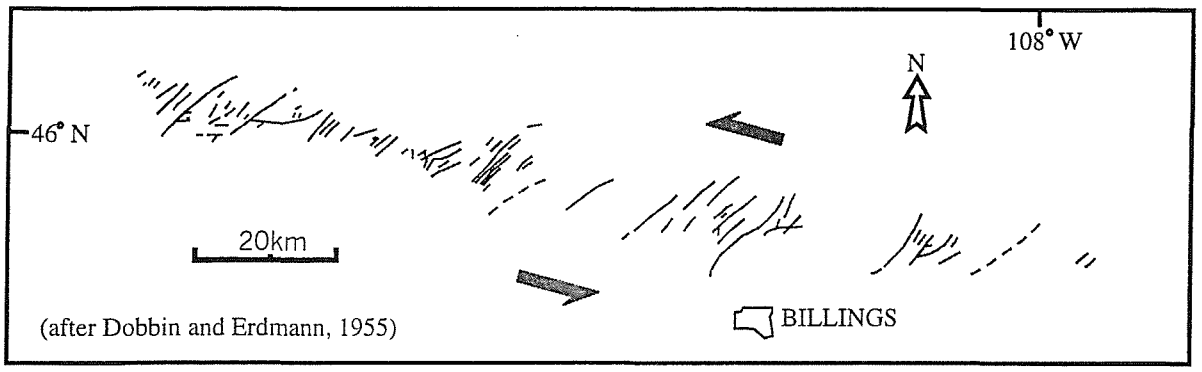

Fig. 6.13. Surface map of Lake Basin fault zone, Montana. Orientations of most en echelon faults correspond with the idealized normal-fault direction for left-lateral strike-slip faulting, but some faults are more nearly transverse and several are less oblique than predicted. This large scale example is similar to the distributed wall zone damage from Gozo, Malta. Modified from Harding *et al.*(1985).

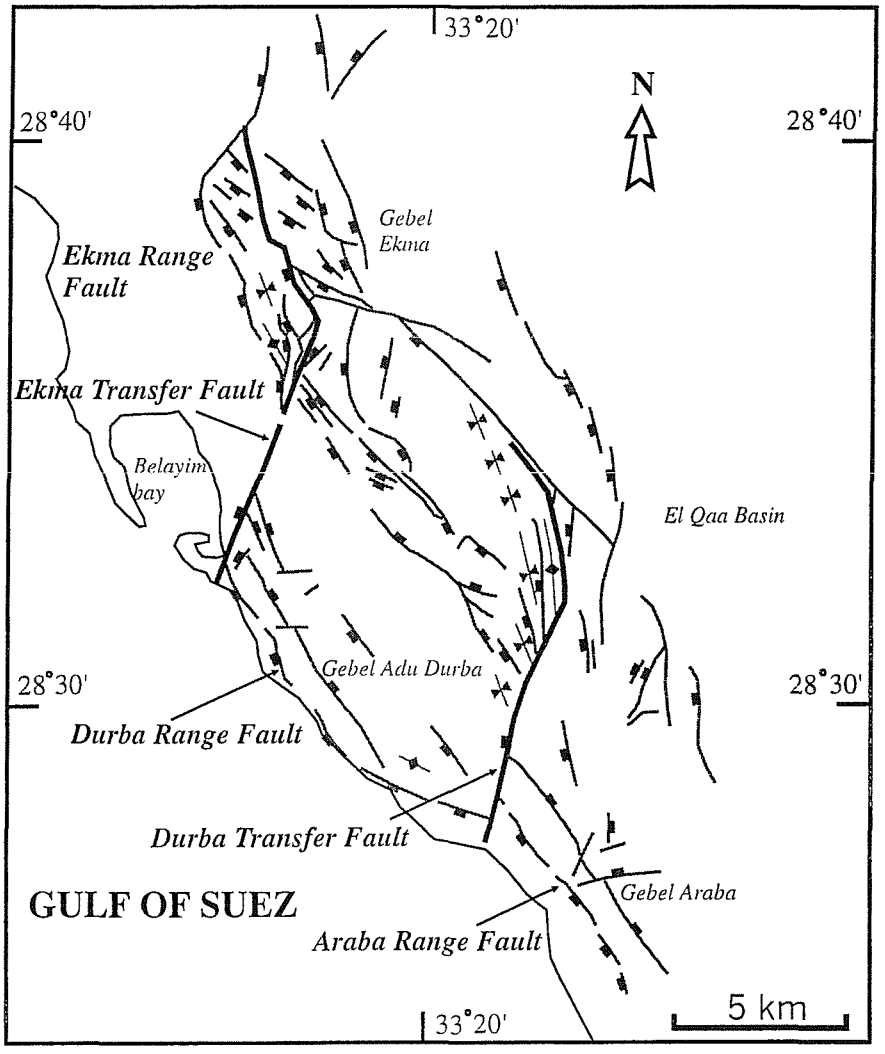

Fig. 6.14. Simplified fault map of the Durba and Ekma transfer faults. This map shows a large scale example of horsetail splays at transfer fault tips. Modified from McClay and Khalil (1998).

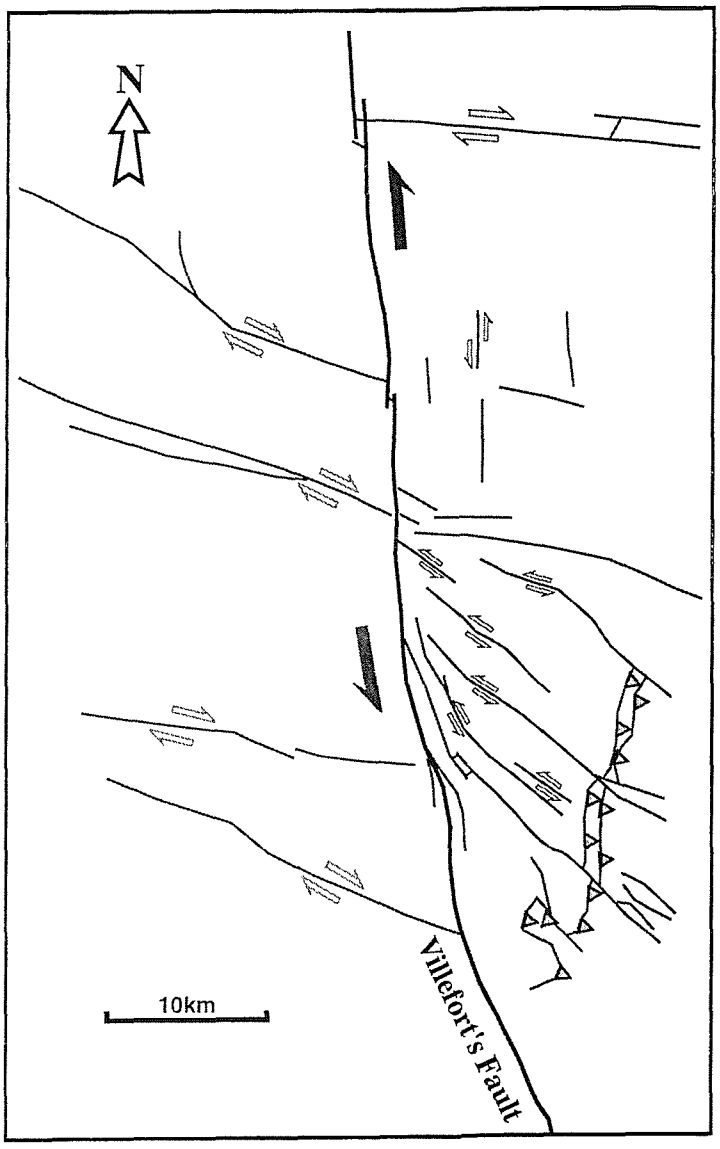

Fig. 6.15. Simplified structutal map of Villefort's region according to Arthaud and Matte (1975). It shows antithetic faults, thrust faults and horsetail splays around a left-lateral strike-slip fault. Modified from Granier (1985).

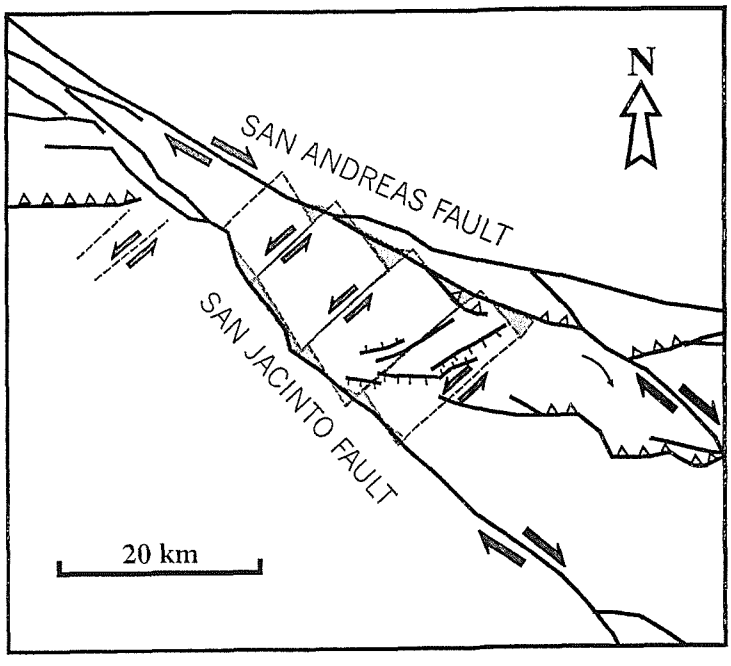

Fig. 6.16. Block model for shear rotation near the intersection of the San Jacinto and San Andreas faults inferred from geology and seismicity (Matti *et al.*, 1985; Nicholson *et al.*, 1986a, 1986b). Two sub-parallel faults make a wedge-shaped block between the two faults. Modified from Nicholson *et al.*, 1986b.

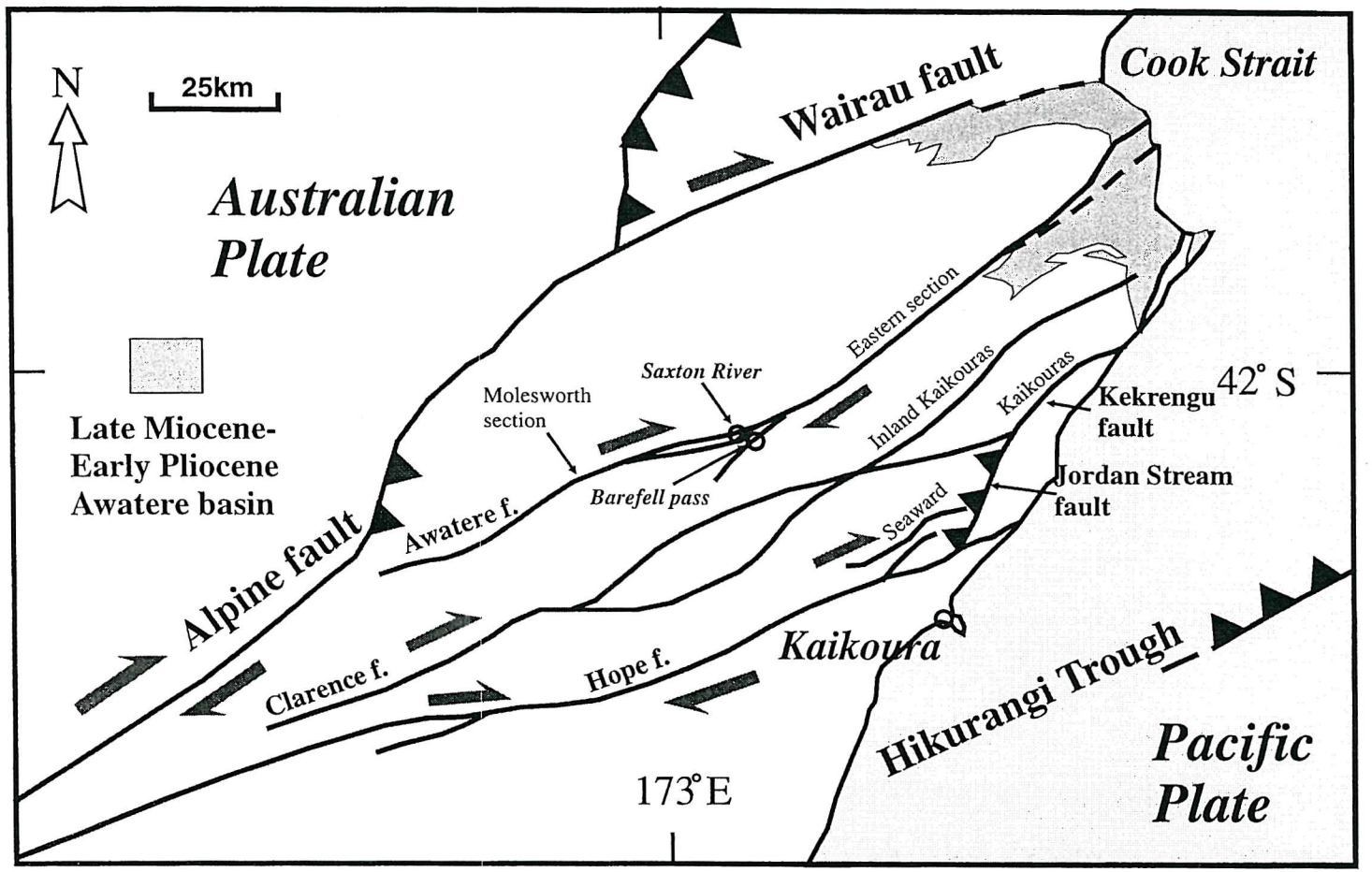

Fig. 6.17. Simplified tectonic map of northeastern South Island, New Zealand showing principal elements of the Marlborough fault system and location of the late Miocene-early Pliocene Awatere basin. It shows a couple of lens-shaped fault geometry pattern. Modified from Little *et al.* (1998).

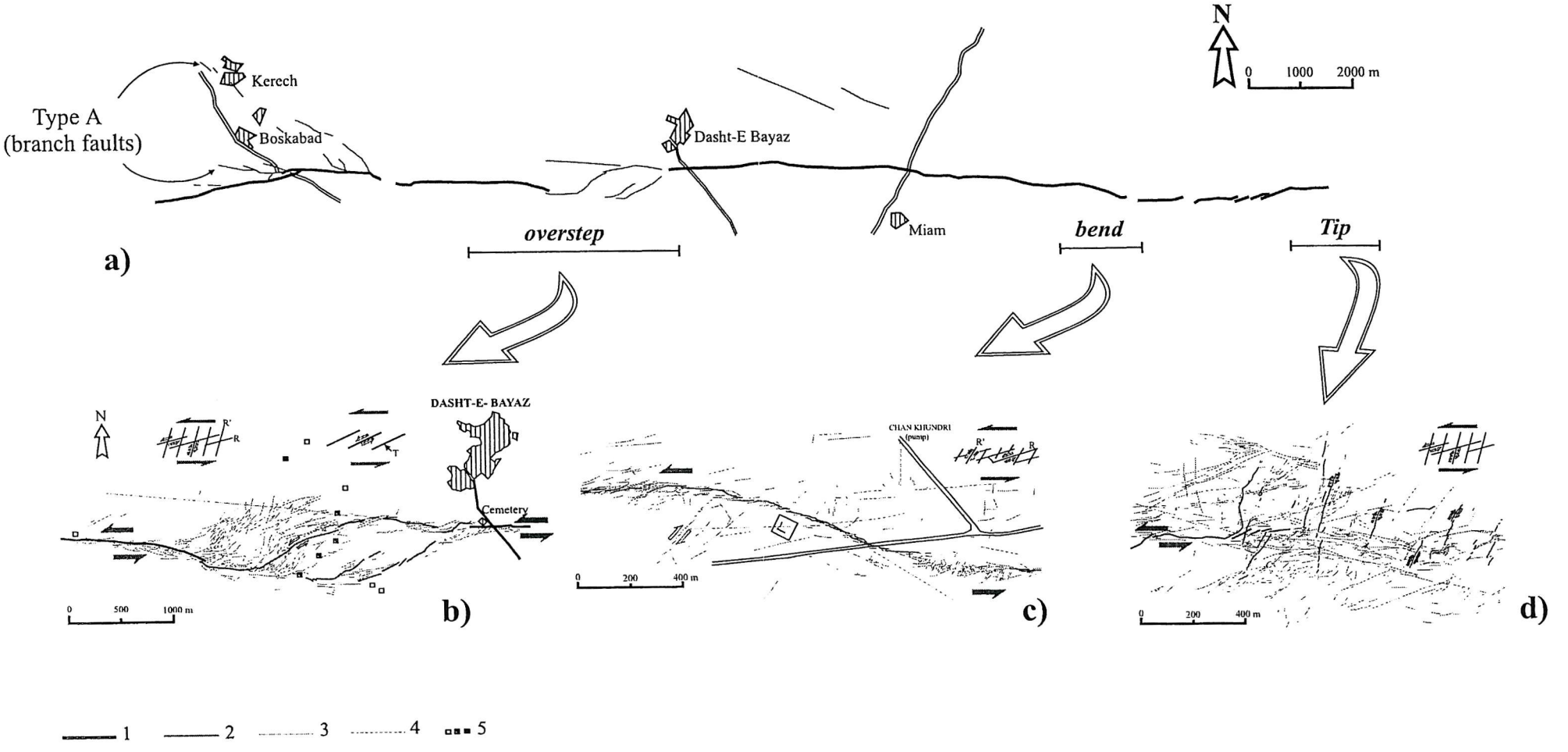

Fig. 6.18. Map and structural analysis of the fault zone in the Nimbluk Valley (modified from Tchalenko and Ambraseys, 1970).
1. Main fault. 2. Fracture showing great amount of relative displacement. 3. Small fracture. 4. Pre-earthquake fault lineament.
5. Isolated mud houses respectively undamaged, damaged, and destroyed.

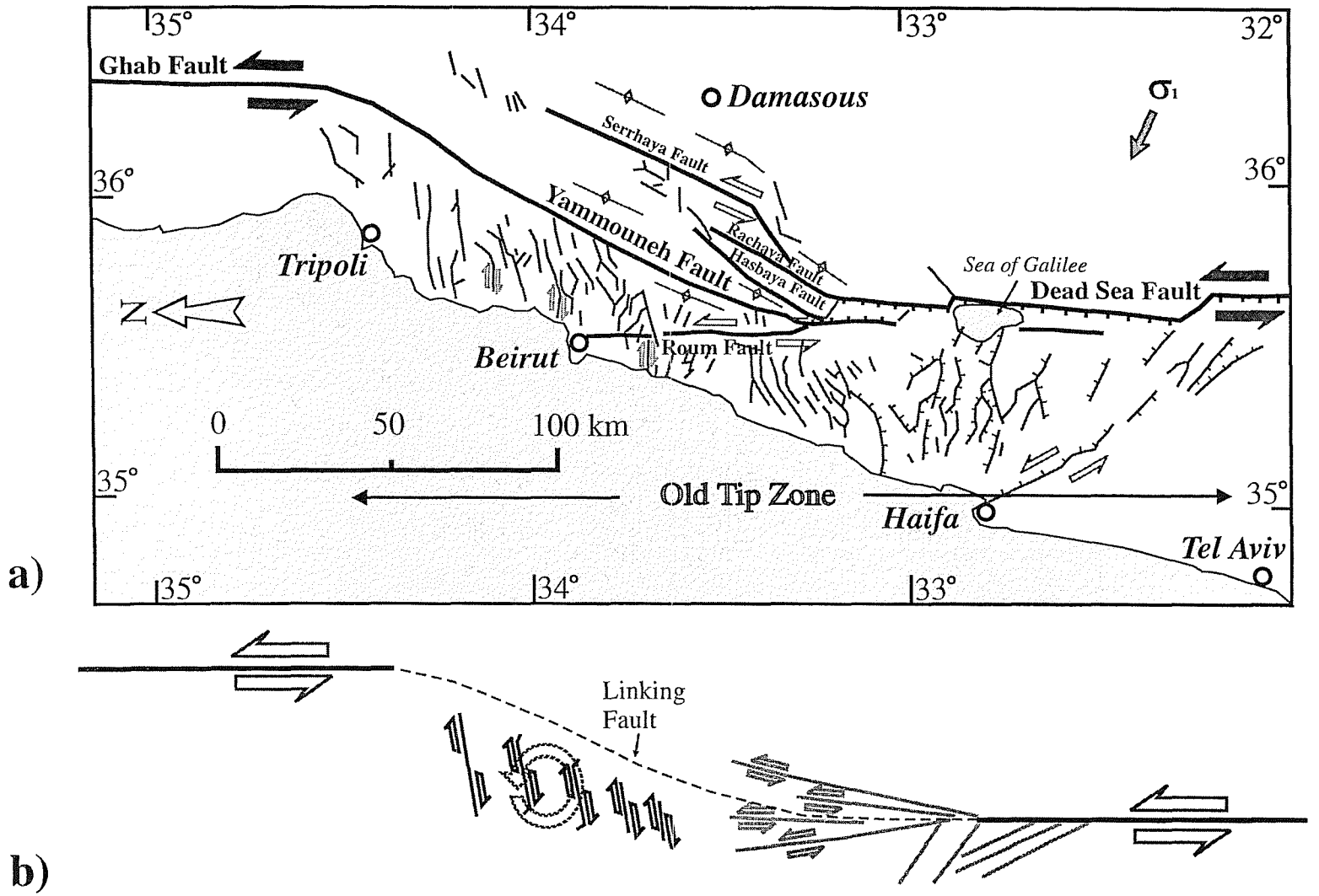

Fig. 6.19. a) Fault pattern of the Galilee and Lebanon. This shows that the fault deformation can be explained by a large left-hand shear along the Dead Sea rift. Modified from Dubertret (1962), Freund *et al.* (1970), Girdler (1990) and Butler *et al.* (1997). b) A simple cartoon showing the linkage of the two old fault tips in the Lebanon region.

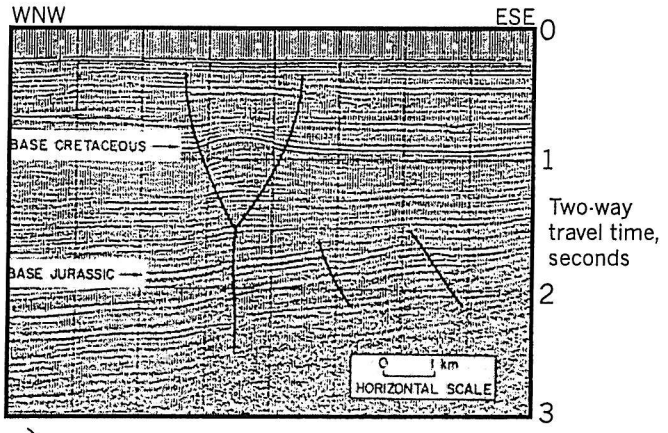

a)

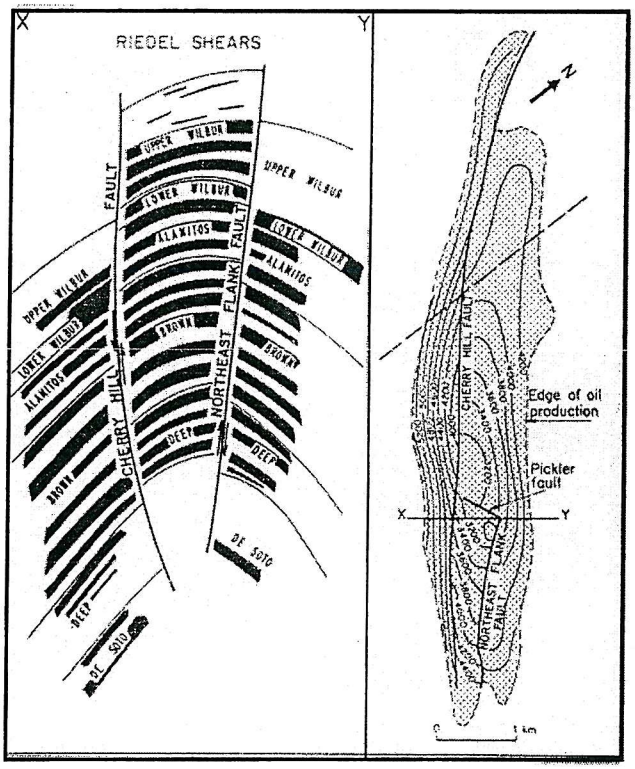

b)

Fig. 6.20. Flower structures showing similar fracture patterns to mode III fault tips in cross sections. a) Seismic line in the Moray Firth, Scotland. b) Long Beach oilfield, California (after Naylor *et al.*, 1986).

CHAPTER 7: SIMILARITIES AND EVOLUTION BETWEEN STRIKE-SLIP FAULTS AT DIFFERENT SCALES

Abstract

Strike-slip faults occur at a wide range of scales. Several strike-slip faults were selected to examine their similarity at different scales. The faults share many similar geometric features over this scale range, and differences in fault style are not related to specific scale ranges. Fractal dimensions are compared for two faults (Gozo and San Andreas) which support the idea of self-similarity. Fractal dimensions for damage zones are higher (D ~ 1.35) than for the main fault traces (D ~ 1.005). Although single event movement in faults typically has u/L (slip / segment length) of ~ 10^{-4}, this can only be established for large faults. Most geologic faults have much higher d_{max}/L (maximum displacement / fault length) of ~ 10^{-2} -10^{-1} (e.g. Gozo ~ 10^{-2} and San Andreas Fault ~ 10^{-1}).

7.1. INTRODUCTION

The aim of this chapter is to examine fault growth and propagation over different scales (e.g. Tchalenko, 1970; Scholz *et al.*, 1993). Limited conclusions have been previously drawn due to insufficient scale range and scattered limited data (Tchalenko, 1970; Cowie and Scholz, 1992b; Dawers *et al.*, 1993; Clark and Cox, 1996; Schlische *et al.*, 1996).

For this study two approaches were carried out; *geological* and *seismological* approaches. (1) *The geological approach* is the study of many examples that are interpreted as part of an evolutionary sequence, and compared at different scales. The study of strike-slip fault damage structures on more than one scale may lead to a better understanding of the general deformation mechanisms involved in strike-slip faults. (2) *The seismological approach* is the study of earthquakes and ground ruptures (single events tend to be at large scale > 1 - 10 km). Okubo and Aki (1987) argued that the detailed seismic fault behaviour, from nucleation of the dynamic instability,

through propagation, to the ultimate arrest of the rupture, is heavily influenced by the complexity of fault geometry. Therefore, the detailed fault geometry is fundamental to an understanding of fault mechanics (Segall and Pollard, 1980).

For selected faults and earthquake ruptures, the maximum displacement (d_{max}) is plotted against fault length (L), or slip (u) against segment length (L), to examine the relationship between slip along earthquake ruptures and cumulative geological displacement.

7.2. COMPARISON OF FAULT GEOMETRIES

Tchalenko (1970) examined the structure of shear zones ranging in size from shear box experiments (~ 10 cm) to that of large tectonic earthquakes (~ 1 km) (Dasht-e Bayaz fault, Iran). Similarities in structural pattern with different magnitudes were interpreted as indicating similarities in the deformation mechanism. In a similar manner, similarities in damage geometry could be interpreted as indicating similarities in the location of damage zone along a fault or the stage of fault evolution (Chapter 4).

The concept of self-similarity is very useful in applying small-scale damage structures to large-scale tectonic interpretation and earthquake hazard prediction. However, there are fundamental differences between several faults with different magnitudes. Some faults in the studied areas will be compared with published examples. The main objective of this chapter is to compare the small-scale examples studied (e.g. Gozo) with larger strike-slip faults (the San Andreas Fault and the North Anatolian Fault), and a detailed study of ground ruptures (e.g. the Dasht-e Bayaz fault, Iran).

7.2.1. Gozo

The M-00 fault in Gozo (Fig. 7.1) shows many of the characteristic features of an overstepping left-lateral strike-slip fault system. The whole fault system is about 40 m in length, and a well-exposed area about 30×15 m^2 has been mapped in detail. Displacement is determined from pre-existed structures such as burrowing trace fossils or veins. The maximum displacement along the fault is ~ 220 mm ($d_{max}/L \approx 6\times10^{-3}$). Most of the main segments (P or PDZ) (Fig. 7.1) are linked through secondary fractures (T), and they can be considered as an transition stage from a soft-linked to a

hard-linked fault system. Though the fault shows two minor contractional oversteps in the eastern part, the segments are mainly linked by dilational left-stepping oversteps. Extensional fractures (mode I) are the predominant fracture pattern at the exposed eastern fault tip.

7.2.2. East Quantoxhead, Somerset

The strike-slip relay ramps at East Quantoxhead, Somerset (Peacock and Sanderson, 1995) show a range of geometries with different amounts of linkage. Several characteristic features are observed around the faults. One of the strike-slip relay ramps developed between two right-lateral strike-slip faults is shown in Figure 7.2.

The mapped faults range from 1 m to 20 m in length. Maximum strike-slip displacement along these mapped faults is about 400 mm ($d_{max}/L \approx 2\times10^{-2}$). The fault zones consist of a series of en echelon segments corresponding to Riedel shears (R) (Peacock and Sanderson, 1995). The relay ramps are developed at contractional oversteps. Veins and antithetic faults occur within the relay ramps at high angles to the fault zones (Fig. 7.2). The antithetic faults (R') are often sigmoidal, indicating rotational strain in the relay ramps, with the sense of rotation consistent with that of the fault zone. Synthetic faults link the en echelon fault segments in several of the zones. These synthetic faults cut and displace the earlier antithetic faults (Fig. 7.2) (Peacock and Sanderson, 1995).

Tension veins (T) are sub-parallel to the final main strike-slip faults with a normal dip slip component. Some of the pull-aparts, filled with vein materials, are composed of two fracture sets (P and R) as seen in Gozo (Chapter 4). It is interpreted that early formed extensional fractures (T) were reactivated as right-lateral strike-slip fault segments (R), and later synthetic faults (P) linked or displaced early formed fractures (R and R') (Fig. 7.2).

7.2.3. Dasht-e Bayaz fault, Iran

Ambraseys and Tchalenko (1969) and Tchalenko and Ambraseys (1970) mapped the Dasht-e Bayaz fault and secondary fractures associated with earthquake ruptures (Fig. 7.3). The earthquake was associated with an east-west, left-lateral fault zone more than 80 km long with some secondary fracturing. The western part of the

fault, over a length of 25 km, crosses Quaternary deposits of the Nimbluk Valley with fractures covering a band 2-3 km wide. The maximum displacement during the single event was ~ 4.5 m left-lateral, and ~ 2.5 m vertical (Ambraseys and Tchalenko, 1969; Tchalenko and Ambraseys, 1970).

The fracture pattern along the fault is well explained by the Riedel shear model (Fig. 7.3) and two- and three-dimensional damage models (Chapter 6). Both Riedel shears (R) and conjugate Riedel shears (R') can be seen, as well as some interconnecting P shears orientated approximately symmetrically to the R shears with respect to the general direction of movement (Fig. 7.3). The relative arrangement of the R, R' and P shears, which constitute the shear zone structure, is seen to be similar at other magnitudes (Tchalenko, 1970; Chapter 6). Detailed maps (Fig. 7.3b - 7.3d) show minor fracture patterns following the Riedel shear model. Figure 7.3b shows a dilational overstep zone being linked by T fractures. A similar fracture pattern is shown in fault M-00, Gozo (Fig. 7. 1). Figure 7.3c shows a contractional bend with R and R' shears. A similar bending structure is shown in Figure 7.2 with a much simpler damage pattern. Figure 7.3d is a fault tip and shows a characteristic pattern composed of P - R - R' shears. It is a predominant mode II tip damage pattern with antithetic shear fractures (R'). Several similar fracture patterns were shown in Chapter 4. The strong similarity between the structures at different scales is evident, so that small-scale structures often provide the best available evidence of the large-scale deformation mechanism.

Tchalenko (1970) described "Riedel within Riedel" structure, in which larger Riedel shears are formed from similar Riedels on a smaller scale. This Riedel shear pattern is well documented in Gozo as a series of ascending fracture orders (Chapter 4) repeating with similar patterns between lower and higher order structures. As a parallel concept, damage structure could contain within it similar damage patterns on smaller (or larger) scales. However, damage patterns are also strongly dependent on locations along the main fault and tip modes (Chapter 4).

The detailed maps of the Dasht-e Bayaz fault zone (Fig. 7.3) (Ambraseys and Tchalenko, 1969; Tchalenko and Ambraseys, 1970) indicate that the fault zone is composed of several underlapping ruptures rather than a hard-linked fault system. Therefore this fault zone is considered as non-coherent soft-linkage (Fossen and Hesthammer, 1997) with a relatively low displacement. Also, most of the faults here

are formed by a single slip event, and the displacement might be relatively low ($d_{max}/L \approx 2\times10^{-4}$) when compared with other geological fault systems.

7.2.4. North Anatolian fault

The North Anatolian fault (NAF) (Fig. 7.4) is the most prominent active fault in Turkey and has been the source of numerous large earthquakes throughout its history. The NAF is about 1500 km in length (Barka and Kadinsky-Cade, 1988; Armijo *et al.*, 1999), and the total displacement over the past 5 m.y. is about 85 km (Sengor *et al.*, 1985; Armijo *et al.*, 1999). The fault is right-lateral and shows a typical right-stepping segmentation (P or PDZ - T style) (Neugebauer, 1995) with splay faults at the western fault tip (Fig. 7.4). One of the main branch faults terminates 100 km east of Ankara. Other branch faults are developed around the Marmara Sea, where the main NAF zone splays into three strands (type A of Chinnery, 1966) to the west of about 30.5°E (Barka and Kadinsky-Cade, 1988; Armijo *et al.*, 1999). Several similar structural patterns have been described from in Gozo (Chapter 4) and Rame Head (Chapter 5).

Several researchers consider the Marmara Sea region as a graben structure (i.e. Crampin and Evans, 1986). To explain the structure of the northern strand of the NAF zone in the Marmara Sea, Barka and Kadinsky-Cade (1988) and Wong *et al.* (1995) develop similar models that consider right-stepping en echelon strike-slip segments giving rise to small open basins and blocks as pull-apart structures.

The curved fault pattern of the NAF is very similar to the fault pattern observed around the India-Asia collision zone (Molnar and Tapponnier, 1975; Sengor *et al.*, 1985). The curved fault pattern with branch faults propagating toward the south-west is interpreted as resulting from the lateral tectonic escape of a collision zone between Arabian platform and Asia around Turkey. A similar fault pattern is also observed at a smaller scale at Crackington Haven (Kim *et al.*, 2000; Chapter 2).

7.2.5. San Andreas fault

The right-lateral San Andreas fault (SAF) (Fig. 7.5) represents perhaps the most studied major fault zone in the world. The SAF is about 1000 ~ 1200 km in length (Hill, 1981; Schulz and Wallace, 1997; SCEC, 2000). The cumulative offset of the SAF since late Oligocene or early Miocene is 300 ~ 330 km (Crowell, 1979; Keller *et*

al., 1982; Christie-Blick and Biddle, 1985; Stanley, 1987; Revenaugh and Reasoner, 1997).

The Pacific Plate moves north-westward relative to the North American Plate, causing earthquakes along the fault. The SAF is the "master" fault of an intricate fault network that cuts through rocks of the California coastal region (Schulz and Wallace, 1997). Many smaller faults branch from and join the San Andreas Fault zone (Jennings, 1994). The SAF forms a continuous narrow break that extends from northern California southward to gulf of California (Fig. 7.5). South-eastward from Cajon Pass are several branching faults, including the San Jacinto and Banning faults. The SAF shows branch style at both ends (P or PDZ - R), and especially around the southern part of the fault a rotated block model (Chapter 4; Nicholson, *et al.*, 1986) is suggested near the intersection of the San Jacinto fault and the SAF (Chapter 6). The Garlock fault showing antithetic (left-lateral) slip sense is interpreted as a conjugate fault set or a rotated R' shear fault. In central California the northern part of the SAF splays out with several branch faults including the Calaveras fault, although it is difficult to talk about 'tips', because the SAF is a plate boundary and links to other structures.

7.2.6. Similarity in fault patterns

Left-stepping of major fault segments is consistent along the left-lateral faults at Gozo (Fig. 7.1), Dasht-e Bayaz, Iran (Fig. 7.3) and Garlock, California (Fig. 7.5) regardless of scale, whereas right-stepping is predominant along the right-lateral North Anatolian fault, Turkey (Fig. 7.4). Therefore, fault linkage is dominated by dilational oversteps rather than contractional oversteps (Chapter 3), suggesting a possible relationship (Aydin and Nur, 1985) between the stepping of the fault trace and the slip sense. The small scale overstep segment pattern is very similar to the large scale overstep pattern. However, this tendency is not consistent for all fault systems, but it depends on moreover local tectonic settings and pre-existing structures (e.g. Bilham and Williams, 1985).

The fault M-00 in Gozo (Fig. 7.1) shows a relatively simple set of left-stepping, left-lateral segments linked by dilational jogs. The segment faults can be considered as P shears or PDZ (principal displacement zones), and the fault system shows a P (or PDZ) - T combination style. The East Quantoxhead fault (Fig. 7.2) shows T fractures

reactivated as R shears, and P shear fractures and some later R' shear fractures. The Dasht-e Bayaz fault (Fig. 7.3) has a P-T combination style in dilational oversteps, P-R-R' style in tip regions, and an R - R' style is predominant in other small fracture patterns.

Although the NAF (Fig. 7.4) and the SAF (Fig. 7.5) have large-scale, more complicated patterns depending on local tectonic settings, the NAF has a predominant P (or PDZ) -T style due to right-lateral right-stepping, and the SAF has a predominant P (or PDZ) -R - R' (Keller *et al.*, 1982) style with several branch faults (R?) and fault bends (P?). Therefore, a variety of fault patterns exist at various scales. They can be classified in terms of their main fault geometry, slip sense and secondary fault pattern. Dominant fault patterns are branch faults (P or PDZ - R), antithetic faults (P or PDZ - R'), and tensional fractures (P or PDZ - T) (Fig. 7.6), but they are not confined to a specific scale range.

The wide range of geometries involving differing components of R-R'-P-T type are present at all scales. It supports the general similarity of fault and fracture patterns over a large range of magnitudes (Tchalenko, 1970), but it is recognised that differences in style may occur in different tectonic settings (e.g. dilational/contractional relays or wall/linkage/tip zones).

7.3. FRACTAL ANALYSIS

When considering the structural similarities of faults, it may also be useful to treat the complexity of fault geometry using fractal concepts. In fractal analysis, a set that exhibits irregularity regardless of the scale can be characterised by a fractal dimension (D). Mandelbrot (1982) realised that fractal geometry has a great potential for characterising the geometry of complex shapes resulting from many natural physical processes. The fractal dimension can be determined in a number of ways, and once determined, provides a quantitative means of characterising the fractal nature of that set. An essential feature of all fractal geometric forms is the persistence of similar complexity in all scales.

Fractal geometry allows a quantitative description of complex fault patterns. The complexity (or irregularity) of a line may be measured by the *ruler method*, for example Aviles *et al.* (1987) use this method for the main trace of the SAF. Okubo and Aki (1987), on the other hand, describe the irregularity of faults along the SAF by

the *circle method* and attribute the resulting fractal dimension to the irregularity, segmentation and damage development along the fault.

The fractal dimension depends on the methods used, the different selection of cut-offs, the different manner of defining the relevant fault traces (Okubo and Aki, 1987), and the selected fault geometry (Zhang *et al.*, 1991; Okubo and Aki, 1987).

In this section the fault zone at Gozo will be analysed by both the ruler and circle methods and compared with similar results obtained for the SAF.

7.3.1. Ruler method

The ruler method uses dividers with an opening (or ruler of length), ε, which is stepped along a continuous curve (Fig. 7.7a). The number of steps (n) multiplied by the ruler length (ε) gives the total measured length $L(\varepsilon) = n\varepsilon$. As ε becomes small, $L(\varepsilon)$ increases, indicating there is no well-defined or true length. The relationship of the divider size ε to the measured length $L(\varepsilon)$ is given by

$$\log L(\varepsilon) = \log F + (1-D)\log\varepsilon \qquad (1)$$

Where D is the fractal dimension which must lie between 1 (a line) and 2 (an area filling fractal curve), and F is a constant.

7.3.2. Circle method

The circle method (Mandelbrot, 1982; Okubo and Aki, 1987; Chapter 4) is used to measure the complexity of a fault system, including secondary fractures. The method has already been explained in Chapter 4 and involves covering all the faults and fractures within the selected zone with circles of decreasing size (Fig. 7.7b). The number of circles required (N) is related to circle radius (r) by:

$$N \propto r^{-D} \qquad (2)$$

Fault M-00 in Gozo was analysed on a computer screen using a zooming technique, so that the errors through small length (or radius) rulers (or circles) could be minimised.

7.3.3. Results

Figure 7.7 illustrates the application of these methods to fault M-00 at Gozo. The ruler method has been applied to the two main fault traces (A and B, Fig. 7.7a)

and the circle method to all the faults and fractures in the area (Fig. 7.7b). For the irregularity of the main fault trace (ruler method), the fractal dimensions (D_r) are 1.008 (trace A) and 1.010 (trace B) (Figs. 7.7 and 7.8). For all faults and fractures around the main fault (circle method), the fractal dimension is 1.37 (D_c) (Table 8.1; Figs. 7.7 and 7.8; Chapter 4). The results are listed in Table 8.1 and compared with similar analysis of SAF data (Fig. 7.9).

For the ruler method, the fractal dimension for the Gozo fault (D_r = 1.008 and 1.010) is higher than that of the San Andreas Fault (D_r = 1.002). This means that the fault trace of the SAF is less complex and less irregular (more linear) than the Gozo fault. The circle method indicates that the fault systems of both the SAF and Gozo fault have D ≈ 1.35, considerably higher than the dimension of the main fault trace.

The fractal dimension from ruler method examines only the irregularity of the main fault trace representing as a single continuous curve, which is very low. The fractal dimension by circle method includes branches, and various minor fault systems, and is relatively high (Table 8.1).

The fractal dimension by the circle method also depends strongly on the sampling location along the fault, because the value is influenced by damage zones, secondary faults or fractures as well as fault trace irregularity itself. The fault complexity and fault trace irregularity may result mainly from oversteps between en echelon segment faults (Chapter 4). La Pointe (1988) argues that the fractal dimension is most sensitive to the number of fractures or blocks, rather than their size, orientation or size variability.

7.3.4 Conclusions

The SAF and Gozo have similar fractal structure at very different scales; i.e. the complexity is similar at different scales. Both faults consist of a 'main trace' embedded in a system of 'damage'. The main fault traces of both strike-slip faults have a low dimension (D <1.02), with some indication of a nearly linear fault trace (D <1.002) for the SAF. This may suggest a smoothing of fault traces as displacement increases.

Table 8.1. Results of fractal analysis for the Gozo and the San Andreas faults.

	Gozo Fault	**San Andreas Fault**	Reference
Circle Method(D_c)	**1.37**	**1.31**	Okubo & Aki, 1987
Ruler Method(D_r)	**A = 1.008** **B = 1.010**	**1.002**	Aviles *et al.*, 1987
d_{max}/L	**~ 0.006**	**~ 0.27**	
Scale	**~ 40 m**	**~ 1200 km**	
Type	P (or PDZ) + T	P + R + R' => PDZ	

7.4. MAXIMUM DISPLACEMENT (d_{max}) AND FAULT LENGTH (L) RELATIONSHIP BETWEEN FAULTS OF DIFFERENT MAGNITUDES

The ratios of maximum displacement / fault length (d_{max}/L) for some selected faults with different magnitudes of displacement are compared. To compare the structural properties of strike-slip faults with different magnitudes, faults from Crackington Haven (Chapter 2; Kim *et al.*, 2000), the fault M-00 in Gozo (Chapter 4) and faults from Rame Head (Chapter 5) are compared with other published examples, such as faults from Gipsy Point and Raeberry (Peacock, 1991), Kilve (Kelly *et al.*, 1998), Dasht-e Bayaz, Iran (Ambraseys and Tchalenko, 1969; Tchalenko and Ambraseys, 1970), the North Anatolian fault, Turkey (Barka and Kadinsky-Cade, 1988; Neugebauer, 1995; Stein *et al.*, 1997; Armijo *et al.*, 1999), and the San Andreas fault, California (Karig and Jensky, 1972; Keller *et al.*, 1982; Working Group on California Earthquake Probabilities, 1995; Zachariasen and Sieh, 1995). These data are plotted on a graph (Fig. 7.10) to compare the influence of magnitudes and slip events. Most of them consist of several interacting segment faults.

The general expression of the relationship between the maximum displacement on a fault (d_{max}) and the fault length (L) is given as;

$$d_{max} = cL^n , \qquad (3)$$

where the value of c is dependent on rock properties (including shear modulus) (Cowie and Scholz, 1992a, 1992b; Gillespie *et al.*, 1992). The range of the exponent value, n, is variable from 0.5 to 2 (Watterson, 1986; Walsh and Watterson, 1988; Marrett and Allmendinger, 1991; Gillespie *et al.*, 1992; Cowie and Scholz, 1992a, 1992b; Dawers *et al.*, 1993; Scholz *et al.*, 1993; Clark and Cox, 1996; Schlische *et al.*, 1996; Fossen and Hesthammer, 1997). The value of the exponent, n, is important as $n = 1$ is consistent with self-similarity.

Small isolated faults (0.2 - 2 m in length) from Crackington Haven have relatively low displacement of $d_{max}/L \approx 10^{-2}$ -10^{-3} , but other interacting small-scale faults (1 - 100 m in length) plot between 10^{-1} and 10^{-2}. The Gozo fault shows a relatively low ratio of $d_{max}/L \approx 6\times10^{-3}$, although each segment shows slightly higher ratios of $d_{max}/L \approx 10^{-1}$ -10^{-2} (Fig. 7.10).

Several ruptures from several km to several hundreds km, associated with earthquakes (m > 6), are plotted in Figure 7.10. They include single slips from the Dasht-e Bayaz fault (Ambraseys and Tchalenko, 1969; Tchalenko and Ambraseys, 1970), the Landers earthquake (Zachariasen and Sieh, 1995), the Owens Valley Independence segment (DePolo *et al.*, 1991) and the North Anatolian Fault (Stein *et al.*, 1997). They show displacements of 1 ~10 m and very low $u/L \sim 10^{-4}$.

The NAF (Fig. 7.4) and the SAF (Fig. 7.5), have relatively high fault lengths and maximum displacements; $d_{max}/L \approx 10^{-1}$. This indicates that larger faults have relatively larger displacements, as already recognised by other works (e.g. Walsh and Watterson, 1988; Cowie and Scholz, 1992b; Clark and Cox, 1996). This does not necessarily mean $n > 1$, but may suggest no single linear relationship is consistent for all combining data sets in different material properties and tectonic settings (Cowie and Scholz, 1992b; Clark and Cox, 1996). Although the SAF has similar fault length (L ~1200 km, Hill, 1981; Schulz and Wallace, 1997; SCEC, 2000) to the NAF ($L \sim$ 1500 km, Barka and Kadinsky-Cade, 1988; Armijo *et al.*, 1999), it has much larger maximum displacement ($d_{max} \sim$ 320 km, Crowell, 1979; Keller *et al.*, 1982; Christie-Blick and Biddle, 1985; Stanley, 1987; Revenaugh and Reasoner, 1997) compared with that ($d_{max} \sim$ 85 km, Sengor *et al.*, 1985; Armijo *et al.*, 1999) of the NAF (Fig. 7.10). Therefore, the ratio of d_{max}/L for the SAF ($d_{max}/L \sim 0.27$) is much higher than that of the NAF ($d_{max}/L \sim 0.06$) (Fig. 7.10). This might result from the relative age of

the faults and/or differing slip rates (Keller *et al.*, 1982; Stanley, 1987; Barka and Kadinsky-Cade, 1988; Working Group on California Earthquake Probabilities, 1995; Revenaugh and Reasoner, 1997; Armijo *et al.*, 1999). Another factor influencing these values might be underestimation of the fault length of the SAF, which extends offshore to the north. However, the general relationship between fault length and maximum displacement for strike-slip faults shows slightly increasing ratio of d_{max}/L in larger magnitude faults. Although it is difficult to confine the relationship of d_{max}/L with limited data, the two alternatives are $2 >> n > 1$ or varieties in d_{max}/L due to result from different material properties and tectonic settings at different scales.

Several incremental slip data for the SAF (e.g. the Landers earthquake, the Owens Valley earthquake) and the NAF are plotted on Figure 7.10. This shows the difference between single earthquake slip (incremental) and cumulative displacement. Single slips have $d_{max}(u)/L \sim 10^{-4}$, whereas small faults have $d_{max}/L \sim 10^{-2}$ (Crackington Haven & Gozo) and large faults have $d_{max}/L \sim 10^{-1}$ (SAF & NAF). These values are within the range of the suggested ratios (Rikitake, 1975; Walsh and Watterson, 1988; Sibson, 1989) for seismic slip and finite displacement.

For earthquake ruptures, the ratio between maximum seismic slip, u, and the rupture length, L, generally lies in the range of $10^{-4} > u/L > 10^{-5}$ (Rikitake, 1975; Sibson, 1989). The ratio of maximum finite displacement, d_{max}, to total fault length, L_f, tends to increase as a fault matures (Walsh and Watterson, 1988) and may eventually reach values, $d_{max}/L_f \sim 10^{-1}$ (Sibson, 1989), as for the SAF and the NAF.

The general expression of the relationship between the cumulative maximum displacement on a fault (d_{max}) and the maximum slip along a rupture for an event (u) is given as;

$$d_{max} \cong \sum u \tag{4}$$

If we consider earthquakes larger than a given moment magnitude (m), the original Gutenberg-Richter distribution is given by

$$N(m) = 10^{a-b \cdot m}, \tag{5}$$

where $N(m)$ is the annual number of earthquakes with magnitude equal to or greater than m, a is the seismicity rate, and b is assumed as unity in most regions (Woking Group on California earthquake Probabilities, 1995). Therefore, earthquakes generally become about 10 times more frequent for every unit decrease in magnitude. From this relationship, the recurrence interval, $I(m)$, of each event larger than any magnitude m

is given as;

$$I(m) = 1/N(m) = 10^{-(a-b \cdot m)} \quad (6)$$

If we know the recurrence interval, $I(m)$, of any particular magnitude (m), we can estimate the age (T) of a fault. If we suppose the same slip for each event during fault growth, the age of the fault is given by

$$T = n(m) \cdot I(m) = n(m)/N(m), \quad (7)$$

where $n(m)$ is the total number of slip events. The value of $n(m)$ can be obtain from the cumulative displacement and slip along an earthquake segment (Fig. 7.10) for a specific fault. However, u increases as fault length (L) increases with a linear relationship (Scholz, 1982; Watterson, 1986), and the recurrence interval, $I(m)$, may also increase with increasing earthquake magnitude (m). However, the annual number of earthquake greater than magnitude m, $N(m)$, decreases as magnitude increases. Sibson (1989) has suggested some structural characteristics and relative frequency of earthquake ruptures of different sizes. He argues that slip and fault length increase and relative frequency decreases as magnitude increases. The relation is given as;

$$u \propto L \cdot \log I(m) / \log N(m), \quad (8)$$

therefore the number of slip events for a specific magnitude is given approximately as;

$$n(m) \cong d_{max} / u, \quad (9)$$

where d_{max} is cumulative maximum displacement and $n(m)$ is obtained from equation (9). It is ~ 3×10^4 for the SAF and the NAF (Fig. 7.10). It means that the SAF and the NAF have activated at least 3×10^4 times, because the number of events is calculated from the recent large magnitude and length of earthquake ruptures. Therefore, the age of fault is given from equation (7) and (9) as,

$$T = d_{max} / u \cdot I(m) \quad (10)$$

The recurrence interval of the NAF for magnitude $m > 6.7$ is range of ~ 450 ±220 yr. (Stein *et al.*, 1997), so that the calculated age of the NAF is 13.5 ± 7 Ma. It is slightly older than the age (13 ~ 4 Ma) proposed by Sengor *et al.* (1985) and Barka and Kadinsky-Cade (1988). This might result from magnitude and slip differences during fault growth. The recurrence interval of the SAF (e.g. Elsinore Fault) for magnitude $m > 7$ is ~ 400 ± 200 yr. (Working Group on California Earthquake Probabilities, 1995), so that the calculated age of the SAF is 12 ± 6 Ma. It is slightly younger than the timing of formation of the transform fault boundary (20 - 30 Ma). However, it is older

than the beginning of separation of Baja California from mainland Mexico at about 5 Ma (Working Group on California Earthquake Probabilities, 1995). However, the calculated age is well matched by the estimated fault age of 12 Ma by Keller *et al.*, (1982).

The values of the ratio of d_{max}/L for the faults and earthquake ruptures (Fig. 7.10) show a variety of distributions. However, there is a tendency for larger faults to have larger maximum displacements, and for hard-linked faults also to have larger maximum displacements than soft-linked faults (thin arrows in Fig. 7.10). Also, most of earthquake rupture slips have very low u/L ratios (~ 10^{-4}) (Rikitake, 1975; Sibson, 1989). If this ratio is assumed for small faults, an inferred similar growth slope to the SAF and the NAF can be drawn for the Gozo fault. From this estimate the relationship between number of events (n) and rupture slip (u) for the Gozo fault is $n \times u = 200$ (d_{max}): e.g. it is 200 ruptures with 1 mm single slip, if about 10 m rupture is considered for the fault (Fig. 7.10).

Schlische *et al.* (1996) argued for a very consistent linear relationship between maximum displacement and fault length using global data, although they accepted that there is a change of the value of c in the equation (3) between small faults and larger faults. Cowie and Scholz (1992b) also plot several data sets from other works and show that there is a non-linear relationship between d_{max} and L with $n = 1$. They recognised the ratio of d_{max}/L as a critical shear strain for fault propagation, and argued that this ratio determines the magnitude of the finite stress concentration at the ends of the faults. For an actively growing fault, this must be just equal to the shear strength of the surrounding rock, σ_0. If a fault grows in a rock with constant stress drop, σ_0, then d_{max}/L must be constant. A non-linear relationship between d_{max} and L implies that σ_0 varies systematically with fault size. On the other hand, the ratio is dependent on the ratio of two material properties (Cowie and Scholz, 1992a, 1992b), and it should be expected to vary between data sets. From the combined data sets (Cowie and Scholz, 1992b) faults with lengths of 1 km or more appear to have systematically higher values of the ratio d_{max}/L than shorter faults, although individual data sets have a near linear relationship (Dawers *et al.*, 1993; Clark and Cox, 1996). They suggested that there might be a cross-over phenomenon between large faults that cut through the entire thickness of the brittle upper crust and small faults that do not. The suggested reasons for this phenomenon are that larger faults are two-dimensional, being only

constrained at their ends, whereas small faults are three-dimensional and are pinned along their entire perimeter, or simply that large faults rupture stronger rock on average (Cowie and Scholz, 1992b).

Slip along a fault may also vary as a result of lithologic variations (Bürgmann *et al.*, 1994), interaction with nearby structures (Willemse *et al.*, 1996), and irregular fault geometries (Schultz and Aydin, 1990). Heterogeneous loading of the fault, heterogeneous properties of surrounding material, non-planar fault segments, fault segments linkage (Bürgmann *et al.*, 1994), the distribution of friction coefficient (Cooke, 1997), and localisation with increasing magnitudes of faults will all influence fault displacement.

7.5. CONCLUSIONS

1. Strike-slip faults have been examined over a wide range of scales. e.g. Crackington Haven ~ 2×10^0m; Gozo ~ 4×10^1 m; Rame Head ~ 1×10^2; San Andreas Fault ~ 1.2×10^6 m.
2. They share many similar geometric features over this scale range. Differences in styles (e.g. R-P; P-T; T-PDZ) are not confined to specific scale ranges.
3. Fractal analysis supports the idea of self-similarity. Damage zones have higher fractal dimensions (Dc ~ 1.35), whereas the main fault traces have lower fractal dimensions (Dr ~ 1.005). The main fault trace of the SAF is more linear ($Dr \approx$ 1.002) than that at Gozo ($Dr \approx 1.01$) which is consistent with higher displacements leading to smooth fault surfaces.
4. Although single slip events in faults typically have $d_{max}/L \sim 10^{-4}$ (this can only be established for large faults), most geologic faults have much higher $d_{max}/L \sim 10^{-2}$ - 10^{-1} (e.g. Gozo ~ 10^{-2} and SAF ~ 10^{-1}). From the relationship between cumulative maximum displacement and earthquake rupture slip of fault zone evolution, the approximate ages of faults can be determined.

REFERENCES

Ambraseys, N. N. and Tchalenko, J. S. 1969. The Dasht-e Bayaz (Iran) earthquake of August 31, 1968: A field report. *Bulletin of the Seismological Society of America* **59**, 1751-1792.

Armijo, R., Meyer, B. Hubert, A. and Barka, A. 1999. Westward propagation of the North Anatolian fault into the northern Agean: Timing and kinematics. *Geology* **27**, 267-270.

Aviles, C. A., Scholz, C. H., Boatwright, J. 1987, Fractal Analysis Applied to Characteristic Segments of the San Andreas Fault. *J. geophys. Res.* **92**, 331-344.

Aydin, A. and Nur, A. 1985. The types and role of stepovers in strike-slip tectonics. In *Strike-slip Deformation, Basin Formation, and Sedimentation*: eds: Biddle, K. T. and Christie-Blick, N. *Society of Economic Paleontologists and Mineralogists Special Publication*, **37**, 35-44.

Barka, A. A. and Kadinsky-Cade, K. 1988. Strike-slip fault geometry in Turkey and its influence on earthquake activity. *Tectonics* **7**, 663-684.

Bilham, R., and Williams, P. 1985. Sawtooth segmentation and deformation processes on the southern San Andreas Fault, California. *Geophys. Res. Lett.* **12**, 557-560.

Bürgmann, R., Pollard, D. D. and Martel, S. J. 1994. Slip distributions on faults: effects of stress gradients, inelastic deformation, heterogeneous host-rock stiffness, and fault interaction. . *Journal of Structural Geology* **16**, 1675-1690.

Chinnery, M. A. 1966. Secondary faulting: II. Geological aspects. *Canadian Journal of earth Sciences* **3**, 175-190.

Christie-Blick, N. and Biddle, K. T. 1985. Deformation and basin formation along strike-slip faults. In *Strike-slip Deformation, Basin Formation, and Sedimentation*: Eds: Biddle, K. T. and Christie-Blick, N. *Society of Economic Palaeontologists and Mineralogists Special Publication* **37,** 1-34.

Clark, R. M. and Cox, S. J. D. 1996. A modern regression approach to determining fault displacement-length scaling relationships. *Journal of Structural Geology* **18**, 147-152.

Cooke, M. L. 1997. Fracture localization along faults with spatially varying friction. *J. Geophys. Res.* **102**, 22,425-22,434.

Cowie, P. A. and Scholz, C. H. 1992a. Physical explanation for the displacement-length relationship for faults using a post-yield fracture mechanics model. *Journal of Structural Geology* **14**, 1133-1148.

Cowie, P. A. and Scholz, C. H. 1992b. Displacement-length scaling relationship for faults: data synthesis and discussion. *Journal of Structural Geology* **14**, 1149-1156.

Crampin, S. and Evans, R. 1986. Neotectonics of the Marmara Sea region of Turkey. *J. Geol. Soc. London* **143**, 343-348.

Crowell, J. C. 1979. The San Andreas fault system through time. *Journal of Geological Society of London* **136**, 293-302.

Dawers, N. H., Anders, M. H. and Scholz, C. H. 1993. Growth of normal faults: Displacement-length scaling. *Geology*. **21**. 1107-1110.

DePolo, C. M., Clark, D. G., Slemmons, D. B. and Ramelli, A. R. 1991. Historical surface faulting in the Basin and Range province, western North America: implications for fault segmentation. *Journal of Structural Geology* **13**, 123-136.

Fossen, H. and Hesthammer, J. 1997. Geometric analysis and scaling relations of deformation bands in porous sandstone. *Journal of Structural Geology* **19**, 1479-1493.

Gillespie, P. A., Walsh, J. J. and Watterson, J. 1992. Limitations of dimension and displacement data from single faults and the consequences for data analysis and interpretation. *Journal of*

Structural Geology **14**, 1157-1172.

Hill, M. L. 1981. San Andreas fault: History of concepts. *Geol. Soc. Am. Bull.*, **92**, 112-131.

Jennings, C. W. 1994. Fault activity map of California and adjacent areas. *Calif. Geol. Data Map Ser., Map 6.* Calif. Div. of Mines and Geol., Sacramento.

Karig, D. E. and Jensky, W. 1972. The proto-Gulf of California. *Earth and Planetary Science Letters* **17**, 169-174.

Keller, E. A., Bonkowski, M. S., Korsch, R. J. and Shlemon, R. J. 1982. Tectonic geomorphology of the San Andreas fault zone in the southern Indio Hills, Coachella Valley, California. *Geol. Soc. Am. Bull.*, **93**, 46-56.

Kelly, P. G., Sanderson, D. J. and Peacock, D. C. P. 1998. Linkage and evolution of conjugate strike-slip fault zones in limestones of Somerset and Northumbria. *Journal of Structural Geology* **20**, 1477-1493.

Kim, Y. S., Andrews, J. R. and Sanderson, D. J. 2000. Damage zones around strike-slip fault systems and strike-slip fault evolution, Crackington Haven, southwest England. *Geoscience Journal* **4**

La Pointe, P. R. 1988, A Method to Characterize Fracture Density and Connectivity Through Fractal Geometry. *Int. J. Rock Mech. Min. Sci. & Geomech. Abstr.* **25**, 421-429.

Mandelbrot, B. B. 1982 (Rev. ed. of c1977), The Fractal Geometry of Nature, 468pp., W. H. Freeman, San Francisco, Calif.

Marrett, R. and Allmendinger, R. W. 1991. Estimates of strain due to brittle faulting: sampling of fault populations. *Journal of Structural Geology* **13**, 735-738.

Molnar, P. and Tapponnier, P. 1975. Cenozoic tectonics of Asia: effects of a continental collision. *Science* **189**, 419-426.

Neugebauer, J. 1995. Structures and kinematics of the North Anatolian Fault zone, Adapazari-Bolu region, northwest Turkey. *Tectonophysics* **243**, 119-134.

Nicholson, C., Seeber, L., Williams, P. and Sykes, L. R. 1986. Seismic evidence for conjugate slip and block rotation within the San Andreas fault system, southern California. *Tectonics* **5**, 629-648.

Okubo, P. G. and Aki, K. 1987, Fractal Geometry in the San Andreas Fault System. *J. geophys. Res.* **92**, 345-355.

Peacock. D. C. P. 1991. Displacement and segment linkage in strike-slip fault zones. *Journal of Structural Geology* **13**, 1025-1035.

Peacock, D. C. P. and Sanderson, D. J. 1995. Strike-slip relay ramps. *Journal of Structural Geology* **17**, 1351-1360.

Revenaugh, J. and Reasoner, C. 1997. Cumulative offset of the San Andreas fault in central California: A seismic approach. *Geology* **25**, 123-126.

Rikitake, T. 1975. Statistics of ultimate strain of the earth's crust and probability of earthquake occurrence. *Tectonophysics* **26**, 1-21.

SCEC (Southern California Earthquake Center). 2000. Faults of southern California. *http://www.scecdc.scec.org/sanandre.html*

Schlische, R. W., Young, S,. S., Ackermann, R. V. and Gupta, A. 1996. Geometry and scaling relations of a population of very small rift-related normal faults. *Geology* **24,** 683-686.

Scholz, C. H. 1982. Scaling laws for large earthquakes: consequences for physical models. *Bull. Seism. Soc. Am.* **72**. 1-14.

Scholz, C. H., Dawers, N. H., Yu, J.-Z., Anders, M. H. and Cowie, P. A. 1993. Fault Growth and Fault Scaling Laws: Preliminary Results. *Journal of Geophysical Research* **98**. 21,951-21,961.

Schulz, R. A. and Aydin, A. 1990. Formation of interior basins associated with curved faults in Alaska. *Tectonics,* **9**, 1387-1407.

Schulz, S. S. and Wallace, R. E. 1997. The San Andreas Fault. *USGS website.* http://pubs.usgs.gov/gip/earthq3/index.html

Segall, P. and Pollard, D. D. 1980. Mechanics of discontinuous faults. *J. Geophys. Res.* **85**, 4337-4350.

Sengor, A. M. C., Gorur, N. and Saroglu, F. 1985. Strike-slip faulting and related basin formation in zones of tectonic escape: Turkey as a case study. In *Strike-slip Deformation, Basin Formation, and Sedimentation*: Eds: Biddle, K. T. and Christie-Blick, N. *Society of Economic Palaeontologists and Mineralogists Special Publication* **37,** 227-264.

Sibson, R. H. 1989. Earthquake faulting as a structural process. *Journal of Structural Geology* **11**, 1-14.

Stanley, R. G. 1987. New estimates of displacement along the San Andreas fault in central California based on paleobathymetry and paleogeography. *Geology* **15**, 171-174.

Stein, R. S., Barka, A. A. and Dieterich. J. H. 1997. Progressive failure on the North Anatolian fault since 1939 by earthquake stress triggering. *Geophys. J. Int.* **128,** 594-604.

Tchalenko, J. S. 1970, Similarities between shear zones of different magnitudes. *Geol. Soc. Am. Bull.*, **81**, 1625-1640.

Tchalenko, J. S. and Ambraseys, N. N. 1970, Structural analysis of the Dasht-e Bayaz (Iran) earthquake fractures. *Geol. Soc. Am. Bull.*, **81**, 41-60.

Walsh, J. J. and Watterson, J. 1988. Analysis of the relationship between displacements and dimensions of faults. *Journal of Structural Geology* **10**, 239-247.

Watterson, J. 1986. Fault dimensions, displacements and growth. *Pure and Applied Geophysics* **124**, 365-373.

Willemse, E. J. M., Pollard, D. D. and Aydin, A. 1996. Three-dimensional analyses of slip distributions on normal fault arrays with consequences for fault scaling. *Journal of Structural Geology* **18**, 295-309.

Wong, H. K., Ludman, T., Ulug, A. and Gorur, N. 1995. The Sea of Marmara: A plate boundary sea in an escape tectonic regime: Tectonophysics **244**, 231-250.

Working Group on California Earthquake Probabilities, 1995. Seismic hazards in Southern California: Probable earthquakes, 1994 to 2024. *Bull. Seis. Soc. Am.* **85**, 379-439.

Zachariasen, J. and Sieh, K. 1995. The transfer of slip between two en echelon strike-slip faults: A case study from the 1992 Landers earthquake, southern California. *J. Geophys. Res.* **100,** 15,281-15301.

Zhang, P., Slemmons, D. B. and Mao, F. 1991, Geometric pattern, rupture termination and fault segmentation of the Dixie Valley-Pleasant Valley active normal fault system, Nevada, U. S. A. *Journal of Structural Geology* **13**, 165-176.

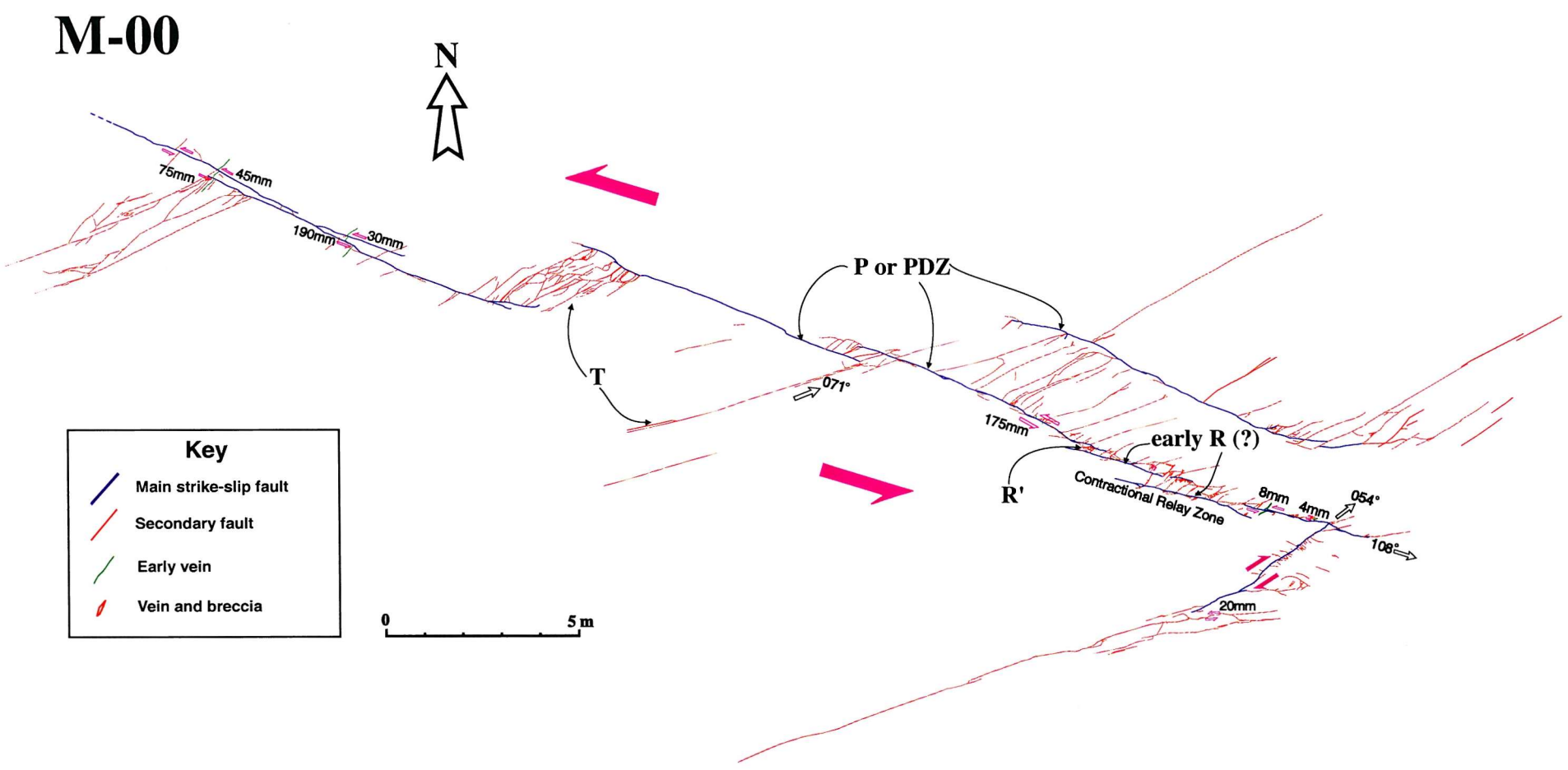

Fig. 7.1. Map of the fault M-00, Marsalforn in Gozo. The master fault trend is N108° and the predominant secondary fractures are extensional fractures striking N071°. This orientation is the same as the orientation of the regional compressive stress in this study area. The main fault system is linked through mainly dilational overstep zones. Linkage zones show high fracture densities. *P*, P shears; *R*, Riedel shears; *R'*, conjugate Riedel shears; *T*, extension fractures; *PDZ*, principal displacement zone for all the following maps.

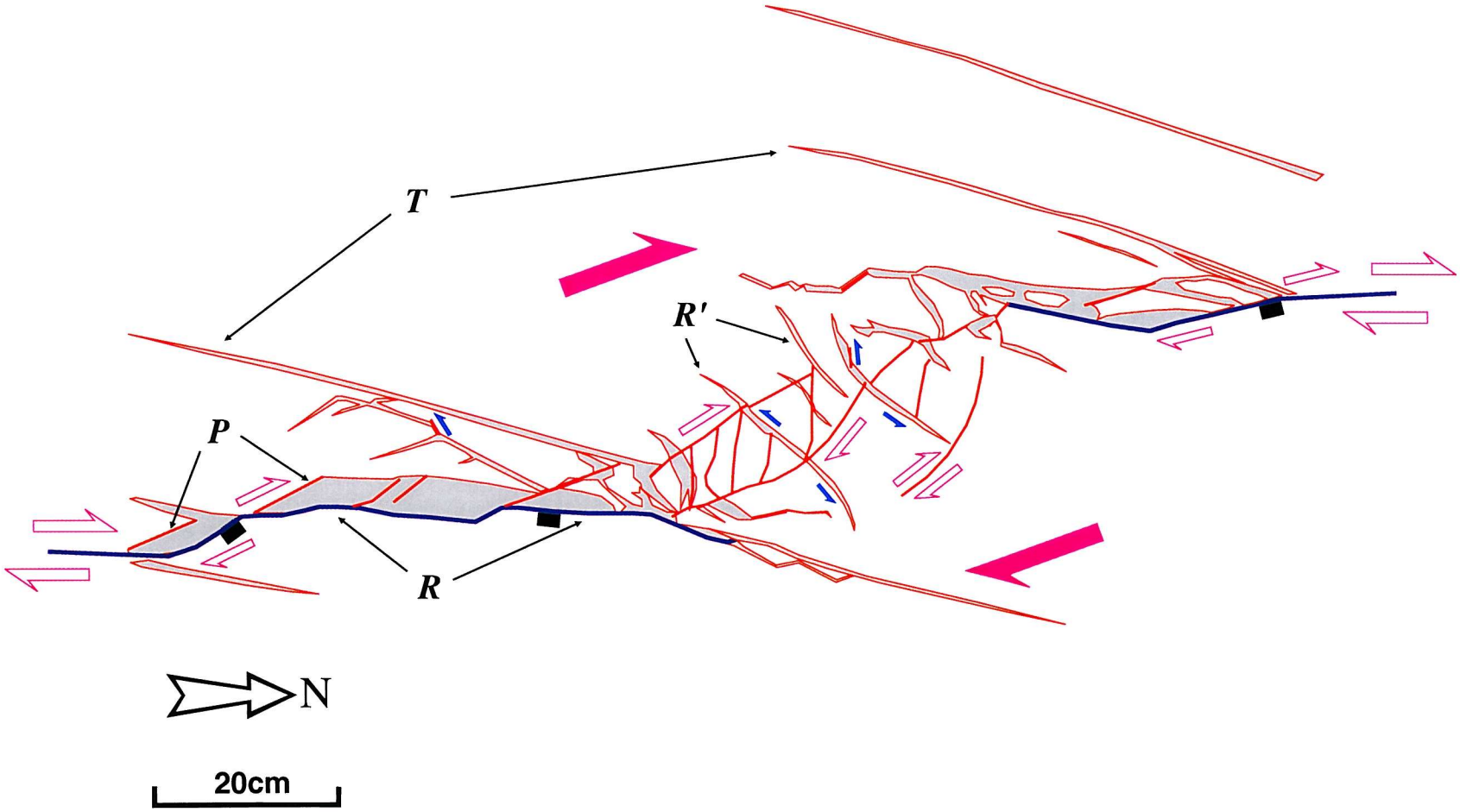

Fig. 7.2. Map of a strike-slip relay ramp at East Quantoxhead, Somerset. Normal faults are reactivated as strike-slip faults. Veins and antithetic faults are concentrated in the relay ramp, which occurs in a contractional overstep between two sinistral faults (modified from Peacock and Sanderson, 1995).

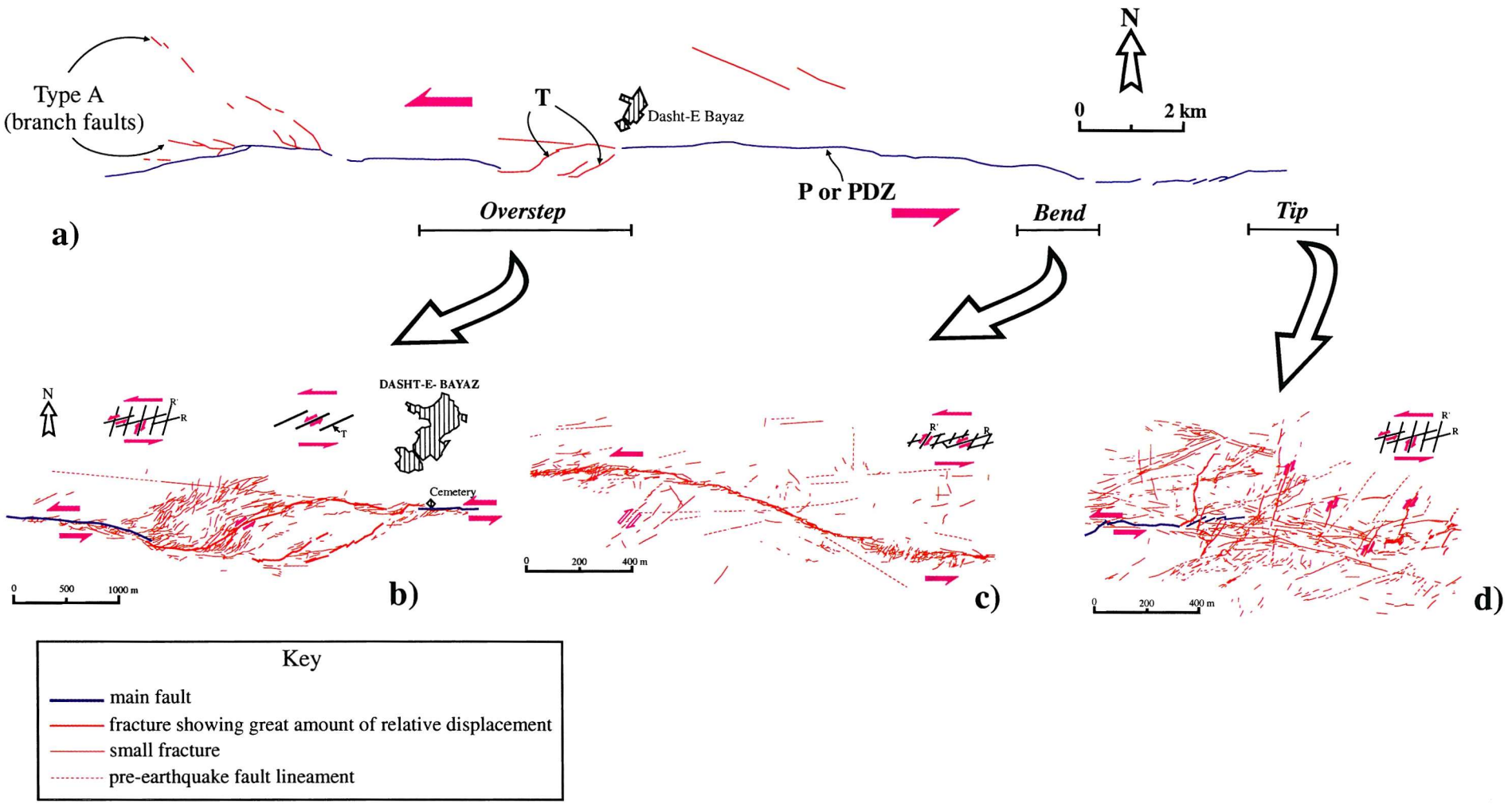

Fig. 7.3. Map and structural analysis of the fault zone in the Nimbluk Valley (modified from Tchalenko and Ambraseys, 1970). a) Main fault segments. b) Dilational overstep. c) Contractional bend. d) Tip region.

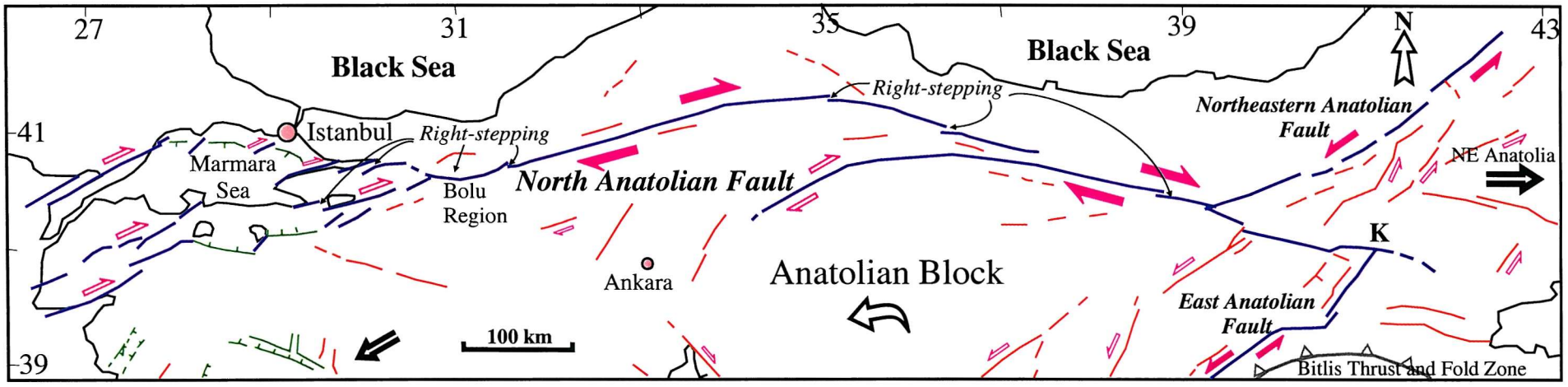

Fig. 7.4. Major tectonic elements around the North Anatolian fault in Turkey. The north and east Anatolian faults intersect at the Karliova triple junction (K). The thick blue, brown, green, and red lines denote major strike-slip fault, thrust fault, normal fault, and minor strike-slip faults, respectively. The large arrows indicate the motion of the Anatolian Block and Northeast Anatolian Block relative to Eurasia. Medium and small arrows denote slip on individual faults. Modified from Barka and Kadinsky-Cade (1988).

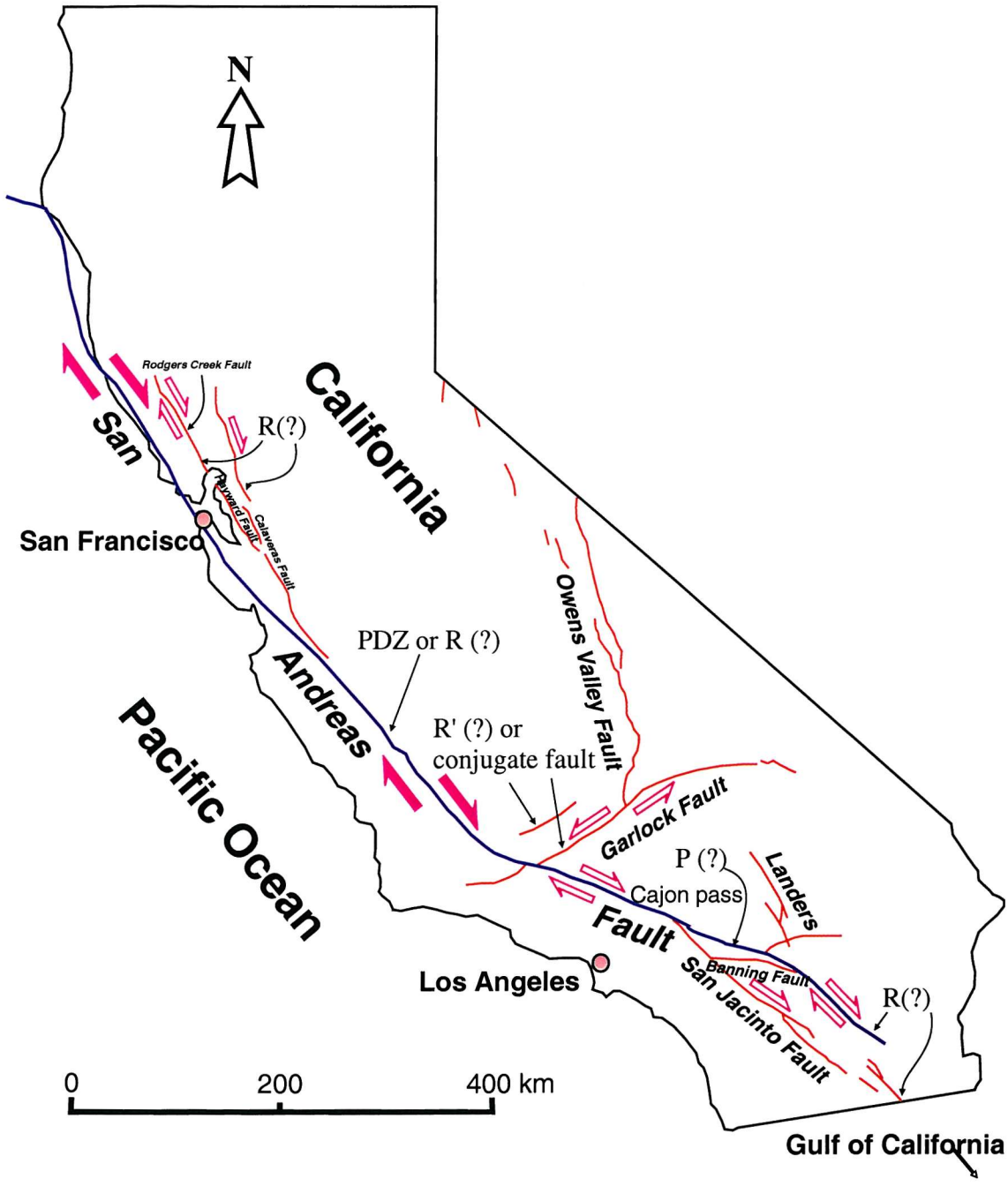

Fig. 7.5. A simplified map of the San Andreas fault system and other large faults in California. The thick blue line indicates the main San Andreas fault, and the thin red line denotes branch faults and other large faults. Modified from Schulz and Wallace (1997).

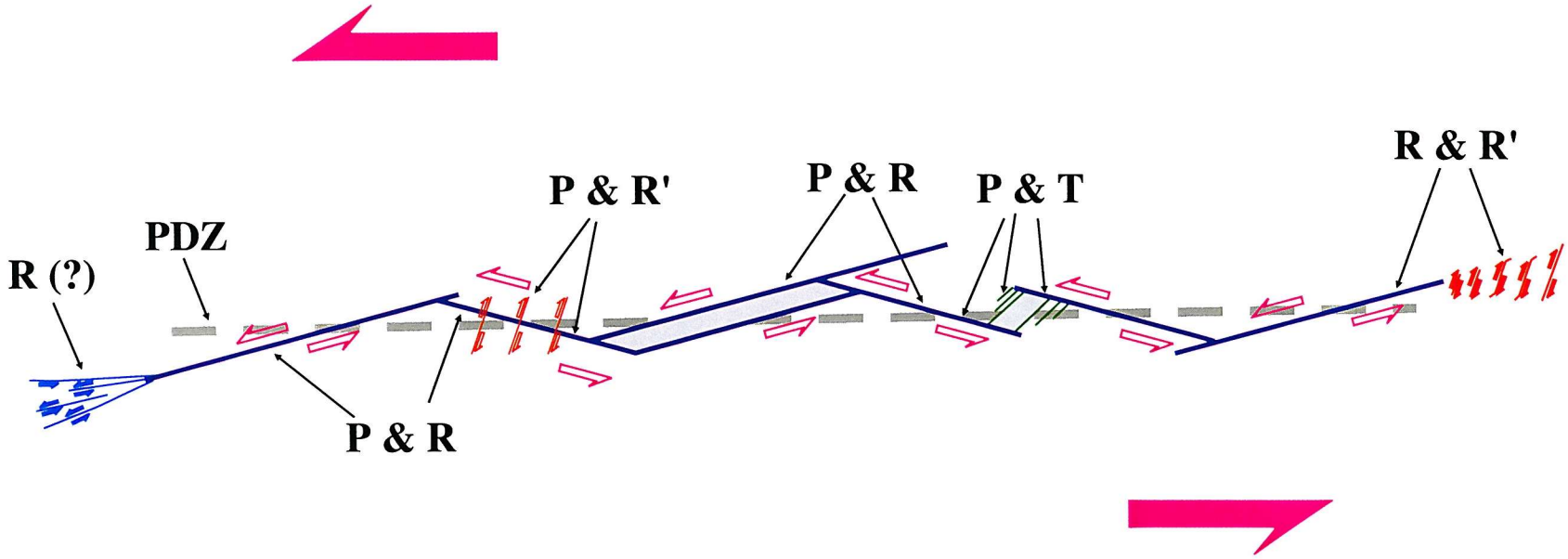

Fig. 7.6. A variety of fault and fracture patterns around strike-slip faults. They are not confined to a specific scale ranges.

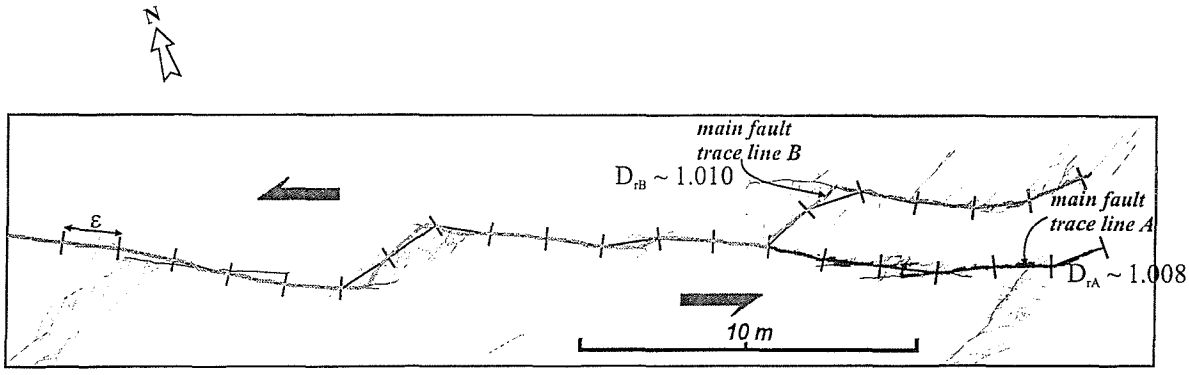

a) Ruler method for the Gozo fault (M-00).

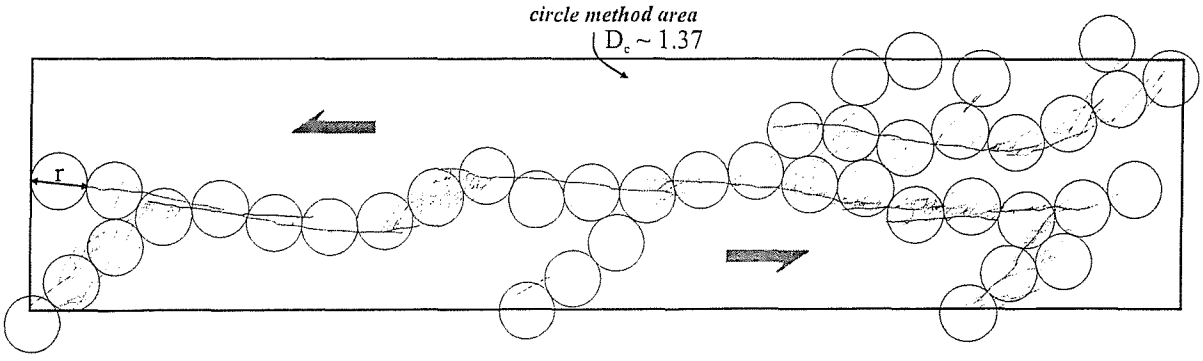

b) Circle method for the Gozo fault (M-00).

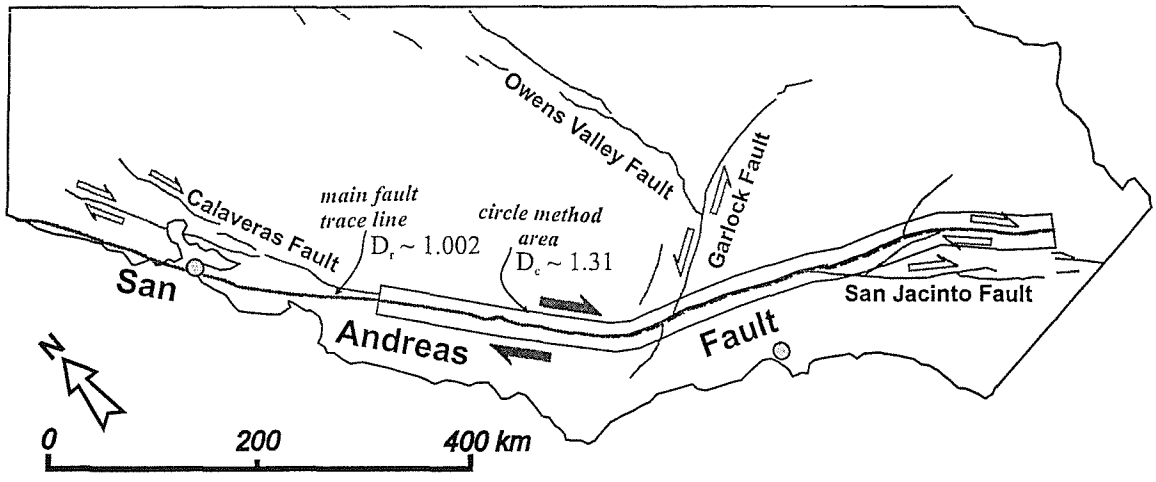

c) Circle and ruler methods for the San Andreas fault.

Fig. 7.7. Fractal analysis for the Gozo and the San Andreas faults. a) Ruler method for the two main fault traces in Gozo.b) Circle method for all faults and fractures within the selected area in Gozo. c) The selected zone for circle method and the analysed main fault trace for ruler method in the San Andreas Fault. Minor faults around the main fault are not drawn in this map. ε and *r* are measuring ruler length and circle diameter, respectively.

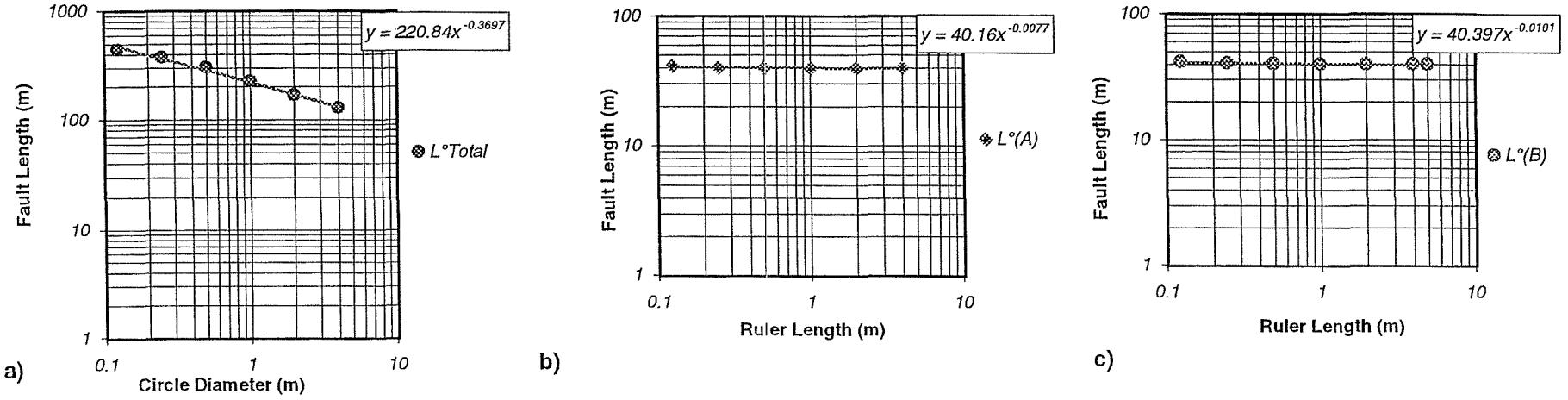

Fig. 7.8. Log fault length $L°(r$ or $\varepsilon)$ versus measuring diameter (r) or ruler length (ε) data for the M-00 fault in Gozo. a) Log fault length $L°(r)$ versus measuring diameter (r) data including secondary fractures by circle method. b) Log fault length $L°(\varepsilon)$ versus ruler length (ε) data for the main fault trace A by ruler method. c) Log fault length $L°(\varepsilon)$ versus measuring ruler length (ε) data for the main fault trace B by ruler method. Lines are best least squares fits to data.

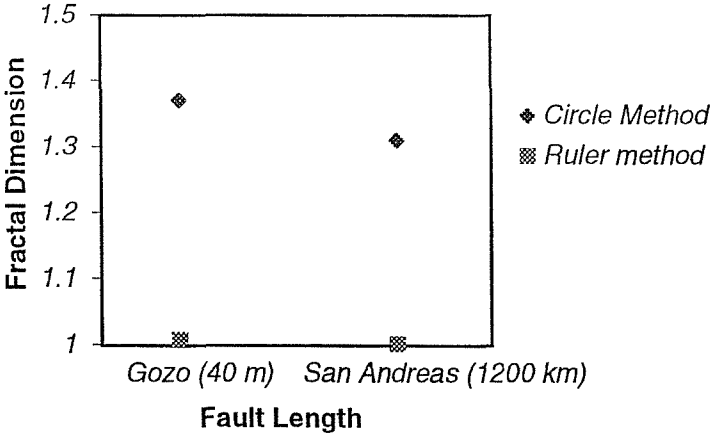

Fig. 7.9. Comparison of fractal dimension (D) data from the fault M-00 in Gozo and the San Andreas Fault. Diamond (square) symbols give dimensions using circle method (ruler method) measurement.

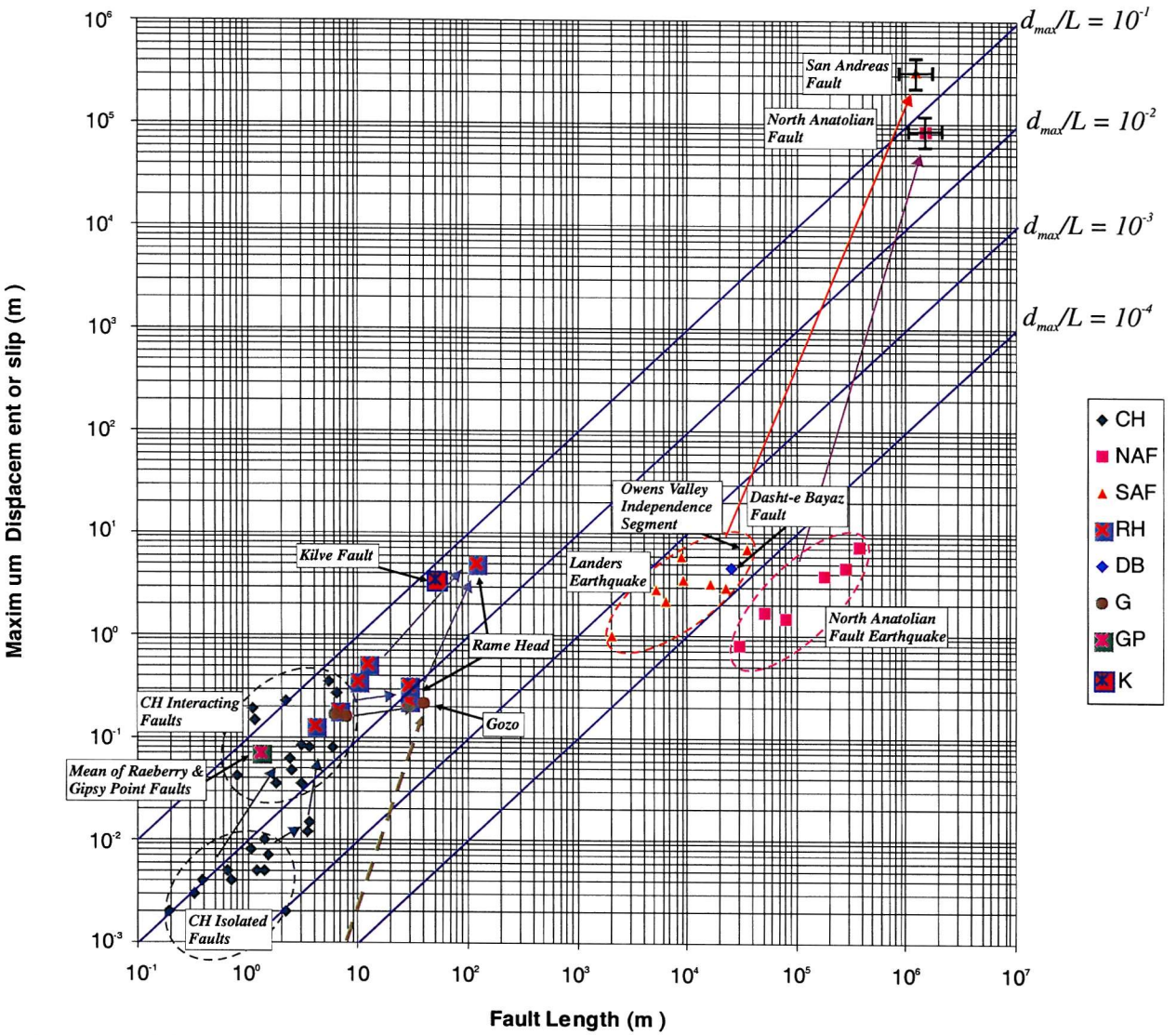

Fig. 7.10. Log-log plot of fault length (L) versus maximum displacement (d_{max}) or slip (u) for selected faults with different magnitudes. CH, Crackington Haven Faults; NAF, North Anatolian Fault and earthquake slips along segements; SAF, San Andreas Fault and earthquake slips in California; RH, Rame Head faults; DB, Dasht-e Bayaz earthquake rupture; G, Gozo faults; GP, mean value of Gipsy Point and Raeberry faults; K, Kilve fault. Arrows denote supposed fault evolution paths.

CHAPTER 8: CONCLUSIONS

1. Damage zones around strike-slip fault show a variety of fracture patterns related to accommodation of strike-slip displacement. Damage zone structures can be classified into three main groups according to their location along strike-slip fault systems; tip zone damage, wall zone damage (distributed damage), and linkage zone damage.

2. The tip damage structures can be classified by geometric patterns of damage structures, which are mainly dependent on the fault tip mode and stress propagation at cohesive end zone of each tip.
   a) Whereas at mode II tip, generally showing asymmetric pattern, a variety of damage structures such as 'wing cracks', 'horsetail splays', 'antithetic shear fractures', 'synthetic branch faults', and their combined types are often observed. A dominant damage pattern at mode II tips is wedge-shaped antithetic shear fractures (R') widening away from a tip, often accompanied by block rotation. Tip cracks develop at the tips of some shear fractures indicating slip sense.
   b) At a mode III fault tip, showing commonly symmetric pattern, the damage pattern is almost similar to the fracture pattern under simple shear. At the tips early developed R' shears intersects later P or R shears. The shear fractures often combined with T fractures to form pull-aparts. This tip damage is a main part of later wall zone damage.

3. Wall zone damage structures are relatively rare, and result from propagation of mode II & III tips, or kinematic damage including joint drag. They are 'en echelon veins', 'tension fractures', 'antithetic faults', 'Riedel shears', 'rotated blocks' and 'triangular openings'. They are increased with increasing displacement and fault growth.

4. Linkage zone damage structures are developed in the overstepped region between two or more parallel or sub-parallel faults. The damage geometries depend on the

nature of oversteps, i.e. dilational or contractional. At dilational oversteps 'tension fractures (mode I)' and 'pull-aparts' form, whereas in contractional oversteps 'composite faults' are developed. 'Rotated blocks' and 'isolated lens' or 'strike-slip duplexes' are observed in both oversteps with slight differences in geometry. Overstepping of fault segments leads to the transfer of fault displacement. At dilational oversteps and jogs, damage is localised within oversteps with displacement on the faults generally being conserved across oversteps with no displacement minimum. Contractional oversteps are characterised by well-defined displacement minima.

5. With increasing displacement, a wide variety of structures develop to accommodate wall-rock strains. Complex zones of veining and block rotation occur in broad regions of fault wall where displacement gradients are relatively constant. Fault bends (λ-faults) are characterised by local patterns of strain controlled by pre-existing structure.

6. Five sub-parallel faults at Crackington Haven show evidence of right-lateral strike-slip movement with tip cracks and dilational jogs, which has been reactivated by left-lateral strike-slip movement.
    a) Evidence for reactivation includes: two slickenside striae on a fault surface; two groups of tip cracks with different orientations; and opposite senses, and low or negative displacement at fault tips. Also, some early tip cracks formed by right-lateral movement show reactivation with a left-lateral slip sense.
    b) The intersection angle of tip cracks with the master fault may depend on the stress state, material properties, and influence of any pre-existing planes of weakness. The angular difference between the two sets of tip cracks is interpreted as due to different far- and near-field stress distribution such as transpression/ transtension and cohesive/non-cohesive. The resulting asymmetric *tree structure* is a useful geometry for recognition of reverse reactivation in the strike-slip fault systems.
    c) Most of the d - x profiles have similar patterns which show low or negative (left-lateral) displacement at the segment fault tips. Profiles that experience two opposing slip movements show various shapes depending on the amount

of displacement and the slip sequence. For a larger slip followed by smaller slip with opposite sense, the profile would be expected to record very low or reverse displacement at fault tips due to late-stage tip propagation. Whereas for a smaller slip followed by larger slip with opposite sense the d - x profile would be M-shape with no negative displacement at the tips.

7. A lot of lens-shaped structures are developed due to segment linkage as faults grow. The displacement along a fault rapidly decreases when the fault meets these structures. The d-x profiles show very variable and irregular relationship. This originates from segment linkage through lens-shaped structures and branch faults. If the fault system as a whole is considered, the d-x relationship more or less resembles that for a single fault. Where displacement minima occur, they indicate relays, lens-shaped structures or branch faults.

8. Three fault growth models are proposed to interpret the observed fracture patterns and damage structures: extensional fracture dominate model, along-strike propagation model, and up- and down-dip propagation model. These models are dependent on the master fault tip modes as well as exposed surface level across the master fault.

9. A three dimensional conceptual model is proposed for strike-slip fault damage structures, which shows different damage patterns depending on the fault tip mode and exposed section level. Different fault tips have different slip properties, so that different tip damage structures occur. Also, on the same tip mode, damage structures vary depending on location, and evolution stages.

10. Several large-scale strike-slip faults and their damage structures are compared with the classification from small-scale damage structures. Most of the large-scale examples are consistent with the classification and interpretation.

11. Although single-slip events in faults typically have $d_{max}/L \sim 10^{-4}$ (that can only be established for large faults), most geologic faults have much higher $d_{max}/L \sim 10^{-2}$ - 10^{-1} (e.g. Gozo ~ 10^{-2} and SAF ~ 10^{-1}). From the relationship between cumulative

maximum displacement and earthquake rupture slip, fault zone evolution and the approximate ages of faults can be examined.

12. Maximum displacement (d_{max}) - fault length (L) plots of strike-lip faults show a step-like fault evolution from isolated faults through soft-linked, segmented faults to hard-linked, interacting faults as a similar manner to normal fault system.

FUTURE WORK

1. The present study has been based on small-scale (0.1 – 100 m) strike-slip faults, with some comparisons with published large-scale examples. There is a need to analyse faults, particularly in the length range 100 m – 1 km, based on field studies, as these have a major impact on hydrocarbon reservoirs and aquifers.

2. Study of ground rupture associated with active faults would allow the damage patterns to be related directly to displacement events (earthquakes). The extent and nature of damage could be related directly to the slip distribution and the displacement field (from radar interferometry) around the fault.

3. The examples discussed in the present study are essentially 2-dimensional, with 3-dimensional models being inferred from these observations, as in Fig. 4.40. With modern 3-D seismic data, it would be possible to directly test the inferred 3-D models given suitable areas (e.g. Andaman Sea, S. California and Marmara Sea in Turkey, etc.).

4. The models of damage may be used to predict fracture patterns (including orientation, fracture type and density) in relation to major faults. This has major application in fracture prediction in fracture reservoirs. Thus it would be possible to use well data (core analysis, borehole imagery, down-hole logging and pump-test data) to test the applicability of models in suitable hydrocarbon fields (e.g. S. California and Vietnam).

5. The role of different tip modes and fault linkage in controlling damage has been demonstrated for strike-slip faults, but similar controls would be expected to exist for other types of faulting. Studies of areas of extensional (normal) and reverse faulting would allow further development and refinement of these concepts.

6. Damage development around faults has major implications for fluid flow in the crust, which could be examined in several ways:

   a) Numerical modelling of the flow (e.g. Sanderson and Zhang, 1999).

   b) Examination of the production history and well-test in oil fields.

   c) Distribution of hydrothermal mineralisation in relation to faults.